

Development and Assessment of Integrated Powering Systems with Alternative Fuel Choices for Clean Transportation

by

Shaimaa Fouad Mohamed Abdelhamid Seyam

A thesis submitted to the
School of Graduate and Postdoctoral Studies in partial
fulfilment of the requirements for the degree of

Doctor of Philosophy in Mechanical Engineering

Mechanical and Manufacturing Engineering Department
Faculty of Engineering and Applied Science

University of Ontario Institute of Technology (Ontario Tech University)

Oshawa, Ontario, Canada

April 2023

© [Shaimaa F. M. A. Seyam, April 2023](#)

THESIS EXAMINATION INFORMATION

Submitted by: **Shaimaa Fouad Mohamed Abdelhamid Seyam**

Doctor of Philosophy in Mechanical Engineering

Thesis title: Development and Assessment of Alternative Fuel Choices for Clean Transportation Sectors
--

An oral defense of this thesis took place on Mar 28th, 2023, in front of the following examining committee:

Examining Committee:

Chair of Examining Committee	Dr. Ghaus Rizvi
Research Supervisor	Dr. Ibrahim Dincer
Research Co-supervisor	Dr. Martin Agelin-Chaab
Examining Committee Member	Dr. Dipal Patel
Examining Committee Member	Dr. Ahmad Barari
University Examiner	Dr. Jing Ren
External Examiner	Dr. Abdul Hai Alami

The above committee determined that the thesis is acceptable in form and content and that a satisfactory knowledge of the field covered by the thesis was demonstrated by the candidate during an oral examination. A signed copy of the Certificate of Approval is available from the School of Graduate and Postdoctoral Studies.

ABSTRACT

This thesis presents novel engine systems using alternative fuels for aviation, rail, and marine transportation as follows: (i) alternative powering systems, such as fuel cells, on-board hydrogen production (ii) alternative fuel choices with hydrogen, methane, methanol, ethanol, and dimethyl ether; and (iii) different methods for waste retrieval energy, such as absorption refrigeration systems, desalination system, and thermoelectrical generators. The systems are analyzed by three methods: thermodynamic, exergoenvironmental, and exergoeconomic analyses. Besides, the multi-objective particle swarm optimization (MOPSO) is applied for different operating conditions to choose the optimal design characteristic of the transportation systems. For aviation transportation, the base turbofan produces a power of 9144 kW and thrusting energy of 38 MW, with 43.4% and 52% energetic and exergetic efficiency, respectively, under cruising conditions. However, the maximum power of SOFC-turbofan is 48MW, including 7.3 MW of turbofan power, 39.8 MW of thrust energy, and 0.94 MW of the SOFC. The overall energetic and exergetic efficiencies of the hybrid turbofan are 48.1% and 54.4%, respectively. For rail transportation, the traditional rail engine produces a power of 3355 kW with 45 % energetic and 57% exergetic efficiency. A new design of gas turbine combined with SOFC and PEMEC produces about 5590 kW with 90% energy efficiency and 50% exergy efficiency. This engine is optimized to produce a power of 7502 kW with exergetic efficiency of 82% with reducing specific fuel and product exergy cost to 11.5 \$/GJ and 14.5\$/GJ, respectively. For marine transportation, the traditional marine engine produces a power of 10,524 kW with 23% energetic efficiency. However, a steam Rankine cycle combined with a hybridized gas turbine produces a power of 15546 kW with 61% energetic efficiency and 43% exergetic efficiency. This engine is optimized to produce a power of 16725 kW with exergetic efficiency of 70% and reducing specific fuel and product exergy cost of 18 and 28 \$/GJ, respectively. In addition, all five fuel blends in the eight engines were able to reduce carbon emissions by more than 60% compared to traditional fuels. Also, the specific fuel consumption was reduced by 10-20% compared to the utilization of traditional fuels.

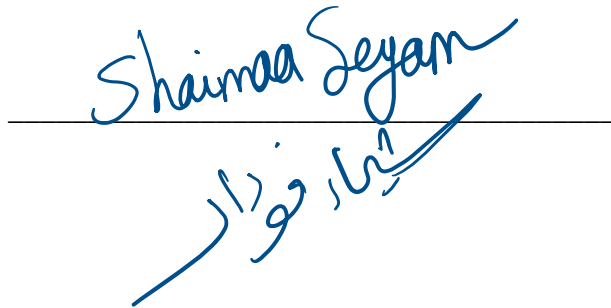
Keywords

Transportation; thermodynamic analysis; exergoenvironmental analysis; exergoeconomic analysis; alternative fuels.

AUTHOR'S DECLARATION

I hereby declare that this thesis consists of original work which I have authored. This is a true copy of the thesis, including any required final revisions, as accepted by my examiners.

I authorize the University of Ontario Institute of Technology (Ontario Tech University) to lend this thesis to other institutions or individuals for the purpose of scholarly research. I further authorize the University of Ontario Institute of Technology (Ontario Tech University) to reproduce this thesis by photocopying or by other means, in total or in part, at the request of other institutions or individuals for the purpose of scholarly research. I understand that my thesis will be made electronically available to the public.



Shaimaa Fouad Mohamed Abdelhamid
Seyam

STATEMENT OF CONTRIBUTIONS

Part of the work described in Chapter 2, 3, 4, and 5 has been published as the following:

Aviation Transportation:

- S. Seyam, I. Dincer, M. Agelin-Chaab, Environmental impact assessment of a newly developed solid oxide fuel cell-based system combined with propulsion engine using various fuel blends for cleaner operations. *Sustain Mater Technol* 35 (2023) e00554. <https://doi.org/10.1016/j.susmat.2022.e00554>.
- S. Seyam, I. Dincer, M. Agelin-Chaab, Economic and environmental impact assessments of hybridized aircraft engines with hydrogen and other fuels, *Int. J. Hydrogen Energy*. 47 (2022) 11669–11685. <https://doi.org/10.1016/j.ijhydene.2022.01.171>.
- S. Seyam, I. Dincer, M. Agelin-Chaab, Exergetic assessment of a newly designed solid oxide fuel cell-based system combined with a propulsion engine, *Energy*. 239 (2022) 122314. <https://doi.org/10.1016/j.energy.2021.122314>.
- S. Seyam, I. Dincer, M. Agelin-Chaab, Investigation of potential fuels for hybrid molten carbonate fuel cell-based aircraft propulsion systems, *Energy & Fuels*. (2021). <https://doi.org/10.1021/acs.energyfuels.1c00915>.
- S. Seyam, I. Dincer, M. Agelin-Chaab, Investigation of two hybrid aircraft propulsion and powering systems using alternative fuels, *Energy*. 232 (2021) 121037. <https://doi.org/10.1016/j.energy.2021.121037>.
- S. Seyam, I. Dincer, M. Agelin-Chaab, Novel hybrid aircraft propulsion systems using hydrogen, methane, methanol, ethanol and dimethyl ether as alternative fuels, *Energy Convers. Manag.* 238 (2021) 114172. <https://doi.org/10.1016/j.enconman.2021.114172>.

Rail Transportation:

- S. Seyam, I. Dincer, M. Agelin-Chaab, Modelling of a New Fuel Cell Based Rail Engine System Using Green Fuel Blends. *Appl Therm Eng* (2023) 120527. <https://doi.org/10.1016/j.applthermaleng.2023.120527>. (In press)
- S. Seyam, I. Dincer, M. Agelin-Chaab, Efficiency, economic and environmental impact assessments of a new integrated rail engine system using hydrogen and other sustainable fuel blends. *E-Prime - Adv Electr Eng Electron Energy* 3 (2023) 100109. <https://doi.org/10.1016/j.prime.2023.100109>.
- S. Seyam, I. Dincer, M. Agelin-Chaab, Analysis of a newly developed locomotive engine employing sustainable fuel blends with hydrogen, *Fuel*. 319 (2022) 123748. <https://doi.org/10.1016/j.fuel.2022.123748>.
- S. Seyam, I. Dincer, M. Agelin-Chaab, Development and assessment of a unique hybridized gas turbine locomotive engine operated by sustainable fuel blends, *Fuel*. 330 (2022) 125638. <https://doi.org/10.1016/j.fuel.2022.125638>.
- S. Seyam, I. Dincer, M. Agelin-Chaab, Exergetic, exergoeconomic and exergoenvironmental analyses of a hybrid combined locomotive powering system for rail transportation, *Energy Convers. Manag.* 245 (2021) 114619. <https://doi.org/10.1016/j.enconman.2021.114619>.

S. Seyam, I. Dincer, M. Agelin-Chaab, Development and assessment of a cleaner locomotive powering system with alternative fuels, *Fuel*. 185 (2021) 120529. <https://doi.org/10.1016/j.applthermaleng.2020.116432>.

Conference papers:

S. Seyam, I. Dincer, M. Agelin-chaab, Analysis of an integrated gas turbine-locomotive engine using sustainable fuel blends with hydrogen, in: 23rd World Hydrog. Energy Conf., WHEC 2022, Istanbul (2022) 1032–1034.

S. Seyam, I. Dincer, M. Agelin-Chaab, Exergoenvironmental analysis of hybridized gas turbine locomotive engine operated by a sustainable fuel blend, in: 10th Glob. Conf. Glob. Warm., Sharjah, United Arab Emirates (2022) 10–12.

Marine Transportation:

S. Seyam, I. Dincer, M. Agelin-chaab, An innovative study on a hybridized ship powering system with fuel cells using hydrogen and clean fuel blends, *Appl. Therm. Eng.* 221 (2023) 119893. <https://doi.org/10.1016/j.applthermaleng.2022.119893>.

S. Seyam, I. Dincer, M. Agelin-Chaab, Investigation and comparative evaluation of a hybridized marine engine powered by eco-friendly fuels including hydrogen, *Int. J. Hydrogen Energy*. (2022). <https://doi.org/10.1016/j.ijhydene.2022.11.008>.

S. Seyam, I. Dincer, M. Agelin-Chaab, Investigation of a hybridized combined cycle engine with SOFC system for marine applications, *J. Therm. Anal. Calorim.* (2022). <https://doi.org/10.1007/s10973-022-11765-y>.

Conference papers:

S. Seyam, I. Dincer, M. Agelin-Chaab, A hybridized ship powering system with fuel cells using hydrogen and methane, in: 13th Int. Conf. Hydrog. Prod., Pakistan, 2022: pp. 13–15.

For all the journal articles mentioned above, I performed the majority of the modelling, simulation of the proposed systems, and writing of the manuscript.

ACKNOWLEDGEMENTS

I thank Allah for the opportunity that He almighty gave to me to pursue my Ph.D. studies at Ontario Tech University since I requested and supplicated to my Lord for this journey to benefit the humanity and more specific the Muslim countries who suffered pollutions and instability before I was born. My whole dream is that this thesis will be a great contribution to humanity for better living. I asked Allah to accept this thesis for his sake and forgive my shortcomings and sins.

I thank my supervisors, Prof. Ibrahim Dincer and Dr. Martin Agelin-Chaab, for their sharing knowledge, guidance, support, and patience. Their guidance in my research was very important to achieve better performance. I also acknowledge the financial support provided by Transport Canada through its Clean Transportation Program-Research and Development and the Natural Sciences and Engineering Research Council of Canada (NSERC). In addition, my gratitude to the Ph.D. defense committee, Dr. Dipal Patel, Dr. Ahmad Barari, the university examiner, Dr. Jing Ren, and the external examiner, Dr. Abdul Hai Alami, for their comments and guidance to excel my writing for better quality.

Also, I thank my family, especially my husband, Prof. Amro Ibrahim, who supported me during my journey with passion and love, and financial assistance. I thank my kids, Fatema, Alhasan, and Rokayya who were trying to keep a quite environment for studying and supporting each other while I am busy and away from home. Special thanks to Fatema, who helped me in preparing food and cleaning our tiny and lovely house.

TABLE OF CONTENTS

THESIS EXAMINATION INFORMATION	i
ABSTRACT	ii
Keywords	ii
AUTHOR'S DECLARATION	iii
STATEMENT OF CONTRIBUTIONS	iv
ACKNOWLEDGEMENTS	vi
TABLE OF CONTENTS	vii
LIST OF TABLES	x
LIST OF FIGURES	xiv
LIST OF ABBREVIATIONS AND SYMBOLS	xxi
Chapter 1. Introduction	1
1.1 Type of Transportation Engines	1
1.2 Fuel Consumption and Environmental Impact	3
1.3 Potential Solutions for Sustainable Transportation	7
1.4 Potential of alternative fuels in transportation systems	7
1.5 Motivation and Research Objectives	9
1.6 Novelties	10
1.7 Thesis Outline	11
Chapter 2. Literature Review	12
2.1 Aviation Transportation	12
2.2 Rail Transportation	17
2.3 Marine Transportation	21
Chapter 3. Details of Transportation Systems	29
3.1 Aviation Engine Systems	30
3.1.1 System A-1: Hybrid molten carbonate fuel cell and turbofan engine	31
3.1.2 System A-2: Hybrid solid oxide fuel cell and turbofan engine	32
3.2 Rail Engine Systems	33
3.2.1 System R-1: Hybrid combined locomotive engine	34
3.2.2 System R-2: Hybrid SOFC- gas turbine and PEMFC-AEC locomotive engine	36
3.2.3 System R-3: Hybrid SOFC-PEMFC- gas turbine engine	37
3.3 Marine Engine Systems	39
3.3.1 System M-1: Hybrid combined marine engine	40
3.5.2 System M-2: Hybrid compound cycles (SRC-SOFC-GT) marine engine	41
3.3.3 System M-3: Hybrid gas turbine combined with binary systems	43
Chapter 4. System Modelling	45
4.1 Modelling of Engines	45
4.1.1 Modelling of internal combustion engine	46
4.1.2 Modelling of gas turbine engine	48
4.1.3 Modelling of a turbofan engine	48
4.1.4 Steam Rankine Cycle Modelling	50
4.1.5 Modelling of a binary system	52
4.2 Modelling of Fuel Cells	54
4.2.1 Modelling of molten carbonate fuel cell	54
4.2.2 Modelling of solid oxide fuel cell	57

4.2.3 Proton Exchange Membrane Fuel Cell (PEMFC).....	61
4.2.4 Aluminum Electrolysis Cell (AEC)	64
4.3 Modelling of Energy Recovery System	66
4.3.1 Modelling of thermoelectric generator (TEG)	66
4.3.2 Modelling of the absorption refrigeration system (ARS).....	67
4.3.3 Desalination Unit (DSWR)	68
4.4 Combustion Modelling	69
4.5 Analyses and Assessments.....	71
4.5.1 Thermodynamic Analysis	71
4.5.2 Exergy Analysis	83
4.5.3 Exergoeconomic Analysis (Economic Assessment)	91
4.5.4 Environmental Impact Assessment	102
4.6 Multi-objective Optimization.....	117
4.6.1 Optimization Procedure.....	117
4.6.2 Evolutionary Algorithm: MOPSO	118
4.6.3 Algorithm Specifications.....	120
Chapter 5. Results and Discussion	122
5.1 Results of System A-1.....	122
5.1.1 Results of Thermodynamic Analysis	122
5.1.2 Results of Exergy Analysis	127
5.1.3 Results of Exergoeconomic Analysis.....	128
5.1.4 Results of Exergoenvironmental Analysis	130
5.2 Results of System A-2.....	134
5.2.1 Results of Thermodynamic Analysis	134
5.2.2 Results of Exergy Analysis	140
5.2.3 Results of Exergoeconomic Analysis.....	143
5.2.4 Results of Exergoenvironmental Analysis	147
5.3 Results of System R-1.....	155
5.3.1 Results of Thermodynamic Analysis	156
5.3.2 Results of Exergy Analysis	161
5.3.3 Results of Exergoeconomic Analysis.....	164
5.3.4 Results of Exergoenvironmental Analysis	167
5.4 Results of System R-2.....	171
5.4.1 Results of Thermodynamic Analysis	171
5.4.2 Results of Exergy Analysis	176
5.4.3 Results of Exergoeconomic Analysis.....	178
5.4.4 Results of Exergoenvironmental Analysis	182
5.5 Results of System R-3.....	189
5.5.1 Results of Thermodynamic Analysis	189
5.5.2 Results of Exergy Analysis	199
5.5.3 Results of Exergoeconomic Analysis.....	201
5.5.4 Results of Exergoenvironmental Analysis	204
5.6 Results of System M-1.....	211
5.6.1 Results of Thermodynamic Analysis	211
5.6.2 Results of Exergy Analysis	220
5.6.3 Results of Exergoeconomic Analysis.....	222
5.6.4 Results of Exergoenvironmental Analysis	225

5.7 Results of System M-2.....	230
5.7.1 Results of Thermodynamic Analysis	231
5.7.2 Results of Exergy Analysis	241
5.7.3 Results of Exergoeconomic Analysis.....	243
5.7.4 Results of Exergoenvironmental Analysis	247
5.8 Results of System M-3.....	254
5.8.1 Results of Thermodynamic Analysis	254
5.8.2 Results of Exergy Analysis	263
5.8.3 Results of Exergoeconomic Analysis.....	265
5.8.4 Results of Exergoenvironmental Analysis	268
5.9 Comparison and Optimization	274
5.9.1 Aviation Systems.....	274
5.9.2 Rail Systems	279
5.9.3 Marine Systems	284
Chapter 6. Conclusions and Recommendations.....	290
6.1 Conclusions.....	290
6.2 Recommendations	300
REFERENCES.....	302
APPENDICES	320
Appendix A: Similarity of Papers.....	320
Appendix B: Cost Equations of major components	324
Appendix C: Life cycle analysis of material processing.....	325
Appendix D: Life cycle analysis of material production	326

LIST OF TABLES

Table 3.1 The system design for the transportation sectors.....	29
Table 3.2 The specification of a traditional turbofan aircraft engine	31
Table 3.3 The specifications of the locomotive engine	34
Table 3.4 The specification of a tanker ship and its engine for marine transportation ([18,19])	39
Table 4.1 The thermodynamic equations for the dual cycle processes.....	47
Table 4.2 Energy and exergy balance equations for basic components in turbofan engines.	49
Table 4.3 The specifications of SRC	52
Table 4.4 Refrigerants used in the binary system of TORC/BORC [143,144]	52
Table 4.5 The specifications of MCFC.....	57
Table 4.6 The specifications of SOFC [151]	60
Table 4.7 The specifications of PEMFC [154]	63
Table 4.8 The specifications of AEC [159]	65
Table 4.9 Partial mass balance and energy balance equations of ARS	68
Table 4.10 The specifications of baseline fuels for baseline transportation systems	70
Table 4.11 The specifications of alternative fuels for developed transportation systems	70
Table 4.12 The stoichiometric combustion reactions for the fuels	70
Table 4.13 Steam reforming, water gas shift and catalytic burner of SOFC and MCFC systems.....	71
Table 4.14 The fuel and product exergy equations for A-1 system components	84
Table 4.15 The fuel and product exergy equations for A-2 system components	85
Table 4.16 The fuel and product exergy equations for R-1 system components.....	86
Table 4.17 The fuel and product exergy equations for R-2 system components.....	87
Table 4.18 The fuel and product exergy for R-3 system components	88
Table 4.19 The fuel and product exergy for M-1 system components	89
Table 4.20 The fuel and product exergy for M-2 system components	90
Table 4.21 The fuel and product exergy for M-3 system components	91
Table 4.22 The exergoeconomic balance equations for equipment of A-1 system	94
Table 4.23 The exergoeconomic balance equations for A-2 system components.....	95
Table 4.24 The exergoeconomic balance equations for R-1 system components.....	96
Table 4.25 The exergoeconomic balance equations for R-2 system components.....	97
Table 4.26 The exergoeconomic balance equations for R-3 system components.....	98
Table 4.27 The exergoeconomic balance equations for M-1 system components.....	99
Table 4.28 The exergoeconomic balance equations for M-2 system components.....	100
Table 4.29 The exergoeconomic balance equations for M-3 system components.....	101
Table 4.30 The normalization of TRACI V2.1 Categories.....	105
Table 4.31 The cost and environmental impact of fuels and substances	108
Table 4.32 The specific exergoeconomic and exergoenvironmental impact of fuels.....	108
Table 4.33 The exergoenvironmental balance equations for A-1 system components ..	109
Table 4.34 The exergoenvironmental balance equations for A-2 system components ..	110
Table 4.35 The exergoenvironmental balance equations for R-1 system components...	111
Table 4.36 The exergoenvironmental balance equations for R-2 system components...	112

Table 4.37 The exergoenvironmental balance equations for R-3 system components...	113
Table 4.38 The exergoenvironmental balance equations for M-1 system components..	114
Table 4.39 The exergoenvironmental balance equations for M-2 system components..	115
Table 4.40 The exergoenvironmental balance equations for M-3 system components..	116
Table 5.1 The thermodynamic data of system components of MCFC-turbofan using fuel F1	123
Table 5.2 The results of MCFC performance using different fuels.....	124
Table 5.3 CO ₂ production and emission of hybrid-turbofan engine	126
Table 5.4 The exergetic analysis for components of aircraft system.....	127
Table 5.5 The exergoeconomic analysis of components of combined aircraft system ..	129
Table 5.6 The exergoenvironmental results of components of combined aircraft system	131
Table 5.7 The exergoenvironmental performance of components	131
Table 5.8 The thermodynamic results of components in the base-turbofan engine	135
Table 5.9 Results of the SOFC using F1 (75% methane and 25% hydrogen).....	135
Table 5.10 The performance of the SR, WGS, and SOFC with respect to fuels	136
Table 5.11 Mass flow rates using alternative fuels.....	137
Table 5.12 The exit conditions of the hot nozzle using different fuels.....	137
Table 5.13 The exergetic results of components in the SOFC-turbofan system	140
Table 5.14 The capital cost and annual levelized investment cost of components.....	144
Table 5.15 The exergoeconomic results of components in SOFC-turbofan system.....	144
Table 5.16 The specific exergetic cost [\$/GJ] of electricity and exhaust gases.	147
Table 5.17 The percentage Weight of Rolls Royce parts [214].....	147
Table 5.18 The component-related exergoenvironmental impact of SOFC turbofan engine	148
Table 5.19 The exergoenvironmental impact results for components	149
Table 5.20 The exergoenvironmental impact results for components	149
Table 5.21 Specific exergoenvironmental impact [mPt/MJ] of electricity and exhaust gases.....	153
Table 5.22 The energy loads and efficiencies of components using F1 fuel.	157
Table 5.23 The hybrid combined engine performance using F1 fuel.	158
Table 5.24 The MCFC performance with respect to different fuels.....	159
Table 5.25 The absorption Refrigeration system performance with respect to fuels.	160
Table 5.26 The exergy flow analysis for the components	163
Table 5.27 The results of exergoeconomic analysis of the system components	166
Table 5.28 The component-related environmental impact results.....	167
Table 5.29 The exergoenvironmental analysis results of the components	169
Table 5.30 The results of the performance of components in the hybrid engine.....	172
Table 5.31 The performance of the major systems/components	172
Table 5.32 The fuel and air mass flowrates with respect to fuels.....	173
Table 5.33 The CO ₂ emissions using diesel and sustainable fuels.	176
Table 5.34 The exergy analysis of rail engine components.....	177
Table 5.35 The components' costs of R-2 rail engine.	179
Table 5.36 The primary economic assessment of the rail engine	180
Table 5.37 Economic results of the rail engine.....	180

Table 5.38 The exergoeconomic analysis of rail engine components	181
Table 5.39 The exergoenvironmental analysis of rail engine components.....	183
Table 5.40 The exergoenvironmental performance of rail engine components	184
Table 5.41 The performance of the engine components.....	191
Table 5.42 Performance of the subsystems and overall engine	192
Table 5.43 CO ₂ emissions with respect to fuels	195
Table 5.44 The exergy performance of R-3 system.....	200
Table 5.45 The components' costs of R-3 rail system.....	202
Table 5.46 The exergoeconomic analysis of R-3 rail engine components	203
Table 5.47 The component-related environmental impact results.....	205
Table 5.48 The exergoenvironmental analysis of R-3 rail engine components.....	206
Table 5.49 The exergoenvironmental performance of R-3 rail engine components	207
Table 5.50 The detailed performance of system component.	212
Table 5.51 The performance of combined engines and overall system.....	213
Table 5.52 Comparison of traditional marine engine and sustainable fuels hybrid marine engines	220
Table 5.53 Exergy performance of M-1 marine engine.....	221
Table 5.54 The components' costs of M-1 marine engine.....	223
Table 5.55 The exergoeconomic analysis of M-1 marine engine components.....	223
Table 5.56 The component-related environmental impact results of M-1 marine engine	226
Table 5.57 The exergoenvironmental analysis of M-1 marine engine components	227
Table 5.58 The exergoenvironmental performance of M-1 marine engine components	227
Table 5.59 The component performance for the SRC and GBC engines.....	233
Table 5.60 The component units for desalination unit (DSWR)	234
Table 5.61 Comparison of traditional marine engines and sustainable fuels hybrid marine engines	240
Table 5.62 The exergy performance of M-2 marine engine	243
Table 5.63 The components' costs of M-2 marine engine.....	245
Table 5.64 The exergoeconomic analysis of M-2 marine engine components.....	246
Table 5.65 The component-related environmental impact results of M-2 marine engine	249
Table 5.66 The exergoenvironmental analysis of M-2 marine engine components	250
Table 5.67 The exergoenvironmental performance of M-2 marine engine components	251
Table 5.68 The equipment performance in the developed marine engine	255
Table 5.69 The performance of subsystems and overall marine engine	256
Table 5.70 Exhaust temperature of GBC including streams G8 to G11	260
Table 5.71 Comparison of traditional marine engine and sustainable fuels hybrid marine engines	263
Table 5.72 The exergy performance of M-3 marine engine	264
Table 5.73 The components' costs of M-3 marine engine.....	266
Table 5.74 The exergoeconomic analysis of M-3 marine engine components.....	267
Table 5.75 The component-related environmental impact results of M-3 marine engine	270
Table 5.76 The exergoenvironmental analysis of M-3 marine engine components	270
Table 5.77 The exergoenvironmental performance of M-3 marine engine components	271

Table 5.78 Comparison between aviation aircraft engines	275
Table 5.79 Decision variables of SOFC-turbofan with lower and upper constrains.	277
Table 5.80 The objective functions of SOFC-turbofan optimization	278
Table 5.81 The optimal solutions and decision variables for SOFC-turbofan engine....	279
Table 5.82 Comparison between three developed and traditional rail engines.	281
Table 5.83 The decision variables of SOFC-PEMFC-GT (R-3) rail engine.	282
Table 5.84 The objective functions of hybridized gas turbine rial engine for optimization.	283
Table 5.85 The optimal solutions and optimal decision variables for R-3 rail system...	284
Table 5.86 Comparison of three designed marine engine and traditional marine engine.	286
Table 5.87 The decision variables of SRC-GT-SOFC (M-2) marine engine.	288
Table 5.88 Objective functions of SRC-GT-SOFC marine engine for optimization	288
Table 5.89 The optimal solutions and decision variables of M-2 marine engine.	289

LIST OF FIGURES

Figure 1.1 Types of aircraft engines of atmospheric dependent type (adapted from [4]) ..	2
Figure 1.2 Types of locomotive engines (adapted from [5])	3
Figure 1.3 Types of marine propulsion engines (adapted from [6])	3
Figure 1.4 The physical properties of different fuel transportation (adapted from [7,8]) ..	4
Figure 1.5 Fuel mix of the transportation sector, 2021 (adapted from [9])	5
Figure 1.6 The GHG emissions and energy use for rail transportation (a) the activity of passenger and freight rail transportation (b), the GHG emissions and energy use for aviation transportation (c) and the activity of passenger and freight aviation transportation (d), the GHG emissions and energy use for marine transportation (e), and the activity of freight marine transportation (f).....	6
Figure 3.1 The configuration of the aviation base (A-Base) system	30
Figure 3.2 The configuration of hybrid MCFC-turbofan engine (A-1) system.....	32
Figure 3.3 The configuration of hybrid SOFC-turbofan engine (A-2) system	33
Figure 3.4 The configuration of R-Base system	34
Figure 3.5 The configuration of the proposed hybrid combined engine (R-1) system.....	35
Figure 3.6 The schematic diagram of the hybrid locomotive engine (R-2) system.....	37
Figure 3.7 The schematic layout of the proposed hybridized gas turbine locomotive engine (R-3) system	38
Figure 3.8 The layout of traditional marine engine	40
Figure 3.9 The layout of the proposed hybrid marine engine (M-1) system.	41
Figure 3.10 The schematic diagram of the hybrid combined marine engine (M-2) system.	42
Figure 3.11 The schematic layout of the hybridized integrated marine engine (M-3) system	44
Figure 4.1 The layout of system modelling throughout the thesis.....	45
Figure 4.2 The diagrams of dual fuel cycle without a turbocharger: (a) P-v diagram and (b) T-s diagram	46
Figure 4.3 The T-s diagram for base-turbofan engine.	49
Figure 4.4 The MCFC diagram with steam reforming and water gas shift	55
Figure 4.5 The SOFC diagram with steam reforming and water gas shift	58
Figure 4.6 The schematic diagram of PEMFC diagram	62
Figure 4.7 The flow chart analyses and assessments.....	72
Figure 4.8 The flow chart of Aspen Plus simulation for hybrid MCFC-turbofan systems.	75
Figure 4.9 The Aspen Plus flow chart for the SOFC-turbofan systems	75
Figure 4.10 The Aspen flow chart for: (a) the hybrid combined engine and (b) the absorption refrigeration system.....	77
Figure 4.11 The Aspen flowcharts for hybrid engine: (a) the GT and SOFC, (b) onboard hydrogen production, and (c) ARS system.	78
Figure 4.12 The flowchart of the Aspen Plus simulation of system R-3 locomotive engine.....	79

Figure 4.13 The simulation diagram of the developed marine engine using the Aspen Plus	80
Figure 4.14 The Aspen PLUS flowchart of the SRC. The stream B2 exits from the burner boiler (BR-BL) to the heat exchanger boiler (HXBL) (see Figure 4.14).....	81
Figure 4.15 The Aspen Plus flowchart of the hybrid GBC. The stream B2 flows to the heat exchanger boiler (HXBL).....	82
Figure 4.16 The Aspen Plus flowchart for the desalination unit (DSWR)	82
Figure 4.17 The Aspen flowchart for hybridized GBC. Stream G9 goes to CN1 in Figure 4.18.....	83
Figure 4.18 The Aspen flowchart of the ORCs. Stream G9 comes from GTHX.	83
Figure 4.19 Life cycle analysis frameworks	102
Figure 4.20 Vehicle and Fuel cycles for three transportation sectors	102
Figure 4.21 LCIA for fuel blends to estimate bf for fuel blends Y for some components.	108
Figure 4.22 The optimization procedure for clean transportation systems.....	117
Figure 4.23 The pseudo-code for the PSO algorithm	119
Figure 5.1 The total power of the hybrid-MCFC turbofan engine.	125
Figure 5.2 The performance of the hybrid-MCFC turbofan engine with respect to fuels	125
Figure 5.3 The total specific fuel consumption and thrust-to-weight ratio of the hybrid-MCFC turbofan engine.	126
Figure 5.4 (a) Total exergy rates of fuel, product, and destruction and (b) the exergetic efficiency ε and exergy destruction ratio y	128
Figure 5.5 (a) Total exergetic rates of fuel, product, and destruction and (b) the overall specific exergetic cost of fuel, product and fuel blends.....	129
Figure 5.6 (a) The relative cost difference, r , and exergoeconomic factor, f and (b) the specific exergetic cost of electricity cel	130
Figure 5.7 (a) Total exergoenvironmental rates of fuel, product, and destruction and (b) the overall specific exergoenvironmental impact of fuel, product, and fuel blends.	132
Figure 5.8 (a) Relative environmental difference, rb , and exergoenvironmental factor, fb and (b) the specific exergoenvironmental impact of electricity $belec$	132
Figure 5.9 (a) The exergetic cost rate of thrust and (b) the exergoenvironmental rate of thrust.	133
Figure 5.10 The thrust force and the TSFC of the base- and SOFC-turbofans with respect to fuels.....	138
Figure 5.11 The net power of the GT and thrust energy of the base- and SOFC-turbofans.	138
Figure 5.12 Overall energetic and exergetic efficiencies of the base- and SOFC-turbofans.	139
Figure 5.13 The CO ₂ emission with respect to fuels	139
Figure 5.14 The Sankey diagram for exergy flow rate [kW].....	141
Figure 5.15 The exergy results of hybrid SOFC-turbofan engine: (a) fuel, product, and destruction exergy rate, and (b) ε and y	142
Figure 5.16 The Sankey diagram for exergoeconomic flow rates [\$/h].	145

Figure 5.17 The exergoeconomic analysis results of hybrid SOFC-turbofan engine: (a) exergoeconomic rates for fuel, product, and destruction, and (b) overall specific exergoeconomic fuel, product, and selected fuel.....	146
Figure 5.18 The relative cost difference r and exergoeconomic factor f	146
Figure 5.19 The Sankey diagram for exergoenvironmental flow rates [mPt/h]	148
Figure 5.20 Total exergoenvironmental rates for fuel, product, and destruction	150
Figure 5.21 The specific exergoenvironmental impact for fuel and product for engine and fuels.....	151
Figure 5.22 Environmental impact due to pollution formation, BPF	152
Figure 5.23 Total environmental impact, BT	152
Figure 5.24 Relative environmental impact difference r_b and exergoenvironmental factor f_b	153
Figure 5.25 (a) Exergy rates and (b) exergoenvironmental rates of the Exit Nozzle (EN)	154
Figure 5.26 (a) Exergy rates and (b) exergoenvironmental rates of the FAN Nozzle (FN)	154
Figure 5.27 (a) The thrust forces and (b) exergoenvironmental impact due to nozzle thrust forces.....	155
Figure 5.28 The fuel and steam mass flow rate entering the SR and the S/C ratio.	158
Figure 5.29 (a) Net power and (b) specific fuel consumption for subsystems and overall system	160
Figure 5.30 (a) Overall efficiencies for the engine and (b) CO ₂ emissions for the subsystems	161
Figure 5.31 The Sankey Diagram for exergy flow rate in kW	162
Figure 5.32 (a) The total exergy fuel, product, destruction, and loss and (b) the total exergy efficiency (ε_t) and destruction ratio (y_t).	164
Figure 5.33 The Sankey diagram for the cost exergy flow rates in [\$ /h]	165
Figure 5.34 (a) The total cost rate of exergy fuel CF , product CP , and destruction CD and (b) the total exergoeconomic factor (f) and relative cost difference (r).....	166
Figure 5.35 The Sankey diagram for exergoenvironmental impact flow rate for streams [mPt/h]	168
Figure 5.36 (a) The total exergoenvironmental impact rate of fuel BF , product BP , destruction BD , and total related to components BT , and (b) the total exergoenvironmental factor f_b and the relative environmental impact difference r_b ...	170
Figure 5.37 The performance of hybrid engine: (a) heat and power, (b) electric power of major components, and (c) overall energetic and exergetic efficiency of the hybrid engine.....	173
Figure 5.38 (a) The heating load of the combustion chamber (CC), afterburner (BR) and cooling load and (b) the duty of SR and WGS reactors with respect to fuel blends	175
Figure 5.39 The performance of SOFC: (a) heat and power and a number of stacks and energetic and (b) exergetic efficiencies and amount of required hydrogen.....	175
Figure 5.40 The exergy analysis based on fuel blends: (a) Fuel, product, destruction, and losses exergetic rates, and (b) exergetic efficiency and exergy destruction ratio	178
Figure 5.41 Exergoeconomic rates with respect to fuel blends	182
Figure 5.42 The exergoeconomic performance of the hybridized engine: (a) specific fuel and product exergy cost, and (b) relative cost difference and exergoeconomic factor...	182

Figure 5.43 Four exergoenvironmental rates with respect to fuel blends	185
Figure 5.44 (a) Pollution formation exergoenvironmental rates and (b) total environmental impact rates of components with respect to fuel blends	186
Figure 5.45 The exergoenvironmental performance: (a) specific exergoenvironmental impact, and (b) relative environmental difference and exergoenvironmental factor	187
Figure 5.46 Economic and environmental impact of hydrogen production and exhaust gases: (a) specific exergetic cost, and (b) specific environmental impact	187
Figure 5.47 Economic and environmental impact of power and heat components: (a) specific exergy cost of power and heat, and (b) specific environmental impact of power and heat	189
Figure 5.48 The power and heat of engine (a) and the performance of hybrid engine...	193
Figure 5.49 The power and heat of the engine components	193
Figure 5.50 Comparison of energetic efficiency of the GT-only, GT+SOFC, and the overall engine	195
Figure 5.51 The performance of the SOFC system: (a) The power and heat of SOFC, and (b) the efficiencies of SOFC	196
Figure 5.52 The performance of PEMFC system: (a) power and heat, and (b) efficiencies	197
Figure 5.53 Number of stacks (a) and amount of hydrogen (b) for the fuel cells	197
Figure 5.54 The TEG1 performance: (a) power and exhaust heat, and (b) efficiencies.	198
Figure 5.55 The TEG2 performance: (a) power and heat, and (b) efficiencies	198
Figure 5.56 The Sankey flowchart of exergy rates of R-3 rail engine system.....	199
Figure 5.57 The exergy analysis based on fuel blends: (a) fuel, product, destruction, and losses exergetic rates, and (b) exergetic efficiency and exergy destruction ratio	200
Figure 5.58 Sankey flowchart of exergoeconomic rates of R-3 rail engine.	201
Figure 5.59 (a) Exergoeconomic rates and (b) specific exergy costs of the hybridized rail engine with respect to fuel blends.....	203
Figure 5.60 Exergoeconomic performance of a hybridized rail engine: (a) relative cost difference and exergoeconomic factor, and (b) specific exergy cost of exhaust	204
Figure 5.61 Sankey flowchart of exergoenvironmental rates [Pt/h]	204
Figure 5.62 (a) Exergoenvironmental rates and (b) specific exergy costs of the hybridized rail engine with respect to fuel blends	208
Figure 5.63 Pollution formation exergoenvironmental rates (a) and total environmental impact rates (b) of components with respect to fuel blends.....	209
Figure 5.64 The exergoeconomic performance of a hybridized R-3 rail engine: (a) relative environmental difference and exergoenvironmental factor, and (b) specific exergy environmental impact of exhaust	209
Figure 5.65 (a) Exergy cost and (b) environmental impact of electricity and heat of R-3 engine	210
Figure 5.66 (a) Power and (b) heat of the ICE processes	214
Figure 5.67 (a) ICE Efficiencies and (b) specific fuel consumption (SFC) and carbon emissions.....	214
Figure 5.68 (a) Power and (b) heat of GT engine with respect to fuel blends.....	215
Figure 5.69 (a) Efficiencies and (b) SFC and carbon emissions of GT engine	216

Figure 5.70 Performance of SOFC with respect to fuel blends: (a) reforming heat, (b) Cell and loss voltage, (c)) Heat and power of SOFC, (d) Number of stacks and hydrogen amount, (e) Efficiencies of SOFC, and (f) SFC and carbon emissions	217
Figure 5.71 (a) Overall power and (b) Overall efficiencies of hybrid ICE and GT engines	218
Figure 5.72 The arrangement of two engine systems in the Aframax engine room	219
Figure 5.73 The Sankey flowchart of exergy rates of M-1 engine [kW].....	220
Figure 5.74 The exergy analysis of M-1 marine engine based on fuel blends: (a) fuel, product, destruction, and losses exergetic rates, and (b) exergetic efficiency and exergy destruction ratio	221
Figure 5.75 The Sankey flowchart of exergoeconomic rates of M-1 engine.....	222
Figure 5.76 (a) Exergoeconomic rates and (b) specific exergy costs of the hybridized rail engine with respect to fuel blends.....	224
Figure 5.77 The exergoeconomic performance of a hybridized rail engine: (a) relative cost difference and exergoeconomic factor, and (b) specific exergy cost of exhaust.....	225
Figure 5.78 The Sankey flowchart of exergoenvironmental rates of M-1 engine [Pt/h]	225
Figure 5.79 (a) Exergoenvironmental rates and (b) specific exergy costs of M-1 marine engine with respect to fuel blends.....	228
Figure 5.80 (a) Pollution formation rates and (b) total environmental impact rates of components of M-1 marine engine with respect to fuel blends	229
Figure 5.81 The exergoeconomic performance of a hybridized M-1 engine: (a) relative environment difference and exergoenvironmental factor, and (b) specific exergy environmental impact of exhaust	229
Figure 5.82 (a) Exergy cost and (b) environmental impact of electricity and heat for M-1 engine	230
Figure 5.83 (a) The net power and (b) the net required heat for three marine subsystems	235
Figure 5.84 The heat rates of SRC components for all fuels	236
Figure 5.85 (a) Exergy destruction rates and (b) energetic and exergetic efficiencies for three subsystems	236
Figure 5.86 The overall energetic and exergetic efficiency of the engine	237
Figure 5.87 The distribution of heat and power of SOFC	238
Figure 5.88 (a) Electric performance of SOFC and (b) required stack numbers and amount of hydrogen in SOFC	239
Figure 5.89 (a) Fuel mass flow rates, (b) SFC, and (c) carbon emissions of three marine subsystems	240
Figure 5.90 The Sankey flowchart of exergy rates of M-2 engine	242
Figure 5.91 Exergy analysis of M-2 marine engine based on fuel blends: (a) Fuel, product, destruction, and losses exergetic rates, and (b) Exergetic efficiency and exergy destruction ratio.	242
Figure 5.92 The Sankey flowchart of exergoeconomic rates of M-2 engine.....	244
Figure 5.93 (a) Exergoeconomic rates and (b) specific exergy costs of the M-2 marine engine with respect to fuel blends.....	247
Figure 5.94 Exergoeconomic performance of an M-2 marine engine. (a) Relative cost difference and exergoeconomic factor, and (b) specific exergy cost of products	247

Figure 5.95 The Sankey flowchart of exergoenvironmental rates of M-2 marine engine [Pt/h]	248
Figure 5.96 (a) Exergoenvironmental rates and (b) specific exergy costs of the hybridized M-2 marine engine with respect to fuel blends.....	249
Figure 5.97 The pollution formation rates (a) and total environmental impact rates (b) of components of M-2 marine engine with respect to fuel blends	250
Figure 5.98 Exergoenvironmental performance of a hybridized M-2 marine engine: (a) Relative environment difference and exergoenvironmental factor, and (b) Specific exergy environmental impact of product	252
Figure 5.99 (a) Exergy cost and (b) environmental impact of electricity and heat of M-2 marine engine.....	253
Figure 5.100 The exergy destruction rates [kW] of group of components in the integrated hybridized M-3 marine engine.....	255
Figure 5.101 (a) The net power and (b) required heat of subsystems in the engine	257
Figure 5.102 (a) Total exergy destruction rate and (b) efficiencies of subsystems in M-3 engine.....	257
Figure 5.103 The SOFC Performance and its direct components: (a) Heat and power of SOFC components, and (b) cell and loss voltage and electrical efficiency.....	258
Figure 5.104 (a) Number of SOFC stacks according to amount of hydrogen and (b) SOFC efficiencies.	259
Figure 5.105 The GBC performance with respect to fuel blends: (a) heat and power, and (b) efficiencies	260
Figure 5.106 The Performance of TORC, BORC, and LNG: (a) temperature of EVs and LNG, (b) heat and power, and (c) efficiencies.....	261
Figure 5.107 (a) Fuel mass flow rates, (b) SFC, and (c) CO ₂ emissions of GBC, SOFC, and entire engine	262
Figure 5.108 The Sankey flowchart of exergy rates of M-3 marine engine	264
Figure 5.109 Exergy analysis of M-3 engine based on fuel blends: (a) fuel, product, destruction, and losses exergetic rates, and (b) exergetic efficiency and exergy destruction ratio	265
Figure 5.110 The Sankey flowchart of exergoeconomic rates of M-3 engine.....	266
Figure 5.111 (a) Exergoeconomic rates and (b) specific exergy costs of the M-3 marine engine with respect to fuel blends.....	268
Figure 5.112 Exergoeconomic performance of a hybridized M-3 marine engine: (a) relative cost difference and exergoeconomic factor, and (b) Specific exergy cost of exhaust.	268
Figure 5.113 The Sankey flowchart of exergoenvironmental rates of M-3 engine [Pt/h]	269
Figure 5.114 (a) Exergoenvironmental rates and (b) specific exergy costs of the hybridized M-3 marine engine with respect to fuel blends.....	271
Figure 5.115 (a) Pollution formation rates and (b) total environmental impact rates of M-3 marine engine components with respect to fuel blends	272
Figure 5.116 Exergoenvironmental performance of a hybridized M-3 marine engine: (a) relative environment difference and exergoenvironmental factor, and (b) specific exergy environmental impact of exhaust	273

Figure 5.117 (a) Exergy cost and (b) environmental impact of electricity of M-3 marine engine.....	273
Figure 5.118 The sensitivity analysis of fuel cost on: (a) exergoeconomic rates, (b) specific exergy cost, and (c) exergoeconomic factor and relative cost difference of aviation systems.....	276
Figure 5.119 The sensitivity analysis of fuel environmental impact on: (a) exergoenvironmental rates, (b) specific exergy environment, and (c) exergoenvironmental factor and relative environment difference of aviation systems.	277
Figure 5.120 The sensitivity analysis of fuel cost on: (a) exergoeconomic rates, (b) specific exergy cost, and (c) exergoeconomic factor and relative cost difference of rail systems.....	281
Figure 5.121 The sensitivity analysis of fuel environmental impact on: (a) exergoenvironmental rates, (b) specific exergy environment, and (c) exergoenvironmental factor and relative environment difference of rail systems.....	282
Figure 5.122 The sensitivity analysis of fuel cost on: (a) exergoeconomic rates, (b) specific exergy cost, and (c) exergoeconomic factor and relative cost difference of marine systems.....	286
Figure 5.123 The sensitivity analysis of fuel environmental impact on: (a) exergoenvironmental rates, (b) specific exergy environment, and (c) exergoenvironmental factor and relative environment difference of marine systems.	287

LIST OF ABBREVIATIONS AND SYMBOLS

Abbreviations

A	Aviation
AEC	Ammonia electrolysis cell
AP	Pump in the absorption refrigeration system
ARS	Absorption refrigeration system
BR	Afterburner
C	Compressor
CEPCI	Chemical engineering plant cost index
CC	Combustion chamber
CN	Condenser
EV	Evaporator
EX	Expansion valve
F-P	Fuel and product principal.
GBC	Gas Brayton cycle
GHG	Green house gases
GT	Gas turbine
HP	High-pressure
HX	Heat Exchanger
ICE	Internal combustion engine
IP	Intermediate pressure
LCA	Life cycle assessment
LCIA	Life cycle impact assessment
LP	Low pressure
M	Marine
MCFC	Molten carbonate fuel cell
MGO	Marine gas oil
MOPSO	Multi-objective particle swarm optimization
MX	Mixer
PEMFC	Proton exchange membrane fuel cell
R	Rail
RH	Reheater

S	Splitter
SOFC	Solid oxide fuel cell
SR	Steam reforming
SRC	Steam Rankine Cycle
ST	Steam turbine
T	Turbine
TEG	Thermoelectric generator
TRACI	Tool for reduction and assessment of chemicals and other environmental impacts
ULSD	Ultra-low sulfur diesel
WGS	Water gas shift
<i>Symbols</i>	
A	Area [cm^2]
b	Specific environmental impact [mPt/MJ]
\dot{B}	Exergoenvironmental rate [mPt/h]
c	Specific exergy cost [$\$/\text{GJ}$]
\dot{C}	Exergoeconomic rate [$\$/\text{h}$]
D	Diffusivity [m^2/s]
E	Nernst voltage [V]
\dot{E}	Energy rate [kW]
ex	Specific exergy [kJ/kg]
$\dot{E}x$	Exergy flow rate [kW]
F	Faraday constant [C/mol]
\bar{g}	Gibbs free energy [kJ/mol]
h	Specific enthalpy [kJ/kg]
i and j	Current density [A/cm^2]
I	Thermoelectric current [A]
K	Thermal conductance [$\text{W}/(\text{m.K})$]
La	Base temperature lapse rate per kilometre [K/km]
N	Number of cells or stacks, and revolution of engine speed [rpm]
m	Mass [kg]
\dot{m}	Mass flow rate [kg/s]

M	Mach number
P	Pressure [kPa]
\dot{Q}	Heat rate [kW]
r	Electric resistance [Ω]
R	Resistive loss [$\Omega - \text{cm}^2$]
\bar{R}	Molar gas constant [J/(mol.K)]
s	Specific entropy [kJ/(kg.K)]
T	Temperature [K]
U	Flight speed [m/s]
V	Voltage [V] and Volume [m^3]
\dot{W}	Power [kW]
Y	Component-related environmental impact [mPt]
\dot{Y}	Component-related environmental impact rate [mPt/h]
\dot{Z}	Levelized component cost rate [\$/h]

Subscripts

act	Activation
an	Anode
ca	Cathode
CCL	Cathodic catalyst layer
D	Destruction
e	Electrical
eff	Effective
L	Losses
mem	Membrane
o	Overall
ref	Reference
t	Total

Greek letters

ψ	Exergy efficiency [%]
η	Energy efficiency [%]
δ	Thickness [μm]
ε	Porosity [-] and exergetic efficiency [%] based on F-P principal.
κ	Conductivity of Nafion [$1/(\Omega.\text{cm})$]

Chapter 1. Introduction

The population of Canada is increasing at a rate of 1% [1]. This increase in population in addition to the vast distances between the farms, urban cities, and mine, will force the importance of transportation in Canada. Therefore, the number of vehicles increases in different transportation modes to ensure communication and facilitate the services among different cities and the whole world. Thus, a significant impact is provided on the economic, social, and political state of the country. A government report on the transportation sector shows that it contributed to an increase in the gross domestic product by 3.2%, which is equivalent to 1.5 times the growth rate for all industries [2].

The five principal modes of transportation in Canada consist of motor carriers, water, rail, and air [3]. Motor carrier transportation is represented by trucks in different shapes to transport consumer goods, petroleum, logs, and industrial products. Water transportation is used to transport bulk commodities and customers through the Pacific and Atlantic oceans, inland waterways as in canals and the Great Lakes, and coastal along the British Columbia coastal water. Rail transportation is also used for bulk merchandizes and transferring passengers over long distances to connect the east to the west and north to south of Canada. Air transportation is used for large and small items for remote distances and in a short time. The primary purpose of all transportation modes is to ensure the transport of passengers and goods with a high degree of safety despite the distance and time.

1.1 Type of Transportation Engines

The prime movers of the vehicles are the engines that can be classified into engines with moving parts, including positive displacement motion and rotational motion and non-moving parts, such as jet engines. The energy cycle in the engine, in many cases, contains four processes: compression, ignition, expansion, and cooling to provide motion to pistons, blades, and propulsive force. There are specific engines according to the transportation sector. For example, in aviation, the main force is the propulsive force and lift force in the air. The types of aircraft engines can be classified as moving and stationary components, as shown in Figure 1.1. The moving components include reciprocating and rotary engines

(e.g., piston and Wankel) and gas turbines. The aircraft gas turbines comprise a turboprop, turbojet, turbofan, and turbo-ram. The stationary components are represented as scramjet, ramjet and pulsejet aircraft engines.

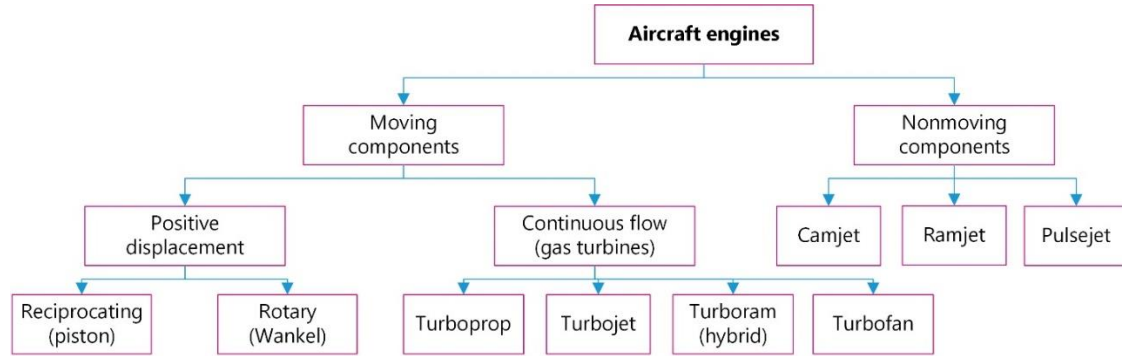


Figure 1.1 Types of aircraft engines of atmospheric dependent type (adapted from [4])

For the rail transportation sectors, the locomotive engine is the prime mover of the train. There are three main types of locomotive engines, as shown in Figure 1.2, including internal combustion, external combustion engines, electric engines, and other engines. Internal combustion engines can be classified into reciprocating as in diesel engines and other fuel engines such as kerosene and petrol, as well as rotational engines and gas turbines. External combustion engines are steam locomotive that uses boilers to heat water to the vapour and superheated phases. This energy moves pistons in a reciprocating motion to move the train wheels. Electric engines use electric motors with different types of current instead of combustion engines. Nowadays, new trends are represented consisting of combustion and electric motors or sustainable fuel cells to reduce the train's gas emissions and provide high driving power. All the engines are connected to the gearbox to transfer the motion to the train's wheel.

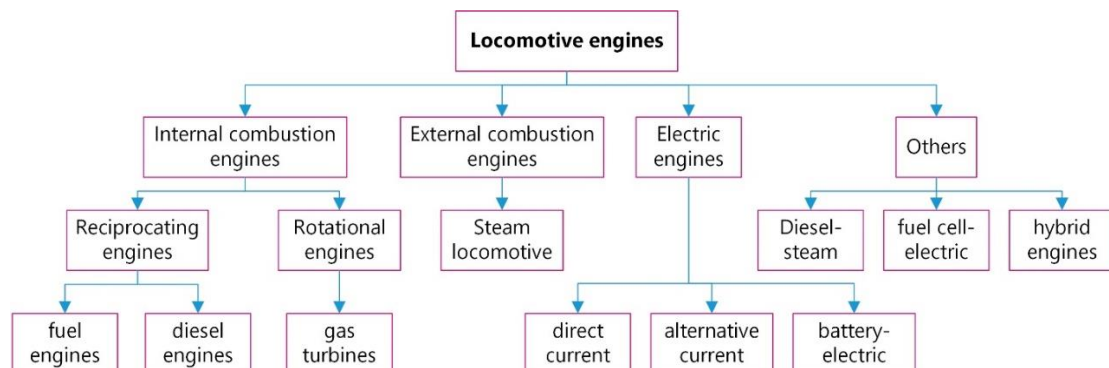


Figure 1.2 Types of locomotive engines (adapted from [5])

Similarly, marine transportation engines are similar to rail transportation engines, which involve internal and external combustion engines, electric engines, and other engines, as shown in Figure 1.3. Therefore, all marine engines should be connected to a propulsion system such as a propeller, a paddle wheel, a pump jet, or a sail. The internal reciprocating combustion engines used in marine transportation contain diesel, dual-fuel, and LNG engines, while the rotational combustion engine can be represented as a gas turbine. The external combustion system includes a steam turbine and a Stirling engine. Diesel engines are most used in freight marine transportation because of the high propulsive power to transport massive loads in the water. Other types include electric engines operating by electric motors. Hybrid engines combine diesel and electric engines and fuel-cell engines can be used in marine transportation.

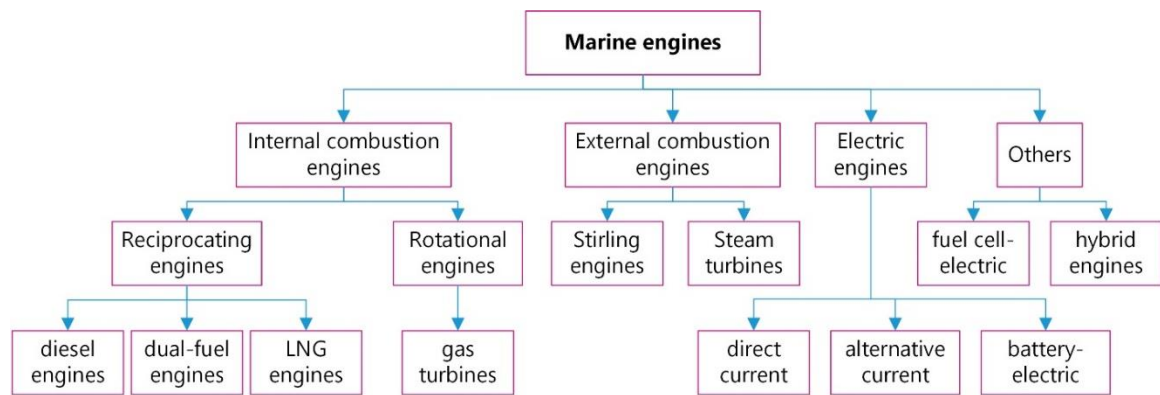


Figure 1.3 Types of marine propulsion engines (adapted from [6])

1.2 Fuel Consumption and Environmental Impact

Different types of fuels in the transportation sector contain conventional and alternative fuels relevant to clean transportation. The least carbon-emissive fuel is hydrogen, whether compressed, liquified or hydrides. Hydrogen exists abundantly in the atmosphere and the seas and oceans. In addition, hydrogen can be considered the lowest specific energy density and volumetric energy density, among other fuels. This is because of its lower density compared to others ranging from 10 to 70.8 kg/m³, as shown in Figure 1.4. However, ammonia has a higher volumetric and gravimetric energy density than hydrogen. Nitrogen gas has tremendous potential as a fuel since liquefied nitrogen has higher specific and volumetric energy density than compressed gas. Additionally, diesel and gasoline products

are mostly used in fueling vehicles despite the higher carbon emissions because of substantial volumetric and gravimetric energy densities, as shown in Figure 1.4. To reduce emissions from these fuels, diesel from natural resources and lower sulfur content are produced, such as biodiesel (B100) from soy, waste oil, and fats and ultra-low-sulfur-diesel (ULSD) fuels from crude oil.

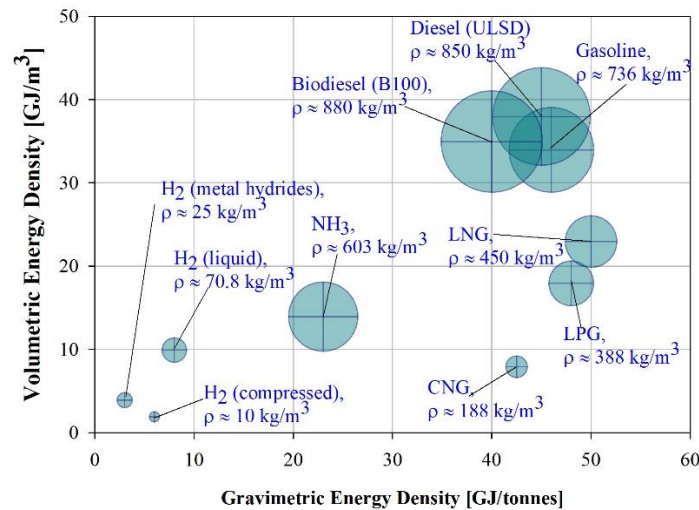


Figure 1.4 The physical properties of different fuel transportation (adapted from [7,8])

The fuel distribution in the transportation sector is shown in Figure 1.5, as presented in the Natural Resources Canada report of 2021 [9]. The total transportation energy use increased by 16% from 2000 to 2016 to a total of 2,683 PJ in 2020. The significant contribution of fuels to the total energy use is motor gasoline at 58% and diesel fuel oil at 28%. Aviation turbo fuels contribute to energy use by 10%, while heavy fuel, ethanol, and propane are consumed by less than 5% in total. The report has also shown that energy efficiency improvements in the transportation sector saved Canadians 763 PJ of energy and almost \$21 billion in energy costs in 2021.

Fuel consumption has a significant impact on the environment, and it is essential to measure the greenhouse gas (GHG) equivalent for each economic and transportation sector. The total GHG emissions from all economic sectors reached 709 Mt CO₂e in 2017, which decreased by 1.6% from 2000 [10]. The main contributors to these emissions were the oil and gas industry and transportation. The emission from transportation sectors has increased by 39% from 131 to 182 Mt of CO₂e as a consequence of the increase in population and the economic sector [10].

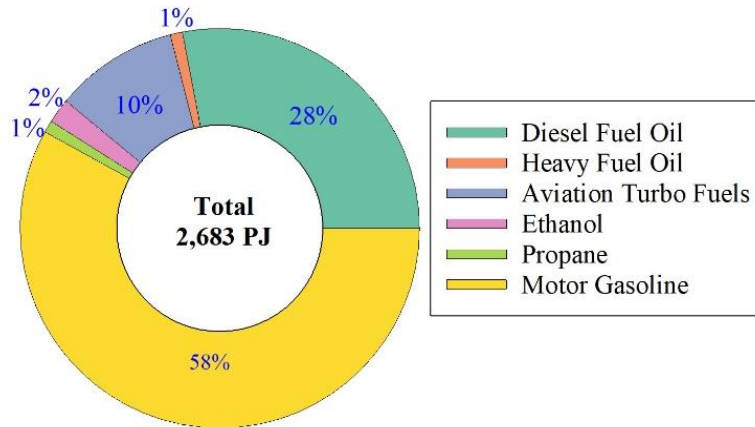


Figure 1.5 Fuel mix of the transportation sector, 2021 (adapted from [9])

For the transportation sector, passenger transportation contributes 54% to the total emissions, freight emissions are 41%, and off-road emissions are 5% [10]. Emissions from passenger transportation have continued to rise because of an increased number of vehicles due to the increase in travelling and trading. Also, freight emissions have increased because of many factors, including increasing trade and globalization and on-line shopping. The main contributor to this number of emissions is cars and buses, which have 48% of the total emissions from all transportation sectors. However, rail, aviation and marine emit about 26% of the total emission of all transportation sectors. This amount is equivalent to 27.0 to 32.2 Mt of CO₂e from 1990 to 2017 [10]. The significant emission from vehicles compared to others is because the number of vehicles and buses in Canada is more than the number of trains, airplanes, and ships.

For rail transportation, the GHG emissions and energy used and train activity and presented in Figure 1.6-a and -b. The GHG emission decreased from 7 to 6 Mt of CO₂e from 1990 to 1998, then spiked up to 8 Mt of CO₂e in 2008, then decreased to 6.5 Mt of CO₂e in 2018. The energy use curve has similar behaviour to the GHG emission curve, which represents the amount of energy consumption by trains. Figure 1.6-b explains the reason behind the distribution of GHG emissions and energy use over the years. The activities for passenger and freight trains have significantly increased over the 17 years. For aviation transportation, Figure 1.6-c and -d display the GHG emissions, energy use, and activities. The GHG emission has increased substantially from 12 to 20 Mt of CO₂e. Similarly, energy use has increased from 180 to 280 PJ from 1990 to 2017. The reason for

that is the number of passenger and freight flights has significantly increased over the past years due to travelling and globalization trading.

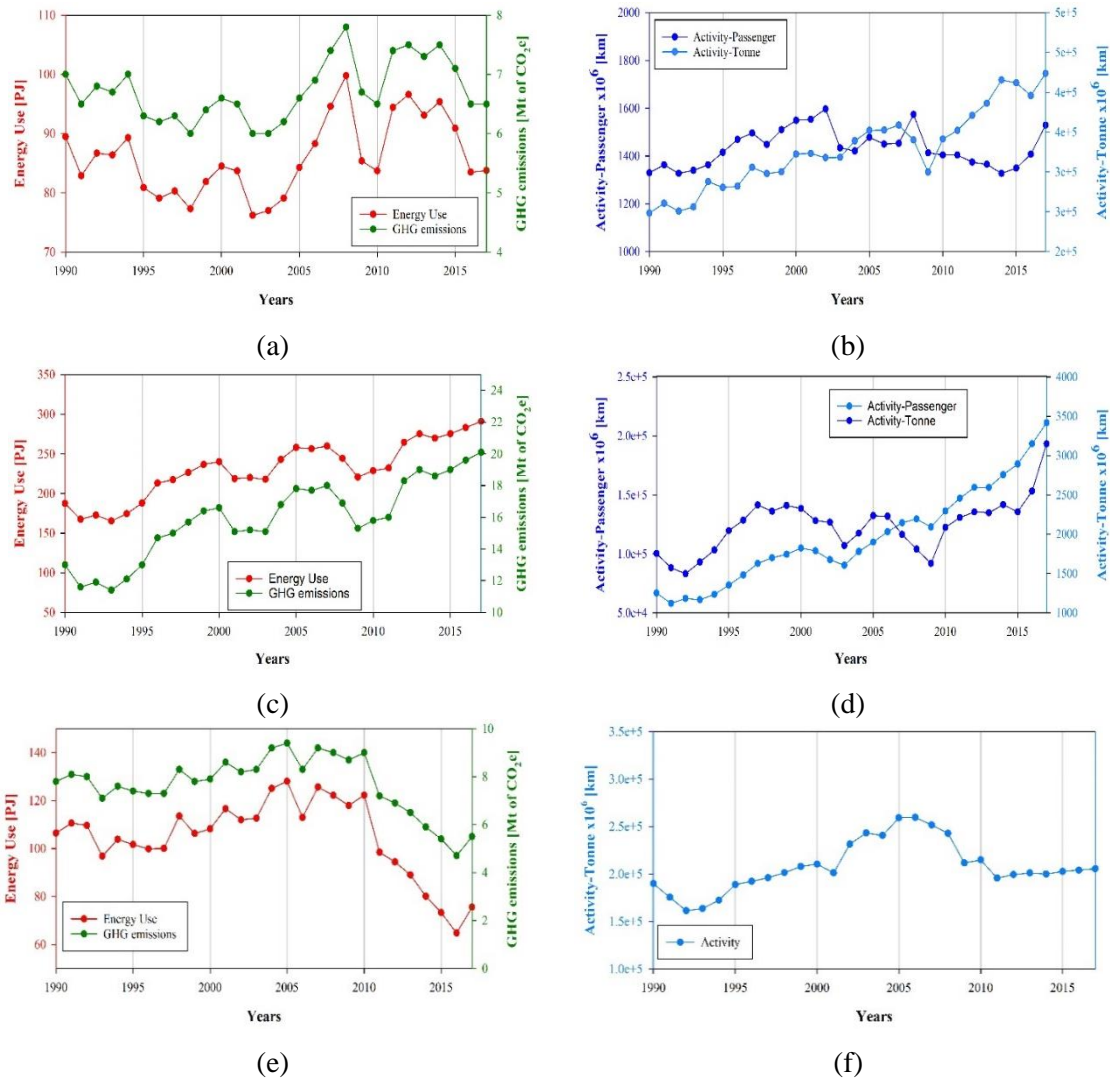


Figure 1.6 The GHG emissions and energy use for rail transportation (a) the activity of passenger and freight rail transportation (b), the GHG emissions and energy use for aviation transportation (c) and the activity of passenger and freight aviation transportation (d), the GHG emissions and energy use for marine transportation (e), and the activity of freight marine transportation (f).

The GHG emissions and energy use for marine transportation are explained in Figure 1.6-e. The emissions from freight marine significantly decreased from 8 to 5.5 Mt of CO₂e. Also, energy use decreases from 108 to 80 PJ. That is because the activity of freight marine increased from 170000 million km to 250000 million km from 1990 to 2005, then decreased to 200000 million km, as shown in Figure 1.6-f.

The Canada GHG emission plan is to reduce the total emissions to 517 Mt CO₂e by 2050 [11]. The carbon emissions were lowered from 815 Mt CO₂e in 2016 to 722 Mt CO₂e in 2017. However, a considerable reduction of 205 Mt CO₂e should be implemented by 2030, which includes 30 Mt CO₂e by all transportation sectors to achieve the total reduction. Therefore, this thesis will contribute to GHG emission reduction by tackling the research gap in the transportation sectors (rail, aviation, and marine) and utilizing alternative fuels instead of fossil fuels.

1.3 Potential Solutions for Sustainable Transportation

The government of Canada is concerned about the environment and natural resources [12]. Much information has been collected through years of measurements in order to investigate, analyze and predict the weather and climate issues [13] to have a better understanding of the effects and causes of climate change [14], and that was presented by measuring the GHG emissions through different economic sectors and more focus on transportation sector from 2000 to 2017. Therefore, the Canadian government has proposed Canada's climate plan [15] include some strategic plans for the transportation sector [16], such as (a) providing a 2016 budget of \$62.5 million to invest in electric charging stations for electric vehicles and providing alternative fuel stations using natural gas and hydrogen; (b) providing a 2016 budget of \$ 3.4 billion to expand public transit; and (c) implementing a zero-emissions vehicle strategy. The main goal of this plan is to achieve a reduction of greenhouse gas emissions of up to 512 Mt CO₂e by 2030. That means the GHG emissions from transportation should achieve 150 Mt CO₂e by reducing 30 Mt CO₂e within the next ten years. As a result, Transport Canada [17] has established many programs to provide a safe and secure and ecofriendly transportation system, such as a clean transportation system-research and development program [18].

1.4 Potential of alternative fuels in transportation systems

The design of transportation systems covers the aspect of fuel-system design, which considers the fuel selection and system components. The fuel selection should be clean fuels without fossil fuels such as diesel or kerosene. Five alternative fuels are considered with their combinations in this thesis, such as hydrogen, ethanol, methanol, dimethyl ether,

and methane. Since Canada's plan for GHG emissions is to reduce the emissions to 517 Mt of CO₂e by 2050. therefore, the usage of fossil fuels should be eliminated to reach that goal. The reasons for the selected alternative fuels are explained below.

Hydrogen is colourless, odourless, non-toxic, and zero-emission fuel burned with oxygen and can be used in fuel cells and internal combustion engines. Hydrogen can be produced from fossil fuels by steam reforming or partial oxidation of methane and coal and by electrolysis of water. Hydrogen has been used in internal combustion engines by blending with other hydrocarbon fuels, such as reducing carbon emissions because of its high octane ratio (>130) [19–21].

Methane is the simplest alkane and the primary substance of natural gas or biomethane, which is upgraded to biogas to be similar to fossil natural gas [22]. Methane has a low carbon intensity rating which can significantly reduce carbon emissions. In California, methane has replaced fossil natural gas in transportation sectors and households to reduce GHG emissions [23].

Methanol is considered an alternative fuel, and its properties are like ethanol. Methanol is generally produced by steam-reforming natural gas to create a synthesis gas, which is fed by a catalyst to produce methanol and water. It may be produced by renewable sources such as biomass and feedstocks. The benefits of methanol include lower production cost, lower risk of flammability compared to gasoline, and can be produced from feedstocks to reduce fuel use and clean the environment [24,25].

Ethanol fuel is ethyl alcohol used as fuel. It is most often used as a motor fuel, mainly as a biofuel additive for gasoline. Bioethanol is a form of renewable energy that can be produced from agricultural feedstocks from biomass, such as corn or sugarcane. Ethanol contains approximately 34% less energy per unit volume than gasoline, but the engine efficiency is increased compared to gasoline alone because ethanol has a higher-octane rating to raise the compression ratio [26,27].

Dimethyl ether is an organic compound simplest ether, and a colourless gas being used in a variety of fuel applications. It is produced by the dehydration of methanol, which is obtained from synthesis gas. It is a second-generation synthetic biofuel which can be produced from lignocellulosic biomass, which is made of animal, food and agricultural waste. It is potentially used as a substitute for propane in liquified petrol gas in households

and industry. DME can be a promising fuel in diesel engines and gas turbines because of its higher cetane number of 55 than diesel fuels (40-53), which is a measure of fuel ignitability in compression ignition engines [28,29].

1.5 Motivation and Research Objectives

The primary purpose of this proposal is to provide environmental solutions in rail, aviation, and marine transportation sectors for many reasons: (a) there is a research gap for these sectors as presented in the literature, (b) the greenhouse emissions must be reduced from transportation sectors, (c) the idea of zero-emission vehicles is required to be fulfilled, (d) transportation energy performance must be improved, and (e) sustainable and clean resources are implemented. To achieve these research goals, this thesis focuses on the following:

- a. The utilization of alternative fuels in transportation.
- b. The development of transportation engine systems (rail, aviation, and marine).
- c. The usage of renewable powering systems.

The specific objectives of this thesis study can be stated as follows:

- To develop new systems in three transportation sectors (rail, marine, and aviation). Aviation includes two developed systems, and each rail and marine include three developed systems. Traditional engines, internal combustion engines for rail and marine, and traditional turbofans for aviation. New powering systems are combined with or replace the existing engines, such as Rankine cycles, fuel cells, and gas turbines. Also, energy recovery systems are implemented in the engine exhaust to reduce the waste heat. The combination of systems will increase the net power and energy efficiency.
- To use alternative fuels, such as hydrogen H_2 , methane CH_4 , methanol CH_3OH , ethanol CH_3OHCH_2 , and dimethyl ether CH_3OCH_3 , as a replacement for fossil fuels. The alternative fuels are composed of five hydrogen-based fuel blends with different mass fractions. The utilization of these fuel blends guarantees the reduction of carbon emissions since they have less carbon content, high heating values, and are produced from renewable sources such as animals, agriculture feedstocks and wastewater.
- To analyze the developed systems using three methods such as:
 - a. Thermodynamic analysis by analyzing the system energetically and exergetically, estimating both energetic and exergetic efficiencies for the overall engine and its components, evaluating exergy destruction rates and irreversibility for all system

components, conducting parametric studies to some operating conditions in order to study the engine behaviour and overall efficiencies.

- b. Economic assessment by providing exergoeconomic analysis by considering the exergy cost rating for inlet and outlet streams, work done and produced, and heat added and rejected by the components.
 - c. An environmental impact assessment by providing life cycle assessment including the vehicle and fuel cycles, environmental impact assessment by the tool for reduction and assessment of chemicals and other environmental impacts (TRACI V2.1) impact method, and exergoenvironmental analysis.
- To provide an optimization study using multi-objective particle swarm algorithm (MOPSO) for each transportation sector with different operating conditions to choose the best design of the transportation engines.

1.6 Novelties

Previous research covers whether modifications of traditional engines or mixing some additives to traditional fuels increase engine performance and reduce carbon emissions, but the reduction of carbon emissions was not sufficient to reduce the GHG and global carbon emissions. The previous studies can be categorized into two aspects: fuel-based design and system-based design. However, this thesis is categorized as system-fuel-based design. The novelties of this study are as follows:

- It designs renewable powering systems using environment-friendly fuel cells. The proposed fuel cells are solid oxide fuel cells (SOFC), molten carbonate fuel cells (MCFC), and proton exchange membrane fuel cells (PEMFC). These fuel cells will combine with other powering systems such as internal combustion engines, gas turbines, and Rankine cycle systems to increase the output power and reduce carbon emissions.
- It develops solutions for energy recovery to increase energy performance and decrease energy losses. The energy recovery will be utilized by transferring the waste heating load into a cooling load using an absorption refrigeration system, electric power using thermoelectric generators, and producing fresh water using a desalination system.
- It employs alternative fuels instead of fossil fuels, such as hydrogen, methane, methanol, ethanol, and dimethyl ether, to eliminate carbon emissions. These fuels are

formed into five hydrogen-based fuel blends with various mass fractions to moderate the dependency on carbon content and reduce carbon emissions.

- It investigates the designed systems using three analyses, such as thermodynamic, exergoeconomic, and exergoenvironmental analyses. The eight developed engines are also compared to the commonly used engines in each transportation sector regarding energy performance, cost, and environmental impact to be an excellent asset for decision-makers.
- It contributes to a significant increase in engine efficiency, enhancing transportation performance, and great reduction of carbon emissions because of the newly developed engines and utilization of clean fuels.

1.7 Thesis Outline

This thesis presents five chapters. Chapter One is an introduction to the topic of transportation sectors and their effect on the environment. It also includes the research motivation, research objectives, and novelties. Chapter Two presents a comprehensive literature review for three sectors. It includes the current engines with different configurations and investigations conducted on them. To facilitate the reading of this chapter, the chapter splits into three major sections, in which each sector is discussed separately. Chapter Three displays the description of transportation systems, which are eight engines: two aviation engines, three rail engines, and three marine engines. Chapter Four introduces the system modelling, including modelling of subsystems in engines separately, as follows: (1) engines: internal combustion engine, turbofan, gas turbine engine, steam Rankine cycle, and binary systems; (2) fuel cells: SOFC, PEMFC, MCFC, and aluminum electrolysis cell (AEC); (3) energy recovery systems: an absorption refrigeration system, thermoelectric generators, and desalination unit. Also, this chapter presents analyses and assessments, such as thermodynamic analysis, exergy analysis, exergoeconomic analysis, and exergoenvironmental analysis, and optimization algorithm. Chapter Five presents the results and discussions of the eight engine systems based on four analyses and compares the results of the developed engines with traditional engines in each sector. It also includes a comparison between systems and optimization results for the least weight engine configurations to provide maximum performance with the least cost rates and the least environmental impact. Lastly, Chapter Six concludes the results and discussions of each system.

Chapter 2. Literature Review

This chapter presents a comprehensive literature review for each transportation sector. This review will cover studies conducted on aviation engines, rail engines, and marine engines. The review focuses on the reduction of carbon emissions, the possibilities of using alternative fuels only, different engine configurations, and the usage of fuel cells and other powering systems. It will also provide an overview of different analyses besides thermodynamic analysis and the cost and environmental impact of engines.

2.1 Aviation Transportation

Aviation is an essential link to connect countries globally and plays a vital role in economic activities. The number of passenger and freight flights has significantly increased over the past years due to global travelling and globalization. This rapid growth rate increased the carbon emissions seven-times to 1034 Tg CO₂/yr [30]. Focusing on Canada, the energy use of aviation transportation in Canada has increased from 180 to 300 PJ from 1990 to 2019 [31]. This energy use relies on aviation turbo fuels, which are kerosene-based fuels. Consequently, greenhouse gas (GHG) emissions have increased substantially from 15 to 22 Mt of CO₂e [32,33], which contributes about 2% of total GHG emissions from all transportation sectors in Canada.

Several studies have been conducted on clean aviation transportation. For example, Kousoulidou and Lonza [34] collected data from actual flight information EUROCONTROL and Eurostat statistics for European flights to predict the consumption of biokerosene and conventional kerosene and their impact on carbon emission. They discovered that the total fuel consumption was obtained to be about 170 million tonnes resulting in 400 million tonnes of CO₂ emissions by 2030, and the main contribution to these data is the conventional fuels. Therefore, the European Union planned for the use of biofuels such as clustered in hydro-processed esters and fatty acids (HEFA), hydrotreated vegetable oils (HVO) and biomass-to-liquid (BTL) biojet fuels to reduce the global CO₂ emissions from aviation sector. Also, Schripp et al. [35] analyzed the use of ternary alternative jet fuel blends in a practical flight of an A300-600 aircraft with PW4158 engine at the airport Leipzig/Halle. The first fuel blend is a mixture of Jet A-1, 30%vol HEFA,

and 8% vol alcohol-to-jet (ATJ), and the second blend is Jet A-1, Jet A-1, HEFA, ATJ, and synthesized iso-paraffins (SIP). Thus, the soot formation has significantly lessened, and the particle emissions have reduced by 29% to 37% according to the flight conditions.

Moreover, adding hydrogen (20%v/v) to kerosene in a Scramjet engine has improved the performance of kerosene supersonic combustion under 3.8 Mach number inlet conditions. The heat released is intensified, resulting in higher exit temperature and pressure and more OH radicals at low-temperature conditions. That is because the hydrogen addition promotes the pre-evaporation and combustion heat release and CO oxidation [36]. Furthermore, Badami et al. [37] conducted a small-size turbojet engine performance using a traditional Jet-A with two alternative fuels, such as synthetic Gas to Liquid and a blended biofuel of Jet-A and Jatropha Methyl Ester. A similar performance was achieved despite the lower heat value for alternative fuels. However, the unburned hydrocarbon emissions were reduced by 25% to 35% using alternative fuels.

Alternative fuels such as hydrogen and methane have been investigated in research to test their ability to operate aircraft engines. Hydrogen is a carbon-free fuel with a high heating value and high energy carrier with less volume, and methane has a low carbon intensity rating, which can significantly reduce carbon emissions. Adding hydrogen to methane or other hydrocarbon fuels has been tested experimentally. Hydrogen can decrease the ignition delay and increase laminar burning velocities [38]. A mixture of ammonia, methane, and hydrogen has been conducted experimentally in a high-pressure combustion test rig for gas turbines. The mixture can achieve high stability flame with low emissions at a low equivalence ratio [39]. Bicer and Dincer [40] performed a life cycle assessment of a well-to-wake approach for conventional and alternative aircraft fuels, such as hydrogen, ammonia, methanol, ethanol, and liquified natural gas. They showed that hydrogen and liquified natural gas have the lowest environmental impact compared to other fuels because of their clean and renewable fuel production.

Ekici et al. [41] conducted a thermodynamic analysis on a turboprop engine using methanol and compared its performance with kerosene. The methanol and oxygen mixture flow rate should be increased to compensate for the low heating value but negatively impact the environmental effect factor. Also, Ekici [42] analyzed a turbofan engine of A321-200 by exergy analysis and sustainability analysis. The combustion chamber has the

lowest exergetic efficiency and high exergetic depletion ratio. In addition, the climb, cruise, and descent phases recorded the lowest product depletion ratio, while the landing and take-off phases recorded the highest depletion ratio. In addition, Ekici [43] studied the performance map of B707-JT3D pairing by thermodynamic analysis and exergetic analysis to make aircraft-engine more environmentally benign.

Fuel cells are introduced into aircraft engines as powering systems to increase engine performance. Many efforts are executed to reduce the fuel cell size by eliminating the external steam reformer and water gas shift. This can be implemented by fabricating direct fuel cells by implementing new catalysts before the anode electrode to apply the two reactions (steam reforming and water gas shift) as internal reactors while maintaining the cathode electrode as it is. For example, Direct methanol fuel cells have been studied and applied in the industry because of their high energy density and avoiding the extra requirement of fuel reforming [24]. Also, a direct DME fuel cell has been investigated using different compositions of platinum (Pt) and ruthenium (Ru), and 50% of Pt and Ru catalyst provides the best overall performance at a wide range of cell voltages [44]. Also, new catalysts were developed for (DME) steam reforming by impregnation of copper with cerium and nickel additives using mordenite (MOR) and alumina as supports [45]. In addition, adding a DME to propane in the SOFC and SR systems has increased the power and cell voltage by 70% without changing the reactor structure [46].

Molten carbonate fuel cells (MCFC) are the most effective method of converting chemical energy into electrical energy using molten carbonate electrolytes [47]. They are used for large-scale power plants and for powering transportation to provide electric power and reduce carbon emissions. For example, Ansarinasab et al. [48] conducted a study on a combined power plant that utilized a gas turbine, a Stirling engine, and a MCFC. The plant provided a power of about 6.5 MW, and the rejected heat of the MCFC equipment was used to heat a Stirling engine to increase the energetic efficiency of the plant. Also, Hosseini et al.[49] developed an integrated power plant consisting of MCFC, steam methane reforming (SR), methanol synthesis process (MSP) and combined heat and power system containing gas turbine and Rankine cycle. The overall power plant can produce about 110 MW and other facilities, such as pure water and methanol, with 83% and 58.4% energetic and exergetic efficiencies, respectively. Other power generation systems are

incorporated with the MCFC system, such as a hybrid solar parabolic power generation [50], a hybrid production process of liquified natural and helium [51], a biodiesel production [52], and a multiple-effect desalination plant[53]. The use of the MCFC unit has significantly reduced the CO₂ by about 30% to 70% and increased the overall efficiency compared to other traditional systems.

They have been used in land transportation [54,55]. However, few studies have combined fuel cells with aircraft engines. For example, Ji et al. [56] compared thermodynamically three configurations of turbojet engines using kerosene fuel. The configurations are two-shaft turbojet, two-shaft turbojet with afterburner, two-shaft turbojet with a solid oxide fuel cell (SOFC) and afterburner. The last design has achieved the best energetic efficiency between 36% to 42% according to different turbine inlet temperatures from 1550 to 1700K and a pressure ratio of 24. Besides, Waters and Cadou [57] presented three aircraft engines of the unmanned aerial vehicle combined with SOFC and catalytic partial oxidation reactors to reduce fuel burn. The engines are turbojet, with high bypass ratio and low bypass ratio of turbofans. The fuel used in the system is JP-5. They found that fuel efficiency increased by about 8% for a 90 kW high bypass turbofan with a modest cost. Also, Jia et al. [58] investigated the effect of hydrogenation degree on jet fuel (RP-3). Combining hydrogen and additive catalyst has slightly reduced the density and sulfur content but enhanced the thermal oxidation stability of jet fuel. In addition, a mixture of hydrogen ammonia and air has been combusted and numerically investigated. Cai and Zhao found that increasing the hydrogen to ammonia ratio to about 50% dramatically decreased the NO_x emission and increased the flame length closer to the combustor inlet [59]. Luo et al. [36] studied the addition of hydrogen and fuel additive effects on kerosene for dual-mode scramjet under flight Mach 3.8 inflow conditions. The results show that adding hydrogen has increased heat released from the scramjet at low combustion conditions yielding improved combustion efficiency and flame stabilization.

Moreover, Ji et al. [60] conducted their study on unmanned aerial vehicles. They proposed the concept of turbine-less jet engines combined with SOFC and battery to operate the fuel cell. The proposed design showed better performance than a traditional turbojet engine with a maximum pressure ratio of 33 and a Mach number of 0.3. Also, Bakalis et al. [61] studied a hybrid SOFC-GT and conducted an optimization to achieve

the best performance in the whole operating range. The optimized hybrid system can produce a net power of 246.4 kW (192.2 kW for SOFC and 57.2 kW for GT) with 58.5 % thermal efficiency.

Aircraft manufacturers are concerned about the extra weight that affect the aerodynamic performance of airplanes due to changing fuel types and engine systems. However, studies have proven the opposite. Verstraete [62] investigated the utilization of hydrogen fuel in the aviation sector. It was found that hydrogen storage capacity can be performed in a smaller span and wing area. The gross weight of the hydrogen-fueled aircraft is less than 30% than that of kerosene-fueled, which reduces the direct operating costs from 6.65 to 6.53 €/seat. In addition, the improvements in engine specific fuel consumption were 20% fewer sensitives for a hydrogen-fueled than that kerosene-fueled aircraft. Also, the ratio of operating empty weight between the hydrogen-fueled to kerosene-fueled is 95.9%. Further, the lift/drag ratio of the airplane is less by 15.3% for using hydrogen fuel. However, the energy utilization was higher for the hydrogen fuel of 643.4 kJ/seat than that of kerosene fuel by 68%.

Wang et al.[63] reviewed different configurations of hybrid UAV, mainly focusing on three fuel cells, such as the proton exchange membrane fuel cell (PEMFC), solid oxide fuel cell (SOFC), and direct methanol fuel cell (DMFC). All the fuel cells can increase the aircraft's performance but also increase the total engine weight. They recommended that the weight be reduced to reduce the engine weight and increase the total thrust. In addition, other power sources are included, such as batteries, solar cells, and internal combustion engines. Some challenges are discussed, including slow response, low efficiency at low power output and fuel storage and accessories. Also, a new lightweight design of fuel cells should be introduced to overcome weight problems.

A few researchers have focused on combining the MCFC with gas turbines. Liu et al. [64] studied a micro gas turbine with MCFC in addition to the catalytic burner to utilize the waste energy from the combined system. They used a platinum catalyst with additives of ceria–zirconia mixed oxide (CeZrO_2) Lanthanum manganite (LaMnO_3) coated with alumina $\gamma\text{-Al}_2\text{O}_3$. They found that the additives to the catalytic burner have improved the combustibility at lower temperatures and reduced the catalyst reactivity, and increased the performance of the hybrid micro gas turbine system. Recently, direct MCFC has been

intensively investigated with different fuels, such as direct ethanol MCFC. Devianto et al. [65] prepared a new anodic electrode by pressing magnesium oxide (MgO) and lead monoxide (PbO) into a disc-shaped specimen and mixing it with nickel-based catalyst. A mixture of ethanol and water is fed to the anodic electrode. They found that the Ni/MgO converts 99.8% of ethanol with 57.3% hydrogen selectivity achieving the highest performance among other specimens of direct ethanol MCFC.

2.2 Rail Transportation

Rail transportation is a convenient method to link distant cities and countries to transfer passengers and goods. However, rail transportation counts on fossil fuels such as diesel and gasoline for about 83%, and also freight emissions contribute about 42% to the total amount of emissions from transportation [9]. Unfortunately, this growth in carbon emissions affects the occurrences of natural disasters, especially in developing countries [66] and continues to be a global matter since they also impact developed countries [67]. Many efforts are consumed to enhance the combustion quality of fossil fuels; for instance, lowering the flame temperature and increasing the excess air decreases NO_x emissions [68]. Also, blending and adding some additives such as nitro ethanol to diesel changes the properties of diesel and reduces emissions such as NO_x, SO_x, and carbon emissions [69]. Furthermore, urea is usually injected into the exhaust of a rail diesel engine before the selective catalytic reduction to reduce NO_x emissions [70]. However, these efforts are not sufficient to significantly reduce global warming and the overall emissions. Therefore, not only are fossil fuels needed to be replaced by renewable and green fuels, but also new powering systems must be introduced in rail transportation to increase engine performance.

For rail transportation, the popular locomotive engine is an internal combustion engine operated by diesel fuel, which emits greenhouse gas emissions to the environment. Several studies have been conducted on alternative fuels and engines to reduce GHG emissions. For example, Hogerwaard and Dincer [71] have studied the effect of ammonia-ultra low sulfur diesel (NH₃-ULSD) dual fuel as an alternative replacement to diesel fuel in a locomotive engine. Also, hydrogen production was added onboard to reuse the heat recovery from ammonia decomposition to reduce diesel fuel consumption. They have found that heat recovery has improved the energy and exergy efficiencies for the new

locomotive system. The alternative fuel has reduced GHG emissions by 53% and air contaminants emissions.

Marin et al. [72] conducted their research on the usage of hydrogen for passenger locomotives in the GO Transit Lakeshore corridor through Oshawa, Toronto, and Hamilton, in the province of Ontario in Canada. They compared three types of engines: diesel internal combustion engines, electrification, and hydrogen fuel cell. They found that the hydrogen fuel cell increased the weight of electric locomotives by 30%, but it has higher flexibility and is more economical than electrification. Their study has been extended to include energy supply and distribution. Marin et al. [73] have investigated the economic impact and flexibility of hydrogen production and distribution on the Bombardier ALP-46A locomotives. Four hydrogen production processes are included in their study: proton exchange membrane fuel cell, thermochemical Cu-Cl cycle, electrolysis, and steam methane reforming. They reported that the usage of hydrogen fuel cells has some drawbacks: the life expectancy of a fuel cell is one-third of that of diesel engines, and hydrogen storage at a higher energy density is less efficient than diesel on-board space utilization. Also, the implementation of fuel cells has an expected cost for high power transportation of 500 \$/kW. Marin et al. [73] have recommended internal combustion engines operating on hydrogen despite low efficiency to overcome the high operational cost of fuel cells.

In order to reduce hydrogen consumption and increase the efficiency of fuel cells in locomotive engines, Hong et al. [74] constructed a small-scale locomotive system. The prototype locomotive comprises a proton exchange membrane fuel cell and battery. They simulated different driving cycles and investigated the performance of the hybrid engine. They found that maintaining the charge state of the battery can achieve self-adaption function to improve efficiency by 2% and reduce hydrogen consumption by 0.86g. Similarly, Meegahawatte et al. [75] analyzed a hybrid fuel cell series of commuter railway vehicles by analyzing power flow models of a hydrogen fuel cell stack, battery pack and hybrid drive controller based on a typical return journey between Stratford Upon Avon and Birmingham in the United Kingdom. In addition, fuel consumption was compared among different types of engines, such as diesel engines and hybrid engines. They have found that pure fuel cell engines can consume 38 kg of hydrogen for a long journey with a power of

355 kWh. However, the diesel-battery hybrid engine can consume 82 l of diesel oil for a small journey with a power of 294 kWh. Also, the CO₂ emission was obtained from the hybridized fuel cell with a battery of 148.5 kg CO₂, which was a less amount compared to that of the diesel engine, diesel hybrid, and pure fuel cell engine.

In addition, Shinde et al. [76] performed the life cycle assessment for Mumbai Suburban Railway in India to include the construction and maintenance of railway infrastructures such as power supply installations, bridges and platforms. It was found that the main contribution to the total environmental impact was the operation of the multiple electric units that feed the railway stations with electricity. The main reason for that was the dependence on power supply from conventional sources such as charcoals and fossil fuels. To reduce GHG emissions, renewable energy sources should be considered in the operation phase. Moreover, Zhang et al. [77] investigated the proportion limit of coal power consumption for rail transit in 18 cities in China from 2015 to 2017. This investigation was performed to measure the carbon emission reduction in rail transit. They have found that the environmental impact of rail transits is decreased compared to other transit modes due to the application of different sustainable strategies.

Another way is to remove ICE and use a gas turbine engine only or integrated with fuel cells to increase the power and energetic efficiency. That is because fuel cells are devices operated by electrochemical reactions to produce electricity rather than mechanical systems accompanied by mechanical motions and mechanical friction. For example, Guo et al. [78] combined a gas turbine engine with a SOFC operated with a mixture of ammonia and water for hydrogen production in order to allow the SOFC to generate electricity. The performance of the combined engine is increased by increasing the sharing power of the SOFC to 25% and reducing the fuel consumption of the GT by about 20%. Another method to replace the ICE is to use hybrid-electric commuters combined with PEMFC and battery, as studied by Sarma and Ganguly [79]. Fan et al. [80] presented a recent review study focused on air emissions, especially in transportation, that can be minimized by using zero-carbon fuels such as hydrogen, which can enhance engine performance in a safe and clean environment for passengers. Hence, hydrogen storage is a vital obstacle in transportation power due to its enormous size. Thus, on-board hydrogen production could be an answer to this dilemma by applying aluminum electrolysis cells (AEC). It is operated by

electrochemical reactions of liquid aluminum, which will separate into amide ions (NH_2^-) and ammonium ion (NH_4^+) by combining amide salts to the ammonium solution like potassium amide, lithium amide, and sodium amide [81,82].

Transportation engines use massive heat to combust fuel with air and produce power. However, a fraction of this immense heat is transferred to power by expansion leaving behind a huge waste of energy, which results in lowering the overall energetic efficiency of the engines. This waste energy can be utilized by converting heat to cooling load or electricity, such as a thermoelectric generator (TEG) and absorption refrigeration systems (ARS). For example, Luo et al. [83] installed TEG units in the exhaust pipes of a vehicle, which were able to generate electric power of 40W at a speed of 120 km/h. Moreover, Ma et al. [84] constructed a small-scale of geothermal system that contains 32 TEG modules to be connected to a geothermal exhaust pipe. The inlet temperature ranged from 100°C to 300 °C with a mass flowrate of a maximum of 24 kg/h. The net power of TEG modules is from 0.66 to 3.17 W with 0.67% of energetic efficiency. Similarly, Alegria et al. [85] established an experimental model of a geothermal pipe connected with TEG units to produce a power of 10 to 20 W from an input heat of 330 to 480 W. In conclusion, TEG units can be attached to exhaust lines to convert some of the excessive heat into electric power and reduce waste energy.

Few studies have conducted exergoeconomic analysis and exergoenvironmental analysis to address engine systems economically and environmentally. Uysal and Keçebaş [86] performed an exergoeconomic analysis on a real gas turbine engine in order to reduce the exergy destruction cost rate of the system. In addition, Chitgar and Emadi [87] applied exergoeconomic analysis on a hybrid SOFC and gas turbine system combined with a desalination and organic flash cycle for a residential building. The obtained costs were 3.4 ¢/ kWh for electricity, 37.8 ¢/m³ for fresh water and 1.7 \$/kg for hydrogen. Aghbashlo et al. [88] performed exergoeconomic analysis on a single-cylinder Ricardo diesel engine using different biodiesel concentrations (B5) blended with diesel fuel. They found that the pure diesel decreased to the specific exergy cost 48.81 \$/MJ for a full load compared to 53 \$/MJ for 3% emulsified water-biodiesel (B6W3m). However, the fuel blend of B5W3m had high exergetic efficiency of 28% to 33% according to the engine load percentage and higher exergoeconomic factor of 4% and a minimum relative cost difference of 1.6. That

showed the fuel blend of B5W3m was exergetically and economically effective fuel. Cavalcanti et al. [89] performed exergoeconomic and exergoenvironmental analysis on different mixtures of biodiesel and diesel in a direct-injection engine of 27 kW. They found that low biodiesel concentration had a slightly higher exergy efficiency of 33% than pure diesel 32%. Also, the exergoeconomic factor was higher for 5% biodiesel (D95B5) of 0.36% than for pure biodiesel (B100) of 0.16%. However, biodiesel had a lower environmental impact of 55.8 mPt/kg than 240 mPt/kg of diesel. Increasing the biodiesel concentration decreased the environmental impact from 33.7 mPt/MJ to 19.41 mPt/MJ.

Similar studies have been conducted in hybrid power plants. Lee et al. [90] developed a hybrid power generation system and performed exergetic and exergoeconomic analyses. The hybrid system comprises solid oxide fuel cell (SOFC) and ICE, and other additional devices such as heat exchangers and blowers. They used liquified natural gas (LNG). The unit exergy cost of LNG was \$12.62 /GJ. The researchers found that extensive exergy destruction occurred in the ICE, followed by heat exchangers and then SOFC. Also, the SOFC had the highest exergoeconomic factor of 93%. However, the heat exchanger had the lowest exergoeconomic factor of 7%. The ICE and SOFC produced a power of 11.36 kW and 93 kW, respectively. The net power was 101 kW with an overall system efficiency of 62.1% and exergetic efficiency of 57.0%. In addition, the combination of SOFC and turbomachinery improved the energetic efficiency of the overall cycle to reach to 65% [91,92].

2.3 Marine Transportation

Marine transportation is recognized as another source of global warming due to the pollutants emitted, and sometimes it can be considered as conditional marine pollution for international shipping [93]. However, greenhouse gas (GHG) emissions are anticipated to rise by 50% in 2050, and an international mitigation governance system should be the initiative to ease some challenges to reducing emissions [94]. An allometric approach is adopted to discover the correlation between the ship size and speed and the amount of GHG emissions. It is worth noting that slowing down the ships and applying energy-saving strategies can drastically reduce GHG emissions [95]. Therefore, two emission regulations as, International Maritime Organization Data Collection System and European Union

Monitoring, Recording, and Verification, become essential for ships above 5000 GRT (gross register tonnage) to inspect the carbon emissions in addition to applying energy efficiency management systems [96].

Different methods to improve efficiency and reduce emissions, such as changing fuels, using energy recovery techniques, and developing hybridization designs, may exist. First, many strategies have been applied to reduce carbon emissions. For example, CO₂ reduction can be achieved by adding an absorber solvent (such as mono-ethanolamine) with a reduction of specific energy consumption to increase the CO₂ capture rate in the combustion chamber of an engine, as reported in [97]. In addition, Liu et al. [98] examined the combustion performance of two fuels such as ammonia/ammonium nitrite and ammonia/hydrogen, under different conditions. They found that ammonia nitrite decreases the ignition of ammonia and shortens the ignition delay time of the mixture fuel. The compression ignition can be reduced by mixing hydrogen and ammonium nitrite. The addition of ammonia nitrite reduces the intake temperature to 300-360K. Moreover, Tipanluisa et al. [99] investigated the impact of blending diesel/n-butanol on a heavy-duty diesel engine. They found that the concentration of n-butane at 10% of the volume ratio increases the maximum pressure and maximum heat release rate of the combustion chamber but decreases the in-cylinder temperature without significant changes in ignition delay. In addition, the existence of n-butanol reduces brake-specific energy consumption and carbon emission. Also, Zhao et al. [100] studied the effect of hydroxyl (HHO) on the conventional marine diesel engine by blending waste cooking oil and hydroxyl gas with diesel and with diesel and kerosene. They found that this fuel blend can increase the brake thermal efficiency to its maximum of 38%, with a brake specific fuel consumption of 228 g/kWh and can reduce the carbon emission and eliminate others. Moreover, recent studies have been conducted on enhancing combustion performance. For example, Mueller et al. [101] investigated a ducted fuel injection of a diesel engine using pure diesel fuel, diesel and 25% vol methyl carbonate, diesel and 25% vol glycol ethers. Adding oxygenated fuel to diesel significantly reduces NO_x and SO_x emissions. Also, Monsalve-Serrano et al. [102] studied dual-fuel combustion performance by using diesel mixed with methane. They found that the carbon emissions have been reduced during high load conditions only. This review includes the well-to-wake life cycle elements. In addition, Xing et al. [103]

presented a technological review to determine whether encouraging alternative marine fuels that can reduce the most dangerous emissions, such as sulphur oxides, carbon dioxide, and nitrogen oxides, has significant benefits. They found that the usage of fossil fuels with any additives still produces fewer emissions compared with that only fossil fuels but still higher than what regulations have permitted. In addition, hydrogen and ammonia are great choices for a small shipping and domestic application despite their high price tag. Methanol is also a boundless opportunity for international shipping instead of biofuels and modified fossil fuels.

A hybridization is a great approach to increasing engine performance. For instance, Wang et al. [104] presented a review of marine renewable energy storage evolving pumped hydro, hydrogen, battery and buoyancy energy storages and need more contribution to enhance the energy performance with economic benefits. In another example, Miretti et al. [105] investigated the air quality of hybridized waterbuses. They found that parallel or series hybridization by using batteries, electric generators, and electric motors can reduce engine emissions and increase air quality. In addition, Long et al. [106] designed a system for an exhaust gas-reformer that is attached to LNG marine engine to produce hydrogen on-board. The reformer uses methane and oxygen. They found that hydrogen-rich gases are obtained by reforming a mixture of methane and engine exhaust gases with a catalyst of $\text{Ni}/\text{Al}_2\text{O}_3$ to reach a maximum hydrogen concentration of 12.6% by increasing the methane concentration with acceptable excess air. This hydrogen production was able to get the benefit of waste energy-yielding to increase the overall engine performance. Also, Yao et al. [107] presented a combined system of on-board cold storage, air conditioning and desalination with about 55% of utilization efficiency and 50% exergy efficiency. Moreover, Sürer and Arat [108] presented on-board hydrogen storage using desalination of seawater and electrolysis for hydrogen production combined with a proton membrane fuel cell (PEMFC) in order to provide electric power for operating a ship and for running the electrolysis. They found that the hydrogen fuel consumption is 460 kg/day for a FLAGSHIP project, and there will be 3×200 kW PEMFC modules to transport 199 passengers and 60 cars or 6 trucks. Most studies have introduced electrolysis, desalination, and hydrogen production to utilize the waste energy of marine internal combustion engines,

whether operated by diesel or LNG. However, no new marine engine configurations have been implemented to increase the engine efficiency using clean fuels.

Combining fuel cells with marine engines becomes more interesting as introducing new efficient powering systems instead of traditional marine diesel engines. For example, Ahn et al. [109] provided different analyses of the effect and failure mode for a tanker operated using a molten carbonate fuel cell (MCFC) and gas turbine. The tanker uses two fuels natural gas and liquified hydrogen. Also, the MCFC is located before the combustor and power turbine. The propulsion receives a total power of a gas turbine and MCFC. They found that the power of gas turbines and MCFC are 4.5 and 24 MW, respectively. In addition, the mentioned analysis found that mechanical failure can occur during leakages, and the dangerous areas are around the hydrogen storage, and extra precautions and maintenance must be applied to reduce any future malfunctions. In addition, Lin et al. [110] designed three configurations of indirect ammonia proton exchange membrane fuel cell (IA-PEMFC) using liquid ammonia, ammonia decomposition reactor (AMR), ammonia removal unit, PEMFC, and tail gas combustion in order to provide hydrogen to PEMFC to produce electrical power. They found that the net power of this cycle is 10 kW, and using tail gas combustion was helpful in reducing the AMR heat addition yielding to increase in the cycle efficiency from 30% to 50%. Moreover, Ahn et al. [111] developed two marine engine configurations using two gas turbine engines and a steam Rankine cycle (SRC). One of them uses only LNG, and the other uses a mixture of liquified hydrogen and LNG. They also replaced the two gas turbine engines with MCFC using only LNG fuel. The net power of the MCFC configuration is about 66 MW which is almost the same as other configurations with electric efficiency of 54%. Also, combining gas turbines with SRC and operating using only LNG is more economical and feasible and more efficient than any other configurations. Furthermore, Sürer and Arat [108] presented a literature review of hybridized marine engines combined with fuel cells, especially PEMFC to provide a net power varying from 12 kW to 300 kW from PEMFC and 400 kW from the electric motor. The hydrogen production was from steam reforming or gasification of methane and coal, pyrolysis of methane, and electrolysis of seawater after desalination. The challenge of such systems is the limited output power of PEMFC with respect to its size and large storage of hydrogen gas.

Waste energy is a great concern to many leaders of industry and must be reduced as much as possible to increase engine efficiency. Nawi et al. [112] studied possible methods of recovering waste exhaust heat from marine diesel engines of 996 kW by combining the organic Rankine cycle and marine. The working fluid is bioethanol production from some microalgae. They found that the net power is 5.10 kW with an energetic efficiency of 2.3%. In addition, Tian et al. [113] investigated a combined organic Rankine cycle (ORC) and liquified natural gas (LNG) marine engine to utilize the waste energy of exhaust gases. They performed thermo-economic analysis over 32 working fluids in order to obtain optimal efficiency and economic benefit. They obtained the best cases in terms of efficiency and power output as of 14% and 210 kW with a combination of three from R1150, R600, R601a, R170, and R290. Also, Liu et al. [114] analyzed a combination of an organic Rankine cycle and thermoelectric generator with a marine diesel engine to make use of the waste energy of exhaust gases. The combined cycle has an energetic efficiency of 6.9% and a net power of 134 W, with a cost of 0.461 \$/kWh, which is lower than each bottom cycle.

Vedachalam et al. [115] and Ampah et al. [116] have reviewed marine regulations to restrict the sulphur contents in marine fuels such as distillate marine fuels (DM), ultra-low sulphur fuel oil (ULSFO-DM), residual marine fuel (RM), and high-sulphur heavy fuel oil (HSHFO). They also discussed the role of the international marine organization (IMO) in lowering the border of carbon emissions, nitrogen oxides, sulphur oxides, and particulate matter. Some combinations and processing can be performed for marine fuels; hence, alternative fuels can be introduced and have the potential for better propulsion and power performance, such as hydrogen, liquified natural gas, alcohol fuels (i.e., ethanol and methanol), hydrocarbons (i.e., dimethyl ether), ammonia, and biodiesel and biofuels with the addition of nano particles on biodiesel-diesel blends to reduce emissions.

Some studies have implemented a combination of Rankine cycles with marine diesel or dual engines. For example, Hountalas et al. [117] combined a Rankine bottoming cycle with the exhaust of a marine diesel engine to utilize waste energy. This integration increases the net power and overall efficiency and reduces fuel consumption. Aghdoudchaboki et al. [118] combined an organic Rankine cycle and a multi-effect desalination unit with a marine diesel engine to recover the waste heat. The integrated

engine can produce a net power of about 390 kW and 7 m³/h of freshwater, and it has maximum exergy efficiency of 36%. Jafarzad et al. [119] introduced a topping cycle and two bottoming cycles to be combined with the marine diesel engine to recover waste heat. The topping cycle is a steam turbocharger, and the bottoming cycles are an organic Rankine cycle (ORC) and reverse-osmosis desalination unit. The overall performance was raised to 82% and 54% energetic and exergetic efficiencies, respectively, and the cogenerated engine can generate a net electric power of 668 kW and a heating load of 650 kW.

Tsougranis and Wu [120] developed a power plant system of a vessel consisting of four dual-fuel engines and two LNG tanks to be connected to a bottom ORC that depends on a cryogenic pump at the affluent of LNG tanks for cooling the condenser. They used one-stage and two-stage ORC. They found that both ORCs can produce a net power of more than 400 kW for one-stage and 550 kW for the two-stage ORC, with energetic and exergetic efficiencies of about 28% for one-stage and more than 35% for two-stage. The cost of this system can be increased due to the heat exchanger and expanders; however, the fuel consumption saving per year is 344285 \$/year with a payback of four years.

The diesel engine is still in use despite its low efficiency compared to other powering systems. Therefore, some studies have been conducted to investigate the performance of other powering systems. For instance, Gonca [121] analyzed an SRC containing three turbines, one open and two closed feedwater heaters. He found that pressure is a necessary condition to consider in the design to gain maximum performance. Gude [122] used the engine exhaust's waste energy to desalinate the ships' ballast water to produce 1000 m³/d freshwater that is sufficient for 2000 to 4000 occupants. Also, Singh and Singh [123] combine a gas turbine cycle with an SRC by using a recovery heat exchanger for steam generation. The energetic efficiency of this combination ranges from 38% to 33%, according to the excess air in the combustion of natural gas.

Some state-of-art powering systems have been introduced to marine transportation. For example, Long et al. [106] [20] designed hydrogen gas production by utilizing the exhaust gases of a diesel engine that operated using LNG. The process can produce a maximum hydrogen concentration of about 13%, and the energetic efficiency of a steam reformer (SR) ranges from 63 to 94%, according to the amount of excess air. Lion et al. [124] studied a two-stroke marine diesel engine of 13.6 MW. They found a massive amount

of waste heat is rejected in the atmosphere. Therefore, they designed SRC and ORC to recapture two energy sources: the high heat of exhaust to the boiler and the rejected heat of condensers by using seawater. The first scenario is SRC and ORC, and the second scenario is only ORC. The first scenario can produce 848 kW, while the second can give 678 kW. This shows the combination of two cycles is a better choice than the other. Chitgar et al. [125] combined a solid oxide fuel cell (SOFC) with freshwater desalination by reverse osmosis process, and they selected methane for hydrogen production from a fuel cell. The combined system can produce a net power of 1.3 MW and about 230 m³/day of freshwater with an exergetic rate of 54%.

Utilization of waste energy is a great approach to improving the overall engine performance. It can be executed in various techniques. For example, Zhu et al. [126] combined a steam Rankine cycle (SRC) and a gas Brayton cycle (GBC) with a two-stroke MAN diesel engine of 28 MW at 60% load to use the waste energy of engine exhaust. For a full load, the diesel engine can produce 4800 kW, while the SRC and GBC can generate a power of 400 kW and 200 kW, respectively, at a bypass ratio of 12% of waste exhaust. This results in a reduction in fuel consumption by 7.3%. Furthermore, Wang et al. [127] combined the organic Rankine cycle (ORC) with the exhaust of a marine diesel engine. The working fluid is a zeotropic mixture of benzene/m-xylene and cyclopentane/toluene. The exergy efficiency of ORC is improved by 7 to 22%, while the power is increased by an average of 20% using zeotropic mixture compared to individual refrigerants at low and high exhaust engine temperatures ranging from 225 to 380 °C. They also found that the higher the exhaust temperature, the lower the ORC performance. In addition, the lowest performance occurs in the summer than in the winter season.

Additionally, Liu et al. [128] connected the exhaust line of a diesel engine to the hot junction of thermoelectric generator (TEG) modules, while the cold junction of TEG is connected to an organic Rankine cycle with R22 working fluid. In addition, the charge air of the engine is used to preheat the pump exit before the evaporator. This cycle can produce an output power of 134 W, with an energy efficiency of about 7%. Also, Pallis et al. [129] used the organic Rankine cycle with R134a working fluid attached to the hot marine diesel engine to benefit from the waste heat. This design was able to produce net electrical power of about 165 kWe with an energy efficiency of about 7%. In addition,

Abbas et al. [130] constructed two cascaded ORCs to use the waste energy. The topper ORC is a high-temperature (HT) cycle with a working fluid of cyclopentane, while the bottomer ORC is the low-temperature (LT) cycle using propane, butane, or pentane. The energy efficiency is obtained to be 5.5%, while the exergetic efficiency is 20%. The best fluid option is pentane for better performance. Moreover, Qu et al. [131] used a steam Rankine cycle, power turbine, and ORC using R25fa in order to take benefit from the waste energy of a marine diesel engine of 9960 kW. The additional net power generated from this cycle is about 1 MW at full load with energetic and exergetic efficiencies of about 28% and 66%, respectively. Another method to use the existing energy source is the usage of cooling load from the liquified natural gas (LNG) as reported by Yao et al. [107] in designing combined system for a containership to on-board cold storage, desalination, and air conditioning. The exergy efficiency of this combination increases to about 55% and it is economically beneficial at 50%.

Fuel cells are electrochemical engines with no mechanical part movement, and they are efficient compared to turbomachinery and internal combustion engines. However, still, hybridization of existing engines is more acceptable than standalone fuel cells for its reliability and cheapness. For example, Ahn et al. [132] designed an engine system for a tanker to include a molten carbonate fuel cell and a gas turbine or steam Rankine cycle. The main fuel in the system is natural gas. The energy efficiency reaches 54% using gas turbine and 50% using steam Rankine cycle. In another instance, Choi et al. [133] introduced a polymer electrolyte membrane fuel cell combined with a lithium-ion battery to deliver power to a waterjet propulsion system of a tourist boat with a maximum power of 86 kW. The PEMFC can deliver 56 kW (28 kW for each stack), which can be combined with the batteries to provide full power or can work alone for low-speed voyages. It is better to manage all energy sources for the best engine performance. For example, Si et al. [134] presented energy management of a hybrid engine that contains a diesel engine, fuel cell, battery, hydrogen storage, and solar panels for a bulker ship. The management system was able to allow each subsystem to operate to its maximum performance to reduce carbon emissions, management cost, and fuel consumption by more than 40%.

Chapter 3. Details of Transportation Systems

This chapter presents the description of the newly developed engine systems in three transportation sectors in addition to the most common engine in the sector. The detailed modelling of each subsystem will be described in the following chapter. The system components are selected for the internal combustion engine, gas turbine, Rankine cycle, and fuel cells, as shown in Table 3.1.

These are powering systems that deliver power to the generator, which is connected to the motor for the required motion. The aviation transportation sector has a baseline traditional turbofan engine (A-Base) and two hybrid turbofan engines, A-1 of MCFC-turbofan and A-2 of SOFC-turbofan engine. The rail transportation sector has a baseline internal combustion engine (ICE) for the traditional locomotive engine (R-Base) and three developed rail engines, which are hybrid gas turbines combined with ICE (MCFC-GT, ICE) as R-1 engine, hybrid gas turbine combined with on-board hydrogen (SOFC-GT, AEC-PEMFC) as R-2 engine, and hybrid gas turbine (SOFC-PEMFC-GT) as R-3 engine. The marine transportation sector has a baseline internal combustion engine (ICE) for traditional marine engines (M-Base) and three developed marine engines, which are ICE combined with a hybrid gas turbine engine (ICE, SOFC-GT) as M-1 engine, steam Rankine cycle combined with a hybrid gas turbine (SRC, SOFC-GT) as M-2 engine, and hybrid gas turbine combined with a binary system of two organic Rankine cycles (SOFC-GT, 2ORCs) as M-3 engine.

Table 3.1 The system design for the transportation sectors

Transportation	System #	System	Main Engines
Aviation	A-Base	Original	Turbofan
	A-1	Hybrid	MCFC-turbofan
	A-2	Hybrid	SOFC-turbofan
Rail	R-Base	Original	ICE
	R-1	Hybrid	ICE, MCFC-GT
	R-2	Hybrid	SOFC-GT, AEC-PEMFC
	R-3	Hybrid GT	SOFC-PEMFC-GT
Marine	M-Base	Original	ICE
	M-1	Hybrid	ICE, SOFC-GT
	M-2	Hybrid combined	SRC, SOFC-GT
	M-3	Hybrid combined	SOFC-GT, 2ORCs

3.1 Aviation Engine Systems

A turbofan aircraft engine is operating Boeing 787 Dreamline in Air Canada, which is a baseline aviation system of a turbofan aircraft with a high bypass ratio (high-BPR), as shown in Figure 3.1. It consists of an inlet diffuser (ID), low-pressure compressor (FAN), intermediate-pressure compressor (IPC), high-pressure compressor (HPC), combustion chamber (CC), high-pressure turbine (HPT), intermediate-pressure turbine (IPT), low-pressure turbine (LPT), and exit nozzle (EN).

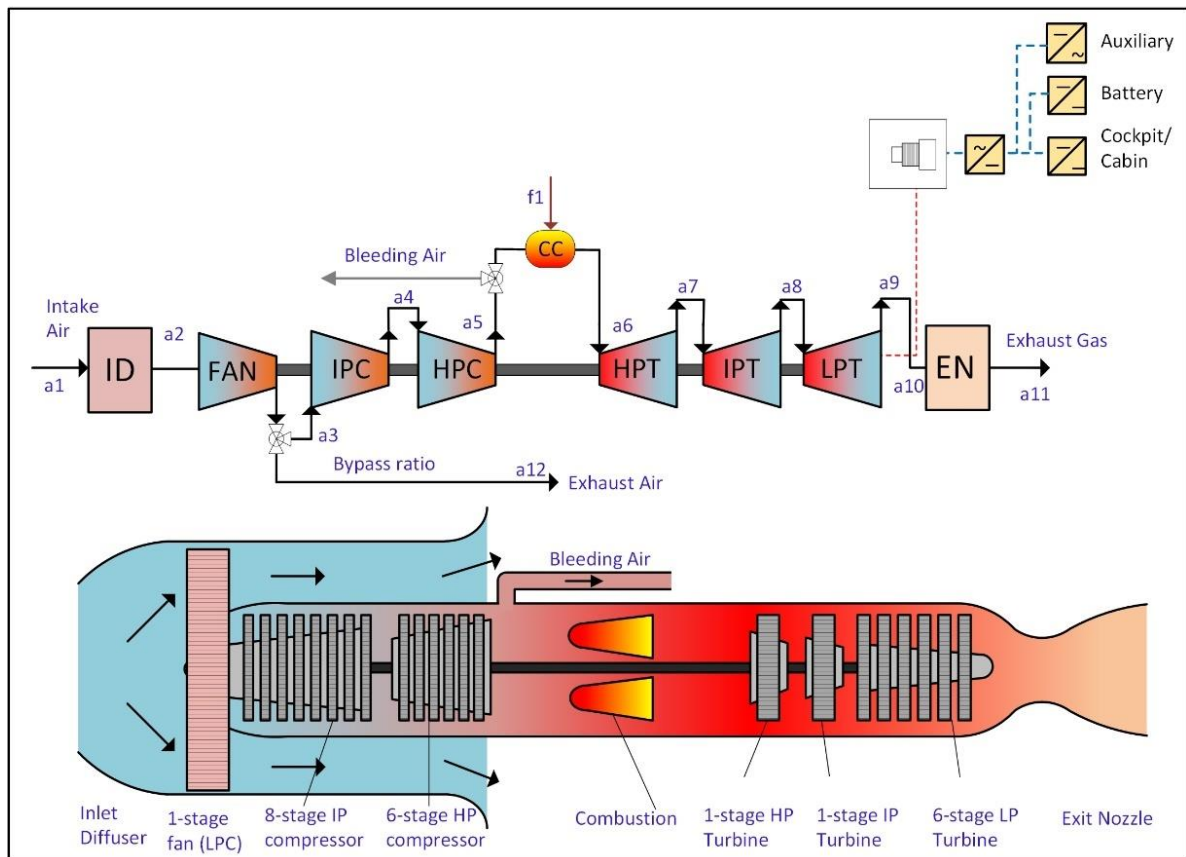


Figure 3.1 The configuration of the aviation base (A-Base) system

The traditional fuel used in the aviation system is kerosene. The power generated from the turbofan engine is used to operate the cockpit of the airplane, any auxiliary systems, and the battery for storage and emergency cases. The specifications of a traditional turbofan are listed in Table 3.2. These specifications include some general characteristics, such as

engine type, dimension and dry weight, major components, like compressors, turbines, and combustors, and overall aircraft engine performance.

Table 3.2 The specification of a traditional turbofan aircraft engine

Specifications	Turbofan [135]		
Aircraft engine	Rolls-Royce Trent 1000		
General Characteristics:			
Type	Three-spool high-bypass turbofan		
Dimension	Length: 4.738m, diameter: 2.85 m (fan)		
Dry weight	5,936 – 6,120 kg		
Components:			
compressor	One-stage LP (fan), 8-stage IP, 6-stage HP compressor		
combustors	Single annular combustor with 18-off fuel spray nozzles		
turbine	Single-stage HP (13391 RPM), single-stage IP turbine (8937 rpm), and 6-stage LP turbine (2683 rpm)		
Performance:			
Overall pressure ratio	50:1	Thrust-to-weight ratio	6.01:1
TIT	920°C	Air mass flow	1,090 – 1,210 kg/s
Thrust	265.3–360.4 kN	BPR	>10:1
SFC	479.16 kg/(h.kN)		
TIT... Turbine inlet temperature		SFC... Specific fuel consumption	BPR... Bypass ratio

3.1.1 System A-1: Hybrid molten carbonate fuel cell and turbofan engine

The hybrid MCFC-turbofan engine consists of a turbofan aircraft engine with an MCFC and a catalytic burner or an oxidizer, as shown in Figure 3.2. The air flows through the turbofan. A portion of exhaust gas after the LPT flows through the afterburner and then the MCFC, while the remaining exits to the atmosphere after mixing with the exhaust of the MCFC and afterburner. The fuel blend with the steam injection enters the anode of the MCFC. The catalytic burner receives exhaust gases to oxidize the fuels and produce carbon dioxides. The exhaust from the catalytic burner enters the cathode of MCFC that chemically react with the electrolyte to produce clean exhaust gases. If any carbon dioxide or monoxide exits as by-products in the exhaust gases, then the exhaust gas returns to the burner and re-oxidizes into the cathode of the MCFC. The clean exhaust gas leaves the turbofan through the hot exit nozzle.

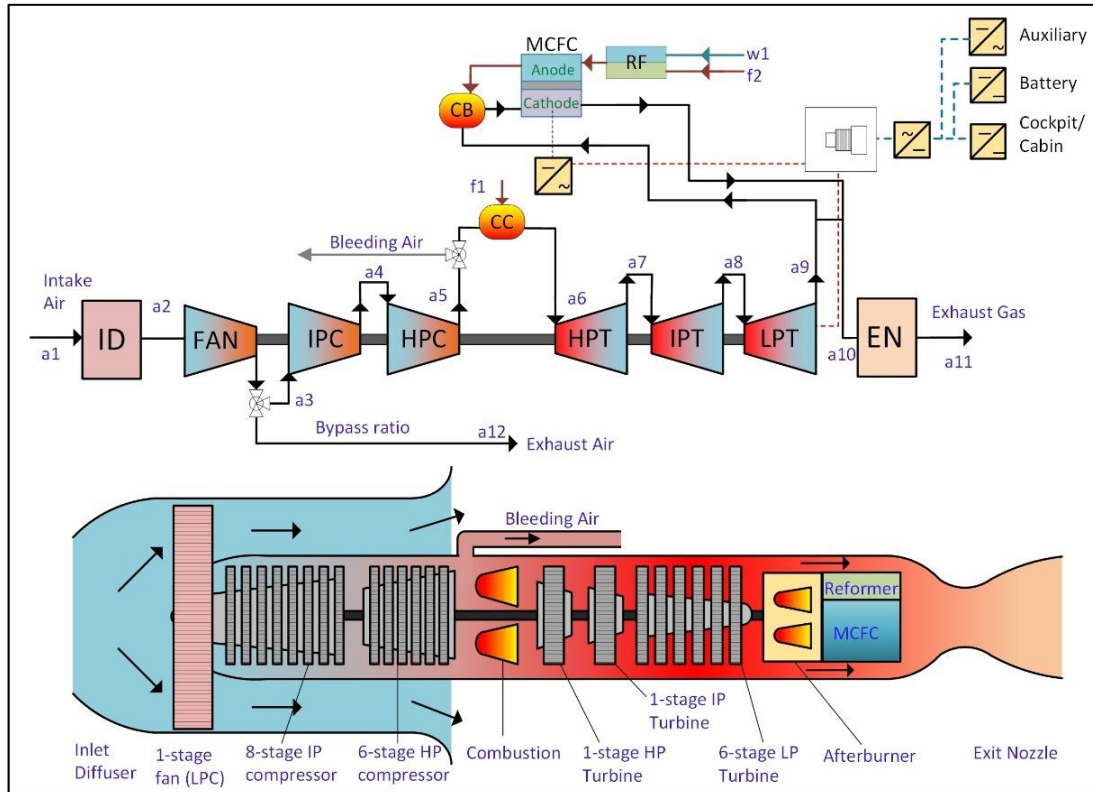


Figure 3.2 The configuration of hybrid MCFC-turbofan engine (A-1) system

3.1.2 System A-2: Hybrid solid oxide fuel cell and turbofan engine

The hybrid SOFC-turbofan consists of a turbofan aircraft engine with a high bypass ratio (high-BPR) and a SOFC, as shown in Figure 3.3. The airflow enters the diffuser. Some of air is bypassed around the turbofan through the high-pressure compressors (HPC) through the bypass after the low-pressure compressor (FAN) to the atmosphere, while the remaining air flows through the core of the turbofan. The compressed air from the IPC and HPC compressors flows through the cathode of SOFC and the combustion chambers. There is also bleeding air with a small ratio of the compressed air that flows to any auxiliary systems and balances the required air for aircraft. The fuel blend, and the steam enter the reformer and the anode of SOFC. The exit flows from the SOFC burn with the compressed air in the combustion chamber. The exhaust gases flow through the HPT, IPT and LPT turbines and the hot exit nozzle.

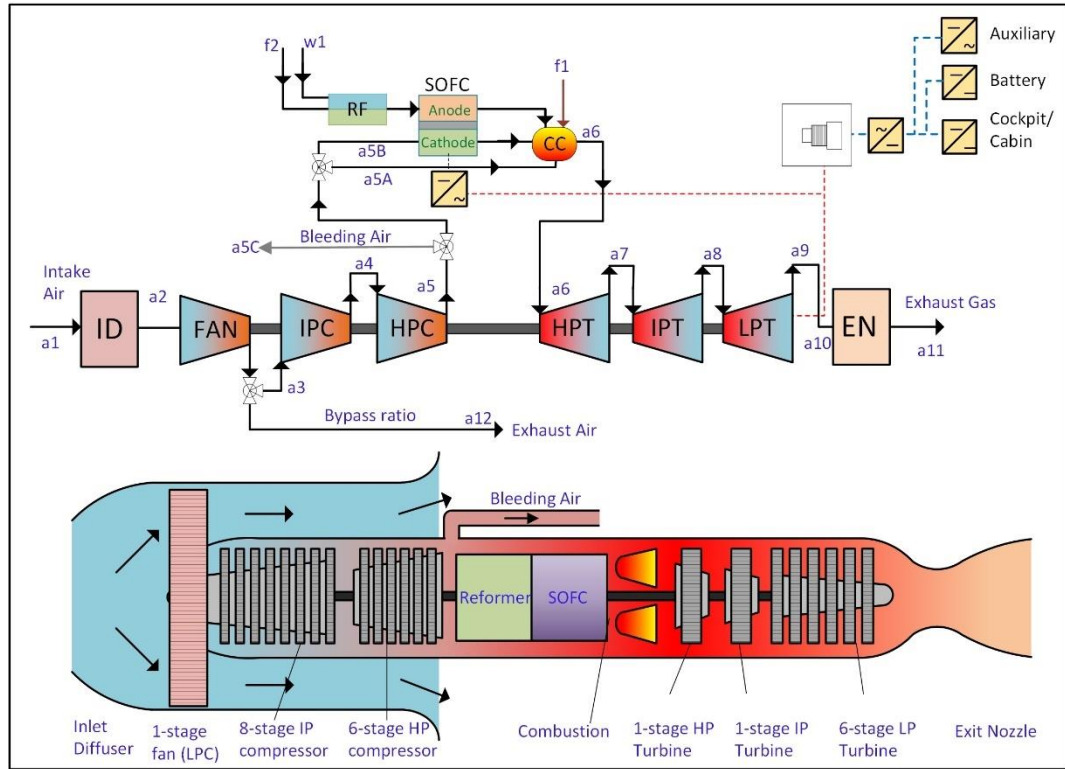


Figure 3.3 The configuration of hybrid SOFC-turbofan engine (A-2) system

3.2 Rail Engine Systems

The traditional rail engine is a diesel internal combustion engine (ICE), which is the baseline engine (R-Base), as illustrated in Figure 3.4. Air is compressed into the compressor of a turbocharger and then flows to an aftercooled heat exchanger into the ICE at state point a3. A turbocharger turbine expands the exhaust of ICE. It runs the compressor and delivers the remaining power to a starting generator. Other subsystems include jacket water cooling and oil cooling subsystems. The fuel consumption is adjusted by the governor to control the engine speed. The traditional engine is commonly operated by ultra-low-sulfur diesel (ULSD) fuel. The ICE is connected to the generator to deliver the power to a traction motor, battery for storage, and auxiliary supplies. The engine model is selected based on the most common engine types in rail transportation sectors in the province of Ontario and Quebec. It was found that the engine model of EMD 16-710-G3 is the most common engine that operates freight, passenger, and commuter trains in the two provinces. The specification and other technical details of the EMD 16-710-G3 are listed in Table 3.3.

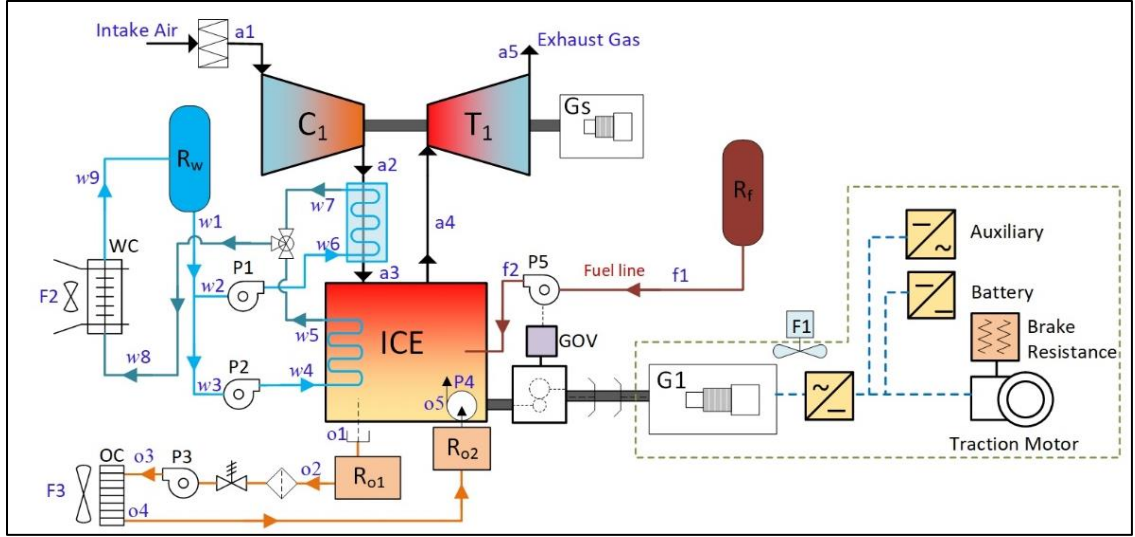


Figure 3.4 The configuration of R-Base system

Table 3.3 The specifications of the locomotive engine

Specifications	Values [136,137]	Units
Engine Model (EMD)	EMD 16-710G3	--
Engine Horsepower, EHP	4,500	hp
Engine Power, \dot{W}_E	3,355	kW
Output power per cylinder, \dot{W}_{E-cy}	210	kW
Engine Speed, N_{ICE1}	950	rpm
Brake mean effective pressure, b_{mep}	1,069	kPa
Displacement Volume per cylinder, V_d	11.635	l
Compression Ratio, r	15:1	---
Bore	0.23019	m
Stroke	0.2794	m
Number of cylinders, n_{cyl}	16	---
Fuel Tank Volume, V_{RES1}	8,410	l
Turbocharger Pressure Boost, ϕ_{TC}	1.25	---
Cooling water reservoir temperature, T_{RES3}	49	°C
Engine jacket cooling water outlet temp, T_{12}	85	°C
Maximum cylinder pressure, P_{max}	10,800	kPa

3.2.1 System R-1: Hybrid combined locomotive engine

A hybrid combined engine (R-1) is proposed, which consists of ICE with a turbocharger and gas turbine cycle combined with a molten carbonate fuel cell (MCFC), as shown in Figure 3.5. The ICE and GT are separate engines. The air is compressed in the turbocharger compressor and cooled down by the aftercooler heat exchanger before entering the ICE. Also, the fuel blend of hydrogen and hydroxyl is pumped to the ICE to be burnt with the compressed air in the pistons. The exhaust gas released from ICE enters the turbocharger turbine and is used in the gas turbine system.

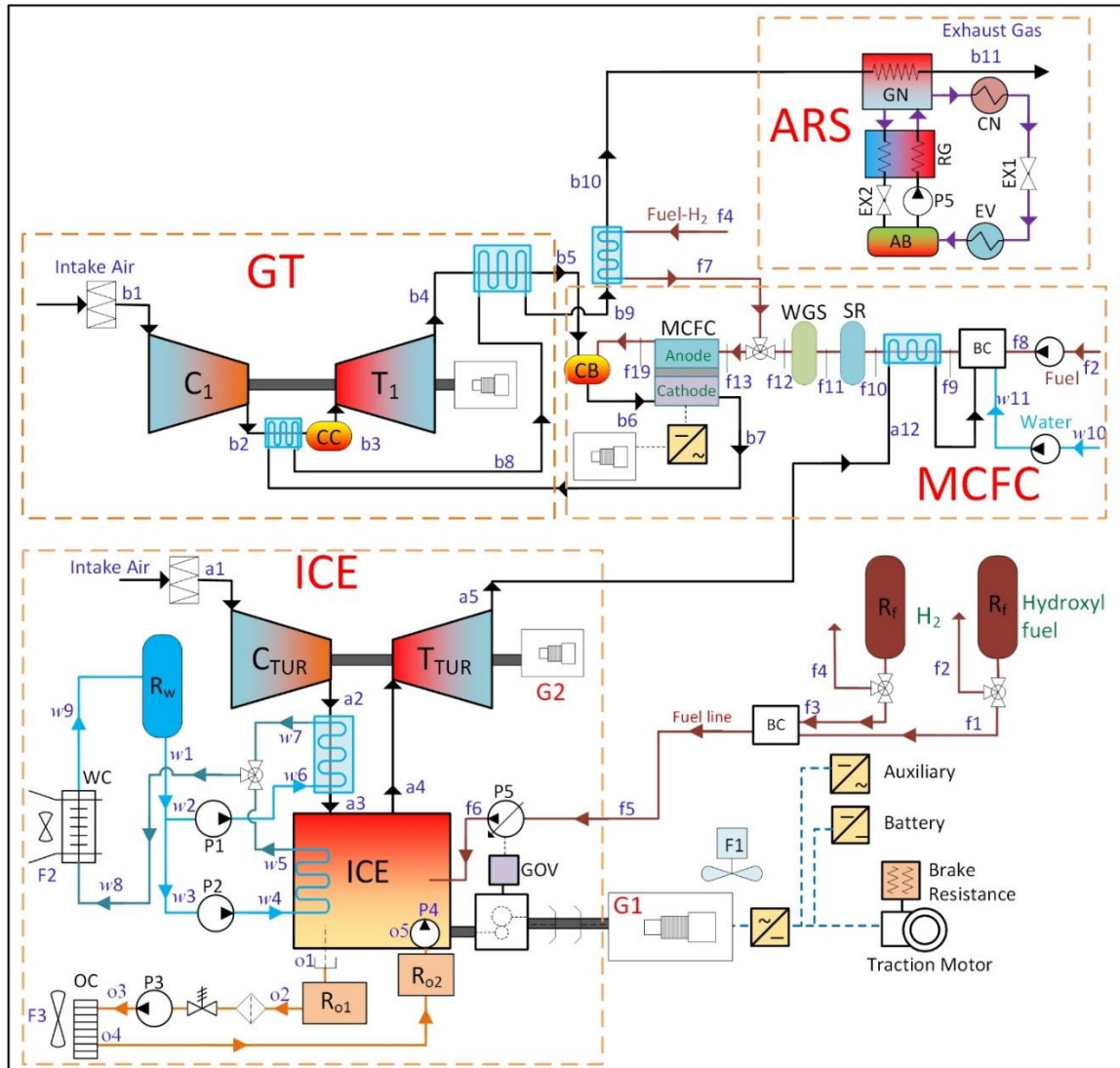


Figure 3.5 The configuration of the proposed hybrid combined engine (R-1) system.

The gas turbine (GT) consists of a compressor and a turbine and is combined with a molten carbonate fuel cell (MCFC). Another amount of air is compressed, then cooled, then expanded in the GT cycle, and then used in the MCFC system. In the MCFC, the fuel is blended with water and exhaust gas from the ICE system and heated by that exhaust gas before entering the steam reforming (SR) and water gas shift (WGS) and then entering the anode of MCFC. Note that additional hydrogen gas may be added to the fuel stream before the MCFC. The anode flow exit enters a catalyst burner to burn the fuel with the expanded air from the turbine of GT, and the combustion results will enter the cathode to extract the carbon monoxide and carbon dioxide gases. Therefore, the exhaust gas has fewer carbon

emissions and provides electrical power from the MCFC. The excessive heat of the exhaust gas is utilized to produce cooling by an ammonia absorption refrigeration system. The net power is generated from the ICE, GT, and MCFC systems, which are connected to the generator to deliver the electric power to the traction motor and auxiliary systems. The excess electric power can be stored in batteries.

3.2.2 System R-2: Hybrid SOFC- gas turbine and PEMFC-AEC locomotive engine

The hybrid locomotive engine is designed as shown in Figure 3.6. This hybrid engine consists of three subsystems working together with another auxiliary system for hydrogen production. The hybrid engine composes of the following: a gas turbine (GT) comprising of a compressor (C1), a combustion chamber (CC), and a turbine (T1); a SOFC system comprising of a steam reforming (SR), a water gas shift (WGS), SOFC units, and afterburner (BR); and energy recovery system comprising of a thermal generator (TG) and an absorption refrigeration system (ARS).

The intake air is compressed by C1 and used in the combustion with fuel blends and expanded by T1 to be exhausted into the atmosphere. The exhaust gas releases the GT system at a very high temperature with high emissions as well. Therefore, the exhaust gas is split to enter the SOFC system, which also uses a mixture of fuel blend and water to be reformed and electrochemically transformed into steam to produce electricity. Any unburned fuels will be completely re-combusted in the BR at a lower temperature than the exit of the turbine. The exhaust gases still have excessive heat, which can be transferred into electricity by the TG and cooling load by ARS.

The hydrogen production system is executed on board the train, separated from the engine to refill to store the hydrogen fuel. This system consists of an aluminum electrolysis cell (AEC) that uses aluminum solution ($\text{NH}_3\text{-H}_2\text{O}$) and potassium hydroxide solution ($\text{KOH-H}_2\text{O}$) to produce two gases: hydrogen and nitrogen gases. The nitrogen gases are released into the atmosphere after expanding by T2. Some of the hydrogens can be stored; the remaining hydrogen can be used for electrochemical reactions of PEMFC with compressed oxygen by the compressor (C2) to produce hot steam and electricity.

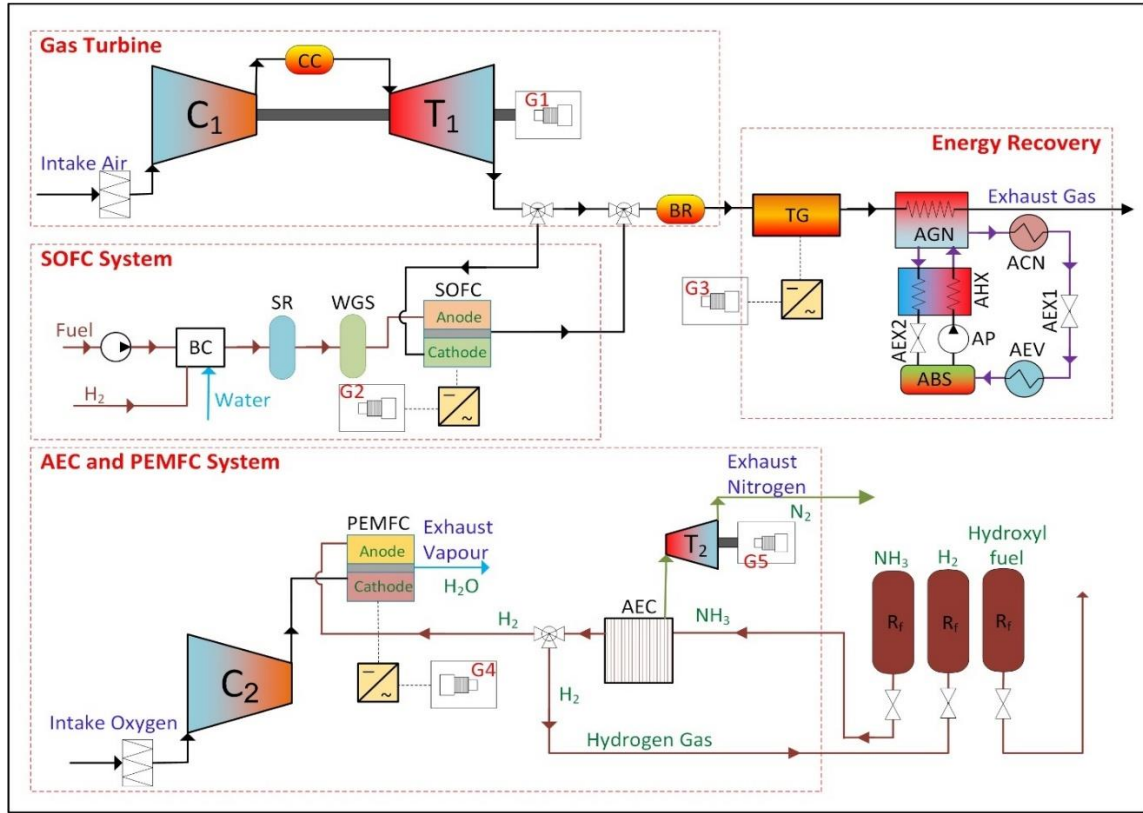


Figure 3.6 The schematic diagram of the hybrid locomotive engine (R-2) system

3.2.3 System R-3: Hybrid SOFC-PEMFC- gas turbine engine

The proposed design of the rail engine is presented in Figure 3.7, which consists of an intercooled gas turbine system, an energy recovery system, and a fuel cell system. The gas turbine comprises two compressors (C1 and C2), two turbines (T1 and T2), an intercooler (IC), a combustion chamber (CC), and an afterburner (BR). The fuel cell system involves high-temperature proton exchange membrane (PEMFC) and solid oxide fuel cell (SOFC). The energy recovery system contains two thermoelectric generators (TEG1 and TEG2) and an absorption refrigeration system (ARS) containing a generator (AGN), condenser (ACN), an evaporator (AEV), an absorber (ABS), and a heat exchanger (AHX).

The intake air passes through the first compressor C1, which is pressurized in the intermediate pressure. Then the air is cooled by IC and split into two parts; the main part passes through the second compressor to be pressurized to high pressure, and the second part passes through the high-temperature PEMFC. Then the fuel blend is burnt with compressed air in the CC to reach its high temperature producing exhaust gases. These gases are expanded by the high-pressure turbine (T2) to generate electricity. After that,

some of the exhaust gases are utilized in the SOFC to produce electricity, while the remaining is combusted in the afterburner (BR) with the exhaust of the SOFC to ensure the complete combustion of the fuel blends before expanding in the low-pressure turbine (T1) to be released to the surroundings.

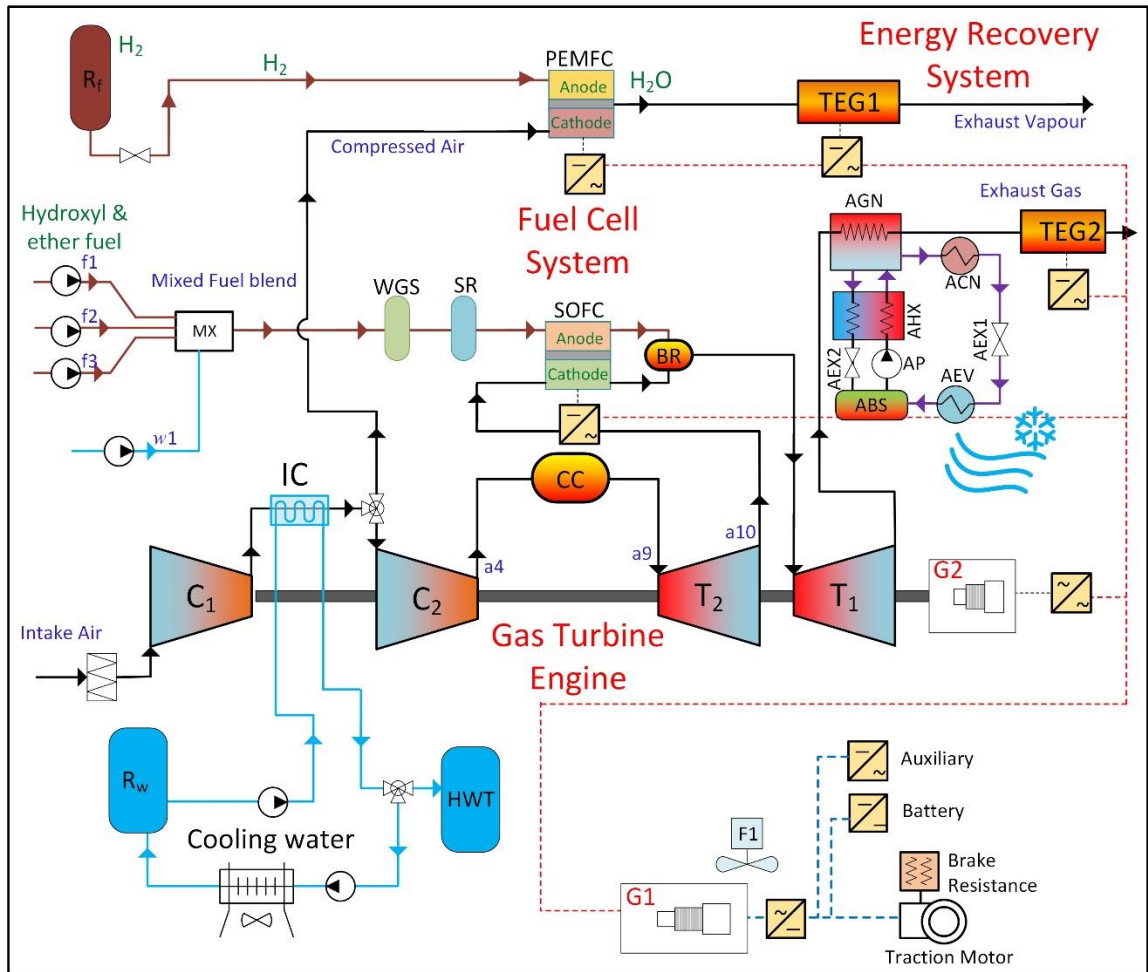


Figure 3.7 The schematic layout of the proposed hybridized gas turbine locomotive engine (R-3) system

The exhaust gases leave the engine at a high temperature with large thermal waste energy, which can be recovered by the energy recovery system (ERS) by transferring thermal energy into electric power using TEG1 and TEG2 and into a cooling load for air conditioning the trains by the ARS, using an ammonia-water refrigerant. A simplified layout of the proposed system is shown in Figure 3.7. It shows a block of a gas turbine engine, which has two outlets: the first is attached to ARS and TEG2, while the second outlet is attached to the PEMFC and expansion and TEG1. The SOFC system uses the

exhaust of the first turbine and returns to the second turbine of the GT. The energy recovery system consists of the ARS and TEGs to transfer the waste energy into cooling loads and electric power.

3.3 Marine Engine Systems

Oil tankers are used for transporting refined or unrefined oils and their derivatives. There are different sizes and capacities, such as Panamax with a length of 230 m and a maximum of 80,000 deadweight tons (DWT), Aframax with a length of 254 m and a maximum of 120,000 DWT, and Ultra-Large Crude Carriers (ULCC) ship with a length of 415 m and a maximum of 550,000 DWT, which are transiting Canadian waters on the east coast of Canada and can carry up to 4 million barrels of oil.

Table 3.4 The specification of a tanker ship and its engine for marine transportation ([18,19])

Ship Specifications	Value	Engine Specifications	Value
Ship model	Aframax WSD 42 111k	Engine model	Wärtsilä 6x62
Ship type	Tanker for oil and products	Output power	10,400 kW
Length overall	252.80 m	Engine Speed	77-103 rpm
Deadweight, max. draft	111,000 DWT	Stroke/bore	4.29
Service speed	14.5 knots	Bore (m)	0.620
Cargo segregation	12 cargo tanks	Stroke (m)	2.658
Fuel oil consumption	41.2 t/day (actual), 82 t/day (theo.)	Number of cylinders	6
Generator sets	3 x 875 kWe	Oil feed rate	0.6 g/kWh
Emerg./harbor generator	1 x 200 kWe	Mean effective pressure	20.5 bar (max. speed)
Engine	2-stroke main engine Wärtsilä 6x62 for 10,400 kW	Engine weight	377 ton

The baseline system for the marine transportation system is selected to be the Aframax tanker oil, and its specifications are listed in Table 3.4. It is operated by a marine diesel engine, as shown in Figure 3.8, which is a two-stroke ICE engine with a turbocharger. The inlet air is taken for compression in a compressor of the turbocharger unit to be then delivered to the aftercooler for cooling down. This air is compressed by pistons and then combusted with the intake fuel in the dual cycle ICE engine through two processes: at constant pressure and at constant volume. After that, the exhaust air is expanded through an isentropic expansion process and cooled down to the initial state of

the main dual cycle. The difference between the compression and expansion processes generates the required power for propulsion under the sea surface. The generator is connected to the motor to operate the propeller for propulsion force and auxiliary supplies, and the excess power will be stored in batteries. The exhaust gas from the ICE is taken to the turbine of the turbocharger unit and hence released into the atmosphere.

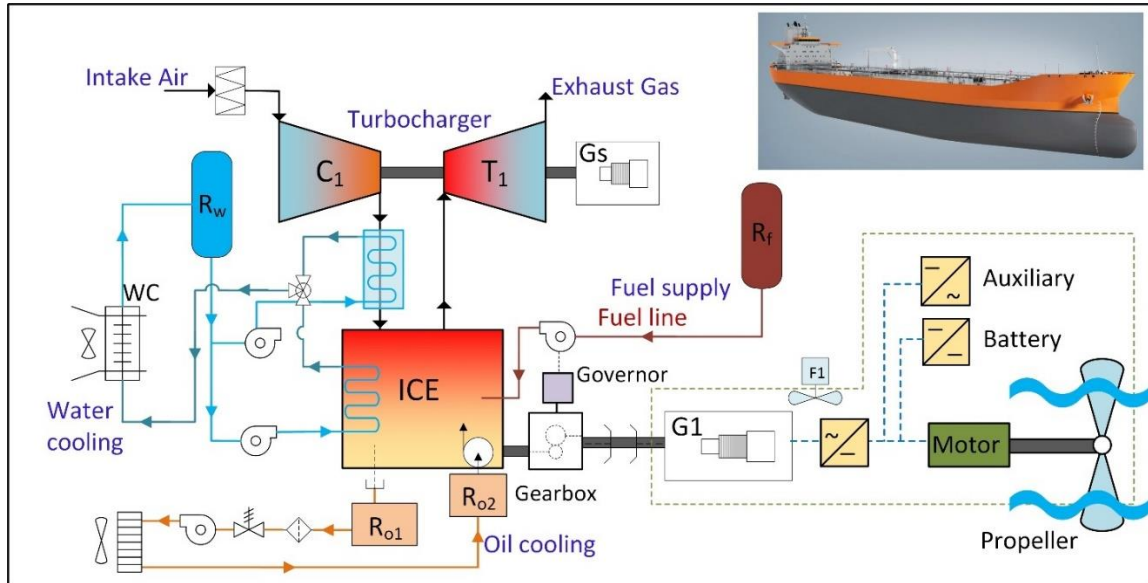


Figure 3.8 The layout of traditional marine engine

3.3.1 System M-1: Hybrid combined marine engine

The hybrid combined engines consist of an ICE, a marine gas turbine (GT), a solid oxide fuel cell (SOFC) system, and two thermoelectric generators (TEGs), as shown in Figure 3.9. The first system is the TEG-ICE system. The intake air goes through a similar process to traditional ICE, but the exhaust gases from the engine are gathered into one large exhaust manifold and then cooled by the first TEG1. The second system is the hybridized GT system, which comprises two compressors with an intercooler and two turbines with a reheater. The air is compressed by the low-pressure compressors, then cooled by an intercooler, then compressed by a high-pressure compressor. The compressed air is added heat by the exhaust air from the last turbine before entering the cathode of the SOFC to be catalytically burned and expanded by the high-pressure turbine. The exhaust air is reheated by the exit of the catalytic burner before entering the low-pressure turbine. The excess heat from exhaust gases can be used for the thermoelectric generator (TEG2) to provide electricity.

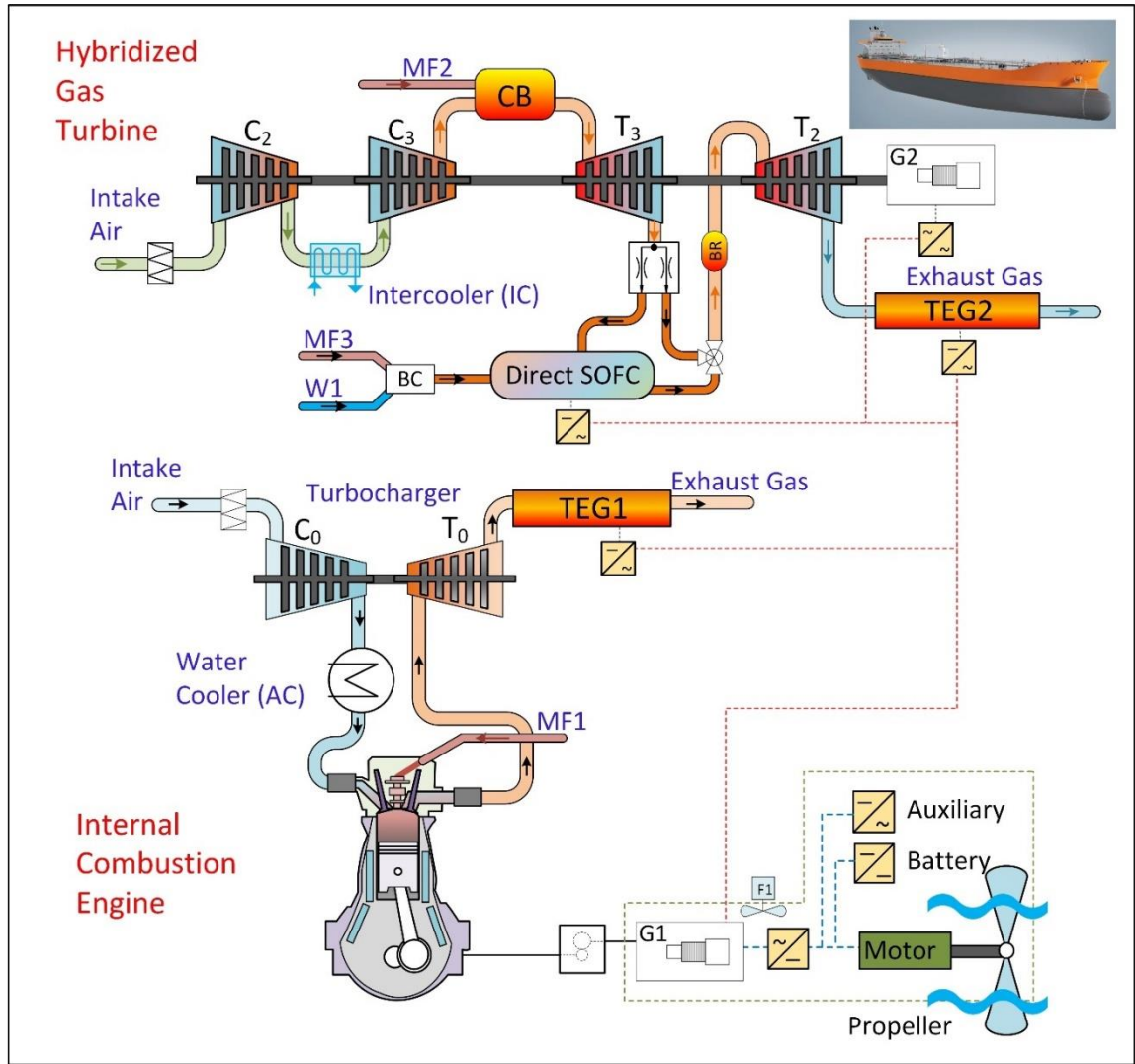


Figure 3.9 The layout of the proposed hybrid marine engine (M-1) system.

3.5.2 System M-2: Hybrid compound cycles (SRC-SOFC-GT) marine engine

The proposed new hybrid compound marine engine consists of a regenerative steam Rankine cycle (SRC), a reheat gas Brayton cycle (GBC) and a solid oxide fuel cell (SOFC), as displayed in Figure 3.10. The first system is GBC [23], where the air is compressed by a low-pressure compressor (LP-C1), cooled by an intercooler (IC), and compressed again through a high-pressure compressor (HP-C2). Then, a bypass from the compressor air is used for the SOFC system, and the remaining is used for combustion with a fuel blend in the combustion chamber (CC). The SOFC system electrochemically reacts the compressed air with hydrogen produced from the steam reforming and water gas shift of fuel blends to produce electric power. At the same time, the exhaust of SOFC flows to the CC to complete

the combustion. The exhaust of CC is used to reheat the outgoing flow of the HP-T1 by a reheater (GTHX) before re-entering the HP-T1. After that, the exhaust gas is expanded again by the LP-T2 and a power turbine (P-T3), which are used in the combustion process of the boiler burner (BR-BL) of the SRC.

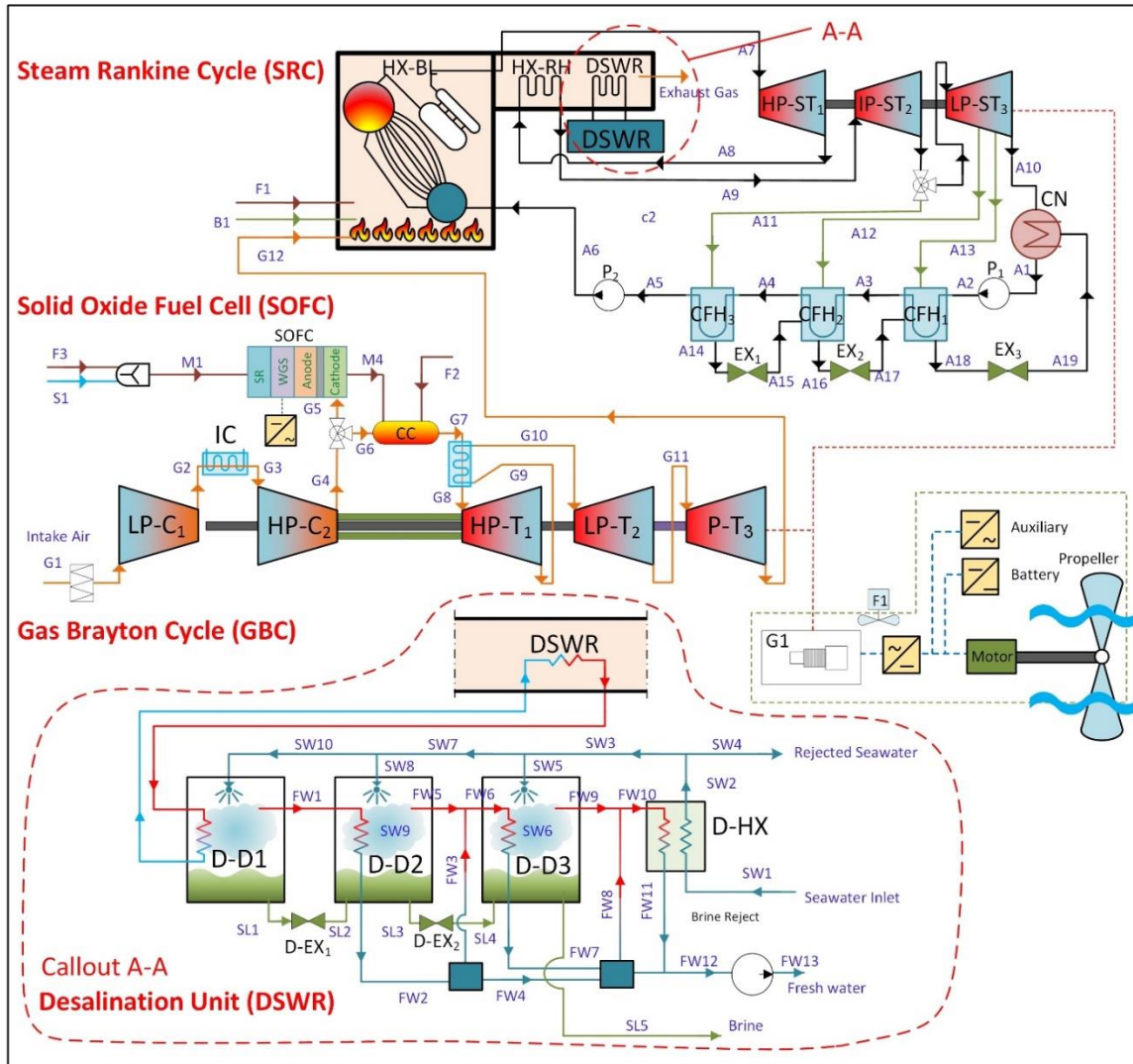


Figure 3.10 The schematic diagram of the hybrid combined marine engine (M-2) system.

The second system is the SRC, where the water is pumped to the heat exchanger boiler (HX-BL) to be heated to superheated steam with high pressure. The superheated steam is expanded by a high-pressure turbine (HP-ST1), reheated in the boiler, and then expanded again by an intermediate-pressure turbine (IP-ST2). After that, the steam exits the IP-ST2 and splits into two pathways: to the third closed feedwater heater (CFH3) and to the low-pressure turbine (LP-ST3) to be expanded to very low pressure of the condenser

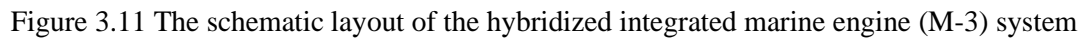
(CN). There are two steam bleeds from the LP-ST3 and one steam bleed from the IP-ST2 that flow to closed feedwater heaters (CFH) and exist to a trap to drop the pressure to the affluent device.

Therefore, the first CFH1 receives a steam bleed to be cooled and expelled to a trap (EX3) to the condenser. The second CFH2 receives a steam bleed at different pressure and exits to the second CFH2 through (EX2). The last one obtains a steam bleed at different pressure and ejects to the third CFH3 through a trap of (EX1). The burner boiler is employed to combust the remaining fuel blend from the GBC with the fuel blend of F1 and air of B1 streams. The exhaust gases inside the boiler are used to heat the pressurized water from A6 to the superheated steam of A7 using the boiler heat exchanger HX-BL before the turbine inlet and heat the steam of the reheater in HX-RH. Also, the waste heat is used for the seawater desalination unit (DSWR) to produce freshwater for the Aframax ship.

3.3.3 System M-3: Hybrid gas turbine combined with binary systems

The proposed system consists of a hybrid gas turbine integrated with a binary system of the topper and bottomer organic Rankine cycle, as shown in Figure 3.11. The hybridized gas turbine involves a gas turbine of Brayton cycle (GBC) with a model of Taurus 6500, combined with a direct SOFC that has direct steam reforming and water gas shift reactors. The GBC consists of one high-pressure compressor (HPC1), a regeneration heat exchanger (GTHX), a combustion chamber (CC), and high-pressure and low-pressure turbines (HPT1 and LPT2). The air is compressed and then passes to the cathode of SOFC, while a blend of fuel and water is reformed in the SR, and WGS then enters the anode of SOFC. Both flows are burnt in the combustion chamber (CC), and the exhaust gases are expanded in HPT1 and LPT2 and exhausted at a significantly high temperature.

The exhaust gases from the GBC system are used to heat the compressed air by GTHX, and the binary system comprises a topper organic Rankine cycle system (TORC) and a bottomer organic reheat Rankine cycle (BORC). These gases are used to transfer heat load in the heat exchanger boiler of the topper cycle and the superheater of the bottomer cycle. The TORC is a simple Rankine cycle, which consists of a turbine (T3) and a pump (P1) and a condenser (CN1) and two evaporators (EV11 and EV12). The bottomer cycle (BORC) is a reheat Rankine cycle, which consists of two turbines, an evaporator EV2, a pump, two heat exchanger condensers EV11 and EV12 and a superheater.



44

Chapter 4. System Modelling

This chapter covers six main topics in system modelling, as shown in Figure 4.1. The first modelling is modelling of engines that includes traditional engines and other powering systems, such as an internal combustion engine for rail and marine, a gas turbine, a traditional turbofan for aviation, a steam Rankine cycle, and a binary system of two organic Rankine cycles. The second modelling is modelling of fuel cells that contains molten carbonate fuel cell (MCFC), solid oxide fuel cell (SOFC), proton exchange membrane fuel cell (PEMFC), and aluminum electrolysis cell (AEC). The third modelling is modelling of energy recovery systems that involves a thermoelectric generator (TEG), absorption refrigeration system (ARS), and desalination unit (DSWR). The fourth modelling is combustion modelling which displays the three traditional fossil fuels, ULSD, kerosene, and MGO, and the characteristic of five alternative fuels, hydrogen, methane, methanol, ethanol, and dimethyl ether, the five fuel blends, the stoichiometric reaction in the combustion chamber, and the chemical reactions in the steam reforming and water gas shift reactors. The fifth modelling is analyses and assessments including thermodynamic, exergy based on fuel and product principal, and exergoeconomic, and exergoenvironmental analyses. Lastly, the sixth modelling is multi-objective optimization using multi-objective-particle-swarm-optimization (MOPSO), including its procedure and algorithm specifications.

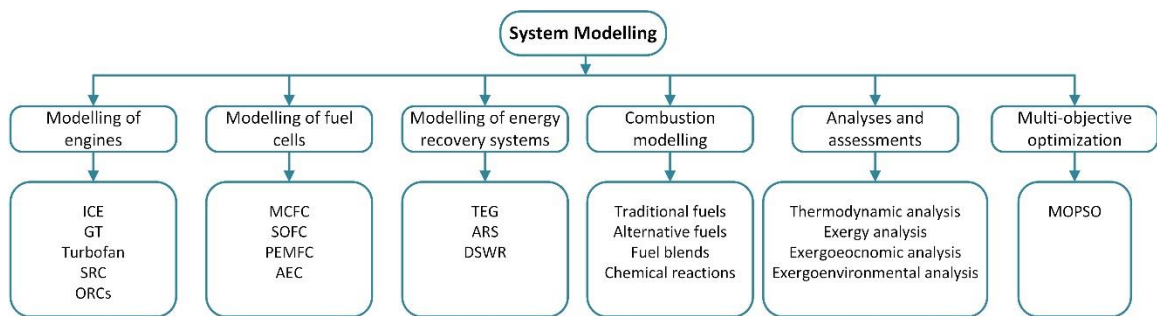


Figure 4.1 The layout of system modelling throughout the thesis.

4.1 Modelling of Engines

This section explains the modelling of all engines and systems used in the thesis. The engines are internal combustion engines, gas turbine engines, turbofan engines, steam Rankine cycle engines, and a binary system of two organic Rankine cycles.

4.1.1 Modelling of internal combustion engine

The prime locomotive mover is powered by a large two-stroke compression ignition (CI) diesel-fueled engine dual (limited pressure) cycle [13]. The ideal dual cycle consists of five processes: isentropic compression (1–2), heat addition (2–3) at constant volume, heat addition (3–4) at constant pressure, isentropic expansion (4–5), and constant volume heat rejection (5–1). The P-v diagram and T-s diagram for the ideal dual cycle without a turbocharger is illustrated in Figure 4.2.

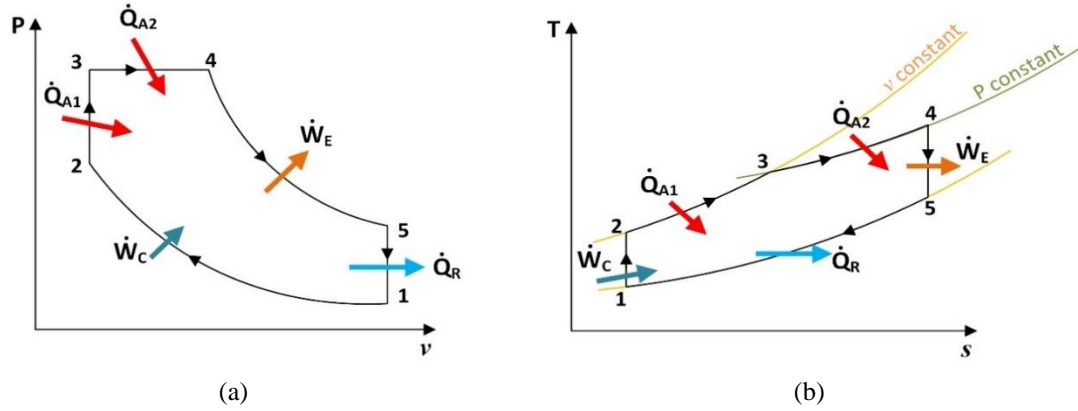


Figure 4.2 The diagrams of dual fuel cycle without a turbocharger: (a) P-v diagram and (b) T-s diagram

The cycle model is developed according to the specification of the locomotive engine geometry and operating conditions like the compression ratio (r), cylinder volumes (V_i), rated traction power, and maximum cylinder pressure ($P_{\max} = P_3$). The mass flow rate of air, \dot{m}_a [141] drawn into the intake manifold is determined based on the engine geometry and rated operating conditions as:

$$\dot{m}_a = \eta_v \left(\frac{P_{in} V_d N_{ICE} n}{R_a T_{in}} \right) \quad (4.1)$$

where P_{in} and T_{in} are the pressure and temperature of the intake air to the ICE engine after the turbocharger, V_d is the total volume displacement of the ICE for all cylinders, R_a is the gas constant of air which is equivalent to 0.287 kJ/kg.K, N_{ICE} is the revolution of the engine speed [rpm] converted to [rev/s], n is the number of cylinders in the engine, and η_v is the volumetric efficiency, which is assumed to be 0.95. The equations describing the cycle processes are outlined in Table 4.1 for the ideal case with a constant specific heat ratio, $\gamma = 1.4$.

Table 4.1 The thermodynamic equations for the dual cycle processes

Process	Description	P/T Relationship	Heat Equations	Work Equations
1 – 2	Isentropic compression	$P_2 = P_1 r^\gamma$ $T_2 = T_1 r^{(\gamma-1)}$	$\dot{Q}_{1-2} = 0$	$\dot{W}_{1-2} = \dot{m}_a \frac{P_1 v_1 - P_2 v_2}{(\gamma - 1)}$
2 – 3	Heat addition at constant volume	$\frac{T_3}{T_2} = \frac{P_3}{P_2}$	\dot{Q}_{2-3} $= \dot{m}_{ex} c_v (T_3 - T_2)$	$\dot{W}_{2-3} = 0$
3 – 4	Heat addition at constant pressure	$\frac{T_4}{T_3} = \frac{v_4}{v_3}$	\dot{Q}_{3-4} $= \dot{m}_{ex} c_p (T_4 - T_3)$	$\dot{W}_{3-4} = \dot{m}_{ex} P_3 (v_3 - v_4)$
4 – 5	Isentropic expansion	$P_5 = P_4 \left(\frac{1}{r}\right)^\gamma$ $T_5 = T_4 \left(\frac{1}{r}\right)^{(\gamma-1)}$	$\dot{Q}_{4-5} = 0$	\dot{W}_{4-5} $= \dot{m}_{ex} \frac{P_4 v_4 - P_5 v_5}{(\gamma - 1)}$
5 – 1	Heat rejection at constant volume	$\frac{T_5}{T_1} = \frac{P_5}{P_1}$	\dot{Q}_{5-1} $= \dot{m}_{ex} c_v (T_5 - T_1)$	$\dot{W}_{5-1} = 0$

The heat addition, \dot{Q}_A , to the engine and the heat rejection, \dot{Q}_R , from the engine can be determined as follows:

$$\dot{Q}_A = \dot{Q}_{2-3} + \dot{Q}_{3-4} \quad \text{and} \quad \dot{Q}_R = \dot{Q}_{5-1} \quad (4.2)$$

The output power of the engine, including the turbocharger turbine and compressor, can be calculated as follows:

$$\dot{W}_{ICE} = \dot{W}_{1-2} + \dot{W}_{3-4} + \dot{W}_{4-5} + \dot{W}_{tur} - \dot{W}_{comp} \quad (4.3)$$

The energetic efficiency, η_{ICE} , and the exergetic efficiency, ψ_{ICE} of the internal combustion engine can be estimated as follows:

$$\eta_{ICE} = \frac{\dot{W}_{ICE}}{\dot{Q}_{ICE}} \quad \text{and} \quad \psi_{ICE} = \frac{\dot{W}_{ICE}}{\left(1 - \frac{T_o}{T_s}\right) \dot{Q}_{ICE}} \quad (4.4)$$

The indicated specific fuel consumption can be defined as:

$$\omega_f = \frac{\dot{m}_f \times 3600}{\dot{W}_{ICE}} \quad (4.5)$$

The chosen formula for ULSD is $C_{12}H_{24}$. The stoichiometric air-fuel (AF) ratio can be given according to the mass basis (AF_m) to be 14.77 kg_a/kg_f and molar basis (AF_M) to be 18 kmol_a/kmol_f.

4.1.2 Modelling of gas turbine engine

The hybrid rail engine is powered by a gas turbine (GT) that contains two compressors (C1 and C2), an intercooler (IC), a combustion chamber (CC), two turbines (T1 and T2), and an afterburner (BR). The GT net power is calculated as the following:

$$\dot{W}_{GT} = \dot{W}_{T1} + \dot{W}_{T2} - \dot{W}_{C1} - \dot{W}_{C2} \quad (4.6)$$

The heat addition of the combustion chamber CC and afterburner BR is written as below:

$$\dot{Q}_{CC} = \dot{m}_{A7}h_{A7} - \dot{m}_{F1}h_{F1} - \dot{m}_{A5}h_{A5} = \eta_{CC}\dot{m}_{F1}LHV_{F1} \quad (4.7)$$

$$\dot{Q}_{BR} = \dot{m}_{A10}h_{A10} - \dot{m}_{A9}h_{A9} - \dot{m}_{D4}h_{D4} \quad (4.8)$$

The heat rejection of intercooler (IC) is given below:

$$\dot{Q}_{IC} = \dot{m}_{A2}h_{A2} - \dot{m}_{A3}h_{A3} \quad (4.9)$$

The gas turbine performance is estimated by energetic efficiency (η_{GT}) and exergetic efficiency (ψ_{GT}), which are written as the following:

$$\eta_{GT} = \frac{\dot{W}_{GT}}{\dot{Q}_{CC} + \dot{Q}_{BR} - \dot{Q}_{IC}} \quad \text{and} \quad \psi_{GT} = \frac{\dot{W}_{GT}}{\dot{E}x_{CC}^Q + \dot{E}x_{BR}^Q - \dot{E}x_{IC}^Q} \quad (4.10)$$

4.1.3 Modelling of a turbofan engine

The ambient condition varies according to the altitude (Z), and both decrease with increasing the altitude. The ambient temperature T_a and ambient pressure P_a are described below [142]:

$$T_a = 288.15 + L_a Z \quad (4.11)$$

$$P_a = 101.325 \left(\frac{288.15}{T_a} \right)^{\frac{g}{R_a L_a}} \quad (4.12)$$

Where L_a is the base temperature lapse rate per kilometre of geopotential altitude and equals to -6.5 K/km, g is the gravitational acceleration, R_a is the gas constant of air in J/kg.K. The flight speed is defined as $U_a = M\sqrt{\gamma R_a T_a}$, where M is a Mach number, γ is the specific heat ratio of air (1.4). The inlet air temperature to the diffuser is described as [142]:

$$T_{02} = T_a \left(1 + \frac{\gamma-1}{2} M^2 \right) \quad (4.13)$$

$$P_{02} = P_a \left(1 + \frac{\gamma - 1}{2} M^2 \right)^{\frac{\gamma}{\gamma - 1}} \quad (4.14)$$

The T-s diagram is graphed in Figure 4.3 for the base-turbofan. The energy balance and exergy balance equations for the components in the turbofan engine are shown in Table 4.2. The isentropic efficiencies are 90% for turbines and compressors and 87% for hot and fan nozzles. The percentage of total pressure drops in the combustion chamber relative to HPC is 2% [4], and the percentage of pressure losses in the jet pipe relative to LPT is 20% [4].

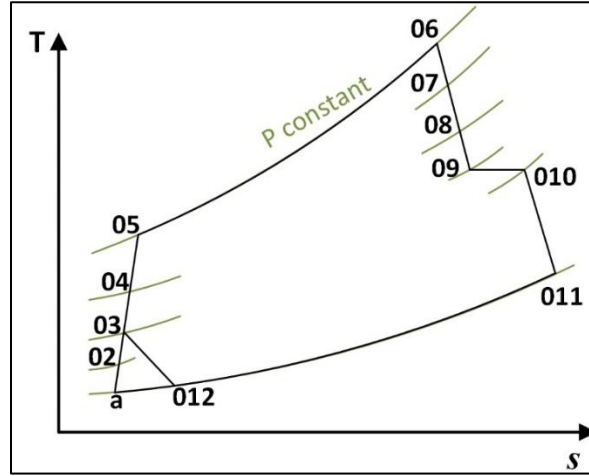


Figure 4.3 The T-s diagram for base-turbofan engine.

Table 4.2 Energy and exergy balance equations for basic components in turbofan engines.

Components	Energy balance	Exergy balance
Inlet Diffuser	$\dot{m}_{i,d} \left(h_{i,d} + \frac{U_a^2}{2} \right) = \dot{m}_{e,d} \left(h_{e,d} + \frac{U_{02}^2}{2} \right)$	$\dot{m}_{i,d} ex_{i,d} + \dot{m}_{i,d} \frac{U_a^2}{2} = \dot{m}_{e,d} ex_{e,d} + \dot{m}_{e,d} \frac{U_{02}^2}{2} + \dot{E}x_{D,d}$
Compressors	$\dot{W}_c = \dot{m}_c (h_{e,c} - h_{i,c}) / \eta_c$	$\dot{m}_{i,c} ex_{i,c} + \dot{W}_c = \dot{m}_{e,c} ex_{e,c} + \dot{E}x_{D,c}$
Turbines	$\dot{W}_t = \eta_t \dot{m}_t (h_{i,t} - h_{e,t})$	$\dot{m}_{i,t} ex_{i,t} = \dot{W}_t + \dot{m}_{e,t} ex_{e,t} + \dot{E}x_{D,t}$
Exit Nozzle	$\dot{m}_{i,n} \left(h_{i,n} + \frac{U_s^2}{2} \right) = \dot{m}_{e,n} \left(h_{e,n} + \frac{U_n^2}{2} \right)$	$\dot{m}_{i,n} ex_{i,n} + \dot{m}_{i,n} \frac{U_s^2}{2} = \dot{m}_{e,n} ex_{e,n} + \dot{m}_{e,n} \frac{U_n^2}{2} + \dot{E}x_{D,n}$
Reactors	$\sum_R \dot{m}_{in,R} h_{in,R} + \dot{Q}_{i,r} = \sum_P \dot{m}_{e,P} h_{e,P}$	$\sum_R \dot{m}_{i,R} ex_{i,R} + (T_o/T_s - 1) \dot{Q}_{i,r} = \sum_P \dot{m}_{e,P} ex_{e,P} + \dot{E}x_{D,r}$

The hot nozzle and fan nozzle should be checked for choking pressure, P_c , which is estimated as the following equation [142]:

$$\frac{P_i}{P_c} = \frac{1}{\left[1 - \left(\frac{1}{\eta} \right) \left(\frac{\gamma - 1}{\gamma + 1} \right) \right]^{\frac{\gamma}{\gamma - 1}}} \quad (4.15)$$

If the ratio of nozzle inlet pressure P_i to the ambient pressure P_a is greater than P_i/P_c , then the nozzle is choking. Therefore, the nozzle exit pressure, temperature, and speed are calculated as the following equations:

$$P_e = \frac{P_i}{P_i/P_c} \quad (4.16)$$

$$T_e = T_i \frac{2}{\gamma + 1} \quad (4.17)$$

$$U_e = \sqrt{\gamma R_a T_e} \quad (4.18)$$

The net power of the gas turbine is determined to be as the following:

$$\dot{W}_{GT} = \sum \dot{W}_T - \sum \dot{W}_C \quad (4.19)$$

The total thrust force is the summation of the inlet thrust force minus the summation of exit thrust force minus the summation of all pressure drops that occurred in by nozzles and diffusers. The thrust force of the turbofan is defined below:

$$\Gamma = \sum_k \dot{m}_{e,k} U_{e,k} - \sum_k \dot{m}_{i,k} U_{i,k} - \sum_k A_{e,k} (P_{e,k} - P_a) \quad (4.20)$$

The thrust specific fuel consumption (TSFC) is determined as the following:

$$\text{TSFC} = \frac{\dot{m}_f}{\Gamma} \quad (4.21)$$

The energetic and exergetic efficiencies of turbofan are described as the following:

$$\eta_{GT} = \frac{\dot{W}_{GT} + \Gamma U_a}{\dot{Q}_{cc}} \quad (4.22)$$

$$\psi_{GT} = \frac{\dot{W}_{GT} + \Gamma U_a}{\dot{Ex}_{cc}^Q} \quad (4.23)$$

4.1.4 Steam Rankine Cycle Modelling

The regenerative steam Rankine cycle contains three turbines (HP-ST1, IP-ST2, and LP-ST3), a condenser (CN), two pumps (P1 and P2), three closed feedwater heaters (CFH1 to CFH3) accompanied by their expansion valves (EX1, EX2, and EX3), and a heat exchanger boiler (HXBL), a reheater (HXRH), and a desalination unit (DSWR). The condenser (CN) is a shell and tube heat exchanger using seawater for cooling media that is pumped from

the sea and rejected back to the sea. The specifications of SCR are listed in Table 4.3. The resultant power of this system is evaluated as the following:

$$\dot{W}_{SRC} = \dot{W}_{HPST1} + \dot{W}_{IPST2} + \dot{W}_{LPST3} - (\dot{W}_{P1} + \dot{W}_{P2}) \quad (4.24)$$

The power of the low-pressure turbine is a function of the bleeding mass fraction to the closed feedwater heaters, which are the equal amount and can be given as y . Therefore, the LP-ST3 is written as:

$$\begin{aligned} \dot{W}_{LPST3} = & \dot{m}_{ST}(1 - y)(h_{A11} - h_{A12}) + \dot{m}_{ST}(1 - 2y)(h_{A12} - h_{A13}) \\ & + \dot{m}_{ST}(1 - 3y)(h_{A13} - h_{A10}) \end{aligned} \quad (4.25)$$

The feedwater heaters have an energy balance as indicated below:

$$\text{CFH1} \quad y\dot{m}_{ST}(h_{A11} - h_{A14}) = \dot{m}_{ST}(h_{A5} - h_{A4}) \quad (4.26)$$

$$\text{CFH2} \quad y\dot{m}_{ST}h_{A12} + y\dot{m}_{ST}h_{A15} - 2y\dot{m}_{ST}h_{A16} = \dot{m}_{ST}(h_{A4} - h_{A3}) \quad (4.27)$$

$$\text{CFH3} \quad y\dot{m}_{ST}h_{A13} + y\dot{m}_{ST}h_{A17} - 3y\dot{m}_{ST}h_{A18} = \dot{m}_{ST}(h_{A3} - h_{A2}) \quad (4.28)$$

The required heat of the exchanger boiler (HXBL) and reheater (HXRH) is calculated as the following:

$$\dot{Q}_{HXBL} = \dot{m}_{ST}(h_{A7} - h_{A6}) \quad (4.29)$$

$$\dot{Q}_{HXRH} = \dot{m}_{ST}(h_{A9} - h_{A8}) \quad (4.30)$$

Another heat exchanger is added to the exhaust gases at the chimney to use the waste energy in the desalination unit of (DSWR) to desalinate the seawater and produce freshwater for the ship, which will be explained in a separate section. The useful heat of DSWR is a function of the exhaust gas flow rate, \dot{m}_{B4} , and the difference in specific enthalpy between the inlet and exit flow of h_{B4} and h_{B5} , respectively, which is written as the following:

$$\dot{Q}_{DSWR} = \dot{m}_{B4}(h_{B4} - h_{B5}) \quad (4.31)$$

The boiler is heated by burning a fuel blend with air mixed with the exhaust of gas Brayton cycle of G12 stream. The input heat of fuel combustion in the burner (BRBL) is estimated as the following:

$$\dot{Q}_{BRBL} = \dot{m}_{B2}h_{B2} - (\dot{m}_{F1}h_{F1} + \dot{m}_{B1}h_{B1} + \dot{m}_{G12}h_{G12}) \quad (4.32)$$

The required power of the two pumps of P1 and P2 are calculated below:

$$\dot{W}_{P1} = \eta_{P1}\dot{m}_{ST}v_{A1}(P_{A2} - P_{A1}) \quad (4.33)$$

$$\dot{W}_{P2} = \eta_{P2}\dot{m}_{ST}v_{A5}(P_{A6} - P_{A5}) \quad (4.34)$$

The performance of SRC is evaluated using energetic efficiency, η_{SRC} , and exergetic efficiency, ψ_{SRC} , as below:

$$\eta_{SRC} = \frac{\dot{W}_{SRC} + \dot{Q}_{DSWR}}{\dot{Q}_{BRBL}} \quad \text{and} \quad \psi_{SRC} = \frac{\dot{W}_{SRC} + \dot{E}x_{DSWR}^Q}{\dot{E}x_{BRBL}^Q} \quad (4.35)$$

Table 4.3 The specifications of SRC

Parameter	Value
Steam mass flow rate	6 kg/s
Maximum temperature before first turbine	536.9 °C
Reheater temperature	526.9 °C
Maximum pressure	7100 kPa
Turbine exit pressures	1700 kPa, 1000 kPa, 5 kPa
Turbine and pump thermal efficiency	85%
Turbine and pump mechanical efficiency	90%
Minimum pressure	5 kPa
First pump pressure ratio	5
Second pump pressure ratio	14.2
Steam bleeding ratio for all CFH	0.1
Steam bleeding pressures	1000 kPa, 600 kPa, and 300 kPa
Condenser cooling media	Seawater enters at 15°C and 500 kPa and leaves at 21 °C and 500 kPa

4.1.5 Modelling of a binary system

The binary system consists of the topper and bottomer organic Rankine cycles (TORC and BORC). The TORC uses R600 and R601 refrigerants, and the BORC uses R290 and 1270 refrigerants, in addition to the liquified natural gas (LNG) for extreme cooling processes. The reason for the selection is that these refrigerants have less global warming effects, less particulate pollution, and a suitable boiling point, critical pressure, and temperature to be combined with the proposed hybridized GBC. The properties of the mentioned refrigerants are listed in Table 4.4.

Table 4.4 Refrigerants used in the binary system of TORC/BORC [143,144]

R#	Name	Formula	Net	RCL/IDLH		Boiling point [°C]	Critical temperature [°C]	Critical pressure (abs.) [kPa]
			GWP 100-yr	ppm	g/m ³			
R-600	Butane	C ₄ H ₁₀	4.0 - 6.5	4,000	9.6	0 ± 1	152.01	3,796
R-601	Pentane	C ₅ H ₁₂	4 ± 2	1,000	2.9	36.1 ± 0.2	196.56	3,358
R-290	Propane	C ₃ H ₈	3.3 - 4.5	5,300	9.5	-42.1 ± 0.2	96.70	4,248
R-1270	Propene	C ₃ H ₆	1.8	1,000	1.7	-47.6	92.42	4,665

The refrigerant concentration limits (RCL) are used to determine the maximum concentration of a refrigerant-occupied space. It must be the lowest of three calculated limits: toxicity, oxygen deprivation, and flammability. The immediately dangerous to life or health (IDLH) is established by the national institute of occupational safety and health (NIOSH) to constrain the acute toxicity exposure limit (ATEL). The workplace should consider the safety precautions and exposure limits in order to use the selected refrigerants safely [144].

The TORC consists of a pump (P1), a condenser (CN1), a turbine (T3), and two evaporators (EV11 and EV12). The BORC comprises a pump (P2), three condensers (EV11, EV12, and CN2), two turbines (T4 and T5) and an evaporator (EV2). The LNG is used to cool the EV12 and EV2 to the saturated liquid of two refrigerant mixtures in the two cycles, and then it will be stored in high-temperature tanks for other uses.

The TORC delivers the net power of \dot{W}_{TORC} , by requiring heat of $\dot{Q}_{A,TORC}$, and rejecting the heat of $\dot{Q}_{R,TORC}$, as the following:

$$\dot{W}_{TORC} = \dot{W}_{T3} - \dot{W}_{P1} \quad (4.36)$$

$$\dot{Q}_{A,TORC} = \dot{Q}_{CN1} = \dot{m}_{TR}(h_{TR3} - h_{TR2}) \quad (4.37)$$

$$\dot{Q}_{R,TORC} = \dot{m}_{TR}(h_{TR4} - h_{TR5}) + \dot{m}_{TR}(h_{TR5} - h_{TR1}) \quad (4.38)$$

where \dot{m}_{TR} is the mass flow rate of the topper Rankine cycle. The energy efficiency and exergetic efficiency are given below:

$$\eta_{TORC} = \frac{\dot{W}_{TORC}}{\dot{Q}_{A,TORC}} \quad (4.39)$$

$$\psi_{TORC} = \frac{\dot{W}_{TORC}}{\dot{Ex}_{A,TORC}^Q} \quad (4.40)$$

Similarly, the BORC can deliver a net power of \dot{W}_{BORC} by adding a heat of $\dot{Q}_{A,BORC}$ from the EV11, EV12, and CN2, which is $\dot{Q}_{CN2} = \dot{m}_{BR}(h_{BR4} - h_{BR3})$ and rejecting heat of $\dot{Q}_{R,BORC}$ by EV2, as shown below:

$$\dot{W}_{BORC} = \dot{W}_{T4} + \dot{W}_{T5} - \dot{W}_{P2} \quad (4.41)$$

$$\dot{Q}_{A,BORC} = \dot{m}_{BR}(h_{BR3} - h_{BR2}) + \dot{m}_{BR}(h_{BR4} - h_{BR3}) + \dot{m}_{BR}(h_{BR6} - h_{BR5}) \quad (4.42)$$

$$\dot{Q}_{R,BORC} = \dot{m}_{TR}(h_{BR7} - h_{BR1}) \quad (4.43)$$

where \dot{m}_{BR} is the mass flow rate of the bottomer Rankine cycle. The BORC energetic and exergetic efficiencies are written below:

$$\eta_{BORC} = \frac{\dot{W}_{BORC}}{\dot{Q}_{A,BORC}} \quad (4.44)$$

$$\psi_{BORC} = \frac{\dot{W}_{BORC}}{\dot{E}x_{B,TORC}^Q} \quad (4.45)$$

The liquified natural gas is assumed to be pure methane and stored at -200°C and 5000 kPa and left the BORC at -83°C and 5000 kPa at the liquid phase. The cooling load of LNG is as the following:

$$\dot{Q}_{LNG} = \dot{m}_{LNG} c_{pLNG} (T_{LNG3} - T_{LNG1}) \quad (4.46)$$

The energy efficiency and exergetic efficiency of LNG can be estimated as the output flow divided by the input flow as expressed below:

$$\eta_{LNG} = \frac{\dot{m}_{LNG} c_{pLNG} T_{LNG3}}{\dot{m}_{LNG} c_{pLNG} T_{LNG1}} \quad (4.47)$$

$$\psi_{LNG} = \frac{\dot{m}_{LNG} ex_{LNG3}}{\dot{m}_{LNG} ex_{LNG1}} \quad (4.48)$$

Also, the utilization of waste energy, \dot{Q}_{WE} , can be evaluated as the following:

$$\dot{Q}_{WE} = \dot{Q}_{GTHX} + \dot{Q}_{CN1} + \dot{Q}_{CN2} \quad (4.49)$$

4.2 Modelling of Fuel Cells

This subsection contains the modelling of four fuel cells, such as a molten carbonate fuel cell, solid oxide fuel cell, proton exchange membrane fuel cell, and aluminum electrolysis cell. The modelling contains the cell voltage, three types of loss voltage like activation, concentration and ohmic losses, and the fuel cell power in detail.

4.2.1 Modelling of molten carbonate fuel cell

The MCFC employs molten salt electrolytes, which are made of eutectic mixtures of Li_2CO_3 , Na_2CO_3 , and K_2CO_3 [145]. The Li_2CO_3 (62 mol%) and K_2CO_3 (38 mol%) eutectic have been widely adopted [146]. These carbonates melt at approximately 500°C to allow transferring ions by the molten carbonates. The operating temperature should be at 923K (650°C) to avoid the volatilization or solidification of the electrolyte. Therefore, the

electrothermal reactions of the MCFC create electricity. The steam reforming (SR) and water gas shift (WGS) reactions occur sequentially to produce H_2 and CO in the MCFC stack [47]. The chemical reactions for SR, WGS, anode, and cathode are written as the followings:

- Anode: $H_2 + CO_3^{2-} \leftrightarrow CO_2 + H_2O + 2e^-$
 $CO + CO_3^{2-} \leftrightarrow 2CO_2 + 2e^-$
- Cathode: $0.5 O_2 + CO_2 + 2e^- \leftrightarrow CO_3^{2-}$
- Overall: $H_2 + 0.5 O_2 + CO_2 \leftrightarrow H_2O + CO_2$ ($\Delta \bar{h}_{298K}^0 = -242 \text{ kJ/mol}$)

Note that the reforming reaction is a highly intensive endothermic process, while others are exothermic processes. Other reactions may occur at the anode, such as CO hydrogenation, methanation, and Boudouard reaction, and others may occur at the cathode, such as polycarbonate, peroxide, and superoxide [146]. After the electrochemical reactions, some byproducts, such as water and CO_2 , whereas the excess air can be emitted from the cathode, as shown in Figure 4.4. Here, CO_2 is consumed to form molten carbonates. Any unreacted fuels flow to the catalytic burner to be combusted with air, and its exhaust of carbon and oxygen gas flows to the cathode.

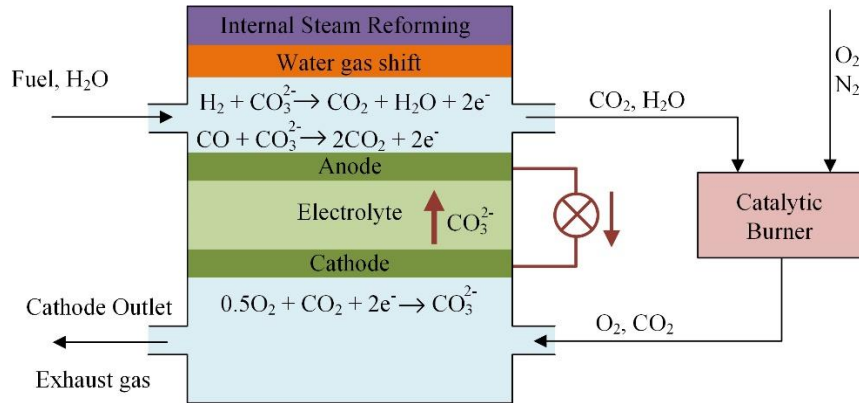


Figure 4.4 The MCFC diagram with steam reforming and water gas shift

The electrochemical phenomenon of a unit fuel cell follows the governing equations. The cell voltage is estimated by the reversible potential taking into account the other losses: the Nernst loss, activation polarization, and concentration loss [132]. The cell voltage V_{cell} of the MCFC [V] can be expressed by:

$$V_{cell} = V^0 - V_{Nernst} - j(R_{an} + R_{ca} + R_{ohm}) \quad (4.50)$$

where V^0 is the reversible potential at standard conditions [V] and V_{Nernst} is the Nernst loss [V]. The maximum Nernst potential can be fulfilled when the summation of V^0 and

V_{Nernst} are considered through the electrochemical reaction. Also, the Nernst potential becomes the open-circuit voltage (OCV) when the current is zero. The j refers to the current density [mA/cm^2]. R_{an} and R_{ca} represent the activation losses of the anode and cathode [$\Omega - \text{cm}^2$], respectively, to break the chemical bonds of H_2 and O_2 molecules in the electrochemical reaction, and R_{ohm} is the ohmic loss. The standard reversible potential is defined using the Gibbs free energy:

$$V^0 = -\frac{\Delta\bar{g}}{nF} \quad (4.51)$$

Where V^0 is the Gibbs free energy [J/mol]; F is the Faraday constant, which is $96,485 \text{ C}/\text{mol}$; and n is the molecular number of H_2 ; and $\Delta\bar{g}$ is function of the MCFC stack temperature [K].

$$\Delta\bar{g} = 0.002474 T^2 + 48.996T - 243730 \quad (4.52)$$

The Nernst loss is a function of the concentrations of the substituents of the reactants and products:

$$V_{Nernst} = \frac{\bar{R}T}{nF} \ln \left(\frac{P_{H_2,an} P_{CO_2,an}}{P_{H_2,an} \sqrt{P_{O_2,ca}} P_{CO_2,ca}} \right) \quad (4.53)$$

where \bar{R} is the molar gas constant, which is $8.314 \text{ J}/\text{mol.K}$, and P is the partial pressure at each electrode. The activation polarization losses that occurred in the anode and cathode are denoted as R_{an} and R_{ca} , which are modeled by Koh et al. [147].

$$R_{an} = 2.27 \times 10^{-5} \times \exp \left(\frac{\Delta\bar{h}_{an}}{\bar{R}T} \right) \times P_{H_2}^{-0.42} P_{CO_2}^{-0.17} P_{H_2O}^{-1.0} \quad (4.54)$$

$$R_{ca} = 7.505 \times 10^{-6} \times \exp \left(\frac{\Delta\bar{h}_{ca}}{\bar{R}T} \right) \times P_{O_2}^{-0.43} P_{CO_2}^{-0.09} \quad (4.55)$$

where $\Delta\bar{h}_{an}$ and $\Delta\bar{h}_{ca}$ are the activation energy values in the anode and cathode, respectively. The ohmic loss [$\Omega - \text{cm}^2$] is the internal resistance due to the ionic and electronic conduction at the electrodes and the contacts. It can be calculated by the Arrhenius-type equation:

$$R_{ohm} = 0.5 \times \exp \left[3016 \left(\frac{1}{T} - \frac{1}{923} \right) \right] \quad (4.56)$$

The net power output of an MCFC [W] is estimated as follows:

$$\dot{W}_{MCFC,AC} = j A_{cell} V_{cell} N \xi_{DC-AC} \quad (4.57)$$

where A_{cell} is the active area [cm²], N is the number of cells, ξ_{DC-AC} is the inverter efficiency to invert the direct current (DC) to alternating current (AC) and is equivalent to 0.95. The specifications of the MCFC are listed in Table 4.5.

The electric efficiency, thermal efficiency, and exergetic efficiency of MCFC can be evaluated below. The added heat of the MCFC, $\dot{Q}_{MCFC,add}$, is considered as the summation of the added heat through the anode, cathode, and catalytic burner.

$$\eta_{MCFC,e} = \frac{\dot{W}_{MCFC,AC}}{\dot{W}_{MCFC,AC} + \dot{W}_{MCFC,loss}} \quad (4.58)$$

$$\eta_{MCFC,th} = \frac{\dot{W}_{MCFC,AC}}{\dot{Q}_{MCFC,add}} \quad (4.59)$$

$$\psi_{MCFC,th} = \frac{\dot{W}_{MCFC,AC}}{\dot{E}x_{MCFC,add}^Q} \quad (4.60)$$

Table 4.5 The specifications of MCFC

Parameter	Value	Units
Operating temperature	923	K
Operating pressure	200	kPa
Current density, j	150	mA/cm ²
Anode activation energy, $\Delta\bar{h}_{an}$	53,500	J/mol
Cathode activation energy, $\Delta\bar{h}_{ca}$	77,300	J/mol
A_{cell}	6700	cm ²
N_{cell}	400 cells	---
N_{stack}	3 stacks	---

4.2.2 Modelling of solid oxide fuel cell

The fuel mixture is mixed with steam and flows to the SOFC anode. The air flows to SOFC cathode. The oxygen molecules diffuse to the triple phase boundary to receive the electrons and produce oxygen ions O^{2-} , which are moved to the anode to produce an electric current. The oxygen is released from the cathode to exit the fuel cell. The oxygen ions react with the hydrogen to produce water on the anode side, as shown in Figure 4.5. The specifications of SOFC are listed in Table 4.6. The electrochemical reactions of the SOFC are listed below:

- Anode: $H_2 + O^{2-} \rightarrow H_2O + 2e^-$
- Cathode: $0.5 O_2 + 2e^- \leftrightarrow O^{2-}$
- Overall: $H_2 + 0.5 O_2 \leftrightarrow H_2O$

The cell voltage of SOFC is expressed as the Nernst potential subtracting the activation losses (η_{act}), the concentration losses (η_{con}), and ohmic losses (η_{ohm}), as shown in Eq. (4.61) [146].

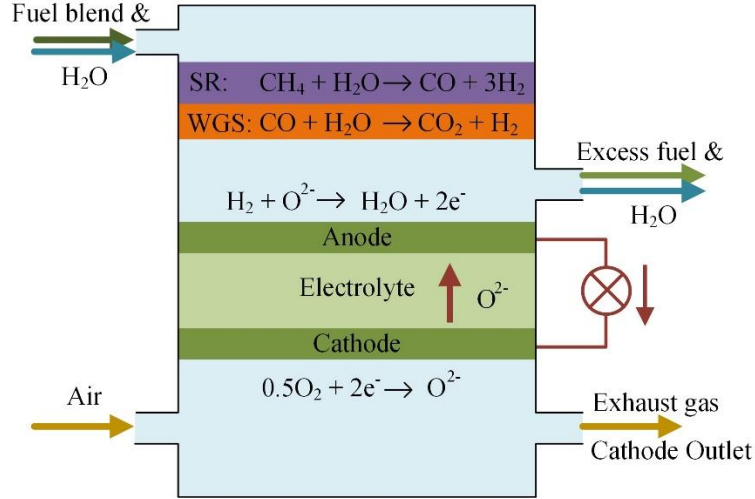


Figure 4.5 The SOFC diagram with steam reforming and water gas shift

$$V_{SOFC,cell} = -\frac{\Delta\bar{g}}{2F} - \frac{\bar{R}T}{2F} \ln \left(\frac{P_{H_2O,an}}{P_{H_2,an}\sqrt{P_{O_2,ca}}} \right) - \eta_{act} - \eta_{con} - \eta_{ohm} \quad (4.61)$$

The activation polarization is produced to overcome the reaction energy barriers between the electrode and electrolyte, which are solved using the Butler-Volmer Equation [146,148]. The activation losses occurred on the anode ($\eta_{act,an}$) and cathode ($\eta_{act,ca}$) as shown below, where α_{an} and α_{ca} are the charge transfer coefficients of anode and cathode, respectively.

$$\eta_{act} = \eta_{act,an} + \eta_{act,ca} = \frac{\bar{R}T}{2\alpha_{an}F} \sinh^{-1} \left(\frac{j}{2j_{0,an}} \right) + \frac{\bar{R}T}{2\alpha_{ca}F} \sinh^{-1} \left(\frac{j}{2j_{0,ca}} \right) \quad (4.62)$$

Here, $j_{0,an}$ and $j_{0,ca}$ are the electrode exchange current densities for the anode and cathode, respectively. They are expressed using Arrhenius' law function of the partial pressure of the reacting species [149]. The γ_{an} and γ_{ca} are the pre-exponential factors, and $E_{act,an}$ and $E_{act,ca}$ are the activation energy for the electrode reactions, and P_{ref} is the reference atmospheric pressure [149].

$$j_{0,an} = \gamma_{an} \left(\frac{P_{H_2}}{P_{ref}} \right) \left(\frac{P_{H_2O}}{P_{ref}} \right) \exp \left(-\frac{E_{act,an}}{\bar{R}T} \right) \quad (4.63)$$

and

$$j_{0,ca} = \gamma_{ca} \left(\frac{P_{O_2}}{P_{ref}} \right)^{0.25} \exp \left(-\frac{E_{act,ca}}{\bar{R}T} \right) \quad (4.64)$$

The ohmic loss is calculated as Eq. (4.65) considering four resistances to the flow of ions and electrons inside the anode ($\rho_{an}\delta_{an}$), cathode ($\rho_{ca}\delta_{ca}$), electrolyte ($\rho_{el}\delta_{el}$), and interconnections ($\rho_{in}\delta_{in}$). They are a function of specific material resistivity ρ and the component thickness δ for planar SOFC [149].

$$\eta_{ohm} = j(\rho_{an}\delta_{an} + \rho_{ca}\delta_{ca} + \rho_{el}\delta_{el} + \rho_{in}\delta_{in})/A_{cell} \quad (4.65)$$

The concentration losses are the voltage drop caused by the mass transfer of the gas phase into and through the electrode [149]. They are given by the following equations for the anode and cathode:

$$\eta_{con,an} = -\frac{\bar{R}T}{2F} \ln \left(1 - \frac{j}{j_{L,an}} \right) + \frac{\bar{R}T}{2F} \ln \left(1 + \frac{P_{H_2}j}{P_{H_2O}j_{L,an}} \right) \quad (4.66)$$

$$\eta_{con,ca} = -\frac{\bar{R}T}{2F} \ln \left(1 - \frac{j}{j_{L,ca}} \right) \quad (4.67)$$

The limiting current densities are defined for the anode and cathode as follows:

$$j_{L,an} = \frac{2FP_{H_2}D_{an(eff)}}{\bar{R}T} \quad (4.68)$$

$$j_{L,ca} = \frac{2FP_{O_2}D_{ca(eff)}}{\bar{R}T} \quad (4.69)$$

where the $D_{an,eff}$ and $D_{ca,eff}$ are the effective diffusivities of reactant species through the porous anode and cathode, respectively. The ordinary diffusion coefficient of each gas is evaluated and converted into an effective value by considering the porosity and the tortuosity of the electrode pores.

$$D_{O,ik} = \frac{1 \times 10^{-7} T^{1.25} (M_i^{-1} + M_k^{-1})^{0.5}}{P(v_i^{1/3} + v_k^{1/3})} \quad (4.70)$$

$$D_{O,i(eff)} = D_{O,i} \left(\frac{\varepsilon}{\xi} \right) \quad (4.71)$$

Where ν is the Fuller diffusion volume of each gas [150]. ε and ξ are the porosity and tortuosity of anode or cathode. The i and k refers to the mixture H_2 and H_2O used for anode and O_2 and N_2 mixture for the cathode. The Knudsen diffusion coefficients were calculated and converted into the effective values as the following equations.

$$D_{K,i} = 97r \sqrt{\frac{T}{M_i}} \quad (4.72)$$

$$D_{K,i(\text{eff})} = D_{K,i} \left(\frac{\varepsilon}{\xi} \right) \quad (4.73)$$

Table 4.6 The specifications of SOFC [151]

Parameter		Value
Operating pressure [kPa]		200
Operating temperature [K]		1123
Current density, j [mA/cm ²]		500
Active cell area, A_{cell} [cm ²]		900 cm ²
N_{cell} in one stack		100 cells
Anode thickness, δ_{an} [m]		5.0E-04
Cathode thickness, δ_{ca} [m]		5.0E-05
Electrolyte thickness, δ_{el} [m]		1.0E-05
Interconnect thickness, δ_{in} [m]		1.0E-05
Pre-exponential coefficient for anode, γ_{an} [A/m ²]		7.0 x 10 ⁹
Pre-exponential coefficient for cathode, γ_{ca} [A/m ²]		2.9 x 10 ⁹
Anode activation energy, $E_{act,an}$ [J/mol]		120,000
Cathode activation energy, $E_{act,ca}$ [J/mol]		120,000
Pore diameter for anode and cathode, r [m]		5.0E-07
Porosity of anode, ε_{ca} [%]		0.5
Porosity of cathode, ε_{ca} [%]		0.5
Tortuosity for anode and cathode, ξ		6
Fuller diffusion volume, ν	H ₂	7.07
	H ₂ O	12.7
	O ₂	16.6
	N ₂	17.9

The overall diffusion coefficient was calculated harmonically averaging the Knudsen effective diffusion coefficient and the ordinary effective diffusion coefficient as described below:

$$\frac{1}{D_{i(\text{eff})}} = \frac{1}{D_{K,i(\text{eff})}} + \frac{1}{D_{O,i(\text{eff})}} \quad (4.74)$$

Therefore, the effective diffusivities of the anode and cathode are described below:

$$D_{an(\text{eff})} = \left(\frac{P_{H_2O}}{P_{an}} \right) D_{H_2(\text{eff})} + \left(\frac{P_{H_2}}{P_{an}} \right) D_{H_2O(\text{eff})} \quad (4.75)$$

$$D_{ca(\text{eff})} = D_{O_2(\text{eff})} \quad (4.76)$$

The resultant power output of SOFC is presented as follows:

$$\dot{W}_{SOFC,AC} = jA_{\text{cell}}V_{\text{cell}}N_{\text{cell}}\xi_{DC-AC} \quad (4.77)$$

where A_{cell} is the total active area of a fuel cell in cm², N_{cell} is the number of cells, ξ_{DC-AC} is the inverter efficiency from direct current (DC) to alternating current (AC) and is

equivalent to 0.95. The electric efficiency of a fuel cell can be determined as Eq. (4.58), while the thermal energetic and exergetic efficiencies can be evaluated as Eq. (36b and c). The added heat of the fuel cell, \dot{Q}_{SOFC} , is considered as the summation of added heat through the anode, cathode, and catalytic burner.

$$\eta_{SOFC,e} = \frac{\dot{W}_{SOFC,AC}}{\dot{W}_{SOFC,AC} + \dot{W}_{SOFC,loss}} \quad (4.78)$$

$$\eta_{SOFC,th} = \frac{\dot{W}_{SOFC,AC}}{\dot{Q}_{SOFC}} \quad (4.79)$$

$$\psi_{SOFC,th} = \frac{\dot{W}_{SOFC,AC}}{\dot{Ex}_{SOFC}^Q} \quad (4.80)$$

4.2.3 Proton Exchange Membrane Fuel Cell (PEMFC)

The proton exchange membrane fuel cell (PEMFC) consists of a membrane electrode assembly (MEA), and each large side of a membrane has a gas diffusion layer (GDL), a bipolar plate, a current collector plate, and a compression plate. These plates formed one cell of PEM. Air and hydrogen are brought to the bipolar plates and flow into the channels of plates [152]. Then the gases are diffused by the GDL on either side of MEA, which is made of platinum. At the contact of platinum of electrodes, the dihydrogen is split into protons H^+ and electrons, which flow through the GDL, bipolar, current collectors and the circuit, while the MEA acts as a barrier to them. These electrons are combined with dioxygen at contact with the platinum of the electrode to form O^{2-} . Then the H^+ travels through the MEA and combines with O^{2-} to form water, which is transferred out of the fuel cell with the airflow, as shown in Figure 4.6. The electrochemical reactions of PEMFC are the following:

- Anode: $H_2 \rightarrow 2H^+ + 2e^-$
- Cathode: $0.5O_2 + 2H^+ + 2e^- \rightarrow H_2O$
- Overall: $H_2 + 0.5O_2 \rightarrow H_2O$

The specifications of PEMFC are listed in Table 4.7 [153]. The gross power of PEMFC (\dot{W}_{PEMFC}), which is function of cell voltage, activation losses, ohmic losses, and concentration losses of PEMFC are expressed as:

$$\dot{W}_{PEMFC} = jA_t V_c \xi \quad (4.81)$$

$$V_c = E_N - \eta_{act} - \eta_{\Omega} - \eta_{con} \quad (4.82)$$

$$E_N = -\frac{\Delta \bar{g}}{2F} - \frac{\bar{R}T_c}{2F} \ln \left(\frac{p_{H_2O}}{p_{H_2} \sqrt{p_{O_2}}} \right) \quad (4.83)$$

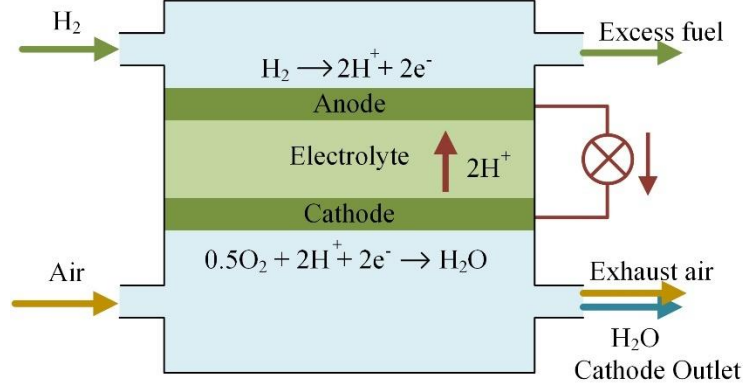


Figure 4.6 The schematic diagram of PEMFC diagram

The activation losses are considered the losses from the cathodic only since they are negligible from the anodic electrode. The activation losses are a function of the exchange current density of cathode ($j_{0,ca}$), which is a function of oxygen concentration in this electrode ($C_{O_2,ca}$) and they can be described as the following:

$$\eta_{act} = \eta_{act,an} + \eta_{act,ca} \quad (4.84)$$

$$\eta_{act,ca} = \frac{\bar{R}T_c}{2\alpha_{ca}F} \ln \left(\frac{j}{j_{0,ca}} \right) \quad (4.85)$$

$$j_{0,ca} = j_{0,ref} \times \frac{C_{O_2,ca}}{C_{O_2,ref}} \quad (4.86)$$

$$C_{O_2,ref} = \frac{P_0 x_{O_2,ref}}{\bar{R}T_0} \quad \text{and} \quad C_{O_2,ca} = \frac{P_c x_{O_2,ca}}{\bar{R}T_c} \quad (4.87)$$

The ohmic losses are considered the resistive losses in the membrane and cathode catalyst layer (CCL) due to the proton transport, and they can be described as the following:

$$\eta_{\Omega} = \left(\frac{\delta_{mem}}{\kappa_{mem}} + \frac{\delta_{CCL}}{f_{CCL}^{1.5} \kappa_{CCL}} \right) j \quad (4.88)$$

, where ionomer fraction (f_{CCL}) is assumed to be equal to 0.15. The conductivity of Nafion (κ) is a function of the water content (λ) with respect to membrane and CCL, and it can be written as below:

$$\kappa = (0.005139\lambda - 0.00326) \times \exp\left(1268\left(\frac{1}{303} - \frac{1}{T_c}\right)\right) \quad (4.89)$$

The concentration losses (η_{con}) are also negligible for the anode and count only for the cathode layer, and are given as:

$$\eta_{con,ca} = \left(1 + \frac{1}{\alpha_{ca}}\right) \frac{\bar{R}T_c}{4F} \ln\left(\frac{j_L}{j_{L,ca} - j}\right) \quad (4.90)$$

, where the limiting current density of the cathode ($j_{L,ca}$) is a function of the concentration and diffusivity of oxygen and, as shown below:

$$j_{L,ca} = j_{L,ref} \times \frac{C_{O_2,ca}}{C_{O_2,ref}} \times \frac{D_{O_2,ca}}{D_{O_2,ref}} \quad (4.91)$$

$$D_{O_2,eff} = D_{O_2,N_2}|_{(T_c,P_c)} \varepsilon^{3.6} (1 - S_{av})^3 \quad (4.92)$$

, where the reference diffusion coefficient ($D_{O_2,ref}$) and reference diffusion coefficient ($D_{O_2,ref}$) of oxygen are written below, and liquid water saturation (S_{av}) is assumed to be 0.1.

$$D_{O_2,ref} = D_{O_2,N_2}|_{(T_0,P_0)} \varepsilon^{3.6} (1 - S_{av})^3 \quad (4.93)$$

$$D_{O_2,ref} = D_{O_2,N_2}|_{(T_0,P_0)} \varepsilon^{3.6} \quad (4.94)$$

Table 4.7 The specifications of PEMFC [154]

Parameters	Symbols	Units	Value
Cell temperature	T_c	K	343
Cell pressure	P_c	kPa	200
Current density	j	A/m ²	7700
Exchange current density	j_o	A/m ²	2290
Active cell area	A_c	m ²	0.3
# of cells per stack	Nc	-	50
# of stacks	Ns	-	2
Total area	A_t	m ²	30
Anode thickness	δ_{an}	μm	125
Cathode thickness	δ_{ca}	μm	350
Electrolyte thickness	δ_{el}	μm	350
Interconnect thickness	δ_{in}	μm	30
Effective GDL thickness	δ_{GDL}	μm	500
Effective hydrogen (or water) diffusivity	D_{eff,H_2-H_2O}	m ² /s	0.0000149
Effective oxygen & water diffusivity	D_{eff,O_2-H_2O}	m ² /s	0.00000295
Water diffusivity in Nafion	D_λ	m ² /s	3.81E-10
Cathode Transfer Coefficient	α	-	0.3
Porosity of anode	ε_{na}	-	0.5
Porosity of cathode	ε_{ca}	-	0.5
Porosity of GDL	ε_{GDL}	-	0.6
Tortuosity for anode and cathode	ξ	-	6

The binary diffusion coefficient can be estimated based on [155] and written below, where $a = 2.75 \times 10^{-4}$ and $b = 1.823$.

$$D_{ij}|_{(T,P)} = \frac{a}{P} \left(\frac{T}{\sqrt{T_{cr,i}T_{cr,j}}} \right)^b \times (P_{cr,i}P_{cr,j})^{\frac{1}{3}} \times (T_{cr,i}T_{cr,j})^{\frac{5}{12}} \times \left(\frac{1}{M_i} + \frac{1}{M_j} \right)^{\frac{1}{2}} \quad (4.95)$$

The electric efficiency of PEMFC is the ratio of cell voltage and Nernst voltage, and the thermal and exergetic efficiency is the ratio of electric power of PEMFC to the low heating value of hydrogen and exergetic flow rate of H₁, respectively [156].

$$\eta_{PEMFC,e} = \frac{V_c}{E_N} \quad (4.96)$$

$$\eta_{PEMFC,th} = \frac{\dot{W}_{PEMFC}}{\dot{m}_{H_1} LHV_{H_2}} \quad \text{and} \quad \psi_{PEMFC,th} = \frac{\dot{W}_{PEMFC}}{\dot{E}x_{H_1}} \quad (4.97)$$

4.2.4 Aluminum Electrolysis Cell (AEC)

This electrolysis cell decomposes ammonia into hydrogen and nitrogen gases by electrochemical reactions [157]. Two solutions flow into the cell: potassium hydroxide solution (5M of KOH) to the cathode and ammonium solution (5M of NH₃) to the anode at room temperature. KOH is strong alkali to make the water alkaline and produces hydroxide ions. At that moment, the ammonia in the anode side reacts with hydroxide ions to produce nitrogen gas, water, and free electrons. Therefore, the electrons pass through the electrolyte solution of alkalized water to electrochemically decompose water into hydrogen gas and OH⁻. Hence, nitrogen gas releases from the anode side and hydrogen gas releases from the cathode side. The specifications of AEC are listed in Table 4.8, and the electrochemical reaction is formed as follows:

- Anode: $2\text{NH}_3 + 6\text{OH}^- \rightarrow \text{N}_2 + 6\text{H}_2\text{O} + 6\text{e}^-$
- Cathode: $6\text{H}_2\text{O} + 6\text{e}^- \rightarrow 3\text{H}_2 + 6\text{OH}^-$
- Overall: $2\text{NH}_3 \rightarrow 3\text{H}_2 + \text{N}_2$

The cell voltage is evaluated based on the experimental data done by [158] by evaluating the trendline equations of all activation, ohmic, and concentration losses to predict the cell voltage after verifying multiple experimental values of cell voltage based on electrodes of platinum carbon nanotubes (Pt-CNT) films. Therefore, the cell voltage, the Nernst voltage, activation loss, ohmic loss, and concentration loss are described below:

$$V_c = E_N - \eta_{act} - \eta_\Omega - \eta_{con} \quad (4.98)$$

$$E_N = -\frac{\Delta \bar{g}}{3F} - \frac{\bar{R}T_c}{3F} \ln \left(\frac{1}{p_{N_2}^{0.5} p_{H_2}^{1.5}} \right) \quad (4.99)$$

$$\eta_{act} = \frac{2.3\bar{R}T_c}{3\alpha F} \ln \left(\frac{j}{j_o} \right) \quad (4.100)$$

$$\eta_\Omega = A_e \times i \times R \quad (4.101)$$

$$\eta_{con} = \left(1 + \frac{1}{\beta} \right) \frac{\bar{R}T_c}{3F} \ln \left(\frac{j_L}{j_L - j} \right) \quad (4.102)$$

where j_o is the exchange current density, which is estimated as 1.16×10^{-8} mA/cm². α is the transfer coefficient, and it is calculated to be 0.85, and β is a function of the transfer coefficient and equals to $k\alpha$, where k is a constant of 0.0218. The limiting current density j_L equals to 1.35 A/cm². A_e is the electrode surface area which is equal to 1.75 cm², and R is the resistance of Pt-CNT electrode, which is measured to be 0.701 Ω [158]. The required power of AEC is defined as:

$$\dot{W}_{AEC} = j A_t V_c \xi \quad (4.103)$$

Table 4.8 The specifications of AEC [159]

Parameters	Symbols	Units	Value
Cell temperature	T_c	K	333
Cell pressure	P_c	kPa	1000
Current density	j	A/m ²	8000
Exchange current density	j_o	A/m ²	3287
Active cell area	A_c	m ²	0.3
# of cells per a stack	Nc	-	100
# of stacks	Ns	-	4
Total area	A_t	m ²	120
Porosity of anode	ε_{na}	-	0.5
Porosity of cathode	ε_{ca}	-	0.5
Tortuosity for anode and cathode	ξ	-	6

The electric efficiency of AEC is the ratio of Nernst voltage to cell voltage since it requires more voltage to operate the cell. The energetic and exergetic efficiency is the ratio of the hydrogen energy produced by the cell and exergetic flow rate of H₂ divided by the amount required power to operate this cell.

$$\eta_{AEC,e} = \frac{E_N}{V_c} \quad (4.104)$$

$$\eta_{AEC,th} = \frac{\dot{m}_{H_2} LHV_{H_2}}{\dot{W}_{AEC}} \quad \text{and} \quad \psi_{AEC,th} = \frac{\dot{E}x_{H_2}}{\dot{W}_{AEC}} \quad (4.105)$$

4.3 Modelling of Energy Recovery System

This section includes the modelling of three parts of the energy recovery systems, such as thermoelectric generator, absorption refrigeration system, and desalination system. The modelling of these systems contains thermodynamic analysis in terms of required and added heat transfer, the produced power, and the device efficiency.

4.3.1 Modelling of thermoelectric generator (TEG)

The energy recovery system consists of two subsystems: thermoelectric generator (TEG) and absorption refrigeration system (ARS). The TEG is a device that converts excessive waste heating load into electrical power. It is based on a thermoelectric module, which comprises p- and n-type semiconductors connected in series or parallel. The principle of electricity generation of TEG is governed by the Seebeck effect. The amount of heat transferred from the exhaust to the TG is expressed as \dot{Q}_{TEG} , and the hot and cold junction heat transferred is defined as $\dot{Q}_{H,TEG}$ and $\dot{Q}_{L,TEG}$, respectively. The resultant power of TEG is defined as \dot{W}_{TEG} , while the performance of TG can be measured by electric efficiency ($\eta_{e,TEG}$), energetic efficiency ($\eta_{th,TEG}$), and exergetic efficiency (ψ_{TEG}), as defined below [160].

$$\dot{Q}_{TEG} = \dot{m}_{Ex} (h_{Ex,i} - h_{Ex,o}) \quad (4.106)$$

$$\dot{Q}_{H,TEG} = N \left(\beta I T_H - \frac{I^2 r}{2} + K(T_H - T_L) \right) \quad (4.107)$$

$$\dot{Q}_{L,TEG} = N \left(\beta I T_L + \frac{I^2 r}{2} + K(T_H - T_L) \right) \quad (4.108)$$

$$\dot{W}_{TEG} = \dot{Q}_{H,TEG} - \dot{Q}_{L,TEG} \quad (4.109)$$

$$\eta_{e,TEG} = \frac{\dot{W}_{TEG}}{\dot{Q}_{H,TEG}} \quad \text{and} \quad \eta_{th,GT} = \frac{\dot{W}_{TEG}}{\dot{Q}_{TEG}} \quad (4.110)$$

$$\psi_{TG} = \frac{\dot{W}_{TEG}}{\dot{E}x_{TEG}^Q} \quad (4.111)$$

where β is the Seebeck coefficient, N is the number of thermoelectric units (100), I is the thermoelectric current, the current density of TEG (i) is 3000 A/m², and the active area of TEG (A_t) is 33.6 m² [161]. T_H is the hot junction temperature, which is the average

temperature of B7 and B8, and T_L is the cold junction temperature, which is the ambient temperature, r is electric resistance, K is thermal conductance. Thermoelectric properties are function of temperature and can be expressed as the following [162]:

$$\beta = 2 \times (2224 + 930.6 T_m - 0.9905 T_m^2) \times 10^{-9} \quad (4.112)$$

$$\rho_P = \rho_N = (5112 + 163.4 T_m - 0.6279 T_m^2) \times 10^{-9} \quad (4.113)$$

$$\lambda_P = \lambda_N = (62605 - 277.7 T_m + 0.413 T_m^2) \times 10^{-9} \quad (4.114)$$

$$T_m = \frac{T_H + T_L}{2} \quad (4.115)$$

$$r = \frac{\rho_P + \rho_N}{C} \quad (4.116)$$

$$K = \frac{\lambda_P + \lambda_N}{C} \quad (4.117)$$

where ρ is the electrical resistivity, λ is the heat transfer coefficient, C is the geometry factor and equals 0.5 m, and T_m is the mean temperature [163]. The maximum efficiency of TEGs can be estimated from the following equations [161]:

$$\eta_{max} = \frac{T_h - T_c}{T_h} \times \frac{\sqrt{1 + Z\bar{T}} - 1}{\sqrt{1 + Z\bar{T}} + \frac{T_c}{T_h}} \quad (4.118)$$

$$Z\bar{T} = \frac{(\alpha_p - \alpha_n)^2 \bar{T}}{\left[\left(\frac{\kappa_p}{\alpha_p} \right)^{\frac{1}{2}} + \left(\frac{\kappa_n}{\alpha_n} \right)^{\frac{1}{2}} \right]^2} \quad (4.119)$$

where $(T_h - T_c)/T_h$ is the Carnot efficiency of the TEG, and the second term of maximum efficiency is called the reduced efficiency. The $Z\bar{T}$ is the figure of merit, which depends on the Seebeck coefficient of α . α_p and α_n are the Seebeck coefficient or electric conductivity of p- and n- semiconductors, respectively. κ_p and κ_n are the specific thermal conductivity of p- and n- semiconductors, respectively, and \bar{T} is the mean temperature.

4.3.2 Modelling of the absorption refrigeration system (ARS)

The ARS uses ammonia-water refrigerant and consists of a generator (AGN), absorber (ABS), two expansion valves (AEX1 and AEX2), an evaporator (AEV), a pump (AP), and condenser (ACN). Table 4.9 displays the partial mass balance and energy balance

equations. In the ARS systems, three solutions are considered: pure ammonia solution (y_{pure}), weak ammonia solution (y_{ws}) and strong ammonia solution (y_{ss}) [164,165]. The performance of ARS is measured based on energetic and exergetic COP of the cycle as written below:

$$COP_{en} = \frac{\dot{Q}_{AEV}}{\dot{Q}_{AGN} + \dot{W}_{AP}} \quad \text{and} \quad COP_{ex} = \frac{\dot{E}x_{AEV}^Q}{\dot{E}x_{AGN}^Q + \dot{W}_{AP}} \quad (4.120)$$

Table 4.9 Partial mass balance and energy balance equations of ARS

Comp#	Partial Mass Balance	Energy Balance
ACN	$y_{NH_3,R7} = y_{NH_3,R8} = y_{pure}$	$\dot{Q}_{ACN} = \dot{m}_{R8}(h_{R7} - h_{R8})$
AEV	$y_{NH_3,R7} = y_{NH_3,R8} = y_{pure}$	$\dot{Q}_{AEV} = \dot{m}_{R9}(h_{R9} - h_{R10})$
AGN	$\dot{m}_{R3}y_{NH_3,R3} = \dot{m}_{R4}y_{NH_3,R4} + \dot{m}_{R7}y_{NH_3,R7}$	$\dot{Q}_{AGN} = \dot{m}_{R7}h_{R7} + \dot{m}_{R4}h_{R4} - \dot{m}_{R3}h_{R3}$
AHX	$y_{NH_3,R2} = y_{NH_3,R3} = y_{ss}$ $y_{NH_3,R4} = y_{NH_3,R5} = y_{ws}$	$\dot{Q}_{AHX} = \dot{m}_{R4}(h_{R4} - h_{R5})$
ABS	$\dot{m}_{R6}y_{NH_3,R6} + \dot{m}_{R10}y_{NH_3,R10} = \dot{m}_{R1}y_{NH_3,R1}$	$\dot{Q}_{ABS} = \dot{m}_{R6}h_{R6} + \dot{m}_{R10}h_{R10} - \dot{m}_{R1}h_{R1}$
AP	$y_{NH_3,R1} = y_{NH_3,R2} = y_{ss}$	$\dot{W}_{AP} = \dot{m}_{R1}(h_{R2} - h_{R1})$

4.3.3 Desalination Unit (DSWR)

The Multi-effect desalination system (DSWR) consists of three stages (D-D#) under the same temperature difference. The brine temperature, T_i , is decreased for the next unit by the temperature difference.

$$\Delta T = \frac{T_{D-D1} - T_{D-D3}}{3 - 1} \quad (4.121)$$

The condensation temperature inside each stage is the difference between the brine temperature and the boiling point elevation (BPE). The feed seawater flow rate, \dot{m}_{SW} , is equally distributed to all stages. A constant salinity of seawater x_i is assumed throughout all effects. The brine leaving the stage (i), \dot{m}_{SLi} , is introduced into the next stage ($i + 1$). Therefore, pure water, \dot{m}_{FWi} , leaves the stage and heats the next stage. This is repeated until the last stage has no salinity. The mass flow rate of desalinated water, \dot{m}_{FWi} , is calculated as:

$$\dot{m}_{FWi} = \sum_{k=1}^i \dot{m}_{SWi} - \dot{m}_{SLi} \quad (4.122)$$

The first stage can be analyzed thermodynamically by estimating the mass balance, partial mass balance, and energy balance equations, as indicated below:

$$\dot{m}_{FW,1} = \dot{m}_{SW,1} - \dot{m}_{SL,1} \quad (4.123)$$

$$x_{SW}\dot{m}_{SW} = x_{SL}\dot{m}_{SL} = x_{SL}(\dot{m}_{SW} - \dot{m}_{FW}) \quad (4.124)$$

$$\dot{Q}_{DSWR} = \dot{m}_s c (T_{s,in} - T_{s,ex}) \quad (4.125)$$

$$\dot{Q}_{DSWR} = \dot{m}_{FW,1} h_{fg,1} + \dot{m}_{SW,1} c (T_1 - T_{SW}) \quad (4.126)$$

The desalinated water is used to heat the next stage, while the brine of the previous stage enters the next one and heats the seawater to remove its salinity. The mass balance and the energy balance equations of the following stages are explained below:

$$\dot{m}_{SL,i} = \dot{m}_{SW,i} - (\dot{m}_{SL,i} - \dot{m}_{SL,i-1}) \quad (4.127)$$

$$x_{SW}\dot{m}_{SW} + x_{SL,i-1}\dot{m}_{SL,i-1} = x_{SL,i}\dot{m}_{SL,i} \quad (4.128)$$

$$\dot{Q}_{s,i} = \dot{m}_{FW,i-1} h_{fg,i-1} + \dot{m}_{SL,i-1} c (T_{i-1} - T_i) \quad (4.129)$$

$$\dot{Q}_{s,i} = \dot{m}_{FW,i} h_{fg,i} + \dot{m}_{SW,i} c (T_i - T_F) \quad (4.130)$$

The energetic efficiency of the desalination (DSWR), η_{DSWR} , and its exergy efficiency, ψ_{DSWR} , can be described below. Also, the gained output ratio (GOR) is calculated by the ratio of the latent heat of fresh water exiting the last stage to the input heat of steam entering the first stage.

$$\eta_{DSWR} = \frac{\dot{m}_{FW15} h_{FW16}}{\dot{Q}_{DSWR}} \quad (4.131)$$

$$\psi_{DSWR} = \frac{\dot{m}_{FW15} ex_{FW16}}{\dot{Ex}_{DSWR}^Q} \quad (4.132)$$

$$GOR = \frac{\dot{m}_{FW15} h_{fg}}{\dot{Q}_{DSWR}} \quad (4.133)$$

4.4 Combustion Modelling

The baseline fuels for the baseline system are ultra-low-sulfur diesel (ULSD), kerosene, marine gas oil (MGO-DMA), which comprises 75% saturated hydrocarbons containing paraffin and naphthenes, 24% unsaturated hydrocarbons as benzene rings, 1% Asphaltenes. The properties of the baseline fuels are presented in Table 4.10. The alternative fuels are selected to be hydrogen, methanol, ethanol, dimethyl-ether (DME), and methane, which their properties are listed in Table 4.11. The Stoichiometric combustion reactions for the baseline fuels and alternative fuels are listed in Table 4.12.

Table 4.10 The specifications of baseline fuels for baseline transportation systems

Specifications	ULSD [166]	Kerosene [167]	MGO-DMA [168,169]
Molecular formula	C ₁₂ H ₂₄	C ₁₀ H ₂₂	---
Molecular weight, M _i [kg/kmol]	168.3	142	220 - 238
Adiabatic flame temperature [°C]	1977	2093	2101
Auto-ignition temperature [°C]	~ 225	640	256
Density at 40°C [kg/m ³]	876	760-810	815-870
Viscosity at 40°C [mm ² /S]	4.1	1-1.9	4.5
High heating value [MJ/kg]	45.6	46.2	45.9
Low heating value [MJ/kg]	43.3	43.0	42.8

Table 4.11 The specifications of alternative fuels for developed transportation systems

Specifications	Hydrogen [170]	Methanol [24]	Ethanol [171]	DME [44]	Methane [140]
Molecular formula	H ₂	CH ₃ OH	CH ₃ OHCH ₂	CH ₃ OCH ₃	CH ₄
Molecular weight, M _i [kg/kmol]	2.016	46.069	46.07	46.07	16.043
Adiabatic flame temperature [°C]	2000	1949	2082	2100	1963
Auto-ignition temperature [°C]	571	470	365	350	537
Density at 40°C [kg/m ³]	0.0773	792	789	2.11	0.657
Viscosity at 40°C [mm ² /s]	109	0.75	1.056	0.184	18.72
High heating value [MJ/kg]	141.9	22.7	29.7	31.67	55.5
Low heating value [MJ/kg]	119.0	18.1	26.7	28.87	50

Table 4.12 The stoichiometric combustion reactions for the fuels

Fuel	Stoichiometric combustion reaction	Heat of combustion (ΔH _c)
ULSD	C ₁₂ H ₂₄ + 18 O ₂ → 12 CO ₂ + 12 H ₂ O	-7674.5 kJ/mol
Kerosene	C ₁₀ H ₂₂ + 15.5 O ₂ → 10 CO ₂ + 11 H ₂ O	-6652.8 kJ/mol
MGO	Paraffins (C _n H _{2n+2}): C ₆ H ₁₄ + 9.5 O ₂ → 6 CO ₂ + 7 H ₂ O Naphthenes (C _n H _{2n}): C ₆ H ₁₂ + 9 O ₂ → 6 CO ₂ + 6 H ₂ O Aromatics (C ₆ H ₆): C ₆ H ₆ + 7.5 O ₂ → 6 CO ₂ + 3 H ₂ O	-10557 kJ/mol
Hydrogen	2 H ₂ + O ₂ → 2 H ₂ O	-286 kJ/mol
Methanol	CH ₃ OH + 1.5 O ₂ → CO ₂ + 2 H ₂ O	-726 kJ/mol
Ethanol	CH ₃ OHCH ₂ + 3 O ₂ → 2 CO ₂ + 3 H ₂ O	-1366.91 kJ/mol
DME	CH ₃ OCH ₃ + 3 O ₂ → 2 CO ₂ + 3 H ₂ O	-2726.3 kJ/mol
Methane	CH ₄ + 2 O ₂ → CO ₂ + 2 H ₂ O	-891 kJ/mol

Five combinations of fuels are used in the study based on the mass fractions: F1 (75% natural gas and 25% hydrogen); F2 (75% methanol and 25% hydrogen); F3 (60% ethanol and 40% hydrogen); F4 (60% DME and 40% hydrogen); and F5 (15% natural gas, 40% hydrogen, 15% methanol, 15% ethanol, and 15% DME). The steam reforming, water gas shift, and catalytic burner for the five combination fuels are listed in Table 4.13.

Table 4.13 Steam reforming, water gas shift and catalytic burner of SOFC and MCFC systems.

Fuels	SR	WGS	CC and BR
F1	$\text{CH}_4 + \text{H}_2\text{O} \rightarrow \text{CO} + 3\text{H}_2$	$\text{CO} + \text{H}_2\text{O} \rightarrow \text{CO}_2 + \text{H}_2$	$\text{CH}_4 + 2\text{O}_2 \rightarrow \text{CO}_2 + 2\text{H}_2\text{O}$ $2\text{H}_2 + \text{O}_2 \rightarrow 2\text{H}_2\text{O}$ $2\text{CO} + \text{O}_2 \rightarrow 2\text{CO}_2$
F2	$\text{CH}_3\text{OH} \rightarrow \text{CO} + 2\text{H}_2$	$\text{CO} + \text{H}_2\text{O} \rightarrow \text{CO}_2 + \text{H}_2$	$\text{CH}_3\text{OH} + 1.5\text{O}_2 \rightarrow \text{CO}_2 + 2\text{H}_2\text{O}$ $2\text{H}_2 + \text{O}_2 \rightarrow 2\text{H}_2\text{O}$ $2\text{CO} + \text{O}_2 \rightarrow 2\text{CO}_2$
F3	$\text{CH}_3\text{OHCH}_2 \rightarrow \text{CH}_4 + \text{CO} + \text{H}_2$ $\text{CH}_4 + \text{H}_2\text{O} \rightarrow \text{CO} + 3\text{H}_2$	$\text{CO} + \text{H}_2\text{O} \rightarrow \text{CO}_2 + \text{H}_2$	$\text{CH}_3\text{OHCH}_2 + 3\text{O}_2 \rightarrow 2\text{CO}_2 + 3\text{H}_2\text{O}$ $2\text{H}_2 + \text{O}_2 \rightarrow 2\text{H}_2\text{O}$ $2\text{CO} + \text{O}_2 \rightarrow 2\text{CO}_2$
F4	$\text{CH}_3\text{OCH}_3 \rightarrow \text{CH}_4 + \text{CO} + \text{H}_2$ $\text{CH}_4 + \text{H}_2\text{O} \rightarrow \text{CO} + 3\text{H}_2$	$\text{CO} + \text{H}_2\text{O} \rightarrow \text{CO}_2 + \text{H}_2$	$\text{CH}_3\text{OCH}_3 + 3\text{O}_2 \rightarrow 2\text{CO}_2 + 3\text{H}_2\text{O}$ $2\text{H}_2 + \text{O}_2 \rightarrow 2\text{H}_2\text{O}$ $2\text{CO} + \text{O}_2 \rightarrow 2\text{CO}_2$
F5	$\text{CH}_4 + \text{H}_2\text{O} \rightarrow \text{CO} + 3\text{H}_2$ $\text{CH}_3\text{OH} \rightarrow \text{CO} + 2\text{H}_2$ $\text{CH}_3\text{OHCH}_2 \rightarrow \text{CH}_4 + \text{CO} + \text{H}_2$ $\text{CH}_3\text{OCH}_3 \rightarrow \text{CH}_4 + \text{CO} + \text{H}_2$	$\text{CO} + \text{H}_2\text{O} \rightarrow \text{CO}_2 + \text{H}_2$	$\text{CH}_4 + 2\text{O}_2 \rightarrow \text{CO}_2 + 2\text{H}_2\text{O}$ $\text{CH}_3\text{OH} + 1.5\text{O}_2 \rightarrow \text{CO}_2 + 2\text{H}_2\text{O}$ $\text{CH}_3\text{OHCH}_2 + 3\text{O}_2 \rightarrow 2\text{CO}_2 + 3\text{H}_2\text{O}$ $\text{CH}_3\text{OCH}_3 + 3\text{O}_2 \rightarrow 2\text{CO}_2 + 3\text{H}_2\text{O}$ $2\text{H}_2 + \text{O}_2 \rightarrow 2\text{H}_2\text{O}$ $2\text{CO} + \text{O}_2 \rightarrow 2\text{CO}_2$

4.5 Analyses and Assessments

This subsection is important since it includes the three assessments such as energy performance, economic, and environmental assessments. The energy performance is evaluated by using thermodynamic analysis to estimate energy (power and heat), energy and exergy efficiencies, and the effect of fuels on energy performance. This step is essential and a prerequisite to other analyses. Then, the exergy analysis based on Fuel and Product (F-P) principle is conducted on each component of the systems to estimate the overall fuel, product, and destruction exergy rates and exergy efficiency of the whole engine. After that exergoeconomic analysis and exergoenvironmental analysis are conducted based on fuel and product principal to estimate the fuel and product costs and fuel and product environmental impact. Figure 4.7 shows the path of analyses for each system in the three transportation sectors.

4.5.1 Thermodynamic Analysis

The energy consumption and analysis are studied by using the thermodynamic analysis for each transportation sector by considering the most common powering system used in each sector. The thermodynamic analysis is governed by the first and second law of thermodynamics and compare each system to the ideal case.

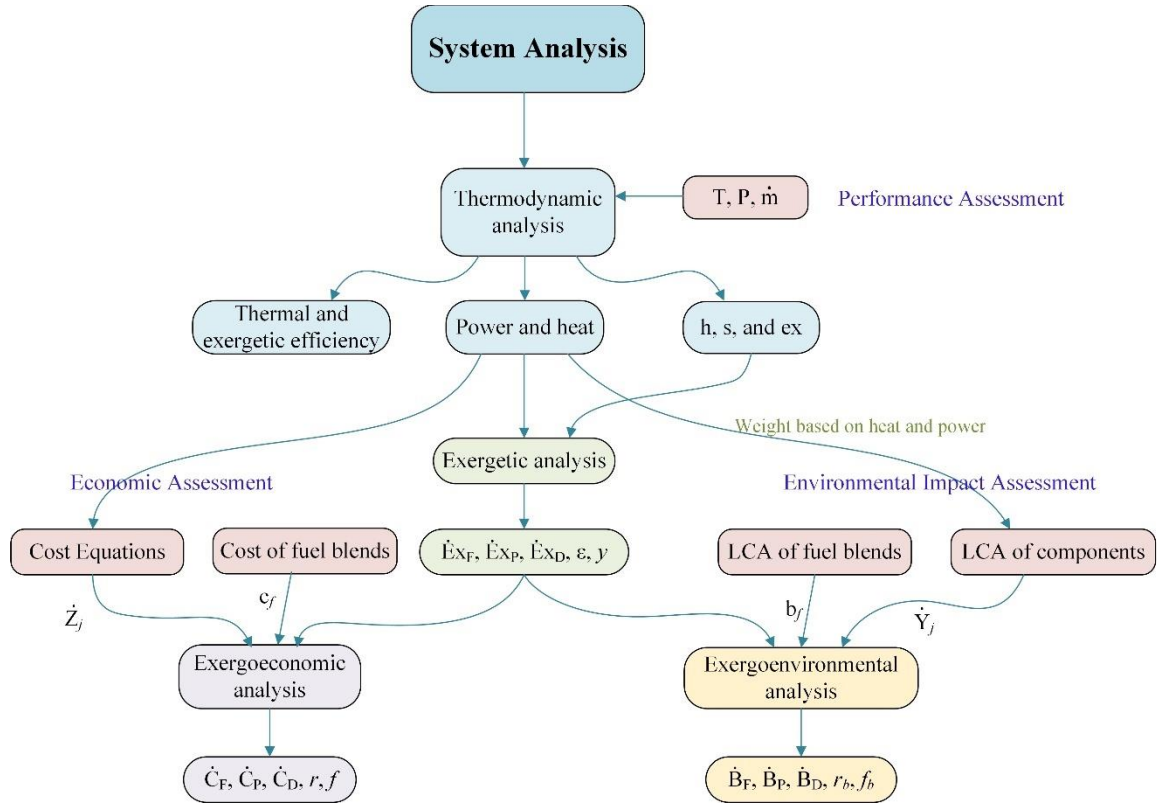


Figure 4.7 The flow chart analyses and assessments

The first law of thermodynamics is formulated by the conservation of mass and energy, while the second law of thermodynamics is formulated by the entropy and exergy balance equations. The software programs used in the analyses are EES (Engineering Equation solver) and Aspen-Plus software because of their reliable thermodynamic properties as well as the calculation methods, and they have been excessively used by researchers for thermodynamic analysis for several systems.

The thermodynamic balance equations can be expressed in general forms since the processes of each component are at steady-state equilibrium. Therefore, the mass balance equation can be expressed as:

$$\sum \dot{m}_{in} = \sum \dot{m}_{out} \quad (4.134)$$

The general form of the energy balance equation in a steady state can be expressed as the following equation, where \dot{Q}_{cv} and \dot{W}_{cv} represents the heat transfer and the work crossing the boundaries of a closed system of each component. The steady energy flow is expressed as $\left(h + \frac{1}{2}V^2 + gZ\right)$, which represents the internal energy of the media, the specific kinetic

energy, and the specific potential energy, respectively. h is the specific enthalpy, V is the stream velocity of the working fluid, g is the gravitational acceleration, and Z is the elevation from the datum.

$$\begin{aligned} \sum_{in} \dot{Q}_{cv} + \sum_{in} \dot{W}_{cv} + \sum_i \dot{m}_i \left(h_i + \frac{1}{2} V_i^2 + gZ_i \right) \\ = \sum_{out} \dot{Q}_{cv} + \sum_{out} \dot{W}_{cv} + \sum_e \dot{m}_e \left(h_e + \frac{1}{2} V_e^2 + gZ_e \right) \end{aligned} \quad (4.135)$$

The general form of the second law of thermodynamics can be represented in two primary general forms: the entropy balance equation and the exergy balance equation in a steady-state condition for each process. The entropy balance equation can be expressed in a general form as the following:

$$\sum_{in} \frac{\dot{Q}_{cv}}{T_s} + \sum_i \dot{m}_i s_i + \dot{S}_{gen} = \sum_e \dot{m}_e s_e + \sum_{out} \frac{\dot{Q}_{cv}}{T_s} \quad (4.136)$$

, while the general form of the exergy balance equation can be written as follows:

$$\sum_i \dot{m}_i ex_i + \sum_{in} \dot{E}x_Q + \sum_{in} \dot{E}x_W = \sum_e \dot{m}_e ex_e + \sum_{out} \dot{E}x_Q + \sum_{out} \dot{E}x_W + \dot{E}x_D \quad (4.137)$$

where $\dot{E}x_W$ denotes the work done or required by the process, and $\dot{E}x_Q$ is thermal exergy due to the heat transfer within the boundaries ($\dot{Q}_{cv,i}$) and depends on the reference temperature T_o . They can be defined as the following:

$$\dot{E}x_W = \dot{W}_{cv} \quad , \text{ and } \quad \dot{E}x_{Q,i} = \left(1 - \frac{T_o}{T_{s,i}} \right) \dot{Q}_{cv,i} \quad (4.138)$$

The specific exergy of each stream is comprised of physical specific exergy, $ex_{ph,i}$, and chemical specific exergy, $ex_{ch,i}$, and are described as the following:

$$\bar{ex}_i = \bar{ex}_{ph,i} + \bar{ex}_{ch,i} = \sum_i [(\bar{h}_i - \bar{h}_o) - T_o(\bar{s}_i - \bar{s}_o)] + \bar{ex}_{ch,i} \quad (4.139)$$

while the chemical exergy depends on the chemical changes of a component composition during the chemical reaction. It depends on the Gibbs function of a unit mole of a substance \bar{g} which consists of the Gibbs function of the formation of each substance \bar{g}_f^o , Gibbs function of a substance at a specific temperature \bar{g}_{T_o} and Gibbs function at a reference temperature \bar{g}^o . The chemical exergy can be expressed as:

$$\overline{ex}_{ch,i} = \sum_i n_i (\bar{g}_f^o + \bar{g}_{T_o} - \bar{g}^o) \quad (4.140)$$

The performance of a system can be evaluated by the overall energy efficiencies η and exergy efficiencies ψ for each component and the entire system. Besides, the irreversibility ratio (IR), which is defined as the ratio of exergy destruction of a component to that of the entire system, can show the highest contribution to irreversibility, which later can be minimized by manipulating the thermodynamic parameters to enhance the overall system performance.

$$\eta = \frac{\text{Useful Energy Output}}{\text{Energy Required}} \quad (4.141)$$

$$\psi = \frac{\text{Useful Exergy Output}}{\text{Exergy Required}} \quad (4.142)$$

$$IR = \frac{\dot{Ex}_{des,i}}{\sum \dot{Ex}_{des,i}} \quad (4.143)$$

The performance of all engine systems is summarized below, starting with aviation engine systems, followed by rail engine systems and marine engine systems. The software programs used in the analyses are the EES (Engineering Equation solver) and the Aspen-Plus software because of their reliable thermodynamic properties as well as the calculation methods and are extensively used by many researchers for thermodynamic analysis for several systems. The equation of state is chosen to be the Soave-Redlick-Kwong (SRK) for the thermodynamic properties because it is the most widely accepted equation for modern chemical processes and recommended for gas mixtures and electrolytes (such as carbonate electrolyte CO_3^{2-}) at high temperature and pressure conditions [172–174]. Also, the equation of states is chosen to be the electrolyte property method (ELECRTL) for modelling the AEC [175]. The first step is to evaluate the thermodynamic data, including the mass flow rate, temperature, pressure, specific enthalpy, specific entropy, specific physical and chemical exergy, and total exergy rate for each stream. Then, use EES software to evaluate the fuel and product exergy, exergoeconomic rates, and exergoenvironmental rates for each stream. The Aspen PLUS flowcharts are represented before in in the system performance since the exergy analysis, exergoeconomic analysis, and exergoenvironmental analysis are written with the stream names of those charts.

System A-1: The flow chart of Aspen PLUS for hybrid MCFC-turbofan is presented in Figure 4.8. The total engine power, \dot{W}_{eng} , overall energetic efficiency, η_{eng} , and exergetic efficiency, ψ_{eng} , of the hybrid MCFC-turbofan engine are explained by:

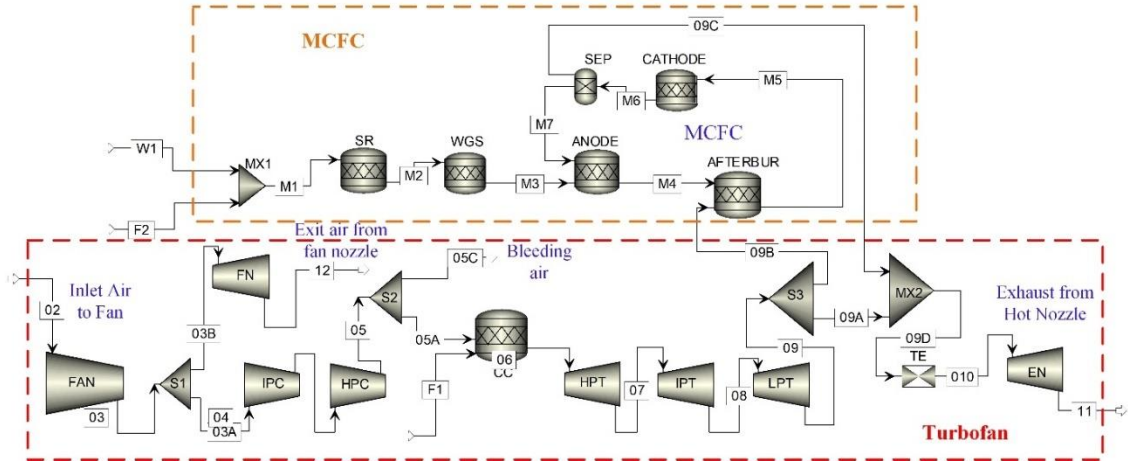


Figure 4.8 The flow chart of Aspen Plus simulation for hybrid MCFC-turbofan systems.

$$\dot{W}_{eng} = \dot{W}_{MCFC} + \dot{W}_{GT} + \Gamma U_a \quad (4.144)$$

$$\eta_{eng} = \frac{\dot{W}_{eng}}{\dot{Q}_{MCFC} + \dot{Q}_{CC} + \dot{Q}_{SR} + \dot{Q}_{WGS}} \quad (4.145)$$

$$\psi_{eng} = \frac{\dot{W}_{eng}}{\dot{Ex}_{MCFC}^Q + \dot{Ex}_{CC}^Q + \dot{Ex}_{SR}^Q + \dot{Ex}_{WGS}^Q} \quad (4.146)$$

System A-2: The flowchart of hybrid SOFC-turbofan is shown in Figure 4.9. The performance of the developed turbofan systems can be determined as the overall energetic efficiency η_{eng} , and the overall exergetic efficiency ψ_{eng} , as the following:

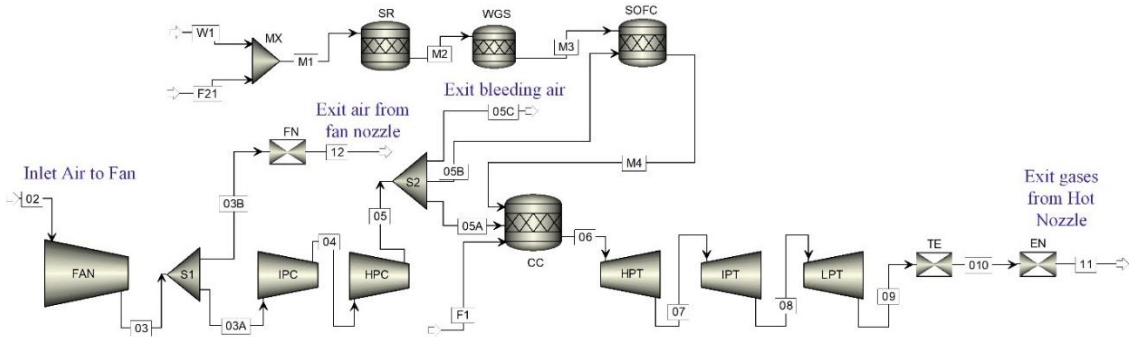


Figure 4.9 The Aspen Plus flow chart for the SOFC-turbofan systems

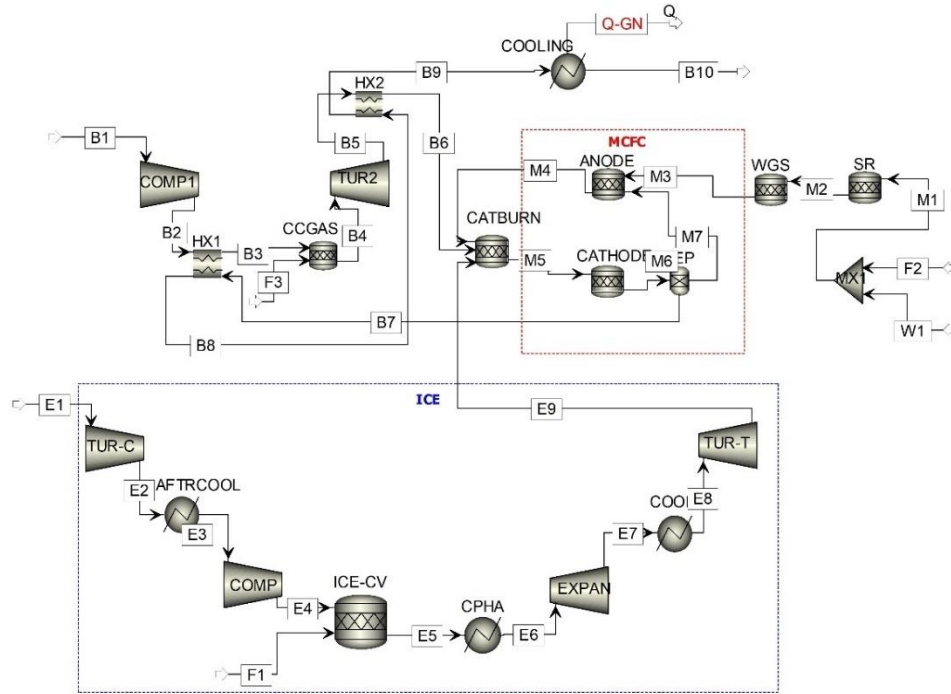
$$\eta_{eng} = \frac{\dot{W}_{SOFC,AC} + \dot{W}_{GT} + \Gamma U_a}{\dot{Q}_{CC} + \dot{Q}_{SOFC,add} + \dot{Q}_{SR} + \dot{Q}_{WGS}} \quad (4.147)$$

$$\psi_{eng} = \frac{\dot{W}_{SOFC,AC} + \dot{W}_{GT} + \Gamma U_a}{\dot{Ex}_{CC}^Q + \dot{Ex}_{SOFC,add}^Q + \dot{Ex}_{SR}^Q + \dot{Ex}_{WGS}^Q} \quad (4.148)$$

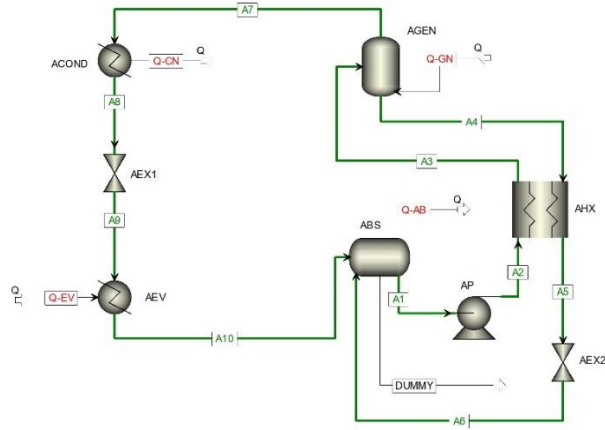
System R-1: The Aspen PLUS flow chart for modelling system R-1 of the hybrid combined locomotive engine is displayed in Figure 4.10, where Figure 4.10-a presents the flow charts for the MCFC-GT and ICE, and Figure 4.10-b shows the ARS. The overall performance of the rail engine system can be expressed by energetic and exergetic efficiencies. The useful energy sources are the net electric power of MCFC, ICE, GT, pump, and the cooling load, while the required energy sources in the engine are the added heat of ICE, GT, and endothermic heat of the steam reformer and water gas shift.

$$\eta_{eng} = \frac{\dot{W}_{MCFC,AC} + \dot{W}_{GT} + \dot{W}_{ICE} - \dot{W}_{AP} + \dot{Q}_{cooling}}{\dot{Q}_{ICE} + \dot{Q}_{GT} + \dot{Q}_{SR} + \dot{Q}_{WGS}} \quad (4.149)$$

$$\eta_{eng} = \frac{\dot{W}_{MCFC,AC} + \dot{W}_{GT} + \dot{W}_{ICE} - \dot{W}_{AP} + \dot{Ex}_{cooling}^Q}{\dot{Ex}_{ICE}^Q + \dot{Ex}_{GT}^Q + \dot{Ex}_{SR}^Q + \dot{Ex}_{WGS}^Q} \quad (4.150)$$



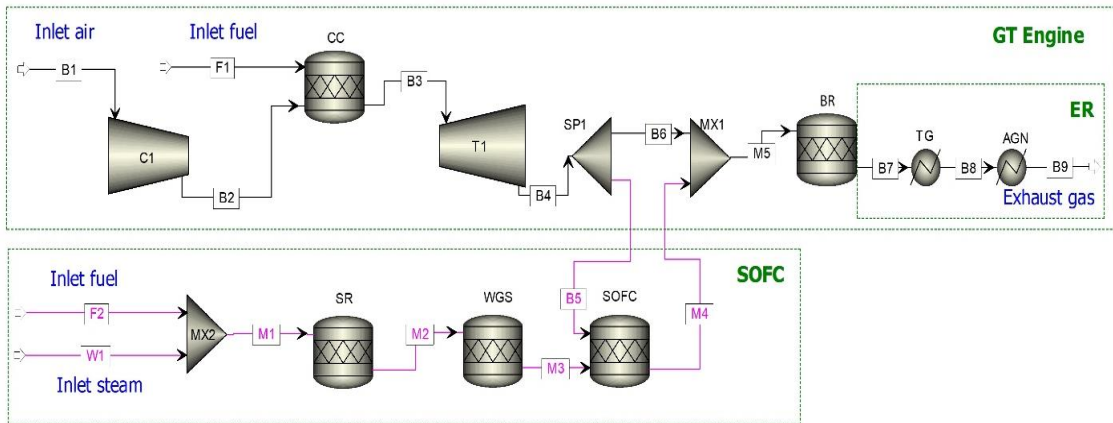
(a)



(b)

Figure 4.10 The Aspen flow chart for: (a) the hybrid combined engine and (b) the absorption refrigeration system.

System R-2: The flow chart of the hybrid SOFC- GT-PEMFC-AEC locomotive engine (system R-2) is drawn in Figure 4.11. Figure 4.11-a shows the flow chart of SOFC-GT, while Figure 4.11-b and -c shows the flow chart of hydrogen production using PEMFC-AEC system and the absorption refrigeration system (ARS). The engine power (\dot{W}_{eng}) and heat required (\dot{Q}_{eng}) are given below. The power and heat exergy rates are defined by \dot{Ex}_{eng}^W and \dot{Ex}_{eng}^Q , respectively. The overall performance of the hybrid locomotive engine can be measured using energetic efficiency (η_{eng}) and exergetic efficiency (ψ_{eng}) of the engine, which are explained below:



(a)

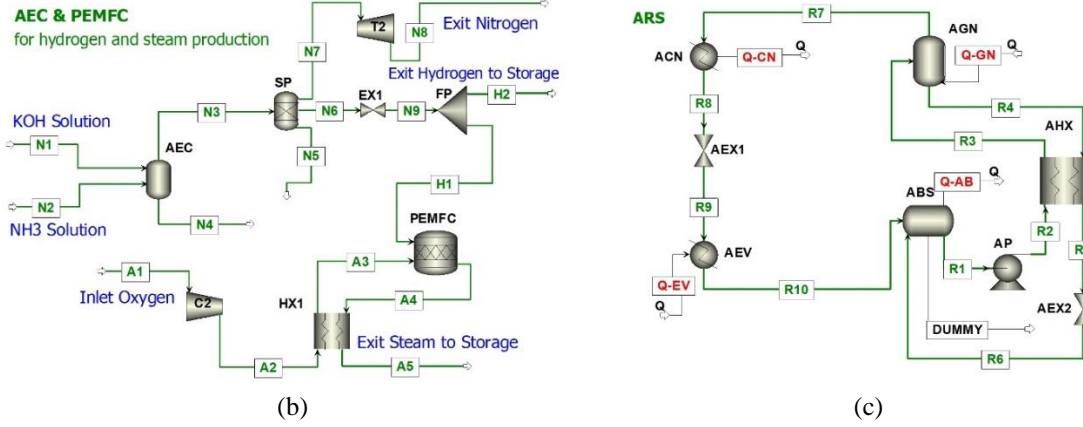


Figure 4.11 The Aspen flowcharts for hybrid engine: (a) the GT and SOFC, (b) onboard hydrogen production, and (c) ARS system.

$$\dot{W}_{eng} = \dot{W}_{GT} + \dot{W}_{TG} + \dot{W}_{SOFC} + \dot{W}_S - \dot{W}_{AP} \quad (4.151)$$

$$\dot{Q}_{eng} = \dot{Q}_{CC} + \dot{Q}_{BR} \quad (4.152)$$

$$\dot{Ex}_{eng}^W = \dot{W}_{eng} \quad (4.153)$$

$$\dot{Ex}_{eng}^Q = \dot{Ex}_{CC}^Q + \dot{Ex}_{BR}^Q \quad (4.154)$$

$$\eta_{eng} = \frac{\dot{Ex}_{out,eng}^Q}{\dot{Ex}_{in,eng}^Q} = \frac{\dot{W}_{eng} + \dot{Q}_{AEV}}{\dot{Q}_{eng}} \quad (4.155)$$

$$\psi_{eng} = \frac{\dot{Ex}_{out,eng}^Q}{\dot{Ex}_{in,eng}^Q} = \frac{\dot{Ex}_{eng}^W + \dot{Ex}_{AEV}^Q}{\dot{Ex}_{eng}^Q} \quad (4.156)$$

System R-3: The flow chart of the hybrid SOFC-PEMFC-GT locomotive engine (system R-3) is shown in Figure 4.12. The rail engine power (\dot{W}_{eng}) is the total power generated from GT, SOFC, PEMFC, TEG1, and TEG2, while the heat required (\dot{Q}_{eng}) are total heat of CC and BR, subtracting the IC. The power and heat exergy rates are defined by \dot{Ex}_{eng}^W and \dot{Ex}_{eng}^Q , respectively. The hybrid rail engine has an overall performance of energetic efficiency (η_{eng}) and exergetic efficiency (ψ_{eng}), which are expressed below.

$$\dot{W}_{eng} = \dot{W}_{GT} + \dot{W}_{TEG1} + \dot{W}_{TEG2} + \dot{W}_{SOFC} + \dot{W}_{PEMFC} \quad (4.157)$$

$$\dot{Q}_{eng} = \dot{Q}_{CC} + \dot{Q}_{BR} - \dot{Q}_{IC} \quad (4.158)$$

$$\dot{Ex}_{eng}^W = \dot{W}_{eng} \quad (4.159)$$

$$\dot{Ex}_{eng}^Q = \dot{Ex}_{CC}^Q + \dot{Ex}_{BR}^Q - \dot{Ex}_{IC}^Q \quad (4.160)$$

$$\eta_{eng} = \frac{\dot{E}_{out,eng}}{\dot{E}_{in,eng}} = \frac{\dot{W}_{eng} + \dot{Q}_{AEV}}{\dot{Q}_{eng}} \quad (4.161)$$

$$\psi_{eng} = \frac{\dot{E}x_{out,eng}}{\dot{E}x_{in,eng}} = \frac{\dot{E}x_{eng}^W + \dot{E}x_{AEV}^Q}{\dot{E}x_{eng}^Q} \quad (4.162)$$

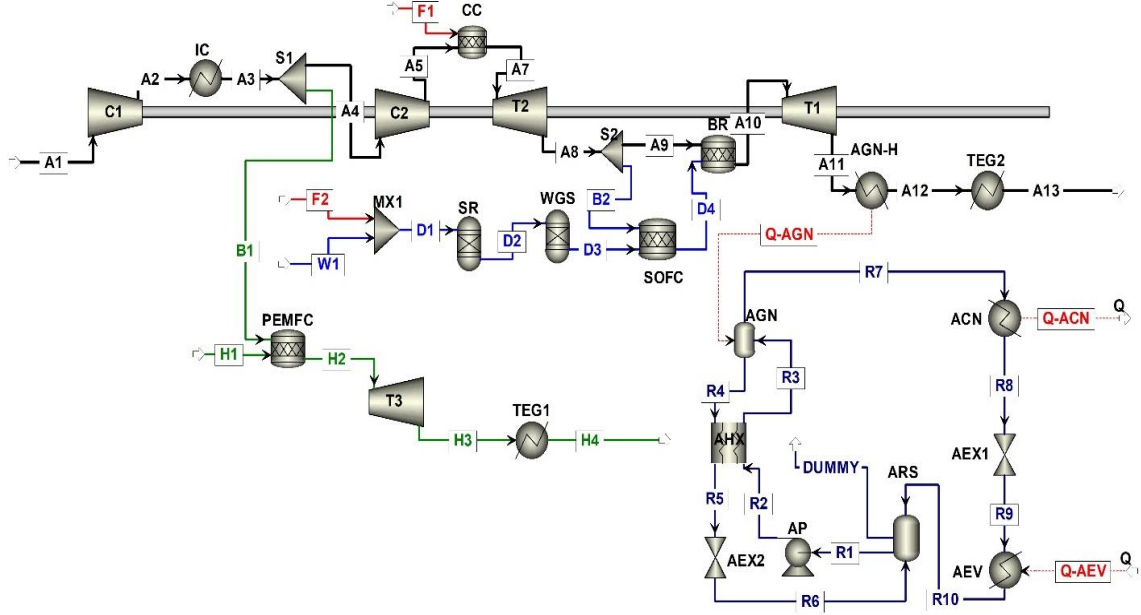


Figure 4.12 The flowchart of the Aspen Plus simulation of system R-3 locomotive engine.

System M-1: The flowchart of the hybrid combined marine engine (system M-1) is presented in Figure 4.13. The hybridized marine engine system is a combination of TEG-ICE engine and a hybrid GT, each of which can fulfill the power of Aframax, and adding them can increase the total power to double without increasing the overall engine weight. Therefore, the performance of each engine system is considered, as well as the combination of them.

The TEG-ICE has a net energetic efficiency of $\eta_{ICE,net}$ and a net exergetic efficiency of $\psi_{ICE,net}$ that includes the power and heat reduction of TEG1, while the hybrid GT has a net energetic and exergetic efficiency of $\eta_{GT,net}$ and $\psi_{GT,net}$, respectively. If the two engines are totally combined and utilized, then the total energetic and exergetic efficiency can be given as η_t and ψ_t , as mentioned below.

$$\eta_{ICE,net} = \frac{\dot{W}_{ICE} + \dot{W}_{TEG1}}{\dot{Q}_{ICE} - \dot{Q}_{TEG1}} \quad (4.163)$$

$$\psi_{ICE,net} = \frac{\dot{W}_{ICE} + \dot{W}_{TEG1}}{\dot{E}x_{ICE}^Q - \dot{E}x_{TEG1}^Q} \quad (4.164)$$

$$\eta_{GT,net} = \frac{\dot{W}_{GT} + \dot{W}_{SOFC} + \dot{W}_{TEG2}}{\dot{Q}_{GT} + \dot{Q}_{SOFC} - \dot{Q}_{TEG2}} \quad (4.165)$$

$$\psi_{GT,net} = \frac{\dot{W}_{GT} + \dot{W}_{SOFC} + \dot{W}_{TEG2}}{\dot{E}x_{GT}^Q + \dot{E}x_{SOFC}^Q - \dot{E}x_{TEG2}^Q} \quad (4.166)$$

$$\eta_t = \frac{\dot{W}_{ICE} + \dot{W}_{TEG1} + \dot{W}_{GT} + \dot{W}_{SOFC} + \dot{W}_{TEG2}}{\dot{Q}_{ICE} - \dot{Q}_{TEG1} + \dot{Q}_{GT} + \dot{Q}_{SOFC} - \dot{Q}_{TEG2}} \quad (4.167)$$

$$\psi_t = \frac{\dot{W}_{ICE} + \dot{W}_{TEG1} + \dot{W}_{GT} + \dot{W}_{SOFC} + \dot{W}_{TEG2}}{\dot{E}x_{ICE}^Q - \dot{E}x_{TEG1}^Q + \dot{E}x_{GT}^Q + \dot{E}x_{SOFC}^Q - \dot{E}x_{TEG2}^Q} \quad (4.168)$$

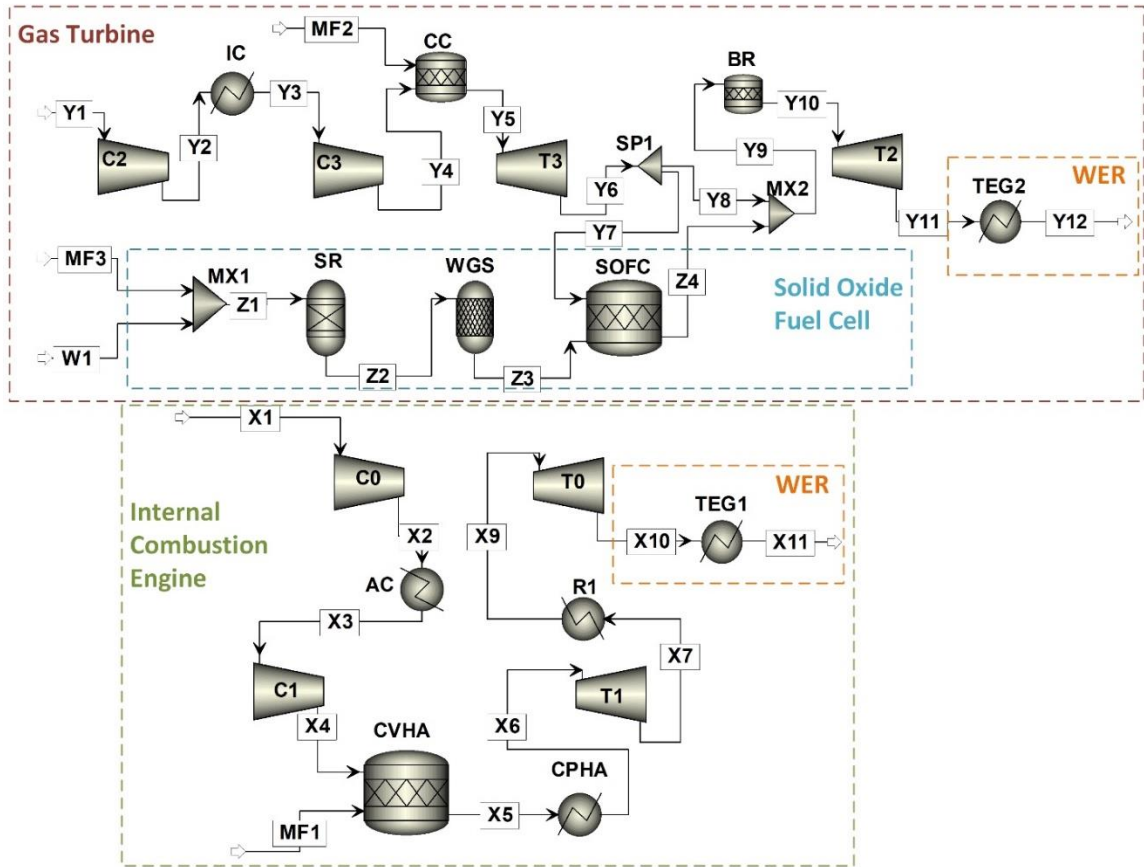


Figure 4.13 The simulation diagram of the developed marine engine using the Aspen Plus

The specific fuel consumption (SFC) is another parameter addressing the engine performance in terms of fuel consumption, which can follow the general form as below. It is calculated for each engine and for the total number of engines altogether.

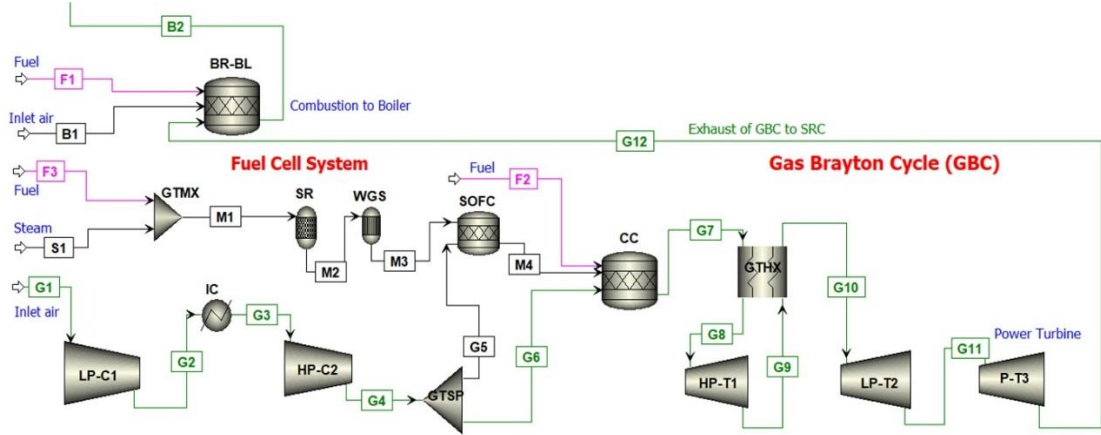


Figure 4.15 The Aspen Plus flowchart of the hybrid GBC. The stream B2 flows to the heat exchanger boiler (HXBL).

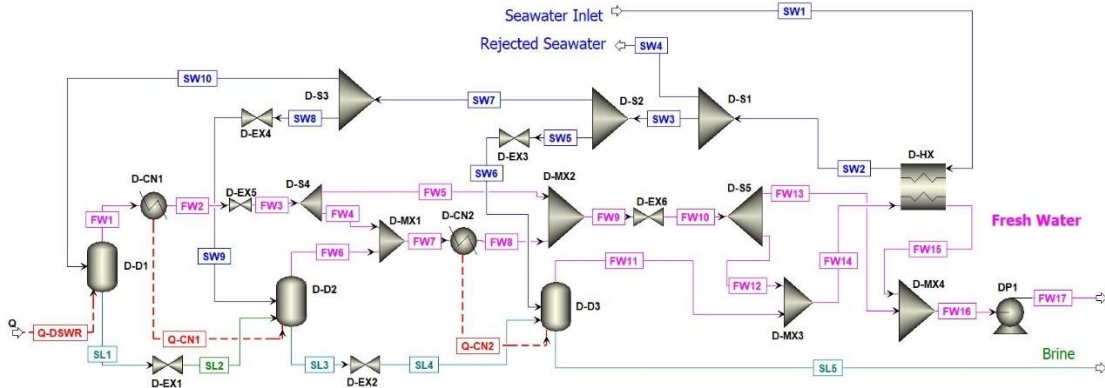


Figure 4.16 The Aspen Plus flowchart for the desalination unit (DSWR)

System M-3: The flowchart of system M-3 of a hybrid gas turbine combined with two binary systems is illustrated in Figure 4.17 for the hybridized gas Brayton cycle (GBC) and Figure 4.18 for the two organic Rankine cycles (ORCs). The overall performance of the proposed engine can be estimated by evaluating the overall energy and exergy efficiencies and the specific fuel consumption (SFC) [183]. These are written as:

$$\eta_{ME} = \frac{\dot{W}_{GBC} + \dot{W}_{SOFC} + \dot{W}_{TORC} + \dot{W}_{BORC} + \dot{m}_{LNG} c_{pLNG} T_{LNG3}}{\dot{Q}_{CC} + \dot{Q}_{SOFC} + \dot{m}_{LNG} c_{pLNG} T_{LNG1}} \quad (4.172)$$

$$\psi_{ME} = \frac{\dot{W}_{GBC} + \dot{W}_{SOFC} + \dot{W}_{TORC} + \dot{W}_{BORC} + \dot{m}_{LNG} ex_{LNG3}}{\dot{Q}_{CC} + \dot{Q}_{SOFC} + \dot{m}_{LNG} ex_{LNG1}} \quad (4.173)$$

$$SFC_{ME} = \frac{\dot{m}_{F1} + \dot{m}_{F2}}{\dot{W}_{GBC} + \dot{W}_{SOFC} + \dot{W}_{TORC} + \dot{W}_{BORC}} \quad (4.174)$$

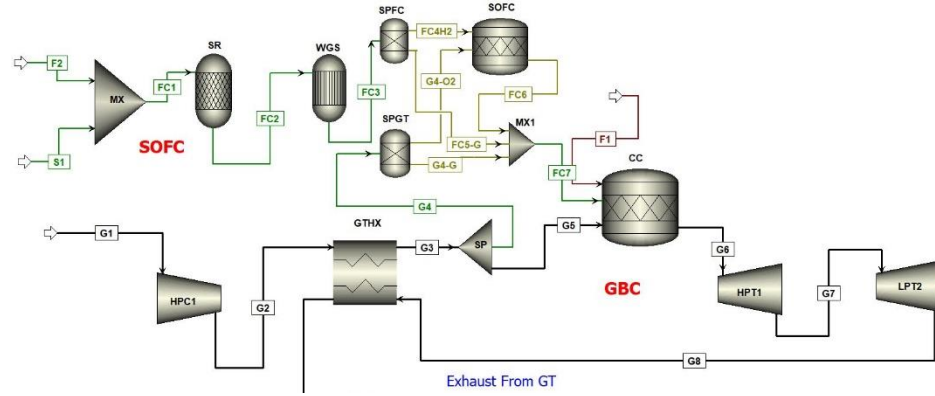


Figure 4.17 The Aspen flowchart for hybridized GBC. Stream G9 goes to CN1 in Figure 4.18.

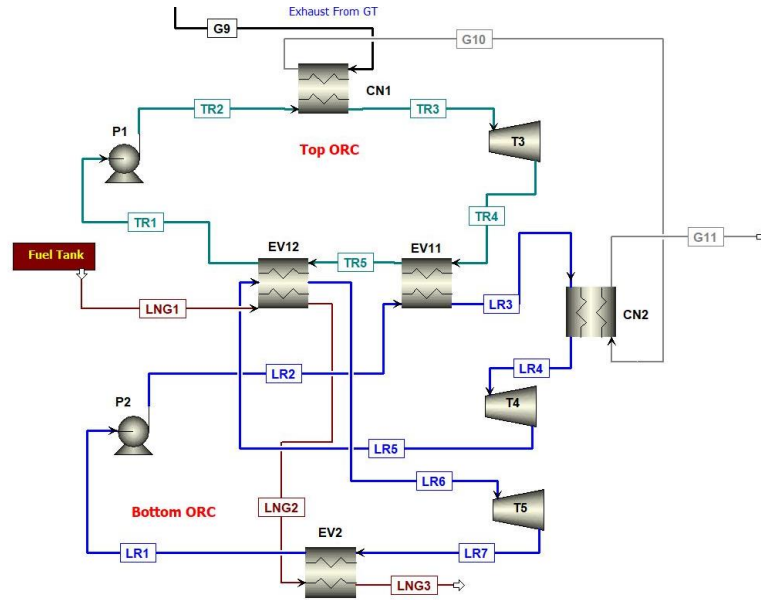


Figure 4.18 The Aspen flowchart of the ORCs. Stream G9 comes from GTHX.

4.5.2 Exergy Analysis

The exergetic performance of this new locomotive engine is studied according to fuel and product exergy analysis. The fuel exergy rate ($\dot{E}x_{F,j}$) is the total input exergy rate, input work exergy and input thermal exergy, whereas the product exergy rate ($\dot{E}x_{P,j}$) is total output exergy rates, output work exergy, and output thermal exergy. The difference between $\dot{E}x_{F,j}$ and $\dot{E}x_{P,j}$ is known as $\dot{E}x_{D,j}$, which is the destruction exergy rate. The irreversibility ratio (γ_j^*) is the ratio of exergy destruction of a component to its total, and the exergy destruction ratio (γ_j) is the ratio of exergy destruction to the total fuel exergy rate. The component exergetic efficiency (ϵ_j) is the ratio of product to fuel exergy, whereas (ϵ_t) is the ratio of the total product exergy rate to the total fuel exergy rate. All these parameters are written below:

$$\dot{Ex}_{D,j} = \dot{Ex}_{F,j} - \dot{Ex}_{P,j} \quad (4.175)$$

$$y_j^* = \frac{\dot{Ex}_{D,j}}{\sum \dot{Ex}_{D,j}} \quad \text{and} \quad y_j = \frac{\dot{Ex}_{D,j}}{\sum \dot{Ex}_{F,j}} \quad (4.176)$$

$$\varepsilon_j = \frac{\dot{Ex}_{P,j}}{\dot{Ex}_{F,j}} \quad \text{and} \quad \varepsilon_t = \frac{\sum \dot{Ex}_{P,j}}{\sum \dot{Ex}_{F,j}} \quad (4.177)$$

System A-1: The fuel and product exergy analysis are explained for each component for the hybrid MCFC-turbofan aircraft engine, and the equations are listed in Table 4.14. This table presents the fuel and exergy flows, including the heat and power for the turbofan engine, followed by the fuel cell SOFC system.

Table 4.14 The fuel and product exergy equations for A-1 system components

Equipment	F-Exergy	P-Exergy
Turbofan Engine		
Compressor (FAN)	$\dot{Ex}_{FAN}^W = \dot{W}_{FAN}$	$\dot{Ex}_{a3} - \dot{Ex}_{a2}$
Splitter (S1)	\dot{Ex}_{a3}	$\dot{Ex}_{a3A} + \dot{Ex}_{a3B}$
Compressor (IPC)	$\dot{Ex}_{IPC}^W = \dot{W}_{IPC}$	$\dot{Ex}_{a4} - \dot{Ex}_{a3A}$
Compressor (HPC)	$\dot{Ex}_{HPC}^W = \dot{W}_{HPC}$	$\dot{Ex}_{a5} - \dot{Ex}_{a4}$
Splitter (S2)	\dot{Ex}_{a5}	$\dot{Ex}_{a5A} + \dot{Ex}_{a5C}$
Combustor (CC)	$\dot{Ex}_{f1} + \dot{Ex}_{a5A}$	\dot{Ex}_{a6}
Turbine (HPT)	$\dot{Ex}_{a6} - \dot{Ex}_{a7}$	$\dot{Ex}_{HPT}^W = \dot{W}_{HPT}$
Turbine (IPT)	$\dot{Ex}_{a7} - \dot{Ex}_{a8}$	$\dot{Ex}_{IPT}^W = \dot{W}_{IPT}$
Turbine (LPT)	$\dot{Ex}_{a8} - \dot{Ex}_{a9}$	$\dot{Ex}_{LPT}^W = \dot{W}_{LPT}$
Splitter (S3)	\dot{Ex}_{a9}	$\dot{Ex}_{a9A} + \dot{Ex}_{a9B}$
Mixer (MX1)	$\dot{Ex}_{a9A} + \dot{Ex}_{a9C}$	\dot{Ex}_{a9D}
Turbine exit (TE)	\dot{Ex}_{a9D}	\dot{Ex}_{a10}
Fan Nozzle (FN)	\dot{Ex}_{a3B}	$\dot{Ex}_{a12}^{PH} + \dot{Ex}_{FN}^{KE}$
Exit Nozzle (EN)	\dot{Ex}_{a10}	$\dot{Ex}_{a11}^{PH} + \dot{Ex}_{EN}^{KE}$
Fuel Cell (MCFC)		
Mixer (MX2)	$\dot{Ex}_{f2} + \dot{Ex}_{w1}$	\dot{Ex}_{b1}
Steam Reformer (SR)	\dot{Ex}_{b1}	\dot{Ex}_{b2}
Water Gas Shift (WGS)	\dot{Ex}_{b2}	\dot{Ex}_{b3}
Fuel cell (MCFC)	$\dot{Ex}_{b3} + \dot{Ex}_{a9B} - \dot{Ex}_{a9C}$	$\dot{W}_{MCFC} + \dot{Ex}_{MCFC}^L$

System A-2: The fuel and product exergy analysis are explained for each component for the hybrid SOFC-turbofan aircraft engine, and the equations are listed in Table 4.15. The

first section of the table explains the fuel and product exergy flows for the turbofan engine, while the second section displays the fuel and product exergy flows of the SOFC.

Table 4.15 The fuel and product exergy equations for A-2 system components

Component	F-Exergy	P-Exergy
Turbofan Engine		
Compressor (FAN)	$\dot{Ex}_{FAN}^W = \dot{W}_{FAN}$	$\dot{Ex}_{03} - \dot{Ex}_{02}$
Splitter (S1)	\dot{Ex}_{03}	$\dot{Ex}_{03A} + \dot{Ex}_{03B}$
Compressor (IPC)	$\dot{Ex}_{IPC}^W = \dot{W}_{IPC}$	$\dot{Ex}_{04} - \dot{Ex}_{03A}$
Compressor (HPC)	$\dot{Ex}_{HPC}^W = \dot{W}_{HPC}$	$\dot{Ex}_{05} - \dot{Ex}_{04}$
Combustor (CC)	$\dot{Ex}_{M4} + \dot{Ex}_{F1} + \dot{Ex}_{05A}$	\dot{Ex}_{06}
Splitter (S2)	\dot{Ex}_{05}	$\dot{Ex}_{05A} + \dot{Ex}_{05B} + \dot{Ex}_{05C}$
Turbine (HPT)	$\dot{Ex}_{06} - \dot{Ex}_{07}$	$\dot{Ex}_{HPT}^W = \dot{W}_{HPT}$
Turbine (IPT)	$\dot{Ex}_{07} - \dot{Ex}_{08}$	$\dot{Ex}_{IPT}^W = \dot{W}_{IPT}$
Turbine (LPT)	$\dot{Ex}_{08} - \dot{Ex}_{09}$	$\dot{Ex}_{LPT}^W = \dot{W}_{LPT}$
Turbine exit (TE)	\dot{Ex}_{09}	\dot{Ex}_{010}
Fan Nozzle (FN)	\dot{Ex}_{03B}	$\dot{Ex}_{12} + \dot{Ex}_{FN}^{KE}$
Exit Nozzle (EN)	\dot{Ex}_{010}	$\dot{Ex}_{11} + \dot{Ex}_{EN}^{KE}$
Fuel Cell (SOFC)		
Mixer (MX1)	$\dot{Ex}_{F2} + \dot{Ex}_{W1}$	\dot{Ex}_{M1}
Steam Reformer (SR)	\dot{Ex}_{M1}	\dot{Ex}_{M2}
Water Gas Shift (WGS)	\dot{Ex}_{M2}	\dot{Ex}_{M3}
Fuel cell (SOFC)	$\dot{Ex}_{M3} + \dot{Ex}_{05B} - \dot{Ex}_{M4}$	$\dot{W}_{SOFC} + \dot{Ex}_{SOFC}^L$

System R-1: The fuel and product exergy analysis are explained for each component for ICE combined with a hybrid MCFC-GT, and the equations are shown in Table 4.16. This table divides into four parts. The first part displays the fuel and product exergy of gas turbine components. The second part lists the fuel and product exergy of fuel cell systems containing the mixer (MX1), steam reformer (SR), water gas shift (WGS) and fuel cell (MCFC). The third part displays the fuel and product exergy for ICE. Lastly, the fourth part explains the fuel and product exergy of the absorption refrigeration system (ARS) containing a pump, a condenser, an evaporator, a generator, and an absorber.

Table 4.16 The fuel and product exergy equations for R-1 system components

Component	F-Exergy	P-Exergy
Gas Turbine		
Compressor (C2)	$\dot{E}x_{C2}^W = \dot{W}_{C2}$	$\dot{E}x_{B2} - \dot{E}x_{B1}$
HX-1	$\dot{E}x_{B7} - \dot{E}x_{B8}$	$\dot{E}x_{B3} - \dot{E}x_{B2}$
Combustion Chamber (CC)	$\dot{E}x_{B3} + \dot{E}x_{F3} + \dot{E}x_{CC}^Q$	$\dot{E}x_{B4}$
Turbine (T2)	$\dot{E}x_{B4} - \dot{E}x_{B5}$	$\dot{E}x_{T2}^W = \dot{W}_{T2}$
HX-2	$\dot{E}x_{B8} - \dot{E}x_{B9}$	$\dot{E}x_{B6} - \dot{E}x_{B5}$
Fuel Cell (MCFC)		
Mixer (MX1)	$\dot{E}x_{F2} + \dot{E}x_{W1}$	$\dot{E}x_{M1}$
Steam Reformer (SR)	$\dot{E}x_{M1} + \dot{E}x_{SR}^Q$	$\dot{E}x_{M2}$
Water Gas Shift (WGS)	$\dot{E}x_{M2} + \dot{E}x_{WGC}^Q$	$\dot{E}x_{M3}$
MCFC	$\dot{E}x_{M5} - \dot{E}x_{B7}$	$\dot{E}x_{M4} - \dot{E}x_{M3} + \dot{W}_{MCFC} + \dot{E}x_{MCFC}^L$
Catalytic burner (BR)	$\dot{E}x_{B6} + \dot{E}x_{E9} + \dot{E}x_{M4} + \dot{E}x_{BR}^Q$	$\dot{E}x_{M5}$
Internal Combustion Engine (ICE)		
ICE Engine	$\dot{E}x_{E1} + \dot{E}x_{F1} - \dot{E}x_{E9}$	$\dot{E}x_{ICE}^W = \dot{W}_{ICE}$
Absorption Refrigeration Cycle (ARC)		
Generator (AGN)	$\dot{E}x_{B9} - \dot{E}x_{B10} + \dot{E}x_{A3}$	$\dot{E}x_{A7} + \dot{E}x_{A4}$
Condenser (ACN)	$\dot{E}x_{A7} - \dot{E}x_{A8}$	$\dot{E}x_{CN}^Q$
Evaporator (AEV)	$\dot{E}x_{EV}^Q$	$\dot{E}x_{A9} - \dot{E}x_{A10}$
Absorber (ABS)	$\dot{E}x_{A10} + \dot{E}x_{A6}$	$\dot{E}x_{AB}^Q + \dot{E}x_{A1}$
Pump (AP)	$\dot{E}x_P^W = \dot{W}_P$	$\dot{E}x_{A2} - \dot{E}x_{A1}$
Regenerator (AHX)	$\dot{E}x_{A4} - \dot{E}x_{A5}$	$\dot{E}x_{A3} - \dot{E}x_{A2}$

System R-2: The fuel and product exergy analysis are explained for each component of hybrid SOFC-GT combined with PEMFC-AEC locomotive engine, and the equations are shown in Table 4.17. The table displays four subsystems. The first part presents the fuel and product exergy flows for the gas turbine components. The second part explains the fuel and product exergy flows of the fuel cell subsystem containing a mixer (MX2), steam reformer (SR), water gas shift (WGS), and a fuel cell (SOFC). The third part lists the fuel and product exergy of the energy recovery system involving a thermoelectric generator (TEG) and the components of the absorption refrigeration system. The Last part tabulates

the fuel and product exergy of the hydrogen production system comprising AEC, PEMFC, T2, C2 and HX2.

Table 4.17 The fuel and product exergy equations for R-2 system components

Component	F-Exergy	P-Exergy
Gas Turbine		
Compressor (C1)	$\dot{E}x_{C1}^W = \dot{W}_{C1}$	$\dot{E}x_{B2} - \dot{E}x_{B1}$
Combustion Chamber (CC)	$\dot{E}x_{B2} + \dot{E}x_{F1} + \dot{E}x_{CC}^Q$	$\dot{E}x_{B3}$
Turbine (T1)	$\dot{E}x_{B3} - \dot{E}x_{B4}$	$\dot{E}x_{T1}^W = \dot{W}_{T1}$
Splitter (SP1)	$\dot{E}x_{B4}$	$\dot{E}x_{B5} + \dot{E}x_{B6}$
Mixer (MX1)	$\dot{E}x_{M5} + \dot{E}x_{B6}$	$\dot{E}x_{B7}$
Fuel Cell (SOFC)		
Mixer (MX2)	$\dot{E}x_{F2} + \dot{E}x_{W1}$	$\dot{E}x_{M1}$
Steam Reformer (SR)	$\dot{E}x_{M1} + \dot{E}x_{SR}^Q$	$\dot{E}x_{M2}$
Water Gas Shift (WGS)	$\dot{E}x_{M2} + \dot{E}x_{WGS}^Q$	$\dot{E}x_{M3}$
SOFC	$\dot{E}x_{M3} + \dot{E}x_{B5} - \dot{E}x_{M4} + \dot{E}x_{SOFC}^Q$	$\dot{E}x_{SOFC}^W = \dot{W}_{SOFC}$
Afterburner (BR)	$\dot{E}x_{M4} + \dot{E}x_{BR}^Q$	$\dot{E}x_{M5}$
Energy Recovery		
Thermoelectric generator (TEG)	$\dot{E}x_{B7} - \dot{E}x_{B8}$	$\dot{E}x_{TEG}^W = \dot{W}_{TEG}$
Generator (AGN)	$\dot{E}x_{R3} + \dot{E}x_{AGN}^Q$	$\dot{E}x_{R4} + \dot{E}x_{R7}$
Condenser (ACN)	$\dot{E}x_{R7} - \dot{E}x_{R8}$	$\dot{E}x_{ACN}^Q$
Expansion valve (AEX1)	$\dot{E}x_{R8}$	$\dot{E}x_{R9}$
Evaporator (AEV)	$\dot{E}x_{AEV}^Q$	$\dot{E}x_{R10} - \dot{E}x_{R9}$
Absorber (ABS)	$\dot{E}x_{R10} + \dot{E}x_{R6}$	$\dot{E}x_{ABS}^Q + \dot{E}x_{R1}$
Pump (AP)	$\dot{E}x_{AP}^W = \dot{W}_{AP}$	$\dot{E}x_{R2} - \dot{E}x_{R1}$
Regenerator (AHX)	$\dot{E}x_{R4} - \dot{E}x_{R5}$	$\dot{E}x_{R3} - \dot{E}x_{R2}$
Expansion valve (AEX2)	$\dot{E}x_{R6}$	$\dot{E}x_{R5}$
Hydrogen Production (PEMFC-AEC)		
Ammonia electrolysis cell (AEC)	$\dot{E}x_{AEC}^W + \dot{E}x_{N1} + \dot{E}x_{N2} - \dot{E}x_{AEC}^Q$	$\dot{E}x_{N7} + \dot{E}x_{H1} + \dot{E}x_{H2}$
PEMFC	$\dot{E}x_{A3} + \dot{E}x_{H1} - \dot{E}x_{A4} + \dot{E}x_{PEMFC}^Q$	$\dot{E}x_{PEMFC}^W = \dot{W}_{PEMFC}$
Turbine (T2)	$\dot{E}x_{N7} - \dot{E}x_{N8}$	$\dot{E}x_{T2}^W = \dot{W}_{T2}$
Compressor (C2)	$\dot{E}x_{C2}^W = \dot{W}_{C2}$	$\dot{E}x_{A2} - \dot{E}x_{A1}$
Heat exchanger (HX2)	$\dot{E}x_{A3} - \dot{E}x_{A2}$	$\dot{E}x_{A5} - \dot{E}x_{A4}$

System R-3: The fuel and product exergy analysis are explained for each component of the hybrid SOFC-PEMFC-GT locomotive engine, and the equations are presented in Table 4.18. The presented table contains three parts. The first part displays the fuel and product exergy flows for the gas turbine engine, the second part lists the fuel and product exergy flows for the fuel cell subsystem, and the third part displays the fuel and product exergy flows for the components of the energy recovery subsystem.

Table 4.18 The fuel and product exergy for R-3 system components

Component	F-Exergy	P-Exergy
Gas Turbine		
Compressor (C1)	$\dot{E}x_{C1}^W = \dot{W}_{C1}$	$\dot{E}x_{A2} - \dot{E}x_{A1}$
Intercooler (IC)	$\dot{E}x_{A2} - \dot{E}x_{IC}^Q$	$\dot{E}x_{A3}$
Splitter (S1)	$\dot{E}x_{A3}$	$\dot{E}x_{B1} + \dot{E}x_{A4}$
Compressor (C2)	$\dot{E}x_{C2}^W = \dot{W}_{C2}$	$\dot{E}x_{A5} - \dot{E}x_{A4}$
Combustion Chamber (CC)	$\dot{E}x_{A5} + \dot{E}x_{F1} + \dot{E}x_{CC}^Q$	$\dot{E}x_{A7}$
Turbine (T2)	$\dot{E}x_{A7} - \dot{E}x_{A8}$	$\dot{E}x_{T2}^W = \dot{W}_{T2}$
Splitter (S2)	$\dot{E}x_{A8}$	$\dot{E}x_{B2} + \dot{E}x_{A9}$
Turbine (T1)	$\dot{E}x_{A10} - \dot{E}x_{A11}$	$\dot{E}x_{T1}^W = \dot{W}_{T1}$
PEMFC	$\dot{E}x_{B1} + \dot{E}x_{H1} - \dot{E}x_{H2} + \dot{E}x_{PEMFC}^Q$	$\dot{E}x_{PEMFC}^W = \dot{W}_{PEMFC}$
Turbine (T3)	$\dot{E}x_{H2} - \dot{E}x_{H3}$	$\dot{E}x_{T3}^W = \dot{W}_{T3}$
Thermoelectric generator (TEG1)	$\dot{E}x_{H3} - \dot{E}x_{H4}$	$\dot{E}x_{TEG1}^W = \dot{W}_{TEG1}$
Fuel Cell (SOFC)		
Mixer (MX1)	$\dot{E}x_{F2} + \dot{E}x_{W1}$	$\dot{E}x_{D1}$
Steam Reformer (SR)	$\dot{E}x_{D1} + \dot{E}x_{SR}^Q$	$\dot{E}x_{D2}$
Water Gas Shift (WGS)	$\dot{E}x_{D2} + \dot{E}x_{WGS}^Q$	$\dot{E}x_{D3}$
SOFC	$\dot{E}x_{D3} + \dot{E}x_{B2} - \dot{E}x_{D4} + \dot{E}x_{SOFC}^Q$	$\dot{E}x_{SOFC}^W = \dot{W}_{SOFC}$
Afterburner (BR)	$\dot{E}x_{D4} + \dot{E}x_{A9}$	$\dot{E}x_{A10}$
Energy Recovery		
Thermoelectric generator (TEG2)	$\dot{E}x_{A11} - \dot{E}x_{A12}$	$\dot{E}x_{TEG2}^W = \dot{W}_{TEG2}$
Generator (AGN)	$\dot{E}x_{R3} + \dot{E}x_{AGN}^Q$	$\dot{E}x_{R4} + \dot{E}x_{R7}$
Condenser (ACN)	$\dot{E}x_{R7} - \dot{E}x_{R8}$	$\dot{E}x_{ACN}^Q$
Heat exchanger (AHX1)	$\dot{E}x_{R4} - \dot{E}x_{R5}$	$\dot{E}x_{R3} - \dot{E}x_{R2}$
Expansion valve (AEX1)	$\dot{E}x_{R8}$	$\dot{E}x_{R9}$
Evaporator (AEV)	$\dot{E}x_{AEV}^Q$	$\dot{E}x_{R10} - \dot{E}x_{R9}$
Absorber (ABS)	$\dot{E}x_{R10} + \dot{E}x_{R6}$	$\dot{E}x_{ABS}^Q + \dot{E}x_{R1}$
Pump (AP)	$\dot{E}x_{AP}^W = \dot{W}_{AP}$	$\dot{E}x_{R2} - \dot{E}x_{R1}$
Regenerator (AHX2)	$\dot{E}x_{R4} - \dot{E}x_{R5}$	$\dot{E}x_{R3} - \dot{E}x_{R2}$
Expansion valve (AEX2)	$\dot{E}x_{R6}$	$\dot{E}x_{R5}$

System M-1: The fuel and product exergy analysis are explained for each component of the hybrid combined marine engine, and the equations are listed in Table 4.19. The table contains three subsystems. The first part explains the fuel and product exergy flows for the gas turbine engine, the second part displays the fuel and product exergy flows for the SOFC fuel cell subsystem, and the third part contains the fuel and product exergy flows for the ICE engine.

Table 4.19 The fuel and product exergy for M-1 system components

Component	F-Exergy	P-Exergy
Gas Turbine		
Compressor (C2)	$\dot{E}x_{C2}^W = \dot{W}_{C2}$	$\dot{E}x_{Y2} - \dot{E}x_{Y1}$
Intercooler (IC)	$\dot{E}x_{Y2} - \dot{E}x_{IC}^Q$	$\dot{E}x_{Y3}$
Compressor (C3)	$\dot{E}x_{C3}^W = \dot{W}_{C3}$	$\dot{E}x_{Y4} - \dot{E}x_{Y3}$
Combustion chamber (CC)	$\dot{E}x_{Y4} + \dot{E}x_{MF2} + \dot{E}x_{CC}^Q$	$\dot{E}x_{Y5}$
Turbine (T3)	$\dot{E}x_{Y5} - \dot{E}x_{Y6}$	$\dot{E}x_{T3}^W = \dot{W}_{T3}$
Splitter (SP1)	$\dot{E}x_{Y6}$	$\dot{E}x_{Y7} + \dot{E}x_{Y8}$
Turbine (T2)	$\dot{E}x_{Y10} - \dot{E}x_{Y11}$	$\dot{E}x_{T2}^W = \dot{W}_{T2}$
Thermoelectric generator (TEG2)	$\dot{E}x_{Y11} - \dot{E}x_{Y12}$	$\dot{E}x_{TEG2}^W = \dot{W}_{TEG2}$
Fuel Cell (SOFC)		
Mixer (MX1)	$\dot{E}x_{MF3} + \dot{E}x_{W1}$	$\dot{E}x_{Z1}$
Steam reformer (SR)	$\dot{E}x_{Z1} + \dot{E}x_{SR}^Q$	$\dot{E}x_{Z2}$
Water gas shift (WGS)	$\dot{E}x_{Z2} + \dot{E}x_{WGS}^Q$	$\dot{E}x_{Z3}$
SOFC	$\dot{E}x_{Z3} + \dot{E}x_{Y7} - \dot{E}x_{Z4} + \dot{E}x_{SOFC}^Q$	$\dot{E}x_{SOFC}^W = \dot{W}_{SOFC}$
Mixer (MX2)	$\dot{E}x_{Z4} + \dot{E}x_{Y8}$	$\dot{E}x_{Y9}$
Afterburner (BR)	$\dot{E}x_{Y9} + \dot{E}x_{BR}^Q$	$\dot{E}x_{Y10}$
Internal Combustion Engine (ICE)		
Internal combustion engine (ICE)	$\dot{E}x_{X1} + \dot{E}x_{MF1} - \dot{E}x_{X10} - \dot{E}x_{AC}^Q - \dot{E}x_{R1}^Q$	$\dot{E}x_{ICE}^W = \dot{W}_{ICE}$
Thermoelectric generator (TEG1)	$\dot{E}x_{X10} - \dot{E}x_{X11}$	$\dot{E}x_{TEG1}^W = \dot{W}_{TEG1}$

System M-2: The fuel and product exergy analysis are explained for each component of the hybrid compound cycles (SRC-SOFC-GT) marine engine, and the equations are listed in Table 4.20. The table contains fuel and product exergy flows for three subsystems: a steam Rankine cycle (SRC), a gas Bryton cycle (GBC), and a fuel cell subsystem of the SOFC package.

Table 4.20 The fuel and product exergy for M-2 system components

Component	F-Exergy	P-Exergy
Steam Rankine Cycle (SRC)		
HP-ST1	$\dot{E}x_{A7} - \dot{E}x_{A8}$	$\dot{E}x_{HPST1}^W = \dot{W}_{HPST1}$
IP-ST2	$\dot{E}x_{A9} - \dot{E}x_{A11E}$	$\dot{E}x_{IPST2}^W = \dot{W}_{IPSP2}$
LP-ST3	$\dot{E}x_{A11T} - \dot{E}x_{A12} - \dot{E}x_{A13} - \dot{E}x_{A10}$	$\dot{E}x_{LPST3}^W = \dot{W}_{LPST3}$
CN	$\dot{E}x_{A22} + \dot{E}x_{A10} - \dot{E}x_{A1}$	$\dot{E}x_{CN}^Q$
P1	$\dot{E}x_{P1}^W = \dot{W}_{P1}$	$\dot{E}x_{A2} - \dot{E}x_{A1}$
P2	$\dot{E}x_{P2}^W = \dot{W}_{P2}$	$\dot{E}x_{A6} - \dot{E}x_{A5}$
CFH1	$\dot{E}x_{A13} + \dot{E}x_{A18} - \dot{E}x_{A20}$	$\dot{E}x_{A3} - \dot{E}x_{A2}$
CFH2	$\dot{E}x_{A12} + \dot{E}x_{A15} - \dot{E}x_{A17}$	$\dot{E}x_{A4} - \dot{E}x_{A3}$
CFH3	$\dot{E}x_{A11} - \dot{E}x_{A14}$	$\dot{E}x_{A5} - \dot{E}x_{A4}$
EX1	$\dot{E}x_{A14}$	$\dot{E}x_{A15}$
EX2	$\dot{E}x_{A17}$	$\dot{E}x_{A18}$
EX3	$\dot{E}x_{A20}$	$\dot{E}x_{A21}$
BR-BL	$\dot{E}x_{G12} + \dot{E}x_{B1} + \dot{E}x_{F1} + \dot{E}x_{BRBL}^Q$	$\dot{E}x_{B2}$
HX-BL	$\dot{E}x_{B2} - \dot{E}x_{B3}$	$\dot{E}x_{A7} - \dot{E}x_{A6}$
HX-RH	$\dot{E}x_{B3} - \dot{E}x_{B4}$	$\dot{E}x_{A9} - \dot{E}x_{A8}$
DSWR	$\dot{E}x_{B4} - \dot{E}x_{B5} + \dot{E}x_{SW1} - \dot{E}x_{SW4}$	$\dot{E}x_{FW16} + \dot{E}x_{SL5}$
Gas Brayton Cycle (GBC)		
LP-C1	$\dot{E}x_{LPC1}^W = \dot{W}_{LPC1}$	$\dot{E}x_{G2} - \dot{E}x_{G1}$
IC	$\dot{E}x_{G2} - \dot{E}x_{IC}^Q$	$\dot{E}x_{G3}$
HP-C2	$\dot{E}x_{HPC2}^W = \dot{W}_{HPC2}$	$\dot{E}x_{G4} - \dot{E}x_{G3}$
GTSP	$\dot{E}x_{G4}$	$\dot{E}x_{G5} + \dot{E}x_{G6}$
CC	$\dot{E}x_{M4} + \dot{E}x_{F2} + \dot{E}x_{G6} + \dot{E}x_{CC}^Q$	$\dot{E}x_{G7}$
GTHX	$\dot{E}x_{G7} - \dot{E}x_{G8}$	$\dot{E}x_{G11} - \dot{E}x_{G10}$
HP-T1	$\dot{E}x_{G8} - \dot{E}x_{G9}$	$\dot{E}x_{HPT1}^W = \dot{W}_{HPT1}$
LP-T2	$\dot{E}x_{G10} - \dot{E}x_{G11}$	$\dot{E}x_{LPT2}^W = \dot{W}_{LPT2}$
P-T3	$\dot{E}x_{G11} - \dot{E}x_{G12}$	$\dot{E}x_{PT3}^W = \dot{W}_{PT3}$
Fuel Cell (SOFC)		
GTMX	$\dot{E}x_{F3} + \dot{E}x_{W1}$	$\dot{E}x_{M1}$
SR	$\dot{E}x_{M1} + \dot{E}x_{SR}^Q$	$\dot{E}x_{M2}$
WGS	$\dot{E}x_{M2} + \dot{E}x_{WGS}^Q$	$\dot{E}x_{M3}$
SOFC	$\dot{E}x_{G5} + \dot{E}x_{M3} - \dot{E}x_{M4} - \dot{E}x_{SOFC}^Q$	$\dot{E}x_{SOFC}^W = \dot{W}_{SOFC}$

System M-3: The fuel and product exergy analysis are explained for each component of the hybrid gas turbine combined with binary systems marine engine, and the equations are shown in Table 4.21.

Table 4.21 The fuel and product exergy for M-3 system components

Component	F-Exergy	P-Exergy
Gas Brayton Cycle (GBC)		
HPC1	$\dot{E}x_{HPC1}^W = \dot{W}_{HPC1}$	$\dot{E}x_{G2} - \dot{E}x_{G1}$
GTHX	$\dot{E}x_{G3} - \dot{E}x_{G2}$	$\dot{E}x_{G9} - \dot{E}x_{G8}$
SP	$\dot{E}x_{G3}$	$\dot{E}x_{G4} + \dot{E}x_{G5}$
CC	$\dot{E}x_{G5} + \dot{E}x_{FC7} + \dot{E}x_{F1} + \dot{E}x_{CC}^Q$	$\dot{E}x_{G6}$
HPT1	$\dot{E}x_{G6} - \dot{E}x_{G7}$	$\dot{E}x_{HPT1}^W = \dot{W}_{HPT1}$
LPT2	$\dot{E}x_{G7} - \dot{E}x_{G8}$	$\dot{E}x_{LPT2}^W = \dot{W}_{LPT2}$
Fuel Cell (SOFC)		
MX	$\dot{E}x_{F2} + \dot{E}x_{S1}$	$\dot{E}x_{FC1}$
SR	$\dot{E}x_{FC1} + \dot{E}x_{SR}^Q$	$\dot{E}x_{FC2}$
WGS	$\dot{E}x_{FC2} + \dot{E}x_{WGS}^Q$	$\dot{E}x_{FC3}$
SOFC	$\dot{E}x_{G4} + \dot{E}x_{FC3} - \dot{E}x_{FC7} + \dot{E}x_{SOFC}^Q$	$\dot{E}x_{SOFC}^W = \dot{W}_{SOFC}$
Organic Rankine Cycles (TORC and BORC)		
CN1	$\dot{E}x_{G9} - \dot{E}x_{G10}$	$\dot{E}x_{TR3} - \dot{E}x_{TR2}$
CN2	$\dot{E}x_{G10} - \dot{E}x_{G11}$	$\dot{E}x_{LR4} - \dot{E}x_{LR3}$
T3	$\dot{E}x_{TR3} - \dot{E}x_{TR4}$	$\dot{E}x_{T3}^W = \dot{W}_{T3}$
T4	$\dot{E}x_{LR4} - \dot{E}x_{LR5}$	$\dot{E}x_{T4}^W = \dot{W}_{T4}$
T5	$\dot{E}x_{LR6} - \dot{E}x_{LR7}$	$\dot{E}x_{T5}^W = \dot{W}_{T5}$
P1	$\dot{E}x_{P1}^W = \dot{W}_{P1}$	$\dot{E}x_{TR2} - \dot{E}x_{TR1}$
P2	$\dot{E}x_{P2}^W = \dot{W}_{P2}$	$\dot{E}x_{LR2} - \dot{E}x_{LR1}$
EV11	$\dot{E}x_{LR2} - \dot{E}x_{LR3}$	$\dot{E}x_{TR5} - \dot{E}x_{TR4}$
EV12	$\dot{E}x_{LR5} - \dot{E}x_{LR6} + \dot{E}x_{LGN1} - \dot{E}x_{LNG2}$	$\dot{E}x_{TR1} - \dot{E}x_{TR5}$
EV2	$\dot{E}x_{LNG2} - \dot{E}x_{LNG3}$	$\dot{E}x_{LR1} - \dot{E}x_{LR7}$

4.5.3 Exergoeconomic Analysis (Economic Assessment)

The exergoeconomic analysis is employed using the specific exergy costing (SPECOC) that can be performed by identification of exergy streams, fuel and product, and writing cost equations [184]. The exergy costing is the cost rate correlated with each exergy stream, work exergy, and thermal exergy crossing the boundary of the system. Therefore, the cost rate \dot{C} of exergoeconomic analysis of the system is written as follows:

$$\dot{C}_{in} = c_{in} \dot{E}x_{in} \quad (4.178)$$

$$\dot{C}_{out} = c_{out} \dot{E}x_{out} \quad (4.179)$$

$$\dot{C}_W = c_W \dot{W} \quad (4.180)$$

$$\dot{C}_Q = c_Q \dot{E}x_Q \quad (4.181)$$

where \dot{C} and c is the exergoeconomic rate and specific exergy cost. The cost balance is described as below:

$$\sum \dot{C}_{out,j} + \dot{C}_{W,j} = \sum \dot{C}_{in,j} + \dot{C}_{Q,j} + \dot{Z}_j^T \quad (4.182)$$

$$\dot{Z}_j^T = \dot{Z}_j^{CI} + \dot{Z}_j^{OM} = \dot{Z}_j^{CI} \times \varphi = \frac{Z_j \times CRF \times \varphi_{CO}}{\tau} \quad (4.183)$$

where \dot{Z}_j^T is the total levelized cost rate combined with the capital cost rate (\dot{Z}_j^{CI}) and operating-maintenance cost rate (\dot{Z}_j^{OM}) for each component (j). φ_{CO} denotes operation-maintenance factor. The CRF is the capital recovery factor and is defined in the following equation:

$$CRF = \frac{i(1+i)^n}{(1+i)^n - 1} \quad (4.184)$$

where i , and n are the real interest rate and lifetime in years. The i is described as $1 + i = (1 + i_n)/(1 + r)$, where i_n and r are the nominal interest rate and inflation rate. The Z_j is a component purchase equipment cost in May-2022. It is estimated by a component cost equation [185,186] at its reference year and normalized by the cost index (CEPCI), as below:

$$Z_j = C_{ref} \frac{CEPCI_{May-2022}}{CEPCI_{ref}} \quad (4.185)$$

Due to the total number of exergy streams exiting the component being considered, there are an equal number of unknowns and only one equation, which is the exergy cost balance equation. Thus, a sufficient number of auxiliary equations should be formulated with the aid of the F and P principles of the SPECO method [184]. The F principle states the specific cost (cost per unit exergy) associated with the removal of exergy from a fuel stream supplied to the same stream in the upstream component, while the P principle refers to that of product exergy at the same average cost. Since each exiting exergy stream is associated either with fuel or with a product, the number of exiting streams (n) equals the total number of exiting fuel streams and product streams. Thus, the F and P principles provide $(n - 1)$ auxiliary equations. The average unit cost of fuel, the average unit cost of

a product, the cost rate of exergy destruction, and the cost rate of exergy loss can be mathematically expressed as follows:

$$c_{F,j} = \frac{\dot{C}_{F,j}}{\dot{E}x_{F,j}} \quad (4.186)$$

$$c_{P,j} = \frac{\dot{C}_{P,j}}{\dot{E}x_{P,j}} \quad (4.187)$$

$$\dot{C}_{D,j} = c_{F,j} \dot{E}x_{D,j} \quad (4.188)$$

$$\dot{C}_{L,j} = c_{F,j} \dot{E}x_{L,j} \quad (4.189)$$

$$\dot{C}_{P,j} = \dot{C}_{F,j} + \dot{Z}_j^T \quad (4.190)$$

where the subscripts F, P, D, and L are correlated with fuel, product, destruction, and loss, respectively. The total specific fuel and product exergetic cost ($c_{F,t}$ and $c_{P,t}$) are described below:

$$c_{F,t} = \frac{\sum \dot{C}_{F,j}}{\sum \dot{E}x_{F,j}} \quad (4.191)$$

$$c_{P,t} = \frac{\sum \dot{C}_{P,j}}{\sum \dot{E}x_{P,j}} \quad (4.192)$$

In an exergoeconomic evaluation, the relative cost difference, r_j , is the difference between the average cost per exergy unit of product and fuel divided by the specific fuel exergy cost. The exergoeconomic factor, f_j , is used in making key decisions concerning the improvement of the system, can be defined respectively as follows:

$$r_j = \frac{c_{P,j} - c_{F,j}}{c_{F,j}} = \frac{c_{F,j} \dot{E}x_{D,j} + \dot{Z}_j^T}{c_{F,j} \dot{E}x_{P,j}} \quad (4.193)$$

$$f_j = \frac{\dot{Z}_j^T}{\dot{Z}_j^T + \dot{C}_{D,j}} = \frac{\dot{Z}_j^T}{\dot{Z}_j^T + c_{F,j} \dot{E}x_{D,j}} \quad (4.194)$$

System A-1:

The cost balance equations and auxiliary equations are explained for each component of the hybrid MCFC-turbofan aircraft engine, and the equations are listed in Table 4.22. This table displays the cost balance equations and auxiliary equations for two subsystems: the turbofan engine, containing compressors, combustors, turbines, and nozzles, and the fuel

cell (MCFC) subsystem, containing MCFC, steam reforming (SR) and water gas shift (WGS).

Table 4.22 The exergoeconomic balance equations for equipment of A-1 system

Equipment	Cost Balance Equations	Auxiliary Equations
Turbofan Engine		
Compressor (FAN)	$\dot{C}_{a2} + \dot{C}_{FAN}^W + \dot{Z}_{FAN} = \dot{C}_{a3}$	$c_{a2} = 0 \text{ \& } c_{e,FAN} = c_{e,LPT}$
Splitter (S1)	$\dot{C}_{a3} = \dot{C}_{a3A} + \dot{C}_{a3B}$	$c_{a3} = c_{a3A} = c_{a3B}$
Compressor (IPC)	$\dot{C}_{a3A} + \dot{C}_{IPC}^W + \dot{Z}_{IPC} = \dot{C}_{a4}$	$c_{e,IPC} = c_{e,IPT}$
Compressor (HPC)	$\dot{C}_{a4} + \dot{C}_{HPC}^W + \dot{Z}_{HPC} = \dot{C}_{a5}$	$c_{e,HPC} = c_{e,HPT}$
Splitter (S2)	$\dot{C}_{a5} = \dot{C}_{a5A} + \dot{C}_{a5C}$	$c_{a5} = c_{a5A} = c_{a5C}$
Combustor (CC)	$\dot{C}_{f1} + \dot{C}_{05A} + \dot{Z}_{CC} = \dot{C}_{a6}$	$c_{f1} = \text{fuel cost}$
Turbine (HPT)	$\dot{C}_{a6} - \dot{C}_{a7} + \dot{Z}_{HPT} = \dot{C}_{HPT}^W$	$c_{a7} = c_{a6}$
Turbine (IPT)	$\dot{C}_{a7} - \dot{C}_{a8} + \dot{Z}_{IPT} = \dot{C}_{IPT}^W$	$c_{a8} = c_{a6}$
Turbine (LPT)	$\dot{C}_{a8} - \dot{C}_{a9} + \dot{Z}_{LPT} = \dot{C}_{LPT}^W$	$c_{a8} = c_{a6}$
Splitter (S3)	$\dot{C}_{a9} = \dot{C}_{a9A} + \dot{C}_{a9B}$	$c_{a9} = c_{a9A} = c_{a9B}$
Mixer (MX1)	$\dot{C}_{a9A} + \dot{C}_{a9C} + \dot{Z}_{MX1} = \dot{C}_{a9D}$	$\dot{Z}_{MX1}=0, c_{a9A} = c_{a9C} = c_{a9D}$
Turbine exit (TE)	$\dot{C}_{a9D} + \dot{Z}_{TE} = \dot{C}_{a10}$	$\dot{Z}_{TE}=0$
Fan Nozzle (FN)	$\dot{C}_{a3B} + \dot{Z}_{FN} = \dot{C}_{a12}$	$\dot{Z}_{FN}=0$
Exit Nozzle (EN)	$\dot{C}_{a10} + \dot{Z}_{EN} = \dot{C}_{a11}$	$\dot{Z}_{EN}=0$
Fuel Cell (MCFC)		
Mixer (MX2)	$\dot{C}_{f2} + \dot{C}_{w1} + \dot{Z}_{MX2} = \dot{C}_{b1}$	$\dot{Z}_{MX2}=0, c_{w1} = 0$
Steam Reformer (SR)	$\dot{C}_{b1} + \dot{Z}_{SR} = \dot{C}_{b2}$	
Water Gas Shift (WGS)	$\dot{C}_{b2} + \dot{Z}_{WGS} = \dot{C}_{b3}$	
Fuel cell (MCFC)	$\dot{C}_{b3} + \dot{C}_{a9B} - \dot{C}_{a9C} + \dot{Z}_{MCFC}$ $= \dot{C}_{MCFC}^W + \dot{C}_{MCFC}^L$	$c_{e,MCFC} = \frac{\dot{C}_{b3} + \dot{C}_{a9B} - \dot{C}_{a9C}}{\dot{E}x_{b3} + \dot{E}x_{a9B} - \dot{E}x_{a9C}}$ $c_{l,MCFC} = 2 \text{ \$/GJ (assumed)}$

System A-2:

The cost balance equations and auxiliary equations are explained for each component of the hybrid SOFC-turbofan aircraft engine, and the equations are listed in Table 4.23. This table lists the cost balance equations and auxiliary equations for two main subsystems: the turbofan engine, containing compressors such as FAN, IPC, and HPC; combustors like CC, turbines like HPT, IPT, LPT, and nozzles as FN and EN; and the SOFC subsystem,

containing a mixer (MX1), a fuel cell of SOFC, steam reformer (SR), and a water gas shift reactor (WGS).

Table 4.23 The exergoeconomic balance equations for A-2 system components.

Component	Cost Balance Equation	Auxiliary Equations
Turbofan		
Compressor (FAN)	$\dot{C}_{02} + \dot{C}_{FAN}^W + \dot{Z}_{FAN} = \dot{C}_{03}$	$c_{02} = 0 \text{ \& } c_{e,FAN} = c_{e,LPT}$
Splitter (S1)	$\dot{C}_{03} = \dot{C}_{03A} + \dot{C}_{03B}$	$c_{03} = c_{03A} = c_{03B}$
Compressor (IPC)	$\dot{C}_{03A} + \dot{C}_{IPC}^W + \dot{Z}_{IPC} = \dot{C}_{04}$	$c_{e,IPC} = c_{e,IPT}$
Compressor (HPC)	$\dot{C}_{04} + \dot{C}_{HPC}^W + \dot{Z}_{HPC} = \dot{C}_{05}$	$c_{e,HPC} = c_{e,HPT}$
Splitter (S2)	$\dot{C}_{05} = \dot{C}_{05A} + \dot{C}_{05B} + \dot{C}_{05C}$	$c_{05} = c_{05A} = c_{05B} = c_{05C}$
Combustor (CC)	$\dot{C}_{M4} + \dot{C}_{F1} + \dot{C}_{05A} + \dot{Z}_{CC} = \dot{C}_{06}$	$c_{F1} = \text{fuel cost}$
Turbine (HPT)	$\dot{C}_{06} - \dot{C}_{07} + \dot{Z}_{HPT} = \dot{C}_{HPT}^W$	$c_{07} = c_{06}$
Turbine (IPT)	$\dot{C}_{07} - \dot{C}_{08} + \dot{Z}_{IPT} = \dot{C}_{IPT}^W$	$c_{08} = c_{06}$
Turbine (LPT)	$\dot{C}_{08} - \dot{C}_{09} + \dot{Z}_{LPT} = \dot{C}_{LPT}^W$	$c_{08} = c_{06}$
Turbine exit (TE)	$\dot{C}_{09} + \dot{Z}_{TE} = \dot{C}_{010}$	$\dot{Z}_{TE}=0$
Fan Nozzle (FN)	$\dot{C}_{03B} + \dot{Z}_{FN} = \dot{C}_{12}$	$\dot{Z}_{FN}=0$
Exit Nozzle (EN)	$\dot{C}_{010} + \dot{Z}_{EN} = \dot{C}_{11}$	$\dot{Z}_{EN}=0$
Fuel Cell (SOFC)		
Mixer (MX1)	$\dot{C}_{F2} + \dot{C}_{W1} + \dot{Z}_{MX1} = \dot{C}_{M1}$	$\dot{Z}_{MX1}=0, c_{W1} = 0$
Steam Reformer (SR)	$\dot{C}_{M1} + \dot{Z}_{SR} = \dot{C}_{M2}$	
Water Gas Shift (WGS)	$\dot{C}_{M2} + \dot{Z}_{WGS} = \dot{C}_{M3}$	
Fuel cell (SOFC)	$\dot{C}_{M3} + \dot{C}_{05B} - \dot{C}_{M4} + \dot{Z}_{SOFC}$ $= \dot{C}_{SOFC}^W$ $+ \dot{C}_{SOFC}^L$	$c_{e,SOFC} = \frac{\dot{C}_{M3} + \dot{C}_{05B} - \dot{C}_{M4}}{\dot{E}x_{M3} + \dot{E}x_{05B} - \dot{E}x_{M4}}$ $c_{l,SOFC} = 2 \text{ \$/GJ (assumed)}$

System R-1:

The cost balance equations and auxiliary equations are explained for each component of a hybrid combined locomotive engine, and the equations are listed in Table 4.24. This table displays the cost balance equations and auxiliary equations for four subsystems. The first part contains the exergoeconomic balance equations for the gas turbine engine, the second part displays the exergoeconomic balance equations for the MCFC fuel cell, the third part lists the exergoeconomic balance equations for the internal combustion engine, and the last part explains exergoeconomic balance equations for the absorption refrigeration system.

Table 4.24 The exergoeconomic balance equations for R-1 system components.

Component	Cost Balance Equation	Auxiliary Equations
Gas Turbine		
Compressor (C2)	$\dot{C}_{B1} + \dot{C}_{C2}^W + \dot{Z}_{C1} = \dot{C}_{B2}$	$c_{B1} = 0$
HX-1	$\dot{C}_{B7} - \dot{C}_{B8} + \dot{Z}_{HX1} = \dot{C}_{B3} - \dot{C}_{B2}$	$\frac{\dot{C}_{B2}}{\dot{E}x_{B2}} = \frac{\dot{C}_{B3}}{\dot{E}x_{B3}}$
Combustion Chamber (CC)	$\dot{C}_{B3} + \dot{C}_{F3} + \dot{C}_{CC}^Q + \dot{Z}_{CC} = \dot{C}_{B4}$	$c_{F3} = \text{fuel cost}$
Turbine (T2)	$\dot{C}_{B4} - \dot{C}_{B5} + \dot{Z}_{T2} = \dot{C}_{T2}^W$	$c_{B5} = c_{B4}$
HX-2	$\dot{C}_{B8} - \dot{C}_{B9} + \dot{Z}_{HX2} = \dot{C}_{B6} - \dot{C}_{B5}$	$\frac{\dot{C}_{B6}}{\dot{E}x_{B6}} = \frac{\dot{C}_{B5}}{\dot{E}x_{B5}}$
Fuel Cell (MCFC)		
Mixer (MX1)	$\dot{C}_{F2} + \dot{C}_{W1} + \dot{Z}_{MX1} = \dot{C}_{M1}$	$\dot{Z}_{MX1}=0, c_{W1} = 0$
Steam Reformer (SR)	$\dot{C}_{M1} + \dot{C}_{SR}^Q + \dot{Z}_{SR} = \dot{C}_{M2}$	
Water Gas Shift (WGS)	$\dot{C}_{M2} + \dot{Z}_{WGS} + \dot{C}_{WGS}^Q = \dot{C}_{M3}$	
Fuel cell (MCFC)	$\dot{C}_{M5} - \dot{C}_{B7} + \dot{Z}_{MCFC} = \dot{C}_{MCFC}^W + \dot{C}_{M4}$ $-\dot{C}_{M3} + \dot{C}_{MCFC}^L$	$c_{B7} = c_{M4}$
Catalytic burner (BR)	$\dot{C}_{B6} + \dot{C}_{E9} + \dot{C}_{M4} + \dot{Z}_{BR} + \dot{C}_{BR}^Q = \dot{C}_{M5}$	
Internal Combustion Engine (ICE)		
ICE Engine	$\dot{C}_{E1} + \dot{C}_{F1} - \dot{C}_{E9} + \dot{Z}_{ICE} = \dot{C}_{ICE}^W$	$c_{F1} = \text{fuel cost}, c_{E1} = 0$
Absorption Refrigeration Cycle (ARS)		
Generator (AGN)	$\dot{C}_{B9} - \dot{C}_{B10} + \dot{C}_{A3} + \dot{Z}_{AGN} = \dot{C}_{A7} + \dot{C}_{A4}$	$c_{A4} = 0, c_{B9} = c_{B10}$
Condenser (ACN)	$\dot{C}_{A7} - \dot{C}_{A8} + \dot{Z}_{ACN} = \dot{C}_{CN}^Q$	$c_{A7} = c_{A8}$
Evaporator (AEV)	$\dot{C}_{EV}^Q + \dot{Z}_{AEV} = \dot{C}_{A9} - \dot{C}_{A10}$	$c_{A9} = c_{A10}$
Absorber (ABS)	$\dot{C}_{A10} + \dot{C}_{A6} + \dot{Z}_{ABS} = \dot{C}_{A1} + \dot{C}_{AB}^Q$	
Pump (AP)	$\dot{C}_P^W + \dot{Z}_{AP} = \dot{C}_{A2} - \dot{C}_{A1}$	
Regenerator (AHX)	$\dot{C}_{A4} - \dot{C}_{A5} + \dot{Z}_{AHX} = \dot{C}_{A3} - \dot{C}_{A2}$	$c_{A4} = c_{A5}$

System R-2:

The cost balance equations and auxiliary equations are explained for each component of the hybrid SOFC-GT combined with PEMFC-AEC locomotive engine, and the equations are presented in Table 4.25. The table displays the cost balance equations and auxiliary equations for four subsystems like a gas turbine, SOFC, energy recovery, and hydrogen production.

Table 4.25 The exergoeconomic balance equations for R-2 system components.

Component	Cost Balance Equation	Auxiliary Equations
Gas Turbine		
Compressor (C1)	$\dot{C}_{B1} + \dot{C}_{C1}^W + \dot{Z}_{C1} = \dot{C}_{B2}$	$c_{B1} = 0$
Combustion Chamber (CC)	$\dot{C}_{B2} + \dot{C}_{F1} + \dot{Z}_{CC} = \dot{C}_{B3}$	$c_{F1} = \text{fuel cost}$
Turbine (T1)	$\dot{C}_{B3} - \dot{C}_{B4} + \dot{Z}_{T1} = \dot{C}_{T1}^W$	$c_{B3} = c_{B4}, c_{el,C1} = c_{el,T1}$
Splitter (SP1)	$\dot{C}_{B4} + \dot{Z}_{SP1} = \dot{C}_{B5} + \dot{C}_{B6}$	$c_{B4} = c_{B5} = c_{B6}, \dot{Z}_{SP1} = 0$
Mixer (MX1)	$\dot{C}_{B8} + \dot{C}_{B9} + \dot{Z}_{MX1} = \dot{C}_{B7}$	$c_{B7} = c_{B6} = c_{M5}, \dot{Z}_{MX1} = 0$
Fuel Cell (SOFC)		
Mixer (MX2)	$\dot{C}_{F2} + \dot{C}_{W1} + \dot{Z}_{MX1} = \dot{C}_{M1}$	$\dot{Z}_{MX1}=0, c_{W1} = 0$
Steam Reformer (SR)	$\dot{C}_{M1} + \dot{Z}_{SR} = \dot{C}_{M2}$	---
Water Gas Shift (WGS)	$\dot{C}_{M2} + \dot{Z}_{WGS} = \dot{C}_{M3}$	---
SOFC	$\dot{C}_{M3} - \dot{C}_{B5} + \dot{Z}_{SOFC} - \dot{C}_{M4} = \dot{C}_{SOFC}^W$	$c_{B7} = c_{M4}$
Afterburner (BR)	$\dot{C}_{M4} + \dot{Z}_{BR} = \dot{C}_{M5}$	---
Energy Recovery		
Thermoelectric generator (TG)	$\dot{C}_{B7} - \dot{C}_{B8} + \dot{Z}_{TG} = \dot{C}_{TG}^W$	$c_{B8} = c_{B7}$
Generator (AGN)	$\dot{C}_{R3} + \dot{C}_{B8} - \dot{C}_{B9} + \dot{Z}_{AGN} = \dot{C}_{R4} + \dot{C}_{R7}$	$c_{R3} = \text{refrigerant cost}$
Condenser (ACN)	$\dot{C}_{R7} - \dot{C}_{R8} + \dot{Z}_{ACN} = \dot{C}_{ACN}^Q$	$c_{R7} = c_{R8}$
Expansion valve (AEX1)	$\dot{C}_{R8} + \dot{Z}_{AEX1} = \dot{C}_{R9}$	$\dot{Z}_{AEX1} = 0, c_{R8} = c_{R9}$
Evaporator (AEV)	$\dot{C}_{EV}^Q + \dot{Z}_{AEV} = \dot{C}_{R10} - \dot{C}_{R9}$	$c_{A9} = c_{A10}$
Absorber (ABS)	$\dot{C}_{R10} + \dot{C}_{R6} + \dot{Z}_{ABS} = \dot{C}_{R1} + \dot{C}_{ABS}^Q$	---
Pump (AP)	$\dot{C}_{AP}^W + \dot{Z}_{AP} = \dot{C}_{R2} - \dot{C}_{R1}$	$c_{R2} = c_{R1}, c_{el,AP} = c_{el,T1}$
Regenerator (AHX)	$\dot{C}_{R4} - \dot{C}_{R5} + \dot{Z}_{AHX} = \dot{C}_{R3} - \dot{C}_{R2}$	$c_{R2} = c_{R3}, c_{R4} = c_{R5}$
Expansion valve (AEX2)	$\dot{C}_{R5} + \dot{Z}_{AEX2} = \dot{C}_{R6}$	$\dot{Z}_{AEX2} = 0, c_{R5} = c_{R6}$
Hydrogen Production		
Ammonia electrolysis cell (AEC)	$\dot{C}_{AEC}^W + \dot{C}_{N1} + \dot{C}_{NH3} + \dot{Z}_{AEC} = \dot{C}_{N8} + \dot{C}_{H1} + \dot{C}_{H2}$	$c_{NH3} = \text{ammonia cost}$ $c_{H1} = c_{H2} = 3c_{N7},$ $c_{el,AEC} = c_{el,T1}$
Expansion valve (EX1)	$\dot{C}_{N6} + \dot{Z}_{EX1} = \dot{C}_{N9}$	$\dot{C}_{EX1} = 0, c_{N9} = c_{N6}$
Splitter (FP)	$\dot{C}_{N9} + \dot{Z}_{FP} = \dot{C}_{H2} + \dot{C}_{H1}$	
PEMFC	$\dot{C}_{A3} + \dot{C}_{H1} - \dot{C}_{A4} + \dot{Z}_{PEMFC} = \dot{C}_{PEMFC}^W$	---
Turbine (T2)	$\dot{C}_{N7} - \dot{C}_{N8} + \dot{Z}_{T2} = \dot{C}_{T2}^W$	$c_{N7} = c_{N8}$
Compressor (C2)	$\dot{C}_{A1} + \dot{C}_{C2}^W + \dot{Z}_{C2} = \dot{C}_{A2}$	$c_{A1} = 0, c_{el,C2} = c_{el,T2}$
Heat exchanger (HX2)	$\dot{C}_{A3} - \dot{C}_{A2} + \dot{Z}_{HX2} = \dot{C}_{A5} - \dot{C}_{A4}$	$c_{A4} = c_{A5}, c_{A3} = c_{A2}$

System R-3:

The cost balance equations and auxiliary equations are explained for each component of the hybrid SOFC-PEMFC gas turbine locomotive engine, and the equations are tabulated in Table 4.26.

Table 4.26 The exergoeconomic balance equations for R-3 system components.

Component	Cost Balance Equation	Auxiliary Equations
Gas Turbine (GT)		
Compressor (C1)	$\dot{C}_{A1} + \dot{C}_{C1}^W + \dot{Z}_{C1} = \dot{C}_{A2}$	$c_{A1} = 0$
Intercooler (IC)	$\dot{C}_{A2} - \dot{C}_{IC}^Q + \dot{Z}_{IC} = \dot{C}_{A3}$	$c_{A2} = c_{A3}$
Splitter (S1)	$\dot{C}_{A3} + \dot{Z}_{S1} = \dot{C}_{A4} + \dot{C}_{B1}$	$c_{A3} = c_{A4} = c_{B1},$ $\dot{Z}_{S1} = 0$
Compressor (C2)	$\dot{C}_{A4} + \dot{C}_{C2}^W + \dot{Z}_{C2} = \dot{C}_{A5}$	
Combustion Chamber (CC)	$\dot{C}_{A5} + \dot{C}_{F1} + \dot{Z}_{CC} = \dot{C}_{A7}$	$c_{F1} = \text{fuel cost}$
Turbine (T2)	$\dot{C}_{A7} - \dot{C}_{A8} + \dot{Z}_{T2} = \dot{C}_{T2}^W$	$c_{A7} = c_{A8}, c_{el,C2} = c_{el,T2}$
Splitter (S2)	$\dot{C}_{A8} + \dot{Z}_{S2} = \dot{C}_{A9} + \dot{C}_{B2}$	$c_{A8} = c_{A9} = c_{B2},$ $\dot{Z}_{S2} = 0$
Turbine (T1)	$\dot{C}_{A10} - \dot{C}_{A11} + \dot{Z}_{T1} = \dot{C}_{T1}^W$	$c_{A11} = c_{A12}, c_{el,C1} =$ $c_{el,T1}$
PEMFC	$\dot{C}_{B1} + \dot{C}_{H1} - \dot{C}_{H2} + \dot{Z}_{PEMFC} = \dot{C}_{PEMFC}^W$	---
Turbine (T3)	$\dot{C}_{H2} - \dot{C}_{H3} + \dot{Z}_{T3} = \dot{C}_{T3}^W$	$c_{H3} = c_{H2}$
Thermoelectric generator (TEG1)	$\dot{C}_{H3} - \dot{C}_{H4} + \dot{Z}_{TEG1} = \dot{C}_{TEG1}^W$	$c_{H3} = c_{H4}$
Fuel Cell (SOFC)		
Mixer (MX1)	$\dot{C}_{F2} + \dot{C}_{W1} + \dot{Z}_{MX1} = \dot{C}_{D1}$	$\dot{Z}_{MX1}=0, c_{W1} = 0$
Steam Reformer (SR)	$\dot{C}_{D1} + \dot{Z}_{SR} = \dot{C}_{D2}$	---
Water Gas Shift (WGS)	$\dot{C}_{D2} + \dot{Z}_{WGS} = \dot{C}_{D3}$	---
SOFC	$\dot{C}_{D3} + \dot{C}_{B2} + \dot{Z}_{SOFC} - \dot{C}_{D4} = \dot{C}_{SOFC}^W$	$c_{B2} = c_{D4}$
Afterburner (BR)	$\dot{C}_{D4} + \dot{C}_{A9} + \dot{Z}_{BR} = \dot{C}_{A10}$	---
Energy Recovery		
Thermoelectric generator (TEG2)	$\dot{C}_{A12} - \dot{C}_{A13} + \dot{Z}_{TEG2} = \dot{C}_{TEG2}^W$	$c_{A13} = c_{A12}$
Generator (AGN)	$\dot{C}_{R3} + \dot{C}_{A11} - \dot{C}_{A12} + \dot{Z}_{AGN} = \dot{C}_{R4} + \dot{C}_{R7}$	$c_{R3} = \text{refrigerant cost}$
Condenser (CAN)	$\dot{C}_{R7} - \dot{C}_{R8} + \dot{Z}_{ACN} = \dot{C}_{ACN}^Q$	$c_{R7} = c_{R8}$
Expansion valve (AEX1)	$\dot{C}_{R8} + \dot{Z}_{AEX1} = \dot{C}_{R9}$	$\dot{Z}_{AEX1} = 0, c_{R8} = c_{R9}$
Evaporator (AEV)	$\dot{C}_{EV}^Q + \dot{Z}_{AEV} = \dot{C}_{R10} - \dot{C}_{R9}$	$c_{A9} = c_{A10}$
Absorber (ABS)	$\dot{C}_{R10} + \dot{C}_{R6} + \dot{Z}_{ABS} = \dot{C}_{R1} + \dot{C}_{ABS}^Q$	---
Pump (AP)	$\dot{C}_{AP}^W + \dot{Z}_{AP} = \dot{C}_{R2} - \dot{C}_{R1}$	$c_{R2} = c_{R1}, c_{el,AP} =$ $c_{el,T1}$
Regenerator (AHX)	$\dot{C}_{R4} - \dot{C}_{R5} + \dot{Z}_{AHX} = \dot{C}_{R3} - \dot{C}_{R2}$	$c_{R2} = c_{R3}, c_{R4} = c_{R5}$
Expansion valve (AEX2)	$\dot{C}_{R5} + \dot{Z}_{AEX2} = \dot{C}_{R6}$	$\dot{Z}_{AEX2} = 0, c_{R5} = c_{R6}$

System M-1:

The cost balance equations and auxiliary equations are explained for each component of the hybrid combined marine engine, and the equations are shown in Table 4.27.

Table 4.27 The exergoeconomic balance equations for M-1 system components.

Component	Cost Balance Equation	Auxiliary Equations
Gas Turbine (GT)		
Compressor (C2)	$\dot{C}_{Y1} + \dot{C}_{C2}^W + \dot{Z}_{C2} = \dot{C}_{Y2}$	$c_{Y1} = 0$
Intercooler (IC)	$\dot{C}_{Y2} - \dot{C}_{IC}^Q + \dot{Z}_{IC} = \dot{C}_{Y3}$	$c_{Y2} = c_{Y3}$
Compressor (C3)	$\dot{C}_{Y3} + \dot{C}_{C3}^W + \dot{Z}_{C3} = \dot{C}_{Y4}$	
Combustion Chamber (CC)	$\dot{C}_{Y4} + \dot{C}_{MF2} + \dot{Z}_{CC} = \dot{C}_{Y5}$	$c_{MF2} = \text{fuel cost}$
Turbine (T3)	$\dot{C}_{Y5} - \dot{C}_{Y6} + \dot{Z}_{T3} = \dot{C}_{T3}^W$	$c_{Y5} = c_{Y6}, c_{el,C3} = c_{el,T3}$
Splitter (SP1)	$\dot{C}_{Y6} + \dot{Z}_{SP1} = \dot{C}_{Y7} + \dot{C}_{Y8}$	$c_{Y6} = c_{Y7} = c_{Y8},$
Turbine (T2)	$\dot{C}_{Y10} - \dot{C}_{Y11} + \dot{Z}_{T2} = \dot{C}_{T2}^W$	$c_{Y10} = c_{Y11}, c_{el,C2} = c_{el,T2}$
Thermoelectric generator (TEG2)	$\dot{C}_{Y11} - \dot{C}_{Y12} + \dot{Z}_{TEG2} = \dot{C}_{TEG2}^W$	$c_{Y11} = c_{Y12}$
Fuel Cell (SOFC)		
Mixer (MX1)	$\dot{C}_{MF3} + \dot{C}_{W1} + \dot{Z}_{MX1} = \dot{C}_{Z1}$	$\dot{Z}_{MX1}=0, c_{W1} = 0$
Steam Reformer (SR)	$\dot{C}_{Z1} + \dot{Z}_{SR} = \dot{C}_{Z2}$	---
Water Gas Shift (WGS)	$\dot{C}_{Z2} + \dot{Z}_{WGS} = \dot{C}_{Z3}$	---
SOFC	$\dot{C}_{Z3} - \dot{C}_{Z4} + \dot{Z}_{SOFC} + \dot{C}_{Y7} = \dot{C}_{SOFC}^W$	$c_{Y7} = c_{Z4}$
Mixer (MX2)	$\dot{C}_{Z4} + \dot{C}_{Y8} + \dot{Z}_{MX2} = \dot{C}_{Y10}$	
Afterburner (BR)	$\dot{C}_{Y9} + \dot{Z}_{BR} = \dot{C}_{Y10}$	---
Internal Combustion Engine (ICE)		
Internal combustion engine (ICE)	$\dot{C}_{X1} + \dot{C}_{MF1} - \dot{C}_{AC}^Q - \dot{C}_{R1}^Q + \dot{Z}_{ICE} - \dot{C}_{X10} = \dot{C}_{ICE}^W$	$c_{el,ICE}$ $= \frac{\dot{C}_{X1} + \dot{C}_{MF1} - \dot{C}_{X10}}{\dot{E}x_{X1} + \dot{E}x_{MF1} - \dot{E}x_{X10}}$
Thermoelectric generator (TEG1)	$\dot{C}_{X10} - \dot{C}_{X11} + \dot{Z}_{TEG1} = \dot{C}_{TEG1}^W$	$c_{X10} = c_{X11}$

System M-2:

The cost balance equations and auxiliary equations are explained for each component of the hybrid compound cycles (SRC-SOFC-GT) marine engine, and the equations are explained in Table 4.28. This table lists the cost balance equations and auxiliary equations for the steam Rankine cycle (SRC), a gas turbine (GBC), and a fuel cell (SOFC) subsystem.

Table 4.28 The exergoeconomic balance equations for M-2 system components.

Component	Cost Balance Equation	Auxiliary Equations
Steam Rankine Cycle (SRC)		
HP-ST1	$\dot{C}_{A7} - \dot{C}_{A8} + \dot{Z}_{HPST1} = \dot{C}_{HPST1}^W$	$c_{A7} = c_{A8},$ $c_{el,HPT1} = c_{el,P1} = c_{el,P2}$
IP-ST2	$\dot{C}_{A9} - \dot{C}_{A11E} + \dot{Z}_{IPST2} = \dot{C}_{IPST2}^W$	$c_{A9} = c_{A11E}$
LP-ST3	$\dot{C}_{A11T} - \dot{C}_{A12} - \dot{C}_{A13} - \dot{C}_{A10} + \dot{Z}_{LPST3} = \dot{C}_{LPST3}^W$	$c_{A9} = c_{A11E}$
CN	$\dot{C}_{A22} - \dot{C}_{A1} + \dot{Z}_{CN} = \dot{C}_{CN}^Q$	$c_{G2} = c_{G3}$
P1	$\dot{C}_{A1} + \dot{C}_{P1}^W + \dot{Z}_{P1} = \dot{C}_{A2}$	$c_{A1} = c_{A2}$
P2	$\dot{C}_{GA5} + \dot{C}_{LPC1}^W + \dot{Z}_{LPC1} = \dot{C}_{A6}$	$c_{G1} = 0$
CFH1	$\dot{C}_{A13} + \dot{C}_{A18} - \dot{C}_{A20} + \dot{Z}_{CFH1} = \dot{C}_{A3} - \dot{C}_{A2}$	$c_{A3} = c_{A2}$
CFH2	$\dot{C}_{A12} + \dot{C}_{A16} - \dot{C}_{A17} + \dot{Z}_{CFH2} = \dot{C}_{A4} - \dot{C}_{A3}$	$c_{A4} = c_{A3}$
CFH3	$\dot{C}_{A11} - \dot{C}_{A14} + \dot{Z}_{CFH3} = \dot{C}_{A5} - \dot{C}_{A4}$	$c_{A5} = c_{A4}$
EX1	$\dot{C}_{A14} + \dot{Z}_{EX1} = \dot{C}_{A15}$	
EX2	$\dot{C}_{A17} + \dot{Z}_{EX2} = \dot{C}_{G18}$	
EX3	$\dot{C}_{A20} + \dot{Z}_{EX3} = \dot{C}_{A21}$	
BR-BL	$\dot{C}_{G12} + \dot{C}_{B1} + \dot{C}_{F1} + \dot{Z}_{CC} = \dot{C}_{B2}$	$c_{F1} = \text{fuel cost}$
HX-BL	$\dot{C}_{B2} - \dot{C}_{B3} + \dot{Z}_{HXB1} = \dot{C}_{A7} - \dot{C}_{A6}$	$c_{B2} = c_{B3}$
HX-RH	$\dot{C}_{B3} - \dot{C}_{B4} + \dot{Z}_{HXRH} = \dot{C}_{A9} - \dot{C}_{A8}$	$c_{B3} = c_{B4}$
DSWR	$\dot{C}_{B4} - \dot{C}_{B5} + \dot{C}_{SW1} - \dot{C}_{SW4} + \dot{Z}_{DSWR} = \dot{C}_{FW16} - \dot{C}_{SL5}$	$c_{SW1} = 0$
Gas Brayton Cycle (GBC)		
LP-C1	$\dot{C}_{G1} + \dot{C}_{LPC1}^W + \dot{Z}_{LPC1} = \dot{C}_{G2}$	$c_{G1} = 0$
IC	$\dot{C}_{G2} - \dot{C}_{IC}^Q + \dot{Z}_{IC} = \dot{C}_{G3}$	$c_{G2} = c_{G3}$
HP-C2	$\dot{C}_{G3} + \dot{C}_{HPC2}^W + \dot{Z}_{HPC2} = \dot{C}_{G4}$	
GTSP	$\dot{C}_{G4} + \dot{Z}_{GTSP} = \dot{C}_{G5} + \dot{C}_{G6}$	$c_{G4} = c_{G5} = c_{G6}$
CC	$\dot{C}_{M4} + \dot{C}_{F2} + \dot{C}_{G6} + \dot{Z}_{CC} = \dot{C}_{G7}$	$c_{F2} = \text{fuel cost}$
GTHX	$\dot{C}_{G7} - \dot{C}_{G8} + \dot{Z}_{GTHX} = \dot{C}_{G11} - \dot{C}_{G10}$	
HP-T1	$\dot{C}_{G8} - \dot{C}_{G9} + \dot{Z}_{HPT1} = \dot{C}_{HPT1}^W$	$c_{A7} = c_{A8},$ $c_{el,HPT1} = c_{el,HPC2}$
LP-T2	$\dot{C}_{G10} - \dot{C}_{G11} + \dot{Z}_{LPT2} = \dot{C}_{LPT2}^W$	$c_{G10} = c_{G11},$ $c_{el,LPT2} = c_{el,LPC1}$
P-T3	$\dot{C}_{G11} - \dot{C}_{G12} + \dot{Z}_{PT3} = \dot{C}_{PT3}^W$	$c_{G11} = c_{G12}$
Fuel Cell (SOFC)		
GTMX	$\dot{C}_{F3} + \dot{C}_{W1} + \dot{Z}_{GTMX} = \dot{C}_{M1}$	$c_{W1} = 0, c_{F3} = \text{fuel cost}$
SR	$\dot{C}_{M1} + \dot{Z}_{SR} = \dot{C}_{M2}$	---
WGS	$\dot{C}_{M2} + \dot{Z}_{WGS} = \dot{C}_{M3}$	---
SOFC	$\dot{C}_{G5} + \dot{C}_{M3} + \dot{Z}_{SOFC} - \dot{C}_{M4} = \dot{C}_{SOFC}^W$	$c_{M4} = c_{G5}$

System M-3:

The cost balance equations and auxiliary equations are explained for each component of a hybrid gas turbine combined with binary systems marine engine, which the equations are shown in Table 4.29. The table displays cost balance equations and auxiliary equations for three subsystems: a gas turbine engine (GBC), a fuel cell (SOFC), and two organic Rankine cycles (TORC and BORC).

Table 4.29 The exergoeconomic balance equations for M-3 system components.

Component	Cost Balance Equation	Auxiliary Equations
Gas Brayton Cycle (GBC)		
HPC1	$\dot{C}_{G1} + \dot{C}_{HPC1}^W + \dot{Z}_{HPC1} = \dot{C}_{G2}$	$c_{A1} = 0$
GTHX	$\dot{C}_{G3} - \dot{C}_{G2} + \dot{Z}_{GTHX} = \dot{C}_{G9} - \dot{C}_{G8}$	$c_{G2} = c_{G3}$
SP	$\dot{C}_{G3} + \dot{Z}_{SP} = \dot{C}_{G4} + \dot{C}_{G5}$	$c_{G3} = c_{G4} = c_{G5}$
CC	$\dot{C}_{G5} + \dot{C}_{FC7} + \dot{C}_{F1} + \dot{Z}_{CC} = \dot{C}_{G6}$	$c_{F1} = \text{fuel cost}$
HPT1	$\dot{C}_{G6} - \dot{C}_{G7} + \dot{Z}_{HPT1} = \dot{C}_{HPT1}^W$	$c_{G6} = c_{G7}, c_{el,HPC1} = c_{el,HPT1}$
LPT2	$\dot{C}_{G7} - \dot{C}_{G8} + \dot{Z}_{LPT2} = \dot{C}_{LPT2}^W$	$c_{G7} = c_{G8}, c_{el,LPT2} = c_{el,P1}$
Fuel Cell (SOFC)		
MX	$\dot{C}_{F2} + \dot{C}_{S1} + \dot{Z}_{MX} = \dot{C}_{FC1}$	$\dot{Z}_{MX}=0, c_{S1} = 0$
SR	$\dot{C}_{FC1} + \dot{Z}_{SR} = \dot{C}_{FC2}$	---
WGS	$\dot{C}_{FC2} + \dot{Z}_{WGS} = \dot{C}_{FC3}$	---
SOFC	$\dot{C}_{FC3} + \dot{C}_{G4} + \dot{Z}_{SOFC} - \dot{C}_{FC7} = \dot{C}_{SOFC}^W$	$c_{FC7} = c_{G4}$
Organic Rankine Cycles (TORC and BORC)		
CN1	$\dot{C}_{G9} - \dot{C}_{G10} + \dot{Z}_{CN1} = \dot{C}_{TR3} - \dot{C}_{TR2}$	$c_{G9} = c_{G10}$
CN2	$\dot{C}_{G10} - \dot{C}_{G11} + \dot{Z}_{AGN} = \dot{C}_{LR4} - \dot{C}_{LR3}$	$c_{G11} = c_{G10}$
T3	$\dot{C}_{TR3} - \dot{C}_{TR4} + \dot{Z}_{T3} = \dot{C}_{T3}^W$	$c_{TR3} = c_{TR4}, c_{el,T3} = c_{el,P1}$
T4	$\dot{C}_{LR4} - \dot{C}_{LR5} + \dot{Z}_{T4} = \dot{C}_{T4}^W$	$c_{LR4} = c_{LR5}, c_{el,T4} = c_{el,P2}$
T5	$\dot{C}_{LR6} - \dot{C}_{LR7} + \dot{Z}_{T5} = \dot{C}_{T5}^W$	$c_{LR6} = c_{LR77}$
P1	$\dot{C}_{TR1} + \dot{Z}_{P1} + \dot{C}_{P1}^W = \dot{C}_{TR2}$	$c_{TR1} = c_{TR2}$
P2	$\dot{C}_{P2}^W + \dot{Z}_{P2} + \dot{C}_{LR1} = \dot{C}_{LR2}$	$c_{LR2} = c_{LR1}$
EV11	$\dot{C}_{LR2} - \dot{C}_{LR3} + \dot{Z}_{EV11} = \dot{C}_{TR5} - \dot{C}_{TR4}$	$c_{LR2} = c_{LR3}$
EV12	$\dot{C}_{LR5} - \dot{C}_{LR6} + \dot{C}_{LGN1} - \dot{C}_{LNG2} + \dot{Z}_{EV12} = \dot{C}_{TR1} - \dot{C}_{TR5}$	$c_{LR5} = c_{LR6}$
EV2	$\dot{C}_{LNG2} - \dot{C}_{LNG3} + \dot{Z}_{EV2} = \dot{C}_{LR1} - \dot{C}_{LR7}$	$c_{LR1} = c_{LR7}$

4.5.4 Environmental Impact Assessment

The environmental impact assessment includes the life cycle assessment for the vehicles in both cycles: vehicle cycle and fuel cycle, environmental impact assessment using TRACI V2.1 impact method, and exergoenvironment analysis.

1. Life cycle Analysis:

The life cycle study comprises four primary steps, as shown in Figure 4.19, including goal and scope definition, inventory analysis, impact assessment, and interpretation. The goal-and-scope definition explains the objective of this thesis, which is to perform the life cycle analysis for the three transportation sectors: rail, marine, and aviation sectors. The life cycle analysis will be implied to both the vehicle cycle and the fuel cycle, as shown in Figure 4.20.

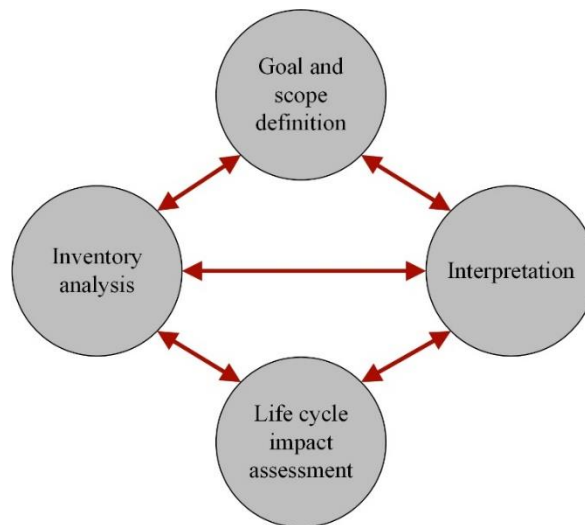


Figure 4.19 Life cycle analysis frameworks

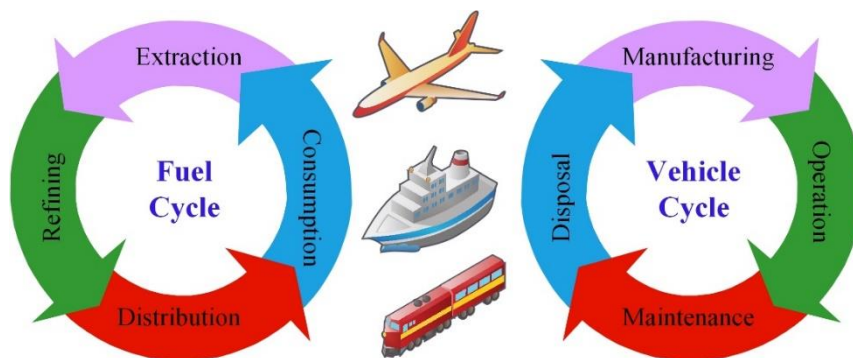


Figure 4.20 Vehicle and Fuel cycles for three transportation sectors

The vehicle cycle comprises four phases in which the functional unit is one-km distance travel for each transportation sector:

- a. Manufacturing of transport (a locomotive, an airplane, and a ship)
- b. Operation of transport (a locomotive, an airplane, and a ship)
- c. Maintenance of transport (a locomotive, an airplane, and a ship)
- d. Disposal of transport (a locomotive, an airplane, and a ship)

While the fuel cycle contains four phases for producing one kilogram of fuel for each fuel type. The four phases of fuel cycles are:

- a. Extraction and transportation of the fuel for its source.
- b. Refining and production process.
- c. Distribution of the fuel production to the required services.
- d. Consumption of fuel based on customer needs.

The inventory analysis presents data for each phase of the vehicle cycle and fuel cycle for the transportation sectors. In the manufacturing phase, the inventory contains processes of energy, water, and material usage, which are utilized in the groundwork of a plant, material consumption, and product production. The inventory for maintenance of transport contains resources used for alternation parts, battery changes, and energy consumption of garages and repair agencies. The inventory of a transport disposal contains disposal processed for bulk materials such as tires, steel, aluminum, copper, waste specific water, plastics, emulsion paint leftovers, and glass. The operation of transport is one of the critical sections of the life cycle analysis. It contains fuel production and consumption processes. Direct airborne emissions of gaseous materials, particulate matters, heavy metals, hydrocarbon emissions, most of them are linked to exhaust emissions, abrasion emissions, and evaporation, which have severe effects on human health, air pollution, and global warming.

In addition, a significant portion of any life cycle analysis requires the collection of reliable data. The quality of data has a profound impact on the quality of the results predicted or estimated by an LCA tool. GHGenius has access to data for Canada from reports produced by Statistics Canada, Natural Resources Canada (NRCan), Environment Canada, and the National Energy Board for power, crude oil, refined petroleum products, and natural gas. Additionally, GHGenius allows the user to provide data for specific steps

in the process to provide the highest degree of flexibility possible in the model without compromising the quality of the results predicted.

2. Environmental impact assessment (TRACI V2.1 impact method):

The environmental assessment is covered by applying the tool for reduction and assessment of chemicals and other environmental impacts (TRACI V2.1) impact method by considering the following categories [187]:

- a. Acidification potential is due to the addition of sulfuric no nitric acid in the atmosphere, which negatively impacts soil, groundwater, surface water, and vegetation, and it can be expressed by SO₂ equivalents/kg emission.
- b. Eutrophication: considers the excessive emissions of micro-nutrients (such as nitrates and phosphates) in the environment, and it is expressed by kg PO₄ equivalent per kg emission, and terrestrial measure differs between local and continental scale.
- c. Global climate change: the greenhouse gases in the air are related to climate change and affect ecosystem health, human health, and material. It can be expressed by a kg of carbon dioxide per kg emission.
- d. Ozone depletion: the ozone depletion potential of several gases within the stratosphere that has an impact on plants, crops, and building materials due to the increase of chlorofluorocarbons (CFCs). This potential can be measured by a kg CFC-11 equivalent per kg emission.
- e. Human heath particulate: it deals with particulate matter and its precursors that appear in ambient air and affect human respiratory systems. It is characterized by a kg of PM_{2.5} equivalent per person.
- f. Human health cancer, non cancer, and ecotoxicity: toxic substances on the human environment are the main concerns and are expressed by CTUcancer, CTUoncancer, and CTUeco, which can be combined as CTUh per emission.
- g. Photochemical smog formation: ground level ozone is caused by different chemical reactions between NO_x, VOCs in sunlight, which cause various respiratory problems. It can be expressed by a kg of O₃ equivalent per person.
- h. Resource depletion: is related to the protection of human wellbeing, human health, and environmental health. It is recognized for every extraction of minerals and fossil fuels,

depending on the concentration of resources and the rate of de-accumulation. It is expressed in MJ surplus per person.

The normalization of TRAC V2.1 is implemented based on the EPA data collected for USA-Canada 2008. Since each category has a unique unit and cannot be added to the total impact, therefore. Each category is normalized and weighted to give a total point of impact (Pt) and can be divided per 1 MJ to 1kg of species, as shown below. The normalization of TRACI V2.1 is expressed in Table 4.30 as established in OpenLCA.

$$\text{Point}_{\text{category}} = \text{Category}_{\text{TRACI}} \times \frac{\text{Normalization Factor}}{\text{Weighting Factor}} \quad (4.195)$$

Table 4.30 The normalization of TRACI V2.1 Categories

Impact category	Normalization factor	Unit	Weighting factor
Acidification	90.9	kg SO ₂ eq (sulphur dioxide) per person per year	0.036
Ecotoxicity	11000	CTUe per person per year	0.084
Eutrophication	21.6	kg N eq (nitrogen) per person per year	0.072
Global warming	24200	kg CO ₂ eq (carbon dioxide) per person per year	0.349
Ozone depletion	0.161	kg CFC-11 eq per person per year	0.024
Carcinogenics	5.07E-05	CTUh per person per year	0.096
Non carcinogenics	0.00105	CTUh per person per year	0.06
Respiratory effects	24.3	kg PM _{2.5} eq (fine particulates) per person per year	0.108
Smog	1390	kg O ₃ eq (ozone) per person per year	0.048
Fossil fuel depletion	17300	MJ surplus per person per year	0.121

3. Exergoenvironmental analysis:

Exergoenvironmental analysis is achieved by estimating stream exergy, life cycle analysis (LCA) of components and fuels, and environmental balance equations. It is an appropriate correlation of exergy and LCA to measure quality and any thermodynamic inefficiencies and offers the environmental impacts with a component or an overall system during its lifetime [188].

An environmental impact rate, \dot{B} , is expressed in points per time unit (Pts/s). It is a weighting method used in the LCA to convert the overall environmental impacts of a component to a single adequate value. Therefore, \dot{B} for an input or output stream is described below:

$$\dot{B}_j = \dot{B}_j^{ch} + \dot{B}_j^{ph} = b_j^{ch} \dot{E}x_j^{ch} + b_j^{ph} \dot{E}x_j^{ph} = b_j \dot{E}x_j \quad (4.196)$$

where b_j is an environmental impact per unit exergy. The exergoenvironmental rate \dot{B}_j might include physical and chemical exergy when a chemical reaction happens. The exergoenvironmental correlated with inlet stream, exit stream, work and heat are described below:

$$\dot{B}_{in} = b_{in} \dot{E}x_{in} \quad (4.197)$$

$$\dot{B}_{out} = b_{out} \dot{E}x_{out} \quad (4.198)$$

$$\dot{B}_W = b_W \dot{W} \quad (4.199)$$

$$\dot{B}_Q = b_Q \dot{E}x_Q \quad (4.200)$$

In addition, pollutant formation occurs during a chemical reaction as only pollutant streams are emitted to the environment, such as CO, CO₂, CH₄, N₂O, NO_x, and SO_x. The value of \dot{B}^{PF} is defined as the pollutant formation exergoenvironmental rate where the environmental impact of emissions is multiplied by the mass difference between the inlet and exit emission of each component:

$$\dot{B}_j^{PF} = \sum_i b_i (m_{out} - m_{in}) \quad (4.201)$$

The component-related environmental impact, \dot{Y}_j , contains three LCA phases of construction, \dot{Y}_j^{CO} ; operation and maintenance, \dot{Y}_j^{OM} ; and disposal, \dot{Y}_j^{DI} , as displayed below:

$$\dot{Y}_j = \dot{Y}_j^{CO} + \dot{Y}_j^{OM} + \dot{Y}_j^{DI} \quad (4.202)$$

This can be described as $\dot{Y}_j = \varphi_{en} (\dot{Y}_j^{CO} + \dot{Y}_j^{DI})$, where φ_{en} is maintenance and operation factor (1.2). The exergoenvironmental balance equation for each component can be written as below:

$$\sum_{k=1}^m \dot{B}_{k,j,in} + \dot{Y}_j + \dot{B}_j^{PF} = \sum_{k=1}^m \dot{B}_{k,j,out} \quad (4.203)$$

The formulated balance equations are not sufficient to solve for unknown variables. Hence, auxiliary equations follow the F and P principle from the exergoeconomic analysis. The specific fuel and product exergoenvironmental impact ($b_{F,j}$ and $b_{P,j}$), and destruction exergoenvironmental rate ($\dot{B}_{D,j}$) for a component are given below:

$$b_{F,j} = \frac{\dot{B}_{F,j}}{\dot{E}x_{F,j}} \quad (4.204)$$

$$b_{P,j} = \frac{\dot{B}_{P,j}}{\dot{E}x_{P,j}} \quad (4.205)$$

$$\dot{B}_{D,j} = b_{F,j} \dot{E}x_{D,j} \quad (4.206)$$

The overall specific fuel exergoenvironmental impact ($b_{F,t}$), overall specific product exergoenvironmental impact ($b_{P,t}$) is written below:

$$b_{F,t} = \frac{\sum \dot{B}_{F,j}}{\sum \dot{E}x_{F,j}} \quad (4.207)$$

$$b_{P,t} = \frac{\sum \dot{B}_{P,j}}{\sum \dot{E}x_{P,j}} \quad (4.208)$$

Therefore, the total environmental impact rates of a component, $\dot{B}_{T,j}$, is given below:

$$\dot{B}_{T,j} = \dot{Y}_j + \dot{B}_j^{PF} + \dot{B}_{D,j} \quad (4.209)$$

The exergoenvironmental factor f_b is the most critical environmental impact scale, and it is defined as the ratio of component exergoenvironmental-impact rate, \dot{Y}_j to the total environmental impact rate ($\dot{Y}_j + \dot{B}_j^{PF} + \dot{B}_{D,j}$) for each component and the entire system.

$$f_{b,j} = \frac{\dot{Y}_j}{\dot{B}_{T,j}} = \frac{\dot{Y}_j}{\dot{Y}_j + \dot{B}_j^{PF} + \dot{B}_{D,j}} \quad (4.210)$$

The relative exergoenvironmental difference, r_b , is a gauge for lowering the environmental impact of a component as expressed below:

$$r_{b,j} = \frac{b_{P,j} - b_{F,j}}{b_{F,j}} \quad (4.211)$$

The costs for electricity, fuels, and water are gathered from various sources, as shown in Table 4.31, and are changed to specific energy cost, $c_{f,en}$ in \$/GJ, and specific exergy cost, $c_{f,ex}$ \$/GJ, ($=c_{f,en}/1.06$) [20, 21]. The environmental impact b_f is calculated based on mining, production, and transportation processes, as shown in Table 4.31. The life cycle impact assessment (LCIA) of the fuels is performed using OpenLCA and GREET software. The environmental impact results of hydrogen and methane are compared to the results of Eco-Indicator E99H [22, 23] and TRACI v2.1 [193] to verify the simulation results in LCA software, as shown in Figure 4.20. The total cost and environmental impact of fuel blends are in Table 4.32.

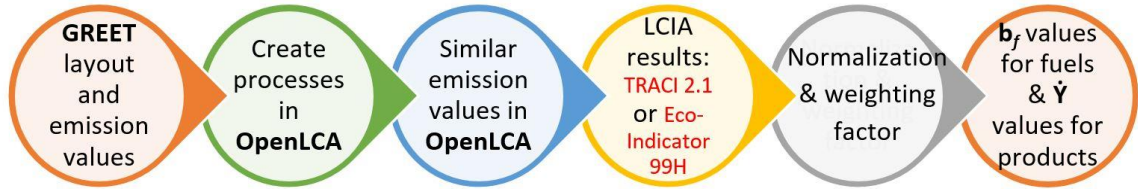


Figure 4.21 LCIA for fuel blends to estimate b_f for fuel blends \dot{Y} for some components.

Table 4.31 The cost and environmental impact of fuels and substances

Fuels	Ref	Value	Unit	$c_{f,en}$		$c_{f,ex}$		b_f	
Electricity	[192,194]	0.082	\$/kWh	22.78	\$/GJ	21.49	\$/GJ	27	mPt/kWh
Water	[192,195]	0.0031	\$/kg	0.0031	\$/kg	0.0029	\$/kg	0.026	mPt/kg
Air		0	\$/GJ	0	\$/GJ	0	\$/GJ	0	mPt/kg
Hydrogen	[196]	2	\$/kg	16.81	\$/GJ	15.86	\$/GJ	731.1	mPt/kg
Ammonia	[197]	1.6	\$/kg	84.66	\$/GJ	79.86	\$/GJ	191.6	mPt/kg
Methanol	[198]	0.599	\$/kg	33.09	\$/GJ	31.22	\$/GJ	153.0	mPt/kg
Ethanol	[199]	0.87	\$/kg	32.58	\$/GJ	30.74	\$/GJ	155.4	mPt/kg
DME	[200]	1.20	\$/kg	41.50	\$/GJ	39.15	\$/GJ	426.7	mPt/kg
Methane	[201]	4.5E-6	\$/kJ	4.50	\$/GJ	4.25	\$/GJ	260.0	mPt/kg
NH ₃ H ₂ O	Cal.	0.80	\$/kg	0.80	\$/kg	0.76	\$/kg	200.0	mPt/kg
Thermal	[192]	2.2	\$/GJ	2.2	\$/GJ	2.08	\$/GJ	5.3	mPt/MJ
KOH solution	[202]	0.089	\$/kg	0.089	\$/kg	0.084	\$/kg	90.0	mPt/kg
NH ₃ solution	cal.	0.058	\$/kg	0.058	\$/kg	0.055	\$/kg	57.5	mPt/kg
Pentane	[203]	3.13	\$/kg	-	-	3.13	\$/kg	245	mPt/kg
Butane	[204]	0.36	\$/kg	-	-	0.36	\$/kg	260	mPt/kg
Propene	[205]	1.00	\$/kg	-	-	1.00	\$/kg	255	mPt/kg
Propane	[206]	0.19	\$/kg	-	-	0.19	\$/kg	250	mPt/kg
LNG	[207]	1.29	\$/kg	-	-	1.29	\$/kg	290	mPt/kg
Emissions:									
CO ₂	[192,208]	-	-	-	-	2.63	\$/GJ	5.454	mPt/kg
CO	[192]	-	-	-	-	0		114.6	mPt/kg
CH ₄	[192]	-	-	-	-	0		8.364	mPt/kg

Table 4.32 The specific exergoeconomic and exergoenvironmental impact of fuels.

Fuels	Methane CH ₄	Hydrogen H ₂	Methanol CH ₃ OH	Ethanol CH ₃ OHCH ₂	DME CH ₃ OCH ₃	$c_{f,ex}$ [\$/GJ]	b_f [mPt/MJ]
F1	0.75	0.25	0	0	0	7.15	5.44
F2	0	0.25	0.75	0	0	27.38	7.88
F3	0	0.4	0	0.6	0	24.79	5.95
F4	0	0.4	0	0	0.6	29.83	11.33
F5	0.15	0.4	0.15	0.15	0.15	22.15	7.6

System A-1: The exergoenvironmental balance equations are explained for each component for hybrid MCFC-turbofan aircraft engine, which the equations are listed in Table 4.33. It presents the exergoenvironmental balance equations and auxiliary equations for tow

subsystems: the turbofan engine containing compressors like FAN, IPC, and HPC, combustor like CC, turbines as HPT, IPT, and LPT, and nozzles, and fuel cell subsystem involving an MCFC, steam reforming (SR), and water gas shift (WGS).

Table 4.33 The exergoenvironmental balance equations for A-1 system components

Equipment	Exergoenvironmental Balance Equations	Auxiliary Equations
Turbofan Engine		
Compressor (FAN)	$\dot{B}_{a2} + \dot{B}_{FAN}^W + \dot{Y}_{FAN} = \dot{B}_{a3}$	$b_{a2} = 0 \text{ \& } b_{e,FAN} = b_{e,LPT}$
Splitter (S1)	$\dot{B}_{a3} = \dot{B}_{a3A} + \dot{B}_{a3B}$	$b_{a3} = b_{a3A} = b_{a3B}$
Compressor (IPC)	$\dot{B}_{a3A} + \dot{B}_{IPC}^W + \dot{Y}_{IPC} = \dot{B}_{a4}$	$b_{e,IPC} = b_{e,IPT}$
Compressor (HPC)	$\dot{B}_{a4} + \dot{B}_{HPC}^W + \dot{Y}_{HPC} = \dot{B}_{a5}$	$b_{e,HPC} = b_{e,HPT}$
Splitter (S2)	$\dot{B}_{a5} = \dot{B}_{a5A} + \dot{B}_{a5C}$	$b_{a5} = b_{a5A} = b_{a5C}$
Combustor (CC)	$\dot{B}_{f1} + \dot{B}_{05A} + \dot{Y}_{CC} + \dot{B}_{CC}^{PF} = \dot{B}_{a6}$	$b_{f1} = \text{fuel}$
Turbine (HPT)	$\dot{B}_{a6} - \dot{B}_{a7} + \dot{Y}_{HPT} = \dot{B}_{HPT}^W$	$b_{a7} = b_{a6}$
Turbine (IPT)	$\dot{B}_{a7} - \dot{B}_{a8} + \dot{Y}_{IPT} = \dot{B}_{IPT}^W$	$b_{a8} = b_{a6}$
Turbine (LPT)	$\dot{B}_{a8} - \dot{B}_{a9} + \dot{Y}_{LPT} = \dot{B}_{LPT}^W$	$b_{a8} = b_{a6}$
Splitter (S3)	$\dot{B}_{a9} = \dot{B}_{a9A} + \dot{B}_{a9B}$	$b_{a9} = b_{a9A} = b_{a9B}$
Mixer (MX1)	$\dot{B}_{a9A} + \dot{B}_{a9C} + \dot{Y}_{MX1} = \dot{B}_{a9D}$	$\dot{Y}_{MX1}=0, b_{a9A} = b_{a9C} = b_{a9D}$
Turbine exit (TE)	$\dot{B}_{a9D} + \dot{Y}_{TE} = \dot{B}_{a10}$	$\dot{Y}_{TE}=0$
Fan Nozzle (FN)	$\dot{B}_{a3B} + \dot{Y}_{FN} = \dot{B}_{a12}$	$\dot{Y}_{FN}=0$
Exit Nozzle (EN)	$\dot{B}_{a10} + \dot{Y}_{EN} = \dot{B}_{a11}$	$\dot{Y}_{EN}=0$
Fuel Cell (MCFC)		
Mixer (MX2)	$\dot{B}_{f2} + \dot{B}_{w1} + \dot{Y}_{MX2} = \dot{B}_{b1}$	$\dot{Y}_{MX2}=0, b_{w1} = 0.012$
Steam Reformer (SR)	$\dot{B}_{b1} + \dot{B}_{SR} + \dot{B}_{SR}^{PF} = \dot{B}_{b2}$	
Water Gas Shift (WGS)	$\dot{B}_{b2} + \dot{Y}_{WGS} + \dot{B}_{WGS}^{PF} = \dot{B}_{b3}$	
Fuel cell (MCFC)	$\dot{B}_{b3} + \dot{B}_{a9B} - \dot{B}_{a9C} + \dot{Y}_{MCFC} + \dot{B}_{MCFC}^{PF} = \dot{B}_{MCFC}^W + \dot{B}_{MCFC}^L$	$b_{e,MCFC} = \frac{\dot{C}_{b3} + \dot{C}_{a9B} - \dot{C}_{a9C}}{\dot{E}x_{b3} + \dot{E}x_{a9B} - \dot{E}x_{a9C}}$ $b_{l,MCFC} = 5.3 \text{ mPt/MJ (assumed)}$

System A-2: The exergoenvironmental balance equations are explained for each component of the hybrid SOFC-turbofan aircraft engine, and the equations are listed in Table 4.34. It contains the exergoenvironmental balance equations and auxiliary equations for two subsystems: the turbofan engine and the fuel cell of the SOFC subsystem.

Table 4.34 The exergoenvironmental balance equations for A-2 system components

Component	Exergoenvironmental Balance Equation	Auxiliary Equations
Turbofan Engine		
Compressor (FAN)	$\dot{B}_{02} + \dot{B}_{FAN}^W + \dot{Y}_{FAN} = \dot{B}_{03}$	$b_{02} = 0 \text{ \& } b_{e,FAN} = b_{e,LPT}$
Splitter (S1)	$\dot{B}_{03} = \dot{B}_{03A} + \dot{B}_{03B}$	$b_{03} = b_{03A} = b_{03B}$
Compressor (IPC)	$\dot{B}_{03A} + \dot{B}_{IPC}^W + \dot{Y}_{IPC} = \dot{B}_{04}$	$b_{e,IPC} = b_{e,IPT}$
Compressor (HPC)	$\dot{B}_{04} + \dot{B}_{HPC}^W + \dot{Y}_{HPC} = \dot{B}_{05}$	$b_{e,HPC} = b_{e,HPT}$
Splitter (S2)	$\dot{B}_{05} = \dot{B}_{05A} + \dot{B}_{05B} + \dot{B}_{05C}$	$b_{05} = b_{05A} = b_{05B} = b_{05C}$
Combustor (CC)	$\dot{B}_{M4} + \dot{B}_{F1} + \dot{B}_{05A} + \dot{Y}_{CC} + \dot{B}_{CC}^{PF} = \dot{B}_{06}$	$b_{F1} = \text{fuel}$
Turbine (HPT)	$\dot{B}_{06} - \dot{B}_{07} + \dot{Y}_{HPT} = \dot{B}_{HPT}^W$	$b_{07} = b_{06}$
Turbine (IPT)	$\dot{B}_{07} - \dot{B}_{08} + \dot{Y}_{IPT} = \dot{B}_{IPT}^W$	$b_{08} = b_{06}$
Turbine (LPT)	$\dot{B}_{08} - \dot{B}_{09} + \dot{Y}_{LPT} = \dot{B}_{LPT}^W$	$b_{08} = b_{06}$
Turbine exit (TE)	$\dot{B}_{09} + \dot{Y}_{TE} = \dot{B}_{010}$	$\dot{Y}_{TE}=0$
Fan Nozzle (FN)	$\dot{B}_{03B} + \dot{Y}_{FN} = \dot{B}_{12}$	$\dot{Y}_{FN}=0$
Exit Nozzle (EN)	$\dot{B}_{010} + \dot{Y}_{EN} = \dot{B}_{11}$	$\dot{Y}_{EN}=0$
Fuel Cell (SOFC)		
Mixer (MX1)	$\dot{B}_{F2} + \dot{B}_{W1} + \dot{Y}_{MX1} = \dot{B}_{M1}$	$\dot{Y}_{MX1}=0, b_{W1} = 0.012$
Steam Reformer (SR)	$\dot{B}_{M1} + \dot{B}_{SR} + \dot{B}_{SR}^{PF} = \dot{B}_{M2}$	
Water Gas Shift (WGS)	$\dot{B}_{M2} + \dot{Y}_{WGS} + \dot{B}_{WGS}^{PF} = \dot{B}_{M3}$	
Fuel cell (SOFC)	$\dot{B}_{M3} + \dot{B}_{05B} - \dot{B}_{M4} + \dot{Y}_{SOFC} + \dot{B}_{SOFC}^{PF} = \dot{B}_{SOFC}^W + \dot{B}_{SOFC}^L$	$b_{e,SOFC} = \frac{\dot{B}_{M3} + \dot{B}_{05B} - \dot{B}_{M4}}{\dot{E}x_{M3} + \dot{E}x_{05B} - \dot{E}x_{M4}}$ $b_{l,SOFC} = 5.3 \text{ mPt/MJ (assumed)}$

System R-1:

The exergoenvironmental balance equations are explained for each component of a hybrid combined locomotive engine, and the equations are listed in Table 4.35. The table displays the exergoenvironmental balance equations and auxiliary equations for three subsystems: the gas turbine engine, a fuel cell of MCFC subsystem including the steam reforming and water gas shift reactors, the internal combustion engine, and the absorption refrigeration system involving a generator, a condenser, an evaporator, an absorber, a pump, and a regenerator heat exchanger.

Table 4.35 The exergoenvironmental balance equations for R-1 system components

Component	Exergoenvironmental Balance Equation	Auxiliary Equations
Gas Turbine (GT)		
Compressor (C2)	$\dot{B}_{B1} + \dot{B}_{C2}^W + \dot{Y}_{C1} = \dot{B}_{B2}$	$b_{B1} = 0$
HX-1	$\dot{B}_{B7} - \dot{B}_{B8} + \dot{Y}_{HX1} = \dot{B}_{B3} - \dot{B}_{B2}$	$\frac{\dot{B}_{B2}}{\dot{E}x_{B2}} = \frac{\dot{B}_{B3}}{\dot{E}x_{B3}}$
Combustion Chamber (CC)	$\dot{B}_{B3} + \dot{B}_{F3} + \dot{B}_{CC}^Q + \dot{Y}_{CC} + \dot{B}_{CC}^{PF} = \dot{B}_{B4}$	$b_{F3} = \text{fuel impact}$
Turbine (T2)	$\dot{B}_{B4} - \dot{B}_{B5} + \dot{Y}_{T2} = \dot{B}_{T2}^W$	$b_{B5} = b_{B4}$
HX-2	$\dot{B}_{B8} - \dot{B}_{B9} + \dot{B}_{HX2} = \dot{B}_{B6} - \dot{B}_{B5}$	$\frac{\dot{B}_{B6}}{\dot{E}x_{B6}} = \frac{\dot{B}_{B5}}{\dot{E}x_{B5}}$
Fuel Cell (MCFC)		
Mixer (MX1)	$\dot{B}_{F2} + \dot{B}_{W1} + \dot{Y}_{MX1} = \dot{B}_{M1}$	$\dot{Y}_{MX1}=0, b_{W1} = 0$
Steam Reformer (SR)	$\dot{B}_{M1} + \dot{B}_{SR}^Q + \dot{Y}_{SR} + \dot{B}_{SR}^{PF} = \dot{B}_{M2}$	
Water Gas Shift (WGS)	$\dot{B}_{M2} + \dot{Y}_{WGS} + \dot{B}_{WGS}^Q + \dot{B}_{WGS}^{PF} = \dot{B}_{M3}$	
Fuel Cell (MCFC)	$\dot{B}_{M5} - \dot{B}_{B7} + \dot{Y}_{MCFC} + \dot{B}_{MCFC}^{PF}$ $= \dot{B}_{MCFC}^W + \dot{B}_{M4} - \dot{B}_{M3} + \dot{B}_{MCFC}^L$	$b_{B7} = b_{M4}$
Catalytic burner (BR)	$\dot{B}_{B6} + \dot{B}_{E9} + \dot{B}_{M4} + \dot{Y}_{BR} + \dot{B}_{BR}^Q + \dot{B}_{BR}^{PF} = \dot{B}_{M5}$	
Internal Combustion Engine (ICE)		
ICE Engine	$\dot{B}_{E1} + \dot{B}_{F1} - \dot{B}_{E9} + \dot{Y}_{ICE} + \dot{B}_{ICE}^{PF} = \dot{B}_{ICE}^W$	$b_{F1} = \text{fuel impact},$ $b_{E1} = 0$
Absorption Refrigeration Cycle (ARC)		
Generator (AGN)	$\dot{B}_{B9} - \dot{B}_{B10} + \dot{B}_{A3} + \dot{Y}_{AGN} = \dot{B}_{A7} + \dot{B}_{A4}$	$b_{A4} = 0, b_{B9} = b_{B10}$
Condenser (ACN)	$\dot{B}_{A7} - \dot{B}_{A8} + \dot{Y}_{ACN} = \dot{B}_{CN}^Q$	$b_{A7} = b_{A8}$
Evaporator (AEV)	$\dot{B}_{EV}^Q + \dot{Y}_{AEV} = \dot{B}_{A9} - \dot{B}_{A10}$	$b_{A9} = b_{A10}$
Absorber (ABS)	$\dot{B}_{A10} + \dot{B}_{A6} + \dot{Y}_{ABS} = \dot{B}_{A1} + \dot{B}_{AB}^Q$	
Pump (AP)	$\dot{B}_P^W + \dot{Y}_{AP} = \dot{B}_{A2} - \dot{B}_{A1}$	
Regenerator (AHX)	$\dot{B}_{A4} - \dot{B}_{A5} + \dot{Y}_{AHX} = \dot{B}_{A3} - \dot{B}_{A2}$	$b_{A4} = b_{A5}$

System R-2:

The exergoenvironmental balance equations and auxiliary equations are explained for each component for hybrid SOFC-GT combined with PEMFC-AEC locomotive engine, which the equations are listed in Table 4.36.

Table 4.36 The exergoenvironmental balance equations for R-2 system components

Component	Cost Balance Equation	Auxiliary Equations
Gas Turbine (GT)		
Compressor (C1)	$\dot{B}_{B1} + \dot{B}_{C1}^W + \dot{Y}_{C1} = \dot{B}_{B2}$	$b_{B1} = 0$
Combustion Chamber (CC)	$\dot{B}_{B2} + \dot{B}_{F1} + \dot{Y}_{CC} + \dot{B}_{CC}^{PF} = \dot{B}_{B3}$	$b_{F3} = \text{fuel impact}$
Turbine (T1)	$\dot{B}_{B3} - \dot{B}_{B4} + \dot{Y}_{T1} = \dot{B}_{T1}^W$	$b_{B3} = b_{B4},$ $b_{el,C1} = b_{el,T1}$
Splitter (SP1)	$\dot{B}_{B4} + \dot{Y}_{SP1} = \dot{B}_{B5} + \dot{B}_{B6}$	$b_{B3} = b_{B5} = b_{B6},$ $\dot{Y}_{SP1} = 0$
Mixer (MX1)	$\dot{B}_{B8} + \dot{B}_{B9} + \dot{Y}_{MX1} = \dot{B}_{B7}$	$b_{B7} = b_{B6} = b_{M5},$ $\dot{Y}_{MX1} = 0$
Fuel Cell (SOFC)		
Mixer (MX2)	$\dot{B}_{F2} + \dot{B}_{W1} + \dot{Y}_{MX1} = \dot{B}_{M1}$	$\dot{Y}_{MX1}=0, b_{W1} = 0$
Steam Reformer (SR)	$\dot{B}_{M1} + \dot{Y}_{SR} + \dot{B}_{SR}^{PF} = \dot{B}_{M2}$	---
Water Gas Shift (WGS)	$\dot{B}_{M2} + \dot{Y}_{WGS} + \dot{B}_{WGS}^{PF} = \dot{B}_{M3}$	---
SOFC	$\dot{B}_{M3} - \dot{B}_{B5} + \dot{Y}_{SOFC} - \dot{B}_{M4} + \dot{B}_{SOFC}^{PF} = \dot{B}_{SOFC}^W$	$b_{B7} = b_{M4}$
Afterburner (BR)	$\dot{B}_{M4} + \dot{Y}_{BR} + \dot{B}_{WGS}^{PF} = \dot{B}_{M5}$	---
Energy Recovery		
Thermoelectric generator (TG)	$\dot{B}_{B7} - \dot{B}_{B8} + \dot{Y}_{TG} = \dot{B}_{TG}^W$	$b_{B8} = b_{B7}$
Generator (AGN)	$\dot{B}_{R3} + \dot{B}_{B8} - \dot{B}_{B9} + \dot{Y}_{AGN} = \dot{B}_{R4} + \dot{B}_{R7}$	$b_{R3} = \text{refrigerant impact}$ $b_{B9} = b_{B8}$ $b_{R7} = b_{R8}$
Condenser (ACN)	$\dot{B}_{R7} - \dot{B}_{R8} + \dot{Y}_{ACN} = \dot{B}_{ACN}^Q$	$b_{R7} = b_{R8}$
Expansion valve (AEX1)	$\dot{B}_{R8} + \dot{Y}_{AEX1} = \dot{B}_{R9}$	$\dot{Y}_{AEX1} = 0, b_{R8} = b_{R9}$
Evaporator (AEV)	$\dot{B}_{EV}^Q + \dot{Y}_{AEV} = \dot{B}_{R10} - \dot{B}_{R9}$	$b_{A9} = b_{A10}$
Absorber (ABS)	$\dot{B}_{R10} + \dot{B}_{R6} + \dot{Y}_{ABS} = \dot{B}_{R1} + \dot{B}_{ABS}^Q$	---
Pump (AP)	$\dot{B}_{AP}^W + \dot{Y}_{AP} = \dot{B}_{R2} - \dot{B}_{R1}$	$b_{R2} = b_{R1}, b_{el,AP} = b_{el,T1}$
Regenerator (AHX)	$\dot{B}_{R4} - \dot{B}_{R5} + \dot{Y}_{AHX} = \dot{B}_{R3} - \dot{B}_{R2}$	$b_{R2} = b_{R3}, b_{R4} = b_{R5}$
Expansion valve (AEX2)	$\dot{B}_{R5} + \dot{Y}_{AEX2} = \dot{B}_{R6}$	$\dot{Y}_{AEX2} = 0, b_{R5} = b_{R6}$
Hydrogen Production		
Ammonia electrolysis cell (AEC)	$\dot{B}_{AEC}^W + \dot{B}_{N1} + \dot{B}_{N2} + \dot{Y}_{AEC} = \dot{B}_{N4} + \dot{B}_{N6} + \dot{B}_{N7}$	$b_{NH3} = \text{ammonia impact}$ $b_{H1} = b_{H2} = 3b_{N7},$ $b_{el,AEC} = b_{el,T1}$
Expansion valve (EX1)	$\dot{B}_{N6} + \dot{Y}_{EX1} = \dot{B}_{N9}$	$\dot{Y}_{EX1} = 0, b_{N9} = b_{N6}$
Splitter (FP)	$\dot{B}_{N9} + \dot{Y}_{FP} = \dot{B}_{H2} + \dot{B}_{H1}$	---
PEMFC	$\dot{B}_{A3} + \dot{B}_{H1} - \dot{B}_{A4} + \dot{Y}_{PEMFC} = \dot{B}_{PEMFC}^W$	---
Turbine (T2)	$\dot{B}_{N7} - \dot{B}_{N8} + \dot{Y}_{T2} = \dot{B}_{T2}^W$	$b_{N7} = b_{N8}$
Compressor (C2)	$\dot{B}_{A1} + \dot{B}_{C2}^W + \dot{Y}_{C2} = \dot{B}_{A2}$	$b_{A1} = 0, b_{el,C2} = b_{el,T2}$
Heat exchanger (HX1)	$\dot{B}_{A3} - \dot{B}_{A2} + \dot{Y}_{HX2} = \dot{B}_{A5} - \dot{B}_{A4}$	$b_{A4} = b_{A5}, b_{A3} = b_{A2}$

System R-3:

The exergoenvironmental balance equations and auxiliary equations are explained for each component for hybrid SOFC-PEMFC-GT locomotive engine in Table 4.37.

Table 4.37 The exergoenvironmental balance equations for R-3 system components

Component	Cost Balance Equation	Auxiliary Equations
Gas Turbine (GT)		
Compressor (C1)	$\dot{B}_{B1} + \dot{B}_{C1}^W + \dot{Y}_{C1} = \dot{B}_{B2}$	$b_{B1} = 0$
Intercooler (IC)	$\dot{B}_{A2} - \dot{B}_{IC}^Q + \dot{Y}_{IC} = \dot{B}_{A3}$	$b_{A2} = b_{A3}$
Splitter (S1)	$\dot{B}_{A3} + \dot{Y}_{S1} = \dot{B}_{A4} + \dot{B}_{B1}$	$b_{A3} = b_{B4} = b_{B1},$ $\dot{Y}_{S1} = 0$
Compressor (C2)	$\dot{B}_{A4} + \dot{B}_{C2}^W + \dot{Y}_{C2} = \dot{B}_{A5}$	
Combustion Chamber (CC)	$\dot{B}_{A5} + \dot{B}_{F1} + \dot{Y}_{CC} + \dot{B}_{CC}^{PF} = \dot{B}_{A7}$	$b_{F1} = \text{fuel impact}$
Turbine (T2)	$\dot{B}_{A7} - \dot{B}_{A8} + \dot{Y}_{T2} = \dot{B}_{T2}^W$	$b_{A7} = b_{A8}, b_{el,C2} = b_{el,T2}$
Splitter (S2)	$\dot{B}_{A8} + \dot{Y}_{S2} = \dot{B}_{A9} + \dot{B}_{B2}$	$b_{A8} = b_{A9} = b_{B2},$ $\dot{Y}_{S2} = 0$
Turbine (T1)	$\dot{B}_{A10} - \dot{B}_{A11} + \dot{Y}_{T1} = \dot{B}_{T1}^W$	$b_{A11} = b_{A12}, b_{el,C1} =$ $b_{el,T1}$
PEMFC	$\dot{B}_{B1} + \dot{B}_{H1} - \dot{B}_{H2} + \dot{Y}_{PEMFC} = \dot{B}_{PEMFC}^W$	---
Turbine (T3)	$\dot{B}_{H2} - \dot{B}_{H3} + \dot{Y}_{T3} = \dot{B}_{T3}^W$	$b_{H3} = b_{H2}$
Thermoelectric generator (TEG1)	$\dot{B}_{H3} - \dot{B}_{H4} + \dot{Y}_{TEG1} = \dot{B}_{TEG1}^W$	$b_{H3} = b_{H4}$
Fuel Cell (SOFC)		
Mixer (MX2)	$\dot{B}_{F2} + \dot{B}_{W1} + \dot{Y}_{MX1} = \dot{B}_{D1}$	$\dot{Y}_{MX1}=0, b_{W1} = 0$
Steam Reformer (SR)	$\dot{B}_{D1} + \dot{Y}_{SR} + \dot{B}_{SR}^{PF} = \dot{B}_{D2}$	---
Water Gas Shift (WGS)	$\dot{B}_{D2} + \dot{Y}_{WGS} + \dot{B}_{WGS}^{PF} = \dot{B}_{D3}$	---
SOFC	$\dot{B}_{D3} - \dot{B}_{B2} + \dot{Y}_{SOFC} - \dot{B}_{D4} + \dot{B}_{SOFC}^{PF} = \dot{B}_{SOFC}^W$	$b_{B2} = b_{D4}$
Afterburner (BR)	$\dot{B}_{D4} + \dot{B}_{A9} + \dot{Y}_{BR} + \dot{B}_{WGS}^{PF} = \dot{B}_{A5}$	---
Energy Recovery		
Thermoelectric generator (TG)	$\dot{B}_{A12} - \dot{B}_{A13} + \dot{Y}_{TEG2} = \dot{B}_{TEG2}^W$	$b_{A13} = b_{A12}$
Generator (AGN)	$\dot{B}_{R3} + \dot{B}_{A11} - \dot{B}_{A12} + \dot{Y}_{AGN} = \dot{B}_{R4} + \dot{B}_{R7}$	$b_{R3} = \text{refrigerant impact}$ $b_{A11} = b_{A12}$ $b_{R7} = b_{R8}$
Condenser (ACN)	$\dot{B}_{R7} - \dot{B}_{R8} + \dot{Y}_{ACN} = \dot{B}_{ACN}^Q$	
Expansion valve (AEX1)	$\dot{B}_{R8} + \dot{Y}_{AEX1} = \dot{B}_{R9}$	$\dot{Y}_{AEX1} = 0, b_{R8} = b_{R9}$
Evaporator (AEV)	$\dot{B}_{EV}^Q + \dot{Y}_{AEV} = \dot{B}_{R10} - \dot{B}_{R9}$	$b_{A9} = b_{A10}$
Absorber (ABS)	$\dot{B}_{R10} + \dot{B}_{R6} + \dot{Y}_{ABS} = \dot{B}_{R1} + \dot{B}_{ABS}^Q$	---
Pump (AP)	$\dot{B}_{AP}^W + \dot{Y}_{AP} = \dot{B}_{R2} - \dot{B}_{R1}$	$b_{R2} = b_{R1}, b_{el,AP} =$ $b_{el,T1}$
Regenerator (AHX)	$\dot{B}_{R4} - \dot{B}_{R5} + \dot{Y}_{AHX} = \dot{B}_{R3} - \dot{B}_{R2}$	$b_{R2} = b_{R3}, b_{R4} = b_{R5}$
Expansion valve (AEX2)	$\dot{B}_{R5} + \dot{Y}_{AEX2} = \dot{B}_{R6}$	$\dot{Y}_{AEX2} = 0, b_{R5} = b_{R6}$

System M-1:

The exergoenvironmental balance equations and auxiliary equations are explained for each component for hybrid combined marine engine, which the equations are listed in Table 4.38.

Table 4.38 The exergoenvironmental balance equations for M-1 system components

Component	Cost Balance Equation	Auxiliary Equations
Gas Turbine (GT)		
Compressor (C2)	$\dot{B}_{Y1} + \dot{B}_{C2}^W + \dot{Y}_{C2} = \dot{B}_{Y2}$	$b_{Y1} = 0$
Intercooler (IC)	$\dot{B}_{Y2} - \dot{B}_{IC}^Q + \dot{Y}_{IC} = \dot{B}_{Y3}$	$b_{Y2} = b_{Y3}$
Compressor (C3)	$\dot{B}_{Y3} + \dot{B}_{C3}^W + \dot{Y}_{C3} = \dot{B}_{Y4}$	
Combustion Chamber (CC)	$\dot{B}_{Y4} + \dot{B}_{MF2} + \dot{Y}_{CC} + \dot{B}_{CC}^{PF} = \dot{B}_{Y5}$	$b_{MF1} = \text{fuel impact}$
Turbine (T3)	$\dot{B}_{Y5} - \dot{B}_{Y6} + \dot{Y}_{T3} = \dot{B}_{T3}^W$	$b_{Y5} = b_{Y6}, b_{el,C3} = b_{el,T3}$
Splitter (SP1)	$\dot{B}_{Y6} + \dot{Y}_{SP1} = \dot{B}_{Y7} + \dot{B}_{Y8}$	$b_{Y6} = b_{Y7} = b_{Y8},$
Compressor (C2)	$\dot{B}_{A4} + \dot{B}_{C2}^W + \dot{Y}_{C2} = \dot{B}_{A5}$	
Turbine (T2)	$\dot{B}_{Y10} - \dot{B}_{Y11} + \dot{Y}_{T2} = \dot{B}_{T2}^W$	$b_{Y10} = b_{Y11}, b_{el,C2} = b_{el,T2}$
Thermoelectric generator (TEG2)	$\dot{B}_{Y11} - \dot{B}_{Y12} + \dot{Y}_{TEG2} = \dot{B}_{TEG2}^W$	$b_{Y11} = b_{Y12}$
Fuel Cell (SOFC)		
Mixer (MX1)	$\dot{B}_{MF3} + \dot{B}_{W1} + \dot{Y}_{MX1} = \dot{B}_{Z1}$	$\dot{Y}_{MX1}=0, b_{W1} = 0$
Steam Reformer (SR)	$\dot{B}_{Z1} + \dot{Y}_{SR} + \dot{B}_{SR}^{PF} = \dot{B}_{Z2}$	---
Water Gas Shift (WGS)	$\dot{B}_{Z2} + \dot{Y}_{WGS} + \dot{B}_{WGS}^{PF} = \dot{B}_{Z3}$	---
SOFC	$\dot{B}_{Z3} - \dot{B}_{Z4} + \dot{Y}_{SOFC} + \dot{B}_{Y7} + \dot{B}_{SOFC}^{PF} = \dot{B}_{SOFC}^W$	$b_{Y7} = b_{Z4}$
Mixer (MX2)	$\dot{B}_{Z4} + \dot{B}_{Y8} + \dot{Y}_{MX2} = \dot{B}_{Y9}$	---
Afterburner (BR)	$\dot{B}_{Y9} + \dot{Y}_{BR} + \dot{B}_{BR}^{PF} = \dot{B}_{Y10}$	---
Internal Combustion Engine (ICE)		
Internal combustion engine (ICE)	$\dot{B}_{X1} + \dot{B}_{MF1} - \dot{B}_{AC}^Q - \dot{B}_{R1}^Q + \dot{Y}_{ICE} - \dot{B}_{X10} = \dot{B}_{ICE}^W$	$b_{el,ICE} = \frac{\dot{B}_{X1} + \dot{B}_{MF1} - \dot{B}_{X10}}{\dot{E}x_{X1} + \dot{E}x_{MF1} - \dot{E}x_{X10}}$
Thermoelectric generator (TEG1)	$\dot{B}_{X10} - \dot{B}_{X11} + \dot{Y}_{TEG1} = \dot{B}_{TEG1}^W$	$b_{X10} = b_{X11}$

System M-2:

The exergoenvironmental balance equations and auxiliary equations are explained for each component for hybrid compound cycles (SRC-SOFC-GT) marine engine, which the equations are shown in Table 4.39.

Table 4.39 The exergoenvironmental balance equations for M-2 system components

Component	Cost Balance Equation	Auxiliary Equations
Steam Rankine Cycle (SRC)		
HP-ST1	$\dot{B}_{A7} - \dot{B}_{A8} + \dot{Y}_{HPST1} = \dot{B}_{HPST1}^W$	$b_{A7} = b_{A8},$ $b_{el,HPT1} = b_{el,P1} = b_{el,P2}$
IP-ST2	$\dot{B}_{A9} - \dot{B}_{A11E} + \dot{Y}_{IPST2} = \dot{B}_{IPST2}^W$	$b_{A9} = b_{A11E}$
LP-ST3	$\dot{B}_{A11T} - \dot{B}_{A12} - \dot{B}_{A13} - \dot{B}_{A10} + \dot{Y}_{LPST3} = \dot{B}_{LPST3}^W$	$b_{A9} = b_{A11E}$
CN	$\dot{B}_{G2} - \dot{B}_{G3} + \dot{Y}_{CN} = \dot{B}_{CN}^Q$	$b_{G2} = b_{G3}$
P1	$\dot{B}_{A1} + \dot{B}_{P1}^W + \dot{Y}_{P1} = \dot{B}_{A2}$	$b_{A1} = b_{A2}$
P2	$\dot{B}_{GA5} + \dot{B}_{LPC1}^W + \dot{Y}_{LPC1} = \dot{B}_{A6}$	$b_{G1} = 0$
CFH1	$\dot{B}_{A13} + \dot{B}_{A18} - \dot{B}_{A20} + \dot{Y}_{CFH1} = \dot{B}_{A3} - \dot{B}_{A2}$	$b_{A3} = b_{A2}$
CFH2	$\dot{B}_{A12} + \dot{B}_{A16} - \dot{B}_{A17} + \dot{Y}_{CFH2} = \dot{B}_{A4} - \dot{B}_{A3}$	$b_{A4} = b_{A3}$
CFH3	$\dot{B}_{A11} - \dot{B}_{A14} + \dot{Y}_{CFH3} = \dot{B}_{A5} - \dot{B}_{A4}$	$b_{A5} = b_{A4}$
EX1	$\dot{B}_{A14} + \dot{Y}_{EX1} = \dot{B}_{A15}$	
EX2	$\dot{B}_{A17} + \dot{Y}_{EX2} = \dot{B}_{G18}$	
EX3	$\dot{B}_{A20} + \dot{Y}_{EX3} = \dot{B}_{A21}$	
BR-BL	$\dot{B}_{G12} + \dot{B}_{B1} + \dot{B}_{F1} + \dot{Y}_{CC} + \dot{B}_{BRBL}^{PF} = \dot{B}_{B2}$	$b_{F1} = \text{fuel impact}$
HX-BL	$\dot{B}_{B2} - \dot{B}_{B3} + \dot{Y}_{HXB L} = \dot{B}_{A7} - \dot{B}_{A6}$	$b_{B2} = b_{B3}$
HX-RH	$\dot{B}_{B3} - \dot{B}_{B4} + \dot{Y}_{HXR H} = \dot{B}_{A9} - \dot{B}_{A8}$	$b_{B3} = b_{B4}$
DSWR	$\dot{B}_{B4} - \dot{B}_{B5} + \dot{B}_{SW1} - \dot{B}_{SW4} + \dot{Y}_{DSWR} = \dot{B}_{FW17} - \dot{B}_{SL5}$	$b_{SW1} = 0$
Gas Brayton Cycle (GBC)		
LP-C1	$\dot{B}_{G1} + \dot{B}_{LPC1}^W + \dot{Y}_{LPC1} = \dot{B}_{G2}$	$b_{G1} = 0$
IC	$\dot{B}_{G2} - \dot{B}_{IC}^Q + \dot{Y}_{IC} = \dot{B}_{G3}$	$b_{G2} = b_{G3}$
HP-C2	$\dot{B}_{G3} + \dot{B}_{HPC2}^W + \dot{Y}_{HPC2} = \dot{B}_{G4}$	
GTSP	$\dot{B}_{G4} + \dot{Y}_{GTSP} = \dot{B}_{G5} + \dot{B}_{G6}$	$b_{G4} = b_{G5} = b_{G6}$
CC	$\dot{B}_{M4} + \dot{B}_{F2} + \dot{B}_{G6} + \dot{Y}_{CC} + \dot{B}_{CC}^{PF} = \dot{B}_{G7}$	$b_{F2} = \text{fuel impact}$
GTHX	$\dot{B}_{G7} - \dot{B}_{G8} + \dot{Y}_{GTHX} = \dot{B}_{G11} - \dot{B}_{G10}$	
HP-T1	$\dot{B}_{G8} - \dot{B}_{G9} + \dot{Y}_{HPT1} = \dot{B}_{HPT1}^W$	$b_{A7} = b_{A8},$ $b_{el,HPT1} = b_{el,HPC2}$
LP-T2	$\dot{B}_{G10} - \dot{B}_{G11} + \dot{Y}_{LPT2} = \dot{B}_{LPT2}^W$	$b_{G10} = b_{G11},$ $b_{el,LPT2} = b_{el,LPC1}$
P-T3	$\dot{B}_{G11} - \dot{B}_{G12} + \dot{Y}_{PT3} = \dot{B}_{PT3}^W$	$b_{G11} = b_{G12}$
Fuel Cell (SOFC)		
GTMX	$\dot{B}_{F3} + \dot{B}_{W1} + \dot{Y}_{GTMX} = \dot{B}_{M1}$	$b_{W1} = 0, b_{F3} = \text{fuel impact}$
SR	$\dot{B}_{M1} + \dot{Y}_{SR} + \dot{B}_{SR}^{PF} = \dot{B}_{M2}$	---
WGS	$\dot{B}_{M2} + \dot{Y}_{WGS} + \dot{B}_{WGS}^{PF} = \dot{B}_{M3}$	---
SOFC	$\dot{B}_{G5} + \dot{B}_{M3} + \dot{Y}_{SOFC} + \dot{B}_{SOFC}^{PF} - \dot{B}_{M4} = \dot{B}_{SOFC}^W$	$b_{M4} = b_{G5}$

System M-3:

The exergoenvironmental balance equations and auxiliary equations are explained for each component for hybrid MCFC-turbofan aircraft engine, which the equations are listed in Table 4.40. It covers the equations for three subsystems: a gas turbine engine (GBC), a fuel cell of SOFC subsystem, and two organic Rankine cycles of TORC and BORC subsystems.

Table 4.40 The exergoenvironmental balance equations for M-3 system components

Component	Cost Balance Equation	Auxiliary Equations
Gas Brayton Cycle (GBC)		
HPC1	$\dot{B}_{G1} + \dot{B}_{HPC1}^W + \dot{Z}_{HPC1} = \dot{B}_{G2}$	$b_{A1} = 0$
GTHX	$\dot{B}_{G3} - \dot{B}_{G2} + \dot{Z}_{GTHX} = \dot{B}_{G9} - \dot{B}_{G8}$	$b_{G2} = b_{G3}$
SP	$\dot{B}_{G3} + \dot{Z}_{SP} = \dot{B}_{G4} + \dot{B}_{G5}$	$b_{G3} = b_{G4} = b_{G5}$
CC	$\dot{B}_{G5} + \dot{B}_{FC7} + \dot{B}_{F1} + \dot{Z}_{CC} + \dot{B}_{WGS}^{PF} = \dot{B}_{A5}$	$b_{F1} = \text{fuel impact}$
HPT1	$\dot{B}_{G6} - \dot{B}_{G7} + \dot{Z}_{HPT1} = \dot{B}_{HPT1}^W$	$b_{G6} = b_{G7}, b_{el,HPC1} = b_{el,HPT1}$
LPT2	$\dot{B}_{G7} - \dot{B}_{G8} + \dot{Z}_{LPT2} = \dot{B}_{LPT2}^W$	$b_{G7} = b_{G8}, b_{el,LPT2} = b_{el,P1}$
Fuel Cell (SOFC)		
MX	$\dot{B}_{F2} + \dot{B}_{S1} + \dot{Z}_{MX} = \dot{B}_{FC1}$	$b_{F2} = \text{fuel impact}, b_{S1} = 0$
SR	$\dot{B}_{FC1} + \dot{Z}_{SR} + \dot{B}_{WGS}^{PF} = \dot{B}_{FC2}$	---
WGS	$\dot{B}_{FC2} + \dot{Z}_{WGS} + \dot{B}_{WGS}^{PF} = \dot{B}_{FC3}$	---
SOFC	$\dot{B}_{FC3} + \dot{B}_{G4} + \dot{Z}_{SOFC} + \dot{B}_{WGS}^{PF} - \dot{B}_{FC7} = \dot{B}_{SOFC}^W$	$b_{FC7} = b_{G4}$
Organic Rankine Cycles (TORC and BORC)		
CN1	$\dot{B}_{G9} - \dot{B}_{G10} + \dot{Y}_{CN1} = \dot{B}_{TR3} - \dot{B}_{TR2}$	$b_{G9} = b_{G10}$
CN2	$\dot{B}_{G10} - \dot{B}_{G11} + \dot{Y}_{AGN} = \dot{B}_{LR4} - \dot{B}_{LR3}$	$b_{G11} = b_{G10}$
T3	$\dot{B}_{TR3} - \dot{B}_{TR4} + \dot{Y}_{T3} = \dot{B}_{T3}^W$	$b_{TR3} = b_{TR4}, b_{el,T3} = b_{el,P1}$
T4	$\dot{B}_{LR4} - \dot{B}_{LR5} + \dot{Y}_{T4} = \dot{B}_{T4}^W$	$b_{LR4} = b_{LR5}, b_{el,T4} = b_{el,P2}$
T5	$\dot{B}_{LR6} - \dot{B}_{LR7} + \dot{Y}_{T5} = \dot{B}_{T5}^W$	$b_{LR6} = b_{LR7}$
P1	$\dot{B}_{TR1} + \dot{Y}_{P1} + \dot{B}_{P1}^W = \dot{B}_{TR2}$	$b_{TR1} = b_{TR2}$
P2	$\dot{B}_{P2}^W + \dot{Y}_{P2} + \dot{B}_{LR1} = \dot{B}_{LR2}$	$b_{LR2} = b_{LR1}$
EV11	$\dot{B}_{LR2} - \dot{B}_{LR3} + \dot{Y}_{EV11} = \dot{B}_{TR5} - \dot{B}_{TR4}$	$b_{LR2} = b_{LR3}$
EV12	$\dot{B}_{LR5} - \dot{B}_{LR6} + \dot{B}_{LGN1} - \dot{B}_{LNG2} + \dot{Y}_{EV12} = \dot{B}_{TR1} - \dot{B}_{TR5}$	$b_{LR5} = b_{LR6}$
EV2	$\dot{B}_{LNG2} - \dot{B}_{LNG3} + \dot{Y}_{EV2} = \dot{B}_{LR1} - \dot{B}_{LR7}$	$b_{LR1} = b_{LR7}$

4.6 Multi-objective Optimization

The multi-objective optimization is applied to the transportation systems in order to obtain the optimum system performance. This is a crucial step to provide a optimal objective functions for three transportation engines. The thesis presents four comprehensive analyses that provide many extinctive outputs such as energy performance, cost, and environmental impact, which are correlated in a positive way. However, it is recommended to reduce the cost and environmental impact of engines with increasing the engine performance. The following subsections provide the optimization procedure, the evolutionary algorithm of multi-objective particle swarm algorithm (MOPSO), and algorithm specifications.

4.6.1 Optimization Procedure

The thermodynamic analysis for all systems contains many interrelated equations because the system is considered a closed cycle. Therefore, the number of equations should be reduced to the most valuable equations, which are the objective functions of the system, so that the optimization can be applied. Thus, the optimization procedure is described in Figure 4.22.

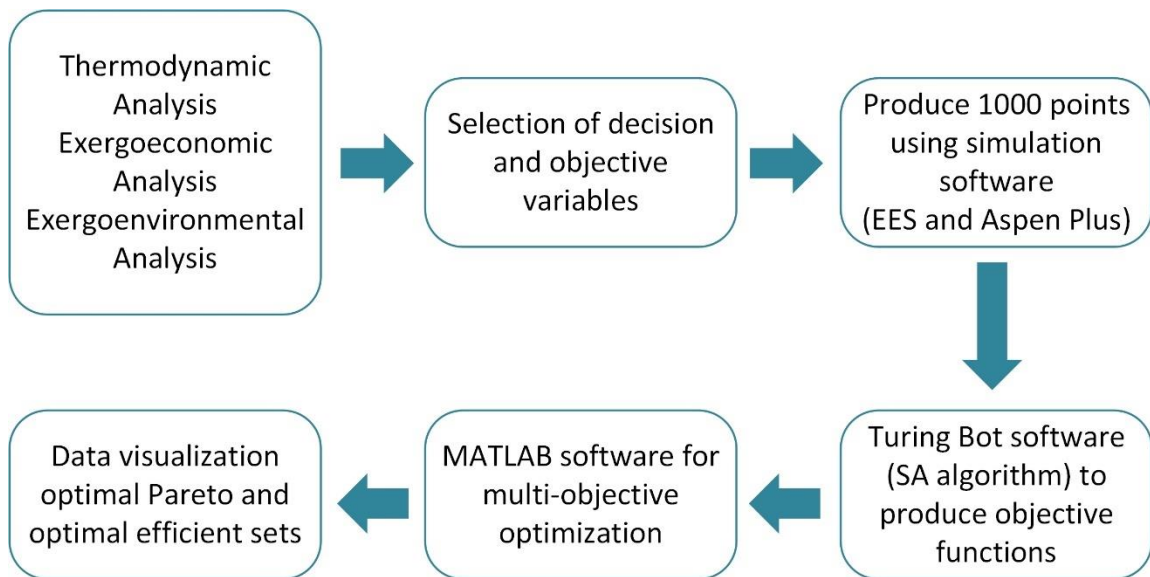


Figure 4.22 The optimization procedure for clean transportation systems

The first step is to design a system based on thermodynamic analysis, exergoeconomic analysis, and exergoenvironmental analysis. This step hundreds of equations covering

energy balance equations, exergy balance equations, exergoeconomic balance equations, and exergoenvironmental balance equations. The second step is to select the decision variables: pressure reduction of turbines, pressure compression ratio of compressors, maximum temperature, and maximum pressure in the cycle. Also, the objective variables are maximizing overall engine power, maximizing exergy efficiency, minimizing the environmental impact, and minimizing the total cost. The third step is to utilize the software of Engineering Equation Solver (EES) and Aspen plus to generate to produce 1000 points or more of results according to the decision variables and objective functions. The fourth step is to use Annealing Algorithm (Turing Bot) software [209], which is based on combining a set of equations to describe the objective functions in terms of the decision variables rather than using thermodynamic analysis equations. The fifth step is to apply the multi-objective particle swarm optimization to obtain a set of trade-off optimal values for the objective functions. Finally, this optimal set is called Pareto optimal efficient set can be tabulated and visualized in different ways.

4.6.2 Evolutionary Algorithm: MOPSO

Evolutionary algorithms are based on computational models of natural selection and genetic operators, like selection, crossover, and mutation. They simulate natural evolution by creating a population of individuals, evaluating their fitness, generating a new population so-called offspring, through genetic operations, and repeating this process many generations. In this thesis, two evolutionary algorithms are employed, namely Simulated Annealing (SA) and multi-objective particle swarm optimization (MOPSO).

Simulated annealing [210] is a method that uses probability to estimate the best possible outcome for a given function. It is a metaheuristic approach to finding the global optimum in a vast search space for optimization problems. The SA is commonly employed when the search space is limited to discrete problems. In situations where getting an approximate global optimum is more significant than obtaining an accurate local optimum in a fixed amount of time, simulated annealing may be preferred over exact algorithms like gradient descent or branch and bound.

A particle swarm optimization (PSO) mimicked the paradigm of birds flocking, which is another stochastic population-based metaheuristic evolutionary algorithm [211].

The core of PSO relies on two simple updating mechanisms: PSO self-updating equations, and the process of updating the individuals per iteration using mutation and crossover operations. Each particle successively adjusts its position x_i toward the global optimum according to the following two factors: the best position visited by itself ($pbest_i$) denoted as $p_i = (p_{i1}, p_{i2}, p_{i3}, \dots, p_{id})$, and the best position visited by the whole swarm ($gbest$) (or $lbest$, the best position for a given subset of the swarm) denoted as $p_g = (p_{g1}, p_{g2}, p_{g3}, \dots, p_{gd})$. The vector $(p_g - x_i)$ represents the difference between the current position of the particle i and the best position of its neighbourhood, as shown in Figure 4.23. Therefore, a particle is composed of three vectors: the x -vector records the current position (location) of the particle in the search space; the p -vector records the location of the best solution found so far by the particle, and the v -vector contains a gradient (direction) for which particle will travel in if undisturbed.

The ρ_1 and ρ_2 are two random variables vectors in the range of $[0,1]$. The constants C_1 and C_2 represent the cognitive learning factor that represents the attraction of the particle toward its own success and the social learning factor that represents the attraction of the particle toward the success of its neighbours, respectively. Because of the updated velocity and the cognitive and social learning factors, the PSO algorithm is faster than the genetic algorithm and reaches the optimal values in a short time, and it performs better in continuous objective functions rather than discrete objective functions.

```

Random initialization of the whole swarm;
Repeat
  Evaluate  $f(x_i)$ 
  For all particles  $i$ 
    Update velocities:
       $v_i(t) = v_i(t-1) + \rho_1 C_1 \times (p_i - x_i(t-1)) + \rho_2 C_2 \times (p_g - x_i(t-1))$ 
    Move to the new position:  $x_i(t) = x_i(t-1) + v_i(t)$ ;
    If  $f(x_i) < f(pbest_i)$  Then  $pbest_i = x_i$ ;
    If  $f(x_i) < f(gbest_i)$  Then  $gbest_i = x_i$ ;
    Update  $(x_i, v_i)$ ;
  End For
Until Stopping criteria

```

Figure 4.23 The pseudo-code for the PSO algorithm

The MOPSO is one of the most promising stochastic search methodologies because of its easy implementation and high convergence speed. The elitism in MOPSO involves two processes: the archiving of good solutions and the selection of $gbest$ for each particle. Diversity must also be considered to encourage and maintain a diverse solution set. The

optimization process of MOPSO starts with the initialization of the swarm, which is followed by an evaluation and density assessment of candidate solutions. Then, good solutions are selected and updated into an external archive. After that, a truncation process will be conducted based on some density assessment to restrict the number of archiving solutions. Next, the current *pbest* position is compared to the former particle position, and the *gbest* selection process involves the set of updated nondominated solutions. Then the PSO updating the exploration and exploitation in the search space for better solutions.

4.6.3 Algorithm Specifications

Algorithms specifications for each algorithm used in the optimization are explained as the following:

- a) The SA algorithm is performed using Turing Bot software [209] four times for the selected objective functions. The population size is more than 20, and mean error is less than 1%, The regression factor (R^2) is more than 0.99.
- b) The MOPSO is run using MATLAB software. The population size is 200, the repository size is 200, maximum number of generations is 500, inertia weight is 0.4, individual confidence or cognitive learning factor C_1 is 2, and swarm confidence or social learning factor C_2 is 2, number of grids in each dimension is 20, maximum velocity percentage is 5%, and uniform mutation percentage is 0.5.

Decision variables:

Few decision variables are considered in the transportation systems. The lower limits and upper limits for each decision variable are restricted to the system limitation design. These variables are listed below as the following:

- The expansion ratio of turbines with a constraint range of (0.02-0.5)
- The compression ratio of compressors with a constraint range of (4-8)
- Maximum temperature of engine cycle with a constraint range of (1500-2200 K)
- Maximum pressure of engine cycle with a constrained range of (800-2000 kPa)

Objective functions:

The objective functions are most likely considered to be related to system performance. They may include four objective functions as the following:

- a) Maximizing the overall engine power,
- b) Maximizing the overall exergetic efficiency based on fuel and product principal,
- c) Minimizing the specific fuel and product exergy cost, yielding to minimizing the overall relative cost difference of the engine, and lastly
- d) Minimizing the overall fuel and product exergy environment, yielding to minimizing the overall relative environment difference of the engine.

In conclusion, this chapter presents modelling of subsystems and engines. The performance system for each engine in the transportation is discussed including the Aspen Plus flowcharts to address the thermodynamic analysis for traditional engines such as internal combustion engine (ICE) for rail and marine transportation and a turbofan engine for aviation. Also, the chapter presents modelling of new powering systems like fuel cells of MCFC, SOFC, PEMFC, and AEC, and energy recovery systems like thermoelectric generator, an absorption refrigeration system, and a desalination system. Three analyses are also conducted for each engine, such as exergy analysis based on fuel and product principal, and exergoeconomic analysis, and exergoenvironmental analysis since the analyses shows the balance equations of fuel and product exergy flows, cost balance equations and their cost auxiliary equations and exergoenvironmental balance equations and their auxiliary equations for each subsystem and its components. Lastly, the multi-objective optimization is addressed in this chapter to increase the engine performance to its optimal conditions.

Chapter 5. Results and Discussion

This chapter presents the results of four analyses for each system in the three sectors of transportation starting from aviation, followed by rail and marine engines. The first analysis is thermodynamic analysis that addresses the net power and required heat of engines and the overall energy and exergy efficiencies. The second analysis is exergy analysis based on fuel and product principal, which is a prerequisite step of the other two analyses. The exergoeconomic analysis is connecting the exergy and cost for flows and components. Lastly, the exergoenvironmental analysis links the exergy and environment impact on flow streams and components.

5.1 Results of System A-1

This section explains the results and discussion of thermodynamic, exergy, exergoeconomic, and exergoenvironmental analyses of hybrid MCFC-turbofan aircraft engine.

5.1.1 Results of Thermodynamic Analysis

Thermodynamic analysis was conducted for the hybrid aircraft engine at a cruising phase at an altitude of 10 km exposed to an ambient temperature of 293.2 K, ambient pressure of 26.4 kPa, and Mach number of 0.83 for the Boeing 787 Dreamline. The thermodynamic results are reported in [176]. After entering the diffuser, the air conditions are 1210 kg/s, 253.8 K, and 40.8 kPa. The mass flow rate of bypass air to the fan nozzle is about 1100 kg/s, while the compressed air has a mass flow rate of 110.11 kg/s, which decreases to 107.91 kg/s because 2% of compressed air is used as bleeding air. The pressure of air increases to 57 kPa by the fan blades, then 340.7 kPa by the IPC, then 2037.6 kPa by the HPC. The air temperature increases to 818.8 K before the combustion chamber and is burning with the fuel of 3.2 kg/s to reach 1800 K to produce an exhaust air of 111.11 kg/s, which is expanded through the HPT, IPT, and LPT turbines. Fuel blend (F1) of 0.15 kg/s is mixed with the steam of 0.3 kg/s and reacts in the steam reformer (SR) at 573 K and 200 kPa. It then reacted in the water gas shift reactor at 673K and 200kPa to produce carbon dioxide and hydrogen. This exhaust gas from SR and WGS enters the anode of MCFC unit,

and about 20% of the exhaust air of the turbines is burnt in a catalytic burner (AFTERBUR) and then in the cathode of MCFC unit.

The equipment results of the hybrid MCFC-turbofan engine is listed in Table 5.1. The required powers are about 31.5 MW for the fan, 23 MW for the IPC, and 39.5 MW for the HPC, while the output powers are 44.5 MW for the HPT, 26.5 MW for the IPT, and 32.3 MW for the LPT. The kinetic energies for fan nozzle and hot nozzle are 21.6 MW and 51.6 MW, respectively. The required heat for the CC, SR, and WGS are obtained to be about 60 MW, 2.5 MW and 21.2 kW, respectively. The MCFC delivers 823.4 kW of electric power and rejects 4.8 MW heat, having electric, energetic and exergetic efficiencies of 63.6%, 17%, and 25%, respectively. The maximum exergy destruction rate can be obtained from the combustion chamber of about 142 MW due to the large difference of temperature and pressure compared to the standard conditions and the chemical reaction heat.

Table 5.1 The thermodynamic data of system components of MCFC-turbofan using fuel F1

Components	\dot{Q} [kW]	\dot{W} [kW]	\dot{KE} [kW]	\dot{Ex}_D [kW]	π	η [%]	Ψ [%]
Compressors							
FAN	0	31546.3	0	336.3	1.4	90	98.9
IPC	0	22981.5	0	1444.1	5.98	90	96.3
HPC	0	39545.6	0	1469.1	5.98	90	93.7
Turbines							
HPT	0	40475.3	0	876.6	0.45	90	97.9
IPT	0	26480.1	0	643.6	0.55	90	97.6
LPT	0	32275.9	0	933.1	0.43	90	97.2
Nozzles & throttling							
EN	0	0	21612.7	22621.7	0.489	87	69.0
FN	0	0	51598.2	61605.0	0.476	87	44.2
TE	0	0	0	239.5	0.977	98	99.7
Reactors							
CC	59956.7	0	0	142373.8	0.982	28.0	55.8
MCFC	4837.2	823.4	0	9324.830	1	63.6 _e , 17.0 _{th}	24.9
SR	2530.5	0	0	90.3	1	73.8	99.2
WGS	21.2	0	0	84.5	1	73.8	99.3

(a) Effect of Fuels on MCFC System Performance:

The use of different fuels impacts the fuel mass flow rates. The highest fuel mass flow rate entering the combustion chamber (\dot{m}_{F1}) is 5 kg/s for kerosene and F2 with fuel-to-air mass ratio (F/A) of 0.046. The F/A decreases to about 0.03 for the remaining fuel blends because of their close values of mass flow rate (about 3.5 kg/s). The reason for this mass variation

is the low heating values of fuels since kerosene and F2 have the lowest LHV at 43.0 and 43.3 MJ/kg, respectively. However, the other fuels, F1, F3, F4, and F5, have large LHV ranging from 63.6 to 67.3 MJ/kg, respectively. The MCFC system is combined with a turbofan at the exit of all turbine stages with a small portion of air that is used for MCFC (M/A), which is called air fraction to MCFC. The values of M/A are 20%, 7% and 8% of total exhaust gas. The exhaust mass flow rates used for the MCFC are about 22 kg/s for F1, 8 kg/s for F2, 9 kg/s for F3 to F5. The fuel blend for the MCFC system, \dot{m}_{F2} , ranges from 0.1 to 0.15 kg/s, while the steam mass flow rates vary from 0.25 and 0.30, making the steam to carbon ratio, S/C, vary from 1.67 to 2.50.

Table 5.2 The results of MCFC performance using different fuels.

MCFC	Units	F1	F2	F3	F4	F5
V_c	V	0.669	0.538	0.764	0.764	0.660
V_{loss}	V	0.384	0.275	0.241	0.241	0.272
VOC	AV	96.31	77.50	110.02	109.96	95.11
\dot{W}_{MCFC}	kW	823.4	662.6	940.7	940.2	813.2
\dot{Q}_{MCFC}	kW	4837.2	4993.3	7576.7	7586.5	7706.4
$\eta_{MCFC,e}$	%	63.6	66.2	76.0	76.0	70.8
$\eta_{MCFC,th}$	%	17.0	13.3	12.4	12.4	10.6
ψ_{MCFC}	%	24.9	19.5	18.3	18.2	15.5
\dot{E}_{x_D}	kW	9324.8	3277.2	2564.6	2409.7	3153.1

The formation of hydrogen, water, carbon dioxide, oxygen should be sufficient to provide an adequate electric power with high electric efficiency. This can be accomplished by adjusting the steam and fuel mass flowrates that mentioned in the previous paragraph. Furthermore, the results of MCFC performance are obtained in Table 5.2. Using fuel blend of F3 (ethanol-base) and F4 (DME-base) can fulfil a maximum power of MCFC of about 940 kW with highest electric efficiency of 76%, but with low energetic efficiency and exergetic efficiency of 12.4% and 18.2%, respectively, because of the maximum required heat of about 7580 kW. Fuels of F1 and F5 produce lower powers of about 820 kW with low electric efficiency of about 64% for F1 and 70% of F5. However, the maximum energetic and exergetic efficiencies can be obtained for F1 of about 17% and 25%, respectively.

(b) Fuel Effect on Turbofan Performance:

The turbofan performance has been simulated using different fuels. The total power of the hybrid turbofan is displayed in Figure 5.1, including the net power of the GT, electric power

of the MCFC, and the thrust power. The highest thrust power occurs using kerosene of about 36 MW because of its large exhaust mass flow rate despite its lower exit pressure and speed. Also, the minimum thrust energy is 31.7 MW for F1. The variety of thrust energy depends on the exhaust speed and exit pressure, which are 610 m/s and 90 kPa for kerosene, 629 m/s and 102 kPa for F1, 640 m/s and 101 kPa for F2, 613 m/s and 105 kPa for F3, 641 m/s for 106 kPa for F4, and 646 m/s and 106 kPa for F5. The minimum and maximum total power are 37.5 MW for F1 and 42.2 MW for F2.

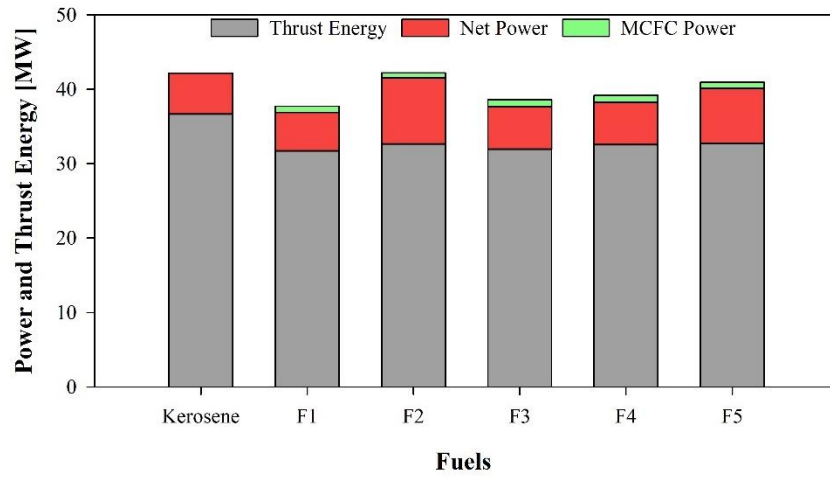


Figure 5.1 The total power of the hybrid-MCFC turbofan engine.

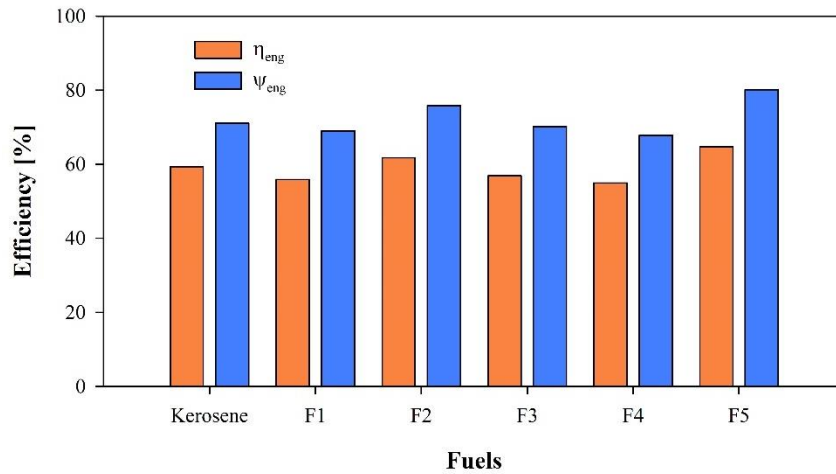


Figure 5.2 The performance of the hybrid-MCFC turbofan engine with respect to fuels

In addition, the hybrid-turbofan performance has been studied. Fueling with kerosene has achieved an energetic and exergetic efficiency of 59% and 71%, respectively, as shown in Figure 5.2. The maximum energetic and exergetic efficiencies are 64.9% and 80.2% for

F5, while the minimum energetic and exergetic efficiencies are 55% and 67% for F4, respectively.

Also, as shown in Figure 5.3, the TSFC ranges from 90 kg/(h.kN) for F1 to 137 kg/(h.kN) for F2. Adding the MCFC system to the turbofan increases the total weight to 11580 kg compared to 6000 kg of turbofan. This weight includes the SR and WGS reactors since they occurred internally before the anode layer. The weight of the MCFC was estimated as the cell weight of 620 g multiplied by the cell number and stack numbers to an overall weight of 5580 kg. Therefore, the thrust-to-weight ratio (T/W) decreases from 2.5 for only the turbofan to about 1.15 for hybrid- MCFC turbofan. In addition, the exergy destruction rates are 268 MW for kerosene and 227 MW for F5 as maximum and minimum total exergy destruction, respectively. The nozzles and combustion chamber are the most contributors of the exergy destruction about 30% and 65%, respectively.

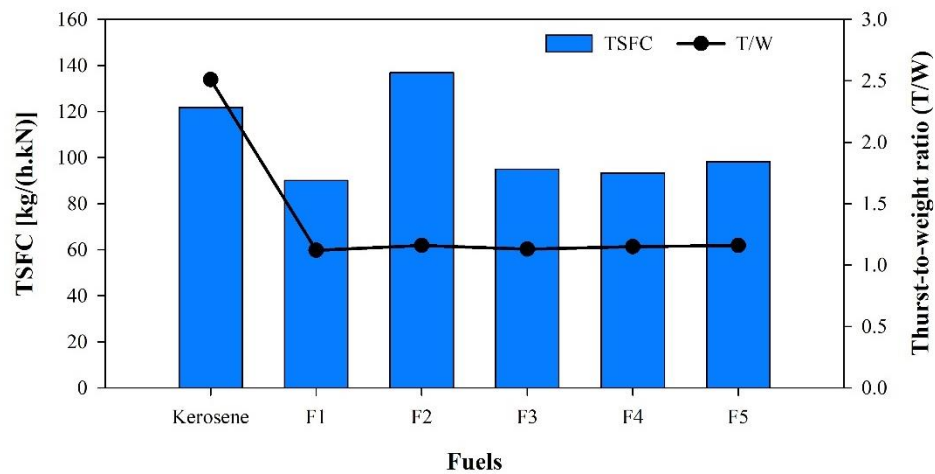


Figure 5.3 The total specific fuel consumption and thrust-to-weight ratio of the hybrid-MCFC turbofan engine.

Table 5.3 CO₂ production and emission of hybrid-turbofan engine

Fuels	Produced CO ₂ [kg/s]	Emitted CO ₂ [kg/s]
Kerosene	18.46	18.46
F1	6.80	5.27
F2	5.26	4.79
F3	3.96	3.59
F4	3.96	3.59
F5	3.92	3.55

(c) Effect of Fuels on Carbon Emissions:

Using alternative fuels has tremendously decreased by 56% for F1, 66% for F2, and 75% for the remaining, as shown in Table 5.3. Using kerosene can produce 18.5 kg/s of CO₂

during the combustion and emit them to the environment. Moreover, the amount of CO₂ has been reduced using MCFC system in the hybrid turbofan by about 9% to a minimum value of 3.55 kg/s.

5.1.2 Results of Exergy Analysis

As shown in Table 5.4, the net power of the combined engine is 5980 kW and total required heat is 67346 kW. The total exergetic rates of fuel, product, and destruction are 1007, 873, and 135 MW, respectively. This system will have an exergetic efficiency of 86.6% and an exergy destruction ratio of 13.4%. Also, the combustion chamber has the highest irreversibility ratio of about 68%, followed by the IPC; then the MCFC has less than 10%.

Table 5.4 The exergetic analysis for components of aircraft system

Comp	\dot{W}_j [kW]	\dot{Q}_j [kW]	\dot{Ex}_F [kW]	\dot{Ex}_P [kW]	\dot{Ex}_D [kW]	\dot{Ex}_L [kW]	ε [%]	y [%]	y^* [%]
FAN	31547	0	31547	31295	252	0	99.20	0.03	0.19
S1	0	0	72602	72602	0	0	100.00	0.00	0.00
FN	0	0	65995	58504	7491	0	88.65	0.74	5.56
IPC	22982	0	22982	10049	12933	0	43.73	1.28	9.60
HPC	39546	0	39546	38077	1469	0	96.29	0.15	1.09
S2	0	0	54732	54732	0	0	100.00	0.00	0.00
CC	0	59957	271805	179462	92343	0	66.03	9.17	68.56
HPT	40475	0	41352	40475	877	0	97.88	0.09	0.65
IPT	26480	0	27124	26480	644	0	97.63	0.06	0.48
LPT	32276	0	33209	32276	933	0	97.19	0.09	0.69
MX1	0	0	10386	10314	72	0	99.31	0.01	0.05
SR	0	2531	11439	10314	1125	0	90.17	0.11	0.84
WGS	0	21.2	11496	11439	57	0	99.50	0.01	0.04
MCFC	823	4837	13581	823	12758	2718	6.06	1.27	9.47
S3	0	0	77777	77777	0	0	100.00	0.00	0.00
MX2	0	0	75692	73208	2484	0	96.72	0.25	1.84
TE	0	0	73208	72969	239	0	99.67	0.02	0.18
EN	0	0	72969	71960	1009	0	98.62	0.10	0.75
Total			1007442	872756	134686	2718	86.63	13.37	100.00

Using fuel blends in the MCFC aircraft shows different total exergetic rates, as presented in Figure 5.4. The total exergetic rates of fuel are 1007, 1032, 1029, 1028, and 1128 MW for F1 to F5, respectively. Also, the total exergetic rates of a product are 873 MW for F1, 900 MW for F2, 901 MW for F3 and F4, and 1006 MW for F5. This makes the exergetic rates of destruction to be within a range of 122 to 134 MW, as shown in Figure 5.4-a. This hybridized system has an exergetic efficiency of 86.6% for F1, 87.3% for F2, 87.6 for F3 and F4, and 89.2% for F5. In addition, the exergy destruction ratio of the system has a range of 10% for F5 to 13.4% for F1, as shown in Figure 5.4-b.

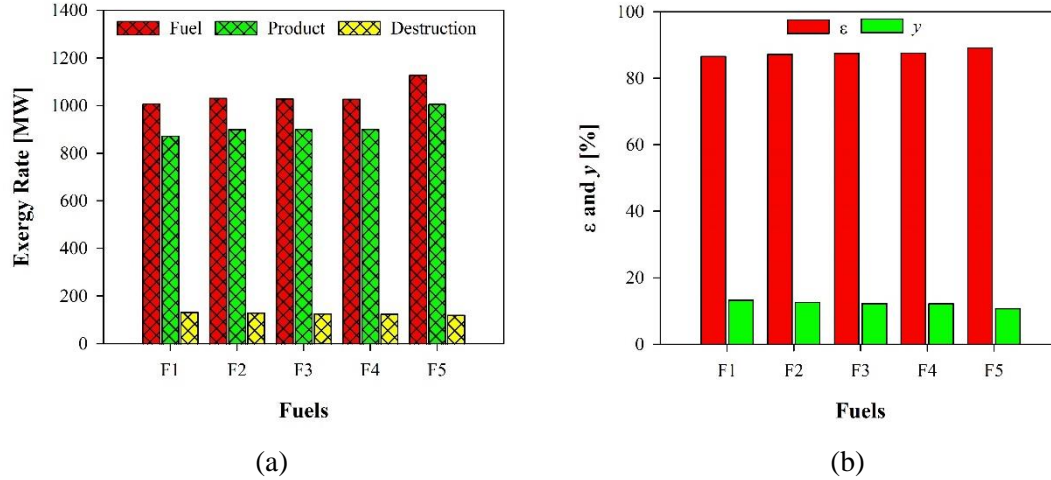


Figure 5.4 (a) Total exergy rates of fuel, product, and destruction and (b) the exergetic efficiency ε and exergy destruction ratio γ .

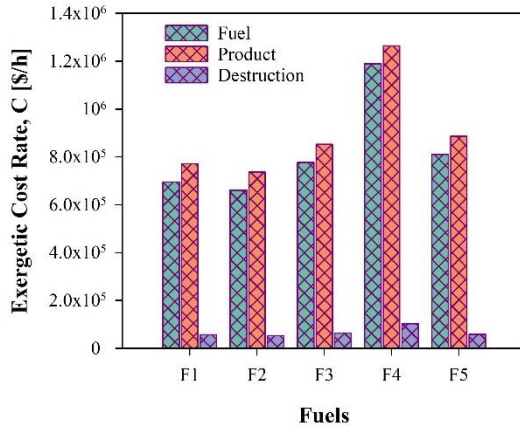
5.1.3 Results of Exergoeconomic Analysis

The exergoeconomic analysis was performed on the combined system. Table 5.5 shows the data results of this analysis for each component using the F1 fuel. The total annual levelized investment, \dot{Z} , is about 76k \$/h where the most investment cost is for the HPT, which is about 71k \$/h, followed by that of the CC of about 5k \$/h. The MCFC has an annual levelized cost of 10. 53 \$/h because of its small size. The total exergetic cost is 697261 \$/h for fuel, 772745 \$/h for product, and 60062 \$/h for destruction. Due to the losses in the MCFC, the exergetic cost of losses is almost negligible (25.3 \$/h). This results in the overall specific exergetic cost of fuel and product of 192.27 and 245.97 \$/GJ, respectively, which yields the exergoeconomic factor to be 55.7% and the relative cost difference to be 21.8%, respectively.

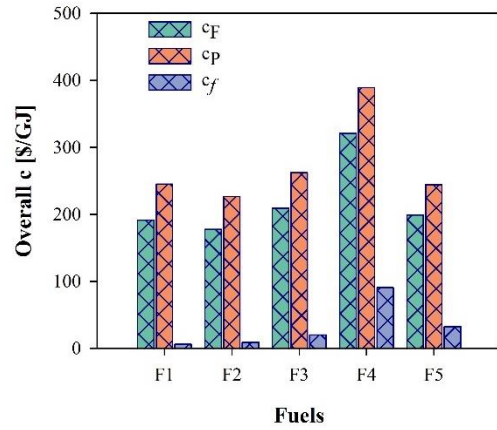
To compare the effect of different fuel blends, we present Figures 5.5 and 5.6. In Figure 5.5, the F4 fuel has the most significant total cost rates at 1265k \$/h for fuel, 1190k \$/h for a product, and 106k \$/h for destruction. However, the F2 has the minimum total cost rates of 663k, 738k, and 56k 4/h for fuel, product, and destruction, respectively, as shown in Figure 5.5-a. The same trend is observed in the overall specific exergetic cost among the fuel blends, as presented in Figure 5.5-b. The values of c_F and c_P are about 192 and 245 \$/GJ for F1, 178 and 227 \$/GJ for F2, 210 and 263 \$/GJ for F3, 321 and 389 \$/GJ for F4, and finally 200 and 245 \$/GJ for F5, respectively.

Table 5.5 The exergoeconomic analysis of components of combined aircraft system

Comp	\dot{C}_j^W [\$/h]	\dot{C}_j^Q [\$/h]	\dot{Z}_j [\$/h]	\dot{C}_F [\$/h]	\dot{C}_P [\$/h]	\dot{C}_D [\$/h]	\dot{C}_L [\$/h]	c_F [\$/GJ]	c_P [\$/GJ]	f [%]	r [%]
FAN	22343	0	17.19	22343	22360	178.5	0	196.75	198.49	8.79	0.87
S1	0	0	0	22360	22360	0.0	0	85.56	85.56	0.00	0.00
FN	0	0	0	20325	20325	2307.1	0	85.56	96.51	0.00	11.35
IPC	16213	0	35.52	16213	16249	9123.8	0	195.98	449.20	0.39	56.37
HPC	96854	0	35.52	96854	96889	3597.8	0	680.37	706.88	0.98	3.75
S2	0	0	0	115173	115173	0.0	0	584.58	584.58	0.00	0.00
CC	0	0	4656.00	118744	123400	40342.1	0	121.36	191.02	10.35	36.47
HPT	99131	0	70697.00	28434	99131	603.0	0	191.02	680.39	99.15	71.93
IPT	18681	0	30.87	18651	18681	442.8	0	191.02	195.98	6.52	2.53
LPT	22859	0	23.86	22835	22859	641.5	0	191.02	196.75	3.59	2.91
MX1	0	0	0	275.4	275	1.9	0	7.37	7.42	0.00	0.69
SR	0	0	0.82	276.3	275	27.2	0	6.71	7.42	2.90	9.54
WGS	0	0	0.82	277	276	1.4	0	6.70	6.71	37.18	0.21
MCFC	117.2	19.6	10.53	126	117	118.5	25.3	2.58	39.54	8.16	93.47
S3	0	0	0	53481	53481	0.0	0	191.02	191.02	0.00	0.00
MX2	0	0	0	53631	53631	1760.0	0	196.83	203.51	0.00	3.28
TE	0	0	0	53631	53631	175.1	0	203.51	204.18	0.00	0.33
EN	0	0	0	53631	53631	741.6	0	204.18	207.04	0.00	1.38
Total			75508.12	697261	772745	60062	25.3	192.27	245.97	55.70	21.83



(a)



(b)

Figure 5.5 (a) Total exergetic rates of fuel, product, and destruction and (b) the overall specific exergetic cost of fuel, product and fuel blends.

Therefore, the values of relative cost difference, r , and exergoeconomic factor f are about 22% and 56% for F1, 21% and 57% for F2, 20% and 53% for F3, 17% and 41% for F4, and 18% and 55% for F5, respectively, as shown in Figure 5.6-a. The electricity generated from the turbines and fuel cells are considered as graphed in Figure 5.6-b. For the HPT, the specific exergetic cost of electricity, c_{elec} , ranges from 637 to 841 \$/GJ, while the c_{elec} for IPT and LPT are almost the same and range from 180.5 to 353.7 \$/GJ. The fuel

cell has the minimum values of c_{elec} varying from 37 to 87 \$/GJ. The F4 records the maximum cost values while F2 has the minimum values.

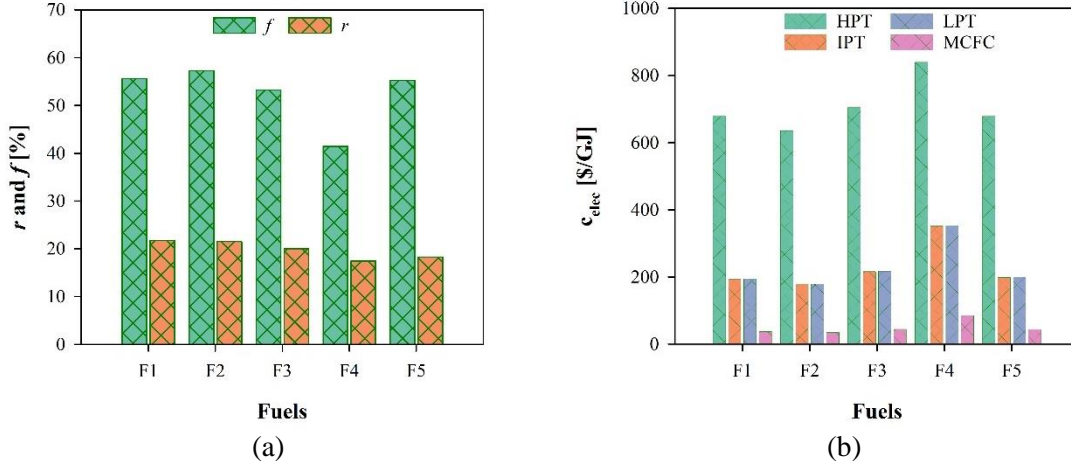


Figure 5.6 (a) The relative cost difference, r , and exergoeconomic factor, f and (b) the specific exergetic cost of electricity c_{el} .

5.1.4 Results of Exergoenvironmental Analysis

The exergoenvironmental analysis is conducted on the proposed system. The results of this analysis are displayed in Table 5.6 for F1 fuel. The total component-related environmental impact rate is 37.17 mPt/h, which is negligible compared to the flowing stream. The total exergoenvironmental rates of fuel, product, destruction, and losses are 29406, 28036, 3350, and 80 Pt/h, respectively. The environmental impact rate of pollution formation, \dot{B}^{PF} , is -964 Pt/h. The negative sign means that the pollution is removed by the entire system. In other words, the exhaust stream of the reactors is free from CO_2 , CO , and CH_4 . The total environmental impact rate, \dot{B}^T , is 2385 Pt/h. Therefore, the specific exergoenvironmental impact for fuel and product are 8.11 and 8.92 mPt/MJ, resulting in -40% of exergoenvironmental factor, f_b , and 10% relative environmental difference, r_b , as displayed in Table 5.7. The exergoenvironmental rates of fuel, product, and destruction are a maximum of 74716, 73853, and 7461 Pt/h for F4, respectively, and a minimum of 29406, 28036, and 3350 Pt/h for F1, respectively, as shown in Figure 5.7-a.

Table 5.6 The exergoenvironmental results of components of combined aircraft system

	\dot{B}_j^W		\dot{Y}_j	\dot{B}_F	\dot{B}_P	\dot{B}_D	\dot{B}_L	\dot{B}_j^{PF}	\dot{B}_j^T
Comp	[mPt/h]	\dot{B}_j^Q [mPt/h]	[mPt/h]	[mPt/h]	[mPt/h]	[mPt/h]	[mPt/h]	[mPt/h]	[mPt/h]
FAN	972990	0	4.35	972990	972994	7772	0	0	7776
S1	0	0	0	972994	972994	0	0	0	0
FN	0	0	0	884451	884451	100393	0	0	100392
IPC	705628	0	1.30	705628	705629	397088	0	0	397090
HPC	1211000	0	0.67	1211000	1211000	44984	0	0	44985
S2	0	0	0	2005000	2005000	0	0	0	0
CC	0	0	2.14	6238000	5379000	2119297	0	-858263	1261036
HPT	1240000	0	0.52	1240000	1240000	26298	0	0	26298
IPT	813049	0	0.49	813049	813049	19304	0	0	19304
LPT	995464	0	1.86	995462	995464	27967	0	0	27969
MX1	0	0	0	200285	200285	1388	0	0	1388
SR	0	0	4.45	163950	200285	16124	0	-36339	-20210
WGS	0	0	3.14	164058	163950	813	0	105	921
MCFC	7	51856	18.35	399973	7	375723	80047	-69739	306002
S3	0	0	0	2331000	2331000	0	0	0	0
MX2	0	0	0	5227000	5227000	171535	0	0	171536
TE	0	0	0	2514000	2367000	8207	0	0	8207
EN	0	0	0	2367000	2367000	32730	0	0	32730
Total			37.27	29405840	28036108	3349627	80047	-964236	2385428

Table 5.7 The exergoenvironmental performance of components

	b_F	b_P	f_b	r_b
Comp	[mPt/MJ]	[mPt/MJ]	[%]	[%]
FAN	8.56	8.64	0.06	0.81
S1	3.72	3.72	0	0
FN	3.72	4.20	0	12.8
IPC	8.53	19.51	0.001	128.7
HPC	8.50	8.83	0.001	3.8
S2	10.18	10.18	0	0
CC	6.38	8.33	-68.06	30.6
HPT	8.33	8.51	0.002	2.2
IPT	8.33	8.53	0.003	2.4
LPT	8.33	8.57	0.007	2.9
MX1	5.36	5.39	0	0.7
SR	3.98	5.39	179.78	35.5
WGS	3.96	3.98	11.75	0.5
MCFC	8.18	0.01	-22.78	-99.9
S3	8.33	8.32	0	0
MX2	19.18	19.83	0	3.4
TE	9.54	9.01	0	-5.5
EN	9.01	9.14	0	1.4
Total	8.11	8.92	-40.42	10.1

The specific exergoenvironmental impact b_F and b_P are 8.1 and 8.9 mPt/MJ for F1, 14.7 and 16.4 mPt/MJ for F2, 10.4 and 11.8 mPt/MJ for F3, 20.2 and 22.8 mPt/MJ for F4, and 13.5 and 14.3 mPt/MJ for F5, respectively, as displayed in Figure 5.7-b. Also, the values of r_b and f_b are 10.1% and -40.4% for F1, 11.5% and 1.5% for F2, 13.8% and 0.6% for F3, 12.7% and 0.3% for F4, and 6% and -2% for F5, as graphed in Figure 5.8-a. The specific exergoenvironmental impact of electricity, b_{elec} , has relative values for HPT, IPT, and LPT of about 8.5, 15.5, 11.7, 22.0 and 12.9 mPt/MJ for F1 to F5, respectively. In contrast, the MCFC has a b_{elec} value ranging from 2.5 to 6.6 mPt/MJ, as shown in Figure 5.8-b.

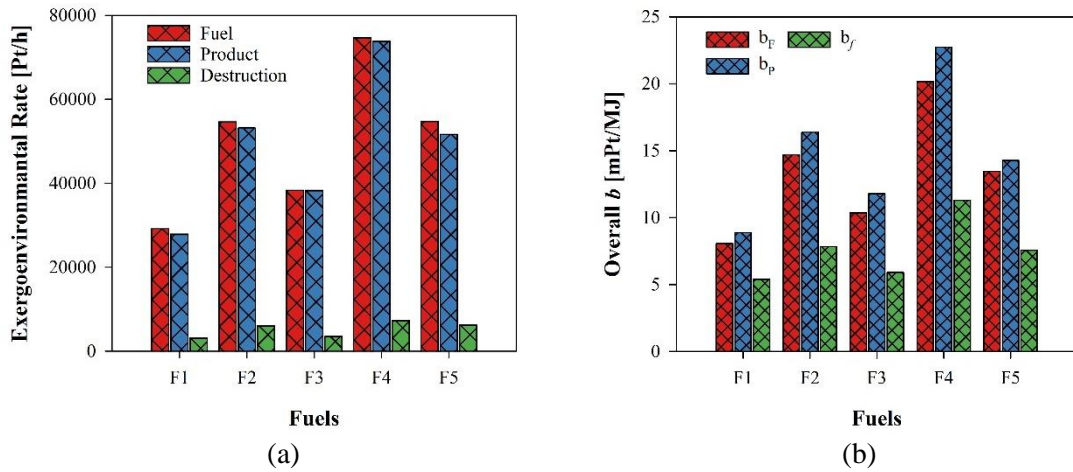


Figure 5.7 (a) Total exergoenvironmental rates of fuel, product, and destruction and (b) the overall specific exergoenvironmental impact of fuel, product, and fuel blends.

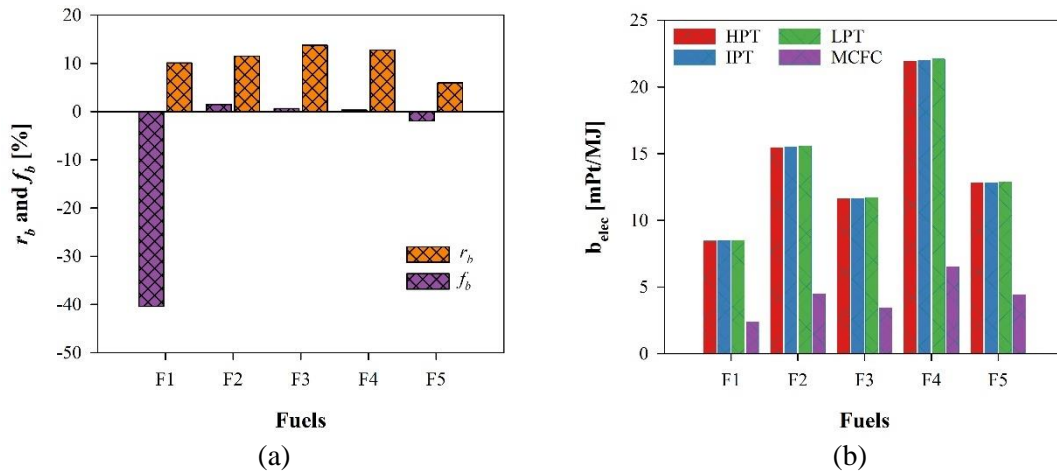


Figure 5.8 (a) Relative environmental difference, r_b , and exergoenvironmental factor, f_b and (b) the specific exergoenvironmental impact of electricity b_{elec} .

The exergoeconomic and exergoenvironmental analyses were conducted on the thrust force of the aircraft. Based on [177], the thrust forces of the hot nozzle (EN) are 63, 67, 64, 66, and 67 kN for F1 to F5, respectively, and the thrust force of the fan nozzle (FN) is almost constant at 64.5 kN for all fuels. That results in the exergetic cost rates of thrust, \dot{C}_{thrust} , for EN to be 849 \$/(h.kN) for F1, 776 \$/(h.kN) for F2, 973 \$/(h.kN) for F3, 1556 \$/(h.kN) for F4, and 1112 \$/(h.kN) for F5. The values of \dot{C}_{thrust} for FN has a range of 291 to 568 \$/(h.kN), which is almost one-third of that for EN, as shown in Figure 5.9-a. On the other hand, the exergoenvironmental rates of the thrusts for EN and FN are 37 and 14 Pt/(h.kN) for F1, 69 and 25 Pt/(h.kN) for F2, 53 and 19 Pt/(h.kN) for F3, 98 and 35 Pt/(h.kN) for F4, and 72 and 21 for F5, respectively, as shown in Figure 5.9-b.

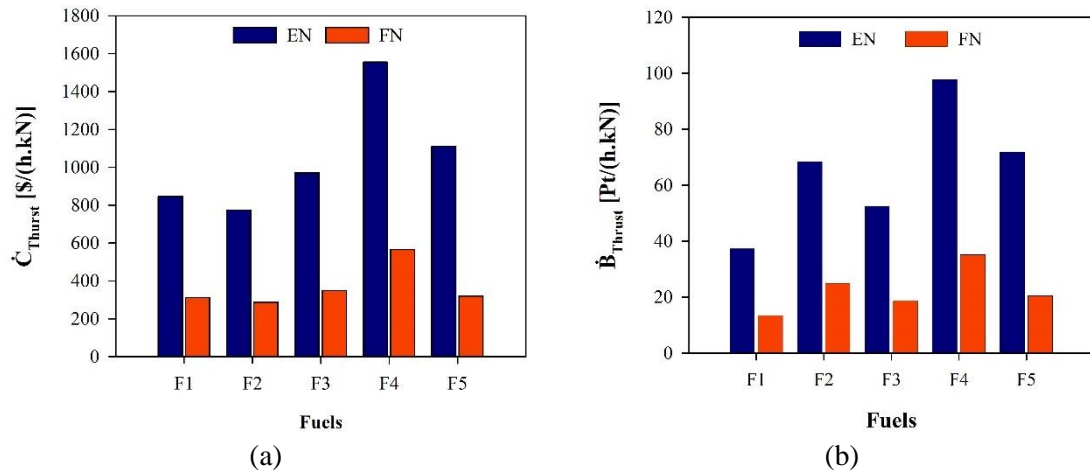


Figure 5.9 (a) The exergetic cost rate of thrust and (b) the exergoenvironmental rate of thrust.

The practical meaning of this proposed study can be summarized. The hybridized system can enhance the overall performance since the irreversibility loss is less than 15% while the exergy efficiency is above 85% for all alternative fuel blends. By combining the exergoeconomic and exergoenvironmental analyses, the fuel blends have an order from the most economical to the most expensive: F2, F1, F3, F5, and F4. However, they differ from the least to the significant environmental impact as F1, F3, F2, F5, and F4. Therefore, the best fuel choice is F3, then F1 F2 to achieve economic and environmental selection. The F2 (a methanol and hydrogen blend) is the most economical fuel, but it has a higher environmental impact than F1 by 50% and F3 by 25%. The F3 achieves a good balance since its exergetic cost is higher than that of F2 by 15%, and its environmental impact is less than that of F2 by 25% but more than that of F1 by 20%. Our system counts of the

specific fuel cost and specific environmental impact of the five fuels and the combinations of fuel blends. These impact factors can be reduced if governments provide incentives and subsidies for dimethyl ether, ethanol, and hydrogen, and they are produced by renewable processes.

5.2 Results of System A-2

This section displays the results of exergetic, exergoeconomic, and exergoenvironmental analysis of compound SOFC turbofan in addition to their discussion. Later, the effect of fuel blends is also explained with respect to these analyses.

5.2.1 Results of Thermodynamic Analysis

The thermodynamic results for the SOFC-turbofan engine are reported in [177] for each state point to include temperature, pressure, mass flow rates, specific enthalpy, specific entropy, and specific exergy. The inlet air conditions to the inlet diffuser are 253.9 K, 40.7 kPa, and 1210 kg/s resulting in the inlet air speed (U_a) of 248.6 m/s. The air exits from two ports: the fan nozzle and the hot nozzle. Consequently, the exit air conditions of the fan nozzle at state 12 are 233.2 K, 27.1 kPa, and 1099.9 kg/s, while the exhaust conditions at the hot nozzle at state 11 are 1127.5 K, 83.6 kPa, and 113.9 kg/s. Therefore, the airspeed at the fan nozzle exit (U_{12}) and hot nozzle exit (U_{11}) are 306.1 m/s and 607.8 m/s, respectively. The choking pressure ratio was checked at the exit nozzles to be 2.046 for the hot nozzle and 2.105 for the fan nozzle. It is found that the inlet to exit pressure ratio is higher for both nozzles, meaning that the thrust force counts for both speed and pressure difference between inlet and exit air.

In addition, the power and heat for components are displayed in Table 5.8. Since the turbofan is designed to have three spools, each spool carries a compressor and a turbine. Therefore, the turbine should deliver more power than that the corresponding required compressor, so the gas turbine configuration can provide net power to operate other systems in an airplane.

Furthermore, the base-turbofan can deliver a net power of 9144.1 kW and thrust energy of 38182.5 kW, but it requires 109082.6 kW of combustion heat to burn 6 kg/s

kerosene fuel. The overall energetic and exergetic efficiencies are 43.4% and 52.0%, respectively.

The solid oxide fuel cell and steam reformer, and water-gas shift are added to the turbofan. The SR and WGS are operated at 673 and 873 K, respectively. The SR uses the heat of 1789 kW with energetic and exergetic efficiency of 78% and 80%, respectively. Also, the WGS needs a total heat of 112 kW with 65% for both energetic and exergetic efficiencies. The results of the SOFC are presented below in Table 5.9 for F1, a mixture of 75% methane and 25% hydrogen. The net power of the SOFC is 944 kW with electric efficiency of 87.0%, the energetic efficiency of 32.3%, and exergetic efficiency of 43.9%.

Table 5.8 The thermodynamic results of components in the base-turbofan engine

Components	\dot{Q} [kW]	\dot{W} [kW]	$\dot{E}x_D$ [kW]	π	η [%]	ψ [%]
FAN	0	31547.2	336.3	1.400	99	98.9
HPC	0	39545.6	1469.1	5.980	90	96.3
HPT	0	44650.2	986.5	0.400	90	97.8
IPC	0	22981.5	1444.1	5.980	90	93.7
IPT	0	25274.8	624.3	0.550	90	97.6
LPT	0	33293.4	989.4	0.400	90	97.1
EN	0	0	7040.7	0.489	87	90.4
FN	0	0	70264.7	0.475	87	41.0
TE	0	0	283.6	0.972	98	99.6
CC	109082.6	0	250639.3	0.982	42.5	41.7

Table 5.9 Results of the SOFC using F1 (75% methane and 25% hydrogen)

Parameters	Values	Units
VOC	262.35	VA
Number of stacks	36	---
V_{cell}	0.833	V
V_{loss}	0.124	V
$\dot{W}_{SOFC,AC}$	944.4	kW
$\dot{W}_{SOFC,loss}$	141.0	kW
$\dot{Q}_{SOFC,add}$	2928.0	kW
$\eta_{SOFC,e}$	87.0	%
$\eta_{SOFC,th}$	32.3	%
$\psi_{SOFC,th}$	43.9	%

(a) *Effect of fuels on the performance of SR, WGS, and SOFC:*

Note that five alternative fuels are used in different combinations with hydrogen as in F1 to F5. All the fuels are used under the same turbofan conditions, which are inlet air conditions, inlet conditions and pressure ratio of compressors, combustion pressure and

temperature, and the turbine pressure ratios. Regarding the reactors, the temperature of SR and WGS remain constant at 673.2 K and 873.2 K, respectively. The performance of the SR, WGS, and SOFC are affected by the fuel combinations are shown in Table 5.10. For the SR, the maximum heat is used for F5, which is 1260.9 kW, while the minimum heat is required for F2 to be 1084.2 kW. The best performance of the SR occurs when using methane and hydrogen mixture of F1, achieving about 78% and 80% of energetic and exergetic efficiencies, respectively. The performance of the SR has been decreased from 55% to 45% as F5, F2, F3, and F4 in this order. For the WSG, the required heat varies from 433.8 kW for F2 to 111.8 kW for F1, fulfilling energetic and exergetic efficiencies of about 60% for F5 to 90% for F2. For SOFC, the minimum heat required occurs using F1 to be 2928 kW to achieve an energetic efficiency of 32.3% and exergetic efficiency of 43.9 %. However, the maximum heat required can be obtained using F3 to be 3959 kW with energetic and exergetic efficiencies of 23.9% and 32.5%, respectively.

Table 5.10 The performance of the SR, WGS, and SOFC with respect to fuels

Parameter	F1	F2	F3	F4	F5
\dot{Q}_{SR} [kW]	1789.0	1084.2	1144.5	1047.1	1260.9
η_{SR} [%]	78.2	47.4	50.0	45.8	55.1
ψ_{SR} [%]	79.5	50.6	50.4	48.7	60.4
\dot{Q}_{WGS} [kW]	111.8	433.8	258.6	353.6	209.2
η_{WGS} [%]	64.8	89.7	86.7	74.3	57.5
ψ_{WGS} [%]	65.1	90.7	89.9	88.5	61.8
$\dot{Q}_{SOFC,add}$ [kW]	2928.0	3102.8	3958.5	3646.4	3360.6
$\eta_{SOFC,th}$ [%]	32.3	30.4	23.9	25.9	28.1
$\psi_{SOFC,th}$ [%]	43.9	41.4	32.5	35.3	38.3

Two reasons for this performance variations are: (a) the mass flowrates of fuels entering the SR with respect to the steam mass flow rate (0.2 kg/s), as shown in Table 5.11, and (b) the chemical reactions of fuel mixture to produce CO and H₂ in the SR which will be reacted to produce CO₂ and H₂ in the WSG, so that the hydrogen can electrochemically react with air to produce electricity and heat in SOFC. The steam to carbon ratio (S/C) is between 1.25 and 2, and the fuel-to-air ratio varies between 0.04 to 0.06 because of the change of fuel mass flow rates. The difference in fuel mass flow rates is owing to the difference of the heating values of the fuels, which are 77.1 MJ/kg for F1, 52.5 MJ/kg for F2, 74.6 MJ/kg for F3, 75.8 MJ/kg for F4, and 77.7 MJ/kg for F5.

Table 5.11 Mass flow rates using alternative fuels.

Parameter	Kerosene	F1	F2	F3	F4	F5
\dot{m}_{F1} [kg/s]	5.968	3.90	5.80	4.00	4.00	3.90
F/A [kg _f /kg _a]	0.055	0.040	0.060	0.041	0.041	0.040
\dot{m}_{F2} [kg/s]	---	0.1	0.16	0.15	0.15	0.12
\dot{m}_{W1} [kg/s]	---	0.2	0.2	0.2	0.2	0.2
S/C [kg _w /kg _f]	---	2	1.25	1.33	1.33	1.67

(b) Effect of fuels on overall turbofan systems:

The alternative fuels are combusted with highly compressed air in the combustion chamber. The existing conditions of the combustion chamber should be 2000 kPa and 1800 K according to the specifications of the Rolls Royce Trent 1000 turbofan engine. In addition, the amount of inlet bypass, and bleeding air is constant throughout the analysis. The fuel mass flow rate varies to ensure adequate combustion based on the heating values of the fuel mixture. Therefore, the fan nozzle conditions are 1099.9 kg/s, 27.1 kPa, 233.2 K, which remain constant. The exhaust conditions vary because of the variation in fuel mass flow rates in the combustion chamber and the fuel cell system, as shown in Table 5.12. The exhaust temperature of alternative fuels is less than that of kerosene, while the exhaust pressure is more than that of kerosene. This yields more exhaust speed by about 6%.

Table 5.12 The exit conditions of the hot nozzle using different fuels.

Parameters	Kerosene	F1	F2	F3	F4	F5
Exhaust mass flow rate, \dot{m}_{11} [kg/s]	113.9	112.1	114.1	112.3	112.3	112.1
Exhaust Pressure, P_{11} [kPa]	1127.5	1007.9	1036.4	1040.5	1026.1	1033.3
Exhaust Temperature, T_{11} [K]	83.6	101.6	113.7	118.0	110.0	113.7
Exhaust speed, U_{11} [m/s]	607.8	643.2	657.5	621.2	648.8	657.5

Using different alternative fuel mixtures affects the thrust force of the hot nozzle. However, the thrust force of the fan nozzle does not change because of the constant air mass flow rate and compressor conditions. As shown in Figure 5.10, the hot thrust force reaches a maximum value of 91.1 kN for F2, and a minimum value of 83.4 for F1, the thrust force using kerosene is 83.7 kN. The fan thrust force is about 69 kN. By dividing the fuel mass flow rate by the total thrust force, the TSFC varies from 88.9 to 130.6 kg/(h.kN) for alternative fuels, which are less than that of kerosene of 139.9 kg/(h.kN).

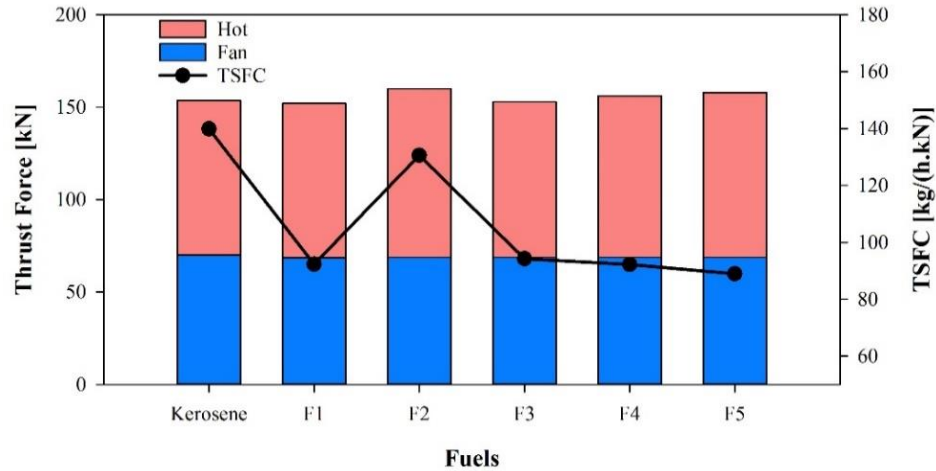


Figure 5.10 The thrust force and the TSFC of the base- and SOFC-turbofans with respect to fuels.

The net power of GT and thrust energy is displayed in Figure 5.11. Using kerosene can achieve a maximum net power of 9144 kW because of the high mass flow rate of 6 kg/s for alternative fuels, the F5 achieves a minimum net power of 5768 kW, and the F1 can achieve a maximum power of 8730 kW. The thrust energy can be obtained to be 38.2 MW for kerosene, while the maximum and minimum thrust energy can be reached 39.8 MW for F3 and 37.8 MW for F1, respectively. The net power of SOFC is constant and equivalent to 944.4 kW. Therefore, the total power of 48 MW can be achieved using F2, which is an increase of 1.5% compared to that of kerosene.

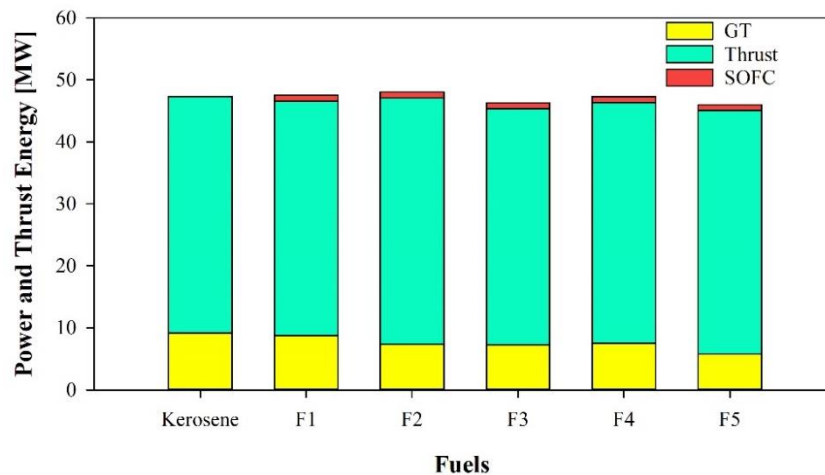


Figure 5.11 The net power of the GT and thrust energy of the base- and SOFC-turbofans.

The overall energetic and exergetic efficiencies of the turbofan engines are displayed in Figure 5.12. Fuel of F3 achieves the highest energetic and exergetic

efficiencies of 48.1% and 54.4%, respectively. Using kerosene fuel reduced the energetic efficiency to 43.4%, but the exergetic efficiency is about 52% and is the third-highest value.

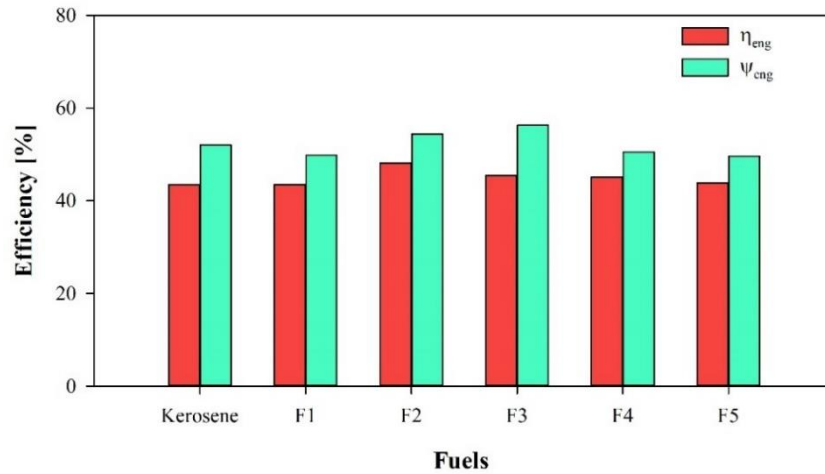


Figure 5.12 Overall energetic and exergetic efficiencies of the base- and SOFC-turbofans.

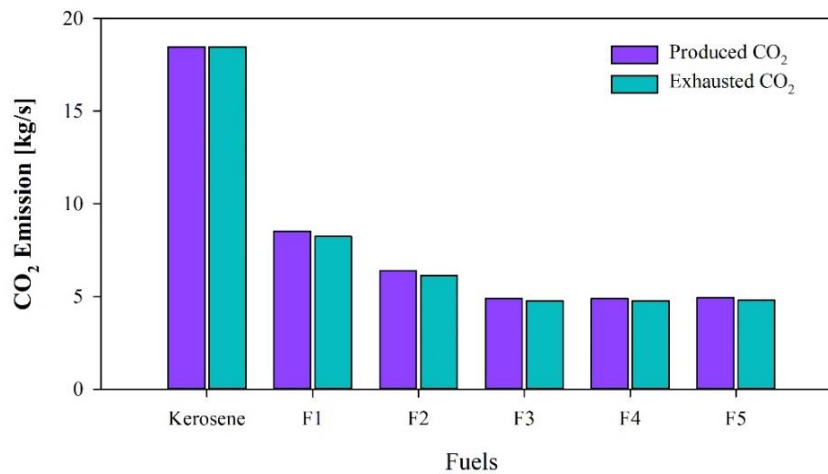


Figure 5.13 The CO₂ emission with respect to fuels

The environmental impact is studied by estimated the CO₂ emissions and presented in Figure 5.13. The kerosene fuel produces CO₂ of 18.5 kg/s and emits the amount to the atmosphere. This amount can be decreased by 54% using F1, 65 % using F2, and about 73% using F3, F4, and F5, reaching 4.9 kg/s without using the SOFC system. SOFC system reduces the CO₂ emission by about 3.5% for all alternative fuel mixtures. The minimum production and exhaustion of CO₂ can be achieved by using F3 and F4, reaching 4.75 kg/s. These fuels are ethanol- and dimethyl ether-based fuels since they have similar chemical formulas and molecular weight.

5.2.2 Results of Exergy Analysis

The data results of state points are reported in [212] including the state conditions such as mass flow rates, temperature, and pressure, exergy flow rate values, and exergoeconomic results such as specific exergetic cost value and exergetic cost rate.

Table 5.13 The exergetic results of components in the SOFC-turbofan system

#	\dot{W}_j	\dot{Q}_j	$\dot{E}x_F$	$\dot{E}x_P$	$\dot{E}x_D$	$\dot{E}x_L$	ε	y	y^*
	[kW]	[kW]	[kW]	[kW]	[kW]	[kW]	[%]	[%]	[%]
FAN	31540	0	31540	31289	251	0	99.20	0.03	0.15
S1	0	0	72589	72589	0	0	100.00	0.00	0.00
FN	0	0	65983	58494	7489	0	88.65	0.83	4.47
IPC	22973	0	22973	10044	12929	0	43.72	1.43	7.71
HPC	39514	0	39514	38046	1468	0	96.28	0.16	0.88
S2	0	0	54696	54696	0	0	100.00	0.00	0.00
CC	0	104276	321071	186820	134251	0	58.19	14.84	80.10
HPT	42566	0	43489	42566	923	0	97.88	0.10	0.55
IPT	27093	0	27752	27093	659	0	97.63	0.07	0.39
LPT	33098	0	34052	33098	954	0	97.20	0.11	0.57
TE	0	0	81527	81275	252	0	99.69	0.03	0.15
EN	0	0	81275	85078	3803	0	104.68	0.42	2.27
MX1	0	0	6923	6877	46	0	99.34	0.01	0.03
SR	0	1789	7670	6877	793	0	89.66	0.09	0.47
WGS	0	111.8	7718	7670	48	0	99.38	0.01	0.03
SOFC	944.4	2928	6139	944.4	3737.6	1457	15.38	0.41	2.23
Total			904911	743456.4	167603.6	1457	82.16	18.52	100.00

Table 5.13 shows the exergetic results for all components used in the system using fuel F1. The highest required power is 31,540 kW to operate the FAN followed by 39,514 kW for HPC then 22,973 kW for IPC. The output power for turbines HPT, IPT, and LPT are 42,566, 27,093, and 33,098 kW, respectively, and 944 kW for SOFC. That results in the net electric power of the SOFC-turbofan being 9,674 kW, while the thrust power is 37,818 kW. Also, the required heat for the combustion chamber CC is about 104 MW. For the SOFC system, the required heat is 1,789 kW for SR, 111.8 kW for WGS, and 2,928 kW for SOFC, with a total of 4829 kW from the entire SOFC system. Therefore, the overall energetic efficiency of the engine is 43.5%, while the exergetic efficiency is 49.8% [177],

which is calculated as the ratio of useful energy/exergy to the required energy/exergy. In Table 5.13, the total fuel, product, and destruction exergy of the whole components are 905, 743, 168 and 1.5 MW yielding the exergetic efficiency for the whole system, ε_t , to be 82.2% and exergy destruction ratio to be 18.5%.

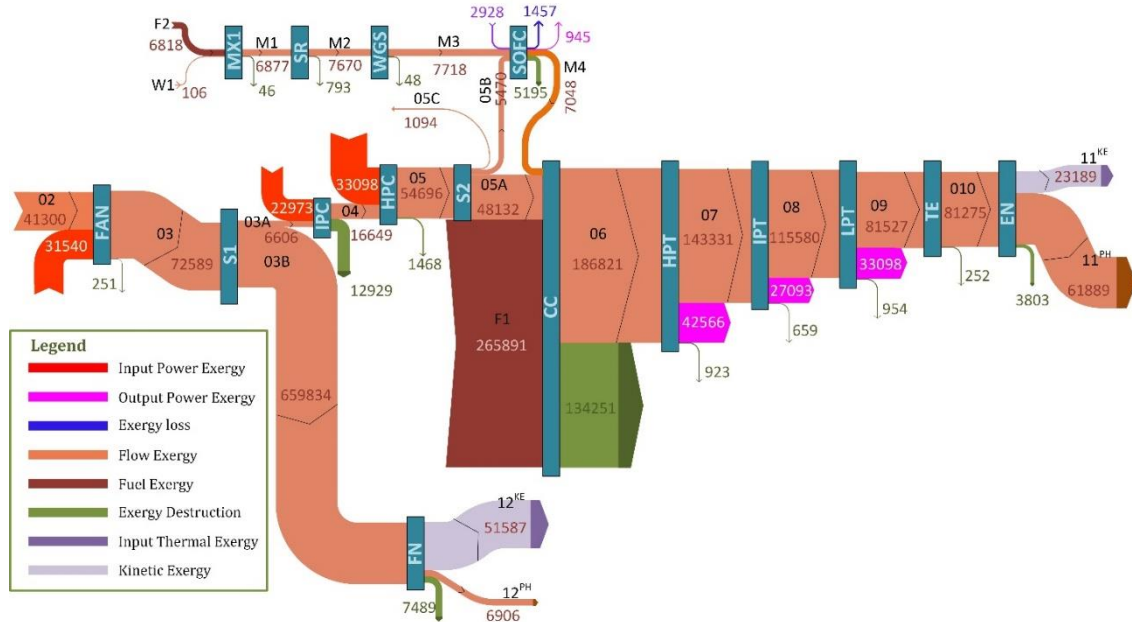


Figure 5.14 The Sankey diagram for exergy flow rate [kW].

Visualizing the exergy flow is presented in the Sankey diagram of Figure 5.14 for the fuel blend F1. All the data in this figure was drawn in a scale of 1000kW/1pt. In this figure, the air enters at 1210 kg/s and an exergy rate of 41300 kW and leaves the fan nozzle (FN) at 6,906 kW for physical exergy rate and 51,587 kW for kinetic exergy rate. The fuel enters the CC at F1 with a mass flow rate of 3.9 kg/s and an exergy rate of 265,891 kW to be combusted with air at 05A and M4 which exits the SOFC. The exhaust flow of 06 has the largest exergy flow of 186,821 kW due to the chemical reaction and huge temperature difference compared to the standard conditions. The exhaust gases exit the SOFC-turbofan engine at physical and kinetic exergy rates of 61,889 kW and 23,189 kW, respectively. The SOFC system utilizes the F1 fuel with a mass flow rate of 0.1 kg/s and 6,818 kW exergy rate combined with a steam of 0.2 kg/s and 106 kW of exergy rate. This fuel blend and steam mixture flows over the SR then the WGS to the SOFC unit to produce a net power of 945 kW and 7,048 kW exergy rate at M4.

The exergetic analysis was performed using five fuel blends (F1 to F5), and the results of this analysis are shown in Figure 5.15-a and 5.15-b. The total exergetic rates of

fuel, product and destruction are relatively close despite changing the fuel blends, as shown in Figure 5.15-a. F2 records the highest fuel exergetic rate, $\dot{E}x_{F,t}$, of 923 MW and the highest product exergetic rate, $\dot{E}x_{P,t}$, of 763 MW. The maximum and minimum destruction exergetic rates are 168 MW for F1 and 159 MW for F3, respectively. Figure 5.15-b illustrates the changes in the overall exergetic efficiency, ε_t , and exergy destruction ratio, y . The ε_t has a range of 82.2% to 82.7%, while the y varies from 17.4% to 18.5% with respect to the fuel blends. This means the selected fuel blends improve the exergetic performance of the system to be 82% and reduce the exergy destruction ratio to be less than 18%, respectively.

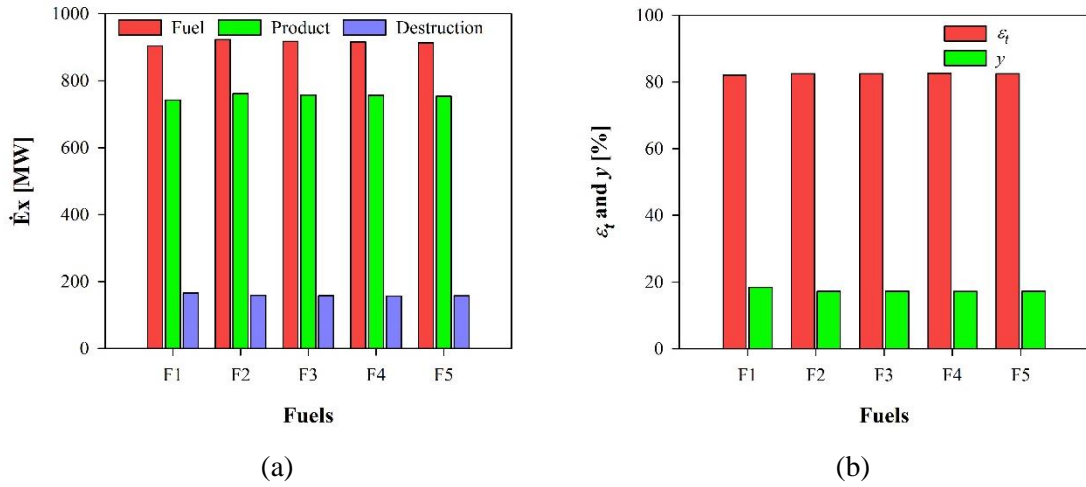


Figure 5.15 The exergy results of hybrid SOFC-turbofan engine: (a) fuel, product, and destruction exergy rate, and (b) ε and y

The most effectual element in the exergetic analysis is from the CC because it has the greatest fuel, product, and destruction exergy rates followed by the turbines, then the compressors. However, the exergy rates of compressors do not change with respect to the fuel blends because of their constant air flow and constant required power. Also, turbines contribute about 10% of the total fuel and product exergy rates, and less than 2% irreversibility ratio. From the other side, the ratios of fuel and product exergy rate of the CC to the total are about 35% and 25%, respectively, but the CC has about 80% irreversibility ratio. Additionally, the CC has fuel and product exergy rates of 321 MW and 187 for F1, 232 and 194 MW for F2, 318 and 190 MW for F3, 317 and 190 MW for F4, and 317.6 and 190 MW for F5. That is because the required heat of the CC is 104, 95, 96,

100, and 100 MW for the fuels F1 to F5 in the order, and the fuel mass flow rates entering the CC are 3.9 kg for F1 and F5, 4 kg for F3 and F4, and 5.48 kg for F2. Consequently, the total exergetic rates using all the fuels are similar because of the similarity of the combustor behavior due to the approximate mass flow rate and approximate required heat despite the change in chemical reactions of those fuels.

5.2.3 Results of Exergoeconomic Analysis

To perform the exergoeconomic analysis, it is required to evaluate the total investment of the system components, as shown in Table 5.14. Some assumptions are considered; the nominal interest rate is 12%, the inflation rate is 3%, the operating time is 20 years, the annual operating hours of flight is 5110 h/year, and the maintenance factor is 6%. The highest cost is for HPT, which is about \$2.1B which increases to \$3.2B because of the maintenance and the CEPCI of 2020 (608). The annual levelized investment cost is the highest for HPT to, be 71,332 \$/h. This huge amount is due to the highest inlet temperature of HPT, which is 1800 K. The total levelized investment of the SOFC-turbofan is about 76,193 \$/h. Also, the exergoeconomic analysis is shown in Table 5.15. The total fuel exergetic cost rate \dot{C}_F is 559k \$/h, while the total product exergetic cost rate, \dot{C}_P , is 635k \$/h resulting destruction exergetic cost rate, \dot{C}_D , to be 66k \$/h. Therefore, the overall specific exergetic cost of fuel and product are about 172 and 237 \$/GJ, respectively. This yields 53.6% of relative cost difference and 53.6% of exergoeconomic factor.

To display the exergetic cost flow rate, we use the Sankey diagram, as shown in Figure 5.16, in a scale of 500 \$/h/pt. The inlet air to the turbofan at 02 is free (0 \$/h). Also, the inlet cost rate of water to the SOFC system is almost free (0.04 \$/h). The exergetic cost rate of fuel F1 at F1 and F2 are 7160 and 184 \$/h, respectively because of the specific exergetic cost of F1 is 7.84 \$/GJ. The largest exergetic cost rates are found in the CC (118,070 \$/h), HPC (108,571 \$/h), and in HPT (90,585 \$/h) because of their largest levelized investment cost as shown in black colour in the figure. The cost rates of input power for compressors are 20,531 \$/h for FAN, 14,898 \$/h for IPC, and 91,732 \$/h for HPC, while the cost rates for the output power are 98,817 \$/h for HPT, 17,570 \$/h for IPT, 21,545 \$/h for LPT, and 380 \$/h for SOFC. The exhaust air at the fan nozzle (FN) and exit nozzle (EN) are 2,206 \$/h for physical exergy and 16,472 \$/h for kinetic exergy, and 37,485 \$/h for physical exergy and 14,040 \$/h for kinetic exergy, respectively.

Table 5.14 The capital cost and annual levelized investment cost of components

#	C_j [\$]	Z_j [\$]	\dot{Z}_j [\$/h]
FAN	509,680	770,859	17.19
S1	0	0	0
FN	0	0	0
IPC	1,053,000	1,593,000	35.52
HPC	1,053,000	1,593,000	35.52
S2	0	0	0
CC	139,300,000	210,700,000	4698.00
HPT	2,115,000,000	3,199,000,000	71332.00
IPT	923,443	1,397,000	31.15
LPT	713,767	1,080,000	24.07
TE	0	0	0
EN	0	0	0
MX1	0	0	0
SR	23,805	36,458	0.81
WGS	23,805	36,458	0.81
SOFC	520,866	797,699	17.79
Total	2,259,121,366	3,417,004,474	76192.87

Table 5.15 The exergoeconomic results of components in SOFC-turbofan system.

#	\dot{C}_j^W [\$/h]	\dot{C}_j^Q [\$/h]	\dot{C}_F [\$/h]	\dot{C}_P [\$/h]	\dot{C}_D [\$/h]	\dot{C}_L [\$/h]	c_F [\$/GJ]	c_P [\$/GJ]	f [%]	r [%]
FAN	20531	0	20531	20548	163.4	0	180.8	182.4	9.5	0.9
S1	0	0	20548	20548	0.0	0	78.6	78.6	0	0
FN	0	0	18678	18678	2119.9	0	78.6	88.7	0	12.8
IPC	14898	0	14898	14933	8384.5	0	180.2	413.0	0.4	129.3
HPC	91732	0	91732	91767	3408.0	0	644.9	670.1	1.1	3.9
S2	0	0	108571	108571	0.0	0	551.4	551.4	0	0
CC	0	0	113372	118070	47404.8	0	98.1	175.6	9.0	79.0
HPT	98817	0	27485	98817	583.3	0	175.6	644.9	99.2	267.3
IPT	17570	0	17539	17570	416.5	0	175.6	180.2	7.0	2.6
LPT	21545	0	21521	21545	602.9	0	175.6	180.8	3.8	3.0
TE	0	0	51525	51525	159.3	0	175.6	176.1	0	0.3
EN	0	0	51525	51525	2410.9	0	176.1	168.2	0	-4.5
MX1	0	0	183.6	183.6	1.2	0	7.4	7.4	0	0.67
SR	0	0	184.4	183.6	19.1	0	6.7	7.4	4.1	11.1
WGS	0	0	185.3	184.4	1.2	0	6.7	6.7	41.4	0.1
SOFC	379.5	10.49	372.2	379.5	226.6	88.3	16.8	111.6	7.3	562.8
Total			558850.5	635028.1	65901.5	88.3	171.6	237.3	53.6	38.3

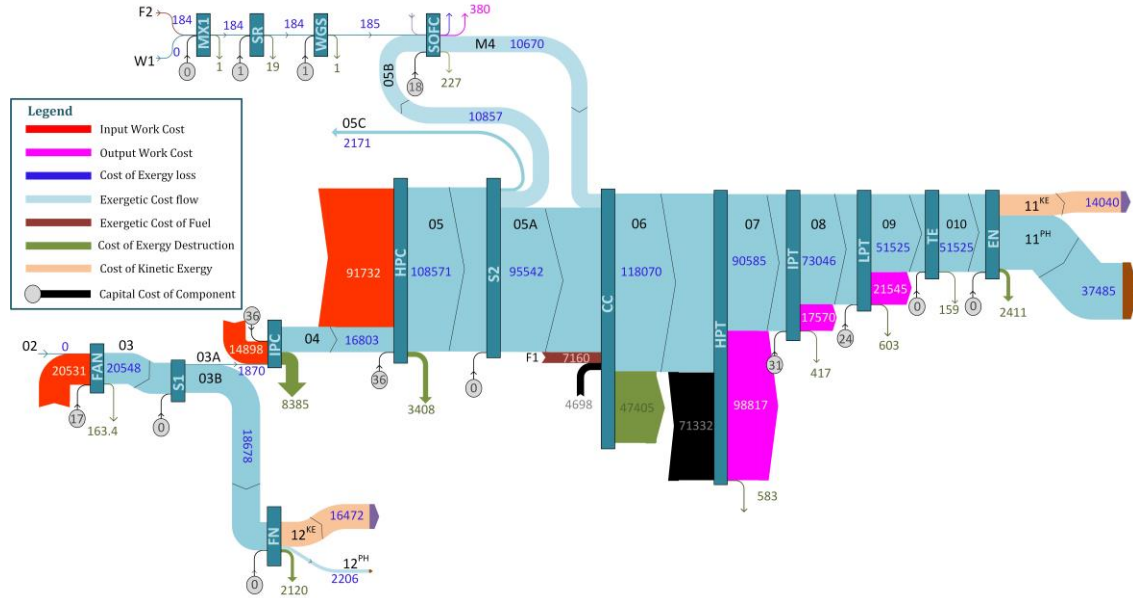


Figure 5.16 The Sankey diagram for exergoeconomic flow rates [\$/h].

The exergoeconomic analysis was conducted on the SOFC-turbofan system using F1 to F5. The total exergoeconomic rates of fuel, product and destruction are the highest for F4 to be 1007k, 1084k, and 125k \$/h, respectively. However, the lowest total exergoeconomic rates are recorded for F2 to be 548k, 625k, 61k \$/h for fuel, product, and destruction exergoeconomic rates, respectively, as shown in Figure 5.17-a. Fuel F4 records the highest values of specific fuel and product exergetic cost as 305 and 398 \$/GJ, respectively, while F2 achieves the minimum values of specific fuel and product exergetic cost as 165 and 228 \$/GJ, respectively, as shown in Figure 5.17-b. The reason behind these maximum and minimum is the exergetic cost of fuel blends, where the DME has the highest fuel cost among other fuels. These values of exergoeconomic rates and specific exergetic cost affects the relative cost difference, r , and exergoeconomic factor, f , as shown in Figure 5.18. The minimum r and f are obtained using F4 as 30% and 38%, respectively, because F4 has the largest destruction exergetic cost rate and the smallest difference between the specific exergetic cost of fuel and product. The maximum f values are reported for F5 as 66%, followed by that of F2 (56%), then of F1 (52%). Also, the maximum r values are about 38% for F1 and F2 and 36% for F3.

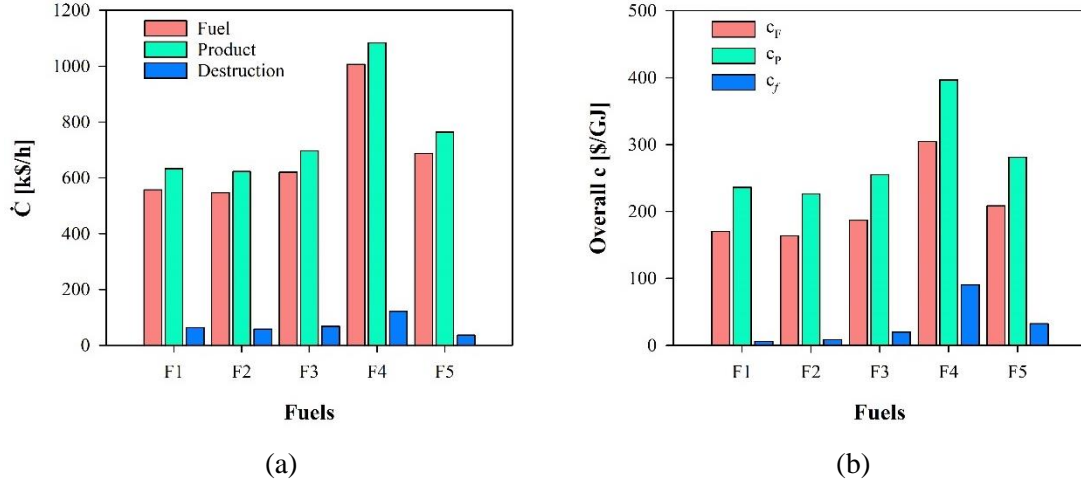


Figure 5.17 The exergoeconomic analysis results of hybrid SOFC-turbofan engine: (a) exergoeconomic rates for fuel, product, and destruction, and (b) overall specific exergoeconomic fuel, product, and selected fuel

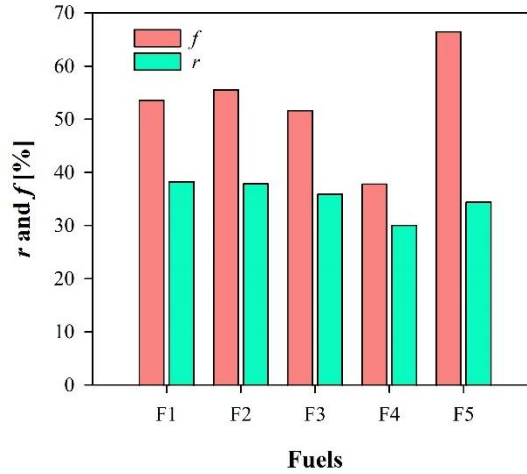


Figure 5.18 The relative cost difference r and exergoeconomic factor f

The output results from economic perspective are compared. The main output parameters of this combined system are the electricity generated from the fuel cell SOFC and turbines of HPT, IPT, and LPT, which deliver the power to compressors of HPC, IPC, and FAN, correspondingly, and the output exhaust gases from fan nozzle (FN) and exit nozzle (EN). Therefore, the economic aspects are discussed in terms of specific exergetic cost, c , as shown in Table 5.16, with respect to the five fuel blends F1 to F5. For electricity, using F2 is the most economic since the electricity cost has the lowest values for the turbines and SOFC. However, the most economic fuel for the exhaust gases is F3. The electricity cost of HPT is the highest cost ranging from 620 to 815 \$/GJ. However, the two

turbines, IPT and LPT, have similar exergetic cost ranging from 170 to 360 \$/GJ. For the SOFC, the specific exergetic cost varies from 108 to 170 \$/GJ. For the exhaust gases, the specific exergetic cost for EN is almost double of that of FN for most of the fuels. The most economical for both nozzles is using F3, which records about 100 and 22 \$/GJ for EN and FN, respectively.

Table 5.16 The specific exergetic cost [\$/GJ] of electricity and exhaust gases.

	HPT	IPT	LPT	SOFC	EN	FN
Fuels	$c_{e,HPT}$	$c_{e,IPT}$	$c_{e,LPT}$	$c_{e,SOFC}$	c_{11}	c_{12}
F1	644.9	180.1	180.8	111.6	168.2	88.7
F2	621.0	171.7	172.3	108.0	169.8	84.5
F3	659.3	203.7	204.4	118.8	100.3	21.5
F4	814.7	359.4	360.8	169.8	355.9	176.9
F5	686.4	230.6	231.4	127.4	228.2	113.5

5.2.4 Results of Exergoenvironmental Analysis

The data results of state points in the SOFC-turbofan including total exergy rate, $\dot{E}x_i$ (physical and chemical), specific exergoenvironmental impact, b_i , and the exergoenvironmental impact rate, \dot{B}_i . exergetic results for all components used in the system using fuel F1 are reported in [213]. In the beginning, the LCA of fuels and components were studied. The weight distributions of the company technical parts are given in Table 5.17 according to [214].

Table 5.17 The percentage Weight of Rolls Royce parts [214]

Component	Percentage [%]	Weight [kg]
Fan	42.4	2544
IPC	12.7	762
HPC	6.5	390
combustor	5.1	306
HPT	6	360
IPT	5.7	342
LPT	21.6	1296
Total engine		6000

Table 5.18 presents the environmental impact of material production, processing, and disposal for each component in mPt/kg. Some assumptions are considered: the operating time is 20 years, the annual operating hours of flight is 5110 h/year, and the maintenance factor is 6%. The total component-related environmental impact rate, \dot{Y}_t , is

26.26 mPt/h, which is a very small amount compared to the exergoenvironmental flow rates.

Table 5.18 The component-related exergoenvironmental impact of SOFC turbofan engine

Comp.	Weight [kg]	Material Production [mPt/kg]	Material Processing [mPt/kg]	Material Disposal [mPt/kg]	Total EI [mPt/kg]	Total Y [mPt]	\dot{Y}_j [mPt/h]
FAN	2544	130.68	11.78	24	166.46	423481.82	4.35
IPC	762	130.68	11.78	24	166.46	126844.79	1.30
HPC	390	130.68	11.78	24	166.46	64920.56	0.67
CC	306	638.08	20.00	24	682.08	208716.51	2.14
HPT	360	104	11.76	24	139.76	50314.67	0.52
IPT	342	104	11.76	24	139.76	47798.94	0.49
LPT	1296	104	11.76	24	139.76	181132.82	1.86
S1	0	86	0	24	110	0	0.00
S2	0	86	0	24	110	0	0.00
MX1	0	86	0	24	110	0	0.00
SR	436	949.6	20.00	24	993.60	433209.64	4.45
WGS	357	811.14	20.00	24	855.14	305283.58	3.14
SOFC	2232	273.89	22.24	24	320.13	714525.82	7.34
Total							26.26

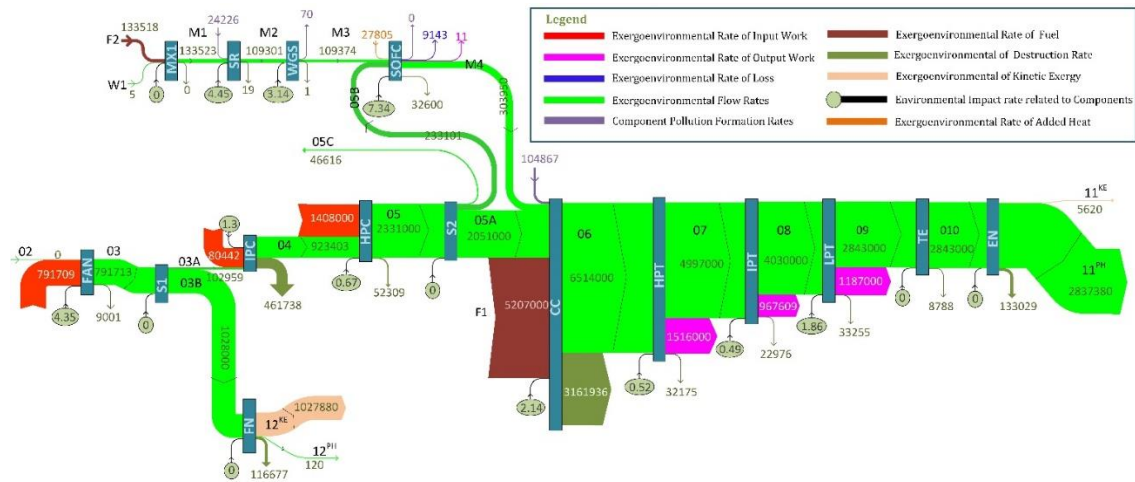


Figure 5.19 The Sankey diagram for exergoenvironmental flow rates [mPt/h]

The exergoenvironmental analysis of components is presented in Table 5.19 and 5.20. The total exergoenvironmental rates for fuel, product, and destruction using F1 fuel are 25159, 24096, and 4077 Pt/h, respectively (note that the values are multiplied by 1000 to convert from mPt to Pt). Also, the total environmental impact rate due to pollution formation, \dot{B}^{PF} , of CC, SR, WGS, and SOFC is -129 Pt/h. The negative value means that the SOFC-turbofan significantly reduces the emissions of CH_4 , CO_2 and CO. Therefore, the total environmental impact, \dot{B}_T , is about 3948 Pt/h, as shown in Table 5.19. The specific

exergoenvironmental impact values of fuel, b_F , and product, b_P , are 7.72 and 9 mPt/MJ, respectively, which results in -3.27% of exergoenvironmental factor, f_b , and 16.5% of relative exergoenvironmental difference, r_b , as shown in Table 5.20.

Table 5.19 The exergoenvironmental impact results for components

Comp.	\dot{B}_j^W [mPt/h]	\dot{B}_j^Q [mPt/h]	\dot{B}_F [mPt/h]	\dot{B}_P [mPt/h]	\dot{B}_D [mPt/h]	\dot{B}_L [mPt/h]	\dot{B}_j^{PF} [mPt/h]	\dot{B}_T [mPt/h]
FAN	1131000	0	1131000	1131000	9001	0	0	9005
S1	0	0	1131000	1131000	0	0	0	0
FN	0	0	1028000	1028000	116677	0	0	116677
IPC	820442	0	820442	820444	461737	0	0	461739
HPC	1408000	0	1408000	1408000	52309	0	0	52310
S2	0	0	2331000	2331000	0	0	0	0
CC	0	0	7562000	6514000	3161936	0	-104867	3057071
HPT	1516000	0	1516000	1516000	32175	0	0	32176
IPT	967609	0	967608	967609	22977	0	0	22977
LPT	1187000	0	1187000	1187000	33255	0	0	33257
TE	0	0	2843000	2843000	8788	0	0	8788
EN	0	0	2843000	2843000	133029	0	0	133029
MX1	0	0	133523	133523	887	0	0	887
SR	0	0	109301	133523	11301	0	-24226	-12921
WGS	0	0	109374	109301	680	0	70	753
SOFC	10.73	27805	38525	10.73	32598	9143	5.92E-12	32606
Total			25158773	24096411	4077350	9143	-129023	3948354

Table 5.20 The exergoenvironmental impact results for components

Comp.	b_F [mPt/MJ]	b_P [mPt/MJ]	f_b [%]	r_b [%]
FAN	9.96	10.04	0.048	0.80
S1	4.33	4.33	0	0
FN	4.33	4.88	0	12.8
IPC	9.92	22.69	0.001	128.7
HPC	9.90	10.28	0.001	3.86
S2	11.84	11.84	0	0
CC	6.54	9.69	-3.43	48.04
HPT	9.68	9.89	0.002	2.2
IPT	9.69	9.92	0.002	2.43
LPT	9.68	9.96	0.006	2.9
TE	9.69	9.72	0	0.31
EN	9.72	9.28	0	-4.47
MX1	5.36	5.39	0	0.67
SR	3.96	5.39	187.46	36.25
WGS	3.94	3.95	9.72	0.56
SOFC	1.74	0.003	0.023	-99.8
Total	7.72	9.00	-3.27	16.5

The exergoenvironmental impact rates are presented in the Sankey diagram of Figure 5.19 with a scale of 30,000 mPt/h/pt. The inlet air has no environmental impact at 02, while the F1 fuel blend has 5207000 mPt/h at F1 and 133518 mPt/h at F2. The

exergoenvironmental rates of input power are 791709 mPt/h for FAN, 80442 mPt/h for IPC, and 1408000 mPt/h for HPC, while the exergoenvironmental rates of output power are 1516000 mPt/h for HPT, 967609 mPt/h for IPT, and 1187000 mPt/h for HPC. The exergoenvironmental rates of exhaust gases in the exit nozzle (EN) are 2837380 mPt/h in physical changes and 5620 mPt/h in kinetic changes. Also, the exhaust air at the fan exit (FN) has an exergoenvironmental rate of 120 mPt/h for physical changes and 1027880 mPt/h for kinetic changes.

The exergoenvironmental study was conducted in the combined turbofan to evaluate the environmental impact of the whole system. The total exergoenvironmental rates for fuel, product, and destruction are the maximum for F4 as (62507, 62508, and 8746 Pt/h, respectively) and the minimum for F1 (25159, 24096, and 4077 Pt/h, respectively), as shown Figure 5.20.

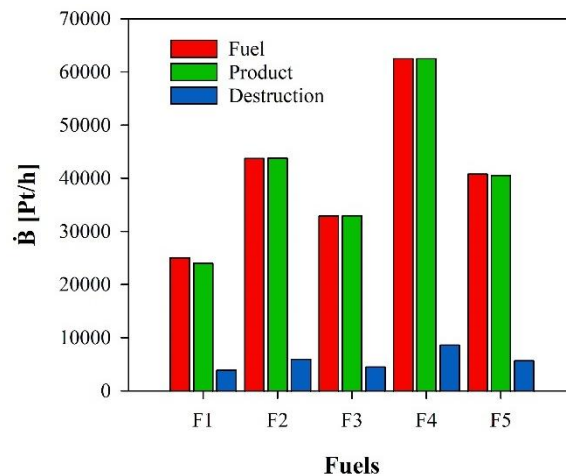


Figure 5.20 Total exergoenvironmental rates for fuel, product, and destruction

The most contribution to the exergoenvironmental fuel is due to the combustion chamber which holds about 30% for F1, and 27% for the other fuel blends. Interestingly, exergoenvironmental product is reduced to 3% compared to that of the fuel, meaning that the system components are reducing the emission through complete chemical reactions to eliminate the carbon monoxide, methane, and NOx. The total exergoenvironmental destruction rate has a range of 4077 mPt/h to 8746 mPt/h, since it was estimated as the difference between the total exergoenvironmental fuel rate and product rate for each fuel utility. This value of the destruction rates contributes about 15% of the fuel rate, which makes efficiency of 85%. The order from highest to lower total exergoenvironmental rates

is F4, F2, F5, F3, and F1. This reflects the overall specific exergoenvironmental impact for fuel and product, as shown in the figure with the same order.

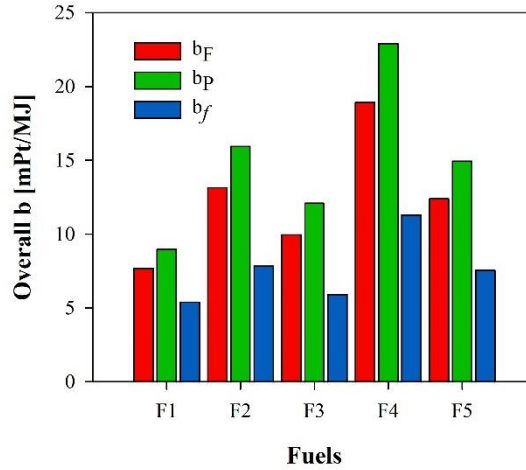


Figure 5.21 The specific exergoenvironmental impact for fuel and product for engine and fuels

Therefore, the maximum b_F and b_P values are 19 and 23 mPt/MJ for F4 and the minimum b_F and b_P values are about 8 and 9 mPt/MJ for F1, respectively. The specific exergoenvironmental impact of fuel and product are computed by the ratio of total exergoenvironmental rate to the total exergetic rate for fuel and product. The total exergetic rates of fuel are 905 MW for F1, 924 MW for F2, 918 MW F3, 917 MW for F4, and 914 for F5, while total exergetic rates of product are 743 MW, 763 MW, 758 MW, 758 MW and 755 MW for F1 to F5, respectively. As shown in Figure 5.21, the trend of the b_F and b_P values is similar to the trend of b_f of fuel blends, which implies that the selection of fuel that has less environmental impact is essential to reduce the overall impact of the system.

In addition, the environmental impact of pollution formation, \dot{B}^{PF} , has been graphed for the chemical reactors and combustion chamber, as shown in Figure 5.22. The \dot{B}^{PF} is estimated as the difference between the output and input of methane, carbon dioxide, and carbon monoxide of the reactors. The figure does not include the SOFC unit because it has zero pollution formation. Since the methane is totally combusted in CC for F1, F4 and F5, the \dot{B}^{PF} is giving negative values of about -105 to -154 Pt/h. The \dot{B}^{PF} of CC using F2 and F3 are 118 and 80 Pt/h, respectively, and these positive values are due to the production of CO_2 and CO in the exhaust of CC. Also, the total \dot{B}^{PF} depends on the emissions from the CC compared to other reactors, such as the SR and WGS since the mass

flow rate of the fuel entering the CC is 27 to 40 times that entering the SOFC system. The total of \dot{B}^{PF} is computed by adding the environmental impact of pollution formation for all reactors. The total of \dot{B}^{PF} has a negative value for F1 and F5 as -129 Pt/h and -154 Pt/h, respectively, because of the huge reduction of emission in the CC since the methane and carbon monoxide have been completely combusted in the CC. In addition, it gains a positive value of 128 Pt/h for F2 and 86 Pt/h and F3, and F4, respectively.

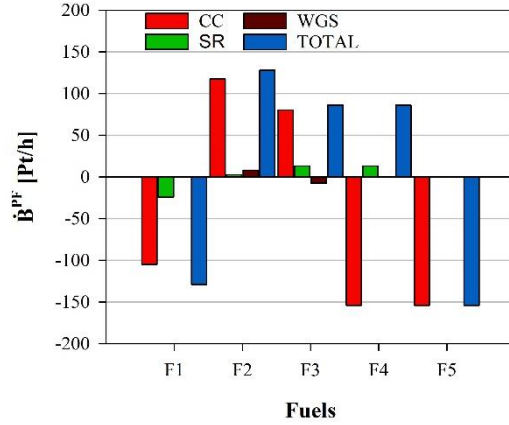


Figure 5.22 Environmental impact due to pollution formation, \dot{B}^{PF}

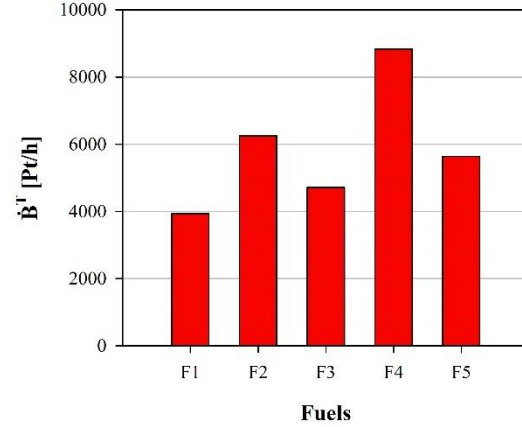


Figure 5.23 Total environmental impact, \dot{B}^T

Furthermore, the total environmental impact, \dot{B}^T , which is the summation of \dot{Y} , \dot{B}^{PF} , and \dot{B}_D for all the components of the SOFC-turbofan engine, is presented in Figure 5.23. The \dot{B}^T counts for the sign of \dot{B}^{PF} , which means that the environmental impact has dramatically decreased since the pollution formation has been decreased by the combined aircraft engine. The minimum and maximum \dot{B}^T are 3948 Pt/h for F1 and 8839 Pt/h for F4. Moreover, the relative environmental impact difference r_b and exergoenvironmental factor f_b are graphed in Figure 5.24. The F1 and F5 have negative values of f_b as -3.27% and -2.73% because f_b counts the sign of \dot{B}^{PF} , while the other fuels have f_b values of 1.06 % for F4, 1.82% for F3 and 2.05% for F2. The last three fuels mentioned have about 21% of r_b , while F1 and F5 have about 17% and 20% of r_b , respectively.

The main output parameters of this combined system are the electricity generated from the fuel cell SOFC and turbines of HPT, IPT, and LPT, which deliver the power to compressors of HPC, IPC, and FAN, correspondingly, and the output exhaust gases from fan nozzle (FN) and exit nozzle (EN). Therefore, the environmental aspects are discussed

as specific exergoenvironmental impact, b , as shown in Table 5.21, with respect to the five fuel blends F1 to F5. For the electricity, F1 has proven as the environmentally friendly option since it records the minimum b value for all the turbines and SOFC, while F4 records the highest specific exergoenvironmental impact for them. The b values of electricity production range from about 10 to 25 mPt/MJ for turbines and 3 to 8 mPt/MJ for SOFC. The b values of exhaust gases vary from 9 to 25 mPt/MJ for EN and 5 to 12 mPt/MJ for FN.

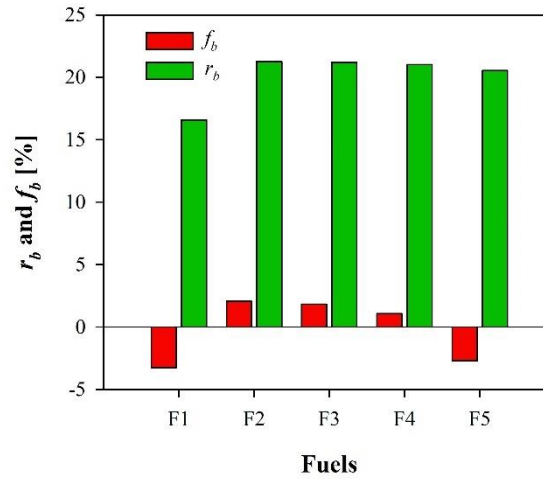


Figure 5.24 Relative environmental impact difference r_b and exergoenvironmental factor f_b

Table 5.21 Specific exergoenvironmental impact [mPt/MJ] of electricity and exhaust gases.

	HPT	IPT	LPT	SOFC	EN	FN
Fuels	$b_{e,HPT}$	$b_{e,IPT}$	$b_{e,LPT}$	$b_{e,SOFC}$	b_{11}	b_{12}
F1	9.9	9.9	10.0	3.2	9.3	4.9
F2	17.4	17.5	17.5	5.7	17.3	8.6
F3	13.3	13.3	13.4	4.4	13.2	6.6
F4	25.2	25.2	25.3	8.3	25.0	12.4
F5	16.4	16.4	16.5	5.3	16.3	8.1

The exergetic rates and exergoenvironmental impact rates are shown in Figure 5.25 for physical and kinetic parts of the Exit nozzle (EN). As shown in Figure 5.25-a, the exhaust gases in EN have physical exergy with a range of 61048 kW at F4 to 64200 kW at F2 and kinetic exergy of 21659 at F3 to 24656 kW to F2. The slight change in physical exergy rate of EN is due to the slight change in mass flow rate of entering the nozzle which is about 112.1 kg/s for F1, 114.1 kg/s for F2, 112.3 for F3 and F4, and 112.1 for F5, which is caused by different fuel rates to CC and SOFC to maintain the reactor operating conditions the same. The kinetic exergy rates equal to the kinetic energy rates for the nozzle

depending on the exhaust speed, ranging from 621 to 657.5 m/s, and mass flow rate ranging from 112 to 114 kg/s. For the environmental impact, as shown in Figure 5.25-b, F1 produces the minimum values of exergoenvironmental impact rates for 2068 Pt/h of physical and 775 Pt/h kinetic parts, while the F4 gives maximum values of physical and kinetic exergoenvironmental rates of 5497 Pt/h and 2127 Pt/h, respectively.

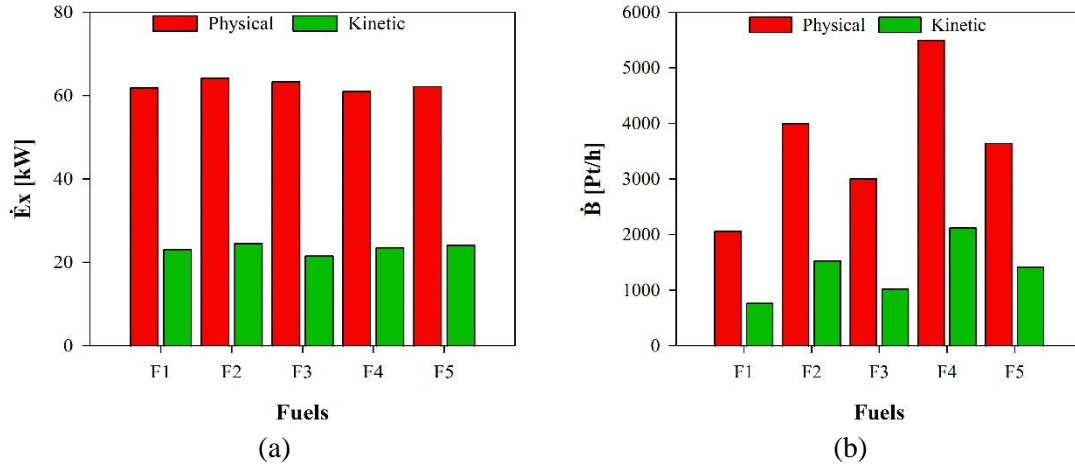


Figure 5.25 (a) Exergy rates and (b) exergoenvironmental rates of the Exit Nozzle (EN)

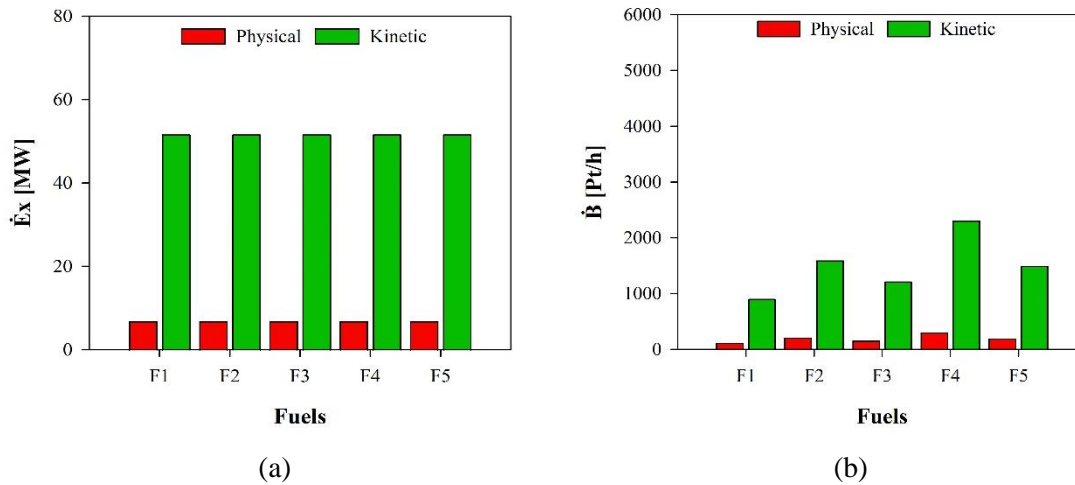


Figure 5.26 (a) Exergy rates and (b) exergoenvironmental rates of the FAN Nozzle (FN)

Similarly, the exhaust air of FAN nozzle (FN) was studied in the exergetic and exergoenvironmental impact rates, as shown Figure 5.26. Figure 5.26-a shows that the exhaust air in FN has a constant physical and kinetic exergy of 6906 and 51587 kW, respectively, because there is no change in the physical conditions of air after the FAN. Also, Figure 5.26-b graphs that F1 produces the minimum values of exergoenvironmental impact rates for 121 Pt/h of physical part and 907 Pt/h for kinetic part for FN, while the F4

gives maximum values of physical and kinetic exergoenvironmental rates of 309 Pt/h and 2307 Pt/h for FN, respectively.

Another important parameter for aircraft applications is thrust force, which is displayed in Figure 5.27-a. The thrust force is stable for FAN Nozzle over the change of the fuels because the operating conditions of compressors were 69 kN, while the thrust force for Exit Nozzle varies from 84 kN for F3 to 91 kN for F2. Therefore, a new parameter is exergoenvironmental impact of thrust force, \dot{B}_{thrust} , which is defined as the total exergoenvironmental impact rate, which is the summation of physical and kinetic parts divided by the thrust force, and its unit is Pt/(h.kN). As shown in Figure 5.27-b, for the EN, the \dot{B}_{thrust} varies from 34 Pt/(h.kN) for F1 to 87 Pt/(h.kN) for F4. That is because the specific exergoenvironmental impact, b_{11} , is the maximum for F4 and minimum for F2, as shown in Table 16, reflecting that the exergoenvironmental rate of \dot{B}_{11} to follow the same trend. Also, the \dot{B}_{thrust} of FN varies from 15 Pt/(h.kN) for F1 to 38 Pt/(h.kN) for F4 because of variation of b_{12} and \dot{B}_{12} .

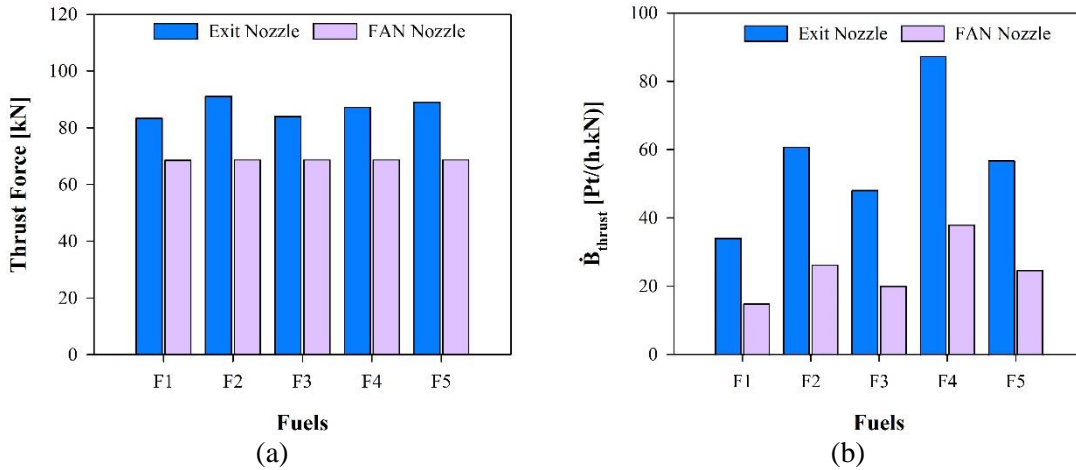


Figure 5.27 (a) The thrust forces and (b) exergoenvironmental impact due to nozzle thrust forces

5.3 Results of System R-1

This section displays the results of exergetic, exergoeconomic, and exergoenvironmental analysis of hybrid combined locomotive engine in addition to their discussion. Later, the effect of fuel blends is also explained with respect to these analyses.

5.3.1 Results of Thermodynamic Analysis

The thermodynamic results of the state points are reported in [178] for the hybrid combined engine. Regarding the ICE system, the air mass flow rate enters the ICE at 3.26 kg/s, while the fuel mass flow rate is 0.15 kg/s. The air is pressurized through the compressor of the turbocharger from 101.3 to 126.63 kPa, then compressed by the piston to 4800 kPa. The air and fuel streams are heated in the combustion chamber at constant volume from 540.33°C to 1150°C and 9000 kPa. The combustion continues under constant pressure to 1350°C. The air is then expanded to 500 kPa and cooled to 350°C and 340 kPa. The exhaust gas is expanded by the turbine of the turbocharger to the atmospheric pressure and 206°C. Regarding the gas turbine system, the air and fuel flow at 2.85 and 0.1 kg/s, respectively. The air is compressed from 101.3 kPa to 1500 kPa. The compressed air has a temperature of 430 °C and is heated to 630°C by the HX1 and combusted with the fuel in CCGAS to increase its temperature to 980°C. The exhaust gas is expanded by the turbine to 100 kPa and 468°C. The exhaust gas is heated again by the heat exchanger HX2 before entering the catalytic burner.

The ammonia-water is pumped from A1 at 10°C and 200 kPa to 2000 kPa. It is in a liquid state with a strong solution of 52.4% ammonia. Then it is heated by the regenerator heat exchanger (AHX) to 72 °C before entering the generator AGEN, which is heated to 125°C to produce a pure ammonia at state A7 (91.9% NH₃) and a weak solution at A4 (32.4% NH₃). The weak solution is flowing through the AHX then expanded through AEX2 to the absorber at 33 °C and 200 kPa. The pure ammonia is cooled down in the condenser at 60°C then expanded by AEX1 to 200 kPa and heated through the evaporator AEV from -6.51°C to 28°C.

The heat transfer and power of the components are presented in Table 5.22. The fuel used in this system is F1 (75% NG+25% H₂). For the ICE turbocharger, the power of the compressor (TUR-C) and turbine (TUR-T) are 82.0 and 592.3 kW, while the thermal load of aftercooling (AFTERCOOL) is 98.7 kW. The load of the ICE engine with turbocharger is separately displayed to show the load of each process. The total net power of the ICE engine including the turbocharger is 2569.2 kW and the added and rejected heat are 7833.5 and 1007.6 kW. That engine has an energetic and exergetic efficiencies of 32.8% and 41.48%, respectively. The gas turbine has a compressor power of 1217.6 kW

and a turbine power of 1865.6 kW to produce a net power of 648.0 kW. It also needs a heating load of 2160.9 kW for a combustion of air and fuel, which has been reduced by using the heat exchanger recovery (HX1) with a duty of 631.8 kW. This GT system has energetic and exergetic efficiencies of about 30 % and 40%, respectively.

Table 5.22 The energy loads and efficiencies of components using F1 fuel.

Component	\dot{Q} [kW]	\dot{W} [kW]	$\dot{E}x_D$ [kW]	η [%]	ψ [%]
<i>ICE-turbocharger</i>					
TUR-C	0	82.0	15.0	80	81.68
AFTRCOOL	98.7	0	3.1	100	34.71
TUR-T	0	592.3	66.6	85	88.76
<i>GT System</i>					
COMP1	0	1217.6	109.5	80	91.01
HX1	631.8	0	23.2	100	99.54
CCGAS	2160.9	0	4246.7	90	41.93
TUR1	0	1865.6	141.9	85	92.39
<i>MCFC system</i>					
MCFC	1758.7	939.6	1965.5	78.71 _e , 53.43 _{th}	78.90
SR	626.4	0	67.8	90	77.44
WGS	58.1	0	9.7	90	99.82
<i>Heat recovery heat exchangers</i>					
COOLING	3358.7	0	787.9	100	52.62
HX2	348.5	0	5.9	100	99.86
<i>ARS system</i>					
ACOND	1215.0	0	83.5	100	88.94
AEV	615.1	0	132.8	100	1.99
AHX	1462.5	0	146.4	100	69.03
AGEN	3346.0	0	157.4	100	81.28
ABS	2763.0	0	170.0	100	21.72
AP	0	17.3	4.2	70	75.97

The MCFC system is modelled with separate steam reforming and water gas shift units. The net power produced by the MCFC is 939.6 kW with a required heat of 1758.7 kW, 626.4 kW of SR and 58.1 kW of WGS. The electric and energetic efficiencies of MCFC are 78.71% and 53.43%, respectively. The exergy efficiency of MCFC is 78.9%. The SR and WGS have 90% of energetic efficiency and above 75% exergy efficiency. For the absorption refrigeration system, the condenser and evaporator have a thermal load of 1215 and 615.1 kW, while the generator and absorber have a thermal load of 3346 and 2763 kW, respectively. The pump power is significantly small of 17.3 kW.

The performance of each subsystem and overall system of the hybrid combined engine are presented in Table 5.23. The overall system has the net power of 4109.3 kW, which is composed of the ICE (2569.2 kW), GS (648 kW), MCFC (939.6 kW), and ARS

(17.3 kW). The required heat for the hybrid engine is 10678.9 kW, combining all the required heat of all subsystems. The rejected heat includes that from the ICE, GC, and MCFC which are rejected to the environment, while the cooling load (615.1 kW) is included in the useful energy to the hybrid combined system. The overall energetic and exergetic efficiency are 44.5 % and 50.4%, respectively. As a result, combining the MCFC and GT with ICE increases the overall net power by 61% and increases the overall heat required by 36% compared to that of ICE. Also, the performance of hybrid combined engine has been increased by 35% energetic efficiency and 25% exergetic efficiency compared to only the ICE engine.

Table 5.23 The hybrid combined engine performance using F1 fuel.

Subsystem	\dot{W} [kW]	\dot{Q}_{add} [kW]	\dot{Q}_{rej} [kW]	η [%]	ψ [%]
ICE	2569.2	7833.5	1106.4	32.8	40.17
GC	648.0	2160.9	0.00	29.99	39.4
MCFC	939.6	0.00	564.8	78.71 _e & 26.0 _{th}	78.9
SR	0.00	626.4	0.00	90	77.44
WGS	0.00	58.1	0.00	90	99.82
ARS	17.3	0.00	615.1	18.29	9.54
Entire System	4139.6	10678.9	615.1	44.52	50.4

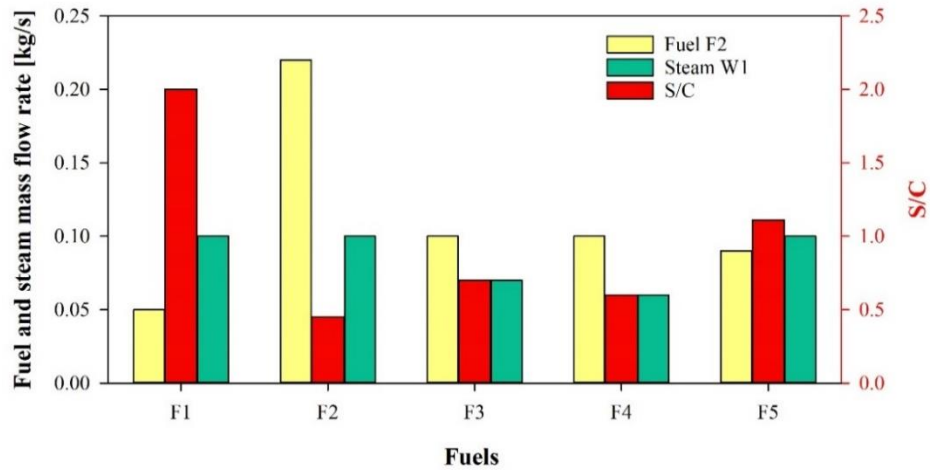


Figure 5.28 The fuel and steam mass flow rate entering the SR and the S/C ratio.

The fuel and steam flow rates entering the MCFC are different for each fuel type as shown in Figure 5.28. The S/C refers to the steam to carbon ratio, which is equivalent to steam to fuel ratio. The steam flow rate at state point (W1) has two values of 0.1 kg/s for F1, F2, and F5 fuels and 0.07 kg/s for F3 and 0.06 kg/s for F4. However, the fuel flow

rates are 0.05 kg/s for F1, 0.09 kg/s for F5, 0.1 kg/s for F3 and F4, and 0.22 kg/s for F2. Accordingly, the S/C is the highest of 0.2 for F2 and the lowest of 0.04 for F2. These values of mass flow rates are chosen to avoid the resulting error in modelling the MCFC using Aspen Plus and to maintain the molar fraction of the substituents in the anode and cathode reactions. The molar fraction of hydrogen in the anode should be above 0.8, while the carbon dioxide and steam slightly above 0.1. however, the molar fraction of oxygen in the cathode is about 0.03 and above 0.05 to 0.08. These molar fraction values have significant impact in Nernst loss potential, activation loss in anode and cathode, since they are function of partial pressures for H₂, CO₂, O₂, and H₂O in anode and cathode plate.

In addition, the effect of fuels on the MCFC performance is investigated as displayed in Table 5.24. The loss voltage is the summation of activation losses of anode and cathode and the ohmic loss. The cell voltage is the difference between the standard reversible potential and Nernst loss and activation. The highest loss voltage is 0.222 V for F1, while the minimum is 0.181 V for F2. Similarly, the maximum and minimum cell voltage is 0.851 and 0.818 V for F2 and F5, respectively. Hence, the cell power is the maximum of 939.6 kW for F1 and the minimum of 937.1 kW for F5. The required heat for the MCFC has a range of 1760 kW for F1 to 5215 kW for F2. Consequently, the maximum and minimum energetic and exergetic efficiencies are about 53% and 79% for F1 and 18% and 27%, respectively.

Table 5.24 The MCFC performance with respect to different fuels.

Parameter	F1	F2	F3	F4	F5
V_{loss} [V]	0.222	0.181	0.193	0.193	0.188
V_{cell} [V]	0.820	0.851	0.822	0.824	0.818
$\dot{W}_{MCFC,AC}$ [kW]	939.6	974.9	942.0	943.7	937.1
$\dot{W}_{MCFC,loss}$ [kW]	254.2	207.5	221.0	221.2	214.8
$\eta_{MCFC,e}$ [%]	78.71	82.45	80.99	81.01	81.35
$\dot{Q}_{MCFC,add}$ [kW]	1758.7	5215.4	2414.3	2430.5	2460.7
$\dot{Q}_{MCFC,loss}$ [kW]	564.8	4033.0	1251.2	1265.7	1308.8
$\eta_{MCFC,th}$ [%]	53.43	18.69	39.02	38.83	38.08
$\psi_{MCFC,th}$ [%]	78.90	27.61	57.62	57.34	56.24

Furthermore, the effect of fuels on the absorption refrigeration system is considered as illustrated in Table 5.25. The exhaust temperature should be cooled to 130°C B10, and the heat rejected is used to increase the generator temperature to 125°C. The heating loads of the generator vary from 2917.8 kW for F5 to 3346 kW for F1. However, the cooling

loads have a range from 439.8 kW for F5 to 615 kW for F1. The resulting COP_{en} is about 15% except for F1 where it is 18%, while the COP_{ex} is about 7.8% and 9.5% for F1. The mass flow rates of ammonia pumped in state A1 are different to suit the generator load.

Table 5.25 The absorption Refrigeration system performance with respect to fuels.

Parameter	F1	F2	F3	F4	F5
\dot{Q}_{AGEN} [kW]	3346.0	3218.9	2944.5	2944.5	2927.8
\dot{Q}_{AEV} [kW]	615.1	483.6	442.3	442.3	439.8
\dot{Q}_{ABS} [kW]	2763.0	2549.3	2332.0	2332.0	2318.8
\dot{Q}_{ACON} [kW]	1215.01	1168.8	1069.2	1069.2	1063.1
\dot{W}_{AP} [kW]	17.26	15.73	14.39	14.39	14.30
COP_{en} [%]	18.29	14.95	14.95	14.95	14.95
COP_{ex} [%]	9.54	7.80	7.8	7.8	7.8
\dot{m}_{ABS} [kg/s]	5	4.81	4.4	4.4	4.375

The net power for subsystems and overall system using different fuels are illustrated in Figure 5.29-a. The overall net power is increased to more than 4000 kW for all fuels compared to 2000 kW of traditional ICE. The specific fuel consumption is displayed in Figure 5.29-b to show the ratio of the fuel mass flow rate to the net power of the system. The traditional ICE has 0.25 kg/kWh for ULSD fuel. However, the GT and MCFC have an average value of 0.32 and 0.35 kg/kWh using ULSD fuel, respectively. The hybrid combined system has different values slightly changing from 0.25 and a maximum of 0.39 kg/kWh for F2 fuel. Using F1 fuel reduced the specific fuel consumption to 0.24 kg/kWh for the whole engine.

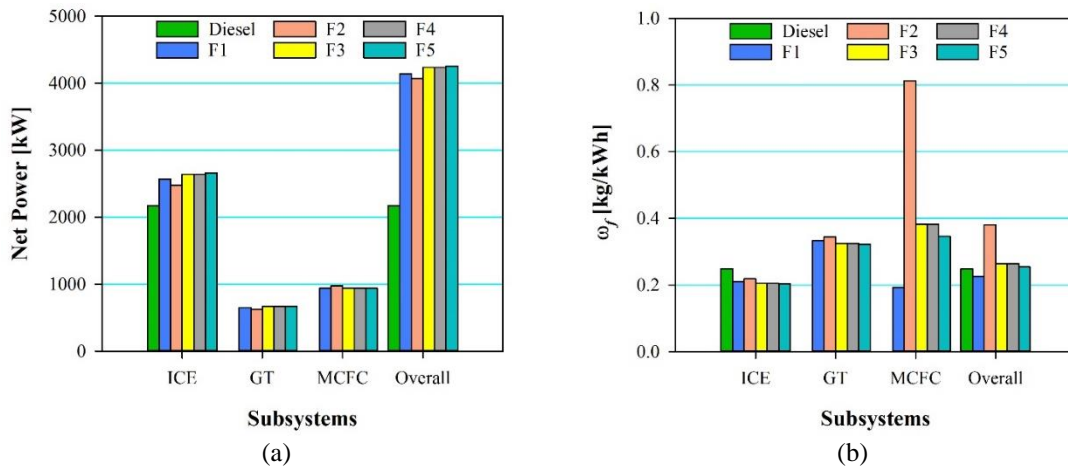


Figure 5.29 (a) Net power and (b) specific fuel consumption for subsystems and overall system

The overall energetic and exergetic efficiencies are similar in values of about 43% and 50%, respectively, for all fuels except F2 (methanol and hydrogen) which has 68%

energetic efficiency and 82% exergetic efficiency, as shown in Figure 5.30-a. However, the CO₂ emissions from ICE using diesel fuel is the most significant of 0.45 kg/s. Using alternative fuels dropped this value by about 30% for F1 and 50% for fuels F2 to F5. The GT system produces less emissions of an average of 0.05 kg/s, as shown in Figure 5.30-b. The emissions from the MCFC are composed of the chemical reactions in the anode, cathode, SR, and WGS, as well as the emissions from ICE and GT. Therefore, the emission of MCFC has values of less than 0.1 kg/s for fuels F2 to F4, 0.15 kg/s for F5, and 0.27 kg/s for F1. That means a total reduction of 60% can be achieved using F2, while 65% F3 and F4 fuels.

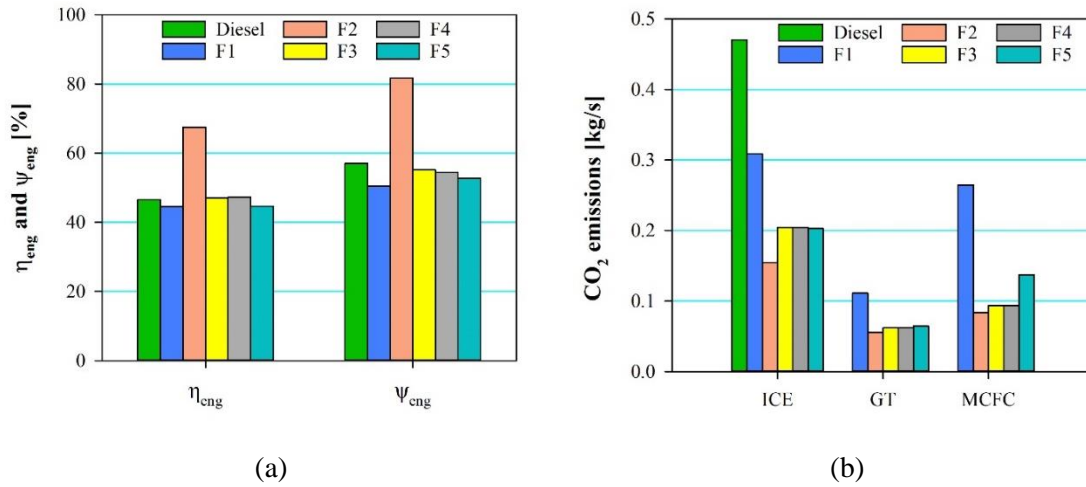


Figure 5.30 (a) Overall efficiencies for the engine and (b) CO₂ emissions for the subsystems

5.3.2 Results of Exergy Analysis

The exergy flow rates for streams are laid out in the Sankey diagram, including the work and thermal exergy rates for the components as reported in [215], as shown in Figure 5.31. The thickness of exergy flow was chosen to be in a scale of 200kW/1mm. Based on the exergy flow, the ICE has the highest exergy flow, then MCFC, then GT, and lastly ARS. The fuel exergy flow, which is represented in brown colour, of the ICE is the highest (10329 kW), followed by the MCFC subsystem entering the mixture at MX1 (5056.3 kW), followed by the combustion chamber (CC) (4149.3 kW). The highest exergy destruction represented in gray is for the ICE, then CC, then MCFC. The thickness of exergy flow increases as the conditions of that flow is far from the standard conditions, and more chemical exergy is added.

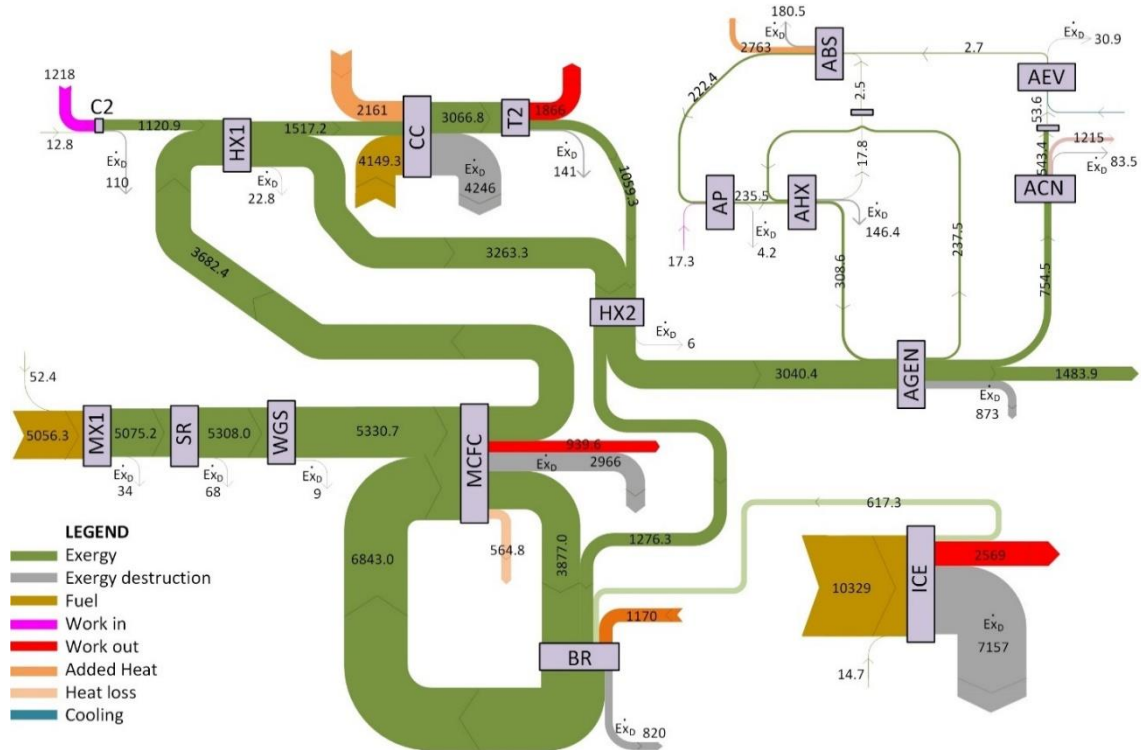


Figure 5.31 The Sankey Diagram for exergy flow rate in kW

In addition, Table 5.26 presents the heat transfer and power of the components as well as the fuel, product, destruction, and loss exergy flow for each component. The net power of the hybrid combined system is 4139.6 kW, which is estimated as the summation of the net power of the gas turbine (648 kW), and the MCFC power (939.6 KW) and the ICE (2569 kW) subtracting the power of pump (17.3 kW). The exergetic efficiency reflects the ratio of exergy product to exergy fuel; as shown in Table 5.26, the compressor (C2), turbine (T2), heat exchangers (HX-1, HX-2), and reactors (SR, WGS, and BR) have a high exergetic efficiency, more than 90%, while other components like MCFC, ACN, AEV, and AP have moderate exergy efficiency between 60% and less than 90%, and around 50% and below for combustion chamber (CC), absorber (ABS) and generator (AGN). This is due to the high-temperature difference between the standard condition and the high heat of chemical reactions. The total exergetic efficiency, ε_t , is 82.68%.

There is another parameter which is used to analyze the system exergetically is γ , referring to the ratio of destruction exergy to the total fuel exergy rates. Most of the components have a low γ value of less than 1%, whereas the ICE, CC, and MCFC have

7.34%, 4.35%, and 3.04%, respectively. The destruction ratio, y_t , is 17.3%. The system was operated using F1 (75% NG and 25% H₂).

Table 5.26 The exergy flow analysis for the components

#	\dot{Q} [Kw]	\dot{W} [kW]	\dot{Ex}_F [kW]	\dot{Ex}_P [kW]	\dot{Ex}_D [kW]	\dot{Ex}_L [kW]	ε [%]	y [%]	y^* [%]
C2	0	1218	1218	1108	110	0	90.97	0.11	0.65
HX-1	631.8	0	419.1	396.3	22.8	0	94.56	0.02	0.13
CC	2161	0	7313	3067	4246	0	41.94	4.35	25.13
T2	0	1866	2007	1866	141	0	92.97	0.14	0.83
HX-2	348.5	0	223	217	6	0	97.31	0.01	0.04
ICE	0	2569	9726	2569	7157	0	26.41	7.34	42.35
MX1	0	0	5109	5075	34	0	99.33	0.03	0.20
SR	626.4	0	5376	5308	68	0	98.74	0.07	0.40
WGS	58.1	0	5340	5331	9	0	99.83	0.01	0.05
MCFC	564.8	939.6	26843	23877	2966	1622	88.95	3.04	17.55
BR	1750	0	31346	30526	820	0	97.38	0.84	4.85
AGN	3346	0	1865	992	873	0	53.19	0.89	5.17
ACN	1215	0	211.2	127.7	83.5	0	60.46	0.09	0.49
AEV	615.1	0	81.9	50.95	30.9	0	62.24	0.03	0.18
ABS	2763	0	227.6	47.2	180.5	0	20.72	0.18	1.07
AP	0	17.3	17.26	13.1	4.2	0	75.96	0.00	0.02
AHX	1463	0	219.6	73.2	146.4	0	33.32	0.15	0.87
Total			97542.6	80644.4	16898.2	1622	82.68	17.3	100

The current hybrid combined system is compared according to different fuels. Figure 5.32 shows the total exergy rates and exergetic efficiency and destruction ratio with respect to fuels. The fuel (F2) has high total exergy fuel and product (107 and 90 MW, respectively) compared to that of F1 (fuel of 97.5 MW and product of 80.6 MW). Note that the minimum fuel and product exergy flow is for F5, about 71 and 54 MW, respectively. The total exergy destruction flow is about 17 MW for all fuels. These yields maximum ε_t and minimum y_t for F2 about 84% and 16%, respectively, whereas F5 has a minimum ε_t and maximum y_t of 76 and 24%, respectively. As presented in Figure 4, the y_t decreases when ε_t increases because the former counts for the exergy destruction, while the latter counts for exergy product. The lower values for exergy fuel and product and higher values of exergy destruction give a high value of y_t and a low value of ε_t .

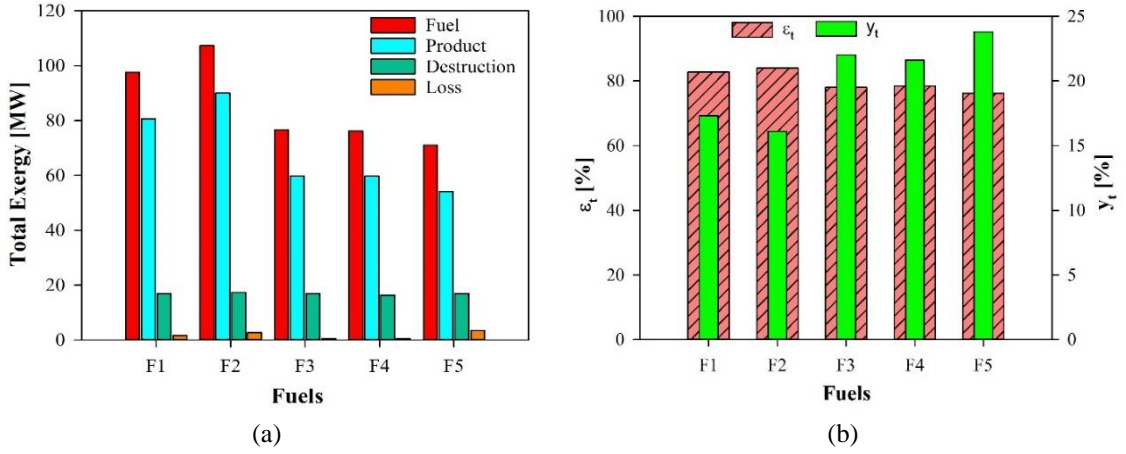


Figure 5.32 (a) The total exergy fuel, product, destruction, and loss and (b) the total exergy efficiency (ε_t) and destruction ratio (γ_t).

5.3.3 Results of Exergoeconomic Analysis

The exergoeconomic analysis for the hybrid combined locomotive engine is performed. Figure 5.33 shows the exergy cost flow rates (\dot{C}_j) including the levelized capital cost (\dot{Z}_k), which are calculated based on cost equations from Table S-1 (Supplementary data), power (\dot{C}_k^W) and thermal exergetic cost rates (\dot{C}_k^Q). Some assumptions are considered to perform the calculations of the exergoeconomic analysis, such as the nominal interest rate being 12%, the lifetime of the engine being 25 years, the annual operation time being 7300 h, the inflation rate being 3%, and the maintenance factor is 6%. The exergetic cost is drawn at a scale of 10 \$/h per 1mm. The fuel exergy costs are 278.1 \$/h for ICE, 136.1 \$/h for MX1 entering the MCFC, and 111.7 \$/h for CC. The component cost rate (\dot{Z}_k) is very small compared to the flow exergy costs of fuel, products, and input and output power. The exergetic cost of the exhaust air to the atmosphere after the generator (AGEN) is estimated to be 185.6 \$/h.

Table 5.27 tabulated the exergoeconomic analysis. The maximum levelized capital cost is for MCFC about 16.52 \$/h followed by the ICE (8.29 \$/h) then the evaporator AEV (2.00 \$/h) then the catalytic burner BR (1.24 \$/h). The total levelized capital cost is 32.15 \$/h, as shown in Table 5.27. The total fuel and product exergetic cost rates are 7962.8 and 7992.2 \$/h, respectively. The destruction and loss of exergetic cost rates are 847.4 and 12 \$/h, respectively. The exergoeconomic factor f for F1 ranges from 0% for the mixer MX1 to 52% for the reactor WGS, while the relative cost difference r ranges from 0.3% for the

LEGEND

- Cost exergy rate
- Total leveled cost, \dot{Z}_k
- Fuel
- Work in cost
- Work out cost
- Added Heat cost
- Heat loss cost
- Cooling cost

minimum total relative cost difference is 19.7% for F2, as shown in Figure 5.34-b, while the maximum total relative cost difference is 31.6% for F5.

Table 5.27 The results of exergoeconomic analysis of the system components

#	\dot{Z}_k [\$/h]	\dot{C}_F [\$/h]	\dot{C}_P [\$/h]	\dot{C}_D [\$/h]	\dot{C}_L [\$/h]	c_F [\$/GJ]	c_P [\$/GJ]	f [%]	r [%]
C2	0.74	52.6	53.3	4.8	0.0	12.00	13.37	13.51	11.47
HX-1	0.09	18.8	18.9	1.0	0.0	12.44	13.22	7.96	6.26
CC	0.57	196.1	196.7	113.9	0.0	7.45	17.82	0.50	139.17
T2	0.58	80.0	80.6	5.6	0.0	11.08	12.00	9.32	8.32
HX-2	0.08	23.8	23.9	0.6	0.0	29.67	30.61	11.65	3.15
ICE	8.29	102.7	111.0	75.6	0.0	2.93	12.00	9.89	309.19
MX1	0.00	136.2	136.2	0.9	0.0	7.41	7.45	0.00	0.67
SR	0.86	138.4	139.3	1.8	0.0	7.15	7.29	32.81	1.94
WGS	0.25	139.5	139.7	0.2	0.0	7.26	7.28	51.67	0.31
MCFC	16.52	3100.0	3114.0	342.5	12.0	32.08	36.23	4.60	12.93
BR	1.24	3515.0	3516.0	92.0	0.0	31.15	31.99	1.33	2.72
AGN	0.07	219.8	219.9	102.9	0.0	32.74	61.58	0.06	88.09
ACN	0.35	59.6	59.9	23.6	0.0	78.36	130.34	1.46	66.33
AEV	2.00	143.6	145.6	54.2	0.0	487.29	793.81	3.56	62.91
ABS	0.07	29.4	29.5	23.3	0.0	35.92	173.80	0.30	383.86
AP	0.11	0.7	0.9	0.2	0.0	12.00	18.10	37.77	50.87
AHX	0.34	6.5	6.9	4.3	0.0	8.25	26.03	7.23	215.69
Total	32.15	7962.8	7992.2	847.4	12.0	22.68	27.53	3.66	21.89

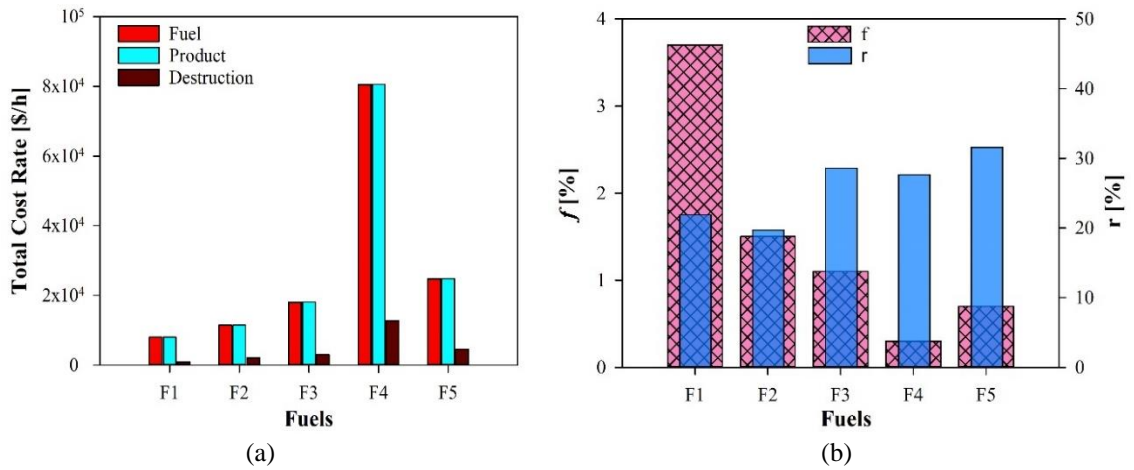


Figure 5.34 (a) The total cost rate of exergy fuel \dot{C}_F , product \dot{C}_P , and destruction \dot{C}_D and (b) the total exergoeconomic factor (f) and relative cost difference (r)

Therefore, the exergoeconomic factor increases when exergy destruction decreases as well as cost exergy destruction decreases. The best economic fuel for the system is pure natural gas, which was assumed as pure methane. In the case that there is no pure natural gas, then the economic fuel is F2, which is a mixture of methanol and hydrogen. In addition,

the specific fuel costs mentioned have a significant impact on exergoeconomic analysis since the F1 has less price among them of 7.48 \$/GJ. Nowadays, fuel prices are not stable because of COVID-19 holding oil production and businesses. They have a significant impact on the economic analysis.

5.3.4 Results of Exergoenvironmental Analysis

The exergoenvironmental analysis is performed on the hybrid combined locomotive engine. Table 5.28 shows the values of the environmental impact of material production, process, disposal, and the total environmental impact as [mPt/kg]. The total Y is calculated as the total environmental impact multiplied by the component weight. The lifetime of the system is 25 years, and the operation time is 7300 hours per year. The weight of the ICE engine is 18,000 kg [216]. The MCFC system, including steam reforming, water gas shift, and catalytic burner, has a weight of 10,336 kg (10 kg/kW [146]). The gas turbine cycle has the least weight of 599 kW [142]. The ABS has a total weight of 4,816 kg (5 ton for 500 kW cooling [164,217,218]). Therefore, the total weight of the hybrid combined locomotive engine is 33,751 kg (~34 ton).

Table 5.28 The component-related environmental impact results

#	Weight [kg]	Material Production [mPt/kg]	Material Processing [mPt/kg]	Material Disposal [mPt/kg]	Total EI [mPt/kg]	Total Y [mPt]	Y [mPt/h]
C2	250.8	131	11.78	24	166.5	41,748.9	0.275
HX-1	67.8	91	12.05	24	127.0	8,610.3	0.057
CC	15	638	20.00	24	682.1	10,231.2	0.067
T2	265.8	104	11.76	24	139.8	37,149.0	0.244
HX-2	12.05	12.05	12.05	24	127.0	347,966.3	2.288
ICE	18000	390	26.02	24	440.2	7,923,816.0	52.102
MX1	0	86.0	0	24	110.0	0	0
SR	1096	911	20.00	24	954.9	1,046,570.5	6.882
WGS	578	811	20.00	24	855.1	494,268.7	3.250
MCFC	4164	274	22.24	24	320.1	1,333,013.2	8.765
BR	1758	656	20.00	24	699.6	1,229,875.9	8.087
AGN	480	92	12.05	24	127.8	61,349.3	0.403
ACN	1140	91	12.05	24	127.3	145,157.3	0.954
AEV	2076	91	12.05	24	126.9	263,342.7	1.732
ABS	360	91	12.05	24	126.9	45,666.4	0.300
AP	100	186	16.87	24	227.0	22,697.0	0.149
AHX	660	91	12.05	24	127.0	83,816.7	0.551
Total							86.10

The component-related environmental impact rate, \dot{Y} , reached the maximum value of 52 mPt/h for ICE, while the values of \dot{Y} for SR, WGS, MCFC, and BR are about 6.9, 3.3, 8.8, and 8.1 mPt/h, respectively. The values of \dot{Y} are dependent on the environmental impact method. However, they can be negligible compared to the environmental impact flow rates of fuel and products [219,220].

The Sankey diagram for exergoenvironmental impact flow rate, \dot{B}_j is illustrated in Figure 5.35 and for fuel F1 (75% NG and 25% H₂). The scale of environmental impact flow is 5000 mPt/h per 1 mm. The pollution formation (\dot{B}^{PF}) and component-related environmental impact (\dot{Y}_k) are included in the figure in gray circle and green arrow, respectively. The fuel exergoenvironmental impact rates are 202,282 mPt/h entering the ICE, 99,022 mPt/h for MX1, and 81,259 mPt/h entering the CC. The exhaust gases for the entire system have an exergoenvironmental rate of 129,000 mPt/h.

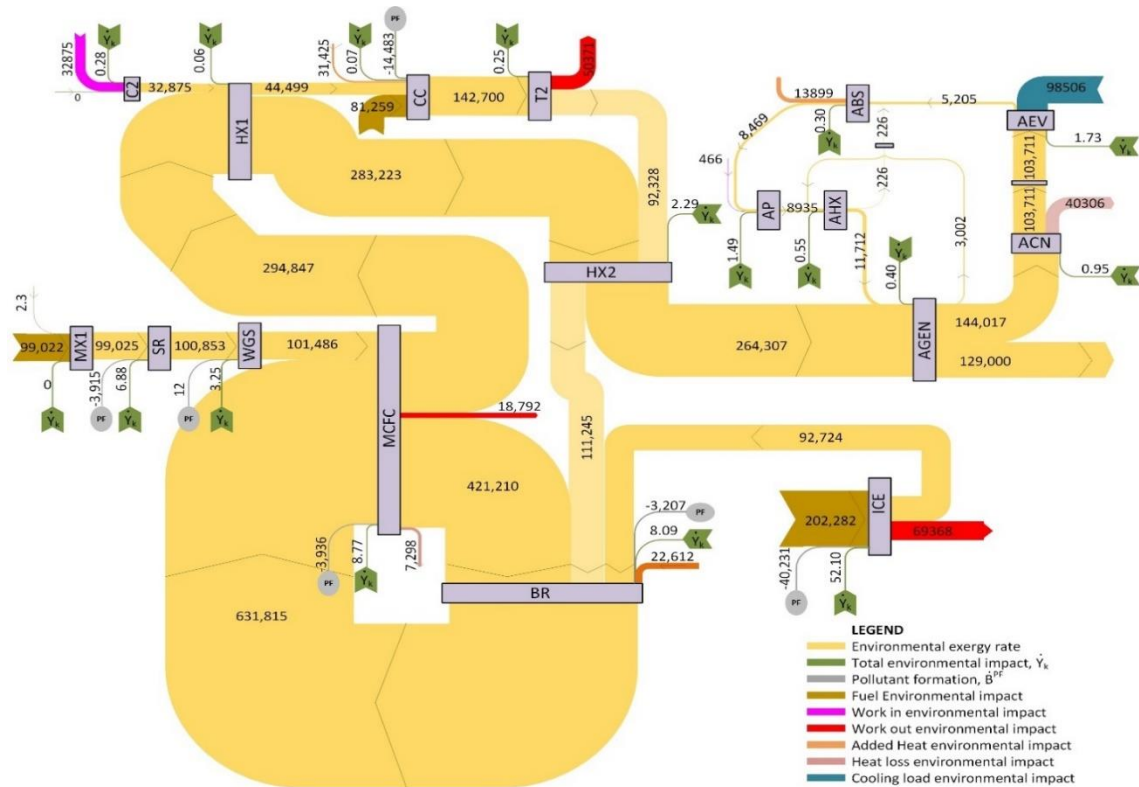


Figure 5.35 The Sankey diagram for exergoenvironmental impact flow rate for streams [mPt/h]

In addition, the exergoenvironmental analysis is listed in Table 5.29. The total component-related environmental impact is 86.10 mPt/h. the total fuel and product environmental impact flowrates are 5670758 and 5598191 mPt/h, respectively. That means

the hybrid combined system reduces the environmental impact. The destruction environmental impact flowrates, \dot{B}_D , is 641788 mPt/h. The total pollution factor, \dot{B}^{PF} , is -65760 mPt/h, which is due to emissions of CO₂, CO, NO_x, and CH₄ to the atmosphere. The specific exergy environment for fuel and product for the entire system are 568.6 and 926.5 mPt/MJ. Therefore, the exergoenvironmental factor, f_b , which is defined as the ratio of the component environmental impact, \dot{Y}_k to the total environmental impact associated with a component, \dot{B}_T .

Table 5.29 The exergoenvironmental analysis results of the components

#	\dot{B}_F [mPt/h]	\dot{B}_P [mPt/h]	\dot{B}_D [mPt/h]	\dot{B}^{PF} [mPt/h]	b_F [mPt/MJ]	b_P [mPt/MJ]	f_b [%]	r_b [%]
C2	32875	32875	3053	0	7.71	8.48	0.009	9.93
HX-1	11624	11624	650	0	7.92	8.38	0.009	5.75
CC	157183	142700	93869	-14483	6.14	13.29	0.000	116.47
T2	50371	50371	3640	0	7.17	7.71	0.007	7.56
HX-2	18916	18916	524	0	24.24	24.91	0.435	2.76
ICE	109558	69368	82923	-40231	3.22	7.71	0.122	139.71
MX1	99025	99025	678	0	5.54	5.57	0	0.67
SR	104762	100853	1363	-3915	5.57	5.43	0.270	2.50
WGS	101471	101486	176	13	5.43	5.44	1.694	0.18
MCFC	2.19E+6	2.18E+6	249124	-3936	23.33	26.10	0.004	11.86
BR	2.49E+6	2.49E+6	66999	-3207	22.70	23.28	0.013	2.56
AGN	147019	147019	70785	0	22.52	42.34	0.0006	88.00
ACN	40306	40306	16391	0	54.53	90.18	0.006	65.39
AEV	98506	98506	38258	0	343.81	552.40	0.005	60.67
ABS	13899	13899	11334	0	17.45	84.22	0.003	382.71
AP	466	466.1	115	0	7.71	10.16	0.129	31.68
AHX	2777	2777	1904	0	3.61	10.84	0.029	200.08
Total	5670758	5598191	641788	-65760	58.14	69.42	0.015	19.41

As shown in Table 5.29, the value of f_b is very small, from 0.003% for the absorber to 1.7% for the water-gas shift. The total f_b for the entire locomotive engine is 0.015% which technically shows a negligible impact of the component-related environmental impact, \dot{Y}_k , compared to the destruction, \dot{B}_D , and pollution formation, \dot{B}^{PF} , of the system components. The relative difference of the specific environmental impact r_b is 63%.

A comparison of the hybrid locomotive engine is considered with respect to different fuels, as displayed in Figure 5.36. The total fuel and product exergoenvironmental

flow rates are the highest when using fuel F4 (9.15×10^6 and 9.11×10^6 mPt/h, respectively), while the lowest fuel and product exergoenvironmental flow rates are 5.39×10^6 and 5.36×10^6 mPt/h, respectively). The destruction and total environmental impact associated with the entire components have similar values ranging from 0.6×10^6 for F1 to 1.7×10^6 mPt/h for F2, respectively.

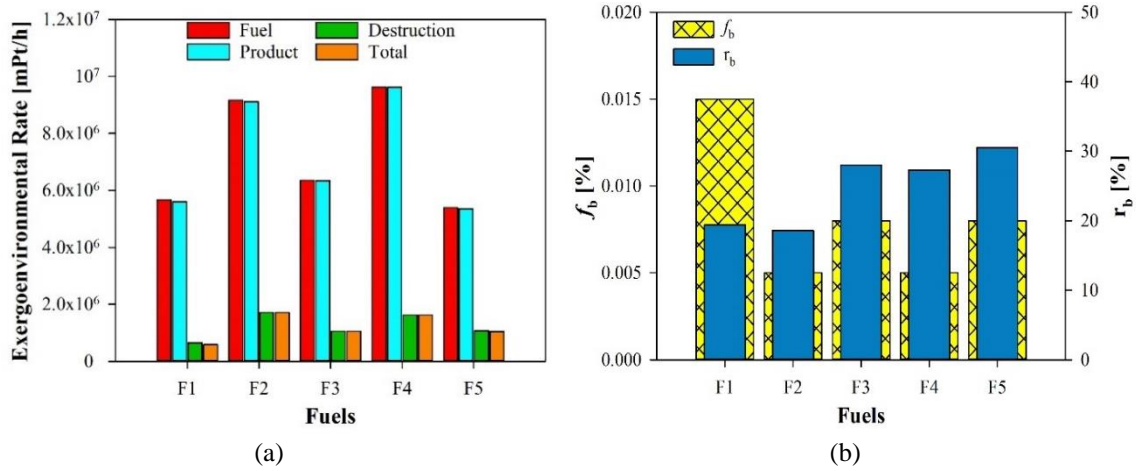


Figure 5.36 (a) The total exergoenvironmental impact rate of fuel \dot{B}_F , product \dot{B}_P , destruction \dot{B}_D , and total related to components \dot{B}_T , and (b) the total exergoenvironmental factor f_b and the relative environmental impact difference r_b

Figure 5.36-b graphs the total values of f_b and r_b and shows the maximum value of f_b is 0.015% for F1 and the minimum value is 0.005% for F2 and F3, while the minimum and maximum values of r_b are 18.6% for F2 and 30.5% for F5. That is because the total specific environmental impact of fuel $b_{F,t}$ is 58.1, 85.3, 82.8, 126.4, and 75.9 mPt/MJ for F1 to F5, respectively, while the total specific environmental impact of product $b_{P,t}$ is 69.4, 101.2, 105.9, 160.9, and 99.0 mPt/MJ for F1 to F5, respectively.

Lowering exergoenvironmental rates for destruction and pollution formation increases the exergoenvironmental impact factor. Therefore, using a mixture of methane and hydrogen has less environmental impact compared to other fuels by 40%. However, all the fuels have a low environmental impact factor of less than 0.015%, which means all the exergoenvironmental rates of pollution formation and destructions are substantially larger than that related to components. This relationship also reflects on the relative exergoenvironmental impact difference since increasing it means increasing the difference between the exergoenvironmental impact of product and fuel due to increasing

environmental impact of destruction and losses. The lower this value, is better and has less impact on the environment.

5.4 Results of System R-2

This section presents the results and discussion of the thermodynamic analysis, exergy analysis, exergoeconomic analysis, and exergoenvironmental analysis of the hybrid SOFC-GT locomotive engine combined with on-board hydrogen production as written in the subsections below.

5.4.1 Results of Thermodynamic Analysis

Thermodynamic data results are reported in [179]. Table 5.30 displays the performance of the system components by evaluating the amount of required and rejected heat, the amount of required and generated power, exergy destruction rate, and energetic and electric efficiency and exergetic efficiency. As shown in this table, the rejected heat varies from 8 kW to 160 kW for SR and WGS reactors to 290 to 1020 kW for fuel cells. Also, the required heat records a similar amount of 7600 kW for combustion in CC and BR. Likewise, the required power was estimated to be <20 kW for AP and C2, and 450 kW for AEC, and 7900 kW for C, while the generated power was obtained to be about 11300 kW for T1, 300 W for T2, 225, 2740, and 960 kW for PEMFC, SOFC, and TG, respectively. The fuel cells have electric efficiency of more than 75%, and energetic efficiency ranging from 30 to 75%. The minimum energetic efficiency was calculated for SOFC to be 33%, while the minimum exergetic efficiency was estimated to be 2% for the AEV.

The performance of the subsystems and overall systems are illustrated in Table 5.31. The performance of GT engine only using F1 is 22.3% energetic efficiency and 32% exergetic efficiency. If this GT engine is operated using diesel oil, the diesel GT can accomplish an overall efficiency of 33.5% and a net power of 3639 kW and combustion heat of 10870 kW, which is higher than the GT only using F1. The SOFC system can attain 34 % and 43% of energetic and exergetic efficiencies, respectively. The energy recovery system consisting of TG and ARS can produce about 940 kW net work and 615 kW of cooling load by converting the net exhaust heat of 5620 kW into electricity and cooling load with 28% efficiency. The hydrogen production can fulfill about 40% overall efficiency by generating electricity of 225.3 kW using PEMFC and producing hydrogen of 367.8 kW

(0.003 kg/s H₂). Therefore, the resultant performance is increased to about 48% energetic efficiency and 51% exergetic efficiency. The total electricity generated by using all these systems is 6844.3 kW without hydrogen flow rate. If we consider only the electric generation, then the overall performance will be 46% energetic efficiency and 48% exergetic efficiency.

Table 5.30 The results of the performance of components in the hybrid engine

Comp. #	\dot{Q} [kW]	\dot{W} [kW]	$\dot{E}x_D$ [kW]	η_{th} [%]	η_e [%]	ψ [%]
C1	0.0	7905.4	1369.4	72.0	0	82.7
T1	0.0	11288.4	2035.9	72.0	0	84.7
C2	0.0	3.6	0.8	72.0	0	78.2
T2	0.0	0.3	0.1	72.0	0	74.0
AEC	1019.7	446.9	1133.5	49.8	79.5	35.7
PEMFC	292.4	225.3	13.2	77.1	77.7	76.6
SOFC	8111.5	2739.7	3600.0	33.8	86.9	43.2
CC	7564.7	0.0	19344.2	49.4	0.0	58.4
BR	7576.7	0.0	10758.1	49.4	0.0	26.1
SR	158.2	0.0	14.6	55.5	0.0	97.9
WGS	8.2	0.0	5.6	95.8	0.0	99.3
TG	1921.1	960.6	303.5	50.0	0.0	76.0
ACN	1215.0	0.0	83.5	100.0	0.0	88.9
AEV	615.1	0.0	132.8	100.0	0.0	2.0
AHX	1462.5	0.0	146.4	100.0	0.0	69.0
AGN	3346.0	0.0	157.4	100.0	0.0	81.3
ABS	2763.0	0.0	170.0	100.0	0.0	21.7
AP	0.0	17.3	4.1	70.0	0.0	76.0

Table 5.31 The performance of the major systems/components

Major Systems	\dot{W}_{net} [kW]	\dot{Q}_{add} [kW]	$\dot{Q}_{cooling}$ [kW]	η_{th} [%]	ψ [%]
<i>GT Engine</i>					
GT	3383.0	15141.5	0	22.3	32.0
<i>SOFC System</i>					
SOFC	2739.7	0	0	33.8	43.2
SR	0	158.2	0	90.0	97.9
WGS	0	8.2	0	90.0	99.3
<i>Energy Recovery</i>					
TG	960.6	0	0	77.1	76.6
ARS	17.3	0	615.1	18.3*	9.5**
<i>Hydrogen Production</i>					
PEMFC	225.3	0	0	77.7	94.7
AEC	446.9 + 367.8 (H ₂)	1019.7	0	30.4	35.7
Resultant Performance	7211.8	16327.6	615.1	47.94	50.98

*COP_{en}

** COP_{ex}

Several parameters were selected to be examined to understand the behavior of the designed system, starting with the effect of different fuel blends, splitting ratio of SP1,

mass flowrates of AEC, current density of fuel cells, and finally constant active area and current density of fuel cells. Five fuel blends are considered in this paper, which is named as F1 to F5, as well as diesel fuel. Table 5.32 displays the mass flowrates of intake air to the GT, intake fuels in streams F1 and F2, and steam in stream W1. These number are considered in that way to fulfill a net power of the GT engine to be greater than or equal to 3355 kW, which is the power of the EMD 16-710G3 [178] that is capable of operating a train. As shown in this table, all the sustainable fuel blends have higher HHV and LHV compared to diesel fuel, reflecting on lower mass flowrates of these fuels than the diesel fuels.

Table 5.32 The fuel and air mass flowrates with respect to fuels.

Parameters	Diesel	F1	F2	F3	F4	F5
\dot{m}_{B1} [kg/s]	15.00	14.00	13.00	13.00	13.00	13.00
\dot{m}_{F1} [kg/s]	1.00	0.58	0.85	0.60	0.56	0.56
\dot{m}_{F2} [kg/s]	0	0.01	0.01	0.01	0.01	0.01
\dot{m}_{W1} [kg/s]	0	0.02	0.01	0.01	0.01	0.01
HHV [MJ/kg]	45.6	77.10	52.50	74.58	75.76	77.70
LHV [MJ/kg]	43.3	67.25	43.33	64.92	64.92	66.15

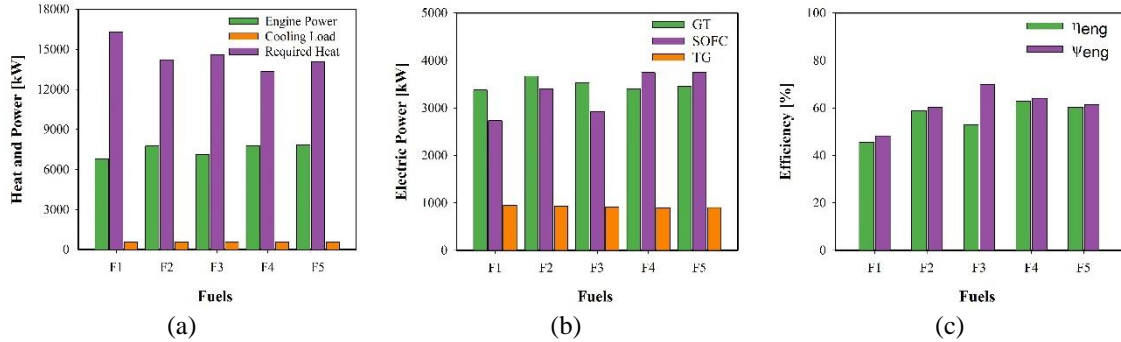


Figure 5.37 The performance of hybrid engine: (a) heat and power, (b) electric power of major components, and (c) overall energetic and exergetic efficiency of the hybrid engine.

In the comparison of fuel blends, Figure 5.37 presents the effect of these fuels on engine performance. By looking at Figure 5.37-a, the highest heat is needed for F1 at 16.3 MW, followed by F3 (14.6 MW), F2 (14.2 MW), F5 (14.1 MW), and the minimum heat is for F4 (13.4 MW). This trend is different in overall engine power, where the highest power is gained by F5 (7.9 MW) and the lowest power is obtained by F1 (6.8 MW). The cooling load is maintained to be constant at 915 kW. Figure 5.37-b illustrates the values of generated power using three subsystems of GT, SOFC, and TG. The TG provides an

average electricity of 925 kW, while the power generated by others change to an average of 3500 kW, while the SOFC generates lower than this value in F1 to F3, with an average of 3020 kW, and higher than 3500 kW using F4 and F5 with an average of 3750 kW. The reason for this variation is the amount of hydrogen produced in the reactors and combustors to be utilized in the SOFC unit. This behavior accomplishes higher efficiencies using F4 and F5 to be above 60%, while the minimum efficiencies are obtained by F1 (below 50%), as shown in Figure 5.37-c.

The equivalence ratio of the fuels considered in this study is about 0.95, which means the stoichiometric air-fuel ratio is less than the actual air-fuel ratio. The excess air is used for the SOFC system and afterburner BR. The combustion heat of F1 is higher than others that is because it is proportional to the ignition temperature of methane (537°C), higher than that of methanol (470°C), ethanol (365°C), and dimethyl ether (350°C). The minimum ignition energy of methane and hydrogen decreases by 30% by increasing the amount of hydrogen blend by 25% [221,222], and it is higher than that of others [223]. The produced work and added heat by fuel is minimum for F1 because the power varies inversely to the specific heat ratio (γ) of fuels, and the γ_{CH_4} is 1.32 and is the highest value [224].

The power required for the compressors is constant for all fuel types because they have same operating conditions and same mass flow rate of air. However, the generated power of turbines varies according to the fuel type. The highest turbine power is by using F1 (11.3 MW) compared to other fuels as 11 MW for F2, 10.9 MW for F3, 10.8 MW for F4, and 10.8 MW for F5. Nevertheless, the fuel F1 produces the lowest SOFC power due to the chemical properties of methane and combustion characteristics of methane. Therefore, the high combustion heat and low resultant power of methane-hydrogen blend decrease the overall energetic efficiency of the entire engine by using F1.

A detailed discussion about the systems is presented focusing on different heating loads, reactor loads, generated and produced power to comprehend the system behavior with respect to fuels blends. As shown in Figure 5.38-a, the heating loads of CC and BR are bar-graphed with an average of 7.2 MW for CC and 6.3 MW for BR; the maximum and minimum values are obtained by F3 and F4 for CC and F1 and F4 for BR, respectively. The cooling load has maintained its value of 915 kW. Additionally, the reforming reactors

(SR) have higher heating loads above 40 kW with a maximum value of 158 kW for F1 and a minimum value of 40 kW for F4, while WGS reactors produce heat with an average of 10 kW, as shown in Figure 5.38-b.

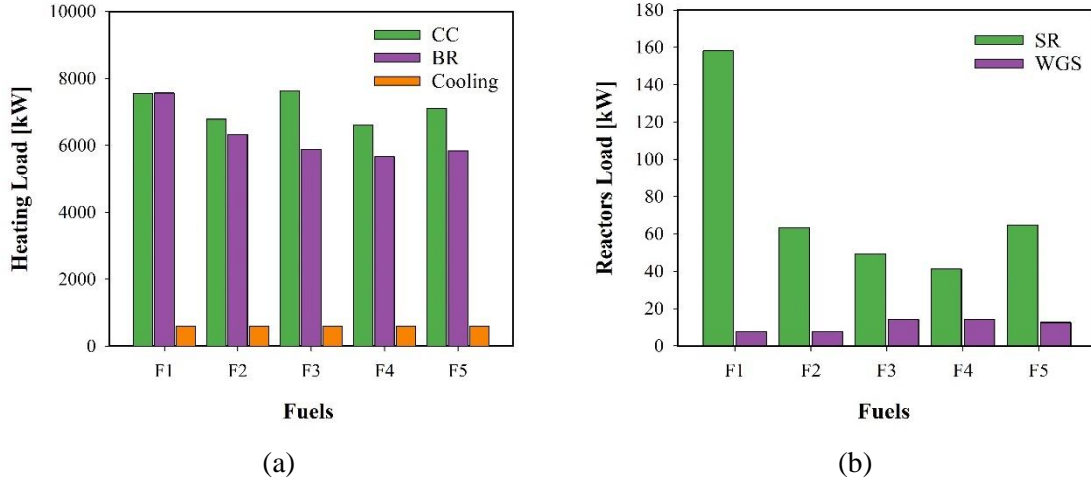


Figure 5.38 (a) The heating load of the combustion chamber (CC), afterburner (BR) and cooling load and (b) the duty of SR and WGS reactors with respect to fuel blends

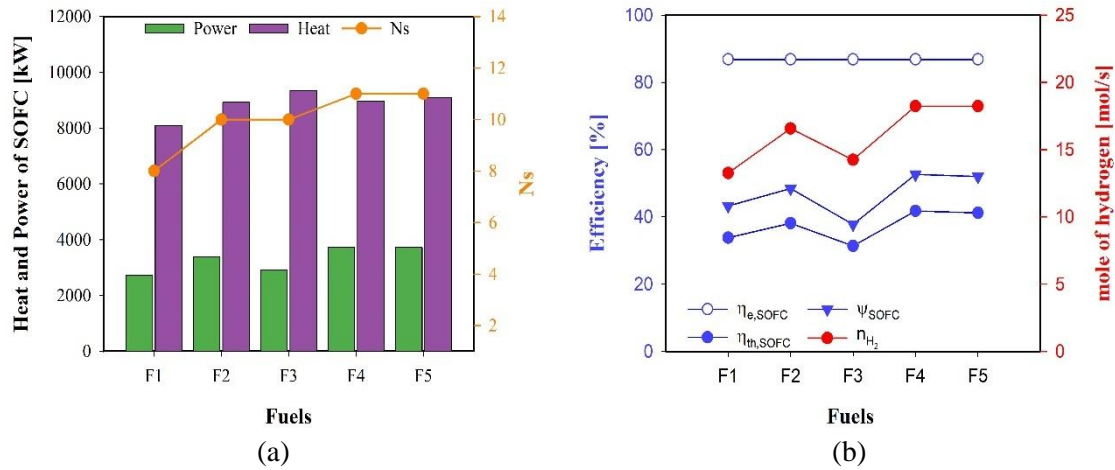


Figure 5.39 The performance of SOFC: (a) heat and power and a number of stacks and energetic and (b) exergetic efficiencies and amount of required hydrogen.

The performance of SOFC has been impacted using fuel blends as graphed in Figure 5.39. The generated power from SOFC is estimated to be with an average of 3000 kW, but their exhaust heat is higher than 8000 kW. The design of SOFC can be executed using two methods: the inner specifications and the moles of required hydrogen, which affect the SOFC size or number of stacks. As shown in Figure 5.39-a, the number of stacks is 11 units for F4 and F5, and dropped to 10 stacks, and again to 8 for F1. Therefore, the moles of required hydrogen in SOFC can be the minimum value of 13 mol/s for F1

followed by F3, and the maximum of 18 mol/s for F4 and F5, as presented in Figure 5.39-b. The electric efficiency is held constant about 87%, while the energetic and exergetic efficiency have the same trend with the highest performance using F4 and lowest performance using F3.

The environmental impact can be compared between this hybrid locomotive engine and traditional GT using diesel fuel as presented in Table 5.33. The mass flow rate of diesel at the B4 is 0.2 kg/s due to 80% of fuel utilization. The net power of GT using diesel is 3639 kW, and the added heat of CC is 10870 kW yielding the energetic efficiency to be 33.48%. Therefore, the CO₂ emission from traditional GT can be 2.51 kg/s and can be increased to 2.82 kg/s if fuel combustion reaches 100%. The proposed hybrid engine can reduce emissions by about 50% using F1, 65% using F2, and more than 70% using F3 to F5.

Table 5.33 The CO₂ emissions using diesel and sustainable fuels.

Emissions	Diesel	F1	F2	F3	F4	F5
CO ₂ [kg/s]	2.510*	1.214	0.886	0.699	0.653	0.679
Reduction [%]	0	51.6	64.7	72.1	74.0	73.0

5.4.2 Results of Exergy Analysis

Exergy, exergoeconomic and exergoenvironmental results of states points are reported in [225]. The exergy analysis is based on fuel and product elements, as shown in Table 5.34, including the power, heat, exergy fuel rates, exergy product rates, exergy destruction rates, and exergy loss rates. These values are important to estimate the irreversibility ratio y^* , exergy destruction ratio y , and exergetic efficiency for each component, as presented in the table. The net power of this rail engine is 4948.6 kW, while the required heat is 12769.8 kW, and the cooling load this is provided by the evaporator is 1927.1 kW, resulting in 53.8% energy efficiency and 50.5% exergy efficiency. However, the exergetic efficiency based on the fuel and product principle is 63.8% because the total fuel and product exergy rates are about 138 M and 88 MW using F1. The difference between these exergy rates is about 50 MW to represent the exergy destruction rate, but the total exergy loss rate is about 0.5 MW due to the power loss of two fuel cells. The exergy destruction ratio between the exergy destruction rate and the fuel exergy rate is 36.2%. The highest exergetic performance is from splitters, mixers, turbines, compressors, and reactors of the SR and

WGS. While the lowest exergetic performance is from the CC, SOFC, AEC, and TG due to the chemical reactions and high temperature differences. In addition, the highest irreversibility ratio can be found in the CC, SOFC, BR, and AEC, which are above 7%.

Table 5.34 The exergy analysis of rail engine components

#	\dot{W}_K	\dot{Q}_K	$\dot{E}x_{F,K}$	$\dot{E}x_{P,K}$	$\dot{E}x_{D,K}$	$\dot{E}x_{L,K}$	ϵ	y	y^*
Units	[kW]	[kW]	[kW]	[kW]	[kW]	[kW]	[%]	[%]	[%]
C1	7341	0	7341	6069	1272	0	82.67	0.92	2.55
CC	0	9908	45934	23431	22503	0	51.01	16.36	45.17
T1	10165	0	12000	10165	1834	0	84.71	1.33	3.68
SP1	0	0	11431	11431	0	0	100.00	0.00	0.00
MX1	0	0	9653	9612	41.3	0	99.58	0.03	0.08
MX2	0	0	4143	4100	41.3	0	98.96	0.03	0.08
SR	0	890.5	4429	4100	329.6	0	92.57	0.24	0.66
WGS	0	41.5	4553	4525	27.23	0	99.39	0.02	0.05
SOFC	3625	3727	14216	3625	10591	475.1	25.50	7.70	21.26
BR	0	3794	11953	6224	5729	0	52.07	4.16	11.50
TG	74.1	1852	1324	74.1	1250	0	5.60	0.91	2.51
AGN	0	3380	2560	1263	1297	0	49.34	0.94	2.60
ACN	0	2394	331.3	216.8	114.5	0	65.44	0.08	0.23
AHX1	0	400.5	8.1	5.9	2.2	0	72.84	0.00	0.00
AEX1	0	0	424.7	389.4	35.3	0	91.69	0.03	0.07
AEV	0	1927	442.3	35.3	407	0	7.98	0.30	0.82
ABS	0	2937	434.7	267	167.7	0	61.42	0.12	0.34
AP	23.1	0	23.1	16.4	6.7	0	71.00	0.00	0.01
AHX2	0	1013	152.5	93.7	58.8	0	61.44	0.04	0.12
AEX2	0	0	345.9	45.3	300.6	0	13.10	0.22	0.60
AEC	1777	1020	4291	609.8	3681	0	14.21	2.68	7.39
EX1	0	0	618.9	608.7	10.23	0	98.35	0.01	0.02
FP	0	0	608.7	608.7	0	0	100.00	0.00	0.00
PEMFC	225.3	292.4	346.6	225.3	121.3	24.5	65.00	0.09	0.24
T2	0.3	0	0.5	0.3	0.2	0	60.00	0.00	0.00
C2	3.6	0	3.6	2.8	0.8	0	77.78	0.00	0.00
HX1	0	1	1.6	0.3	1.3	0	18.75	0.00	0.00
Total	4948.6		137570.5	87744.8	49823.1	499.6	63.8	36.2	100.0

Applying five fuel blends in the proposed system presents a slightly different exergy analysis, as shown in Figure 5.40. The average fuel exergy and product exergy rates are 141 MW and 89 MW, respectively. The average exergy destruction rate is 52 MW with a minimum of 50 MW using F1 and a maximum of 54 MW using F2, and the average exergy loss rate is 0.4 MW with a maximum value of 0.5 MW using F1, as shown in Figure 5.40-a. These exergy values result in an average of 62.7% exergetic efficiency and 37.3% exergy destruction ratio. The highest exergetic performance occurred using F1 and F5 to reach maximum exergetic efficiency of 63% and minimum destruction ratio of 36%, as shown in Figure 5.40-b.

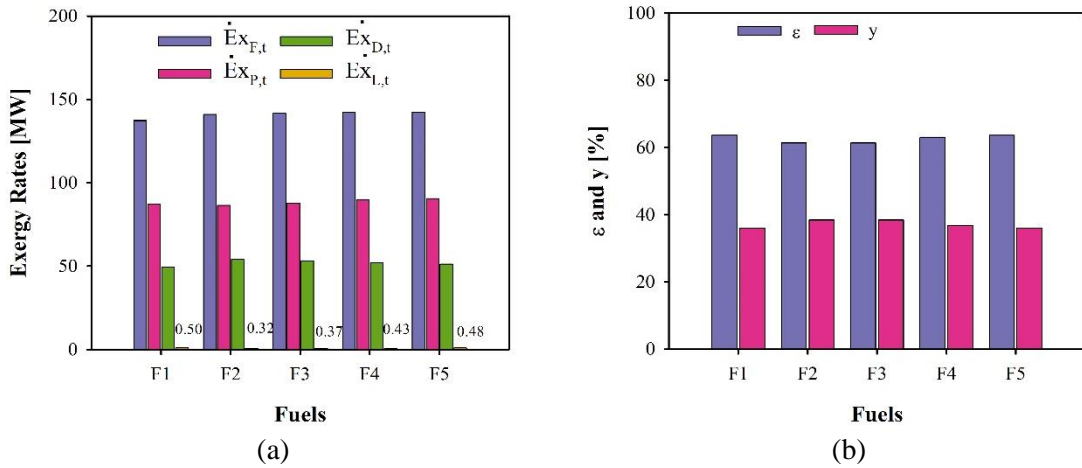


Figure 5.40 The exergy analysis based on fuel blends: (a) Fuel, product, destruction, and losses exergetic rates, and (b) exergetic efficiency and exergy destruction ratio

5.4.3 Results of Exergoeconomic Analysis

The exergoeconomic analysis is conducted on this rail engine using the current prices of fuels as presented in Table 4.31 in 2022, which increases due to inflation, fuel demand, and wars. The components' costs are estimated using the cost equations in the appendix, which are evaluated according to their given year as C_K . The cost of each component is normalized according to this year, 2022. Therefore, the total cost of this new engine is \$10,189,168.47, as presented in Table 5.35. A primary cost assessment is performed to estimate the net present value (NPV), the interest rate of return (IRR), profitability index (PI), return of investment (ROI), discounted payback (DPB), and levelized cost of electricity (LCOE). The LCOE can be defined as the ratio of the total levelized cost rate to the net electrical power of the engine. This assessment includes the direct cost, indirect cost, yearly cash inflow and yearly cash outflow, as presented in Table 5.36. The initial investment is about \$11.3M, while the total cash outflow and inflow are about \$9.4M and \$12.0M, respectively. The NPV is calculated as about \$54M with IRR of 23%, ROI of 56.45, and DPB of 3.36 years. The profitability index is 5.8, and the LCOE is 29.8 \$/MWh., as in Table 5.37.

The exergoeconomic analysis is performed using Engineering Equation Solver (EES) software on the locomotive engine, and its results are listed for each component in Table 5.38. The total fuel and product of exergy cost rates are 6597 \$/h and 6884 \$/h, respectively, while the destruction and loss exergy cost rates are 1834 \$/h and 31\$/h,

respectively. The specific fuel and product exergy cost of this engine using F1 is 13.3 \$/GJ and 21.8 \$/GJ, respectively. The overall specific cost difference, r , is 63.6% meaning that the product cost is 1.6 times the fuel cost, while the exergoeconomic factor, f , is obtained as 7.4% resulting in the exergoeconomic destruction rates being a great amount compared to the components' cost rates.

Table 5.35 The components' costs of R-2 rail engine.

#	C_K [\$]	Year	Z_K [\$] (2022)	\dot{Z}_K [\$/h]
C1	151410	2003	313026	4.529
CC	126114	2003	260730	3.773
T1	1149000	2003	2375000	34.37
SP1	0	---	0	0
MX1	0	---	0	0
MX2	0	---	0	0
SR	57917	2001	121247	1.754
WGS	67470	2001	141246	2.044
SOFC	844389	2003	1746000	25.26
BR	88342	2003	182639	2.643
TG	74100	2003	153195	2.217
AGN	3000	2001	6280	0.0909
ACN	18733	2001	39216	0.5675
AHX1	12894	2001	26994	0.3906
AEX1	382	2001	798.6	0.0116
AEV	164182	2001	343707	4.973
ABS	3164	2001	6623	0.0958
AP	5601	2001	11726	0.1697
AHX2	13882	2001	29060	0.4205
AEX2	191	2001	399.9	0.0058
AEC	2312000	2010	3488000	50.47
EX1	0.57	2001	1.199	0.00002
FP	0	---	0	0
PEMFC	625298	2010	943168	13.65
T2	5.02	2003	7.575	0.00011
C2	21.56	2003	32.52	0.00047
HX1	47.52	2003	71.68	0.00104
Total	5718143.17		10189168.47	147.44

Table 5.36 The primary economic assessment of the rail engine

Parameters	Factor	Values
<i>Direct cost</i>		
Capital cost of components		\$ 10,189,168.47
<i>Indirect cost</i>		
Fixed O &M	6%	\$ 611,350.11
Overheads (contingency)	5%	\$ 509,458.42
<i>Initial cost of investment</i>		\$ 11,309,977.01
<i>Yearly cash outflow</i>		
Variable O&M	\$5/MWh	\$ 180,623.30
Production cost	\$0.003/kWh	\$ 108,373.98
<i>Fuel cost</i>		
F1 (F1 fuel) stream	864.218 \$/h	\$ 6,308,791.40
F2 (F1 fuel) stream	111.618 \$/h	\$ 814,811.40
W1 (water) stream	1.10664 \$/h	\$ 8,078.47
N1 (KOH solution) stream	160.59 \$/h	\$ 1,172,307.00
N2 (NH ₃ solution) stream	104.94 \$/h	\$ 766,062.00
<i>Total cash outflow</i>		\$ 9,359,047.55
<i>Yearly cash inflow cost</i>		
<i>Electricity</i>		
T1	767.33 \$/h	\$ 5,601,538.20
T2	166.95 \$/h	\$ 1,218,735.00
SOFC	112.78 \$/h	\$ 823,323.20
PEMFC	205.85 \$/h	\$ 1,502,719.60
TG	7.81 \$/h	\$ 57,013.58
<i>Cooling</i>		
AEV	4.46 \$/h	\$ 32,546.03
<i>Products</i>		
H ₂	375.88 \$/h	\$ 2,743,894.80
N ₂	0.36 \$/h	\$ 2,660.32
<i>Total cash inflow</i>		\$ 11,982,430.74

Table 5.37 Economic results of the rail engine

Parameters	Values
Interest rate	12%
Inflation rate	3%
CRF	0.0997
Discount rate	10%
Engine lifetime	25 years
Operation hours per year	7300 h/year
Net Present Value (NPV)	\$ 54,274,602.59
Interest rate of return (IRR)	23%
Discounted payback (DPB)	3.36 year
Profitability index (PI)	5.80
Return of investment (ROI)	56.4%
LCOE	29.8 \$/MWh

Table 5.38 The exergoeconomic analysis of rail engine components

#	\dot{C}_K^W [\$/h]	\dot{C}_K^Q [\$/h]	$\dot{C}_{F,K}$ [\$/h]	$\dot{C}_{P,K}$ [\$/h]	$\dot{C}_{D,K}$ [\$/h]	$\dot{C}_{L,K}$ [\$/h]	$c_{F,K}$ [\$/GJ]	$c_{P,K}$ [\$/GJ]	f [%]	r [%]
C1	522.7	0	522.7	527.3	90.6	0.0	19.8	24.1	4.76	21.99
CC	0	0	1343.0	1346.0	657.7	0.0	8.1	16.0	0.57	96.58
T1	723.9	0	689.5	723.9	105.4	0.0	16.0	19.8	24.60	23.93
SP1	0	0	656.9	656.9	0.0	0.0	16.0	16.0	0	0.00
MX1	0	0	681.8	681.8	2.9	0.0	19.6	19.7	0	0.41
MX2	0	0	106.3	106.3	1.1	0.0	7.1	7.2	0	1.07
SR	0	0	106.3	108.1	7.9	0.0	6.7	7.3	18.14	9.82
WGS	0	0	108.1	110.1	0.6	0.0	6.6	6.8	75.97	2.50
SOFC	106.4	0	134.8	106.4	100.4	13.9	2.6	8.2	20.10	209.49
BR	0	0	482.1	484.8	231.0	0.0	11.2	21.6	1.13	93.21
TG	96.16	0	93.9	96.2	88.6	0.0	19.7	360.5	2.44	1729.95
AGN	0	0	167.2	160.6	84.7	0.0	18.2	35.3	0.11	94.66
ACN	0	67.66	67.1	67.7	23.2	0.0	56.3	86.7	2.39	54.12
AHX1	0	0	1.6	16.8	0.0	0.0	0.1	0.8	99.89	1307.57
AEX1	0	0	86.0	86.0	7.1	0.0	56.3	61.4	0.16	9.07
AEV	0	6.697	6.7	1.7	6.2	0.0	4.2	13.6	44.66	222.40
ABS	0	72.29	94.7	76.3	36.5	0.0	60.5	79.4	0.26	31.10
AP	1.645	0	1.6	1.8	0.5	0.0	19.8	30.7	26.24	55.41
AHX2	0	0	3.8	2.4	1.5	0.0	7.0	7.2	22.11	2.69
AEX2	0	0	8.7	8.7	7.6	0.0	7.0	53.5	0.08	664.04
AEC	126.6	0	377.1	643.1	323.5	0.0	24.4	292.9	13.50	1099.92
EX1	0	0	354.6	354.6	5.9	0.0	159.2	161.8	0	1.63
FP	0	0	354.6	354.6	0.0	0.0	161.8	161.8	0	0.00
PEMFC	157.5	0	143.9	157.5	50.3	17.1	115.3	194.2	21.33	68.43
T2	0.2866	0	0.3	0.3	0.1	0.0	159.2	265.4	0.10	66.71
C2	3.439	0	3.4	3.4	0.8	0.0	265.4	341.3	0.06	28.60
HX1	0	0	0.2	0.2	0.2	0.0	33.8	181.2	0.65	436.09
Total			6597.1	6883.6	1834.3	31.1	13.3	21.8	7.4	63.6

The total fuel and product exergoeconomic rates for F1 are 6597 and 6884 \$/h, for F2 are 23310 and 23584 \$/h, for F3 are 21034 and 21299 \$/h, for F4 are 24625 and 24856 \$/h, and for F5 are 18471 and 18714 \$/h, respectively, as shown in Figure 5.41. The exergy destruction cost rates are 1834 \$/h, 6503 \$/h, 5841 \$/h, 6783 \$/h, and 5055 \$/h for F1 to F5 in this order, respectively. The exergy loss cost rates have an average of 55\$/h. As presented in the figure, using F4 produces the highest cost rates, and using F1 produces the lowest cost rates because of the high price of cost fuel of F4 (around 30 \$/GJ) and the low price of methane (around 7\$/GJ).

The exergoeconomic performance is illustrated in Figure 5.42 by evaluating the specific exergy cost, relative cost difference, and exergoeconomic factor. The specific fuel and product exergy costs are an average of 37 \$/GJ and 60 \$/GJ, respectively, and the minimum values are 13.3 \$/GJ and 21.8 \$/GJ using F1, and the maximum values are 48

and 76.7 \$/GJ using F4, respectively, as shown in Figure 5.42-a. This results in the relative cost difference, r , to have an average of 62% because c_P is greater than c_F by a factor of 1.6. However, the lowest r value occurs using F5 to 58.9 %, as shown in Figure 5.42-b. The exergoeconomic factor, f , is its maximum value of 7.4% using F1 because its lowest destruction exergy cost rate, and its minimum value of 2.1% using F4 due to its largest destruction exergy cost rate.

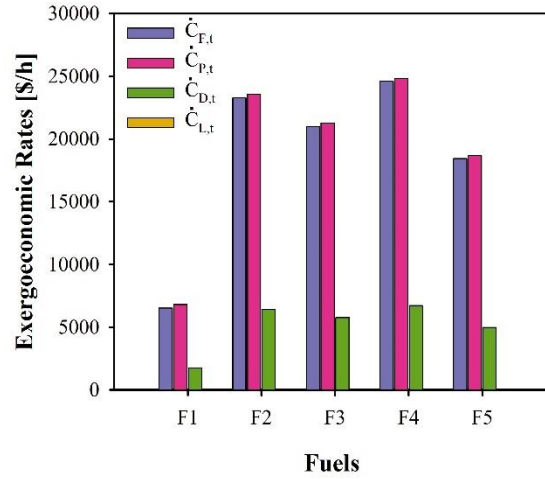


Figure 5.41 Exergoeconomic rates with respect to fuel blends

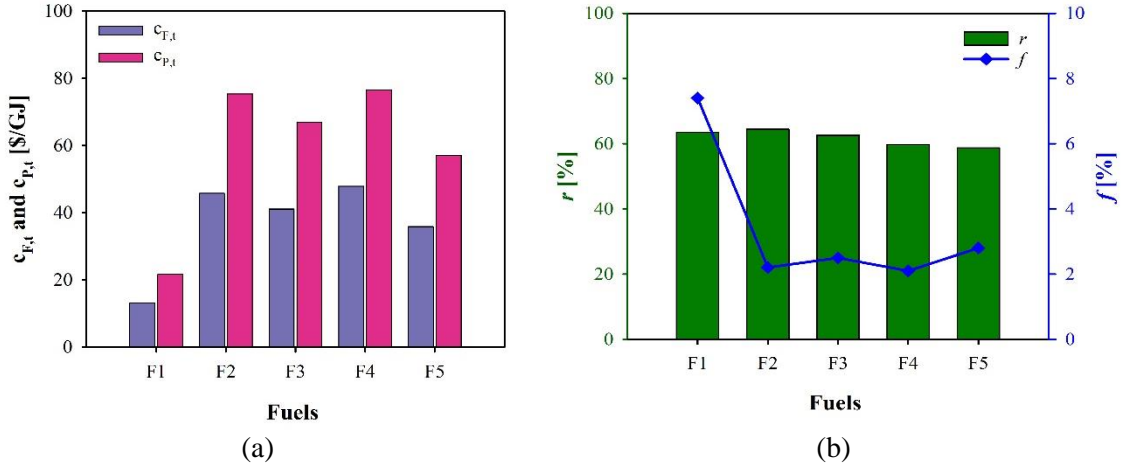


Figure 5.42 The exergoeconomic performance of the hybridized engine: (a) specific fuel and product exergy cost, and (b) relative cost difference and exergoeconomic factor

5.4.4 Results of Exergoenvironmental Analysis

The third analysis in this paper is the exergoenvironmental analysis, which is performed using EES software. Exergoenvironmental analysis of components includes the exergoenvironmental rates of power, heat, fuel, product, destruction, losses, pollution formation, and total environmental impact rates of components, as shown in Table 5.39.

The corresponding component-related environmental rates, \dot{Y}_K , 14.06 mPt/h and the total weight of the engine is 9,256 kg. Also, this table involves specific fuel and product exergoenvironmental impact, relative exergoenvironmental difference, r_b , and exergoenvironmental factors, f_b . This analysis is performed using fuel F1 (75% methane and 25% hydrogen), which has a specific environmental impact of 5.44 mPt/MJ. The component-related environmental impact rates greater than 1 mPt/h are for SR, WGS, SOFC, BR, AEV, and AEC. The power exergoenvironmental rates are high with an order of magnitude of 5 for compressor C1 and turbine T1, and for AEC, SOFC, TG, and PEMFC with an order of magnitude 4.

Table 5.39 The exergoenvironmental analysis of rail engine components

#	\dot{Y}_K	\dot{B}_K^W	\dot{B}_K^Q	$\dot{B}_{F,K}$	$\dot{B}_{P,K}$	$\dot{B}_{D,K}$	$\dot{B}_{L,K}$	\dot{B}_K^{PF}	\dot{B}_K^T
Units	[mPt/h]	[mPt/h]	[mPt/h]	[mPt/h]	[mPt/h]	[mPt/h]	[mPt/h]	[mPt/h]	[mPt/h]
C1	0.876	291651	0	291651	291652	50554	0		50555
CC	0.897	0	0	911985	788610	448710	0	-123375	325336
T1	0.735	403866	0	243369	403866	37198	0	0	37199
SP1	0	0	0	545241	384745	0	0	0	0
MX1	0	0	0	379231	379231	1622	0	0	1622
MX2	0	0	0	80113	80113	799	0	0	799
SR	1.256	0	0	80113	65578	5961	0	-14536	-8573
WGS	1.125	0	0	65578	65626	392	0	47	441
SOFC	1.052	60440	0	68362	60442	27712	7921	0	27713
BR	1.380	0	0	270849	263808	129810	0	-1604	128207
TG	0.032	52249	0	52249	52249	49320	0	0	49320
AGN	0.403	0	0	95376	93600	48326	0	0	48327
ACN	0.954	0	38455	38455	38455	13289	0	0	13290
AHX1	0.551	0	0	940.2	940.7	255	0	0	256
AEX1	0	0	0	49296	49296	4097	0	0	4097
AEV	1.732	0	986	985.7	988.00	907	0	0	909
ABS	0.300	0	49898	53936	53889	20810	0	0	20811
AP	0.149	917.8	0	917.8	917.9	266	0	0	266
AHX2	0.551	0	0	2046	2046	789	0	0	789
AEX2	0	0	0	4640	4640	4032	0	0	4032
AEC	1.523	70617	0	336441	162063	288620	0	0	288621
EX1	0	0	0	87345	87345	1444	0	0	1444
FP	0	0	0	87345	87345	0	0	0	0
PEMFC	0.406	32873	0	36448	32873	12755	3577	0	12756
T2	0.028	212	0	211.7	211.7	85	0	0	85
C2	0.055	2541	0	2541	2541	564	0	0	565
HX1	0.050	0	0	143.8	143.9	117	0	0	117
Total	14.055			3785809	3453215	1148436	11497	-139468	1008982

Three components produce heat as a product, which is ABS, AEV, and ABS and have heat exergoenvironmental rates of 49898 mPt/h, 986 mPt/h, and 38455 mPt/h, respectively. The total fuel and product exergoenvironmental rates are 3,785,809 mPt/h

and 3,453,215 mPt/h, respectively. The total exergy destruction environmental impact rate is 1,148,436 mPt/h, and the total loss exergoenvironmental rate is 11,497 mPt/h. The total environmental rate of pollution formation is -139,468 mPt/h, meaning that the pollution formation of methane, carbon dioxide and carbon monoxide is decreasing by operating the proposed engine. In addition, the total environmental rate of components, \dot{B}_K^T , which is the summation of \dot{Y}_K , \dot{B}_K^{PF} , and $\dot{B}_{D,K}$, is 1,008,982 mPt/h, as shown in Table 5.40. The specific fuel and product exergoenvironmental impact is 8.1 mPt/h and 10.9 mPt/h, respectively.

Table 5.40 The exergoenvironmental performance of rail engine components

K#	$b_{F,K}$	$b_{P,K}$	f_b	r_b
Units	[mPt/MJ]	[mPt/MJ]	[%]	[%]
C1	11.0	13.4	1.73E-03	20.9
CC	5.5	9.3	2.76E-04	70.2
T1	5.6	11.0	1.98E-03	96.0
SP1	13.3	9.3	0	-29.4
MX1	10.9	11.0	0	0.5
MX2	5.4	5.4	0	1.1
SR	5.0	4.4	-1.47E-02	-11.6
WGS	4.0	4.0	2.55E-01	0.7
SOFC	3.1	4.6	3.80E-03	48.7
BR	6.3	11.8	1.08E-03	87.0
TG	11.0	195.9	6.49E-05	1687.4
AGN	10.4	20.6	8.34E-04	98.9
ACN	32.2	49.3	7.18E-03	52.9
AHX1	32.2	44.3	2.15E-01	37.4
AEX1	32.2	35.2	0	9.1
AEV	0.6	0.7	1.91E-01	8.9
ABS	34.5	56.1	1.44E-03	62.6
AP	11.0	15.6	5.59E-02	40.9
AHX2	3.7	6.1	6.98E-02	62.8
AEX2	3.7	28.5	0	663.6
AEC	21.8	73.8	5.28E-04	238.9
EX1	39.2	39.9	0	1.7
FP	39.9	39.9	0	0.0
PEMFC	29.2	40.5	3.18E-03	38.8
T2	117.6	196.0	3.31E-02	66.7
C2	196.0	252.1	9.74E-03	28.6
HX1	25.0	133.2	4.28E-02	433.4
Total	8.1	10.9	1.39E-03	34.8

The exergoenvironmental factor, f_b , is a very low value of an order of magnitude of -3 because the total environmental rate of components is greater than the component-related environmental impact rate by a factor of 82,000. There is also one negative value of f_b in SR because it reduces the pollution formation due to the discarding of methane by the steam reforming process. The relative exergoenvironmental difference, r_b , of the

system is 34.8% because the specific product exergoenvironmental impact is greater than that of fuel by a factor of 1.3, as shown in Table 5.40. There are also two components that have a negative value of r_b , which are SP1 and SR because their product environmental impact values are less than that of fuel values.

The exergoenvironmental analysis is also applied using five fuel blends to understand the effect of fuel selection, as shown in Figure 5.43. The total fuel exergoenvironmental rate records the maximum value of 9248 Pt/h using F3 and reaches the minimum value of 3789 Pt/h using F1. Also, the total product exergoenvironmental rate of the proposed engine ranges from 3453 Pt/h using F1 to 8951 Pt/h using F3. In addition, the destruction exergoenvironmental rate varies from 1148 to 2677 Pt/h with the same trend as fuel and product exergoenvironmental rates. The loss exergoenvironmental rates have an average of 19 Pt/h.

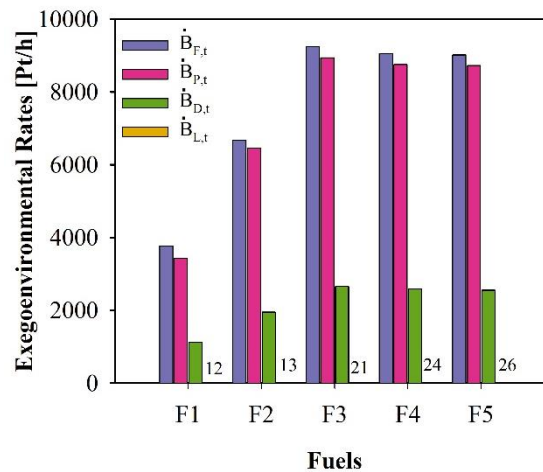


Figure 5.43 Four exergoenvironmental rates with respect to fuel blends

Moreover, the pollution formation exergoenvironmental rate is also studied using the fuel blends, as shown in Figure 5.44-a. Two fuels, F1 and F2, have negative values due to methane reduction reaching -140 Pt/h and -21 Pt/h, respectively, while the average of other fuels is 15 Pt/h. Therefore, the total environmental rate of components is the minimum value of 1009Pt/h using F1 followed by 1992 Pt/h using F2, and followed by an average of 2600 Pt/h for the three fuel blends, as shown in Figure 5.44-b. The total environmental rate of components is estimated by the pollution formation and destruction exergoenvironmental rates since the component-related environmental rate is very small compared to others. If both pollution formation and destruction are positive and high

values, then the total environmental rate of components is high, which means the components of the given system negatively impact the environment. And if the pollution formation is negative, then the total environmental rate of components is the difference between destruction and pollution formation, which is most likely less than the destruction since we are using sustainable fuels, not a fossil fuel. Using fossil fuels produces massive pollution formation and massive destruction exergoenvironmental rates.

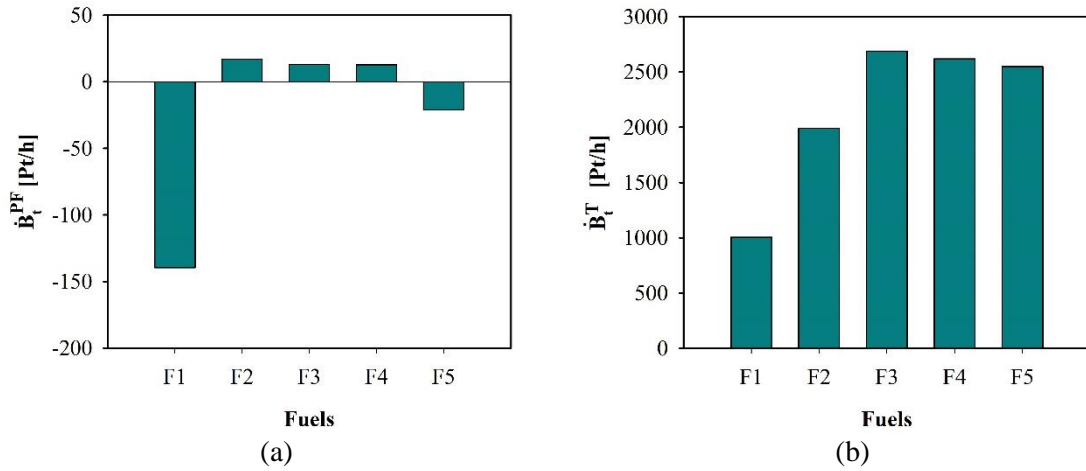


Figure 5.44 (a) Pollution formation exergoenvironmental rates and (b) total environmental impact rates of components with respect to fuel blends

Furthermore, the exergoenvironmental performance is estimated using specific exergoenvironmental impact, as b_F and b_P , relative environmental difference, r_b , and exergoenvironmental factors, f_b , as shown in Figure 5.45. The overall specific fuel environmental impact, $b_{F,t}$, increases from 8.11 mPt/MJ using F1 to 18.08 mPt/MJ using F3 of ethanol and hydrogen mixture, while the overall specific product exergoenvironmental impact, $b_{P,t}$, varies from 10.93 mPt/MJ to 28.16 mPt/MJ, with the same pattern, as graphed in Figure 5.45-a. The specific exergoenvironmental impacts of the present system are increased compared to the specific environmental impact of the fuel blends by about 2 factors for fuel and 3 factors for a product.

The f_b is estimated to be very low with an order of magnitude -3 because of the huge difference of \dot{Y} and \dot{B}^T . The highest f_b value is 1.4×10^{-3} % using F1 and the lowest value is 0.52×10^{-3} % using F3, as shown in Figure 5.45-b. The overall r_b values have an average of 51% where its minimum and maximum values are 35% and 58% using F1 and

F2, respectively. The less r_b and higher f_b values are the less environmental impact and the higher r_b and less f_b values are the higher environmental impact.

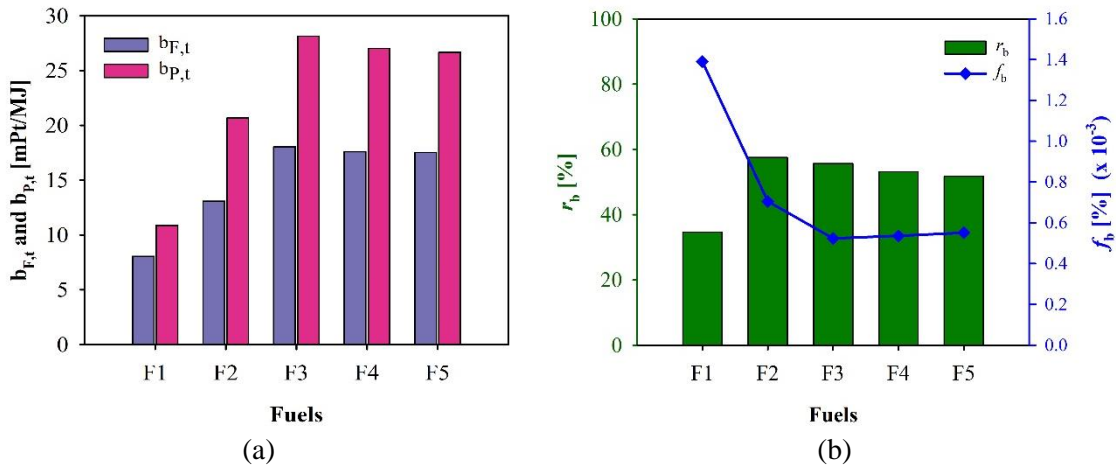


Figure 5.45 The exergoenvironmental performance: (a) specific exergoenvironmental impact, and (b) relative environmental difference and exergoenvironmental factor

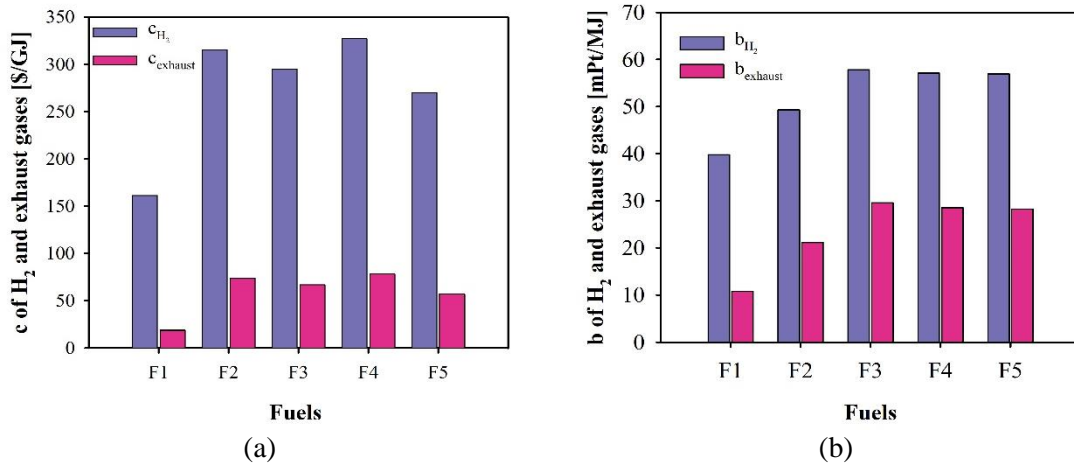


Figure 5.46 Economic and environmental impact of hydrogen production and exhaust gases: (a) specific exergetic cost, and (b) specific environmental impact

On-board hydrogen production system is used to produce hydrogen with a constant mass flowrate of 0.005 kg/s, whereas 0.003 kg/s is stored, and 0.002 kg/s is used to produce electrical energy using PEMFC. However, hydrogen production has different economic and environmental impacts because the fuel exergy, exergoeconomic, and exergoenvironmental rates count on the turbine power of T1 since it provides the electric power to this subsystem. The economic assessment of hydrogen production varies from 162 to 327 \$/GJ of F1 to F4, respectively, as shown in Figure 5.46-a, while its environmental impact has a range of 40 mPt/MJ of F1 to 58 mPt/MJ of F3.

The exhaust gases from the locomotive engine are collected in Stream B9 after passing through the TG and ARS, where its specific exergoeconomic and exergoenvironmental impact are averaged of 60 \$/GJ, as shown in Figure 5.46-a, and 24 mPt/MJ, as shown in Figure 5.46-b. The exhaust gases are more economic and have a less environmental impact than that hydrogen because of the high price and high environmental impact of ammonia and KOH.

The economic and environmental impact of components that deliver or use power and heat following the fuel and product principle is studied and illustrated in Figure 5.47. Based on the fuel and product principle, the specific exergoeconomic and exergoenvironmental impact of electricity of T1, C1, AP, and AEC are equal because the electric power of T1 is distributed to the other three components in addition to the generator to operate the traction motors of the locomotive engine. Also, the specific exergoeconomic and exergoenvironmental impacts of T2 and C2 are equal because T2 is delivering electric power to C2, while the specific exergoeconomic and exergoenvironmental impacts of PEMFC and SOFC are estimated. In addition, following the same principle, the heat of ABS, AEV, and ACN are calculated by solving their balance equations. Therefore, the average of specific exergoeconomic of electricity is 27 \$/GJ for SOFC, 58 \$/GJ for T1, 317 \$/GJ for PEMFC, and 449 \$/GJ for T2. The average of specific exergoeconomic of heat is 1111 \$/GJ for ABS and 270 \$/GJ for ACN, while of cooling load is 7 \$/GJ for AEV, as shown in Figure 5.47-a. Moreover, the average specific exergoenvironmental impact of electricity is 11 mPt/MJ for SOFC, 24 mPt/MJ for T1, 53 mPt/MJ for PEMFC, and 257 mPt/MJ for T2. Also, the average of specific exergoenvironmental impact of heat is 556 mPt/MJ for ABS and 116 mPt/MJ for ACN, while of cooling load is 1 mPt/MJ for AEV, as shown in Figure 5.47-b.

Based on the above discussion, the methane and hydrogen fuel blend are the most economic and have less environmental impact because of the low methane price, which is assumed to be equal to the price of pure natural gas. However, the real price of pure methane is higher than all other fuels reaching 3.24 \$/kg (64.84 \$/GJ) as published in Global Petrol Prices-2022 [226]. That means the fuel prices of F1 and F5 will be higher, and other prices of other fuel blends will remain the same because they do not count on methane. Hence, the best choice must be among three fuel blends (F2, F3, and F4). F2 was

the second least environmental impact after F1, but it is more expensive than F3 and cheaper than F4, which can be a better choice if still the price of methane increases due to the current global political and energy circumstances.

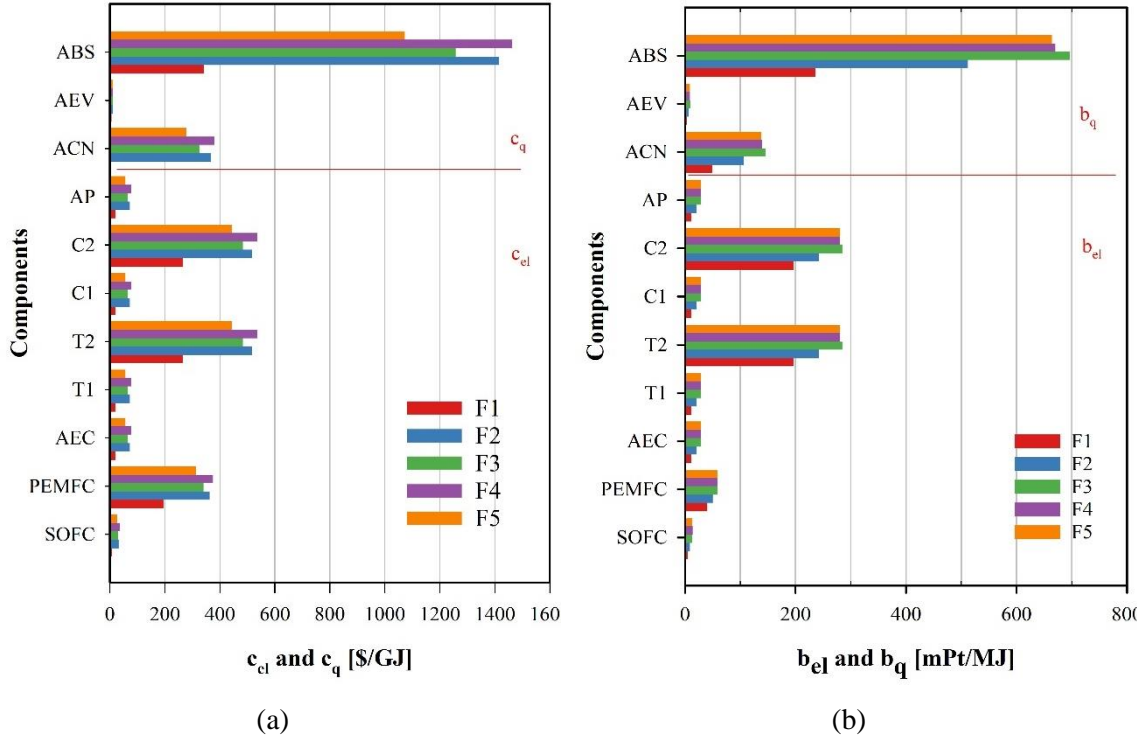


Figure 5.47 Economic and environmental impact of power and heat components: (a) specific exergy cost of power and heat, and (b) specific environmental impact of power and heat

5.5 Results of System R-3

This section presents the results and discussion of the thermodynamic analysis, exergy analysis, exergoeconomic analysis, and exergoenvironmental analysis of the hybrid SOFC-PEMFC-GT locomotive engine as written in the subsections below.

5.5.1 Results of Thermodynamic Analysis

Thermodynamic results of state points are reported in [180]. The air enters the engine at 8 kg/s at standard conditions, then it is compressed by the low-pressure compressor to 720 kPa and intercooled from 571.5 K to 511.5 K. Next, it is compressed by the high-pressure compressor to 5090.4 kPa with a temperature of 948.4 K. A fuel blend of methane, and hydrogen enters the CC at F1 with 0.28 kg/s to be combusted in the CC to increase the temperature to 1573.2 K based on the specifications of Centaur gas turbine [227]. These

exhaust gases are expanded by the high-pressure turbine T2 to 715.5 kPa, and a portion of these exhaust gases is burned again in the afterburner BR to 1073.2 K, which is expanded again in low-pressure turbine T1 to 106.1 kPa. The SOFC system starts with a mixture of steam (W1) at a rate of 0.04 kg/s and a fuel blend (F2) at a rate of 0.025 kg/s. The fuel mixture is steam reformed to 473.2 K and a pressure of 400 kPa, then is water shifted at 673.2 K, so that the hydrogen from this mixture is electrochemically reacted with air to produce electricity by the SOFC at 800 kPa and 1073.2 K. A portion of the air after the intercooler is used for the PEMFC system with a rate of 1.6 kg/s to react with hydrogen with a rate of 0.045 kg/s to produce electricity at 720 kPa and 623.2 K. Then, the exhaust steam is expanded by the low-pressure turbine (T3) to 200 kPa.

In the ARS, the ammonia and water mixture flows at 5 kg/s to the pump at 100 kPa and 283 K to be compressed by the AP to 2000 kPa and heated by the AHX to 345.5 K before entering the generator AGN, which uses the exhaust heat from the GT engine. The AGN discharges the mixture into a weak solution at R4 and a strong solution of ammonia at R7. The strong solution flows to the condenser ACN at 398.2 K and 2000 kPa, which then is expanded by the AEX1 to 100 kPa and 252.8 K to the evaporator to be used for cooling the train. Then, the refrigerant mixture is heated to 301.2 K before entering the absorber ARS. On the other hand, the weak solution from the AGN at R4 flowed to the other side of the AHX to be cooled to 306.1 K and expanded to 100 kPa before entering the absorber ARS.

The analysis of the engine components is displayed in Table 5.41. This analysis contains the heat addition or rejection, required or generated power, exergy destruction rate, energetic and electric efficiency, and exergetic efficiency. The power of the compressors is 2494.7 kW for the C1 and 3402.9 kW for C2, while the turbine power is 2594.1 kW for T1, 5115.1 kW for T2, and 270 kW for T3. The turbines and compressors are designed to have a mechanical efficiency of 80% and an energetic efficiency of 90%, so that their total efficiency is 72%. However, their exergetic efficiency is above 80% except for T3 (70.3%). The BR and CC require heat of 5591 kW and 3050.3 kW, respectively, but they have the greatest value of exergy destruction rate of about 9 MW.

In addition, the fuel cells can convert 5071.4 kW of heat into the power of 1252.5 kW by PEMFC and 4289.1 kW of heat into power of 2321.9 kW by using the SOFC. This

means that the energetic efficiency of PEMFC and SOFC are 24.7% and 54.7%, respectively. However, they have a high electric efficiency of 70% for the PEMFC and 97% for the SOFC. The two electrothermal generators produce 5.7 kW by TEG1 and 31.3 kW by TEG2, making an energetic efficiency of about 5% or less. In the ARS, the AGN utilizes 3346 kW to produce a cooling load of 615.1 kW by the AEV.

Table 5.41 The performance of the engine components

#	\dot{Q} [kW]	\dot{W} [kW]	$\dot{E}x_D$ [kW]	$\eta_{th} (\eta_e)$ [%]	ψ [%]
C1	0.0	2494.7	495.4	72.0	80.1
C2	0.0	3402.9	541.9	72.0	84.1
T1	0.0	2594.1	588.8	72.0	81.5
T2	0.0	5115.1	861.6	72.0	85.6
T3	0.0	270.0	114.3	72.0	70.3
BR	5591.0	0.0	8889.6	60.8	38.4
CC	3050.3	0.0	8666.0	80.0	68.7
PEMFC	5071.4	1252.5	1068.2	24.7 (69.9)	25.2
SOFC	4289.1	2321.9	1249.9	54.1 (96.9)	65.0
SR	340.3	0.0	51.0	45.5	40.5
WGS	23.5	0.0	3.8	11.1	29.3
IC	502.9	0.0	12.2	100.0	94.5
TEG1	104.3	5.7	308.6	5.4	1.6
TEG2	2113.6	31.3	60.4	1.5	10.1
ACOND	1215.0	0.0	83.5	100.0	88.9
AEV	615.1	0.0	132.7	100.0	2.1
AHX	1462.8	0.0	146.3	100.0	69.1
AGN	3346.1	0.0	157.3	100.0	81.4
ABS	2763.1	0.0	170.1	100.0	21.8
AP	0.0	17.4	4.2	69.9	75.9

The subsystems of this hybrid engine are also analyzed as shown in Table 5.42. The GT-only engine has a net power of 1811.5 kW and 8641.3 kW for heat addition and 502.9 for heat rejection by IC. Therefore, this traditional engine has 22.3 % energetic efficiency and 28.1% exergetic efficiency. The SOFC subsystem generates an electric power of 2321.9 kW and requires a heat of 340.3 kW for the SR and 23.5 kW for the WGS. The PEMFC subsystem also generates a total power of 1527.7 kW from the T3, PEMFC, and TEG1. Lastly, the energy recovery subsystem generates a power of 31.3 kW by TEG2 and a cooling load of 615.1 kW from the ARS, which has an energetic and exergetic COP of 18.3 and 9.5%, respectively. This hybrid engine can produce a total power of 5675.7 kW and a cooling load of 615.1 kW by requiring a heat of 9005.1 kW with an overall engine efficiency of 74% energetic efficiency and 46.7% exergetic efficiency.

Table 5.42 Performance of the subsystems and overall engine

System	\dot{W} [kW]	\dot{Q}_{add} [kW]	\dot{Q}_{rej} [kW]	$\dot{E}x_{add}^Q$ [kW]	$\dot{E}x_{rej}^Q$ [kW]	η_{th} [%]	ψ [%]
<i>GT only</i>							
GT	1811.5	8641.3	502.9	6650.3	209.9	22.3	28.1
<i>SOFC subsystem</i>							
SOFC	2321.9	4289.1	0.0	3098.1	0.0	54.1	65.0
SR	0.0	340.3	0.0	126.0	0.0	45.5	40.5
WGS	0.0	23.5	0.0	13.1	0.0	11.1	29.3
<i>Energy recovery subsystem</i>							
TEG2	31.3	0.0	0.0	0.0	0.0	1.5	10.1
ARS	17.3	3346.1	615.1	0.0	81.9	18.3	9.5
<i>PEMFC subsystem</i>							
PEMFC	1252.5	5071.4	0.0	2646.2	0.0	69.9	75.8
T3	270.0	0.0	0.0	0.0	0.0	72.0	70.3
TEG1	5.7	0.0	0.0	0.0	0.0	5.4	1.6
Net	5675.7	9005.1	615.1	12533.6	81.9	74.0	46.7

(a) Effect of fuel blend on engine performance:

The traditional GT locomotive engine uses a 15 kg/s of intake air to produce a net power of 3355 kW, which is a substitute for the internal combustion engine of EMD 16-710G3 [178]. The presented system has reduced the intake air mass flow rate from 14 kg/s, as previously designed in [179], to 8 kg/s to reduce the size of the GT engine by half. Therefore, the fuel mass flowrates of the F1 stream drop from 1 kg/s using diesel to 0.28 kg/s for the F1, 0.46 kg/s for the F2, 0.32 kg/s for the F3 and the F4, and 0.31 kg/s for the F5, to maintain a constant equivalent ratio of 0.95 in the CC. The fuel mass flow rate of F2 is constant for all fuel blends as 0.03 kg/s, while the steam flow rate has two values of 0.04 kg/s for the F1 and 0.01 kg/s for the remaining fuel blends.

The same hybrid system is analyzed with different fuel blends, as shown in Figure 5.48. The engine power is 5675.7 kW for the F1, 6053.1 for the F2, 5984.1 kW for the F3, 5970.4 for the F4, and 5859.6 kW for the F5. The total added heat to the engine is the minimum for the F2 (8915.6kW) and maximum for the F4 (9536.1 kW), while the cooling load is constant at 615.1 kW for all fuels, as shown in Figure 5.48-a. The energetic and exergetic efficiencies are 74% and 46.7% for the F1, 79.3% and 49% for the F2, 76.1% and 46.8% for the F3, 72.9% and 44.5% for the F4, and 74.1% and 44.6% for the F5, respectively, as shown in Figure 5.48-b.

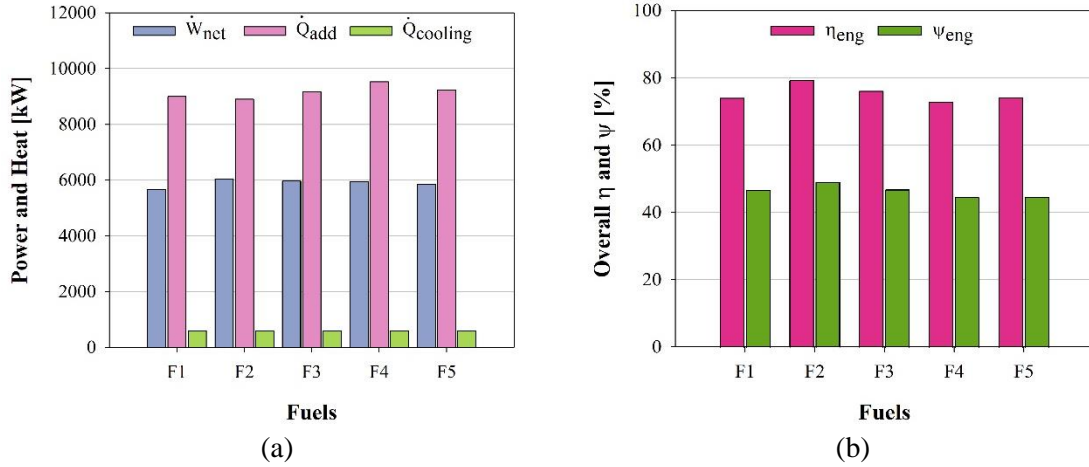


Figure 5.48 The power and heat of engine (a) and the performance of hybrid engine

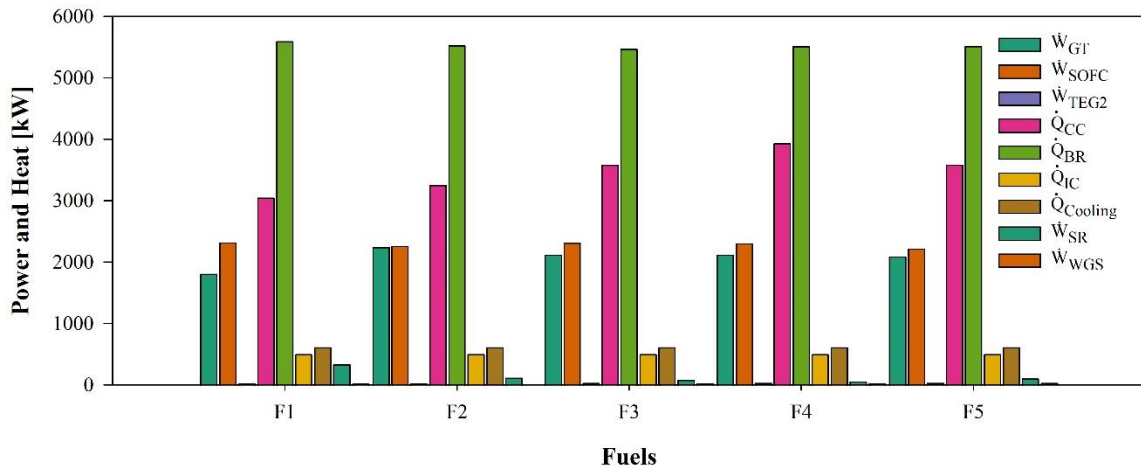


Figure 5.49 The power and heat of the engine components

To examine the engine performance, a detail of engine components for the GT subsystem and the SOFC subsystem is presented in Figure 5.49. The GT engine has a net power of 1811.5 kW by using the F1 and reaches to its maximum of 2248.2 kW for the F2, and the remaining fuels have an average of 2100 kW. The GT requires a heat for the CC, which has an average of 3482 kW with a maximum and minimum of 3933.7 kW for the F4 and 3050.3 kW for the F1, respectively, and a heat for the BR, which has an average of 5520 kW. The intercooler of the GT has a constant value of 503 kW with a temperature reduction of 50°C, and the cooling load of the ARS remains constant at 615 kW. The SOFC unit generates a maximum power of 2332 kW for the F1 and a minimum power of 2220 kW for the F5. The SOFC system contains the SR and WGS to produce hydrogen from different

fuel blends, and they require a heat range of 61 to 340 kW for the SR and 18 to 36 kW for the WGS. The TEG2 produces the lowest power of an average of 34.9 kW.

The weight of the combined engine is the sum of the gas turbine, PEMFC, SOFC, and energy recovery system. The weight of the GT is 1872 kg for 2500 kW without the weight of generators and other accessories. The size of the GT is (6.7m × 2.4 m × 2.7 m) [228]. The weight of once stack of SOFC is 62 kg [176], so the total weight of SOFC is 434 kg for 7 stacks. The weight of one stack of PEMFC is 80 kg [146], then the total weight of PEMFC is 880 kg for 11 stacks, in addition to the weight of turbine T3 is 202 kg. The two fuel cells are distributed on the top of the engine block to ensure air cooling and avoid any obstacles in the engine cabin. Besides, the weight of ARB is 4816 kg, and the weight of the TEGs is about 100 kg. Therefore, the total weight of the engine is about 8304 kg and can increase to 9000 kg to include engine accessories and control system. This weight is less than the weight of the diesel engine locomotive of EMD 16-710G3 (18,000 kg and a size of 5.56 m × 1.75 m × 2.75 m) [216]. The size of the locomotive engine car varies from 10 m to 15 m to include all the engines, batteries, generators, and control cabin as well.

(b) Comparison of different engine modes:

Fuel blends slightly affect the performance of the overall engine, as shown in Figure 5.50. The GT-only engine has an average energetic efficiency of 24.5%, with a minimum and a maximum value of 22.3 % for the F1 and 27.2 % for the F2, respectively. Combining the GT engine with the SOFC subsystem and the energy recovery subsystem of the TEG2 and ARS increases the energetic efficiency to an average of 59%, with a minimum value of 56.8 % for the F4. However, adding the PEMFC subsystem to the combined one as in the proposed system can increase the overall energetic efficiency to an average of 75.3%, which is threefold of the GT-only engine. Not only that, but also the CO₂ emissions have tremendously decreased to 75% using the F1 and 80% for the F2 and 84% for the remaining fuels compared to traditional diesel fuel (2.510 kg/s), as shown in Table 5.43.

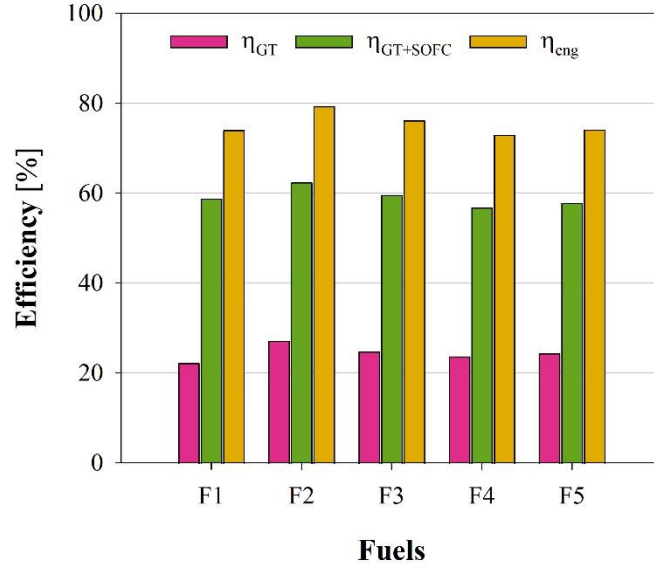


Figure 5.50 Comparison of energetic efficiency of the GT-only, GT+SOFC, and the overall engine

Table 5.43 CO₂ emissions with respect to fuels

Fuels	CO ₂ emission [kg/s]	Reduction percentage [%]
Diesel	2.510	
F1	0.627	75.0
F2	0.499	80.1
F3	0.395	84.2
F4	0.395	84.2
F5	0.393	84.3

(c) Effect of fuel blend on fuel cells:

There are two fuel cells; one is merged with the exit of the high-pressure turbine at B2 with a splitting ratio of 0.5, which is the SOFC and operated at 1073 K. The other uses the compression extraction after the intercooling and before the high-pressure compressor, which is the PEMFC and operated at a temperature of 623 K.

The SOFC modules are operated at 0.6 A/cm² and have a total active area of 350 m² (0.5 m² × 100 cells × 7 stacks). This fuel cell has a Nernst voltage of 1.14 V, while it can produce a cell voltage of 1.11 V to produce a net power of 2322 kW by using the F1. Looking at Figure 5.51, we found that the added heat from the exit of turbine is high reaching 4289 kW for the F1, 4492 kW for the F2, 4769 kW for the F3 and F4, and 4741 kW for the F5. The SOFC can convert this exhaust heat to electric power of 2322 kW for the F1, 2264 kW for the F2, 2318 kW for the F3, 2304 kW for the F4, and 2220 kW for the F5. That means the SOFC uses almost half of the input heat, as shown in Figure 5.51-a. In

other words, The SOFC uses almost 96% of the Nernst voltage, meaning that it has an electric efficiency of 96%. However, the energetic efficiency is below 60 % for the F1 and F2 and below 50% for the remaining, as shown in Figure 5.51-b. The exergetic efficiency of the SOFC is higher with an average of 60% with all fuel blends.

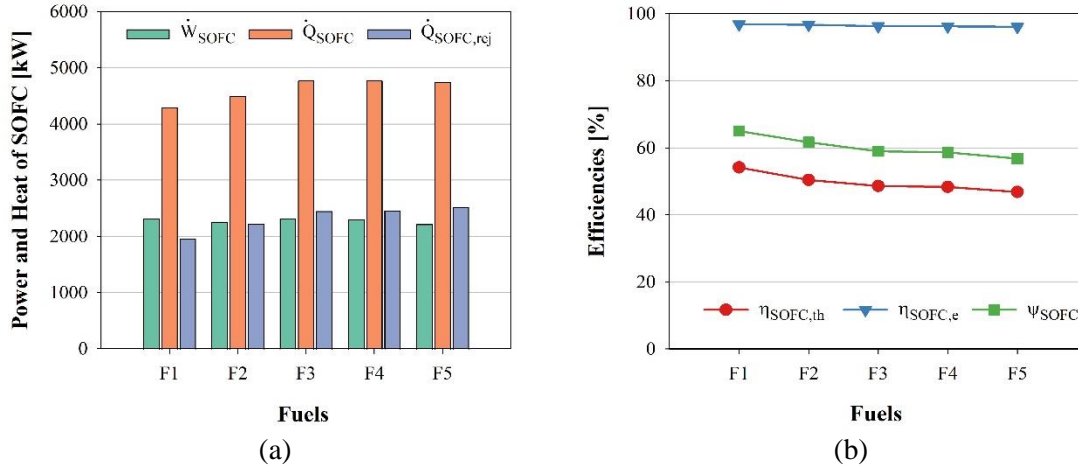


Figure 5.51 The performance of the SOFC system: (a) The power and heat of SOFC, and (b) the efficiencies of SOFC

The PEMFC unit has a constant value with respect to fuel selection because it does not depend on fuel, and the splitting ratio remains constant at 0.2. This PEMFC uses a high current density of 0.8 A/cm² and a total active area of 550 m² (0.5 m² × 100 cells × 11 stacks) based on the amount of hydrogen estimated, which will be discussed later. This PEMFC gives a Nernst voltage of 0.44 V and produces a cell voltage of 0.28 V and an electric power of 1253 kW using the F1. The total input heat to the PEMFC is 5071 kW, while the rejected heat from the PEMFC is 3125 kW, as shown in Figure 5.52-a. Therefore, the thermal, electric, and exergetic efficiencies are 23%, 70%, and 25%, respectively, as shown in Figure 5.52-b.

The active cell and number of cells are the same for all fuel cells to be 0.5 m² and 100 cells. The number of stacks is different depending on the amount of hydrogen entering each cell. As shown in Figure 5.53-a. The number of stacks for SOFC is 7 for F1 and F2, and 8 for F3 to F5, while the number of stacks for PEMFC remains constant at 11 stacks. The amount of hydrogen produced by fuel blends in F1 and F2 streams is minimum of 38 mol/s for F1, maximum of 68.5 mol/s for F3 and F4. The SOFC uses an average of 12 mol/s and about 29% for F1 and 18% for others, as shown in Figure 5.53-b. The PEMFC

uses a fixed amount of 22.3 mol/s that enters separately into the H1 stream to electrochemically react with the air of the B1 stream.

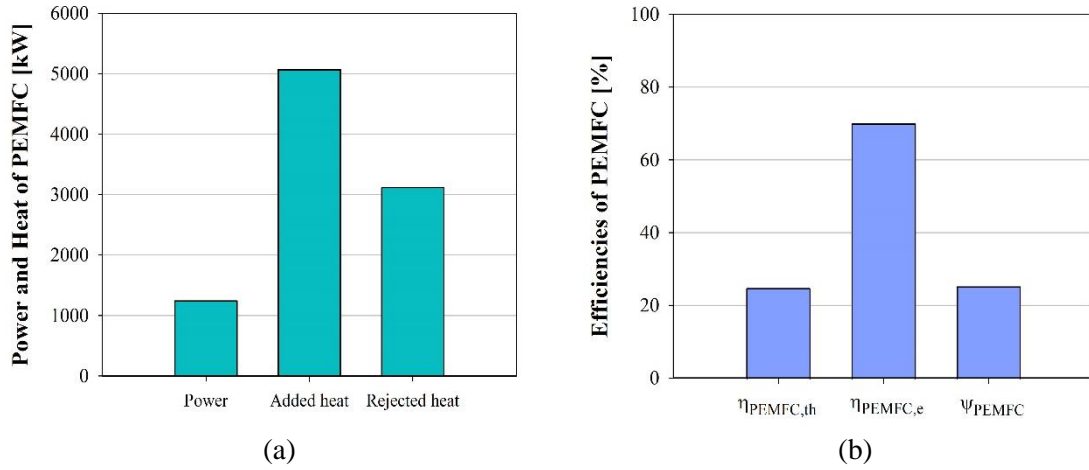


Figure 5.52 The performance of PEMFC system: (a) power and heat, and (b) efficiencies

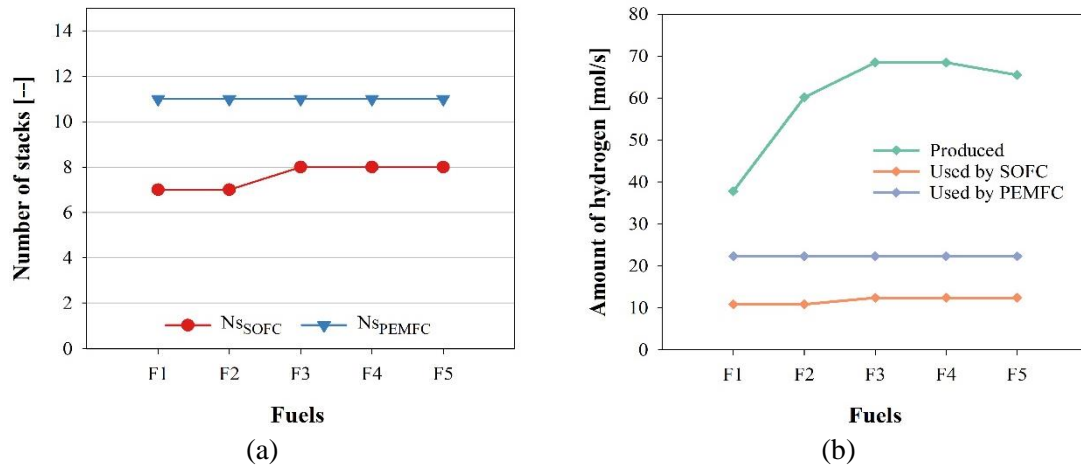


Figure 5.53 Number of stacks (a) and amount of hydrogen (b) for the fuel cells

(d) Effect of fuel blend on TEGs:

The TEGs are used to convert the waste energy of the exhaust gases into electric power, which can be executed by adding modules around the exhaust pipe having a diameter of 0.15 m or 2 m and a length of 1 m that covers about 0.87 circumference area of the pipe. TEG1 is used for the exhaust pipe after the PEMFC subsystem and operated at 3.15 A/m². It uses waste energy of 104 kW to convert to 5.4 kW electric power. The TEG1 can reduce the exhaust temperature by 50 °C and has an energetic and exergetic efficiency of 5.4% and 1.6%, respectively, while the maximum energetic efficiency is 5.8%, as shown in Figure 5.54.

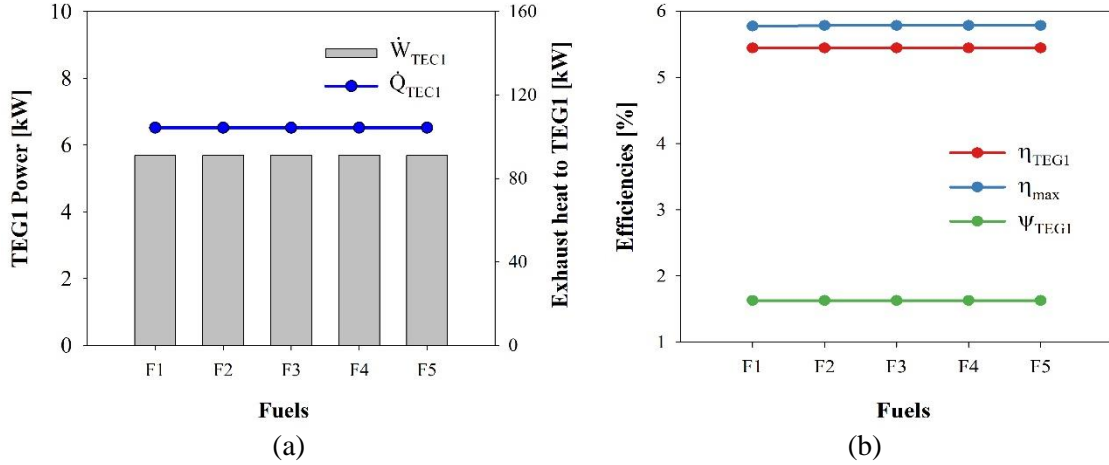


Figure 5.54 The TEG1 performance: (a) power and exhaust heat, and (b) efficiencies

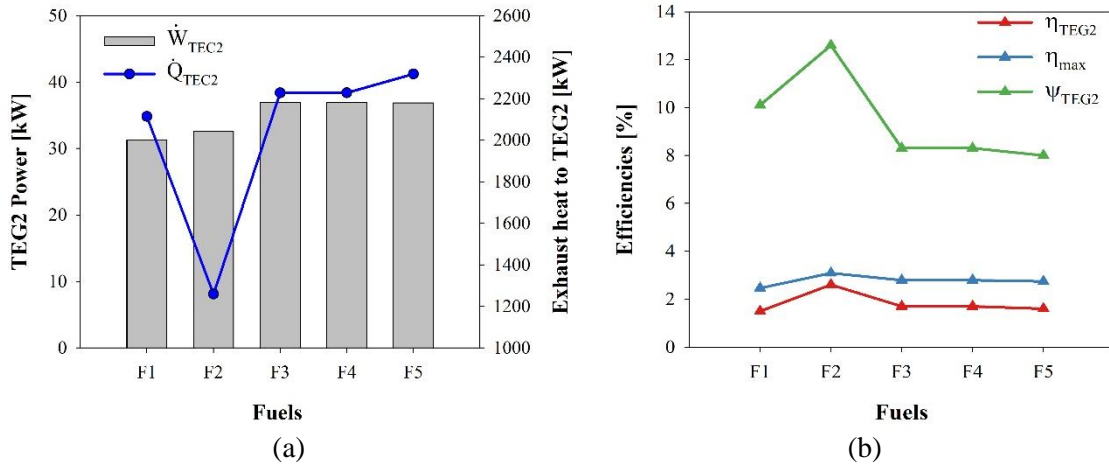


Figure 5.55 The TEG2 performance: (a) power and heat, and (b) efficiencies

On the other hand, the TEG2 was installed at the exit of the GT system after the ARS system and was able to reduce 20 °C of the exhaust gas temperature. The TEG2 is operated at 5 A/m² and uses waste energy of 2200 kW, which is converted to an average electric power of 36 kW, as shown in Figure 5.55. The minimum power of TEG2 is obtained by the F2 of 31.3 kW, and the maximum power is 37 kW for the F3 and F4. F2 has a minimum heat transfer of exhaust gases of 1258 kW because of its relatively high mass flow rate of about 6.9 kg/s with maintaining the same temperature difference between streams A12 and A13. In addition, using F2 has encountered a higher average temperature of 366.3 K than the other. Therefore, the hot conjunction heat transfer and cold conjunction heat transfer are increased yielding to lower the power of TEG2 than that of other fuels of F3 to F5, but more than the power of F1. TEG2 has low energetic efficiency of 1.9 % and

exergetic efficiency of 9%, while the highest efficiency of TEG2 is 2.6%. The maximum efficiency of TEG2 is 2.5 % for the F1, 3% for the F2, and 2.8% for the remaining fuel blends. Because of low heat and relatively low power of TEG2 using F2, its performance is increased to its maximum value using F2, as shown in Figure 5.55-b. The benefit of the energy recovery system ranges from 16 to 20% of useful energy that is coming from the TEGs, cooling load, and turbine power of T3.

5.5.2 Results of Exergy Analysis

The exergy flow rates for streams are drawn with a Sankey diagram incorporating with work, thermal, and destruction exergy rates as shown in Figure 5.56. The exergy rates of fuels are 19 MW entering the CC, 1.7 MW entering the SOFC, and 5.4 MW of hydrogen entering PEMFC. The highest exergy rate is 18 MW exiting the CC. The exhaust has a total exergy rate of 1.4 MW from the GT and PEMFC. The exergy rate of ARS is small with an average of 300 kW. Table 5.44 presents the exergy performance of R-3 system.

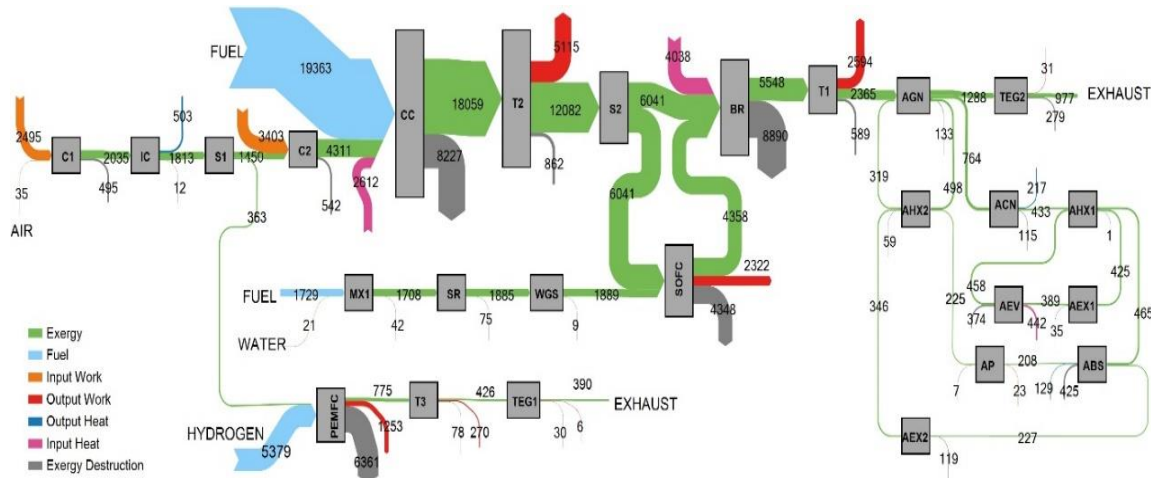
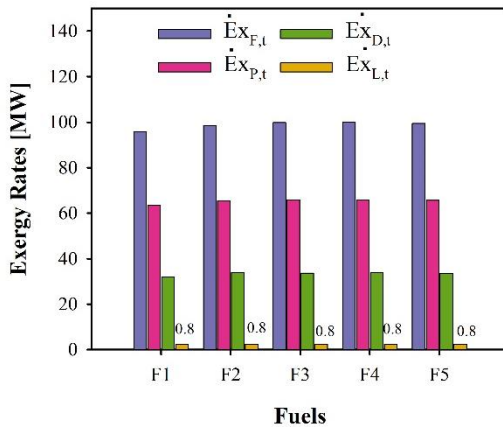


Figure 5.56 The Sankey flowchart of exergy rates of R-3 rail engine system.

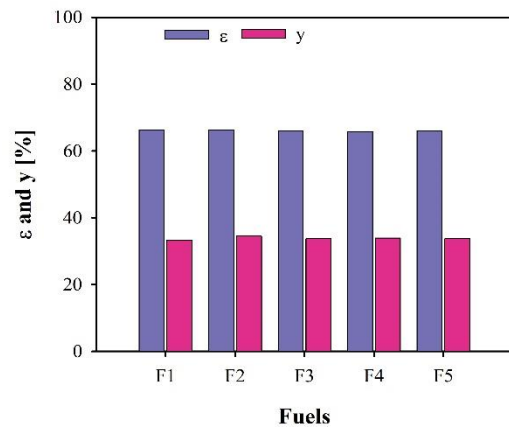
The net power of R-3 using F1 (75% wt. methane and 25% wt. hydrogen) is 5.7 MW, the total fuel, product, losses, and destruction exergy rates are 96 MW, 64 MW, 32 MW, and 0.8 MW, respectively. The exergy efficiency, ϵ , and destruction ratio, γ , are 66.5% and 33.5%, respectively. Using the five fuel blends has slightly affected the exergy rate and exergetic performance as shown in Figure 5.57. The average fuel exergy rate is 98.6 MW, and the product exergy rate is 66.5 MW, which is the difference between the fuel and product, is 33.7 MW, as shown in Figure 5.57-a. The average of exergetic efficiency and destruction ratio are 66% and 34%, respectively, as in Figure 5.57-b.

Table 5.44 The exergy performance of R-3 system

#	W_K	\dot{Q}_K	$\dot{Ex}_{F,K}$	$\dot{Ex}_{P,K}$	$\dot{Ex}_{D,K}$	$\dot{Ex}_{L,K}$	ε	y	y^*
Units	[kW]	[kW]	[kW]	[kW]	[kW]	[kW]	[%]	[%]	[%]
C1	2495	0	2495	1999	495.4	0	80.12	0.52	1.54
IC	0	502.9	1825	1813	12.19	0	99.34	0.01	0.04
S1	0	0	1813	1813	0	0	100.00	0.00	0.00
C2	3403	0	3403	2861	542	0	84.07	0.57	1.69
CC	0	3050	26286	18059	8227	0	68.70	8.58	25.62
T2	5115	0	5977	5115	861.6	0	85.58	0.90	2.68
S2	0	0	12082	12082	0	0	100.00	0.00	0.00
T1	2594	0	3183	2594	588.8	0	81.50	0.61	1.83
PEMFC	1253	0	7613	1253	6361	694	16.46	6.63	19.81
T3	270	0	348.3	270	78.3	0	77.52	0.08	0.24
TEG1	5.7	104.3	36.1	5.7	30.4	0	15.79	0.03	0.09
MX1	0	0	1750	1708	41.8	0	97.60	0.04	0.13
SR	0	340.3	1960	1885	74.99	0	96.17	0.08	0.23
WGS	0	23.5	1898	1889	9.197	0	99.53	0.01	0.03
SOFC	2322	4289	6670	2322	4348	75	34.81	4.53	13.54
BR	0	5591	14438	5548	8890	0	38.43	9.27	27.69
TEG2	31.3	2114	310.5	31.3	279.2	0	10.08	0.29	0.87
AGN	0	3380	1396	1263	133.4	0	90.47	0.14	0.42
ACN	0	2394	331.3	216.8	114.5	0	65.44	0.12	0.36
AHX1	0	400.5	8.1	7.1	1	0	87.65	0.00	0.00
AEX1	0	0	424.7	389.4	35.3	0	91.69	0.04	0.11
AEV	0	1927	442.3	68.5	373.8	0	15.49	0.39	1.16
ABS	0	2937	691.7	267	424.7	0	38.60	0.44	1.32
AP	23.1	0	23.1	16.4	6.7	0	71.00	0.01	0.02
AHX2	0	1013	152.5	93.7	58.8	0	61.44	0.06	0.18
AEX2	0	0	345.9	226.7	119.2	0	65.54	0.12	0.37
Total			95904	63797	32107	769	66.52	33.48	100



(a)



(b)

Figure 5.57 The exergy analysis based on fuel blends: (a) fuel, product, destruction, and losses exergetic rates, and (b) exergetic efficiency and exergy destruction ratio

5.5.3 Results of Exergoeconomic Analysis

The exergoeconomic rate of the R-3 rail engine is plotted for the streams in Figure 5.58. The fuel cost of F1 is 7.15 \$/GJ according to 2022. The exergy cost rates of fuels are 498 \$/h entering the CC, 45 \$/h entering the SOFC, and 326 \$/h of hydrogen entering the PEMFC. The maximum exergy cost rate of 893 \$/h entering the turbine T2. The exhaust gases have a total exergy cost rate of 76 \$/h. Table 5.45 presents the cost of rail engine components. The fuel cells have the maximum prices, followed by the turbine (T2) and combustion chamber (CC). The total initial costs of components according to the corresponding year of cost equation (C_K) is about \$ 2.5M, while the total normalized cost is \$ 4.8M, and the total levelized cost rate is 67 \$/h.

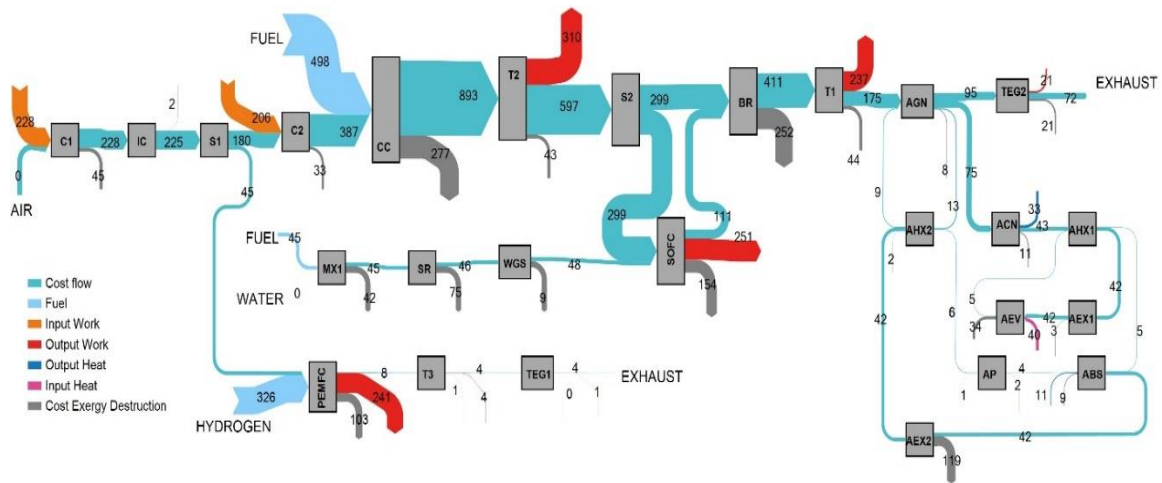


Figure 5.58 Sankey flowchart of exergoeconomic rates of R-3 rail engine.

The exergoeconomic analysis of engine components are discussed and displayed in Table 5.46. The net exergy cost rate of net power is 630 \$/h. While the total exergy cost rate of heat is 85 \$/h. The exergy cost of cooling is 40\$/h. Also, the exergy cost rates of fuel, product, destruction, and losses are 4080, 3990, 1246, and 141 \$/h, respectively. The specific fuel and product exergetic cost are 11.87 and 17.37 \$/GJ, respectively. Therefore, relative cost difference, r , is 47%, which means the specific product exergy cost is higher than the specific fuel exergy cost by 47%. Also, the exergoeconomic factor, f by using the F1 is 5.3%, meaning that the destruction exergy cost rate is significantly larger than the levelized cost rate.

Using different fuel blends affects the exergoeconomic performance. Figure 5.59 shows the exergoeconomic rates and specific exergetic cost. The exergoeconomic rates of

fuel and product are 4080 \$/h and 3990 \$/h using F1, 15571 \$/h and 15636 \$/h using F2, 13433 \$/h and 13273 \$/h using F3, 16041\$/h and 15861 \$/h using F4, and 11943 \$/h and 11793 \$/h using F5, respectively. The average exergoeconomic rate of destruction and loses are 3463 \$/h and 193 \$/h, respectively, as shown in Figure 5.59-a. The specific fuel and product exergetic cost are minimum of 11.8 \$/GJ and 17.4 \$/GJ for F1, maximum of 44.5 \$/GJ and 66.7 \$/GJ, and average of 34 \$/GJ and 51 \$/GJ, respectively, as shown in Figure 5.59-b.

Table 5.45 The components' costs of R-3 rail system

#	C_K [\$]	Z_K [\$] (2022)	\dot{Z}_K [\$/h]
C1	21,504	44,458	0.64
IC	15,061	31,530	0.46
S1	0	0	0
C2	17,203	35,567	0.51
CC	252,608	522,244	7.56
T2	485,255	1,003,000	14.52
S2	0	0	0
T1	18,079	37,377	0.54
PEMFC	534,618	806,390	11.67
T3	2,887	5,969	0.09
TEG1	5,700	11,784	0.17
MX1	0	0	0
SR	44,458	93,071	1.35
WGS	51,794	108,429	1.57
SOFC	781,786	1,616,000	23.39
BR	62,214	128,622	1.86
TEG2	31,300	64,710	0.94
AGN	3,000	6,280	0.09
ACN	13,999	29,305	0.42
AHX1	12,917	27,041	0.39
AEX1	382	799	0.01
AEV	91,286	191,103	2.77
ABS	3,164	6,623	0.10
AP	5,601	11,726	0.17
AHX2	15,114	31,640	0.46
AEX2	191	400	0.01
Total	2,470,121	4,814,068	69.67

Nevertheless, the average relative cost difference of all fuel blends is 49%, as presented in Figure 5.60-a, but the minimum relative cost difference of 47% using F1. The exergoeconomic factor reaches the maximum value of 5.3% using F1 and the minimum

value of 1.5% using F2 and F4. The specific exergetic cost of exhaust gases from combined engine is also plotted in Figure 5.60-b. The minimum specific exergetic cost is 23.5 \$/GJ, while the maximum is 85.65 \$/GJ, and the average of specific exergetic cost of exhaust gases is 65.5 \$/GJ.

Table 5.46 The exergoeconomic analysis of R-3 rail engine components

#	\dot{C}_K^W [\$/h]	\dot{C}_K^Q [\$/h]	$\dot{C}_{F,K}$ [\$/h]	$\dot{C}_{P,K}$ [\$/h]	$\dot{C}_{D,K}$ [\$/h]	$\dot{C}_{L,K}$ [\$/h]	$c_{F,K}$ [\$/GJ]	$c_{P,K}$ [\$/GJ]	f [%]	r [%]
C1	227.5	0	227.5	228.1	45.17	0	25.33	31.69	1.40	25.11
IC	0	1.511	3.165	1.511	0.02	0	0.48	0.23	95.57	-51.92
S1	0	0	225	225	0	0	34.47	34.47	0.00	0.00
C2	206.2	0	206.2	206.7	32.84	0	16.83	20.07	1.54	19.25
CC	0	0	885.1	892.6	277.01	0	9.35	13.73	2.66	46.80
T2	309.9	0	295.4	309.9	42.59	0	13.73	16.83	25.43	22.58
S2	0	0	597.2	597.2	0	0	13.73	13.73	0.00	0.00
T1	236.5	0	236	236.5	43.67	0	20.60	25.33	1.22	22.96
PEMFC	240.7	0	362.4	240.7	302.73	133.4	13.22	53.38	3.71	303.78
T3	3.723	0	3.636	3.723	0.82	0	2.90	3.83	9.56	32.07
TEG1	0.5474	0	0.3769	0.5474	0.32	0	2.90	26.68	34.95	820.00
MX1	0	0	44.92	44.92	1.07	0	7.13	7.31	0.00	2.45
SR	0	0	44.92	46.26	1.72	0	6.37	6.82	43.94	7.10
WGS	0	0	46.26	47.83	0.22	0	6.77	7.03	87.50	3.90
SOFC	250.8	0	235.5	250.8	153.55	8.11	9.81	30.01	13.22	205.91
BR	0	0	409.5	411.3	252.16	0	7.88	20.60	0.73	161.45
TEG2	23.96	0	23.02	23.96	20.71	0	20.60	212.60	4.33	932.04
AGN	0	0	88.78	81.71	8.49	0	17.67	17.98	1.06	1.75
ACN	0	33.13	32.71	33.13	11.30	0	27.42	42.46	3.62	54.85
AHX1	0	0	0.7997	0.07745	0.00	0	0.03	0.00	99.97	-88.95
AEX1	0	0	41.93	41.94	3.48	0	27.42	29.92	0.33	9.12
AEV	0	39.71	39.71	36.94	33.56	0	24.94	149.80	7.61	500.64
ABS	0	10.5	14.4	14.5	8.84	0	5.78	15.08	1.07	160.76
AP	2.106	0	2.106	2.276	0.61	0	25.33	38.55	21.74	52.19
AHX2	0	0	4.11	2.616	1.58	0	7.49	7.76	22.41	3.59
AEX2	0	0	9.322	9.328	3.21	0	7.49	11.43	0.18	52.69
total			4080	3990	1246	141	11.82	17.37	5.30	47.01

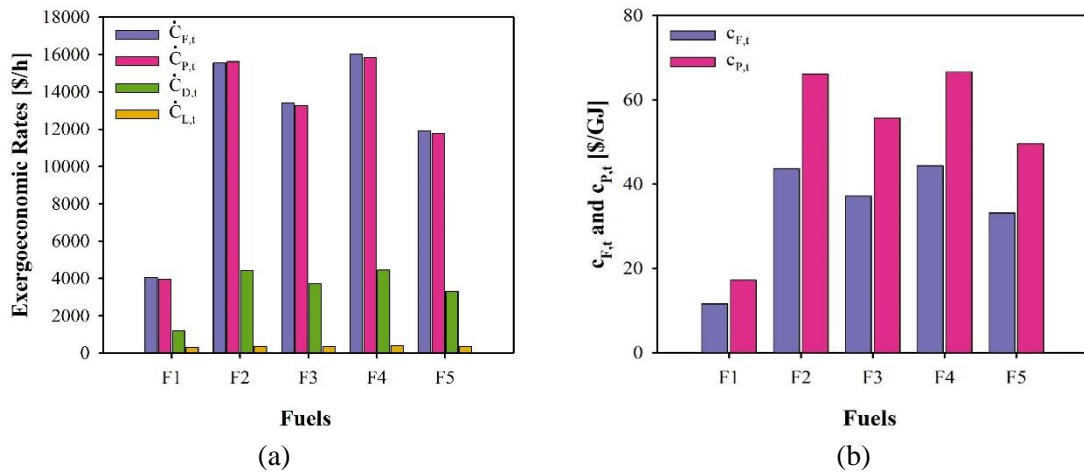


Figure 5.59 (a) Exergoeconomic rates and (b) specific exergy costs of the hybridized rail engine with respect to fuel blends

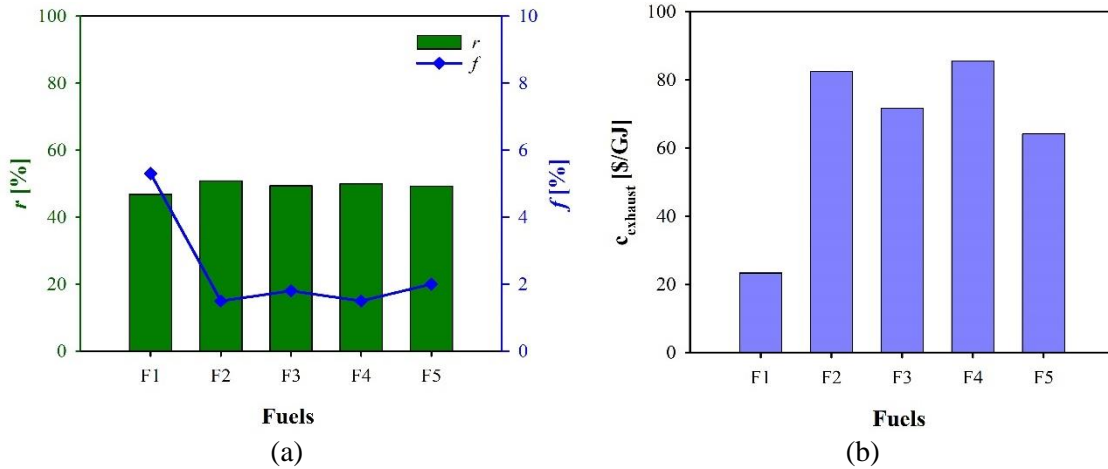


Figure 5.60 Exergoeconomic performance of a hybridized rail engine: (a) relative cost difference and exergoeconomic factor, and (b) specific exergy cost of exhaust

5.5.4 Results of Exergoenvironmental Analysis

The exergoenvironmental rates of streams are drawn using the Sankey diagram, as displayed in Figure 5.61, using fuel blend F1 (75% wt. methane and 25% wt. hydrogen) since b_f of this fuel blend is 5.44 mPt/MJ. The exergoenvironmental rates of fuels are 379 Pt/h entering the CC, 34 Pt/h entering the SOFC, and 119 Pt/h entering the PEMFC. Also, the total exergoenvironmental rates of exhaust gases are 61 Pt/h. In addition, the average exergoenvironmental rates of ARS is 19 Pt/h. Table 5.47 presents the component-related environmental impact. The total weight of the R-3 rail engine is 10944 kg. The material production, process and disposal are also presented in this table. The average of total EI is 253 mPt/kg. The component-related environmental impact, \dot{Y} , of this engine is 15.5 mPt/h, which is almost negligible compared to the rest of the analysis.

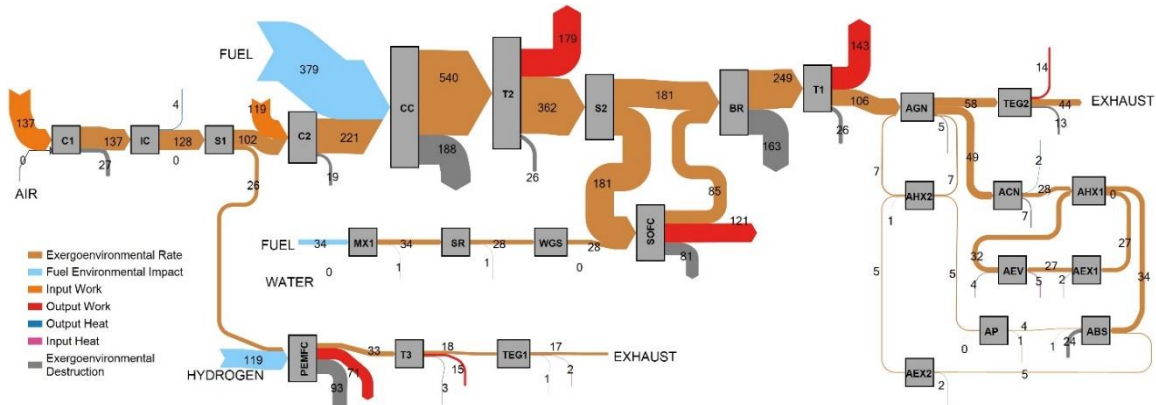


Figure 5.61 Sankey flowchart of exergoenvironmental rates [Pt/h]

Table 5.47 The component-related environmental impact results

#	Weight [kg]	Material Production [mPt/kg]	Material Processing [mPt/kg]	Material Disposal [mPt/kg]	Total EI [mPt/kg]	Total Y [mPt]	\dot{Y} [mPt/h]
C1	400	131	11.78	24	166.5	66,585	0.438
IC	150	91	12.05	24	127.0	19,049	0.125
S1	0	86	11.78	24	121.8	0	0
C2	400	131	12	24	166	66,585	0.438
CC	200	638	20	24	682	136,416	0.897
T2	800	104	12	24	140	111,810	0.735
S2	0	86	11.78	24	121.8	0	0
T1	300	104	12	24	140	41,929	0.276
PEMFC	1,056	279	22	24	325	342,971	2.255
T3	800	104	12	24	140	111,810	0.735
TEG1	50	88	19	24	130	6,505	0.043
MX1	0	86	11.78	24	121.8	0	0
SR	200	911	20	24	955	190,980	1.256
WGS	200	811	20	24	855	171,027	1.125
SOFC	512	274	22	24	320	163,906	1.078
BR	300	656	20	24	700	209,876	1.380
TEG2	100	88	19	24	130	13,010	0.086
AGN	480	92	12	24	128	61,349	0.403
ACN	1,140	91	12	24	127	145,157	0.954
AHX1	660	91	12	24	127	83,817	0.551
AEX1	0	86	11.78	24	121.8	0	0
AEV	2,076	91	12	24	127	263,343	1.732
ABS	360	91	12	24	127	45,666	0.300
AP	100	186	17	24	227	22,697	0.149
AHX2	660	91	12	24	127	83,817	0.551
AEX2	0	86	11.78	24	121.8	0	0
Total							15.51

The exergoenvironmental analysis is also presented in Table 5.48. The net exergoenvironmental rate due to work is 285 Pt/h, and due to the heat is 11.4 Pt/h. The total fuel and product exergoenvironmental rates are 2461.5 Pt/h and 2267.4 Pt/h, respectively, so the destruction exergoenvironmental rate becomes 689 Pt/h, but for the loss is 71 Pt/h. The total pollution formation environmental impact rate, \dot{B}^{PF} is -81.8 Pt/h, where the negative sign means the pollution, such as methane, carbon monoxide, and carbon dioxide, is removed by the existing components. In addition, the total environmental impact rate, \dot{B}^T , which is the summation of \dot{B}^{PF} , \dot{Y} , and \dot{B}_D , is 607.2 Pt/h.

The exergoenvironmental performance can be evaluated using specific environmental impact, relative environmental difference, and exergoenvironmental factor, as displayed in Table 5.49. The minimum specific environmental impact among the components is for intercooler (IC), which is 1.46 mPt/MJ for fuel and 0.61 mPt/MJ for

product, so the relative environmental difference -58% because the specific product environmental impact is less than that of the fuel.

Table 5.48 The exergoenvironmental analysis of R-3 rail engine components

#	\dot{B}_K^W	\dot{B}_K^Q	$\dot{B}_{F,K}$	$\dot{B}_{P,K}$	$\dot{B}_{D,K}$	$\dot{B}_{L,K}$	\dot{B}_K^{PF}	\dot{B}_K^T
Units	[mPt/h]	[mPt/h]	[mPt/h]	[mPt/h]	[mPt/h]	[mPt/h]	[mPt/h]	[mPt/h]
C1	137379	0	137379	137379	27286.6	0	0	27287
IC	0	4005	9595	4005	64.1	0	0	64
S1	0	0	127784	127791	0	0	0	0
C2	118968	0	118968	118969	18948	0	0	18949
CC	0	0	600405	540328	187921	0	-60078	127844
T2	178828	0	178828	178828	25779	0	0	25779
S2	0	0	361500	361497	0	0	0	0
T1	142853	0	142852	142853	26432	0	0	26433
PEMFC	71420	0	110996	71420	92743	0	0	92746
T3	15047	0	15047	15047	3383	70070	0	3383
TEG1	1560	0	1560	1560	1313	0	0	1313
MX1	0	0	33858	33858	809	0	0	809
SR	0	0	33858	28475	1295	0	-5384	-4087
WGS	0	0	28475	28492	138	0	16	155
SOFC	120737	0	124638	120737	81254	1402	0	81255
BR	0	0	265352	248996	163380	0	-16357	147025
TEG2	13936	0	13936	13936	12534	0	0	12534
AGN	0	0	55812	53908	5335	0	0	5336
ACN	0	1910	21091	1910	7288	0	0	7289
AHX1	0	0	515.7	2015	64	0	0	64
AEX1	0	0	27037	27037	2247	0	0	2247
AEV	0	4754	4754	-4756	4018	0	0	4020
ABS	0	694.5	38784	4686	23805	0	0	23806
AP	1272	0	1272	1272	369	0	0	369
AHX2	0	0	2193	2194	846	0	0	846
AEX2	0	0	4975	4975	1714	0	0	1714
Total			2461465	2267412	688966.4	71473	-81803	607179

The average of specific fuel environmental impact of the R-3 engine is 7.33 mPt/MJ, and the average specific product environmental impact is 10.15 mPt/MJ. Therefore, the relative environmental difference, r_b , is about 38.5% because the specific

product's environmental impact is greater than that of the fuel by 38.5%. Also, the exergoenvironmental factor of R-3 engine is 0.003% because the exergoenvironmental rate of destruction is much greater than that of component-related environmental impact rate, which equals 15.5 mPt/h compared to 689 Pt/h.

Table 5.49 The exergoenvironmental performance of R-3 rail engine components

K#	$b_{F,K}$	$b_{P,K}$	f_b	r_b
Units	[mPt/MJ]	[mPt/MJ]	[%]	[%]
C1	15.3	19.09	0.002	24.8
IC	1.46	0.6137	0.195	-58.0
S1	19.58	19.58	0	0
C2	9.711	11.55	0.002	18.9
CC	6.345	8.311	0.001	31.0
T2	8.311	9.711	0.003	16.8
S2	8.311	8.311	0	0
T1	12.47	15.3	0.001	22.7
PEMFC	4.05	15.84	0.002	291.1
T3	12	15.48	0.022	29.0
TEG1	12	76	0.003	533.3
MX1	5.375	5.506	0	2.4
SR	4.798	4.196	-0.031	-12.5
WGS	4.167	4.19	0.727	0.6
SOFC	5.191	14.44	0.001	178.2
BR	5.105	12.47	0.001	144.3
TEG2	12.47	123.7	0.001	892.0
AGN	11.11	11.86	0.008	6.8
ACN	17.68	2.447	0.013	-86.2
AHX1	17.68	78.83	0.858	345.9
AEX1	17.68	19.29	0	9.1
AEV	2.986	-19.29	0.043	-746.0
ABS	15.57	4.875	0.001	-68.7
AP	15.3	21.55	0.040	40.8
AHX2	3.995	6.504	0.065	62.8
AEX2	3.995	6.096	0	52.6
total	7.33	10.15	0.003	38.48

The exergoenvironmental analysis of R-3 rail engine is conducted using five fuel blends named as F1 to F5 by blending hydrogen with other hydrocarbon fuels, as presented before. The fuel blends have superessential effect on exergoenvironmental rates, as shown in Figure 5.62-a. The environmental impact of fuel blends is 5.44 mPt/MJ for F1, 7.88 mPt/MJ for F2, 5.95 mPt/MJ for F3, 11.33 mPt/MJ for F4, and 7.60 mPt/MJ for F5. Therefore, using F1 produces total fuel and product exergoenvironmental rates of 2.5 kPt/h and 2.3 kPt/h, respectively, making a destruction of 689 Pt/h. These values are the

minimum since environmental impact of F1 is the minimum. The maximum exergoenvironmental impact occurs using F4 to reach 6 and 5.5 kPt/h for fuel and product because F4 has the highest environmental impact. The average destruction environmental rate amongst all fuels is 1.1 kPt/h. However, the losses environmental impact is about 73 Pt/h. The specific environmental impact of R-3 engine is copying the trend of environmental impact, as shown in Figure 5.62-b. The hybrid SOFC-PEMFC-GT engine has specific fuel and product environmental impacts of 7.33 and 10.15 mPt/MJ using F1, 12.96 and 19.04 mPt/MJ using F2, 9.23 and 13.41 mPt/MJ using F3, 17.24 and 25.22 mPt/MJ using F4, and 11.38 and 16.46 mPt/MJ using F5, respectively.

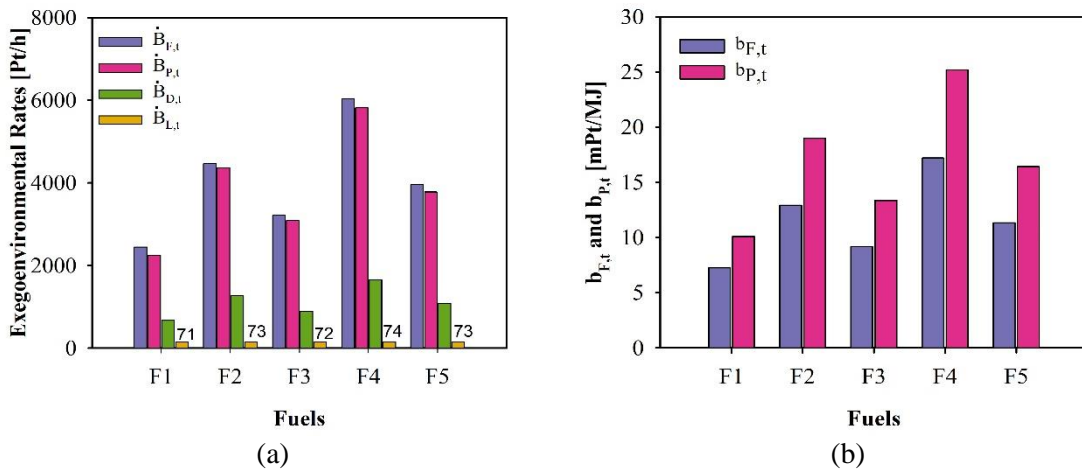


Figure 5.62 (a) Exergoenvironmental rates and (b) specific exergy costs of the hybridized rail engine with respect to fuel blends

The pollution formation and total environmental rates are displayed in Figure 5.63, which both count for the emissions, destruction, and component environmental impact. Figure 5.63-a shows the pollution formation environmental rates. There are two negative values using F1 (-81.8 Pt/h) and F5 (-12.7 Pt/h) because the combustion chamber, afterburner, SOFC, SR, and WGS remove methane to no methane emission from the system, in addition to the removal of carbon monoxide. However, the remaining fuel blends have an average of 8.4 Pt/h due to the removal of carbon monoxide and releasing carbon dioxide emissions. These values are low compared to using traditional fuels since their carbon emissions are higher than that of the selected fuels, as discussed before. Figure 5.63-b plotted the total environmental rates, where the maximum value is 1.7 kPt/h using F4 and the minimum value is 0.6 kPt/h using F1, which significantly count on the destruction exergoenvironmental rates.

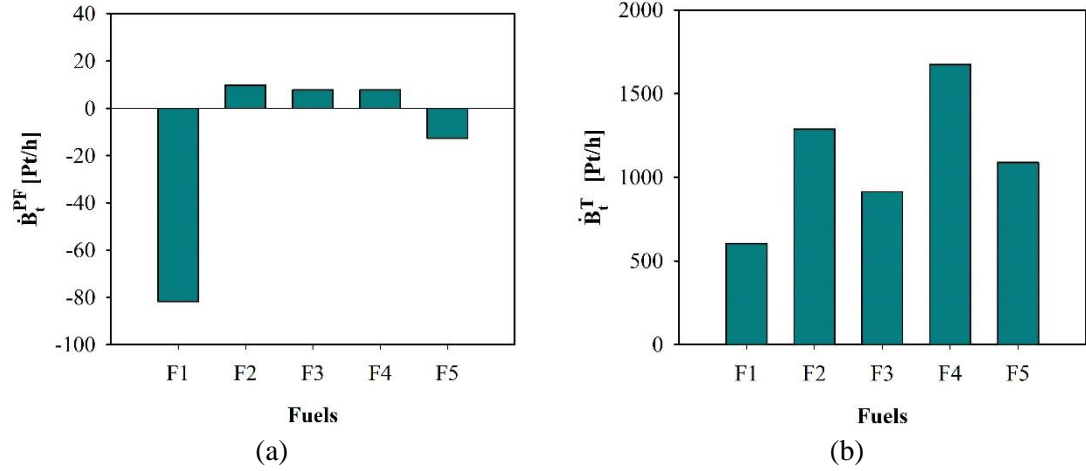


Figure 5.63 Pollution formation exergoenvironmental rates (a) and total environmental impact rates (b) of components with respect to fuel blends

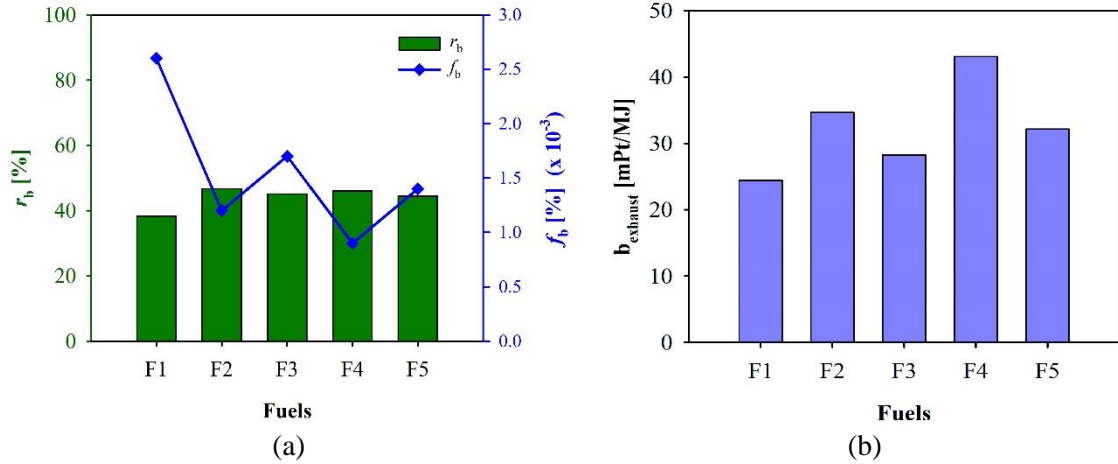


Figure 5.64 The exergoeconomic performance of a hybridized R-3 rail engine: (a) relative environmental difference and exergoenvironmental factor, and (b) specific exergy environmental impact of exhaust

The exergoenvironmental performance of using different fuel blends is explained in Figure 5.64. Figure 5.64-a shows the relative environmental difference, r_b , and exergoenvironmental factor, f_b . The r_b presents the minimum value of 38.5% using F1 and maximum value of 46.9 using F2 with an average of about 44% among the fuel selections. That means the specific product environmental impact increases by less than 50% more than the specific fuel environmental impact. Also, the f_b value shows the opposite pattern with respect to fuel blends since the f_b value is maximum of 0.0026 % using F1 and minimum value using 0.0009 % using F4 because of the destruction exergoenvironmental rates of this engine. Figure 5.64-b presents the specific environmental impact of exhaust

gases, which varies from 24.47 mPt/MJ (using F1) to 43.14 mPt/MJ (using F4). This can be interpreted as the proposed design of rail has less environmental impact in terms of fuel and product and exhaust, but the destruction exergoenvironmental rate is high but less than the traditional engine using traditional fuels.

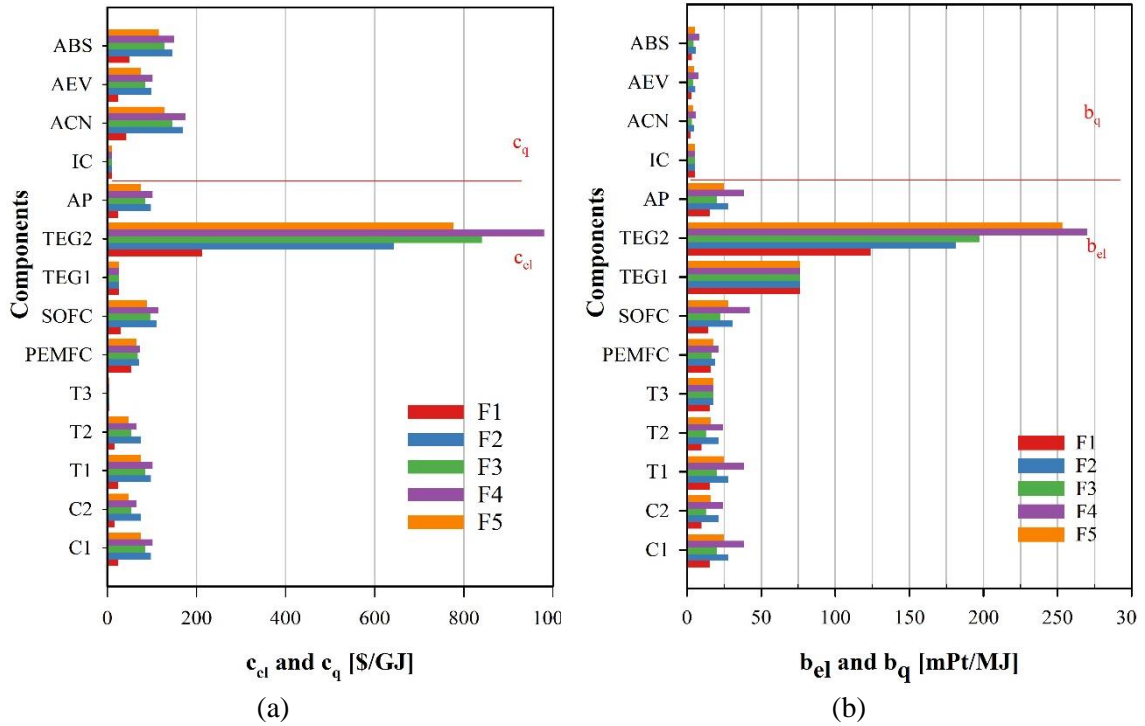


Figure 5.65 (a) Exergy cost and (b) environmental impact of electricity and heat of R-3 engine

Comparing the output and input electric power and heat of this hybrid rail engine, we present the specific exergy cost and specific environmental impact as shown in Figure 5.65. Figure 5.65-a presents the specific exergy cost of electricity and heat. The specific exergy cost of electricity for the compressor C1 and the pump AP equal to that of the turbine T1, which equals an average of 76.9 \$/GJ, and of the compressor C2 equals to that of the turbine T2, which equals an average of 52.0 \$/GJ. The turbine T3 has a specific exergy cost of 4.3 \$/GJ. Regarding the fuel cells, the SOFC has an average specific exergy cost of electricity of 87.5 \$/GJ, which is more than that of PEMFC (66.5 \$/GJ). The thermoelectric generators have two wide range of 26.7 \$/GJ and 696.0 \$/GJ for TEG1 and TEG2, respectively. For the heat, the rejected heat by the intercooler (IC), the condenser (ACN), and the absorber (ABS) have a specific exergy cost of heat of 2.0, 132.4 and 117.9 \$/GJ. The absorbed heat by the evaporator has 76.9 \$/GJ specific exergy cost.

On the other hand, the environmental impact of heat and electricity is given in Figure 5.65-b. Following the same auxiliary equations of electricity, the specific environmental impact of electricity for C1, T1, and AP is 25.2 mPt/MJ, and that for C2 and T2 is 16.7 mPt/MJ. The SOFC and PEMFC have a specific environmental impact of electricity of 27.5 and 18.1 mPt/MJ, respectively. Also, the thermoelectric generators TEG1 and TEG2 have 76.0 and 226.2 mPt/MJ, respectively. Furthermore, the rejected heat by IC, ACN, and ABS has a specific environmental impact of heat of 5.3, 4.1, and 5.5 mPt/MJ, respectively, while the absorbed heat by the evaporator AEV has 5.0 mPt/MJ of specific environmental impact of heat.

5.6 Results of System M-1

This section presents the results and discussion of the thermodynamic analysis, exergy analysis, exergoeconomic analysis, and exergoenvironmental analysis of the hybrid combined marine engine as written in the subsections below.

5.6.1 Results of Thermodynamic Analysis

The thermodynamic results of the hybrid marine engines with a fuel blend of 75% methane and 25% hydrogen are reported in [181]. There are three streams, namely: X# for the ICE engine, Y# for the GT engine, and Z# for the SOFC system. Also, there are three inlet fuel flows named Fs. The air mass flow rate of X1 incoming to the ICE is 14 kg/s, while that of Y1 entering the GT is 27 kg/s. The fuel flows at 0.67 kg/s (F1) to ICE, 0.97 kg/s (F2) to the GT, and 0.25 kg/s (F3) to the SOFC system. The ICE engine is a dual cycle combined with a turbocharger unit, which compresses the air from 303 K and 101.3 kPa to 344.4 K and 152 kPa. Then the air is intercooled to 284K to be pressurized in piston cylinders to 6840 kPa and continued to be compressed for burning with the fuel F1 at a constant specific volume to 1150 K and 9000 kPa. After that, the combustion continues at a pressure of 9000 kPa and 1830 K. Next, the exhaust gases are expanded by pushing the pistons down to 470 kPa and 1059 K. These gases are then cooled to 859K and then expanded in the turbine of the turbocharger to 105 kPa and 621 K, which will be cooled again using the TEG1 to 421 K.

The other GT engine is a hybrid Brayton cycle that uses air at 303 K and 101.3 kPa to be compressed twice to 405 kPa and 2025 kPa, and 626 K. Next, fuel enters at 0.97 kg/s and is combusted with air to 1170 K and 2025 kPa. After the exhausted gases are expanded at Y6 into 300 kPa and 789 K. This Y6 stream is distributed to SOFC with 60% mass flow rate and 40% to the afterburner (BR). Then, the exhausted gases are recombined in the BR for a fully combustion process to be expanded in the second turbine to 105 kPa and 819 K, which is cooled by TEG2 to 619 K. For the SOFC system, the fuel blend of 0.25 kg/s is mixed with steam of 0.4 kg/s to enter the SR at 300 kPa and 400 K and WGS at 600 K and 300 kPa, then to the SOFC at 1073 K and 300 kPa.

Table 5.50 The detailed performance of system component.

#	\dot{Q} [kW]	\dot{W} [kW]	$\dot{E}x_D$ [kW]	$\eta_{th} (\eta_e)$ [%]	ψ [%]
C0	0.0	648.4	115.7	81.0	82.2
C1	0.0	9714.0	1280.9	81.0	86.8
C2	0.0	4943.8	784.8	81.0	84.1
C3	0.0	7546.1	1084.2	81.0	85.6
T0	0.0	4055.0	696.3	81.0	85.4
T1	0.0	15200.5	2241.6	81.0	87.2
T2	0.0	6974.7	1092.7	81.0	86.5
T3	0.0	12650.2	2012.7	81.0	86.3
AC	851.6	0.0	594.7	100.0	48.3
CPHA	14950.8	3157.4	5895.1	21.1	91.4
IC	2216.3	0.0	2576.0	100.0	58.4
R1	3997.6	0.0	6451.2	100.0	57.6
TEG1	3583.3	220.0	1290.7	6.1	6.7
TEG2	7350.3	352.5	3935.5	4.8	5.0
BR	4034.6	0.0	7024.4	83.0	74.0
CC	37650.0	0.0	72995.6	64.5	31.0
CVHA	37599.2	0.0	66548.6	100.0	20.4
SOFC	12134.3	5210.4	7330.1	42.9 (88.3)	59.5
SR	3486.8	0.0	774.2	23.2	53.5
WGS	155.6	0.0	17.8	15.8	22.7
MX1	0.0	0.0	103.8	100.0	99.4
MX2	0.0	0.0	233.6	100.0	99.0
SP1	0.0	0.0	0.0	100.0	100.0

The performance of components and processes is described in Table 5.50. The compressor power is a minimum of 648 kW for C0 and a maximum of 9714 kW for C1, while the power of turbines varies from 4055 kW to 15200 kW. The combustion heat ranges from 37650 kW for CC to 4034 kW for BR. The heat addition of ICE is 37599 kW for a constant specific volume process (CVHA) and 14950 kW for a constant pressure

process (CPHA). The SOFC system requires heat addition of 12134 kW of SOFC unit and heat rejection of 3486 kW of SR and 155 kW of WGS. The TEG1 and TEG2 use heat rejection of 3583 kw and 7350 kW, respectively and provide 220 kW and 353 kW, respectively. As shown in the table, the highest exergy destruction is 73 MW for CC and 67 MW for CVHA due to the huge temperature difference compared to the standard conditions and the chemical reaction of the combustion process. However, the lowest exergy destruction rates are 0 kW for a splitter (SP1), 18 kW for WGS, and 104 kW for a mixer (MX1).

Table 5.51 The performance of combined engines and overall system

Subsystem	\dot{W}_n [kW]	\dot{Q}_a [kW]	\dot{Q}_r [kW]	$\dot{E}x_a^Q$ [kW]	$\dot{E}x_r^Q$ [kW]	η [%]	ψ [%]
ICE	12050.5	52550.0	4849.2	42508.9	4253.2	25.3	31.5
TEG1	220.0	0.0	3583.3	0.0	3285.3	6.1	6.7
<i>net-ICE</i>	12270.5	52550.0	8432.5	42508.9	7538.5	27.8	35.1
GT	7135.0	41684.6	2216.3	30916.4	1918.3	18.1	24.6
SOFC	5210.4	8491.9	0.0	7972.3	0.0	42.9	59.5
TEG2	352.5	0.0	7350.3	0.0	7052.3	4.8	5.0
<i>net-GT</i>	12697.9	50176.5	9566.6	38888.7	8970.6	31.3	42.4
Overall	24968.4	102726.5	17999.1	81397.6	16509.1	29.5	38.5

These components and processes are combined into subsystems, which are analyzed in Table 5.51. The ICE engine has a net power of 12050 kW using the methane and hydrogen blend, with a heat addition of 52550 kW and a heat rejection of 4849 kW. This ICE engine has an energetic and exergetic efficiency of 25.3% and 31.5%, respectively. If the TEG1 is attached to the exhaust pipeline, it provides 220 kW with a energetic and exergetic efficiency of 6%. Therefore, the hybrid ICE engine can provide a total of 12270 kW and has an energetic efficiency of 28% and an exergetic efficiency of 35%. The second engine is the GT hybridized with a fuel cell of SOFC. The GT provides a net power of 7135 kW, while it requires a heat of 41684 kW and rejects some of 2216 kW, so its performance is 18% and 24.6% of energetic and exergetic efficiencies, respectively. The SOFC system generates a power of 5120 kW by using a net heat addition of 8491 kW with energetic and exergy efficiencies of 42.9% and 59.5%, respectively. Also, the exhaust gases have a rejected heat of 7350 kW, which is converted to electricity of 352.5 kW by using TEG2 with an efficiency of 5%. This second engine has a net power of 12697.9 kW, the energetic efficiency of 31.3%, and an exergetic efficiency of 42.4%. The

two combined engines have a net power of 24968 kW, the energy efficiency of 29.5% and exergy efficiency of 38.5%.

(a) *Effect of fuel blends on ICE:*

Five fuel blends are selected and named F1 to F5, as mentioned earlier. The effect of fuel blends is displayed in Figure 5.66. The ICE power is a maximum of 13030 kW for F2 and a minimum of 12050 kW for F1, as shown in Figure 5.66-a. The added heat reaches its maximum of 56314 kW for F4 and a minimum of 50363 kW for F3. The rejected heat is from the aftercooler (AC) and cooling water jacket (R1) reaching its maximum value of 5019 kW for F2 and a minimum of 4033 kW for F3. The net heat has an average of 48598 kW, as shown in Figure 5.66-b.

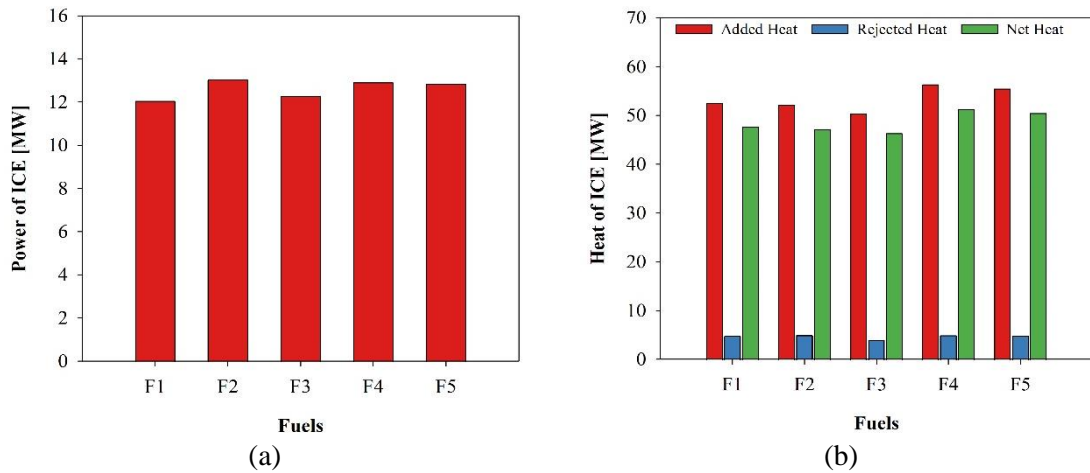


Figure 5.66 (a) Power and (b) heat of the ICE processes

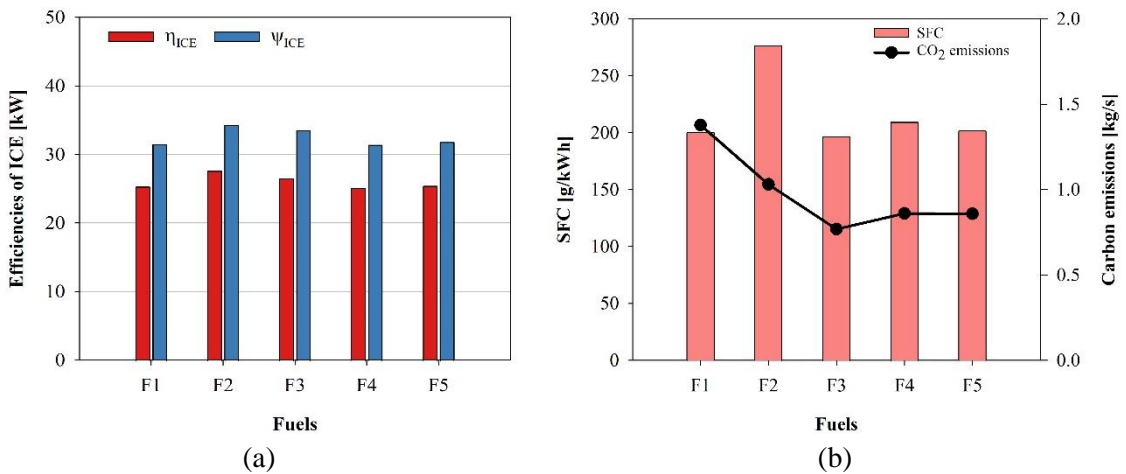


Figure 5.67 (a) ICE Efficiencies and (b) specific fuel consumption (SFC) and carbon emissions.

Therefore, the ICE has an energetic efficiency ranging from 25.1% (F4) to 27.6% (F2), and an exergetic efficiency of 31.4% to 34.3%, as shown in Figure 5.67-a. The specific fuel consumption (SFC) is 200 g/kWh for F1, 276 g/kWh for F2, 197 g/kWh for F3, 209 g/kWh for F4, and 202 g/kWh for F5. Meanwhile, the carbon emission is high, about 1.38 kg/s for F1 and 1.03 kg/s for F2, and below 1 kg/s for the remaining fuel blends, as shown in Figure 5.67-b.

(b) Effect of fuel blends on GT:

The GT engine is also analyzed using five sustainable fuel blends, as shown in Figure 5.68 and 7. The net power of the GT without including the SOFC system is a minimum of 7135 for F1 and a maximum of 8007 kW for F2, as shown in Figure 5.68-a, while the input heat from the CC is about 10 times that of BR reaching its maximum value of 41506 kW using F2 and its minimum value of 37020 kW using F4, as shown in Figure 5.68-b. Also, the input heat of BR has an average of 4140 kW. The rejected heat of the intercooler IC has a constant value of 2216 kW for all fuels. Thus, the net heat is a minimum of 38434 kW using F5 and a maximum of 42272 kW using F2.

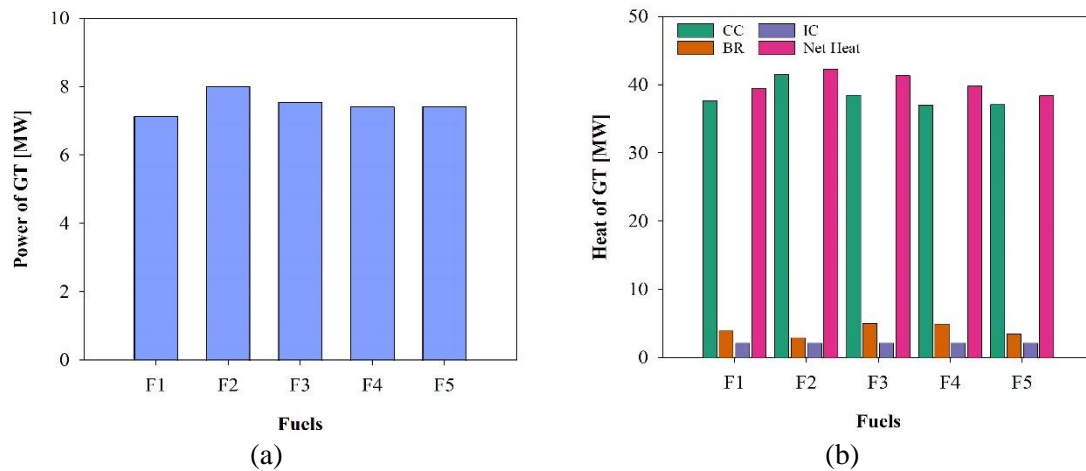


Figure 5.68 (a) Power and (b) heat of GT engine with respect to fuel blends

Therefore, the efficiencies of GT are an average of 18.6% of energetic efficiency and 25.2% of exergy efficiency, as shown in Figure 5.69-a. Since the fuel mass flow rate of F2 stream is increased by 46% compared to F1 stream of the ICE engine and the power is less than that of the ICE, the SFC is also increased by about 150% to reach its maximum value of 719 g/kWh for F2 and its minimum of 486 g/kWh using F4, as shown in Figure

5.69-b. However, using F1 and F2 emit carbon dioxides at a rate of 1.4 and 1.5 kg/s, respectively, while the remaining fuel blends emit around 0.5 kg/s.

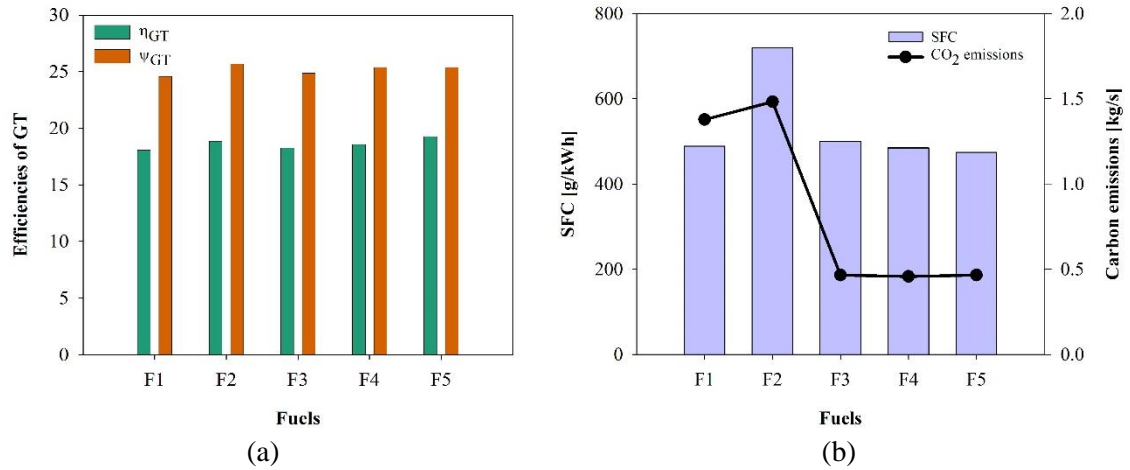


Figure 5.69 (a) Efficiencies and (b) SFC and carbon emissions of GT engine

(c) Effect of fuel blends on SOFC:

The SOFC system has an SR and WGS directly attached to it, but they are represented as separate reactors in the Aspen Plus for simulation purposes. The SR and WGS reactors release heat since most of the reactions are exothermic. The released heat from the SR is 38887 kW, 1354 kW, 777 kW, 390 kW, and 1189 kW using F1 to F5, respectively, to produce carbon monoxide gas, while the average of the released heat from WGS is 253 kW in order to produce hydrogen gas, as shown in Figure 5.70-a. The SOFC unit electrochemically reacts with the hydrogen gas from the WGS (Z3 stream) and oxygen gas from the GT engine (Y7) to generate electric voltage. The cell voltage varies from 0.34 V (F1) to 0.45 V (F4), while the loss voltage due to activation, concentration, and ohmic losses has an average of 0.044V. Thus, the electric efficiency of SOFC varies from 88.5% (F1) to 91.3% (F4), as shown in Figure 5.70-b. Therefore, the net heat of the SOFC system varies from 9259 kW using F2 to 12134 kW using F1, and the electric power ranges from 4791 kW using F2 to 6915 kW using F3 fuel blend, as in Figure 5.70-c.

The amount of hydrogen entering the SOFC unit is a maximum of 80.5 mol/s using F1 and F3, and a minimum of 67.5 mol/s using F2. Because of that, the number of stacks is more than 30 stacks having a cell area of 0.7 cm² and 100 cells; the minimum and maximum stacks are 31 (F2) and 37 stacks (F1 and F3), as graphed in Figure 5.70-d. The average of energetic and exergetic efficiencies of only SOFC units without the SR and

WGS are 48.8% and 74.5%, respectively, but these values have increased to an average of 62.2% and 77%, respectively, as illustrated in Figure 5.70-e. This SOFC system has an SFC value of 173 g/kWh (F1), 225 g/kWh (F2), 156 g/kWh (F3), 157 g/kWh (F4), and 144 g/kWh (F5). Also, it releases carbon emissions of more than 1 kg/s for F1 and F2 and less than 0.75 kg/s for the remaining, as shown in Figure 5.70-f.

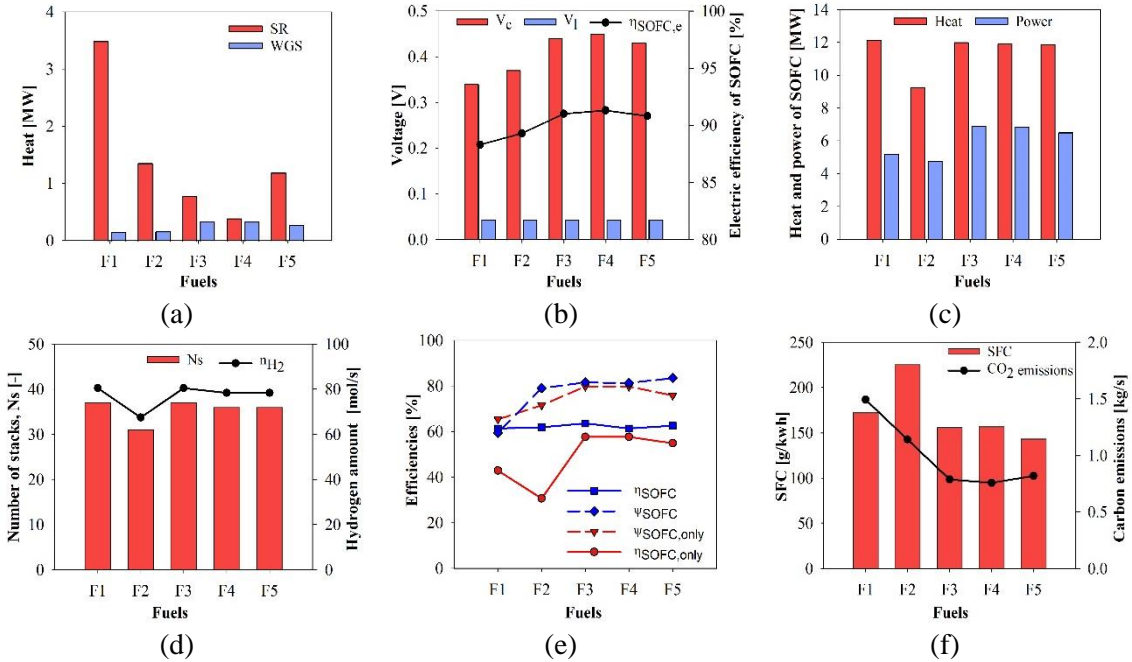


Figure 5.70 Performance of SOFC with respect to fuel blends: (a) reforming heat, (b) Cell and loss voltage, (c)) Heat and power of SOFC, (d) Number of stacks and hydrogen amount, (e) Efficiencies of SOFC, and (f) SFC and carbon emissions

(d) Performance of overall engines:

The performance of the hybrid GT and ICE engines is presented in Figure 5.71. The Aframax oil tanker can be operated with a power of 10400 kW. In this research, the proposed design is to add a hybridized GT engine and attach the exhaust pipes of two engines with TEG modules each. As shown in Figure 5.71-a, the net power of ICE, including TEG 1 modules using five fuel blends, has an average of 12093 kW, and the maximum net power is 13530 kW for F2, while the net power of the GT engine, including the SOFC system and TEG2 modules, has a higher average of 13943 kW and maximum power is produced by using F3, F4, and F5. Figure 5.71-b shows the energetic and exergetic efficiencies of the hybridized ICE and GT and the overall engine. The maximum performance of the hybrid ICE is obtained using the F2 to reach 34% energetic efficiency

and 44% exergetic efficiency, while the minimum performance is found using F1 and F4 to be about 27.6% energetic efficiency and 35.5% exergetic efficiency. For the hybridized GT engine, the minimum and maximum performances are 28% and 41% for F2 and 33.5% and 47.8% using F4 and F5 for energetic and exergetic efficiencies, respectively. The overall performance is obtained by dividing the total net power by the total net heat of two engines. The maximum performance is given by using the fuel blend F3 since the energetic efficiency is 31.2% and the exergetic efficiency is 42%. However, the minimum performance is achieved by the fuel blend of F1 to be 29.5% of energetic efficiency and 38.5% of exergy efficiency.

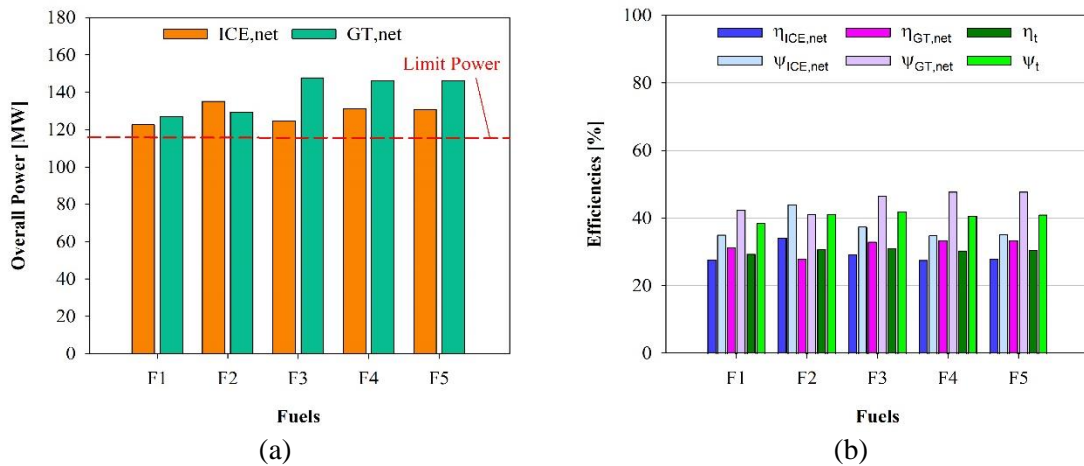


Figure 5.71 (a) Overall power and (b) Overall efficiencies of hybrid ICE and GT engines

The arrangement of engines is described in Figure 5.72. The old configuration is one ICE engine attached to the gearbox with generator sets or an emergency generator. The new arrangement uses two marine gas turbines of 4.6MW to fulfill the required GT output with less engine weight (each of 460 kg). That means the design of the net power of the GT is split into half; each has a small GT engine as MT7, and half of the SOFC modules are attached to a generator. This arrangement is useful to maintain the ship balance in the engine room. Each hybrid GT is attached to a coupling and a gearbox to the main ICE engine. This arrangement is operated in a way to connect or detach the hybrid GT engine with ICE based on the captain's decision.

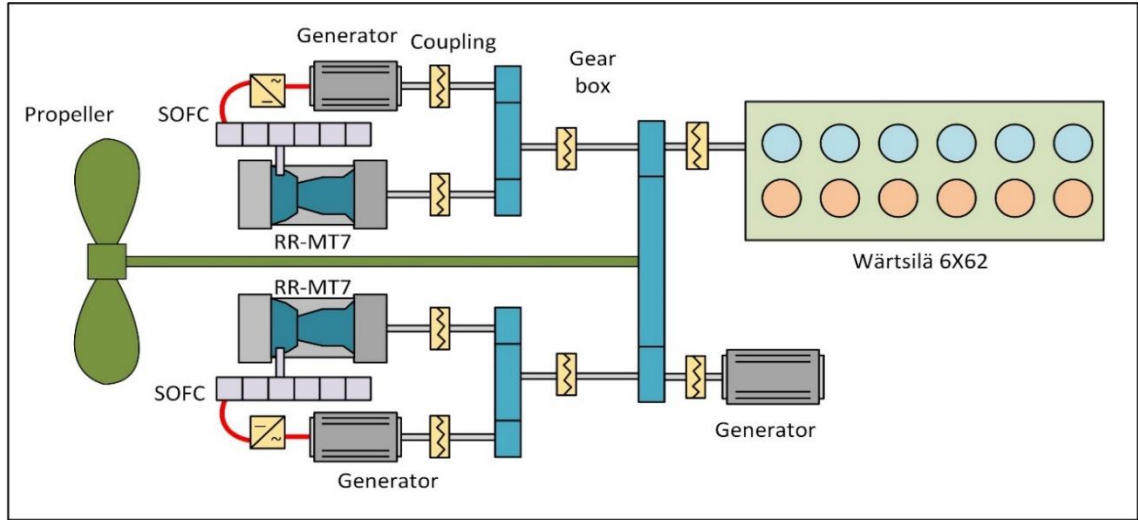


Figure 5.72 The arrangement of two engine systems in the Aframax engine room

After presenting the performance of the overall engines, it is worth noting that the traditional ICE marine engine is operated using an MGO-DMA fuel. Taking into consideration of pressure and temperature of each state and air mass fuel rate, the two ICE using an MGO-DMA fuel have a total power of 21048 kW for maximum engine speed using a total fuel mass flow rate of 1.90 for two ICE engines. The SFC of the traditional engine is 325 g/kWh, and the two engines produce carbon emissions of 6.02 kg/s. Also, this traditional marine engine has a totally energetic and exergetic efficiency of 22.9% and 29%, respectively. In a comparison of the presented design engines with traditional ones, the power of hybridized engines is a maximum of 27773.2 kW using F4 with an increase of 32%, and its minimum of 24968 kW by an increase of 18.6% using F1. The SFC_t of the total engines is a minimum of 272.5 g/kWh, which is decreased by 16.1% and a maximum of 394 g/kWh which is increased by 21.3% compared to the traditional fuel. In addition, the overall energetic (η_o) and exergetic (ψ_o) performance is increased by an average of 33.4% and 40.2%, respectively. Moreover, the carbon emissions are reduced using these fuel blends by an average of 54%, and a maximum reduction is occurred using F3 and F5, as shown in Table 5.52.

In closing, the best fuel blend option is to choose F5 because it helps increase the total power to 27719.5, which is about 31.7%, with almost the same fuel mass flow rate of 1.96, but the SFC is the minimum of 254.5 g/kWh and 61.3% of carbon reduction and 34% and 41.5% increase in the energetic and exergetic performance. It is not recommended to

add another ICE engine besides the existing one for many reasons: the total engine weight will be doubled to 754 tons instead of 377 tons, and the performance will be the same. However, increasing the power and performance can be easily achieved by using two small marine GT, such as MT7 attached to the SOFC stacks on both sides of the propeller to maintain the ship's balance. This will only increase the total weight to less than 1%, as shown in Table 5.52, since one GT engine has a weight of 459 kg and one stack of SOFC has a weight of 62 kg.

Fuels	\dot{W}_o [kW]	\dot{m}_f [kg/s]	SFC _t [g/kWh]	CO _{2,t} [kg/s]	η_o [%]	ψ_o [%]	Weight [kg]
MGO	21047.7	1.90	325.0	6.02	22.9	29.0	754000
F1	24968.4 (↑18.6)	1.89	272.5 (↓16.1)	3.89 (↓35.4)	29.5 (↑28.8)	38.5 (↑32.7)	379815 (↑0.87)
F2	26494.6 (↑25.9)	2.90	394.0 (↑21.3)	2.99 (↓50.4)	30.9 (↑34.9)	41.1 (↑41.8)	379443 (↑0.77)
F3	27277.9 (↑29.6)	2.02	266.6 (↓18.0)	2.32 (↓61.6)	31.2 (↑36.3)	42.0 (↑44.7)	379815 (↑0.87)
F4	27773.2 (↑32.0)	2.05	265.7 (↓18.2)	2.35 (↓61.0)	30.4 (↑33.1)	40.7 (↑40.4)	379691 (↑0.84)
F5	27719.5 (↑31.7)	1.96	254.5 (↓21.7)	2.33 (↓61.3)	30.7 (↑34.1)	41.0 (↑41.4)	379691 (↑0.84)

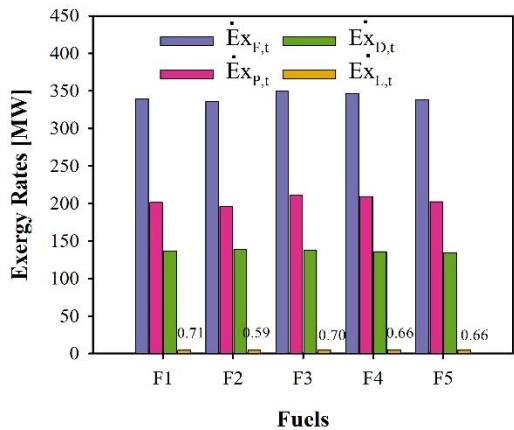
The exergy analysis is based on fuel and product principal, which is conducted on the M-1 hybrid combined marine engine. The exergy rates of streams are displayed for M-1 engine, as shown in Figure 5.73, using the F1 (75% wt methane and 25% wt hydrogen fuel blend).

Figure 5.73 The Sankey flowchart of exergy rates of M-1 engine [kW]

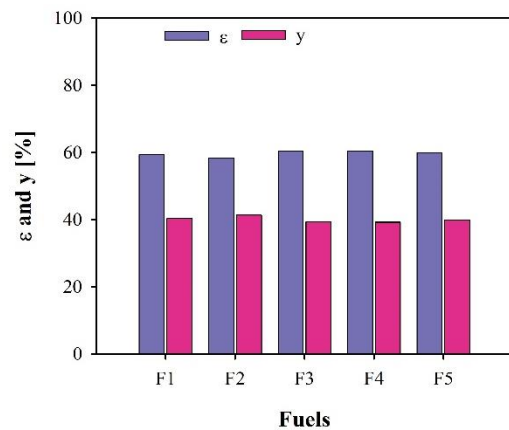
about 30%. The overall fuel and product exergy rates are 339.4 MW and 202 MW, respectively. This makes the destruction exergy rate of the engine to be 137.4 MW. However, the losses exergy rate is 708 kW. This engine has an exergetic efficiency of 59.5%, which is greater than the normal exergy rate of 39%, and destruction ratio of 40.5%.

Table 5.53 Exergy performance of M-1 marine engine

#	\dot{W}_K	\dot{Q}_K	$\dot{Ex}_{F,K}$	$\dot{Ex}_{P,K}$	$\dot{Ex}_{D,K}$	$\dot{Ex}_{L,K}$	ε	y	y^*
Units	[kW]	[kW]	[kW]	[kW]	[kW]	[kW]	[%]	[%]	[%]
ICE	12051	0	42568	12051	30518	0	28.31	8.99	22.20
R1	0	3998	0	0	0	0	0.00	0.00	0.00
AC	0	851.6	0	0	0	0	0.00	0.00	0.00
TEG1	220	3583	1511	220	1291	0	14.56	0.38	0.94
C2	4944	0	4944	4159	784.8	0	84.12	0.23	0.57
IC	0	2216	3780	3623	157.7	0	95.85	0.05	0.11
C3	7546	0	7546	6462	1084	0	85.63	0.32	0.79
CC	0	37650	105804	32808	72996	0	31.01	21.51	53.11
T3	12650	0	14663	12650	2013	0	86.27	0.59	1.46
SP1	0	0	18145	18145	0	0	100.00	0.00	0.00
MX2	0	0	24431	24198	233.6	0	99.05	0.07	0.17
BR	0	4035	27054	20029	7024	0	74.03	2.07	5.11
T2	6975	0	8067	6975	1093	0	86.46	0.32	0.80
TEG2	352.5	7350	4288	352.5	3936	0	8.22	1.16	2.86
MX1	0	0	17328	17224	103.8	0	99.40	0.03	0.08
SR	0	3487	19002	18887	115	0	99.39	0.03	0.08
WGS	0	155.6	18965	18827	138.8	0	99.27	0.04	0.10
SOFC	5351	12134	21305	5351	15954	708	25.12	4.70	11.61
Total			339401	201961.5	137442.7	708	59.51	40.50	100.00



(a)



(b)

Figure 5.74 The exergy analysis of M-1 marine engine based on fuel blends: (a) fuel, product, destruction, and losses exergetic rates, and (b) exergetic efficiency and exergy destruction ratio

The exergy analysis is conducted on marine engine with different fuel blends named as F1 to F5. Using these fuels does a slight change on exergy rates and exergy performance, as shown in Figure 5.74. Figure 5.74-a presents the effect of fuels on exergy rates. The average of fuel and product exergy rates are 342.3 and 204.8 MW, respectively. Also, the destruction and losses exergy rates are 137.5 MW and 0.7 MW, respectively. This results the average exergetic efficiency to be 59.8 % and destruction ratio to be 40.2%, as displayed Figure 5.74-b.

5.6.3 Results of Exergoeconomic Analysis

The exergoeconomic analysis is applied on the hybrid combined marine engine using the F1. The fuel cost is 7.15 \$/GJ. The exergoeconomic rates of the streams are plotted in Figure 5.75 using Sankey flowchart. The fuel exergy cost rates are 1203 \$/h entering ICE engine, 1742 \$/h entering the CC, and 441 \$/h entering the fuel cell. The cost rates of combined exhaust gases are 821 \$/h.

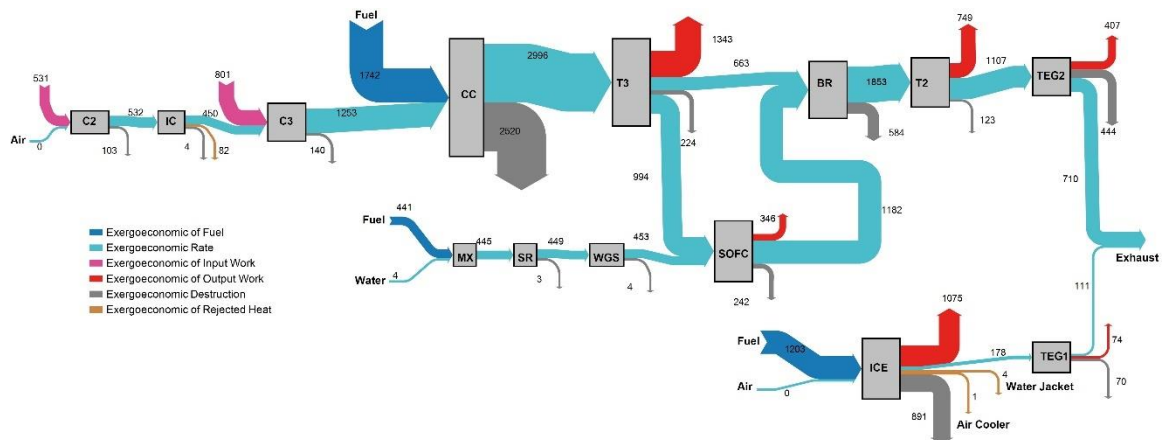


Figure 5.75 The Sankey flowchart of exergoeconomic rates of M-1 engine

The components' costs are listed in Table 5.54. The highest prices are assigned for the ICE (\$ 2.6M) and SOFC (\$ 4.3M), while the total engine cost based on their corresponding year of cost equations is \$8.3M. However, after normalizing the prices of each component to CEPCI of May 2022, the total engine price becomes \$15.7M. Therefore, the total leveled cost rate of this marine engine is 227.6 \$/h.

The exergoeconomic analysis is presented in Table 5.55. The net of exergy cost rate due to the net power of the engine is 2662 \$/h, and the net exergy cost rate of required heat is 87.6 \$/h. The fuel and product exergy cost rates are 14.9K \$/h and 15.1K \$/h,

respectively. The destruction exergy cost rate is 5.4K \$/h, but the losses exergy cost rate is 46 \$/h. This analysis produces specific fuel and product exergy cost of 12.22 and 20.78 \$/GJ, respectively. This results the exergoeconomic factor to be 4.06 % because the destruction exergoeconomic rate is 24 folds of the total levelized cost rate. In addition, the relative cost difference is 70.10%.

Table 5.54 The components' costs of M-1 marine engine

#	C_K [\$]	Z_K [\$] (2022)	\dot{Z}_K [\$/h]
ICE	2,553,000	3,850,000	55.71
TEG1	220,000	454,831	6.581
C2	47,814	98,851	1.43
IC	22,495	47,092	0.6814
C3	69,388	143,454	2.076
CC	51,620	106,721	1.544
T3	122,881	254,046	3.676
SP1	0	0	0
MX2	0	0	0
BR	263,847	545,481	7.893
T2	69,672	144,040	2.084
TEG2	352,500	728,763	10.55
MX1	0	0	0
SR	130,393	272,971	4.0
WGS	151,871	317,934	4.6
SOFC	4,239,000	8,764,000	126.8
Total	8,294,481	15,728,184	227.6

Table 5.55 The exergoeconomic analysis of M-1 marine engine components

#	\dot{C}_K^W [\$/h]	\dot{C}_K^Q [\$/h]	$\dot{C}_{F,K}$ [\$/h]	$\dot{C}_{P,K}$ [\$/h]	$\dot{C}_{D,K}$ [\$/h]	$\dot{C}_{L,K}$ [\$/h]	$c_{F,K}$ [\$/GJ]	$c_{P,K}$ [\$/GJ]	f [%]	r [%]
ICE	1075	5.23	1019	1075	890.9	0	6.65	24.78	5.89	272.64
TEG1	73.97	0	67	74	70.2	0	12.39	93.40	8.57	653.88
C2	530.6	0	531	532	102.7	0	29.81	35.53	1.37	19.19
IC	0	82.41	82	82	4.2	0	6.01	6.32	14.08	5.20
C3	801.1	0	801	803	140.3	0	29.49	34.52	1.46	17.07
CC	0	0	2995	2996	2519.9	0	7.86	25.37	0.06	222.60
T3	1343	0	1339	1343	224.2	0	25.37	29.49	1.61	16.26
SP1	0	0	1657	1657	0	0	25.37	25.37	0	0.00
MX2	0	0	1845	1845	21.5	0	20.98	21.18	0.00	0.96
BR	0	0	1845	1853	584.2	0	18.94	25.70	1.33	35.66
T2	748.5	0	746.4	749	123.3	0	25.70	29.81	1.66	15.98
TEG2	407.3	0	396.7	407	444.1	0	25.70	320.96	2.32	1148.96
MX1	0	0	444.8	449	3.2	0	7.13	7.17	0.00	0.60
SR	0	0	444.8	449	3.3	0	6.50	6.60	54.61	1.49
WGS	0	0	448.7	453	4.0	0	6.57	6.69	53.46	1.77
SOFC	346.3	0	265.3	346	242.3	46	3.46	17.98	34.36	419.71
Total			14926	15109	5378.3	46	12.22	20.78	4.06	70.10

The exergoeconomic analysis is also conducted with respect to the fuel blends, as shown in Figure 5.76. using difference fuel blends has significantly affected the exergoeconomic analysis. The fuel exergy cost rates are 14928 \$/h, 57992 \$/h, 53186 \$/h, 62113 \$/h and 46022 \$/h for F1 to F5 in the same order, respectively. The product exergy cost rates are 15109 \$/h for F1, 58107 \$/h for F2, 53323 \$/h for F3, 62223 \$/h for F4, and 46166 \$/h for F5. The destruction exergy cost rate is the minimum at 5378 \$/h for F1 and the maximum at 22061 \$/h for F4. The loss exergy cost rate is averaged at 98 \$/h, as presented in Figure 5.76-a. The specific fuel and product exergy costs are 12.2 \$/GJ and 20.8 \$/GJ for F1, 47.9 \$/GJ and 82.1 \$/GJ for F2, 42.1 \$/GJ and 69.8 \$/GJ for F3, 49.8 \$/GJ and 82.3 \$/GJ for F4, and 37.7 \$/GJ and 63.1 \$/GJ for F5, as shown in Figure 5.76-b.

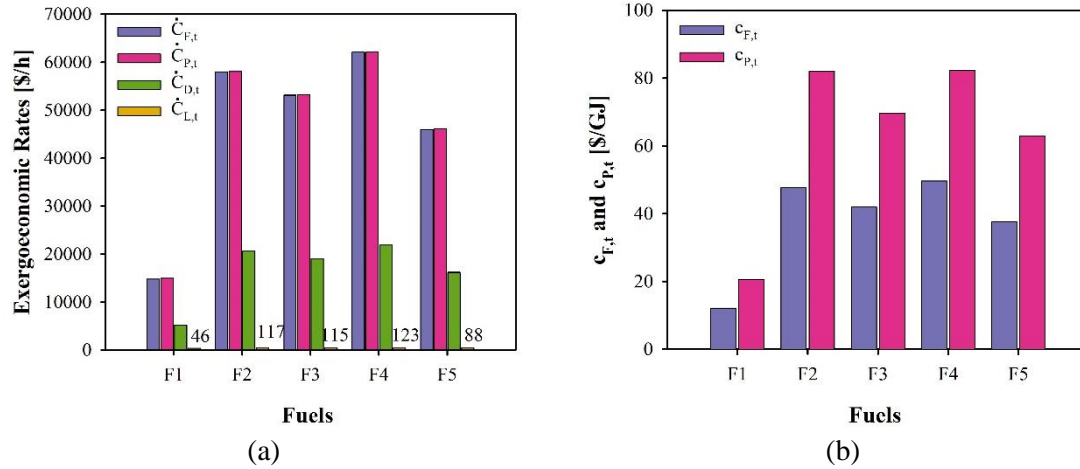


Figure 5.76 (a) Exergoeconomic rates and (b) specific exergy costs of the hybridized rail engine with respect to fuel blends

The exergoeconomic performance can be evaluated by exergoeconomic factor and relative cost difference, and specific exergy cost of exhaust as illustrated in Figure 5.77. Figure 5.77-a provides the average of relative cost difference of 68% because the specific product exergy cost is greater than that the fuel by about 1.7 times. The exergoeconomic factor is the maximum of 4.1% for F1 and minimum of 1% using F4. The combined exhaust gases from the ICE engine and hybrid GT engine have a minimum and maximum specific exergy cost of 38.09 \$/GJ (of F1) and 154.92 \$/GJ (of F4), and an average of 115.24 \$/GJ, as plotted in Figure 5.77-b.

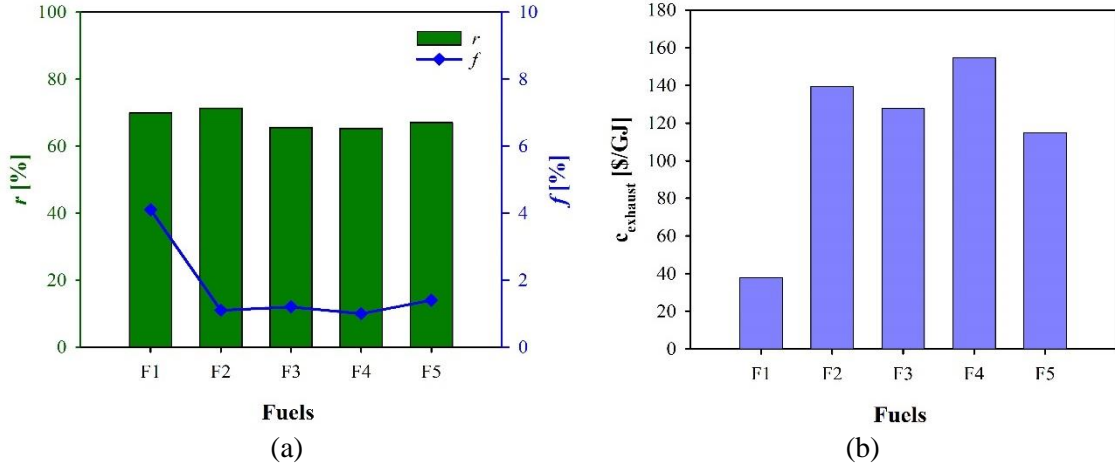


Figure 5.77 The exergoeconomic performance of a hybridized rail engine: (a) relative cost difference and exergoeconomic factor, and (b) specific exergy cost of exhaust

5.6.4 Results of Exergoenvironmental Analysis

The exergoenvironmental analysis is conducted on the hybrid combined marine engine using F1, which has an environmental impact of 5.44 mPt/MJ. The exergoenvironmental rates of streams are plotted using Sankey diagram in Pt/h, as illustrated in Figure 5.78. The fuel streams have exergoenvironmental rates of 915 Pt/h, 1325 Pt/h, and 335 Pt/h entering ICE, CC, and SOFC, respectively. The total exhaust gases have an exergoenvironmental rate of 507 Pt/h. Also, the total pollution formation environmental rate of this engine is reduced by 507 Pt/h.

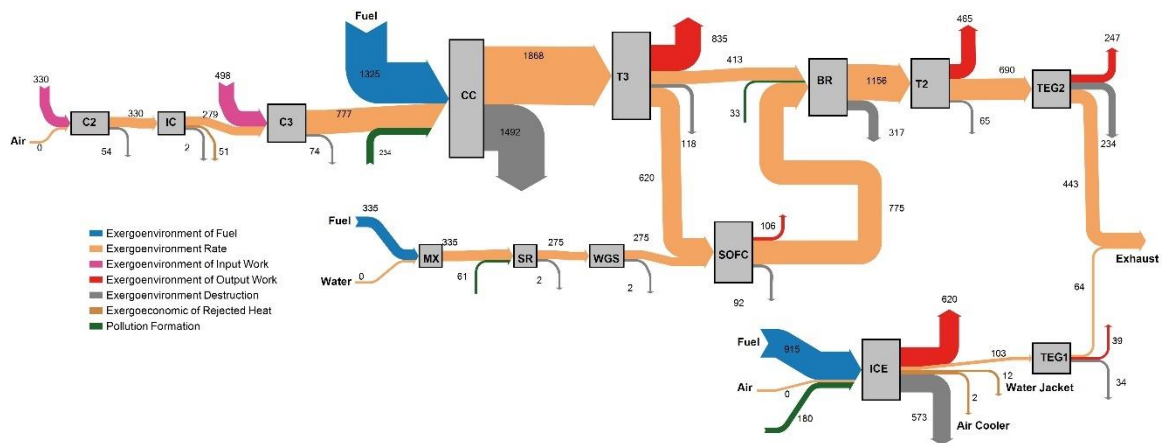


Figure 5.78 The Sankey flowchart of exergoenvironmental rates of M-1 engine [Pt/h]

This analysis requires the life cycle analysis of components that is normalized and converted to mPt, as presented in Table 5.56. The total weight of marine engine is about 413 ton, which the ICE engine contributes about 90% of the total weight. Each component

has an environmental impact of production, processing, and disposal. Therefore, the component-related environmental impact of the total engine is 168,544 Pt, and the component-related environmental impact rate is 1.11 Pt/h, which is a very small amount compared to the rest of the analysis.

Table 5.56 The component-related environmental impact results of M-1 marine engine

#	Weight [kg]	Material Production [mPt/kg]	Material Processing [mPt/kg]	Material Disposal [mPt/kg]	Total EI [mPt/kg]	Total Y [mPt]	\dot{Y} [mPt/h]
ICE	377,000	402	0	24	426	160,673,630	1,056
TEG1	1,000	88	19	24	130	130,100	0.855
C2	7,000	131	12	24	166	1,165,241	7.662
IC	2,000	91	12	24	127	253,990	1.670
C3	5,000	131	12	24	166	832,315	5.473
CC	3,000	638	20	24	682	2,046,240	13.455
T3	7,000	104	12	24	140	978,341	6.433
SP1	0	88	19	24	130	0	0
MX2	0	88	19	24	130	0	0
BR	300	656	20	24	700	209,876	1.380
T2	8,000	104	12	24	140	1,118,104	7.352
TEG2	150	88	19	24	130	19,515	0.128
MX1	0	88	19	24	130	0	0
SR	200	911	20	24	955	190,980	1.256
WGS	200	811	20	24	855	171,027	1.125
SOFC	2,356	274	22	24	320	754,222	4.959
Total	413,206					168,543,581	1,108.2

The exergoenvironmental analysis of this engine for each component can be summarized in Table 5.57. The net exergoenvironmental rates are 1.5 kPt/h due to the net power and 65 Pt/h due to the required heat. The fuel and product exergoenvironmental rates are 9840 Pt/h and 9321 Pt/h, respectively. The destruction and loss exergoenvironmental rates of this engine are 3072 and 4 Pt/h, respectively. The pollution formation environmental rate, \dot{B}^{PF} , and total environmental rate, \dot{B}^T , are -507 and 2566 Pt/h, respectively. The negative value of \dot{B}^{PF} means that the pollutions are reduced and eliminated by the components, such as ICE, CC, SR, WGS, and BR since the methane and carbon monoxide are eliminated.

The exergoenvironmental performance is listed in Table 5.58. The specific fuel and product environmental impact of ICE are 5.21 and 14.29 mPt/MJ, respectively. The SOFC has specific fuel and product environmental impact of 1.61 and 5.65 mPt/MJ, respectively.

Also, the thermoelectric generators have specific fuel and product environmental impact of 7.35 and 49.06 mPt/MJ of TEG1 and 16.48 and 200.52 mPt/MJ of TEG2, respectively. The specific fuel and product environmental impact of the overall engine are 8.28 and 13.19 mPt/MJ, respectively. This makes the relative environment difference to be 59.2% and exergoenvironmental factor to be 0.043 %.

Table 5.57 The exergoenvironmental analysis of M-1 marine engine components

#	\dot{B}_K^W	\dot{B}_K^Q	$\dot{B}_{F,K}$	$\dot{B}_{P,K}$	$\dot{B}_{D,K}$	$\dot{B}_{L,K}$	\dot{B}_K^{PF}	\dot{B}_K^T
Units	[mPt/h]	[mPt/h]	[mPt/h]	[mPt/h]	[mPt/h]	[mPt/h]	[mPt/h]	[mPt/h]
ICE	619875	13867	798518	619875	572505	0	-179699	393864
TEG1	38856	0	38855	38856	34146	0	0	34147
C2	329914	0	329914	329921	53866	0	0	53874
IC	0	50689	50687	50689	2175	0	0	2177
C3	498071	0	498071	498077	73593	0	0	73599
CC	0	0	2102000	1868000	1491640	0	-234145	1257509
T3	834961	0	834955	834961	117901	0	0	117908
SP1	0	0	1033000	1033000	0	0	0	0
MX2	0	0	1188000	1188000	11684	0	0	11684
BR	0	0	1188000	1156000	317252	0	-32699	284554
T2	465441	0	465434	465441	64864	0	0	64871
TEG2	247394	0	247394	247394	233574	0	0	233574
MX1	0	0	335244	335244	2066	0	0	2066
SR	0	0	335244	274680	2087	0	-60566	-58478
WGS	0	0	274680	274878	2068	0	197	2266
SOFC	105872	0	119881	105872	92336	4100	0.00	92341
Total			9839877	9320888	3071757	4100	-506912	2565954

Table 5.58 The exergoenvironmental performance of M-1 marine engine components

#	$b_{F,K}$	$b_{P,K}$	f_b	r_b
Units	[mPt/MJ]	[mPt/MJ]	[%]	[%]
ICE	5.21	14.29	0.268367	174.23
TEG1	7.35	49.06	0.003	567.75
C2	19.07	22.66	0.014	18.88
IC	3.83	4.00	0.077	4.34
C3	18.86	22.02	0.007	16.78
CC	5.68	16.27	0.001	186.59
T3	16.27	18.86	0.005	15.91
SP1	16.27	16.27	0	0
MX2	13.89	14.03	0	0.96
BR	12.55	16.49	0.0005	31.44
T2	16.48	19.07	0.0113	15.66
TEG2	16.48	200.52	0	1116.45
MX1	5.53	5.56	0	0.60
SR	5.04	4.16	-0.002	-17.57
WGS	4.14	4.17	0.050	0.81
SOFC	1.61	5.65	0.005	251.62
Total	8.28	13.19	0.043	59.19

The fuel blends, which are named as F1 to F5, are used in the exergoenvironmental analysis, as produced in Figure 5.79. based on the F1 to F5 of 5.44, 7.88, 5.95, 11.3, and

7.60 mPt/MJ, respectively. Figure 5.79-a presents the exergoenvironmental rates with respect to fuel blends. The fuel and product exergoenvironmental rates are 10 and 9 kPt/h for F1, 17 kPt/h for F2, 13 kPt/h for F3, 24 kPt/h for F4, and 16 and 15 kPt/h for F5, respectively. The destruction exergoenvironmental rates are 3.1 kPt/h, 5.1 kPt/h, 3.9 kPt/h, 7.1 kPt/h, and 4.7 kPt/h for F1 to F5, respectively. The specific fuel and product environmental impacts are 8.28 and 13.19 mPt/MJ for F1, 14.31 and 24.51 mPt/MJ for F2, 10.54 and 17.45 mPt/MJ for F3, 19.57 and 32.31 mPt/MJ for F4, and 13.14 and 21.76 mPt/MJ for F5, respectively, as shown in Figure 5.79-b. The average specific fuel environmental impact of this engine is 13.71 mPt/MJ, and the average specific product environmental impact is 21.84 mPt/MJ.

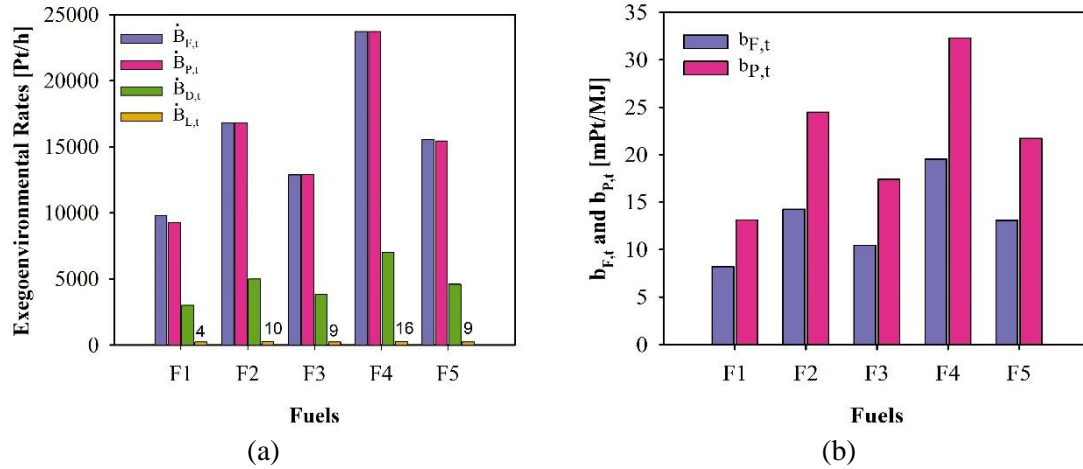


Figure 5.79 (a) Exergoenvironmental rates and (b) specific exergy costs of M-1 marine engine with respect to fuel blends

The pollution formation and total environmental rates are also considered in Figure 5.80. Figure 5.80-a shows the overall pollution formation rates with respect to fuel blends. Using the fuel blend F1 and F5 shows the negative values of pollution formation because of the removal of methane and carbon monoxide, however, the existence of carbon dioxide in F5 is higher than that of F1. The average pollution formation rate of F1 and F5 is -291 Pt/h. The average pollution formation rate for the remaining fuels is 50.1 Pt/h. Figure 5.80-b displays the total environmental rates, \dot{B}^T , is the summation of pollution formation, destruction, and component related environmental rates. As shown in this figure, the \dot{B}^T reaches the minimum of 2566 Pt/h using F1 and the maximum of 7134 Pt/h using F4, and the average of \dot{B}^T is 4635 Pt/h for this engine.

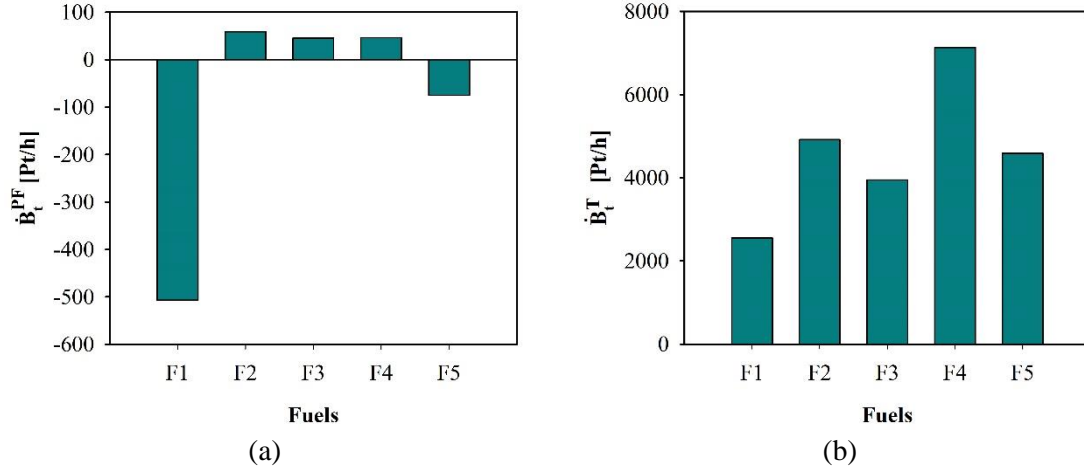


Figure 5.80 (a) Pollution formation rates and (b) total environmental impact rates of components of M-1 marine engine with respect to fuel blends

The exergoenvironmental performance of hybrid combined marine engine is presented in Figure 5.81. The exergoenvironmental factor varies from 0.016% of F4 to 0.043% of F1. In addition, the relative environmental difference has a minimum value of 59.2% of F1 and a maximum value of 71.3% of F2, as illustrated in Figure 5.81-a. The specific environmental impacts of exhaust gases are ranged from 23.17 mPt/MJ to 58.96 mPt/MJ with an average of 38.41 mPt/MJ, as provided in Figure 5.81-b.

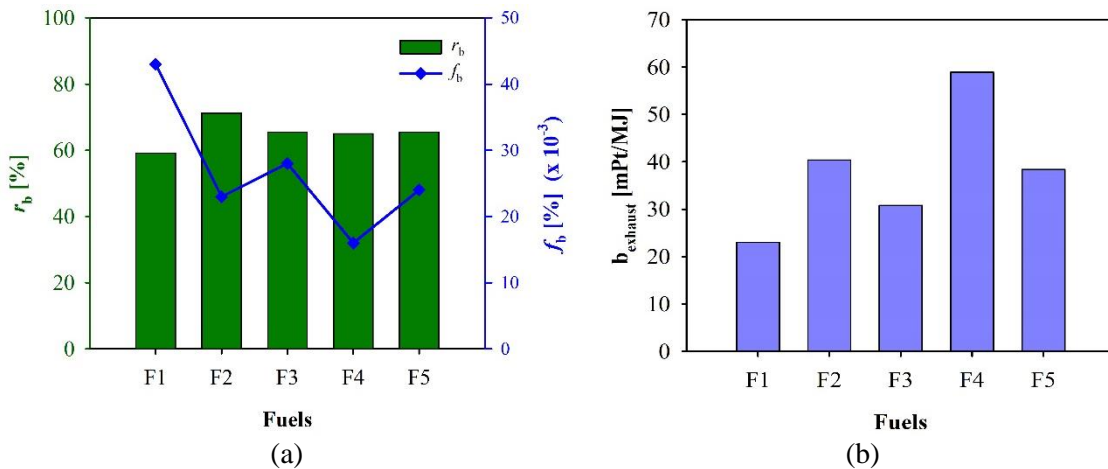


Figure 5.81 The exergoeconomic performance of a hybridized M-1 engine: (a) relative environment difference and exergoenvironmental factor, and (b) specific exergy environmental impact of exhaust

The electrical power and heat are also analyzed by the exergoeconomic and exergoenvironmental analyses, as appeared in Figure 5.82. Figure 5.82-a shows the specific exergy cost of electricity. The compressor C2 and turbine T2 have the same specific exergy

cost of electricity, c_{el} , of 91 \$/GJ, and the compressor C3 and turbine T3 have also the same specific exergy cost of electricity of 90 \$/GJ. The ICE has a low specific exergy cost of electricity of 73 \$/GJ. The fuel cell of SOFC has a specific exergy cost of electricity of 41 \$/GJ. In addition, the thermoelectric generators have a specific exergy cost of electricity of 197 \$/GJ for TEG1 and 562 \$/GJ for TEG2. For the required heat, the ICE and IC have specific exergy costs of heat, c_q , of 4 and 138 \$/GJ, respectively.

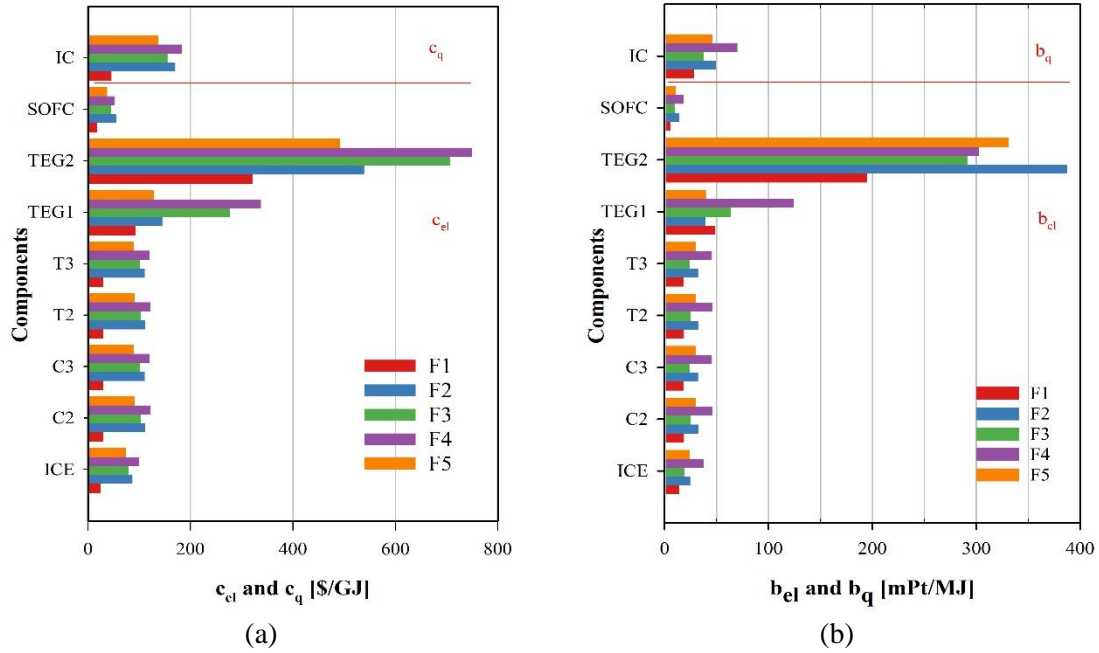


Figure 5.82 (a) Exergy cost and (b) environmental impact of electricity and heat for M-1 engine

Figure 5.82-b presents the specific environmental impact of electricity and heat. The components of ICE, C2 and T2, C3 and T3, TEG1, TEG2, and SOFC have specific environmental impact of electricity, b_{el} , of 24 mPt/MJ, 31 mPt/MJ, 30 mPt/MJ, 63 mPt/MJ, 301 mPt/MJ, and 12 mPt/MJ, respectively. Also, the ICE and IC have specific environmental impact of heat of 11 mPt/MJ and 46 mPt/MJ, respectively.

5.7 Results of System M-2

This section presents the results and discussion of the thermodynamic analysis, exergy analysis, exergoeconomic analysis, and exergoenvironmental analysis of the hybrid compound cycles (SRC-SOFC-GT) marine engine as written in the subsections below.

5.7.1 Results of Thermodynamic Analysis

The thermodynamic properties of streams are evaluated and reported in [182]. The steam enters the boiler at A6 of 7100 kPa and 510.1K and superheats to A7 of 7100 kPa and 810 K. The discharge pressure of turbines is 1700 kPa for HP-ST1, 1000 for IP-ST2, and 5 kPa for LP-ST3. The breeding pressure is 1000 for the CFH1, 600 for the CFH2, and 300 kPa for the CFH3. The steam mass flow rate is 6 kg/s. The mass fraction of bleeding steam is 10% of the feeder. The condenser pressure is 5 kPa and cools the steams using water at 15°C and 400 kg/s to be heated to 21.9°C. The first pump increased the condensed steam from 5 kPa and 37.4°C to 500 kPa and 37.5°C, while the second pump increased the saturated liquid to 7100 kPa. The feedwater heaters increase the low-pressure liquid temperature to 86.1°C by CFH3, 136.8 °C by CFH2, and 152.7 °C by CFH1 to ensure the exit of bleeding steam for the feedwater heaters reach the saturated liquid at their working pressure.

For the GBC, the mass flow rate of intake air of G1 is 30 kg/s at 25°C and 101.3 kPa, which is pressurized to 429.5 kPa and 1823.2 kPa with an overall pressure ratio of 18. The fuel blend is combusted with air under stoichiometric combustion with excess air at a high temperature of 1200°C and 1823 kPa and then decreased to 1100 °C by GTHX for blade safety. The exhaust gases expanded to 750 kPa by HP-T1, 350 kPa by LP-T2, and 200 kPa by P-T3. The exhaust gases are released from the GBC at 730.8 °C and 200kPa of G12 stream to enter the burner boiler (BRBL). The mass flow rate of G5 is 6 kg/s which is 20% of the intake air. The fuel blend and water mass flow rates of F3 and S1 are 0.25 kg/s and 0.4 kg/s. The fuel mixture enters the direct SOFC system to be reformed at 200 °C, then water shifted at 400 °C, and electrochemically reacted with air at 800°C. The fuel blend, 25% wt hydrogen and 75% wt methane, is 1 kg/s at F2 and 0.2 kg/s at F1, while the intake air of B1 is 0.5 kg/s. Finally, the exhaust gases at B5 flow at 32.35 kg/s with 216 °C and 200 kPa.

The desalination unit (DSWR) uses the seawater with a salinity of 0.035 kg/kg at 12 °C and 105 kPa at SW1 to be heated by D-HX to 47°C at SW2. Some of 36 kg/s will be rejected to the sea, while the remaining will be fed to the stages with an equal amount of 8 kg/s. The first stage D-D1 has a pressure of 22.7 kPa and a temperature of 65°C. The following two stages have a pressure of 16.3 kPa and 11.4 kPa for D-D2 and D-D3,

respectively. The temperatures of the last two stages are 56.5 °C (FW6) and 50 °C (FW11). The brine exits the first stage D-D1 at 1.1 kg/s and 65°C (SL1), the second stage D-D2 at 2.4 kg/s and 57.5 °C (SL3), and the third stage D-D3 at 3.7 kg/s and 50 °C with salinity is 0.229 kg/kg. The freshwater exits the desalination system at FW16 with a flow rate of 20.3 kg/s, 48.2 °C and 11.3 kPa with a salinity of 7.1E-25, which is negligible. The steam enters the first stage at S-IN of 7.4 kg/s, 110 °C, and 100 kPa, and leaves it at 99.6 °C to produce heat of 16758 kW to the first stage.

The component performance for the SRC and GBC is displayed in Table 5.59, and for the DSWR in Table 5.60. For the SRC, the turbine power is 1996.8 kW for HP-ST1, 839.1 kW for IP-ST2, and 3840 kW for LP-ST3 combined. The required power of the first pump is 4.3 kW and 1578.6 for the second pump. All thermal efficiencies of turbomachinery components are assumed to be the same 85% isentropic and 90% mechanical efficiency. The required heat for the boiler heat exchanger (HXBL) and reheater (HXRH) are 14887 kW and 2440.8 kW, respectively. The rejected heat by the condenser (CN) is 11492 kW. The feedwater heaters have a duty of 1604 kW for the CFH1, 1490 kW for the CFH2, and 1406 kW for CFH3. The desalination unit (DSWR) has a required heat of 16758 kW. All the heat exchangers and condensers have 100% thermal efficiency because there is no heat loss and no pressure drop in the flow. The boiler burner (BRBL) is 7092 kW, with an energetic efficiency of about 59%. The sum of exergy destruction rates for turbines and pumps is 2245.3 kW, while for the heat exchangers and feedwater heaters is 31596.7, and the maximum rate is recorded for HXBL to be 22271.3 kW.

For the GBC, as shown in Table 5.59, the compressor power is 6017 kW for LP-C1 and 7584 kW for HP-C2, and the turbine power is 8506 kW, 6815.6 kW, and 4163.2 kW for HP-T1, LP-T2, and P-T3, respectively. The rejected heat of the intercooler (IC) is 3079.5 kW, and the required heat of the combustion chamber (CC) is 26885.8 kW. The actual air-to-fuel ratio is 2.5 kg_a/kg_f, while the theoretical air-to-fuel ratio is 1.98 kg_a/kg_f. The required heat of SOFC is 13174.4 kW, and the rejected heat of SR and WGS are 3675.9 kW and 168.8 kW, respectively. The electric efficiency of SOFC is 90.04 %, and its energetic and exergetic efficiencies are 29.4% and 43.5%. All the mixers, splitters, and

expansion valves require no power nor heat with negligible exergy destruction rates. This hybrid combined engine's total exergy destruction rate is about 146,425 kW.

Table 5.59 The component performance for the SRC and GBC engines

#	\dot{Q}_k	\dot{W}_k	$\dot{E}x_{D,k}$	$\eta_{th,k}(\eta_{e,k})$	ψ_k
Units	[kW]	[kW]	[kW]	[%]	[%]
HP-C2	0.0	7584.0	1286.2	76.5	83.0
HP-ST1	0.0	1996.8	417.9	76.5	79.1
HP-T1	0.0	8506.0	1378.8	76.5	83.8
IP-ST2	0.0	839.1	161.6	76.5	80.8
LP-C1	0.0	6017.0	6017.0	76.5	81.3
LP-ST3	0.0	659.9	132.6	76.5	83.3
LP-ST4	0.0	716.7	153.5	76.5	82.4
LP-ST5	0.0	2464.2	714.9	76.5	77.5
LP-T2	0.0	6815.6	1124.8	76.5	85.8
P-T3	0.0	4163.2	490.1	76.5	89.5
P1	0.0	4.3	0.8	76.5	81.2
P2	0.0	1578.6	664.1	76.5	57.9
IC	3079.5	0.0	2056.9	100.0	66.7
CN	11492.2	0.0	1465.8	100.0	68.7
CFH1	1604.5	0.0	1568.7	100.0	22.6
CFH2	1490.9	0.0	965.5	100.0	45.8
CFH3	1406.0	0.0	800.3	100.0	57.6
DSWR	16758.3	0.0	1201.3	86.3	35.4
GTHX	4642.2	0.0	7372.4	100.0	86.0
HXBL	14887.4	0.0	22271.3	100.0	46.8
HXRH	2440.8	0.0	3323.7	100.0	84.4
BRBL	7092.0	0.0	14798.8	58.7	67.3
CC	26885.8	0.0	58158.5	52.8	45.6
SOFC	13174.4	3878.0	18392.3	29.4 (90.04)	43.5
SR	3675.9	0.0	894.4	24.4	60.3
WGS	168.8	0.0	81.5	6.3	86.7
EX1	0.0	0.0	6.0	100.0	98.7
EX2	0.0	0.0	13.2	100.0	98.4
EX3	0.0	0.0	146.6	100.0	86.5
GTMX	0.0	0.0	324.2	100.0	98.1
MX1	0.0	0.0	26.9	100.0	98.0
MX2	0.0	0.0	14.2	100.0	99.1
MX3	0.0	0.0	0.0	100.0	100.0
GTSP	0.0	0.0	0.0	100.0	100.0
SP1	0.0	0.0	0.0	100.0	100.0
SP2	0.0	0.0	0.0	100.0	100.0
SP3	0.0	0.0	0.0	100.0	100.0

Table 5.60 The component units for desalination unit (DSWR)

C# Units	\dot{Q}_k [kW]	$\dot{E}x_{D,k}$ [kW]	$\eta_{th,k}$ [%]	ψ_k [%]
D-CN1	16238.0	222.7	100.0	89.8
D-CN2	16061.9	4.9	100.0	99.7
D-HX	8505.2	366.3	100.0	37.4
D-D1	16758.0	85.5	88.2	95.7
D-D2	16238.0	69.3	76.9	95.7
D-D3	16061.9	65.6	68.1	94.7
D-EX0	0.0	0.9	100.0	97.2
D-EX1	0.0	4.7	100.0	90.2
D-EX2	0.0	4.7	100.0	90.2
D-EX3	0.0	0.0	100.0	99.9
D-EX4	0.0	1.1	100.0	96.9
D-EX5	0.0	2.1	100.0	96.7
D-EX6	0.0	6.9	100.0	92.5
D-MX1	0.0	0.3	100.0	100.0
D-MX2	0.0	0.0	100.0	100.0
D-MX3	0.0	1.3	100.0	99.9
D-MX4	0.0	0.5	100.0	99.9
D-S1	0.0	0.0	100.0	100.0
D-S2	0.0	0.0	100.0	100.0
D-S3	0.0	0.0	100.0	100.0
D-S4	0.0	0.0	100.0	100.0
D-S5	0.0	0.0	100.0	100.0

The DSWR components are also analyzed in Table 5.60. The input heat from the boiler to DSWR is 16758 kW, which is the required heat for D-D1 flash stage. The second and third flashes need an input heat of 16238 kW and 16061.9 kW for D-D2 and D-D3, respectively. The heat exchanger of D-HX has a duty of 8505.2 kW and a maximum destruction rate with a minimum exergetic efficiency of less than 40%. The total exergy destruction rate of DSWR is 1201.3 kW. The GOR is 2.89 since the steam mass flow rate is 7.35 kg/s entering at 110°C and 100 kPa to release its heat to the DSWR and leaving it at the saturated liquid. Based on the datasheet of the Aframax ship, the freshwater tanks are approximately 150 m³, which means the freshwater is reaching its required capacity after 2.1 hours to fill 153.7 m³. Also, the ship demands 600 m³ of technical freshwater tanks, which can be achieved after 8.5 hours to fill 622 m³. The energetic and exergetic efficiency of DSWR unit are 86.3% and 31.6%, respectively.

(a) Effect of fuel blends on engine subsystems:

Five fuel blends are chosen, and hydrogen is the basis of this combination. The net power and net required heat are shown in Figure 5.83. The net power of the SRC is constant at 5094 kW for all fuel blends since the working fluid is steam. The net power of the GBC is

a maximum of 5884 kW using the F1 and a minimum of 4933 kW using F3 and F4. However, the minimum power of the SOFC is given to be 3878 kW using F1, and maximum power is 6667 kW using F5, as shown in Figure 5.83-a. The required heat of the engine is by the BRBL, CC, and net heat of SOFC, including the reforming and water-shifting processes, as shown in Figure 5.83-b. The BRBL heat is its highest value of 7486 kW using F2 and minimum value of 2323 kW using F5 for combustion at 200 kPa and 1273 K.

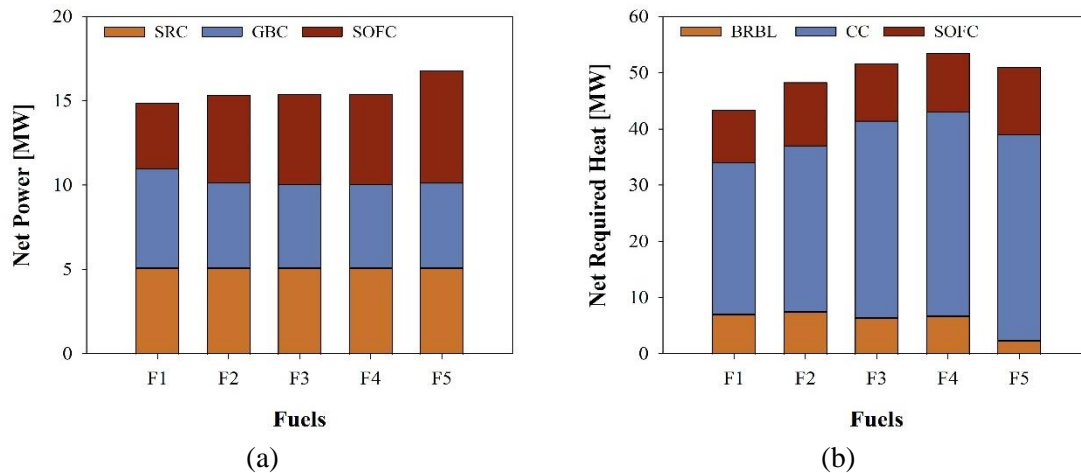


Figure 5.83 (a) The net power and (b) the net required heat for three marine subsystems

However, this trend changes in the CC since the minimum heat is achieved by F1 of 26886 kW and maximum heat is fulfilled by F5 of 36533 kW. The net heat of SOFC is 9330 kW using F1 increased to its maximum of 12036 kW using F5. Therefore, the total engine power is calculated from 14856 kW of F1 to 16780 kW of F5, while the total required heat is obtained to be a minimum of 43308 kW by F1 and a maximum of 53507 kW by F4.

The heat rates of SRC components are displayed in Figure 5.84. The burner boiler added heat of 7092 kW using F1 and varied with fuel blends, as discussed previously. However, the duty of heat exchangers of the boiler, reheater, condensers, feedwater heaters, and desalination remains constant despite the fuel change. The primary source of added heat to the SRC is HXBL of 14887 kW and HXRH of 2440 kW. The feedwater heaters save this much heat (about 4501 kW) from the HXBL. The condenser rejects a heat of 11492 kW from the steam to reach a saturated liquid, and the desalination uses heat of 16758 kW from the waste energy of exhaust gases.

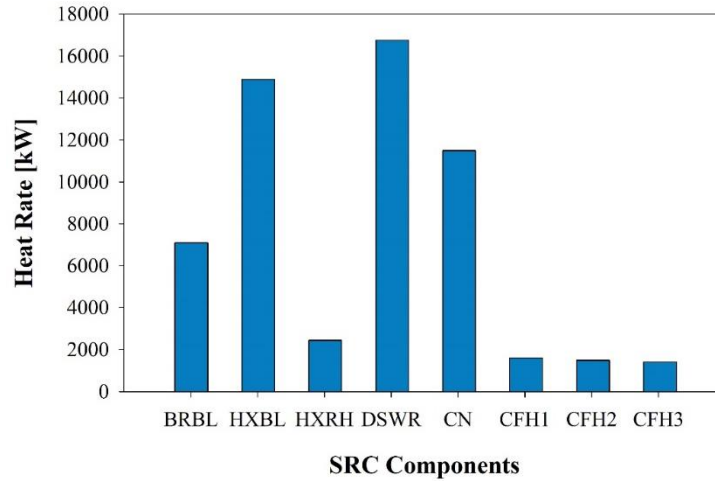


Figure 5.84 The heat rates of SRC components for all fuels

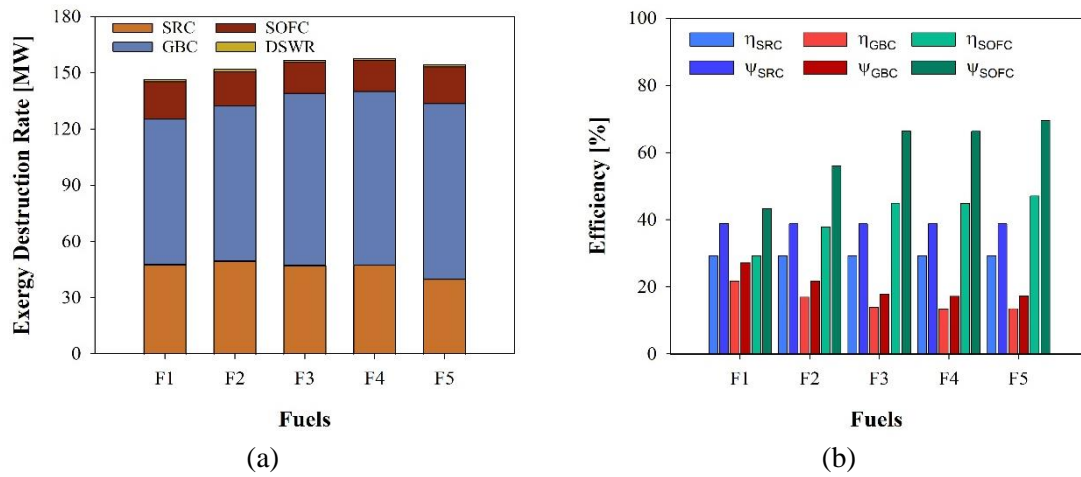


Figure 5.85 (a) Exergy destruction rates and (b) energetic and exergetic efficiencies for three subsystems

The overall performance of each subsystem is also estimated by considering the exergy destruction rates and energetic and exergetic efficiencies, as shown in Figure 5.85. The desalination DSWR has a constant destruction rate of 1201 kW. The GBC has a minimum destruction rate of 77885 kW using F1 and a maximum of 93610 using F5. On the contrary, the SRC has a minimum destruction rate of 39990 kW using F5 and a maximum of 494948 kW using F2. The SOFC has a maximum and a minimum exergy destruction rate of 19692 kW and 16496 kW of F1 and F3, respectively. The destruction rate of the whole engine is more than 145 MW with a maximum of 157737 kW using F4, as shown in Figure 5.85-a. The constant net power and heat of SRC result in unchanging energetic efficiency of 29.4% and unchanging exergetic efficiency of 38.9%. In

comparison, the GBC achieves higher energetic and exergetic efficiency of 21.9% and 27.4%, respectively, using F1 because of its maximum power and minimum heat of CC and destruction rate. For the SOFC, the maximum performance is obtained by using F5 to be 47.2% and 69.6%, respectively, as shown in Figure 5.85-b.

The overall energetic efficiency of the proposed engine is more than 55% and close to 70%, while the exergetic efficiency of the engine is an average of 43%, as shown in Figure 5.86. The performance of this new engine is evaluated as the ratio of useful energy sources, such as net power and energy of freshwater to the required energy as heat of CC, net duty of SOFC, heat of BRBL. The hybrid combined marine engine has a maximum energetic efficiency of 67.7% using F1 and the maximum exergetic efficiency of 45.3%. F1, F2 and F5 positively impacted the engine performance by more than 60% energetic efficiency and more than 43% exergetic efficiency. However, the new engine has minimum performance using F4 (dimethyl ether and hydrogen) for 56% energetic efficiency and 39% exergetic efficiency.

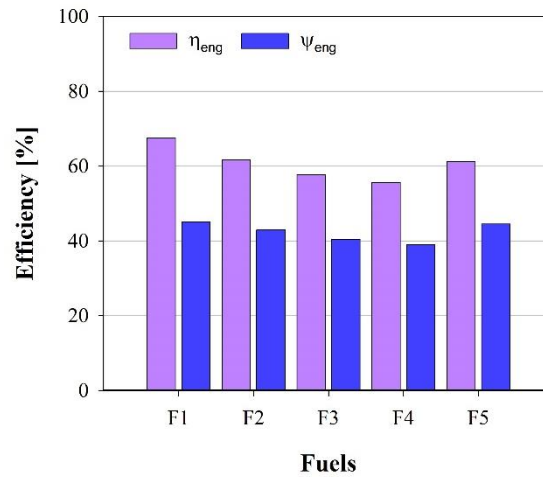


Figure 5.86 The overall energetic and exergetic efficiency of the engine

(b) Effect of fuel blends on the fuel cell:

The marine fuel blends significantly impact SOFC since the fuel cell counts on the Gibbs energy of reactants and products of the fuels and the amount of hydrogen produced in the reforming and water shifting reactors. The SR heat varies from a minimum of 968 kW of F4 to a maximum of 3676 kW of F2, while the minimum heat WGS is obtained by F1 at 169 kW, and its maximum heat is given by 397 by F3 and F4, because they have a similar amount of water and produced carbon monoxide and produced hydrogen, as shown in

Figure 5.87. The heat of the electrochemical reaction of hydrogen and oxygen in the anode and cathode electrodes is produced within a range between 11902 kW (F3 and F4) to 14137 kW (F5). This rejected massive heat will subtract the exothermic reactions of SR and WGS to produce the overall heat rejection of SOFC. The net power of SOFC varies from a minimum value of 3878 kW (F1) to a maximum value of 6667 kW (F5).

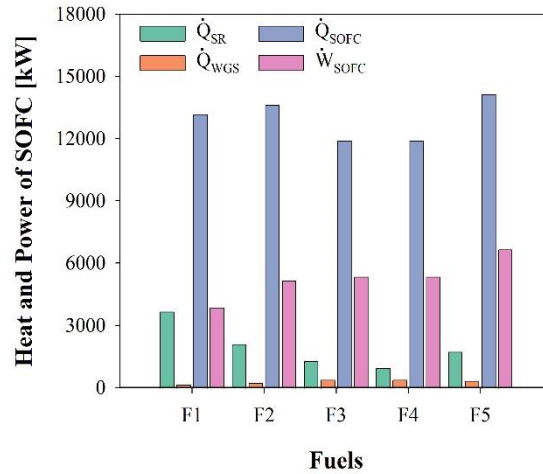


Figure 5.87 The distribution of heat and power of SOFC

The reason for this power is given in Figure 5.88-a. The electrochemical reaction produces a small cell voltage of an average of 0.4 V, because of the high operating pressure of 1823 kPa. Also, F1 makes the fuel cell generate a cell voltage of 0.30 V compared to 0.44 V of F5. The loss voltage that comes from activation losses, ohmic losses, and concentration losses altogether is 0.03 V for all the fuel blends with a still change of ± 0.001 . This represents the high electric efficiency of SOFC to be an average of 92.5%, as presented in Figure 5.88-a. The SOFC power can only be obtained using 34 stacks for F1 and F2, 31 stacks for F3 and F4, and 36 stacks for F5, as shown in Figure 5.88-b. Also, the amount of required hydrogen in SOFC has an average of 72.3 mol/s, which is about 72% of resultant hydrogen from the inlet fuel blend of F3 and reforming and water gas shifting processes. The SOFC system was able to increase the power of GBC from an average of 5165 kW to 10452 kW and increase the efficiency from an average of 16% to 25%. The hybridization of GBC was performed by taking a small fraction of the intake air after the HP-C2 (a constant splitting ratio of 0.2) and a small amount of fuel about 25%, which is a great benefit of enhancing engine performance with less mechanical moving parts and less maintenance.

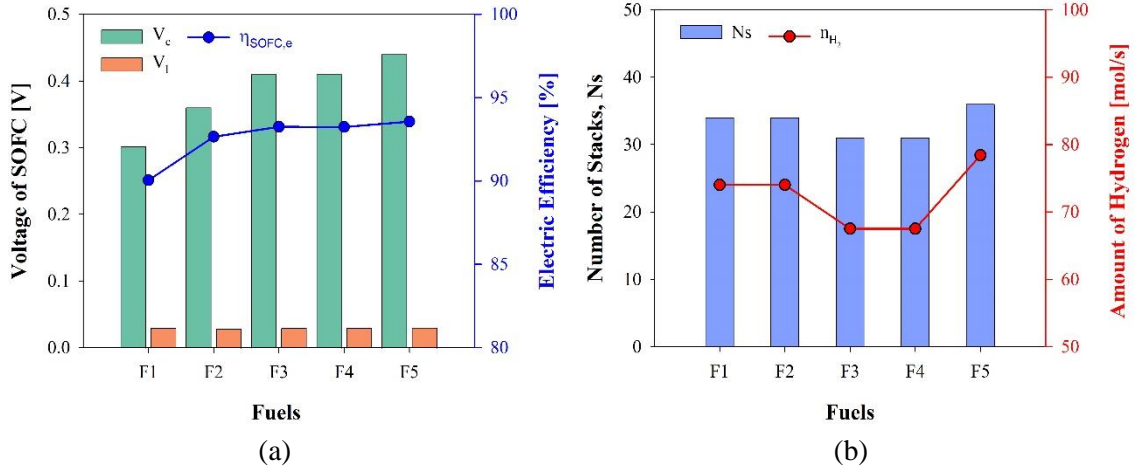


Figure 5.88 (a) Electric performance of SOFC and (b) required stack numbers and amount of hydrogen in SOFC

(c) Fuel consumption and carbon emissions:

Other parameters should be considered in analyzing the engine performance: fuel consumption and carbon emissions. The SRC burner uses the exhaust of GBC by G12 stream combusting with a fuel blend of F1 stream and air of B1 stream. However, in this analysis, the G12 is cancelled, and the SRC must count fully on the fuel blend of F1 and air of B1 only. Therefore, the air mass flow rate of B1 increases 30 kg/s to produce the same power of 5093.7 kW. Hence each system is operating alone and compared with the hybrid combined engine using the same fuel, as shown in Figure 5.89. The fuel mass flow rates of SRC vary from 1.3 to 1.5 kg/s with a minimum record for F1. The GBC uses 1 kg/s for F1 and 1.1 kg/s for F3 to F5 and 1.5 kg/s for F2. The SOFC consumes 0.4 kg/s and less with minimum of F1 (0.25 kg/s) and maximum of F2 (0.4 kg/s). The total fuel flow rate for the proposed engine reaches its maximum value of 2.30 kg/s using F2 and minimum value of 1.45 kg/s using F1, while the remaining F3 to F5 has an average of 1.62 kg/s, as shown in Figure 5.89-a. The specific fuel consumption (SFC) is estimated for the individual subsystem and overall engine as in Figure 5.89-b. The average of SFC is 996.5 g/kWh for the SRC, 815 g/kWh for the GBC, and 215.1 g/kWh for the SOFC, while the average of SFC for the whole engine is 400 g/kWh with a minimum of 337 g/kWh by the F5 and a maximum value of 540 g/kWh by F2. The designed engine's carbon emissions are slightly higher, with an average of 2.2 kg/s compared to 2.1 kg/s for SRC, 1.7 kg/s for the GBC, and 0.2 kg/s for the SOFC. However, high emissions can be produced by fuel F1 and F2, as shown in Figure 5.89-c.

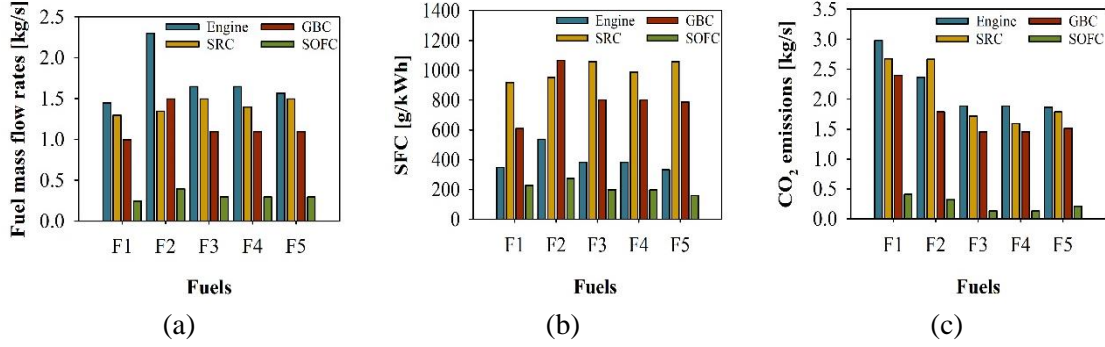


Figure 5.89 (a) Fuel mass flow rates, (b) SFC, and (c) carbon emissions of three marine subsystems

As previously mentioned, the Aframax ship demands a total power of 10400 kW. If the SRC is operated only using the MGO-DMA, the steam mass flow rate will be 13.5 kg/s, the fuel mass flow rate is 1.26 kg/s, and the air mass flow rate is 18.5 kg/s. This operation will generate a net power of 11141.8 kW and an energetic and exergetic efficiency of 29.1% and 38.6%, respectively, as shown in Table 5.61. Also, the carbon emissions will be 3.98 kg/s, which doubles the emissions of the proposed system. On the contrary, this new marine engine emits less carbon dioxide by 25% using F1 and up to 53% using F5. In addition, the SFC of this SRC operated by the MGO-DMA will be about 405.5 g/kWh. The proposed hybrid combined engine has increased the total power by between 30% to 50%, with an increase in fuel mass by 25%, except for F2, which is increased by 83%. The SFC is decreased between 5 to 17% for all fuel blends except for F2. Fortunately, the carbon emissions have reduced significantly to about an average of 50%. In addition, the thermal performance has increased to more than double the traditional system with an increase in exergetic performance of 11%.

Table 5.61 Comparison of traditional marine engines and sustainable fuels hybrid marine engines

Fuels	\dot{W}_o [kW]	\dot{m}_f [kg/s]	SFC _t [g/kWh]	CO _{2,t} [kg/s]	η_t [%]	ψ_t [%]	Weight [kg]
MGO	11141.8	1.26	405.5	3.98	29.1	38.6	91540
F1	14855.5 (↑33.3)	1.45 (↑15.5)	351.4 (↓13.4)	2.98 (↓25.0)	67.7 (↑133)	44.7 (↑15.8)	58016 (↓36.6)
F2	15322.3 (↑37.5)	2.30 (↑83.3)	540.4 (↑33.3)	2.37 (↓40.5)	61.7 (↑112)	42.5 (↑10.1)	58016 (↓36.6)
F3	15389.3 (↑38.1)	1.65 (↑31.5)	386.0 (↓4.8)	1.89 (↓52.5)	57.9 (↑98.9)	41.2 (↑6.9)	57824 (↓36.8)
F4	16382.8 (↑38.1)	1.65 (↑31.5)	386.1 (↓4.8)	1.89 (↓52.3)	55.8 (↑91.7)	39.9 (↑3.5)	57824 (↓36.8)
F5	16779.7 (↑50.6)	1.57 (↑25.1)	336.8 (↓16.9)	1.87 (↓53.0)	61.4 (↑111)	46.1 (↑19.5)	58144 (↓36.5)

The Aframax ship (WSD42 11K) is operated using a diesel engine of Wärtsilä 6X62, which delivers an output power of 10400 kW with a weight of 377000 kg [25]. Suppose the existing engine is replaced by only a steam Rankine cycle engine. In that case,

there are two major components that weigh significantly compared to others: a boiler model of Aalborg D for a capacity of 38800 kW of steam weighs 55,000 kg [38]; and a steam turbine model of MST050 for 5-30MW weighs 36540 kg [39]. Therefore, the total weight of SRC is 91540 kg, as shown in Table 5.61 in the first row. Nevertheless, the proposed engine uses the half capacity of the SRC only and is combined with SOFC units and GBC. Therefore, the SRC that delivers a total turbine power of 5094 kW can be operated by MST020 with a capacity of 1-5 MW weighing 15420 kg and uses a required heat of 17328 kW run by Aalborg D with a capacity of 17600 kW weighing 25000 kg. Hence, the total weight of SRC is 40420 kg, which is almost half the weight of only an SRC engine. The GBC can be operated by Taurus 60, which delivers 5740 kW weighing 15420 kg [33]. Also, a one SOFC stack of 100 cells weighs 64 kg [36], so the total weight of 34 stacks is 2176 kg for F1 and F2. Therefore, the total weight of the proposed engine is 58016 kg for F1 and F2, and so on. This proposed engine weighed less than the traditional SRC only by 36% and less than the traditional diesel engine of 377000 kg by 85%. In conclusion, the proposed engine is more efficient, has less environmental impact, less weight, and is more reliable.

5.7.2 Results of Exergy Analysis

The exergy analysis based on fuel and product is conducted on the hybrid compound marine engine. The Sankey flowchart of exergy rates of this engine is illustrated in Figure 5.90 using F1 (75%wt. methane and 25%wt. hydrogen). The exergy rates of fuels are 13636 kW, 69155 kW, 17191 kW for entering the boiler's burner (BRBL), combustion chamber (CC) of GT, and fuel cell (SOFC). The exhaust of GT has 26186 kW that enters the SRC and releases to the environment at exergy rate of 8592 kW. The exergy rates of cooling seawater of CN are 70465 and 70379 kW for entering and exiting the CN.

Table 5.62 presents the exergy performance of the proposed marine engine. The net power of this engine is 14856 kW by combining the net power of SRC, GT, and SOFC. The net required heat for this engine is 43307 kW, so that the proposed marine engine has an energy efficiency of 68% and exergy efficiency of 45%. The fuel, product, destruction, and losses exergy rates of the overall engine are 292 MW, 179 MW, 113 MW, and 0.43 M, respectively. This engine has an exergetic efficiency, based on fuel and product principal,

of 61.3%, which is higher than the normal exergy efficiency by 15%, and destruction ratio of 38.7%.

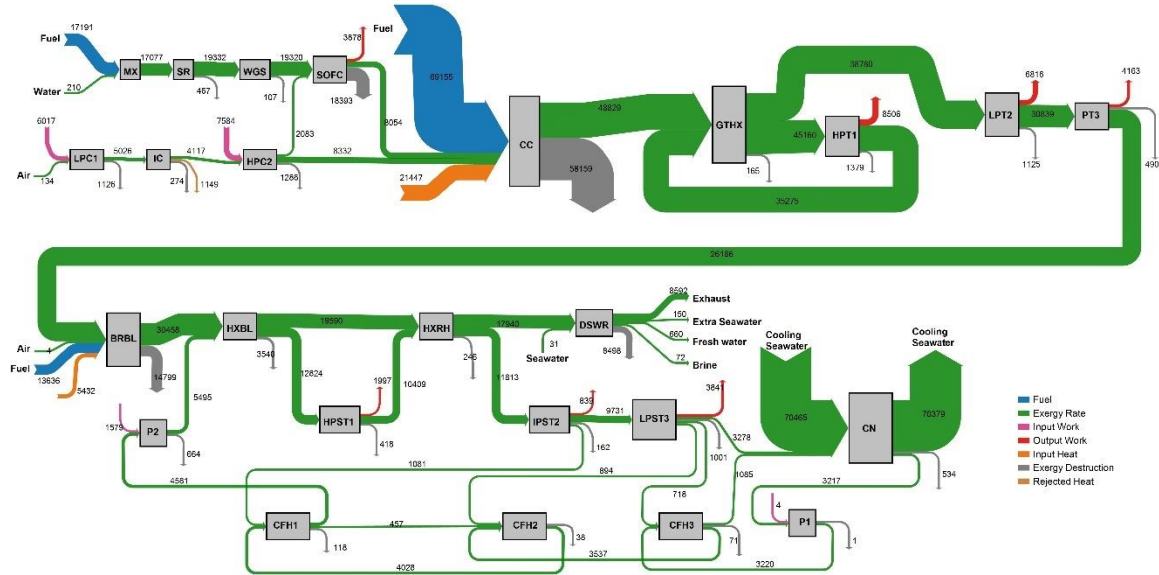


Figure 5.90 The Sankey flowchart of exergy rates of M-2 engine

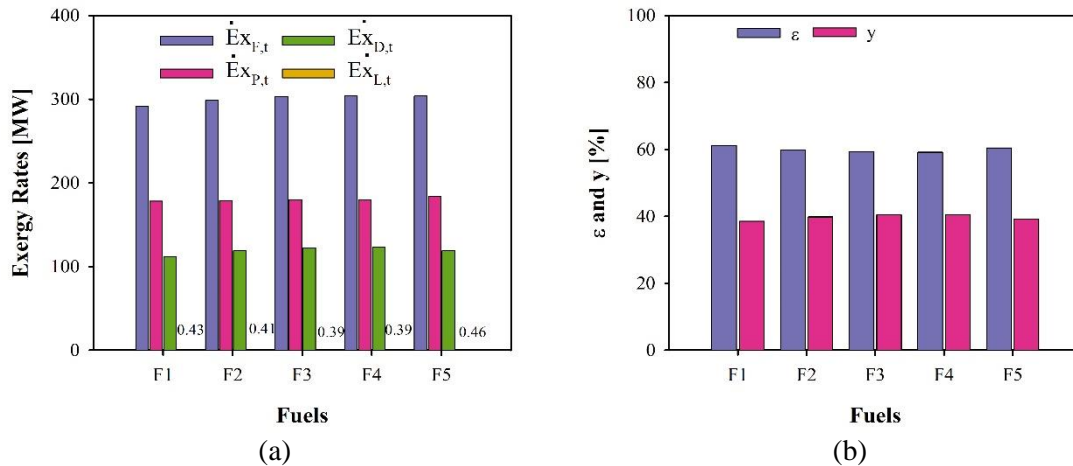


Figure 5.91 Exergy analysis of M-2 marine engine based on fuel blends: (a) Fuel, product, destruction, and losses exergetic rates, and (b) Exergetic efficiency and exergy destruction ratio.

The exergy analysis is also conducted with respect to fuel blends, called as F#s, as presented in Figure 5.91. The fuel exergy rates are 292 MW for F1, 299 MW for F2, 304 MW for F3, 304 MW for F4, and 304 MW for F5. The product exergy rates of the engine have been reduced about 60% to 179 MW, 179 MW, 181 MW, 180 MW, and 184 MW for F1 to F5, respectively. The destruction and losses exergy rates have an average of 120 MW and 0.4 MW, respectively, as shown in Figure 5.91-a. The exergetic efficiency of the

proposed engine has an average of 60.1% and the destruction ratio is about 39.9%, as illustrated in Figure 5.91-b.

Table 5.62 The exergy performance of M-2 marine engine

#	\dot{W}_K	\dot{Q}_K	$\dot{E}x_{F,K}$	$\dot{E}x_{P,K}$	$\dot{E}x_{D,K}$	$\dot{E}x_{L,K}$	ε	γ	γ^*
Units	[kW]	[kW]	[kW]	[kW]	[kW]	[kW]	[%]	[%]	[%]
HPC2	7584	0	7584	6298	1286	0	83.04	0.44	1.14
HPST1	1997	0	2415	1997	417.8	0	82.69	0.14	0.37
HPT1	8506	0	9885	8506	1379	0	86.05	0.47	1.22
IPST2	839.1	0	1001	839.1	161.6	0	83.83	0.06	0.14
LPC1	6017	0	6017	4891	1126	0	81.29	0.39	1.00
LPST3	3841	0	4842	3841	1001	0	79.33	0.34	0.89
LPT2	6816	0	7941	6816	1125	0	85.83	0.39	1.00
PT3	4163	0	4653	4163	490.1	0	89.47	0.17	0.43
P1	4.3	0	4.3	3.5	0.8	0	81.40	0.00	0.00
P2	1579	0	1579	914.5	664.1	0	57.92	0.23	0.59
IC	0	3079	4391	4117	274	0	93.76	0.09	0.24
CN	0	11492	1000	466.2	533.8	0	46.62	0.18	0.47
CFH1	0	1605	435.2	317	118.2	0	72.84	0.04	0.10
CFH2	0	1491	528.5	490.2	38.3	0	92.75	0.01	0.03
CFH3	0	1406	624.3	553.3	71	0	88.63	0.02	0.06
DSWR	0	16758	9229	731.4	8498	0	7.93	2.91	7.52
GTHX	0	4642	3669	3504	164.9	0	95.50	0.06	0.15
HXBL	0	14887	10869	7328	3540	0	67.42	1.21	3.13
HXRH	0	2441	1650	1404	246	0	85.09	0.08	0.22
BR_BL	0	7092	45257	30458	14799	0	67.30	5.07	13.09
CC	0	26886	106988	48829	58159	0	45.64	19.91	51.44
SOFC	3878	13174	22271	3878	18393	429	17.41	6.30	16.27
SR	0	3676	19799	19332	466.8	0	97.64	0.16	0.41
WGS	0	168.8	19426	19320	106.6	0	99.45	0.04	0.09
Total			292058	178997	113060	429	61.29	38.71	100.00

5.7.3 Results of Exergoeconomic Analysis

The exergoeconomic analysis is applied on the hybrid compound cycles of marine engine. The Sankey flowchart of this marine engine is drawn for streams of fuels, air, steam, and exhausts, as shown in Figure 5.92, based on 7.15 \$/GJ of methane and hydrogen fuel blend. The exergy cost rates of fuels are 1780 \$/h for CC, 443\$/h for SOFC, and 351 \$/h for BRBL. The exhaust gases of GT have an exergy cost rate of 1610 \$/h that is reduced to be 554 \$/h that released to the atmosphere. The cooling seawater has an average exergy cost rate of 7370 \$/h, and the freshwater produced by the desalination unit has an exergy cost rate of 498 \$/h, while the exergy cost rate of the brine is 109 \$/h.

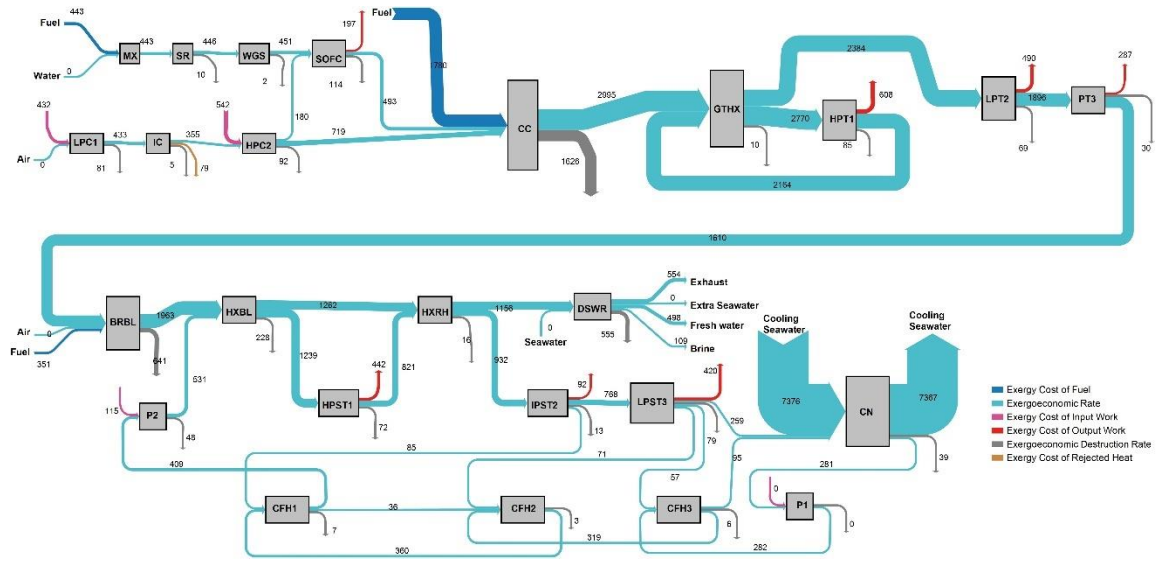


Figure 5.92 The Sankey flowchart of exergoeconomic rates of M-2 engine

The marine engine components' prices are listed in Table 5.63. There are two components with high prices, such as LPST3 of \$1.3M and SOFC of \$2.7M, and the total initial cost of the engine is \$7.3M, and the normalized cost of the overall engine according to May 2022 is \$15.1M. Therefore, the leveled cost rate of the marine engine is 218.61 \$/h.

The exergoeconomic analysis of marine engine is applied, and the results of each component are listed in Table 5.64. The net exergy cost rates are 1446 \$/h for the net power and 169.5 \$/h for the required heat. The fuel and product exergy cost rates are 11230 \$/h and 11432 \$/h, respectively. The destruction and losses exergy cost rates are 3831 \$/h and 2.65\$/h, respectively. The specific fuel and product exergy costs of this hybrid compound marine engine are 10.68 \$/GJ and 17.74 \$/GJ, respectively, which yields the relative cost difference to be 66.1% and the exergoeconomic factor to be 5.4%.

The exergoeconomic analysis has been conducted on the proposed engine with respect to fuel blends, as presented in Figure 5.93. The fuel and product exergy cost rates with respect to the fuel blends are almost the same cost rate of 11 k\$/h, 46 k\$/h, 44 k\$/h, 53 k\$/h, and 39 k\$/h for F1 to F5 in the same order, respectively. The destruction exergy cost rate is not the difference between the fuel and product exergy cost rates, it is the specific fuel exergy cost multiplied by the destruction exergy rates. Therefore, the destruction exergy cost rates are 4 k\$/h, 16 k\$/h, 15 k\$/h, 18 k\$/h, and 13 k\$/h for the fuel blends F1 to F5, respectively.

Table 5.63 The components' costs of M-2 marine engine

#	C_K [\$]	Z_K [\$] (2022)	\dot{Z}_K [\$/h]
HPC2	44,408	91,809	1.34
HPST1	818,904	1,693,000	24.50
HPT1	48,457	100,181	1.45
IPST2	440,106	909,881	13.17
LPC1	44,405	91,804	1.33
LPST3	1,265,000	2,616,000	37.85
LPT2	41,552	85,906	1.24
PT3	30,510	63,077	0.91
P1	3,625	7,495	0.11
P2	226,306	467,868	6.77
IC	23,584	49,372	0.71
CN	601,576	1,244,000	18.00
CFH1	10,526	21,761	0.31
CFH2	14,390	29,750	0.43
CFH3	5,948	12,297	0.18
DSWR	152,513	315,308	4.56
GTHX	16,152	33,394	0.48
HXBL	249,000	514,785	7.45
HXRH	147,937	305,847	4.43
BR_BL	60,117	124,287	1.80
CC	75,866	156,846	2.27
SOFC	2,708,000	5,599,000	81.02
SR	126,709	265,259	3.84
WGS	147,581	308,954	4.47
Total	7,303,172	15,107,881	218.61

The losses exergy cost rates are very low with an average of 6 \$/h, as shown in Figure 5.93-a. The specific fuel and product exergy cost are the minimum of 10.7\$/GJ and 17.7 \$/GJ, and are the maximum of 47.9 \$/GJ and 81.2 \$/GJ, and the average of 35 \$/GJ and 59 \$/GJ, respectively, as displayed in Figure 5.93-b.

The exergoeconomic performance is also considered, as displayed in Figure 5.94. The exergoeconomic factors are very low of 5.4% for F1, 1.4% for F2 and F3, 1.2% for F4, and 1.7% for F5. Also, the relative cost difference for all fuel blends is an average of 68%, as shown in Figure 5.94-a. The products of this engine are exhaust gases, freshwater,

and brine besides the electric power, which will be discussed later. The exhaust specific exergy costs vary from 18 \$/GJ of F1 to 81 \$/GJ of F4, which is small compared to the freshwater and brine. The specific exergy cost of freshwater and brine has an average of 706 \$/GJ and 1412 \$/GJ, respectively, as shown in Figure 5.94-b. That means the freshwater costs an average of 22.90 ¢/kg (22.90 ¢/L), and the brine costs an average of 27.66 ¢/kg.

Table 5.64 The exergoeconomic analysis of M-2 marine engine components

#	\dot{C}_K^W [\$/h]	\dot{C}_K^Q [\$/h]	$\dot{C}_{F,K}$ [\$/h]	$\dot{C}_{P,K}$ [\$/h]	$\dot{C}_{D,K}$ [\$/h]	$\dot{C}_{L,K}$ [\$/h]	$c_{F,K}$ [\$/GJ]	$c_{P,K}$ [\$/GJ]	f [%]	r [%]
HPC2	541.9	0	541.9	543.2	91.9	0	19.85	23.96	1.42	20.71
HPST1	442	0	417.5	442	72.2	0	48.03	61.49	25.33	28.02
HPT1	607.7	0	606.3	607.7	84.6	0	17.04	19.85	1.69	16.49
IPST2	92.11	0	78.94	92.11	12.7	0	21.91	30.49	50.82	39.16
LPC1	432.1	0	432.1	433.4	80.9	0	19.95	24.62	1.62	23.41
LPST3	419.8	0	382	419.8	79.0	0	21.91	30.36	32.40	38.57
LPT2	489.5	0	488.2	489.5	69.2	0	17.08	19.95	1.77	16.80
PT3	287	0	286.1	287	30.1	0	17.08	19.15	2.94	12.12
P1	0.1976	0	0.1976	0.306	0.0	0	12.76	24.29	74.70	90.36
P2	114.8	0	114.8	121.6	48.3	0	20.20	36.93	12.30	82.82
IC	0	79.05	78.34	79.05	4.9	0	4.96	5.33	12.75	7.63
CN	0	90.44	72.44	90.44	38.7	0	20.12	53.89	31.77	167.84
CFH1	0	0	27.49	37.21	7.5	0	17.54	32.61	4.05	85.92
CFH2	0	0	40.55	40.99	2.9	0	21.32	23.23	12.77	8.96
CFH3	0	0	49.25	49.43	5.6	0	21.91	24.81	3.08	13.24
DSWR	0	0	602.4	607	554.6	0	18.13	230.50	0.82	1171.37
GTHX	0	0	225.1	220.8	10.1	0	17.04	17.50	4.56	2.70
HXBL	0	0	700.4	707.8	228.1	0	17.90	26.83	3.16	49.89
HXRH	0	0	106.3	110.8	15.9	0	17.90	21.91	21.83	22.40
BR_BL	0	0	1961	1963	641.4	0	12.04	17.90	0.28	48.67
CC	0	0	2992	2995	1626.2	0	7.77	17.04	0.14	119.39
SOFC	196.8	0	137.6	196.8	113.6	2.65	1.72	14.10	41.62	721.68
SR	0	0	442.5	446.3	10.4	0	6.21	6.41	26.89	3.30
WGS	0	0	446.3	450.8	2.4	0	6.38	6.48	64.61	1.57
Total			11229.71	11432.04	3831.3	2.65	10.68	17.74	5.40	66.10

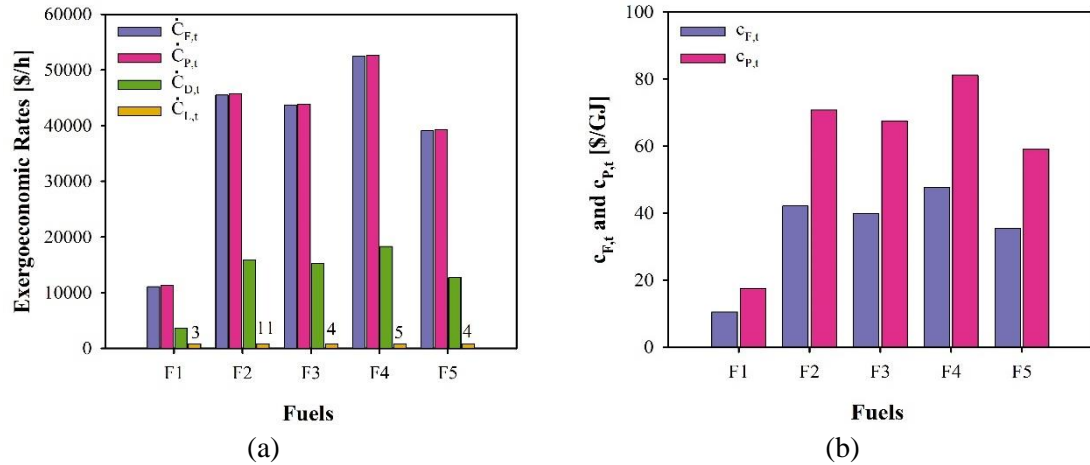


Figure 5.93 (a) Exergoeconomic rates and (b) specific exergy costs of the M-2 marine engine with respect to fuel blends

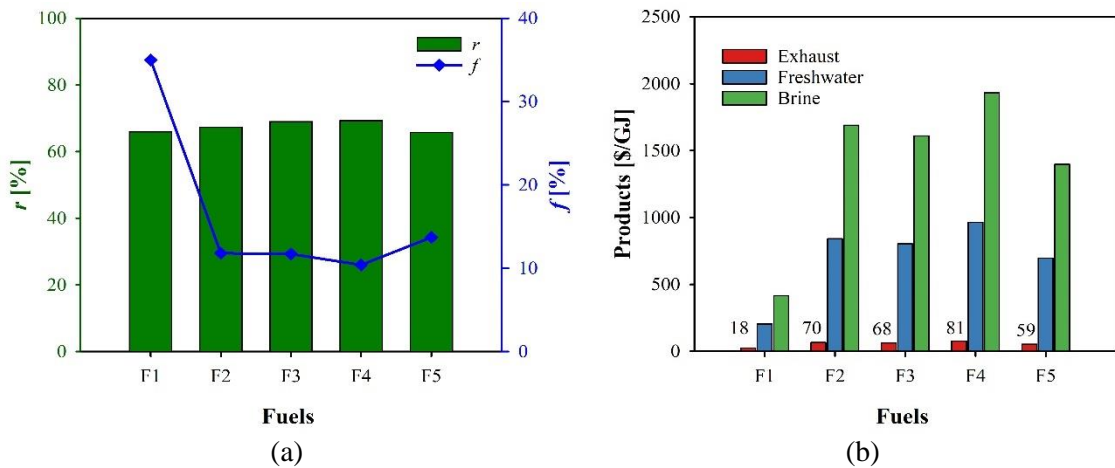


Figure 5.94 Exergoeconomic performance of an M-2 marine engine. (a) Relative cost difference and exergoeconomic factor, and (b) specific exergy cost of products

5.7.4 Results of Exergoenvironmental Analysis

The exergoenvironmental analysis is conducted on hybrid compound systems (SRC and hybrid GT) marine engine. The exergoenvironmental rates is plotted by Sankey flowchart as presented in Figure 5.95 based on the environmental impact of methane and hydrogen, which is 5.44 mPt/MJ. The fuels have exergoenvironmental rates of 1354 Pt/h, 334 Pt/h, and 267 Pt/h for entering CC, SOFC, and BRBL. The exhaust of GT has an exergoenvironmental rate of 999 Pt/h, which is reduced 334 Pt/h by passing through the boilers heat exchangers to the atmosphere. The cooling seaware has an average of exergoenvironmental rate of 3445 Pt/h. In addition, the exergoenvironmental rates of freshwater and brine are 299 Pt/h and 65 Pt/h, respectively.

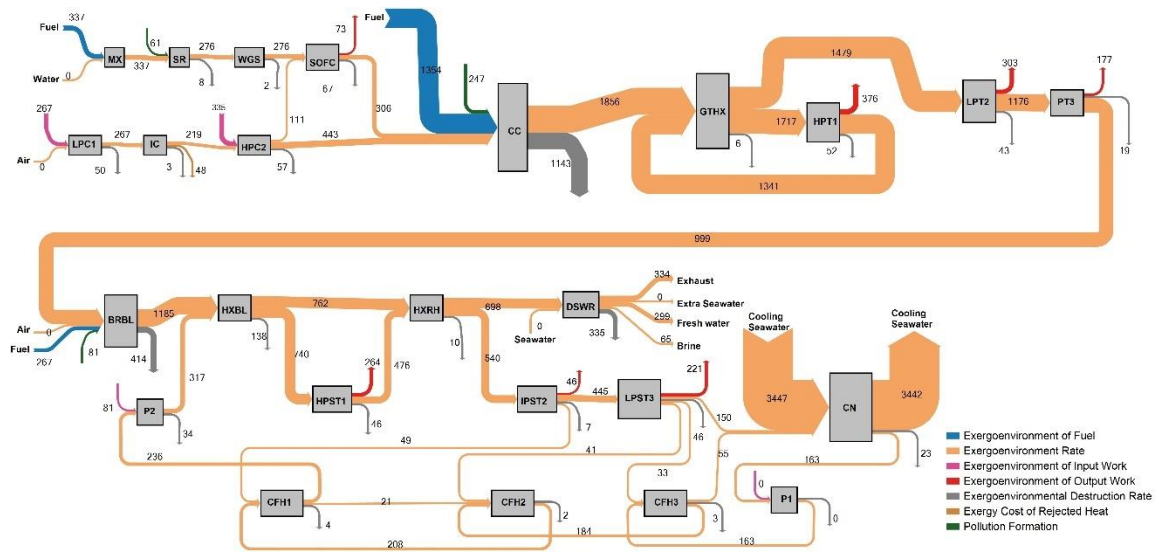


Figure 5.95 The Sankey flowchart of exergoenvironmental rates of M-2 marine engine [Pt/h]

Table 5.65 presents the environmental impact analysis of components based on their weights and their life cycle analysis during the production, processes, and disposal processes of each. The total weight of this engine is 139,304 kg. The total component-related environmental impact, Y , and its rate, \dot{Y} , are 21 kPt and 139 mPt/h.

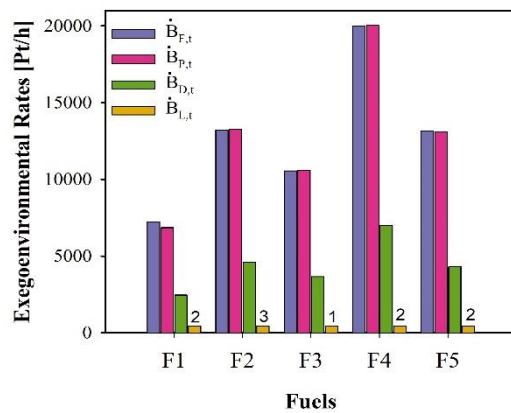
Table 5.66 displays the exergoenvironmental analysis of engine's components. The exergoenvironmental rates of net power and required heat are 777 Pt/h and 91 Pt/h, respectively. Also, the fuel, product, destruction, and losses exergoenvironmental rates are 7282 Pt/h, 6890 Pt/h, 2511 Pt/h, and 2 Pt/h, respectively. The pollution formation, \dot{B}^{PF} , and total environmental impact, \dot{B}^T , of this proposed engine are -389 Pt/h and 2122 Pt/h, respectively. The negative values of \dot{B}^{PF} are for BRBL, SR, and CC since the methane and carbon monoxide are eliminated because of complete combustion reactions. Table 5.67 shows the exergoenvironmental performance of the proposed engine. The specific fuel and product environmental impact are 6.93 and 10.69 mPt/MJ, respectively. The exergoenvironmental factor and relative environmental difference are 0.007% and 54.4%, respectively.

The exergoenvironmental analysis is applied on fuel blends of F1 to F5 of hydrogen-based fuels, as shown in Figure 5.96. The fuel and product exergoenvironmental rates are almost the same and equal to 7 kPt/h, 13 kPt/h, 11 kPt/h, 20 kPt/h, and 13 kPt/h

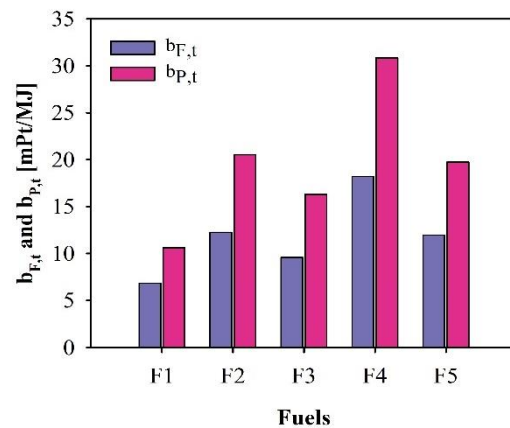
for the fuels of F1 to F5, respectively. The destruction and losses exergoenvironmental rates have an average of 4450 Pt/h and 2 Pt/h, respectively, as presented in Figure 5.96-a. The specific fuel and product environmental impacts are about 7 and 11 mPt/MJ for F1, 12 and 21 mPt/MJ for F2, 10 and 16 mPt/MJ for F3, 18 and 31 mPt/MJ for F4, and 12 and 20 mPt/MJ for F5, as displayed in Figure 5.96-b.

Table 5.65 The component-related environmental impact results of M-2 marine engine

#	Weight [kg]	Material Production [mPt/kg]	Material Processing [mPt/kg]	Material Disposal [mPt/kg]	Total EI [mPt/kg]	Total Y [mPt]	\dot{Y} [mPt/h]
HPC2	3,000	131	12	24	166	499,389	3.284
HPST1	22,000	104	12	24	140	3,074,786	20.218
HPT1	4,000	104	12	24	140	559,052	3.676
IPST2	5,000	104	12	24	140	698,815	4.595
LPC1	5,000	131	12	24	166	832,315	5.473
LPST3	11,000	104	12	24	140	1,537,393	10.109
LPT2	3,000	104	12	24	140	419,289	2.757
PT3	2,000	104	12	24	140	279,526	1.838
P1	1,200	186	17	24	227	272,364	1.791
P2	10,500	186	17	24	227	2,383,186	15.670
IC	500	91	12	24	127	63,498	0.418
CN	20600	91	12	24	127	2616097	17.202
CFH1	2000	91	12	24	127	253990	1.670
CFH2	2,000	91	12	24	127	253,990	1.670
CFH3	8000	91	12	24	127	1015960	6.680
DSWR	9200	91	12	24	127	1168354	7.682
GTHX	1000	91	12	24	127	126995	0.835
HXBL	20600	91	12	24	127	2616097	17.202
HXRH	5000	91	12	24	127	634975	4.175
BRBL	500	656	20	24	700	349,794	2.300
CC	500	638	20	24	682	341,040	2.242
SOFC	2,304	274	22	24	320	737,575	4.850
SR	200	911	20	24	955	190,980	1.256
WGS	200	811	20	24	855	171,027	1.125
Total	139,304					21,096,486	138.72



(a)

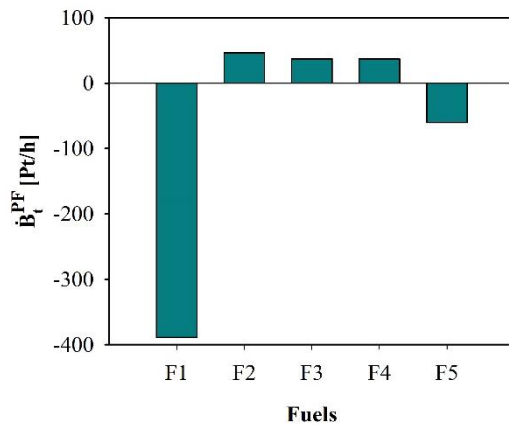


(b)

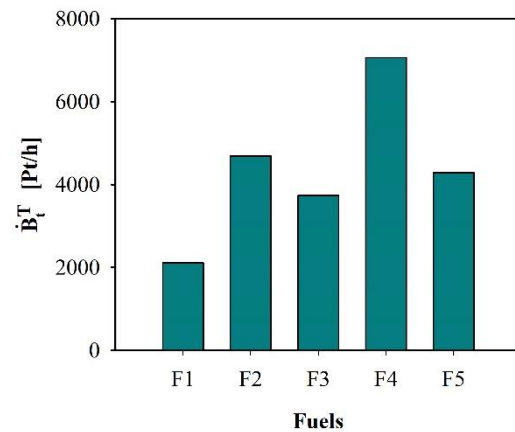
Figure 5.96 (a) Exergoenvironmental rates and (b) specific exergy costs of the hybridized M-2 marine engine with respect to fuel blends

Table 5.66 The exergoenvironmental analysis of M-2 marine engine components

#	\dot{B}_K^W	\dot{B}_K^Q	$\dot{B}_{F,K}$	$\dot{B}_{P,K}$	$\dot{B}_{D,K}$	$\dot{B}_{L,K}$	\dot{B}_K^{PF}	\dot{B}_K^T
Units	[mPt/h]	[mPt/h]	[mPt/h]	[mPt/h]	[mPt/h]	[mPt/h]	[mPt/h]	[mPt/h]
HPC2	335078	0	335078	335082	56805.2	0	0	56808
HPST1	263944	0	263924	263944	45663.9	0	0	45684
HPT1	375814	0	375811	375814	52424.1	0	0	52428
IPST2	45750	0	45745	45750	7388.4	0	0	7393
LPC1	267382	0	267382	267387	50021.4	0	0	50027
LPST3	221346	0	221336	221346	45765.7	0	0	45776
LPT2	302870	0	302867	302870	42930.0	0	0	42933
PT3	177488	0	177487	177488	18702.2	0	0	18704
P1	175.3	0	175.3	177.1	32.6	0	0	34
P2	80661	0	80661	80676	33924.9	0	0	33941
IC	0	48328	48327	48328	3015.4	0	0	3016
CN	0	42261	42243	42261	22541.3	0	0	22559
CFH1	0	0	15930	21381	4327.5	0	0	4329
CFH2	0	0	23501	23502	1702.8	0	0	1704
CFH3	0	0	28539	28546	3246.1	0	0	3253
DSWR	0	0	363583	363591	334685.2	0	0	334693
GTHX	0	0	139503	138005	6268.8	0	0	6270
HXBL	0	0	422736	422753	137635.2	0	0	137652
HXRH	0	0	64178	64182	9564.5	0	0	9569
BRBL	0	0	1266000	1185000	413904.4	0	-81131	332776
CC	0	0	2103000	1856000	1143382.7	0	-247401	895983
SOFC	73198	0	81290	73198	67141.8	1566	0.00	67147
SR	0	0	336683	276119	7938.6	0	-60566	-52626
WGS	0	0	276119	276317	1515.1	0	197	1713
Total			7282098	6889717	2510528	1566	-388901	2121766



(a)



(b)

Figure 5.97 The pollution formation rates (a) and total environmental impact rates (b) of components of M-2 marine engine with respect to fuel blends

The hybrid compound marine engine produces emissions that have environmental impact, which is provided in Figure 5.97. The pollution formation environmental impact rates are evaluated to be two negative values of -389 Pt/h and -60 Pt/h for F1 and F5, and the remaining positive values of 47 Pt/h for F2 and 37 Pt/h for F3 and F4, as presented in Figure 5.97-a. The total environmental rate is calculated as the summation of destruction, pollution formation, and component-related environmental rates without neglecting the negative sign. The minimum and maximum total environmental rates are 2.1 kPt/h and 7.1 kPt/h, respectively, as shown in Figure 5.97-b.

Table 5.67 The exergoenvironmental performance of M-2 marine engine components

# Units	$b_{F,K}$ [mPt/MJ]	$b_{P,K}$ [mPt/MJ]	f_b [%]	r_b [%]
HPC2	12.27	14.78	0.006	20.46
HPST1	30.36	36.72	0.044	20.95
HPT1	10.56	12.27	0.007	16.19
IPST2	12.70	15.15	0.062	19.29
LPC1	12.34	15.19	0.011	23.10
LPST3	12.70	16.01	0.022	26.06
LPT2	10.60	12.34	0.006	16.42
PT3	10.60	11.84	0.010	11.70
P1	11.32	14.05	5.208	24.12
P2	14.19	24.51	0.046	72.73
IC	3.06	3.26	0.014	6.67
CN	11.73	25.18	0.076	114.66
CFH1	10.17	18.74	0.039	84.27
CFH2	12.35	13.32	0.098	7.85
CFH3	12.70	14.33	0.205	12.83
DSWR	10.94	138.10	0.002	1162.34
GTHX	10.56	10.94	0.013	3.60
HXBL	10.80	16.02	0.012	48.33
HXRH	10.80	12.70	0.044	17.59
BR_BL	7.77	10.80	0.001	39.01
CC	5.46	10.56	0.000	93.37
SOFC	1.01	5.24	0.007	417.06
SR	4.72	3.97	-0.002	-16.00
WGS	3.95	3.97	0.066	0.63
Total	6.93	10.69	0.007	54.37

This environmental performance is also considered, as shown in the Figure 5.98. The exergoenvironmental factor is vary low to an average of 0.004% because the destruction exergoenvironmental rate is greater than the component-related environmental impact rate by four orders of magnitude. Also, the relative environmental difference is minimum of 54% of F1 and a maximum of 69% of F4, as displayed in Figure 5.98-a. The products of the marine engine are exhaust gases, brine, and freshwater, and net electric power.

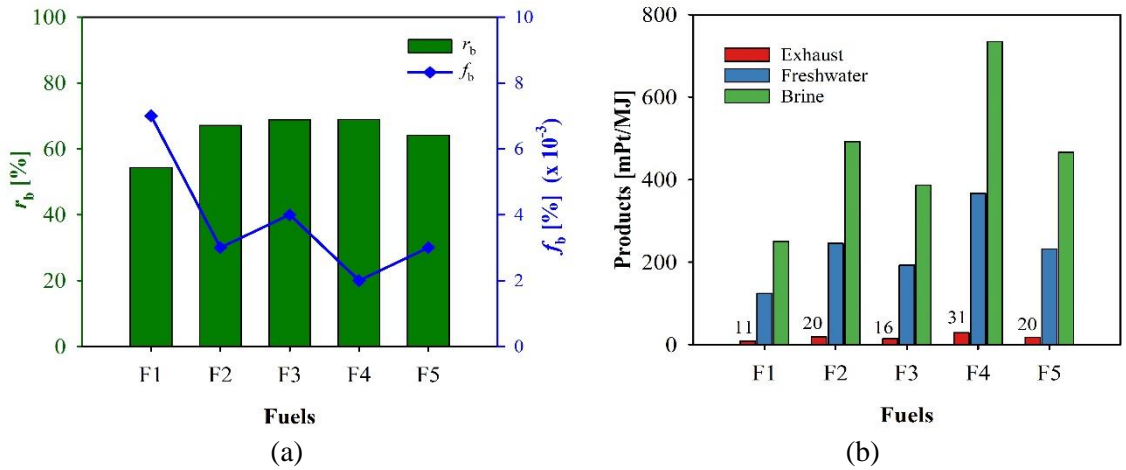


Figure 5.98 Exergoenvironmental performance of a hybridized M-2 marine engine: (a) Relative environment difference and exergoenvironmental factor, and (b) Specific exergy environmental impact of product

However, the last one is discussed later. The specific environmental impact of exhaust is averaged to 20 mPt/MJ, which is 5.92 mPt/kg is greater than the environmental impact of carbon dioxide (5.45 mPt/kg), as shown in Figure 5.98-b. The freshwater and brine have an average specific environmental impact of 233 mPt/MJ and 467 mPt/MJ, respectively. Therefore, the specific environmental impact of freshwater and brine are 7.57 and 9.15 mPt/kg, respectively.

The electric power and required heat are studied by exergoeconomic and exergoenvironmental analyses, as shown in Figure 5.99. The compressors (HPC2 and LPC1) and turbines (HPT1 and LPT2) and almost equal in specific exergy cost and environmental impact of electricity. The specific exergy cost of electricity from the GT engine is 71 \$/GJ. The average specific exergy cost of electricity from SRC is for turbines 201 \$/GJ of HPST1, 89 \$/GJ of IPST2, 92 \$/GJ of LPST3, and 69 \$/GJ of PT3 and for pumps 57 \$/GJ of P1 and 74 \$/GJ of P2, and for fuel cell 19 \$/GJ of SOFC. Also, the average specific exergy cost of heat is 123 \$/GJ of the intercooler (IC) and 151 \$/GJ of the condenser (CN), as shown in Figure 5.99-a. Furthermore, the specific exergy environment of electricity is 23.5 mPt/MJ for GT since all HPC2, HPT1, LPC1, and LPT2 and almost equal. Also, the SRC engine has the average specific exergy environment of electricity of for turbines of 66.5 mPt/MJ for HPST1, 27.7 mPt/MJ for IPST2, 29.3 mPt/MJ for LPST3, and 22.8 mPt/MJ for PT3. The pumps have average specific exergy environment of

electricity of 20.8 mPt/MJ for P1 and 25.6 mPt/MJ for P2. Also, the fuel cell (SOFC) produces 5.6 mPt/MJ of specific exergy environment of electricity. In addition, the intercooler (IC) and condenser (CN) have a specific exergy environment of heat of 40.5 mPt/MJ and 46.0 mPt/MJ, respectively, as presented in Figure 5.99-b.

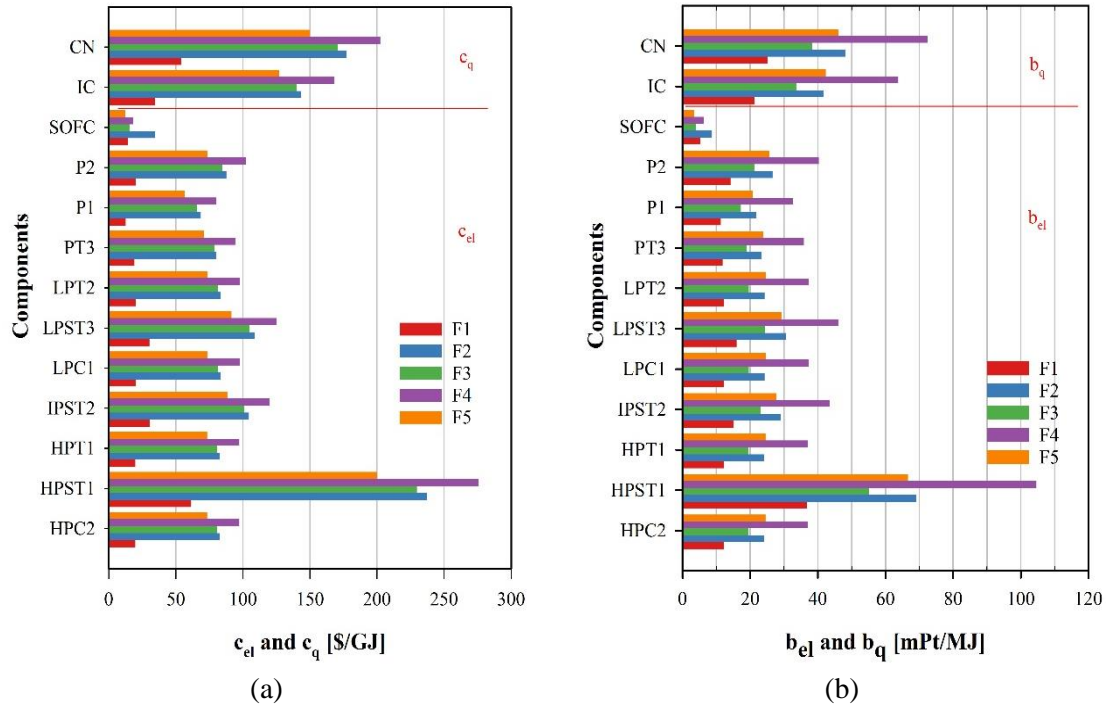


Figure 5.99 (a) Exergy cost and (b) environmental impact of electricity and heat of M-2 marine engine

Based on the above discussion, the methane and hydrogen fuel blend are the most economic and have less environmental impact because of the low methane price, which is assumed to be equal to the price of pure natural gas. However, the real price of pure methane is higher than all other fuels reaching 3.24 \$/kg (64.84 \$/GJ) as published in Global Petrol Prices-2022 [226]. That means the fuel prices of F1 and F5 will be higher, and other prices of other fuel blends will remain the same because they do not count on methane. Hence, the best choice must be among three fuel blends (F2, F3, and F4). F3 was the second least environmental impact and economic after F1, which can be a better choice if still the price of methane increases due to the current global political and energy circumstances.

5.8 Results of System M-3

This section presents the results and discussion of the thermodynamic analysis, exergy analysis, exergoeconomic analysis, and exergoenvironmental analysis of the hybrid gas turbine combined with binary systems marine engine as written in the subsections below.

5.8.1 Results of Thermodynamic Analysis

The state points of the entire system are reported in [183], which includes the mass flow rates, temperature, pressure, specific enthalpy, specific entropy, specific physical, chemical, total exergy, exergy flow rates, and molar Gibb's energy in the mixture. The air enters the GBC in stream G1 at 21 kg/s, 15 °C, and 101.3 kPa, leaves the GBC at G9 of 1130 K and 185 kPa and leaves the entire engine to the atmosphere at G11 of 392 K and 185 kPa. This GBC requires fuel at F1 of 0.75 kg/s, 293 K, and 2000 kPa. However, the fuel blend and water entering the SOFC are under the conditions of 293 kPa and 100 kPa, with mass flow rates of 0.1 kg/s for F2 and 0.15 kg/s for S1, respectively. For the ORCs, the mass flowrates of TORC and BORC are 38 and 16 kg/s, while the mass flow rate of LNG is 35 kg/s. The maximum and minimum pressures in both cycles are 2000 and 200 kPa. In addition, the maximum and minimum temperatures are 423.2 K and 304.6 K in TORC and 338.2 K and 245.9 K in BORC, respectively.

The equipment performance is also shown in Table 5.68, which includes the heat rate, power, exergy destruction rates, energy efficiency, electrical efficiency, and exergetic efficiency. The compressor HPC1 requires a power of 9288 kW and has an exergetic destruction rate of 1510 kW. The turbines HPT1, LPT2, T3, T4, and T5 deliver the power of 9466 kW, 7016 kW, 3011 kW, 439 kW, and 1000 kW, respectively. The pump power is low, about 145 kW and 60 kW for P1 and P2, respectively. The heat of CN1 and CN2 are about 20.5 MPa and 190 kW, respectively. The heat rejected from the evaporators is 8 MW for EV11, 10 MW for EV12, and 7 MW for EV2. The endothermic duty for the reactors is 19 MW for CC and 6 MW for SOFC, while the exothermic duty of SR and WGS is 1.4 MW and 63 kW, respectively. The exergy destruction rates of the groups of components are illustrated in Figure 5.100. The maximum exergy destruction is about 37 MW by the reactors resulting in about 67% of the irreversibility ratio of the destruction rates of 55.3 MW for the entire engine. The second maximum exergy destruction is about

13 MW by heat exchangers of condensers, evaporators, and a regenerator in the engine yielding its irreversibility rate to be 23%. The remaining groups of components, which include turbines, compressors, pumps, splitters, and mixers, have a destruction rate of 5.6MW with an irreversibility rate of 10%.

Table 5.68 The equipment performance in the developed marine engine

Comp#	\dot{Q}_k [kW]	\dot{W}_k [kW]	$\dot{E}x_{D,k}$ [kW]	$\eta_{th,k} (\eta_{e,k})$ [%]	ψ_k [%]
HPC1	0.0	9288.4	1509.7	76.5	83.8
HPT1	0.0	9466.1	1431.0	76.5	84.9
LPT2	0.0	7016.3	1115.8	76.5	84.1
T3	0.0	3011.4	630.0	80.0	79.1
T4	0.0	439.0	106.8	80.0	75.7
T5	0.0	998.7	293.5	80.0	77.3
P1	0.0	146.2	28.8	80.0	80.3
P2	0.0	62.6	15.3	80.0	75.5
CN1	20489.0	0.0	7476.1	100.0	99.6
CN2	190.0	0.0	567.0	100.0	99.9
EV2	6924.0	0.0	3513.1	100.0	99.9
EV11	8017.0	0.0	374.4	100.0	100.0
EV12	9607.0	0.0	300.3	100.0	100.0
GTHX	3452.0	0.0	513.8	100.0	98.1
CC	19340.0	0.0	34204.0	38.2	52.4
SOFC	5897.0	4357.0	1326.1	73.9 (85.7)	76.7
SR	1441.0	0.0	1413.7	65.5	93.5
WGS	63.0	0.0	34.3	38.0	99.5
MX	0.0	0.0	40.6	100.0	99.4
MX1	0.0	0.0	299.0	100.0	91.0
SP	0.0	0.0	0.0	100.0	100.0

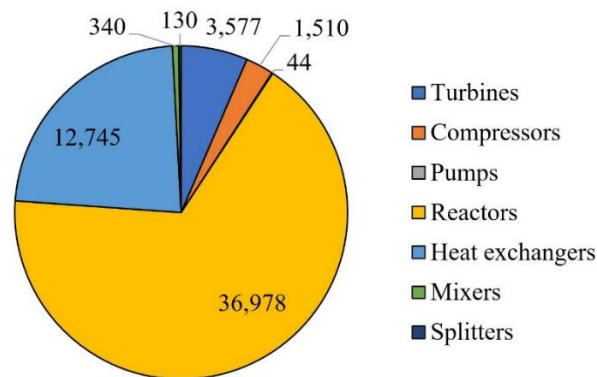


Figure 5.100 The exergy destruction rates [kW] of group of components in the integrated hybridized M-3 marine engine.

The performance of each system and the overall engine is given in Table 5.69. The net power of GBC, SOFC, TORC, and BORC is 7 MW, 4.4 MW, 3 MW, and 1.4 MW, respectively. The net heat of GBC is 19 MW resulting in its energy and exergetic efficiencies of 31.6 and 43.2%, respectively. The required and rejected heat are 20.5 MW

and 18 MW of TORC and 18 MW and 7 MW of BORC, respectively, yielding that their energetic efficiencies are 14 and 7%, respectively, and their exergetic efficiencies are 23% and 13%, respectively.

Table 5.69 The performance of subsystems and overall marine engine

Subsystems	\dot{W}_{net} [kW]	\dot{Q}_A [kW]	\dot{Q}_R [kW]	\dot{Ex}_A^Q [kW]	\dot{Ex}_R^Q [kW]	η [%]	ψ [%]
GBC	7194.0	19340.5	0.0	16154.7	0.0	31.6	43.2
TORC	2865.2	20489.0	17623.8	12506.1	10725.2	14.0	22.9
BORC	1375.1	17814.0	6924.4	10773.5	5162.0	7.72	12.76
SOFC	4357.0	4392.6	0.0	2884.1	0.0	73.9	76.7
LNG	0	0	16438.9	0	14393.5	91.7	98.8
Overall ME	15791.3	23733.1	16438.9	19038.8	14393.5	39.3	47.2

The SOFC required a net heat of 4.4 MW, and its energetic and exergetic efficiencies are 73.9% and 76.7%, respectively. For the LNG, the total rejected energy to the ORCs is 16 MW, resulting in an energy efficiency of 92% and exergetic efficiency of 99%. The overall marine engine can deliver a net power of 15791 kW with an energy efficiency of 39.3% and an exergy efficiency of 47.2%, respectively.

(a) Overall engine performance:

Five fuel blends are applied in streams of F1 and F2; they are named F1, F2, F3, F4, and F5. The mass flow rates of these fuel blends are different based on stoichiometric reactions, so the equivalence ratio is 0.960 and the same air flow rate of GBC. Since the fuels do not affect the ORCs, the net power of BORC and TORC is 2865 kW and 1375 kW, respectively, as shown in Figure 5.101-a. However, the net power of GBC and SOFC changes with the fuel type, as presented in the same figure. The maximum and minimum net power capacities of GBC are found to be 7841 kW by F2 and 7194 kW by F1, respectively, while the maximum and minimum net power values of SOFC are 4357 kW by F1 and 3980 kW by F2. This results in the overall engine power being obtained to be 16087 kW using F3 as a maximum value and a minimum value of 14790 kW using F5.

The required heat for the engine comes from the CC, SOFC, and LNG to fulfill the net power and extreme cooling loads of the evaporators. The LNG provides a constant cooling load of about 16440 kW for ORCs. The combustion chamber needs a maximum heat of 20000 kW by using F4 and a minimum heat of 19163 kW using F2. In addition, the net heat of SOFC, including subtraction of heat from the SR and WGS, is a minimum and maximum value of 4393 kW using F1 and 5471 kW using F4, as illustrated in Figure 5.101-

b. Therefore, the total required heat is calculated as the minimum value of 40.2 MW using F1 and the maximum heat of 41.9 MW using F4.

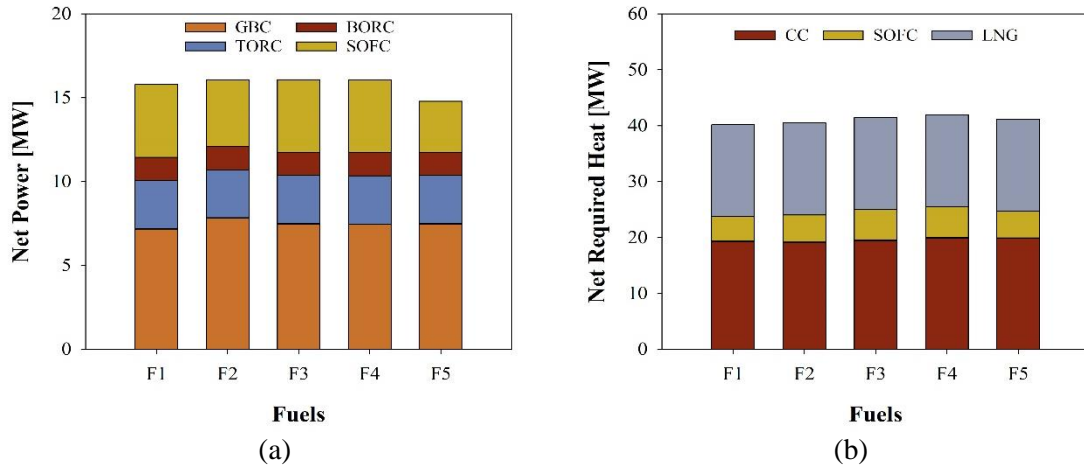


Figure 5.101 (a) The net power and (b) required heat of subsystems in the engine

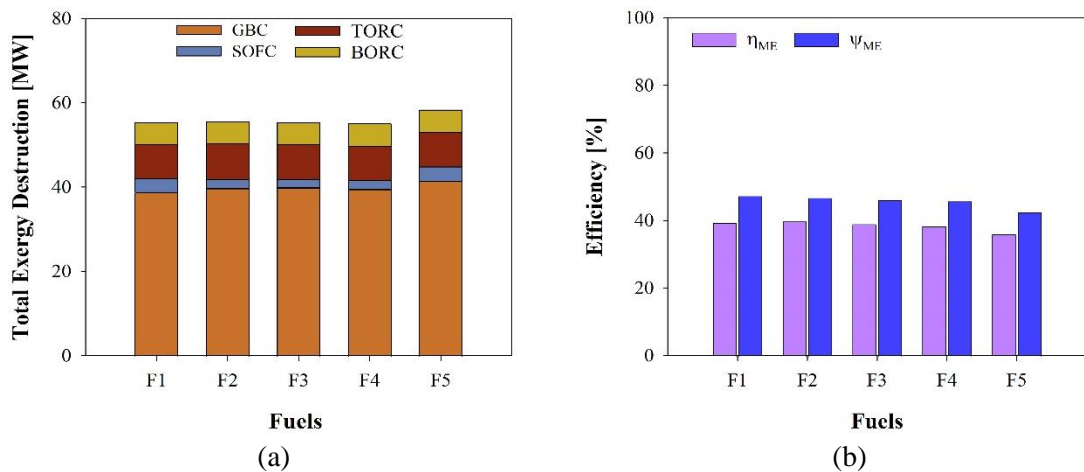


Figure 5.102 (a) Total exergy destruction rate and (b) efficiencies of subsystems in M-3 engine

The exergy destruction rates of the four subsystems are given in Figure 5.102-a. The total exergy destruction rate reaches its maximum value of 58.3 MW using F5, and its minimum value of 55.3 MW using F3, then slightly above 55.3 MW using F1. This increase in F5 is due to the increase of exergy destruction of reactors, especially the CC and SOFC, because of the chemical decomposition and reaction of five fuels. The GBC is the most contributor to the exergy destruction rate at about 70%, followed by the TORC (about 15%), then BORC (9%) and SOFC (6%). By combining the previous discussion, the overall energetic and exergetic efficiencies are explained in Figure 5.102-b. The maximum performance is achieved by using F2 to be 40% energy efficiency and 47% exergetic

efficiency, while the minimum performance is given by using F5 to be 36% and 43% of energetic and exergetic efficiencies, respectively.

(b) Performance of solid oxide fuel cell:

The direct SOFC consists of SR, WGS and SOFC modules. Each component contributes to the reaction duty, whether endothermic or exothermic. The heat of SR is a maximum of 1441 kW by F1 and a minimum of 252 kW by F4, while the heat of WGS is a maximum of 148 kW by F3 and a minimum of 63 kW by F1. The heat of SOFC modules ranges from 5562 kW by F5 to 5900 by F1. Also, the net power of SOFC varies from 3052 kW by F5 to 4357 kW by F1, as shown in Figure 5.103-a.

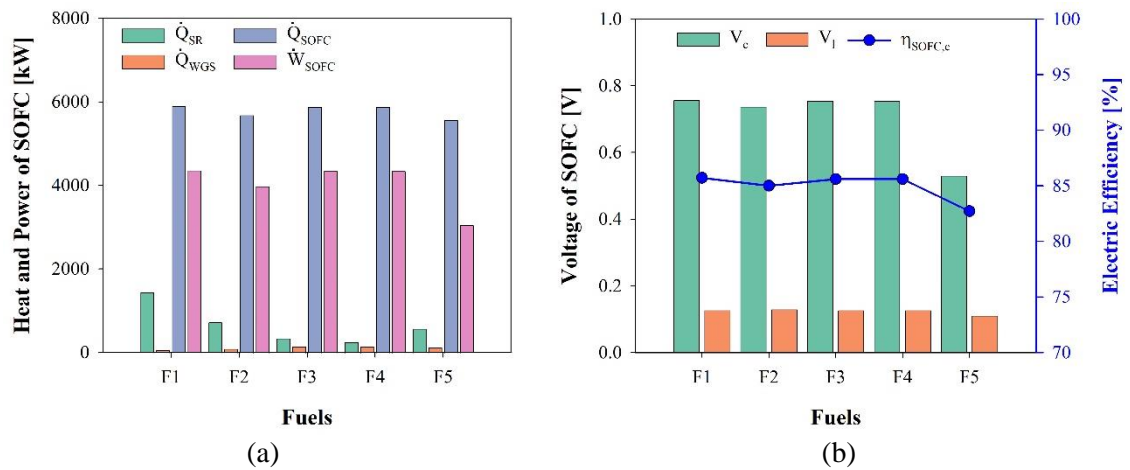


Figure 5.103 The SOFC Performance and its direct components: (a) Heat and power of SOFC components, and (b) cell and loss voltage and electrical efficiency.

This net power is a result of cell voltage and loss voltage of electrochemical reactions of hydrogen and oxygen. The maximum and minimum cell voltage are 0.756 V by F1 and 0.53 V by F5, respectively, while the average loss voltage is 0.124V, resulting in the electric efficiency of SOFC to be an average of 85%, a maximum of 86% by F1 and a minimum of 83% by F5, as shown in Figure 5.103-b.

The amount of hydrogen produced by the SR and WGS is high at 29.8 kg/s by using F1, F3, F4, and F5, and low at 28.0 kg/s by using F2. This amount requires 16 stacks for the maximum amount of hydrogen and 15 stacks for the minimum, as shown in Figure 5.104-a. Therefore, the performance of SOFC system is the maximum by F1, F3, and F4 to be 74% energy efficiency and 86% of exergetic efficiency, and the minimum by F5 to be 55% of energetic and exergetic efficiency together, as plotted in Figure 5.104-b.

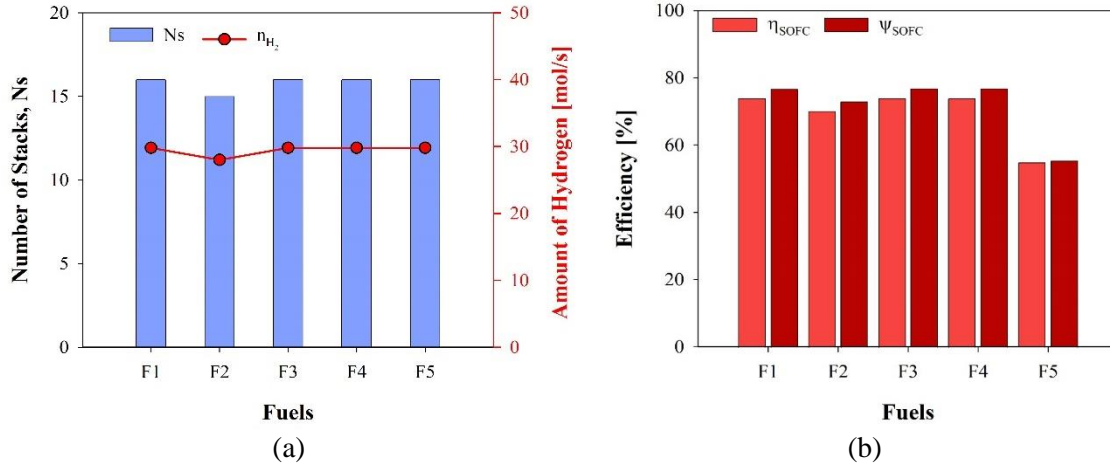


Figure 5.104 (a) Number of SOFC stacks according to amount of hydrogen and (b) SOFC efficiencies.

(c) Performance of gas Brayton cycle:

The GBC power and heat vary with the fuel blends, as shown in Figure 5.105. The required power of the compressor remains constant at 928 kW. The output power of turbines changes from 16482 kW by F1 to 17130 kW by F2. Regarding the heat, the combustion chamber requires a maximum heat of 2000 kW using F4 and a minimum heat of 19163 kW using F2. However, the duty of the regeneration heat exchanger (GTHX) held unchanging with a duty of 3451 kW, as shown in Figure 5.105-a. The performance of GBC is achieved to be a maximum of 35% energy efficiency and 47% exergy efficiency using F2 and to be a minimum of 32% and 43% of energy and exergetic efficiencies of F1, respectively, as illustrated in Figure 5.105-b.

The exhaust temperature at the turbine exit at G8 is an average of 1242 K, which is a very high temperature since the combustion temperature is set to 1536 °C as stated in the manufacturing sheet of Taurus 65 [229]. This is a massive heat lost to the atmosphere; therefore, a regenerative heat exchanger (GTHX) is added before the CC to reduce the combustion heat and increase the GBC efficiency. By then, the temperature drops from 1242 K to 1130 K at G9, as shown in Table 5.70, which again is high temperature and heat and can be utilized by adding two ORCs to reduce the exhaust temperature to about 413 K at G10 and about 406 K at G11. These two systems and GTHX can take the benefit of waste energy and save about an average of 60%.

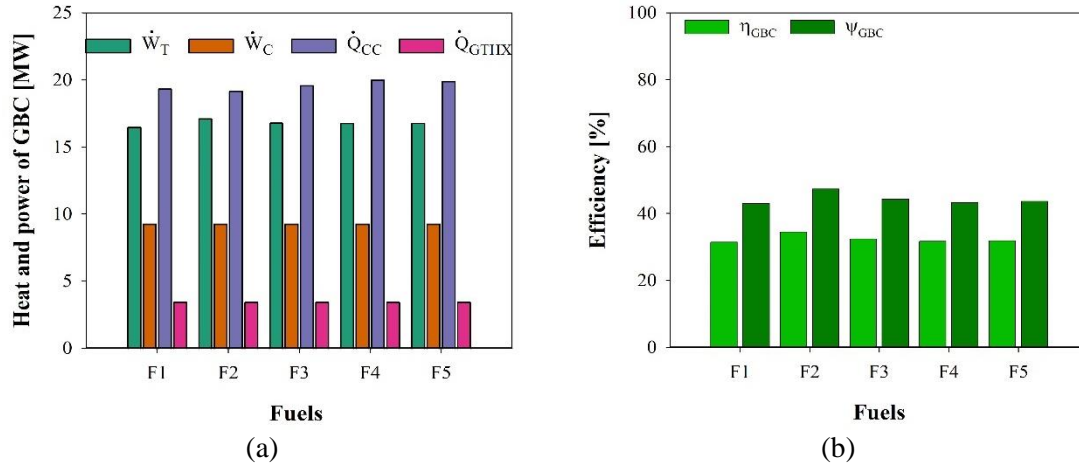


Figure 5.105 The GBC performance with respect to fuel blends: (a) heat and power, and (b) efficiencies

Fuel	Exhaust Temperature of GBC [K]				Waste energy saving (%)
	G8	G9	G10	G11	
F1	1242.3	1130.0	399.7	392.3	59.8
F2	1244.0	1136.2	436.9	429.8	62.5
F3	1240.8	1130.2	411.4	404.1	59.7
F4	1240.4	1129.6	409.0	401.7	59.3
F5	1240.7	1130.1	410.7	403.4	59.7

(d) Performance of organic Rankine cycles:

The ORCs are topper and bottomer ORCs, which are used to provide power at low temperatures. The TORC uses pentane and butane in an equal amount, while BORC uses propene and propane in an equal amount as well. The evaporator temperature of TORC drops from 361K at TR4 to 305 K in the saturated phase by EV11 and then to the liquid phase at 305 K by EV12. Also, the evaporator temperature of BORC declines from 256 K of LR7 to the liquid phase of LR1 at 244 K. This temperature drop was caused by the asset of the BORC condensers and by the LNG, which enters the EV11 at LNG1 of 73 K and leaves it at LNG2 of 151. Also, the LNG continues to cool the BORC evaporator and increases its temperature to LNG3 at 190 K in the liquid state, as shown in Figure 5.106-a.

The Condenser required heat of TORC and BORC are about 21 MW and 18 MW, respectively, while the evaporator rejected heat of TORC and BORC are 18 MW and 7 MW, respectively. The power of turbines and pumps are evaluated as 3 MW and 146 kW for TORC and ~1.4 MW and 63 kW for BORC, respectively, as presented in Figure 5.106-

b. The energetic and exergetic efficiency is estimated to be 14% and 23% for TORC and 8% and 13% for BORC, respectively, as displayed in Figure 5.106-c. However, the LNG enters the ORCs systems in a liquid state so it can be stored for other cooling services. The energetic and exergetic efficiency of LNG is more than 90%.

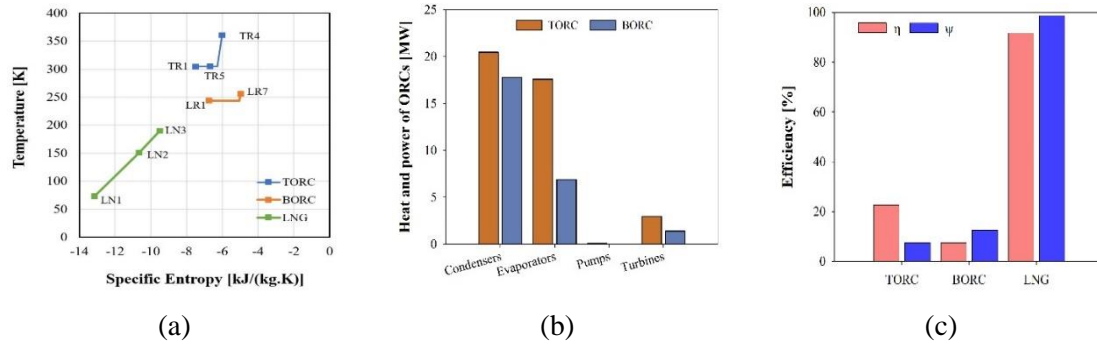


Figure 5.106 The Performance of TORC, BORC, and LNG: (a) temperature of EVs and LNG, (b) heat and power, and (c) efficiencies.

(e) *Fuel consumption and carbon emissions:*

The mass flow rates for air and refrigerants of ORCs remain unchanged, which are 21 kg/s for air, 38 kg/s for TORC, 16 kg/s for BORC, and 35 kg/s of LNG, while the fuel changes according to its substances and mass ratios. The GBC uses fuel mass flow rates of 0.75 kg/s of F1, 1.17 kg/s for F2, 0.79 kg/s for F3, 0.78 kg/s for F4, and 0.77 kg/s for F5. The fuel mass flow rate to the SOFC has an average of 0.12 kg/s with a maximum of 0.15 kg/s for F2 and a minimum of 0.1 kg/s for F1. The mass flow rate of the overall engine is the summation of that of GBC and SOFC, as shown in Figure 5.107-a. The water mass flow rate is 0.15 kg/s, 0.08 kg/s, 0.03 kg/s, 0.03 kg/s, 0.06 kg/s mixed with the fuel blend in the same order as F1 to F5. The SFC is averaged at 113 g/kWh for SOFC, 407 g/kWh for GBC, and 223 g/kWh for the overall engine. The maximum SFC occurred using F2, and the minimum SFC using F1, as shown in Figure 5.107-b. The carbon emissions are maximum using F1 to reach 1.7g kg/s and minimum by 1.04 for F4 for the overall engine and GBC. the carbon emissions released from the fuel cell are about 10% of the overall, as shown in Figure 5.107-c.

As previously mentioned, the Aframax ship demands a total power of 10400 kW operated by a diesel engine of Wärtsilä 6X62. If the GBC is operated only using the MGO-DMA, the fuel and air mass flow rates will be 2.3 kg/s and 42.5 kg/s, respectively, using MAR 100 gas turbine [230]. This operation will generate a net power of 11817kW and use

the heat of 35154 of combustion, resulting that the energy and exergy efficiency will be 33.6% and 40.2%, respectively. Not only that but also the carbon emissions will be 6.56 kg/s, which is quintuple the emissions of the proposed system. In addition, the SFC of this MARs 100 operated by MGO-DMA will be about 700.7 g/kWh, as shown in Table 5.71. The proposed integrated hybridized marine engine has increased the total power by an average of 33%, with decreasing fuel mass by 61% for all fuels. Also, the proposed SFC significantly declined by more than 55% and a maximum of 72.3 by F1. Fortunately, the carbon emissions have substantially reduced to about an average of 80%. In addition, the proposed engine performance has increased by more than 13% by using F1 to F4 and by about 6% using F5.

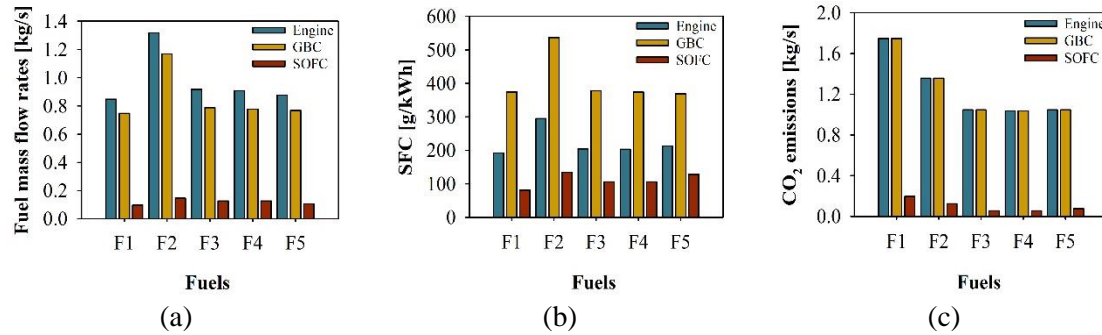


Figure 5.107 (a) Fuel mass flow rates, (b) SFC, and (c) CO₂ emissions of GBC, SOFC, and entire engine

The proposed engine uses a gas turbine to deliver half capacity and is combined with SOFC and ORCs. That means the size of the gas turbine must be lower and changed to another type, such as Taurus 65 [229], to deliver a power of 6500 kW using traditional fuels and more power under the same working conditions but less fuel flow rate. This engine weighs 39600 kg. The SOFC stack of 100 cells weighs 64 kg [212], so the total weight of 15 stacks is 960 kg for F2 and of 16 stacks is 1024 kg for the remaining fuel blends. The ORCs consist of heat exchangers with a maximum duty of 20000 kW that fits all two condensers and three evaporators, in addition to three turbines and two pumps. The weight of a compactable shell and tube heat exchanger of Aalborg MP-C with a length of 1.2 m is 183 kg for 20 °C, 269 kg for 25 °C, and 353 kg for 30 °C [231]. Also, the turbines are chosen to be Turboden gas expanders to deliver a power of 1-5MW with a weight of 7710 kg [232]. Therefore, the weight of ORCs system is the summation of 1072 kg for condensers (CN1, CN2, EV11, and EV12), 183 kg for evaporator (EV2), 23130 kg for

turbines (T3, T4, and T5), and 160 for pumps (P1 and P2). Thus, the total weight of ORCs is 24545 kg. Therefore, the total weight of this proposed engine is 65169 kg for all fuel blends except for F2, which is 65105 kg. This proposed engine weighed less than the traditional MARs 100 only by 21% and less than the traditional diesel engine of 377000 kg by 80%. In conclusion, the proposed engine is more efficient, less environmental impact, and less weight, and more reliable.

Table 5.71 Comparison of traditional marine engine and sustainable fuels hybrid marine engines

Fuels	\dot{W}_o [kW]	\dot{m}_f [kg/s]	SFC _i [g/kWh]	CO _{2,i} [kg/s]	η_t [%]	ψ_t [%]	Weight [kg]
MGO	11817.0	2.30	700.7	6.56	33.6	40.2	82,145
F1	15791.3 (↑33.6)	0.85 (↓63.0)	193.8 (↓72.3)	1.75 (↓73.4)	39.3 (↑17.0)	47.2 (↑17.4)	65169 (↓20.7)
F2	16061.0 (↑35.9)	1.32 (↓42.6)	295.9 (↓57.8)	1.36 (↓79.3)	39.7 (↑18.2)	46.7 (↑15.9)	65105 (↓20.7)
F3	16087.3 (↑36.1)	0.92 (↓60.0)	205.9 (↓70.6)	1.05 (↓83.9)	38.9 (↑15.7)	46.1 (↑14.6)	65169 (↓20.7)
F4	16059.4 (↑35.9)	0.91 (↓60.4)	204.0 (↓70.9)	1.04 (↓84.1)	38.3 (↑14.1)	45.7 (↑13.4)	65169 (↓20.7)
F5	14789.8 (↑25.2)	0.88 (↓61.7)	214.2 (↓69.4)	1.05 (↓84.0)	35.9 (↑6.9)	42.5 (↑5.5)	65169 (↓20.7)

5.8.2 Results of Exergy Analysis

The hybrid gas turbine combined with binary systems is analyzed using the exergy analysis based on fuel and product principal. The exergy rates are plotted for each stream of the proposed marine engine using the Sankey diagram, as shown in Figure 5.108. The exergy rate of (methane and hydrogen) fuel blend is 51866 kW entering the combustion chamber (CC) and 6788 kW entering the fuel cell (SOFC). The exhaust gases from the turbine (LPT2) have an exergy rate of 18613 kW, which has been reduced to 3518 kW after passing through the heat exchanger (GTH), first condenser (CN1) and the second condenser (CN2). The exergy rates of the top organic Rankine cycles (TORC) have an average of 183185 kW (light blue colour), and the BORC and LNG have an average exergy rate of 77168 kW (orange colour) and 184900 kW (pink colour), respectively.

The exergy analysis is applied on marine engine components, as listed in Table 5.72. The net power of this proposed marine engine is 15791 MW, and the required heat is 40172 MW, which makes the energy and exergy efficiencies to be 38% and 47%, respectively. The fuel and product exergy rates of this engine are 177069 kW and 94891 kW, respectively, which makes the destruction exergy rate to be 82178 kW, and the losses exergy rate due to the losses of SOFC is 729 kW. The engine exergetic efficiency is 53.6%, which is greater than the other exergy efficiency of 47%. Also, the destruction ratio is 46.4%.

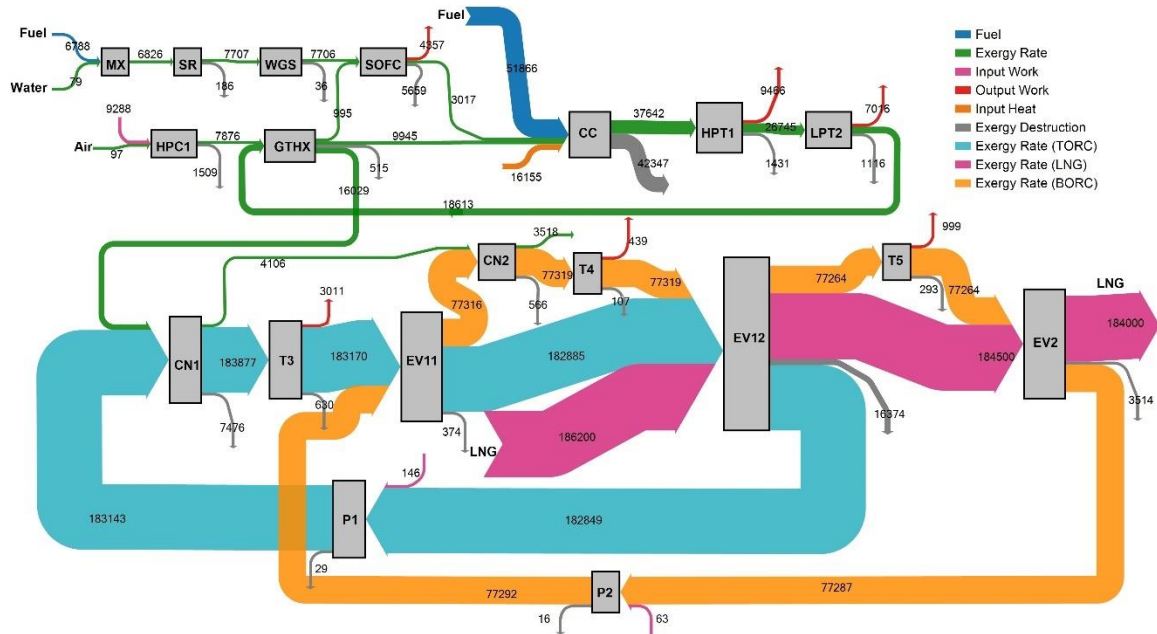


Figure 5.108 The Sankey flowchart of exergy rates of M-3 marine engine

Table 5.72 The exergy performance of M-3 marine engine

#	W_K	\dot{Q}_K	$\dot{E}x_{F,K}$	$\dot{E}x_{P,K}$	$\dot{E}x_{D,K}$	$\dot{E}x_{L,K}$	ϵ	y	y^*
Units	[kW]	[kW]	[kW]	[kW]	[kW]	[kW]	[%]	[%]	[%]
HPC1	9288	0	9288	7779	1509	0	83.75	0.85	1.84
HPT1	9466	0	10897	9466	1431	0	86.87	0.81	1.74
LPT2	7016	0	8132	7016	1116	0	86.28	0.63	1.36
T3	3011	0	3641	3011	629.6	0	82.70	0.36	0.77
T4	439	0	546	439	107	0	80.40	0.06	0.13
T5	998.7	0	1292	998.7	293.3	0	77.30	0.17	0.36
P1	146.2	0	146.2	117	29.2	0	80.03	0.02	0.04
P2	62.6	0	62.6	47	15.6	0	75.08	0.01	0.02
CN1	0	20489	11923	4447	7476	0	37.30	4.22	9.10
CN2	0	190.2	588	22	566	0	3.74	0.32	0.69
EV2	0	6924	5035	1521	3514	0	30.21	1.98	4.28
EV11	0	8017	619	245	374	0	39.58	0.21	0.46
EV12	0	9607	16675	301	16374	0	1.81	9.25	19.93
GTHX	0	3452	2584	2069	515	0	80.07	0.29	0.63
CC	0	19341	79989	37642	42347	0	47.06	23.92	51.53
SOFC	4357	5897	10016	4357	5659	729	43.50	3.20	6.89
SR	0	1441	7893	7707	185.6	0	97.64	0.10	0.23
WGS	0	63.2	7742	7706	36.22	0	99.54	0.02	0.04
Total			177068.8	94891	82178	729	53.59	46.41	100

The exergy analysis is conducted with respect to different fuel blends, as shown in Figure 5.109. The fuel blends have a slight effect on exergy analysis. The fuel, product, and destruction exergy rates are estimated to be 179 MW, 96 MW, and 83 MW, respectively, while the average of loss exergy rate is 0.7 MW, as shown in Figure 5.109-a.

This yields the average of exergetic efficiency and destruction ratio to be 53.6% and 46.4%, respectively, as displayed in Figure 5.109-b.

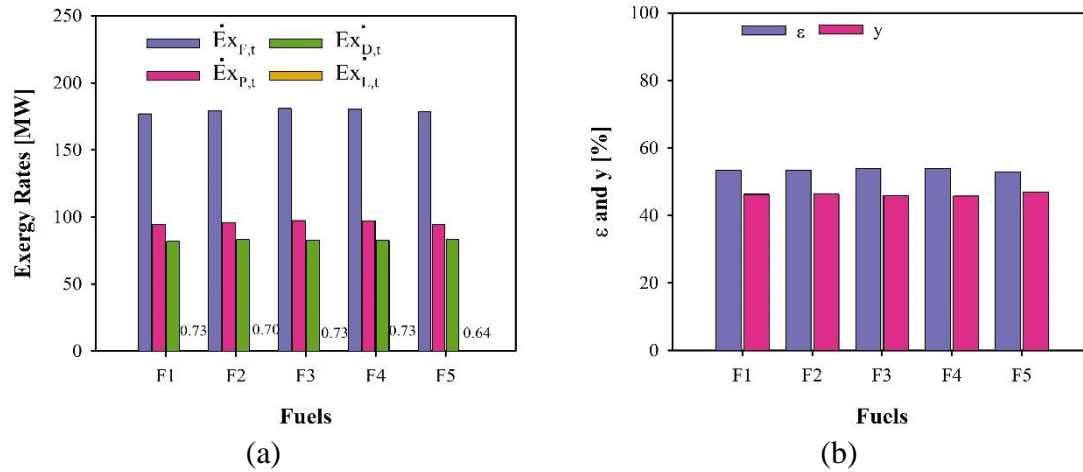


Figure 5.109 Exergy analysis of M-3 engine based on fuel blends: (a) fuel, product, destruction, and losses exergetic rates, and (b) exergetic efficiency and exergy destruction ratio

5.8.3 Results of Exergoeconomic Analysis

The exergoeconomic analysis is conducted on the hybrid GT combined with binary systems, with the fuel blend cost of 7.15\$/GJ of methane and hydrogen. The exergoeconomic rates of streams are drawn by Sankey diagram, as presented in Figure 5.110. The exergy cost rates of fuel blend are 1335 \$/h and 175 \$/h for entering the CC and SOFC, respectively.

The exhaust gases have exergy cost rate of 1242 \$/h, which is lessened to 225 \$/h by passing through the heat exchanger (GTH) and the condensers (CN1 and CN2). The mixture of TORC (propane and propene) and BORC (pentane and butane) have 0.59 \$/kg and 1.74 \$/kg, respectively. Also, the price rate of LNG fluid has 1.29 \$/kg. The average exergy cost rates of BORC and TORC are 3434 \$/h and 23892 \$/h, respectively. In addition, the average LNG exergy cost rate is 16256 \$/h. The engine component costs are tabulated in Table 5.73. The turbine (HPT1) and fuel cell (SOFC) have the maximum initial price of \$3.9M and \$2.0M, respectively. The total initial cost of this marine engine is \$8.1M, and its normalized cost is \$16.8M based on CEPCI of May 2022. The levelized annual cost rate is 242.5\$/h.

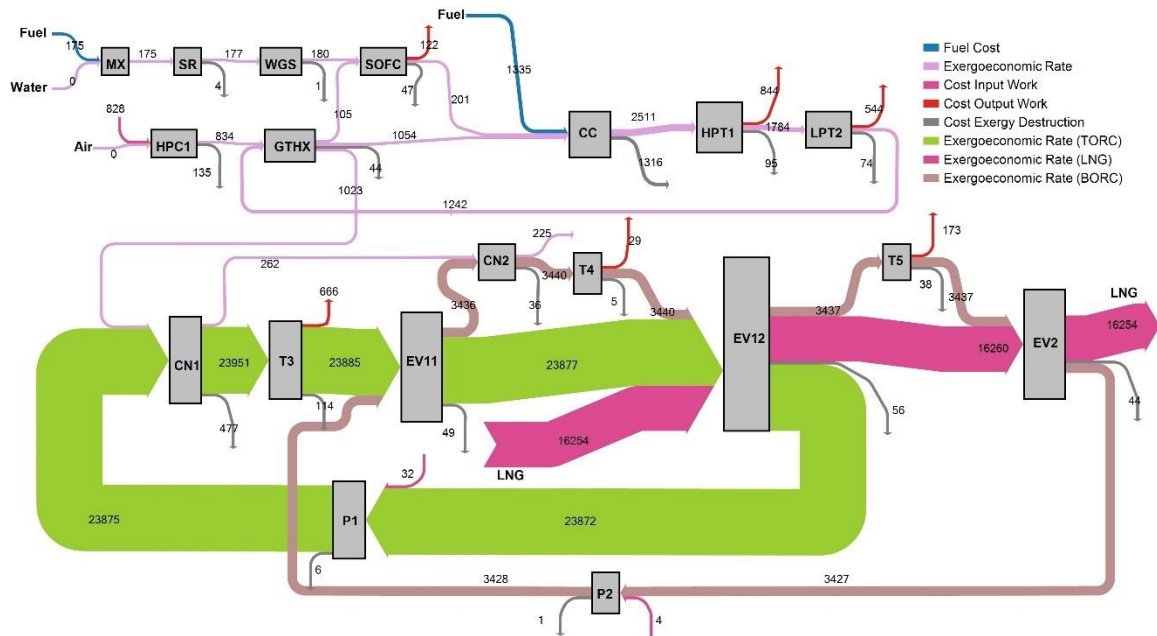


Figure 5.110 The Sankey flowchart of exergoeconomic rates of M-3 engine.

Table 5.73 The components' costs of M-3 marine engine

#	C_K [\$]	Z_K [\$] (2022)	\dot{Z}_K [\$/h]
HPC1	206,158	426,214	6.17
HPT1	3,913,000	8,089,000	117.00
LPT2	39,216	81,076	1.17
T3	305,735	640,042	9.26
T4	155,026	324,538	4.70
T5	222,172	465,105	6.73
P1	16,831	35,234	0.51
P2	9,592	20,081	0.29
CN1	38,004	78,570	1.14
CN2	3,487	7,208	0.10
EV2	69,637	143,968	2.08
EV11	81,663	168,830	2.44
EV12	21,779	45,026	0.65
GTHX	7,109	14,696	0.21
CC	892,260	1,845,000	26.69
SOFC	1,952,000	4,036,000	58.40
SR	75,951	158,999	2.30
WGS	88,473	185,213	2.68
Total	8,098,093	16,764,800	242.53

The exergoeconomic analysis of the hybrid combined marine engine is displayed in Table 5.74. The net exergy cost rate of the net power is 1513 \$/h, and the exergy cost rate is 0 \$/h for required heat. The fuel, product, destruction, and loss exergy cost rates are

7121 \$/h, 7341 \$/h, 2542 \$/h, and 6 \$/h, respectively. In addition, the specific fuel and product exergy costs are 11.17 and 21.49 \$/GJ, respectively. Therefore, the relative cost difference is 92.37% because the specific product exergy cost is greater than that of fuel by 1.9 times. Also, the exergoeconomic factor is 8.71% since the destruction exergy cost rate is greater than the levelized cost rate by about 10 times.

Table 5.74 The exergoeconomic analysis of M-3 marine engine components

#	\dot{C}_K^W [\$/h]	\dot{C}_K^Q [\$/h]	$\dot{C}_{F,K}$ [\$/h]	$\dot{C}_{P,K}$ [\$/h]	$\dot{C}_{D,K}$ [\$/h]	$\dot{C}_{L,K}$ [\$/h]	$C_{F,K}$ [\$/GJ]	$C_{P,K}$ [\$/GJ]	f [%]	r [%]
HPC1	828.2	0	828.2	834.3	134.6	0	24.77	29.79	4.38	20.28
HPT1	844.0	0	727.0	844.3	95.5	0	18.53	24.77	55.07	33.64
LPT2	543.7	0	542.5	543.7	74.5	0	18.53	21.53	1.55	16.16
T3	666.3	0	657.0	666.3	113.6	0	50.12	61.47	7.54	22.63
T4	29.0	0	24.3	29.0	4.8	0	12.36	18.34	49.66	48.44
T5	172.9	0	166.2	172.9	37.7	0	35.73	48.09	15.14	34.58
P1	32.4	0	32.4	32.9	6.5	0	61.47	78.02	7.31	26.93
P2	4.1	0	4.1	4.4	1.1	0	18.34	26.15	22.01	42.57
CN1	0	0	760.8	761.9	477.0	0	17.72	47.59	0.24	168.50
CN2	0	0	37.5	37.6	36.1	0	17.73	475.00	0.29	2579.85
EV2	0	0	62.9	65.0	43.9	0	3.47	11.87	4.53	241.98
EV11	0	0	80.9	83.3	48.9	0	36.29	94.45	4.76	160.28
EV12	0	0	57.4	56.8	56.4	0	0.96	52.38	1.14	5376.19
GTHX	0	0	219.0	219.2	43.6	0	23.54	29.43	0.48	25.01
CC	0	0	2485.0	2511.0	1315.6	0	8.63	18.53	1.99	114.72
SOFC	121.8	0	83.8	121.8	47.4	6.1	2.33	7.77	55.21	233.97
SR	0	0	174.7	177.0	4.1	0	6.15	6.38	35.90	3.76
WGS	0	0	177.0	179.7	0.8	0	6.35	6.48	76.40	2.00
Total			7121.0	7341	2542	6.1	11.17	21.49	8.71	92.37

The exergoeconomic analysis has been applied on the marine engine based on different fuel blends named by F1 to F5, as presented in Figure 5.111. The product exergy cost rate is slightly increased more than the fuel exergy cost rate by about 3% among all the fuel blends. The fuel exergy cost rates are about 7 k\$/h for F1, 25 k\$/h for F2, 23 k\$/h for F3, 27 k\$/h for F4, and 20 k\$/h for F5. The destruction exergy cost rates have an average of 7164 \$/h with a maximum and minimum of 9493 \$/h and 2542 \$/h, respectively, as illustrated in Figure 5.111-a. The specific fuel and product exergy costs are 11.2 and 21.5 \$/GJ, 38.1 and 71.8 \$/GJ, and 35.6 and 66.6 \$/GJ, 42.2 and 78.7 \$/GJ, and 31.0 and 59.0 \$/GJ for F1 to F5, respectively, as shown in Figure 5.111-b.

The exergoeconomic performance of the engine is performed with respect to the fuel blends, as displayed in Figure 5.112. The relative cost difference in is within the range of 86.9 to 92.4%. Also, the exergoeconomic factor is the minimum of 2.5% for F4 and the maximum of 8.7% for F1, as shown in Figure 5.112-a. The exhaust gases form the second

condenser (CN2) have an average specific exergy cost of 51.9 \$/GJ, as presented in Figure 5.112-b. The methane and hydrogen fuel blend is the most economic fuel, which produces minimum exergoeconomic performance.

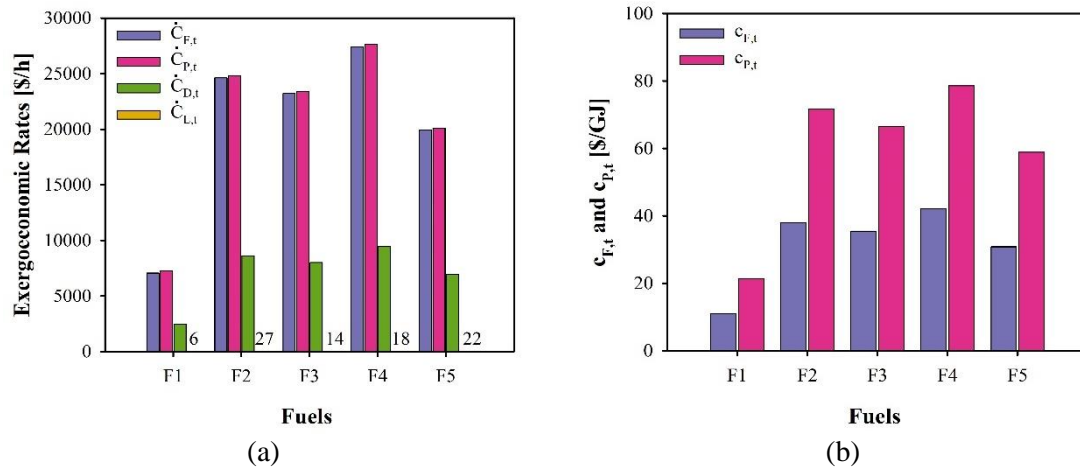


Figure 5.111 (a) Exergoeconomic rates and (b) specific exergy costs of the M-3 marine engine with respect to fuel blends

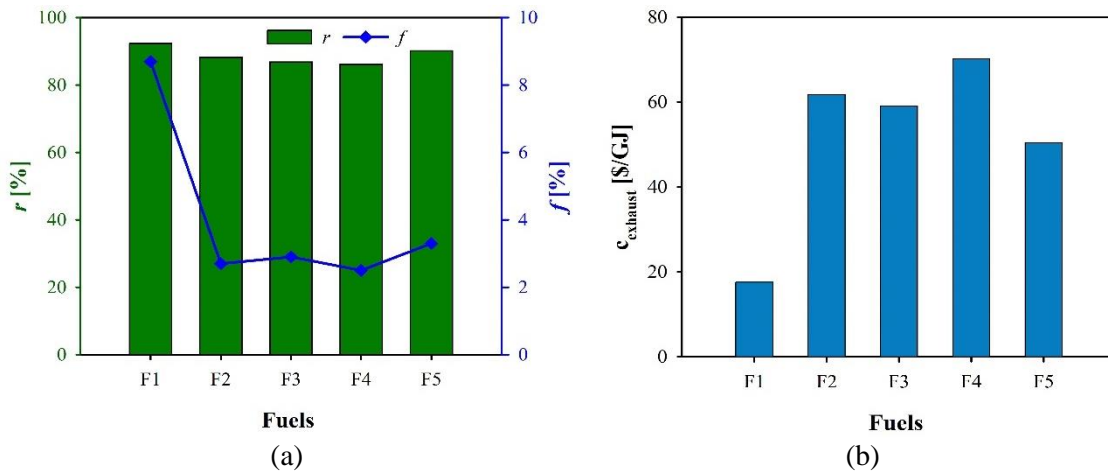


Figure 5.112 Exergoeconomic performance of a hybridized M-3 marine engine: (a) relative cost difference and exergoeconomic factor, and (b) Specific exergy cost of exhaust.

5.8.4 Results of Exergoenvironmental Analysis

The exergoenvironmental analysis is also performed on the proposed marine engine since the methane and hydrogen fuel blend has an environmental impact of 5.44 mPt/MJ. The exergoenvironmental rates of streams are plotted using the Sankey flowchart, as displayed in Figure 5.113. The fuel streams have exergoenvironmental rates of 1016 Pt/h for entering the CC and 133 Pt/h for entering the SOFC. The exergoenvironmental rate of exhaust gases

is evaluated to be 672 Pt/h which is eliminated to 125 Pt/h after crossing the GTHX, CN1, and CN2. The life cycle analysis of components is estimated, as listed in Table 5.75, which considers the production, processing, and disposal phases. The total weight of the proposed marine engine is 115,081 kg. The total environmental impact, \dot{Y} , and its rate, \dot{Y} , are 20k Pt and 131.7mPt/h, respectively.

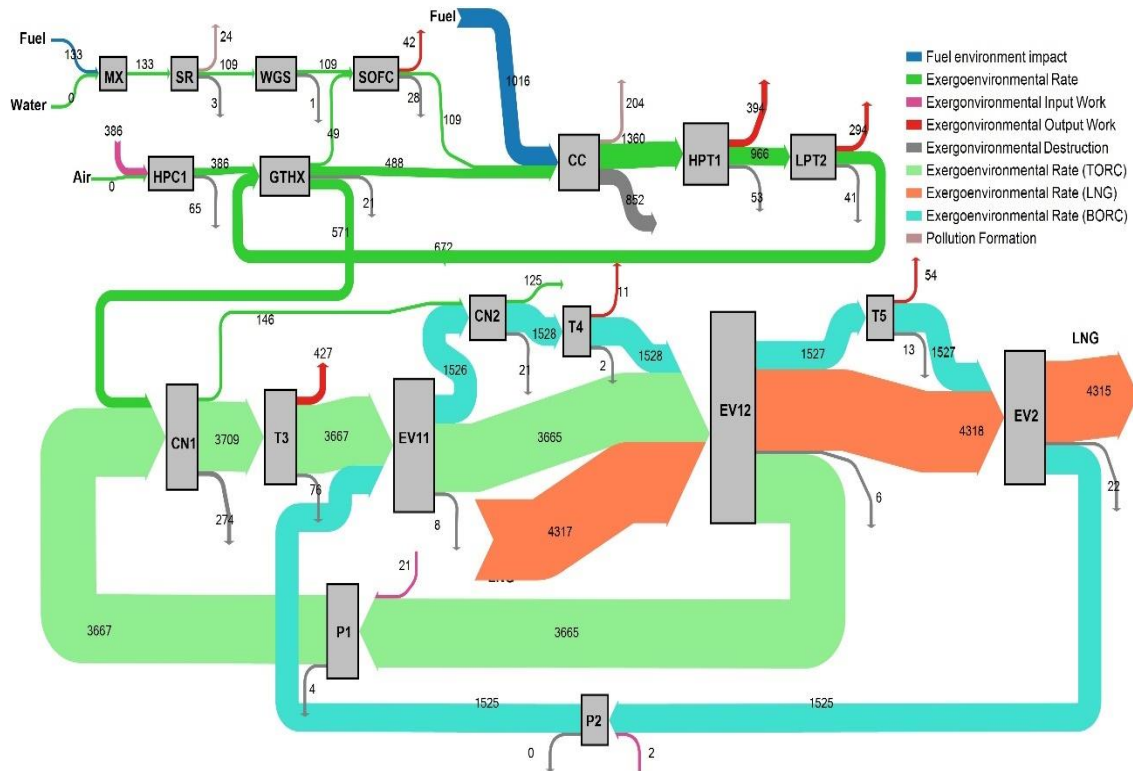


Figure 5.113 The Sankey flowchart of exergoenvironmental rates of M-3 engine [Pt/h]

The exergoenvironmental analysis is calculated for each component of marine engine, as tabulated in Table 5.76. The net marine engine power has an exergoenvironmental rate of 813 Pt/h, but the required heat has no exergoenvironmental rate. The fuel, product, and destruction exergoenvironmental rates are 4038 Pt/h, 3803 Pt/h, and 1489 Pt/h, respectively.

However, the loss exergoenvironmental rate is 3.6 Pt/h. In addition, the pollution formation and total environmental rates are -228 Pt/h and 1261.3 Pt/h, respectively. The negative sign shows the pollution is eliminated by the proposed engine since the methane and carbon monoxide are completely combusted and no by-products of them.

Table 5.75 The component-related environmental impact results of M-3 marine engine

#	Weight [kg]	Material Production [mPt/kg]	Material Processing [mPt/kg]	Material Disposal [mPt/kg]	Total EI [mPt/kg]	Total Y [mPt]	\dot{Y} [mPt/h]
HPC1	13,739	131	12	24	166	2,286,992	15.038
HPT1	25,281	104	12	24	140	3,533,375	23.233
LPT2	20,316	104	12	24	140	2,839,446	18.670
T3	10,956	104	12	24	140	1,531,253	10.069
T4	2,687	104	12	24	140	375,480	2.469
T5	4,895	104	12	24	140	684,189	4.499
P1	695	186	17	24	227	157,761	1.037
P2	311	186	17	24	227	70,476	0.463
CN1	1451	91	12	24	127	184296	1.212
CN2	14	91	12	24	127	1793	0.012
EV2	5,185	91	12	24	127	658,501	4.330
EV11	5729	91	12	24	127	727515	4.784
EV12	6479	91	12	24	127	822761	5.410
GTHX	6855	91	12	24	127	870603	5.725
CC	1,702	638	20	24	682	1,160,872	7.633
SOFC	6,627	274	22	24	320	2,121,366	13.949
SR	1,619	911	20	24	955	1,546,260	10.167
WGS	540	811	20	24	855	461,571	3.035
Total	115,081					20,034,510	131.73

Table 5.76 The exergoenvironmental analysis of M-3 marine engine components

#	\dot{B}_K^W [mPt/h]	\dot{B}_K^Q [mPt/h]	$\dot{B}_{F,K}$ [mPt/h]	$\dot{B}_{P,K}$ [mPt/h]	$\dot{B}_{D,K}$ [mPt/h]	$\dot{B}_{L,K}$ [mPt/h]	\dot{B}_K^{PF} [mPt/h]	\dot{B}_K^T [mPt/h]
HPC1	386346	0	386346	386361	64562.1	0	0	64577.2
HPT1	393737	0	393714	393737	53180.0	0	0	53203.2
LPT2	293832	0	293813	293832	41473.7	0	0	41492.3
T3	426970	0	426961	426970	75939.3	0	0	75949.4
T4	10794	0	10792	10794	2175.3	0	0	2177.8
T5	54182	0	54177	54182	12650.2	0	0	12654.7
P1	20729	0	20729	20731	4258.4	0	0	4259.5
P2	1539	0	1539	1540	394.5	0	0	394.9
CN1	0	0	424737	424738	273929.2	0	0	273930.4
CN2	0	0	20947	20947	20739.4	0	0	20739.4
EV2	0	0	30002	30006	21537.1	0	0	21541.4
EV11	0	0	12412	12417	7713.6	0	0	7718.4
EV12	0	0	6043	6037	6103.5	0	0	6108.9
GTHX	0	0	101490	101496	20805.2	0	0	20811.0
CC	0	0	1564000	1360000	851654.8	0	-203829	647833.6
SOFC	41655	0	48610	41655	28249.2	3638.5	0	28263.1
SR	0	0	132940	108723	3215.3	0	-24226	-21000.8
WGS	0	0	108723	108805	523.2	0	79	605.1
Total			4037975	3802971	1489104	3638.5	-227976	1261259.5

The exergoenvironmental performance is measured by specific environmental impact, exergoenvironmental factor, and relative environment different, as tabulated in Table 5.77. The overall specific fuel and product environmental impact are 6.52 and 11.45 mPt/MJ, respectively. This yields the overall relative environment difference to be 75.7% and the overall exergoenvironmental factor to be 0.010%.

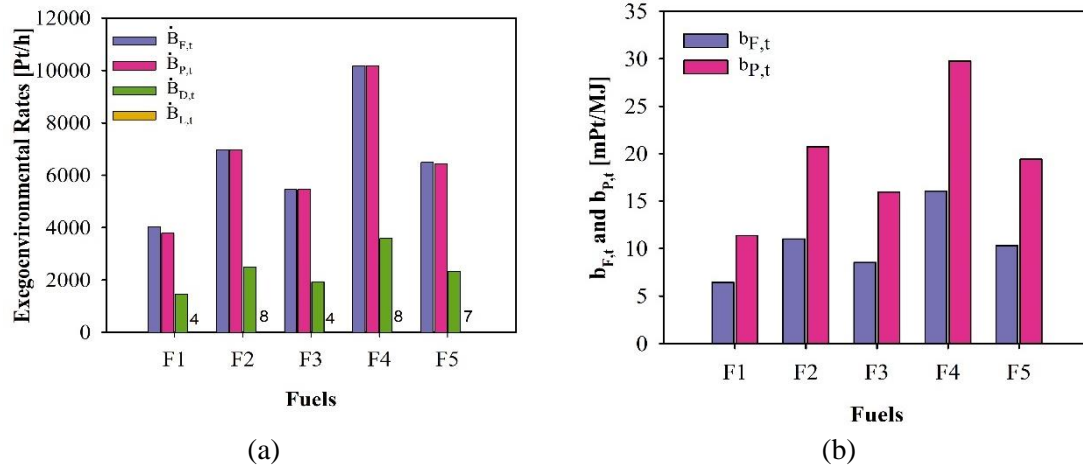


Figure 5.114 (a) Exergoenvironmental rates and (b) specific exergy costs of the hybridized M-3 marine engine with respect to fuel blends

Table 5.77 The exergoenvironmental performance of M-3 marine engine components

#	$b_{F,K}$	$b_{P,K}$	f_b	r_b
Units	[mPt/MJ]	[mPt/MJ]	[%]	[%]
HPC1	11.88	14.19	0.023	19.40
HPT1	10.32	11.88	0.044	15.12
LPT2	10.32	11.97	0.045	15.91
T3	33.50	40.52	0.013	20.93
T4	5.65	7.03	0.113	24.40
T5	11.98	15.50	0.036	29.38
P1	40.51	50.63	0.024	24.97
P2	7.02	9.36	0.117	33.28
CN1	10.18	27.29	0.000	168.11
CN2	10.18	272.04	0.000	2572.73
EV2	1.70	5.64	0.020	231.08
EV11	5.73	14.48	0.062	152.75
EV12	0.10	5.73	0.089	5434.37
GTHX	11.22	14.02	0.028	24.90
CC	5.59	10.32	0.001	84.78
SOFC	1.39	2.73	0.049	96.99
SR	4.81	4.03	-0.048	-16.24
WGS	4.01	4.03	0.502	0.54
Total	6.52	11.45	0.010	75.74

Using different fuel blends affects the exergoenvironmental analysis as, described in Figure 5.114. The fuel and product exergoenvironmental rates are approximate equal

but variable with fuels. The fuel exergoenvironmental rates are about 4 kPt/h for F1, 7 kPt/h for F2, 5 kPt/h for F3, 10 kPt/h for F4 and 6.5 kPt/h for F5. The destruction and losses exergoenvironmental rates have an average of 2.4 kPt/h and 6.2 Pt/h, respectively, as displayed in Figure 5.114-a. The maximum specific fuel and product exergoenvironmental impacts are 16.11 and 29.8 mPt/MJ with F4, respectively, and the minimum impacts are 6.52 and 11.45 mPt/MJ occurring with F1, respectively, as produced in Figure 5.114-b.

The pollution formation and total environmental rates are displayed in Figure 5.115. The F1 and F5 have a negative value of -228 Pt/h and -34 Pt/h, respectively. That means the inlet emissions is greater than outlet emissions, in other ways the components can reduce the emissions. The fuels F2, F3, and F4 produces emissions with an average of 22.6 Pt/h, as shown in Figure 5.115-a. The total environmental rates have ascended from 1261 Pt/h for F1, 1971 Pt/h for F3, 2322 Pt/h for F5, 2543 Pt/h for F2, and 3627 Pt/h for F4, as presented in Figure 5.115-b.

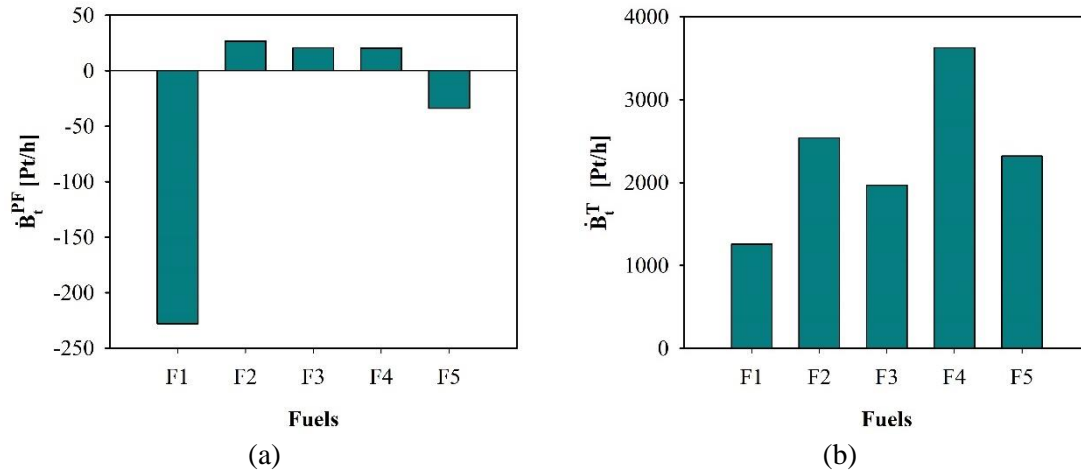


Figure 5.115 (a) Pollution formation rates and (b) total environmental impact rates of M-3 marine engine components with respect to fuel blends

The exergoenvironmental performance is displayed in Figure 5.116. The relative environmental difference is the minimum of 75.7% of F1 and the remaining fuels have almost the same value of 86%. The exergoenvironmental factor is almost the opposite direction of relative environmental difference, where the maximum value is 0.010% of F1 and the minimum value is 0.004% for F4, as shown in Figure 5.116-a. In addition, the exhaust gases have an average specific environment impact of 16.86 mPt/MJ, where the minimum and maximum are for F1 and F4, as presented in Figure 5.116-b.

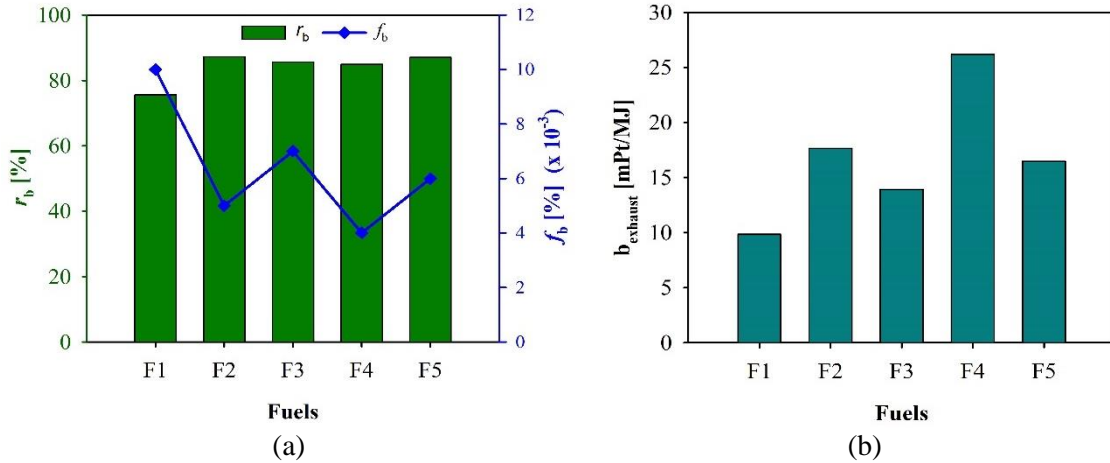


Figure 5.116 Exergoenvironmental performance of a hybridized M-3 marine engine: (a) relative environment difference and exergoenvironmental factor, and (b) specific exergy environmental impact of exhaust

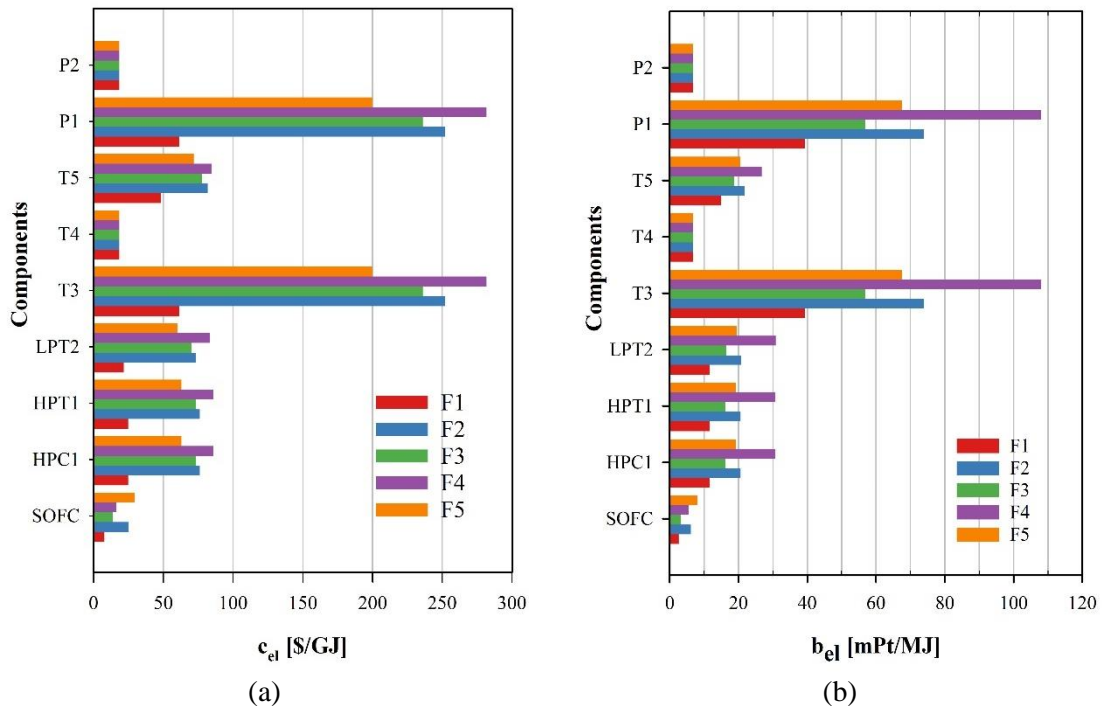


Figure 5.117 (a) Exergy cost and (b) environmental impact of electricity of M-3 marine engine

The electrical power has been studied in the exergoeconomic and exergoenvironmental analyses, as displayed in Figure 5.117. The electric power of turbine (HPT1) delivers the power to the compressor (HPC1), the same for turbine (T3) and pump (P1), and turbine (T4) and pump (P2), so that the specific cost and environment of electricity are the same. The compressor (HPC1), turbine (LPT2), fuel cell (SOFC),

turbines (T3, T4, and T5), have specific exergy cost of electricity of 64.6 \$/GJ, 61.6 \$/GJ, 18.5 \$/GJ, 206.2 \$/GJ, 18.4 \$/GJ, and 72.8 \$/GJ, respectively, as presented in Figure 5.117-a. The specific environment impact of HPC1, LPT2, SOFC, T3, T4, and T5 have the average of 19.68 mPt/MJ, 19.81 mPt/MJ, 5.12 mPt/MJ, 69.12 mPt/MJ, 6.84 mPt/MJ, and 20.56 mPt/MJ, as illustrated in Figure 5.117-b. The fuel F1 produces the least price and least environmental impact, and the second least economic is provided using F5, while the second least environmental impact is produced by F3.

5.9 Comparison and Optimization

This subsection presents a comparison between systems in each sector and choosing one system for optimization based on minimum weight and maximum performance that resulted during thermodynamic analysis and minimum exergoeconomic and exergoenvironmental analysis.

5.9.1 Aviation Systems

Two aviation systems are designed and analyzed. Both A-1 and A-2 are hybrid turbofans that consist of MCFC and SOFC, respectively. As presented in Table 5.78, the SOFC-turbofan (A-2) can produce a total power of 47 MW, which is higher than that of MCFC-turbofan (A-1), but less than the traditional turbofan of Rolls Royce Trent 1000. Also, the weight of a traditional turbofan is 6 tons and increased to about 8 tons by adding SOFC stacks and increased to about 12 tons by adding MCFC stacks. The SOFC stacks are 36 stacks and have a total cell area of 324 m² (900 cm²×100 cells×36 stacks). However, it is disturbed within a surface area of 3.24 m² (around 1.62 m² inside each wing of a plane). The MCFC system requires 90 stacks to produce around 840 kW, less than that of SOFC, and these stacks have the same cell number (100 cells) and same cell area (900 cm²). Therefore, the total cell area of MFCF is 810 m² and can be disturbed over 8.1 m² (around 4.04 m² for each wing). It should be arranged to be two or three rows to fit the wing width and length.

Thrust-to-weight ratio (T/W) is another factor that must be considered in the aviation industry. For the traditional aviation, the T/W is 1.70, which is higher than 1.4 since the thrust force is more than 90 kN [233]. The SOFC-turbofan has the highest T/W

about 1.9, and the MCFC-turbofan has the lowest value of about 1.2, which is lower than 1.4 during the cruise condition. The thrust force can be increased more by decreasing the pressure ratio of turbines, which will be done in the optimization study.

Regarding the carbon emissions, the traditional turbofan emits 18.5 kg/s of CO₂, while the hybrid turbofans emit about 4.2 kg/s of CO₂ for MCFC-turbofan and 5.73 kg/s for SOFC-turbofan. Based on the presenting values, there is a relationship between the engine weight and carbon emissions. It is a negative linear regression of a correlation coefficient of -0.739, meaning that increasing the engine weight using fuel cells will decrease the carbon emissions. However, the probability value (p-value) is high of 0.471 showing that the data is not significantly statistical and requires more data points to show the exact correlation between the weight and carbon emissions. By observing the given table, MCFC-turbofan has better performance of 59 and 73% of energy and exergy efficiency, higher exergetic efficiency (88%), less exergoeconomic factor and exergoenvironmental factor. Nevertheless, the heavy weight of MCFC is a troublesome and can cause a significant issue for a safe flight of Boeing 787 carrying passengers and their luggage. Therefore, it is better to focus the optimization study on SOFC-turbofan to increase its performance with minimum cost and environmental impact.

Table 5.78 Comparison between aviation aircraft engines

Element	A-1	A-2	Traditional turbofan
Thrust energy [MW]	32.34	38.60	38.18
Turbofan Power [MW]	6.55	7.71	9.14
Fuel cell Power [MW]	0.84	0.94	0
Total energy [MW]	39.72	47.00	47.33
Thrust force [kN]	130.08	155.79	115.4
Engine weight [kg]	11,580	8,232	6,000
Thrust-to-weight ratio	1.15	1.93	1.70
CO ₂ emissions [kg/s]	4.15	5.73	18.5
η [%]	58.9	45.2	43.4
ψ [%]	72.7	51.02	52.0
ε [%]	87.66	82.55	56.0
\dot{Z}_{eng} [\$/h]	76192.9	75508.12	75495.96
\dot{Y}_{eng} [mPt/h]	37.72	26.26	11.33
r_{eng} [%]	19.92	35.37	38.2
f_{eng} [%]	52.63	53.04	45.20
$r_{b,eng}$ [%]	10.80	20.13	25.05
$f_{b,eng}$ [%]	0.0016	0.0004	0.0002

There are many parameters affecting the thermodynamic analysis, such as compression and expansion ratios of compressors and turbines and the maximum pressure and temperature of the engine cycle. Also, there are two other parameters, such as the fuel cost, c_f , and fuel environmental impact, b_f , which are very sensitive to the market price and source and life cycle of the fuel. Therefore, a sensitivity analysis is performed for the fuel cost and fuel environmental analysis for the aviation systems as shown in Figure 5.118 and 5.119. Changing the fuel cost from 5 to 90 \$/GJ increases the total fuel, product, and destruction exergoeconomic rates with a linear trend, as presented in Figure 5.118-a. Also, these changing increases the specific fuel and product exergy costs with a constant rate from 200 to 350 \$/GJ, as illustrated in Figure 5.118-b. However, the relative cost difference decreases slightly from 40 to 35%, and the exergoeconomic factor declines from 55% to 40%, as plotted in Figure 5.118-c.

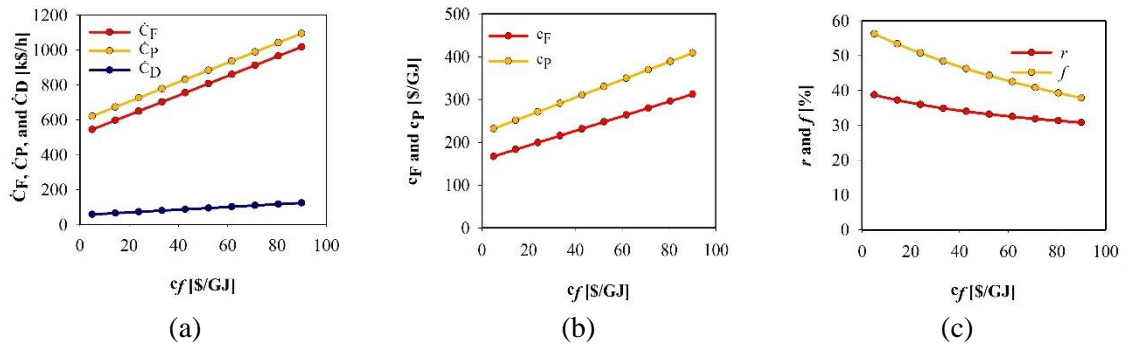


Figure 5.118 The sensitivity analysis of fuel cost on: (a) exergoeconomic rates, (b) specific exergy cost, and (c) exergoeconomic factor and relative cost difference of aviation systems.

Similarly, the fuel environmental impact varies from 5 to 90 mPt/MJ. This change affects the increase of exergoenvironmental rates from in a linear trend, as shown in Figure 5.119-a. Also, the variation increases the specific fuel and product exergy environment of the aviation system with a constant rate, as presented in Figure 5.119-b, but have a slight effect on relative environment difference that changes from 15 to 20 and plateaus at 20 % and decreases the exergoenvironmental factor from 0.001 to 0.0001%, as displayed in Figure 5.119-c.

Therefore, the results of exergoeconomic and exergoenvironmental analyses will significantly change based on the changes of fuel cost and fuel environmental impact. However, the most valuable parameter is the relative cost difference and exergoeconomic factor for exergoeconomic analysis and similar parameters in exergoenvironmental

analysis that shows how the product cost/environment and destruction cost/environment changes with respect to the fuel cost/environment and component cost/environment. This can be translated into if the engine is economic and ecofriendly or not.

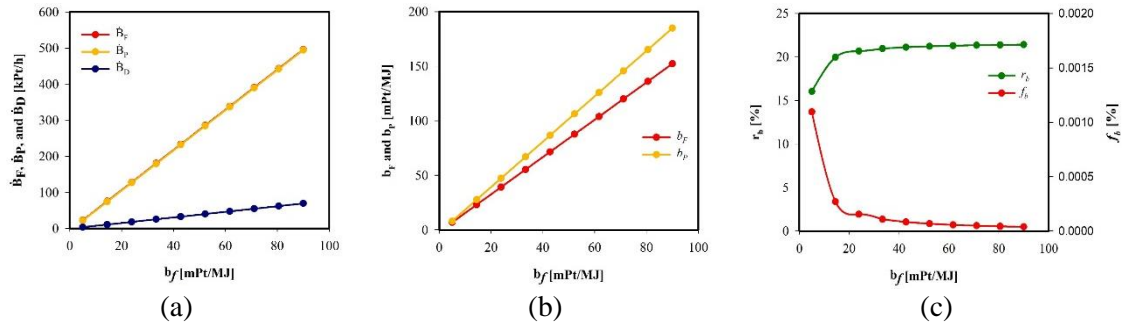


Figure 5.119 The sensitivity analysis of fuel environmental impact on: (a) exergoenvironmental rates, (b) specific exergy environment, and (c) exergoenvironmental factor and relative environment difference of aviation systems.

Table 5.79 Decision variables of SOFC-turbofan with lower and upper constrains.

Variables	Symbols	Lower limit	Upper limit
Compression ratio of compressors	r_{FAN} [-]	1.2	1.6
	r_{IPC} [-]	4	6
	r_{HPC} [-]	4	6
Expansion ratio of turbines	r_{HPT} [-]	0.4	0.6
	r_{IPT} [-]	0.4	0.6
	r_{LPT} [-]	0.4	0.5
Maximum Temperature	T_{CC} [°C]	1227	1827
Maximum pressure	P_{CC} [kPa]	781.44	2334.32

This sensitivity analysis is essential in choosing decision variables for SOFC-turbofan engine. Some parameters are not necessary such as air mass flow rate and fuel mass flow rate because they are selected based on the engine capacity, which will be included in the decision variable. The main parameters are compression ratio of compressors, expansion ratio of turbines, and maximum pressure and maximum temperature of the combustion chamber. These parameters are listed with lower and upper constrains as shown in Table 5.79, which are permissible according to the manufacture recommendation of the Rolls Royce Trent 1000.

The decision variables are operated using Aspen Plus linked with MATLAB to produce many data such as the power of compressors and turbines, thermodynamic analysis of components and the overall system, exergy analysis using fuel and product principal, exergoeconomic analysis, and exergoenvironmental analysis. There are about 13500 points of data that can be produced from Aspen Plus without any error messages. The data are

gathered and analyzed using an Excel sheet to submitted to Turing Bot software to find a symbolic regression analysis of the four main objective variables, as presented in Table 5.80, to describe the engine power, \dot{W}_{eng} , exergetic efficiency, ε_{eng} , relative cost difference, r_{eng} , and relative environment difference, $r_{b,eng}$, of the aviation engine.

Table 5.80 The objective functions of SOFC-turbofan optimization

Objective functions
$\dot{W}_{eng} = \left(3.79398 \left(-2.11557 - \left((-0.956837 + \text{asinh}(r_{HPT}) + r_{LPT} + (r_{FAN} - 0.988296 + \text{asinh}(r_{IPT})) \right) \times 47.6857(2.76022 + r_{HPC}) \right) \right) + T_{CC} \Big/ (0.018772 - (r_{IPC} + 4.9094 r_{HPT} r_{IPT})^{-3.66279})$
$\varepsilon_{eng} = (3.41368 + \text{atanh}(\cos(r_{FAN} - (T_{CC} - 0.41026)))) \times (r_{FAN} - 1.34704) + \left(\frac{-1.07506 + \frac{0.0152535}{\cos(e^{r_{IPC}})}}{77.7134 - \frac{\cos(T_{CC})}{\cos(T_{CC})}} \right) + 4.301 \times 10^{-4} \times P_{CC}$
$r_{eng} = \left(38.683 - \tan(-1.05121 - T_{CC}) + \left((5.27324 * \cos(T_{CC} + 0.815368) + (5.6675 - \text{atanh}(\cos(1.99733 r_{HPC}))) \right) \times \tan(-0.087005 - r_{HPT}) \times r_{HPC} \right) \times \cos(r_{FAN} + 5.21544)$
$r_{b,eng} = \frac{\tan(\cos(1.41998 - 0.502172 \cos(r_{IPC}) - T_{CC}) - 0.206691) - 0.894949 r_{IPC}}{36516.02} + \left(\frac{67.8023 (r_{HPT} + r_{LPT}) r_{HPT} r_{FAN} r_{IPT} + \left(T_{CC} - \left(\frac{94.3166}{r_{FAN} - 0.712888} \right) \right) - 189.346}{\left(\frac{94.3166}{r_{FAN} - 0.712888} \right) - 189.346} \right)$

The objective functions are optimized to find two maximum variables, such as \dot{W}_{eng} and ε_{eng} , and two minimum variables, such as r_{eng} and $r_{b,eng}$ to fulfil the maximum energy performance and minimum cost and environmental impact. Using MOPSO algorithm, optimal solutions and optimal decision variables are obtained in Table 5.81. The optimal decision variables are 10724.7 kW of engine power, about 86% of exergetic efficiency, 22% of relative cost difference, and 15% of relative environment difference. The optimal engine power is higher than that of MCFC-turbofan by 64% and of the traditional turbofan by 17%. Also, the resultant thrust energy is 43.2 MW, which is greater than both. The relative cost difference is less than 38.2% of the traditional engine but higher than 20% of MCFC-turbofan. However, this relative cost difference results from the specific fuel exergy cost of 197.36 \$/GJ and specific product exergy cost of 240.42 \$/GJ, which are lower than that of other engines. Moreover, the relative environment difference lies between the values

of MCFC-turbofan and traditional turbofan and is obtained from the specific fuel and product exergy environment of 10.97 and 12.67 mPt/M, respectively, that are less than both engines. The new designed variables significantly increase the overall engine power and overall thrust energy, with less cost and less environmental impact. These have improved the engine performance in general compared to the traditional turbofan and its previous design of SOFC-turbofan.

Table 5.81 The optimal solutions and decision variables for SOFC-turbofan engine.

Decision maker points	Symbols and units	Optimal values
Optimal solutions		
Compression ratio of compressors	r_{FAN} [-]	1.4
	r_{IPC} [-]	5.5
	r_{HPC} [-]	5.5
Expansion ratio of turbines	r_{HPT} [-]	0.45
	r_{IPT} [-]	0.5
	r_{LPT} [-]	0.4
Maximum Temperature	T_{CC} [°C]	1827
Maximum pressure	P_{CC} [kPa]	1723.6
Optimal decision variables		
Overall power	\dot{W}_{net} [kW]	10724.7
Exergetic efficiency	ε [%]	85.72
Exergoeconomic factor	r_{eng} [%]	21.82
Exergoenvironmental variable	$r_{b,eng}$ [%]	15.49

5.9.2 Rail Systems

In this thesis, three developed rail engines are analyzed using thermodynamic, exergy, exergoeconomic, exergoenvironmental analyses. The main results of these systems are listed in Table 5.82. The first rail engine (R-1) consists of ICE combined with a GT and MCFC, the second engine (R-2) involves GT-SOFC and onboard hydrogen production using AEC and PEMFC systems, and the third engine (R-3) comprises a GT combined with PEMFC and SOFC systems. All engines are connected to energy waste systems using an absorption refrigeration system or thermoelectric generators. The freight locomotive is commonly operated using and ICE of EMD-16-710G, which produces a net power of 3167 kW using ULSD. The average net power is the maximum of 5905 kW using R-3, followed by 4756 kW using R-2, and 4185 kW using R-1 rail engine. The traditional ICE weighs 18 tons. The maximum engine weight is achieved sing R-1 since it combined ICE and GT to reach 34 tons but replacing the ICE with GT only and relying on it as the main engine

reduced to overall weight to 9.3 tons for R-2 and 9.2 tons for R-3. The number of MCFC stacks of R-1 engine are 3 large stacks, each contains 400 cells of 0.67 m^2 and weighs 10336 kg, while the GT and ARS weigh about 600 kg and 4800 kg, respectively. The generator of ARS is attached to the exhaust pipe of ICE and GT engines, while the condenser is located at the top of the engine cabinet and the evaporator is distributed at the ceiling of other cabinets to provide cooling load. The MCFC can be located above the engine attached to the ceiling and stacked vertically to provide more space for maintenance and movement around the engine. For R-2 engine, the total weight is 9256 kg that contains about 600 kg of onboard hydrogen production, 715 kg of SOFC (9 stacks of 100 cells each of 0.64 cm^2), 2779 kg of GT system, and 4816 kg of ARS. For R-3 engine, The GT and ARS weigh 2779 kg and 4816 kg, respectively, while the SOFC and PEMFC weigh 512 kg and 1056 kg, respectively, since the number of stacks is 11 for SOFC and 20 for PEMFC, and both have 100 cells per stack with a surface area of 0.5 m^2 .

Regarding the carbon emissions, the traditional ICE emits 2.51 kg/s of CO_2 using ULSD fuel, while the developed rails engines emit 1.79 kg/s of CO_2 for the combined ICE and SOFC-GT (R-1) engine, 0.78 kg/s of CO_2 for SOFC-GT and AEC-PEMFC onboard hydrogen production (R-2), and 0.46 kg/s of CO_2 for the SOFC-PEMFC-GT (R-3). It is obvious that increasing the engine weight has increased the carbon emissions, and there is a linear relationship between the engine weight and carbon emissions, with a positive correlation coefficient of 0.608, which is relatively high. Also, replacing the ICE with GT has significantly reduced the weight and reduced the carbon emissions even though using alternative fuels for both engines. However, the probability value (p-value) is high of 0.391 (> 0.05) showing that the data is not statistically significant and requires more data points to show the exact correlation between the weight and carbon emissions.

The traditional ICE engine has 49% and 57% of energy and exergy efficiency, while the best performance can be fulfilled using R-3 reaching 90% of energy efficiency, 50% of exergy efficiency, and 66% of exergetic efficiency. The relative cost difference of R-3 is about 50% which is higher than that of R-1 (26%) and less than that of R-2 and traditional engines. The same trend occurs for the relative environment difference for R-3, which is 51%. However, R-3 engine has the best energy performance but not the best

economic and best eco-friendly engine which can be improved using optimization to choose better design conditions economically and environmentally.

Table 5.82 Comparison between three developed and traditional rail engines.

Element	R-1	R-2	R-3	Traditional rail engine
Total Power [kW]	4185	4756	5905	3355
Engine Weight [kg]	33,751	9,256	9,163	18,000
CO2 emission [kg/s]	1.79	0.78	0.46	2.51
η [%]	50.18	58.98	90.38	48.51
ψ [%]	58.85	72.70	49.08	56.90
ε [%]	79.83	62.72	66.22	32.13
\dot{Z}_{eng} [\$ /h]	32.2	147.44	69.67	7.26
\dot{Y}_{eng} [mPt/h]	86.11	14.06	15.51	40.98
r_{eng} [%]	25.63	61.93	49.39	237.27
f_{eng} [%]	1.44	3.42	2.45	11.0
$r_{b,eng}$ [%]	24.75	50.68	44.31	280.48
$f_{b,eng}$ [%]	0.0084	0.00074	0.0016	0.096

There are many paraments affecting the engine performance that can be manipulated and tuned during the operating conditions, which are under the operator's controls. However, the market prices and life cycle of fuels are out of operator's control and are very sensitive to political and industrial situations, which have a significant impact on economic and environmental aspects.

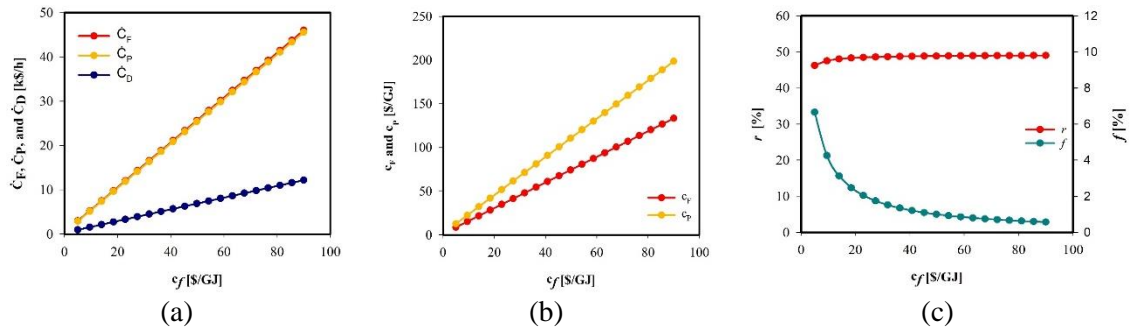


Figure 5.120 The sensitivity analysis of fuel cost on: (a) exergoeconomic rates, (b) specific exergy cost, and (c) exergoeconomic factor and relative cost difference of rail systems.

Therefore, a sensitivity analysis is implemented to observe the effect of fuel cost and fuel environmental impact. Figure 5.120 presents the effect of fuel cost on exergoeconomic analysis. The fuel cost varies from 5 to 90 \$/GJ yielding to increasing the exergoeconomic rates of fuel, product, and destruction with a constant rate, and increasing the specific fuel and product exergy cost form 5\$/GJ to about 150\$/GJ. But this increase of fuel cost does not change the relative cost difference that remains constant at 45% but

decreases the exergoeconomic factor from 7% to 1% because of the increase of destruction exergoeconomic rate of the R-3 rail engine.

Likewise, increasing the fuel environmental impact from 5 to 90 mPt/MJ, as displayed in Figure 5.121, increased the exergoenvironmental rates of fuel and product exergoenvironmental rates from 3 kPt/h to 45 kPt/h, and increases the destruction exergoenvironmental rate from 1 to 10 kPt/h. Also, this change affects the specific exergy environment of fuel and product of the engine to be raised from 5 to about 150 mPt/MJ. Nevertheless, these increased values of constant rates do not affect the relative environment difference, which remains unchanging at 45% but decline the exergoenvironmental factor from 0.0035 to less than 0.001%. This sensitivity analysis explains the importance of relative cost/environment difference, which do not change under sudden market prices because of inflation or life cycle of fuel source.

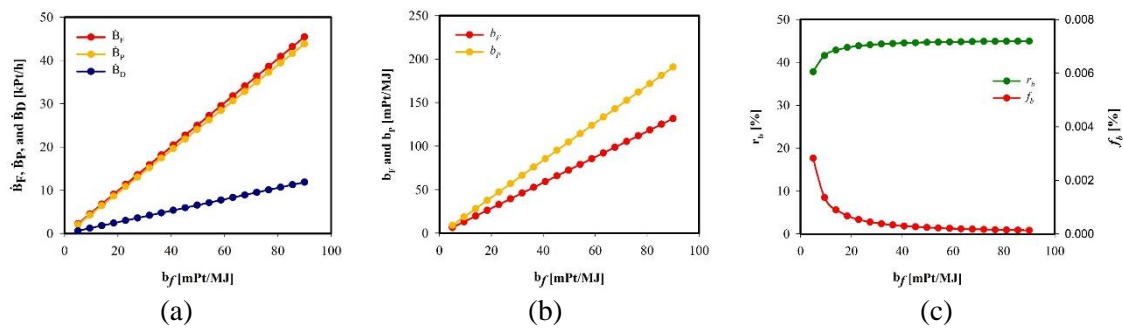


Figure 5.121 The sensitivity analysis of fuel environmental impact on: (a) exergoenvironmental rates, (b) specific exergy environment, and (c) exergoenvironmental factor and relative environment difference of rail systems.

Table 5.83 The decision variables of SOFC-PEMFC-GT (R-3) rail engine.

Variables	Symbols	Lower limit	Upper Limit
Compression ratio of compressors	r_{C1} [-]	4	8
	r_{C2} [-]	4	8
Expansion ratio of turbines	r_{T2} [-]	0.1	0.3
	r_{T1} [-]	0.1	0.3
	r_{T1} [-]	0.1	0.3
	r_{T1} [-]	0.1	0.3
Maximum Temperature	T_{CC} [°C]	1227	2027
Maximum pressure	P_{CC} [kPa]	607.8	4963.7

The sensitivity analysis of fuel cost and environmental impact helps us to lower the decision variables for optimizing the R-3 rail engine for optimal design conditions. Table 5.83 lists the important parameters of decision variables such as compression and expansion ratios, maximum pressure, and maximum temperature of the GT cycle. The

lower and upper limits are also displayed in the given table, and they are selected according to the manufacture recommendation to avoid any fatal errors or damages. These variables do not include the air and fuel mass flow rates because changing them will change the engine capacity yielding to changing the whole engine model with larger size and larger weight.

The seven decision variables are combined to form four objective functions using Turing Bot software, as shown in Table 5.84. They are engine power, \dot{W}_{eng} , and exergetic efficiency, ε_{eng} , which both need to be maximized, relative cost difference, r_{eng} , and relative environment difference, $r_{b,eng}$, which both are required to be minimized. Maximizing the power and exergetic efficiency means maximizing the energy performance, and minimizing the relative cost and environment differences means minimizing the cost and environmental impact of engine product to be more economic and more ecofriendly engine. To obtain these equations, 12040 points are generated using Aspen PLUS to estimate the power of compressors and turbines and the heat addition of combustion chamber. These points are also linked to MATLAB to execute the exergy analysis, exergoeconomic analysis, and exergoenvironmental analysis.

Table 5.84 The objective functions of hybridized gas turbine rial engine for optimization.

Objective functions
$\dot{W}_{eng} = 25.36158 \times r_{c1} \times r_{c2} + 3.01542 T_{cc} \operatorname{asinh} \left(\cos \left(\frac{r_{T1} - 0.98473 \times r_{c2}}{r_{T2} e^{-2.362154 T_{cc}}} \right) \right) \\ + 4.698597 \times P_{cc} \times r_{c1} \times r_{c2} - T_{cc} e^{\frac{524.369887}{-r_{c2} \times r_{T2}}}$
$\varepsilon_{eng} = 2.36548(r_{c1} - 1.836204) + \operatorname{atanh} \left(\sin \left(\frac{r_{c1} - (T_{cc} - 0.41026)}{2.365 \times r_{T1}} \right) \right) (r_{c1} - 1.926504) \\ + 80.7134 - \frac{-1.07506 + \frac{0.0152535}{\sin(e^{r_{c2}})}}{\cos(T_{cc})} + 0.00254 \times P_{cc}$
$r_{eng} = 38.683 \cos(r_{c1} + 5.21544) + \cos(r_{c2} + 5.8544) (-\tan(-1.05121 - T_{cc})) \\ + \cos(r_{c2} + 5.8544) [(6.362 \cos(T_{cc}) \\ + (6.36275 - \operatorname{atanh}(\cos(2.05 r_{T2}))) \tan(-0.0775 - r_{T1}) \times r_{c2}]$
$r_{b,eng} = \tan(-0.206691 + \cos(1.45898 - T_{cc})) - 0.949056 r_{c2} \\ + \frac{5478.3}{76.8123 (r_{T1}^2 r_{T2} r_{c1} + r_{T2}^2 r_{T1} r_{c1}) - \frac{84.3166}{r_{c1} - 0.818} + T_{cc} - 198.245}$

The MOPSO algorithm is selected for optimizing the given objective functions using MATLAB. Table 5.85 displays the optimal solutions and optimal decision variables.

The maximum engine power can reach 7502 kW with maximum exergetic efficiency of 82%, and minimum relative cost difference of 25% and minimum relative environment difference of 24%. The relative cost difference results from specific fuel exergy cost of 11.5 \$/GJ and specific product exergy cost of 14.5 \$/GJ, while the relative environment difference is produced from specific fuel and product exergy environment of 7.2 and 8.9 mPt/MJ, respectively.

Table 5.85 The optimal solutions and optimal decision variables for R-3 rail system.

Decision maker points	Symbols and units	Optimal values
Optimal solutions		
Compression ratio of compressors	r_{c1} [-]	6.5
	r_{c2} [-]	6.5
Expansion ratio of turbines	r_{T2} [-]	0.10
Expansion ratio of turbines	r_{T1} [-]	0.10
	r_{T1} [-]	0.20
Maximum Temperature	T_{CC} [°C]	1600
Maximum pressure	P_{CC} [kPa]	5063
Optimal decision variables		
Overall power	\dot{W}_{net} [kW]	7502
Exergetic efficiency	ε [%]	82.1
Exergoeconomic factor	r_{eng} [%]	25.4
Exergoenvironmental variable	$r_{b,eng}$ [%]	23.9

The optimization results display the ability of the R-3 engine to be enhanced by tuning the compression and expansion ratios of compressor and turbines with changing in fuel and air mass flow rates, fuel cost, and fuel environmental impact. This changing results in reducing the exergy destruction rate yielding to lowering in destruction exergoeconomic and exergoenvironmental rates. This helps the rail engine to be improved with less cost and less environmental impact.

5.9.3 Marine Systems

Three developed marine engines are compared with a traditional marine engine of Wärtsilä 6X62, as listed in Table 5.86. The Aframax ship is operated by a power of 10524 kW. The M-1 marine engine consists of ICE and GT combined with SOFC, the M-2 engine comprises of a SRC combined with a SOFC-GT, and the M-3 engine involves of a SOFC-GT combined with two ORCs. The maximum power can be achieved using M-2 and M-3

marine engines of about 15.5 and 15.8 MW respectively, which are very close to each other, and are higher than M-1 power (13.5 MW). The weight of traditional engine 377 tons of using ICE only, but the M-1 engine, which combines ICE and GT, weighs more by 3.3 tons. However, using SRC as the main engine instead of ICE, as in M-2 engine, makes the new engine weighs about 58 ton. Also, the M-3 engine weighs about 65 tons by combining GT and two ORCs. That means less weight is achieved using SRC and GT-SOFC.

Regarding the carbon emissions, the traditional ICE for marine engine emits 3.98 kg/s of CO₂ using MGO-DMA. The M-1 marine engine, which consists of ICE and SOFC-GT, emits an average 2.77 kg/s of CO₂ using the alternative fuel blends. This emission is decreased by replacing the ICE engine with SRC as in M-2 marine engine to emit 2.2 kg/s of CO₂. Also, the emission has been reduced more using SOFC-GT combined with two ORCs as in M-3 marine engine to reach 1.25 kg/s of CO₂, where comes from the hybrid gas turbine only. That results, reducing the engine weight has dropped the carbon emissions by using alternative fuels and hybrid fuel cells, forming a positive linear relationship between the engine weight and carbon emissions, with a positive correlation coefficient of 0.826, which is relatively high value. However, the probability value (p-value) is high of 0.174 (> 0.05) showing that the data is not statistically significant and requires more data points to show the exact correlation between the weight and carbon emissions.

Regarding the energy performance, the traditional engine achieves 23% of energy efficiency and 29% of exergy efficiency. The maximum energy performance can be fulfilled using M-2 engine reaching 61% of energy efficiency, 43% of exergy efficiency, and 60% of exergetic efficiency. Regarding the exergoeconomic performance, the M-1 and M-2 engines have a relative cost difference of 68%, which is less than that of M-3 engine and traditional marine engine. Also, the exergoeconomic factors are less for all developed marine engines compared to that of the traditional engine. Regarding the exergoenvironmental performance, the relative environment difference trend is similar to that of the exergoeconomic performance to be an average of 70%, and the exergoenvironmental factor of the developed engines varies from 0.006% of M-3 to 0.03% of M-1 engine. The best engine performance can be selected to be M-2 since it has less

weight and maximum energy performance. Other performance can be enhanced using optimization algorithm to choose better decision variables.

Table 5.86 Comparison of three designed marine engine and traditional marine engine.

Element	M-1	M-2	M-3	Traditional marine engine
Total energy [MW]	13,472	15,546	15,758	10,524
Engine Weight [kg]	380,274	58,016	65,169	377,000
CO ₂ emissions [kg/s]	2.77	2.2	1.25	3.98
η [%]	30.6	60.9	38.4	22.9
ψ [%]	40.8	42.6	45.6	29.0
ε [%]	59.81	60.1	53.6	28.3
\dot{Z}_{eng} [\$ /h]	227.58	218.62	242.53	55.71
\dot{Y}_{eng} [mPt/h]	1109	139	132	1057
r_{eng} [%]	68.0	67.6	88.8	272.64
f_{eng} [%]	1.76	2.20	4.03	5.89
$r_{b,eng}$ [%]	65.4	64.7	84.2	174.2
$f_{b,eng}$ [%]	0.03	0.004	0.006	0.268

Cost and environmental impact of selected fuels changes strongly fluctuates according to the market prices and the increase of inflation rates and the life cycle of fuels. A wide range of fuel cost and fuel environmental impact are studied in the sensitivity analysis, as shown below. Figure 5.122 displays the effect of fuel cost that varies from 5 to 90 \$/GJ. This variation increases the exergoeconomic rates of fuel and product from 5 to 140 k\$/h and increases the destruction exergoeconomic rate from 2 to 45 k\$/h with a constant rate to form a linear relationship. Also, the increase of fuel cost increases the fuel exergy cost from 5 to 225 \$/GJ and increases the product exergy cost rate from 4 to 140 \$/GJ. However, this increase stabilizes the relative cost difference above 60%, and declines the exergoeconomic factor from 8 to 1%.

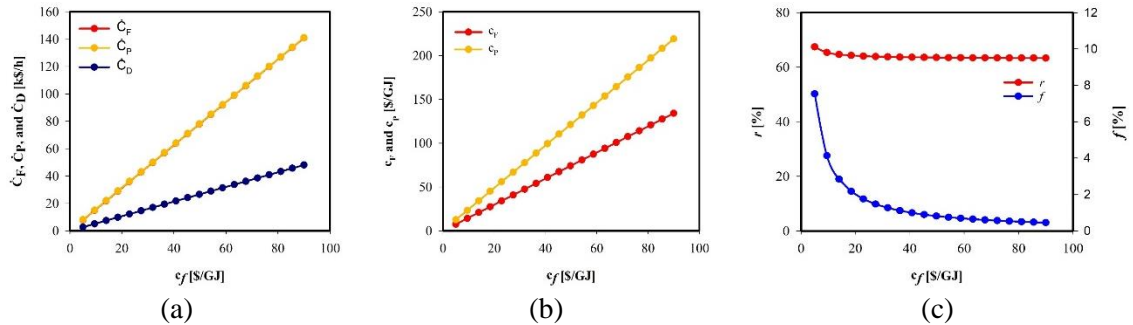


Figure 5.122 The sensitivity analysis of fuel cost on: (a) exergoeconomic rates, (b) specific exergy cost, and (c) exergoeconomic factor and relative cost difference of marine systems.

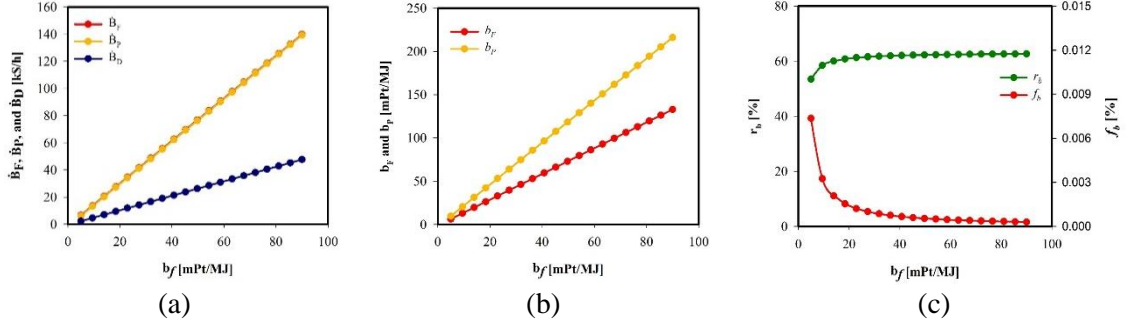


Figure 5.123 The sensitivity analysis of fuel environmental impact on: (a) exergoenvironmental rates, (b) specific exergy environment, and (c) exergoenvironmental factor and relative environment difference of marine systems.

Furthermore, increasing the environmental impact of fuels from 5 to 90 mPt/MJ has a significant effect on increasing the exergoenvironmental rates of fuel, product, and destruction, and on increasing the specific fuel and product exergy environment, as displayed in Figure 5.123. this increase has no effect on relative environment difference (to be 60%) and exergoenvironmental factor (to be less than 0.003%) after 20 mPt/MJ of selected fuels. Therefore, the relative cost and environment difference can remain constant despite the changing of fuel cost and environmental impact, but they can change according to the engine performance and destruction exergy rate.

The sensitivity analysis narrows the decision parameters by cancelling the effect of fuel cost and environmental impact and focusing on compression and expansion ratios of compressors and turbines, and maximum temperature of boiler and combustion chamber, as listed in Table 5.87. Also, the mass flow rate of steam, air, and fuel remain unchanging so that the engine capacity, size, and weight remain the same. Also, the lower and upper limits are displayed in the same table, which are selected according to the manufacture recommendations.

The 12 decision variables are gathered and collected from Aspen Plus and four analyses are applied by connected the results of Aspen Plus to MATLAB and Excel. The resultant data are exported to Turing Bot software to form symbolic regression equations of objective functions, as listed in Table 5.88. These objective functions are maximizing the net power of M-2 engine, \dot{W}_{eng} , and exergetic efficiency, ε_{eng} , and minimizing the relative cost difference, r_{eng} , and relative environment difference, $r_{b,eng}$.

Table 5.87 The decision variables of SRC-GT-SOFC (M-2) marine engine.

Variables	Symbols	Lower limit	Upper Limit
Compression ratio of compressors	r_{LPC1} [-]	4	6
	r_{HPC2} [-]	4	6
Expansion ratio of turbines	r_{HPST1} [-]	0.1	0.3
	r_{IPST2} [-]	0.2	0.6
	$r_{LPST3,1}$ [-]	0.4	0.6
	$r_{LPST3,2}$ [-]	0.4	0.6
	$r_{LPST3,3}$ [-]	0.01	0.03
	r_{HPT1} [-]	0.3	0.5
	r_{LPT2} [-]	0.3	0.5
	r_{PT3} [-]	0.4	0.6
Maximum Temperature	T_{CC} [°C]	900	1800
	T_{BL} [°C]	400	600

Table 5.88 Objective functions of SRC-GT-SOFC marine engine for optimization

Objective functions
$\dot{W}_{eng} = \frac{3.58964 \sin(34.876 r_{HPT1} - 4.365 r_{HPC2})}{2.35 T_{CC} + 2.42 e^{5.326 r_{LPC1} r_{HPC2}} + 5.36985 \ln\left(\frac{r_{HPC2} r_{LPC1}}{r_{HPT1} r_{LPT2} r_{PT3}}\right) + 33.658}$ $+ \operatorname{asinh}\left(\frac{4.5689 r_{HPST1} r_{IPST2} e^{r_{LPST3,1} r_{LPST3,2} r_{LPST3,3}}}{T_{BL} + 2.35 \ln\left(\frac{37.876 r_{LPST3,3}}{r_{LPST3,1} r_{LPST3,2}}\right)}\right)$ $+ 78.365 T_{BL} e^{\frac{r_{HPST1}}{2.365 \times 10^{-4}} + \frac{T_{BL}}{3.569}}$ $\varepsilon_{eng} = 78.5 + \tan\left(\cos\left(5.3647 \frac{r_{HPT1}}{r_{HPC2}} e^{-53.678 \frac{r_{HPT1} r_{LPT2}}{r_{PT3}} + \frac{53.64}{T_{CC}} - 0.02536 T_{CC}}\right)\right) - 45.6963 \left\{\frac{T_{BL}}{25.364} + \cos\left(r_{HPST1} r_{IPST2} + 25.365 (r_{LPST3,1} r_{LPST3,2} r_{LPST3,3} - \ln\left(\frac{0.0025 T_{BL}}{r_{HPST1}}\right))\right)\right\} -$ $5.68925 \operatorname{asinh}(7.3652 r_{HPST1} - r_{LPST2} + 383.65 r_{LPST3,1} r_{LPST3,2} r_{LPST3,3}) +$ $8.09583 T_{BL}^{\frac{5.3715}{e^{-7.36501 r_{IPST2} + 0.3021 T_{CC}}}}$ $r_{eng} = \left\{23.683 - \tan(-1.05121 - T_{CC}) + \left((8.27324 * \cos(T_{CC} + 0.815368) + (5.6075 - \operatorname{atanh}(\cos(1.7383 r_{HPC2}))))\right) \times \tan(-0.201 - r_{HPT1}) \times r_{HPC2}\right\} \cos(r_{LPST2} + 5.21544)$ $- \frac{r_{HPST1}^{-0.25} + 5.326}{\cos\left(\frac{r_{LPST3,1} r_{LPST3,2} r_{LPST3,3}}{r_{HPST1}}\right)} + 7.365 \ln\left(\frac{T_{BL}}{23.65}\right) \tan(4.6028 + r_{HPST1} - r_{IPST2})$ $r_{b,eng} = \tan\left(-\frac{0.206691}{r_{IPST2}} T_{BL} + \cos\left(\frac{1.45898}{r_{HPT1}} - T_{CC}\right)\right) - 0.949056 r_{HPC2}$ $+ \frac{5478.3}{76.8123 (r_{LPST3,1} r_{LPST3,2} r_{LPST3,3} + r_{HPT1} r_{LPC1}) - \frac{84.3166}{r_{LPC1} - 0.818} + T_{BL} - 18.245}$

Using MOPSO algorithm, the optimal solutions and optimal decision variables are obtained in Table 5.89. The maximum marine power can reach to about 16.87 MW with an exergetic efficiency of 70%, and the relative cost difference becomes 56% because the specific fuel and product exergy cost are 18.05 \$/GJ and 28.23 \$/GJ, respectively. Also, the relative environment difference reaches 51% since the specific fuel exergy environment is 6.8 mPt/MJ, and the specific product exergy environment is 10.27 mPt/MJ. Manipulating the compression and expansion ratios has increased the M-2 performance by 59% compared to the traditional engine and by 8% compared to the M-2 design and decreased the cost by 17% and the environmental impact by 15%.

Table 5.89 The optimal solutions and decision variables of M-2 marine engine.

Decision maker points	Symbols and units	Optimal values
Optimal solutions		
Compression ratio of compressors	r_{LPC1} [-]	4.25
	r_{HPC2} [-]	4.25
Expansion ratio of turbines	r_{HPST1} [-]	0.30
	r_{IPST2} [-]	0.50
	$r_{LPST3,1}$ [-]	0.55
	$r_{LPST3,2}$ [-]	0.50
	$r_{LPST3,3}$ [-]	0.01
	r_{HPT1} [-]	0.35
	r_{LPT2} [-]	0.45
	r_{PT3} [-]	0.5
Maximum Temperature	T_{CC} [°C]	1450
	T_{BL} [°C]	550
Optimal decision variables		
Overall power	\dot{W}_{net} [kW]	16724.7
Exergetic efficiency	ε [%]	70.25
Exergoeconomic factor	r_{eng} [%]	56.4
Exergoenvironmental variable	$r_{b,eng}$ [%]	51.0

In conclusion, the eight developed engines in three transportation sectors can achieve higher power and higher exergy and energy performance economically and eco-friendly. Not only this, but also, three optimized engines in three transportation sectors are selected according to less weight and better performance. They are also more improved by manipulating the pressure ratio of compressors and turbines and maximum temperature to reduce the destruction exergy rates yielding to reducing the specific cost and environment.

Chapter 6. Conclusions and Recommendations

This chapter presents conclusions of the work, research, and results in this and then the chapter goes to the recommendation section, which provide recommendations that are inferred from the results of the thesis. Note that the recommendations also introduce ideas for further systems that can be proposed and further analysis ideas that are out of the scope of this thesis and its objectives.

6.1 Conclusions

This chapter provides the conclusion of the presented analyses on transportation sectors, using alternative fuels in different forms with a hydrogen basis. These fuels are ethanol, methane, hydrogen, dimethyl ether, and methanol, with different mass fractions to constitute five fuel blends. These include, F1 (75% CH_4 + 25% H_2); F2 (75% CH_3OH + 25% H_2); F3 (60% CH_3OHCH_2 + 40% H_2); F4 (60% CH_3OCH_3 + 40% H_2); and F5 (15% CH_4 + 15% CH_3OH + 15% CH_3OHCH_2 + 15% CH_3OCH_3 + 40% H_2). Also, there are eight engine systems using different powering systems, such as internal combustion engines, gas turbines, and fuel cells, with different configurations to ensure increasing overall power and energy performance. The following conclusion points are listed according to each engine below:

The system (A-1) investigates a proposed hybrid MCFC-turbofan with alternative fuels. The turbofan engine selected is the Rolls Royce Trent 1000 operating Boeing 747 Dreamline in Air Canada. The following conclusions can be drawn from this study:

- A traditional turbofan performance can produce 42 MW with energetic and exergetic efficiencies of 59% and 71%, respectively.
- The MCFC system produces electric power range between 662.6 kW for F2 and 940.7 kW for F4, with an average of 70% electric efficiency, 13% energetic efficiency, and 20% exergetic efficiency.
- F5 increases the performance to its maximum of 65% and 80% energetic and exergetic efficiencies, respectively.
- The total hybrid turbofan power reaches 42 MW for F2 and 40 MW for F5.

- Alternative fuels reduced the CO₂ emission by more than 55% compared to that of the traditional fuel.
- The exergetic efficiency of the hybridized aircraft varies from 86.6% to 89.2% for the alternative fuel blends.
- The total annual levelized investment of the hybridized system is 76k \$/h because of the high price of the high-pressure turbine and combustion chamber.
- The system achieves an average relative cost difference of 20% and an average exergoeconomic factor of 52%, implying that the proposed system is economical and has low exergetic destruction costs when alternative fuel blends are employed.
- The engine has an average specific exergetic cost of electricity of 710 \$/GJ for the HPT and 230 \$/GJ for the IPT and LPT, and 50 \$/GJ for the MCFC.
- The values of r and f are about 22% and 56% for F1, 21% and 57% for F2, 20% and 53% for F3, 17% and 41% for F4, and 18% and 55% for F5, respectively.
- The hybridized aircraft has an average specific exergoenvironmental impact of electricity of 14 mPt/MJ for the turbines and 4 mPt/MJ for the MCFC.
- The values of r_b and f_b are about 10 % and -40% for F1, 1% and 2% for F2, 14% and ~1% for F3, 13% and <1% for F4, and 6% and -2% for F5, respectively.
- The F3 achieves a good balance for its moderate exergetic cost and environmental impact.

The proposed hybrid turbofan (A-2) consists of the turbofan of Rolls and Royce Trend 1000 and the SOFC system. The SOFC system contains the steam reforming and water gas shift. The conclusions from this study are listed below:

- The base turbofan can produce a net power of 9144 kW and a thrust energy of 38 MW, with 43.4% energetic efficiency and 52% exergetic efficiency at cruising conditions.
- The exhaust speed at the hot nozzle can reach a maximum value of 657.5 m/s using F2 and F5, but F2 can provide the highest thrust force of 160 kN with a high TSFC of 130 kg/(h.kN).
- The maximum total power of 48 MW can be obtained using F2, including 7.3 MW of net power of the GT, 39.8 MW of thrust energy, and 0.94MW of the SOFC.

- The overall energetic and exergetic efficiencies of the hybrid turbofan are 48.1% and 54.4%, respectively, using F2.
- Alternative fuel mixture can reduce CO₂ emission by 54% for F1, 65% using F2 and 73% for F3, F4 and F5.
- The fuel F3, consisting of 60% ethanol and 40% hydrogen can achieve energetic and exergetic efficiencies of 46% and 56%, respectively.
- The overall exergetic efficiency of the combined turbofan is about 82%, while the exergy destruction ratio is about 18% for all fuel blends, F1 to F5.
- The price of the SOFC unit has increased the total price of the turbofan engine by only 0.02%.
- The exergoenvironmental factor is a minimum of -3.27% for F1 and a maximum of 2.05% for F2.
- The relative environmental impact difference is a minimum of 17% for F1 and a maximum of 21.3% for F2.
- The specific exergoenvironmental impact values of electricity production range from about 10 to 25 mPt/MJ for turbines and 3 to 8 mPt/MJ for SOFC.
- The exergoenvironmental impact of thrust force is a minimum of 34 Pt/(h.kN) for F1 and a maximum of 87 Pt/(h.kN) for F4.
- The SOFC-turbofan has been selected for optimization study since it has less weight (8323 kg).
- The optimal output of SOFC-turbofan is increased to 10725 kW of overall power and 86% of exergetic efficiency and decreased to 22% of relative cost difference and 15% of relative environmental impact difference.

The proposed locomotive engine (R-1) system consists of the ICE, GT, and MCFC, in addition to an absorption system. Thus, the main output from this system is electric power and cooling load for air conditioning the trains. Several points can be concluded from this paper as follows:

- The utilization of alternative fuels increases the output power compared to the fossil fuel in the ICE engine by 25%. Also, the net power of the ICE using different fuels is fourfold of that of the GT and threefold of that of the MCFC.

- The proposed hybrid combined engine system has doubled the net power of 4200 kW with less specific fuel consumption like that of USDL fuel (5% difference).
- The overall efficiency of the hybrid combined system is about 43% and 55% energetic and exergetic efficiencies, respectively. The highest performance can be obtained using the fuel with mass fractions of 75% methanol and hydrogen 25%. The performance can reach 68% energetic efficiency and 82% exergetic efficiency.
- As known, the fossil fuel emits more CO₂ to the environment reaching up to 0.48 kg/s. However, the alternative fuels produce less emission by 65% reduction, and the minimum environmental impact can be achieved by the fuel with 75% methanol and 25% hydrogen at less than 0.08 kg/s.
- Combining all alternative fuels as in F5 produces slightly high emissions about 0.15 kg/sCO₂ eq. However, it has less specific fuel consumption of 0.25 kg/kWh and produce high power of 4250 kW.
- The total exergy destruction of the entire system is about 17 MW with 83% exergy efficiency for fuel F1.
- The MCFC and ICE have low exergoeconomic factor of 9.9% and 4.6%, respectively, while the exergoeconomic factor of the system is 3.7% for the F1.
- The F1 fuel shows the highest exergoeconomic factor (3.7%) and least relative cost difference (21.9%), which is the most economical choice because of the least subsidized fuel price.
- The total component-related environmental impact is 86 mPt/h, where the ICE has 52.1 mPt/h.
- The entire system has an exergoenvironmental impact factor for F1 of 0.015% and a relative environmental impact difference of 19.4%. The environmental impact of pollution formation is -65760 mPt/h, which means pollution is removed by the proposed system.
- The specific exergy cost and specific environmental impact of products are 0.1 \$/GJ and 69.4 mPt/MJ, respectively.
- The F1 fuel has the least economic and environmental impact compared to other fuels.

The proposed hybrid engine (R-2) combines a gas turbine with a fuel cell system and an energy recovery system. The following conclusions can be drawn from the study:

- The hybrid locomotive engine can produce a total power of 7211.8 kW with 48% energetic efficiency and 51% exergy efficiency using F1 (methane and hydrogen blend).
- Excluding the hydrogen production system, the overall engine power is a minimum of 6.8 MW using F1 and a maximum of 7.9 MW using F5.
- The SOFC power generates a minimum power of 3 MW using F1 and F3 and a maximum of 3.75 MW using F5.
- The CO₂ emissions are reduced by the designed system and fuel utilization to more than 70% compared to a traditional gas turbine with diesel fuel.
- The onboard hydrogen production using 6 stacks of PEMFC, and 5 stacks of AEC can generate a positive net power of 90 kW and provide 4.32 kg/h hydrogen for storage.
- The hybridized engine has 62.7% exergetic efficiency and 37.3% destruction exergy ratio based on the fuel and product principle.
- The engine normalized cost is \$10.2M, and its levelized cost rate is 147.4 \$/h.
- The levelized cost of electricity is 29.8 \$/MW, which is higher than the specific exergy cost of electricity from the turbine and the SOFC (7.75 \$/MWh) that delivers directly to the generator.
- The overall specific cost difference is 63.6%, and the exergoeconomic factor is obtained as 7.4% using the methane and hydrogen fuel blend.
- The specific fuel and product exergy costs are an average of 37 \$/GJ and 60 \$/GJ, respectively, and the minimum values are 13.3 \$/GJ and 21.8 \$/GJ using F1, and the maximum values are 48 and 76.7 \$/GJ using F4.
- The total weight of the engine is 9,256 kg, and its overall component-related environmental rate is 14.06 mPt/h.
- The specific fuel and product exergoenvironmental impacts are 8.1 mPt/h and 10.9 mPt/h, respectively, using the methane and hydrogen fuel blend.
- The overall specific fuel environmental impact rises from 8.11 mPt/MJ using F1 to 18.08 mPt/MJ using F3 of ethanol and hydrogen mixture, while the overall specific

product exergoenvironmental impact changes from a minimum of 10.93 mPt/MJ for F1 to a maximum of 28.16 mPt/MJ for F3.

- The economic assessment of hydrogen production varies from 162 to 327 \$/GJ for F1 to F4, respectively, while its environmental impact has a range of 40 mPt/MJ for F1 to 58 mPt/MJ for F3.

The proposed hybrid rail engine (R-3) consists of a gas turbine engine of two compressors and two turbines, a direct SOFC subsystem, a high-temperature PEMFC, an expander, and an energy recovery system. The conclusion of this study can be summarized as follows:

- The power of the GT-only engine varies from 1811 kW to 2248 kW, with an average energetic efficiency of 24.5%.
- Combining the GT-only engine with the SOFC subsystem increases the power to an average of 4400 kW and improves the energetic efficiency up to 59%.
- Adding the PEMFC subsystem increases the total power to 5911 kW and the energetic efficiency to 75%.
- Using the F2 (methanol and hydrogen blend) increases the net power of the hybrid engine to its maximum of 6056 kW and maximum energetic efficiency of 79%, as well as an exergetic efficiency of 49%.
- The carbon emission is reduced by more than 80% by using these sustainable fuel blends.
- The SOFC can produce an average electric power of 2262 kW with an electric efficiency of 96%, and PEMFC can generate an average electric power of 1252 kW with an electric efficiency of 70%.
- The energy recovery system can convert 20% of waste energy into electric power and cooling load.
- The average fuel exergy rate is 98.6 MW, and the product exergy rate is 66.5 MW, so the destruction exergy rate is 33.7MW.
- The average of exergetic efficiency and destruction ratio are 66% and 34%, respectively.
- The total normalized cost is \$ 4.8M, and the total levelized cost rate is 67 \$/h.
- The specific fuel and product exergetic cost are minimum of 11.8 \$/GJ and 17.4 \$/GJ for F1, maximum of 44.5 \$/GJ and 66.7 \$/GJ, respectively.

- The average relative cost difference of all fuel blends is 49%, and the exergoeconomic factor reaches an average of 2%.
- The component-related environmental impact is 15.5 mPt/h, which is negligible.
- The rail engine has specific fuel and product environmental impacts of 12 mPt/MJ and 17 mPt/MJ, respectively.
- The relative environmental difference and exergoenvironmental factor of the hybrid rail engine are 44.3% and 0.002%, respectively.
- The SOFC-PEMFC-GT, which is R-3 rail engine, is selected for the optimization study because of its lowest weight (9163 kg) and highest performance.
- The optimal output of SOFC-PEMFC-GT reach 7502 kW of overall power in increased exergetic efficiency of 82% and decreased relative cost difference and relative environmental impact difference of 25% and 24%.

The new design of (M-1) system has replaced one engine of Wärtsilä 6X62 with a hybridized gas turbine engine consisting of low- and high-pressure compressors, a turbine Brayton cycle, and a direct SOFC system. Instead of operating these engines with MGO-DMA. The presented design is analyzed and arrived at the following conclusions:

- The marine engine is operated using two ICE engines for each propeller with a total power of 21047.7 kW with an MGO-DMA with a mass flowrate of 1.9 kg/s and specific fuel consumption of 325 g/kWh.
- The traditional ICEs produce carbon emissions of 6.02 kg/s and have an energetic and exergetic efficiency of 22.9% and 29%, respectively.
- The ICE engine can create an average power of 12619 kW with specific fuel consumption of 217 g/kWh.
- The GT engine has an average of 18.5% energetic efficiency and 25% of exergetic efficiency, and it can produce an average power of 7507 kW with specific fuel consumption of 534 g/kWh.
- The solid oxide fuel cell plays an important role in improving the performance of the GT engine. It increases the GT power to 13944 kW with an average electric efficiency of 90%.

- There are 38 SOFC stacks that use about 80 mol/s of hydrogen. Also, the SOFC cell voltage varies from 0.33 to 0.45V, and its loss voltage is less than 0.05, yielding about 90% of electric efficiency.
- Such a hybridized GT and ICE system can generate a maximum power of 27773 kW using a 60% dimethyl-ether and 40% hydrogen fuel blend with an increase of 32%, while the minimum power is obtained to be 24968 kW using 75% methane and 25% hydrogen blend.
- Using all five fuel blends (i.e., F5) can lower the fuel consumption to 254.5 g/kWh by 21.7%, while increasing the total power to 27719.5 by 31.7%.
- The carbon emissions have drastically declined by 61 % because of the sustainable fuel blend utilization; meanwhile, the performance has increased by more than 35%.
- The average of fuel and product exergy rates are 342.3 and 204.8 MW, respectively. This results the average exergetic efficiency to be 59.8 % and destruction ratio to be 40.2%.
- The total engine price becomes \$15.7M, and the total levelized cost rate is 227.6 \$/h.
- The average specific fuel and product exergy costs are 38 \$/GJ and 64 \$/GJ, respectively.
- The average exergoeconomic factor and relative cost difference of the proposed engine are 2% and 68%, respectively.
- The exergoenvironmental factor varies from 0.016% of F4 to 0.043% of F1, and the relative environmental difference has a minimum value of 59.2% of F1 and a maximum value of 71.3% of F2.

The system (M-2) is a new design of a marine engine comprising a steam Rankine cycle, gas Brayton cycle, and fuel cell systems. The following conclusions can be drawn from the study:

- The SRC can deliver a power of 5094 kW with a energetic efficiency of 29.4% and exergetic efficiency of 39%.
- The GBC can generate an average net power of 5165 kW with average energetic and exergetic efficiencies of 16% and 20.5%, respectively.

- The SOFC can produce 5288 kW with average thermal, electric, and exergetic efficiencies of 41%, 60%, and 93%, respectively.
- The hybrid combined engine can generate a total power of 15546 kW with average energetic and exergetic efficiencies of 61% and 43%, respectively.
- The maximum power is achieved using a mixture of methane, methanol, ethanol, dimethyl ether, and hydrogen (known as F5), which can produce 16780 kW electric power.
- A desalination unit uses the waste energy to produce 154 m³ of freshwater within 2 hours from the seawater with energetic efficiency of 86%, exergetic efficiency of 32%, and a GOR of 2.9.
- The specific fuel consumption is decreased from 405 g/kWh using MGO-DMA to 337 g/kWh using F5, which is a 16.8% improvement in fuel economy.
- Using sustainable fuels reduces carbon emissions by 53% and boosts energetic performance by about 110% and exergetic performance by around 11%, respectively.
- The exergetic efficiency of the proposed engine based on fuel and product principal has an average of 60.1% and the destruction ratio is about 39.9%.
- The normalized cost of the overall engine according to May 2022 is \$15.1M. Therefore, the levelized cost rate of the marine engine is 218.61 \$/h.
- The specific fuel and product exergy cost are the minimum of 10.7\$/GJ and 17.7 \$/GJ and are the maximum of 47.9 \$/GJ and 81.2 \$/GJ, and the average of 35 \$/GJ and 59 \$/GJ, respectively.
- The freshwater costs an average of 22.90 ¢/kg (22.90 ¢/L), and the brine costs an average of 27.66 ¢/kg.
- The exergoeconomic factor is about 2% and the relative cost difference for all fuel blends is an average of 68%.
- The total weight of this engine is 139,304 kg. The total component-related environmental impact and its rate are 21 kPt and 139 mPt/h.
- The fuel and product exergoenvironmental rates are about 13 kPt/h, while the destruction and losses exergoenvironmental rates have an average of 4450 Pt/h and 2 Pt/h, respectively.

- The relative environmental difference is minimum of 54% of F1 and a maximum of 69% of F4, and the exergoenvironmental factor is vary low to an average of 0.004%.

The system (M-3) presents a new design of a marine engine that is comprised of a gas Brayton cycle, fuel cell, and two cascaded organic Rankine cycles. The following conclusions can be drawn from the study:

- The GBC can generate an average net power of 7.5 MW with average energetic and exergetic efficiencies of 32.6% and 44.5%, respectively.
- The SOFC can produce about 4000 kW with average energy, electric, and exergetic efficiencies of 70%, 85%, and 72%, respectively.
- The integrated hybridized engine can produce an average total power of 15758 kW with average energetic and exergetic efficiencies of 38% and 46%, respectively.
- The maximum power is achieved using a mixture of ethanol and hydrogen (known as F2), which can produce 16087 kW of electric power.
- The topper and bottomer organic Rankine cycles can generate a total power of 4240 kW with average energetic and exergetic efficiencies of 11% and 18%, respectively.
- The organic Rankine cycle uses 35 kg of LNG to cool the topper and bottomer cycle and rejects heat of 16440 kW and returns to the liquid phase for storage.
- The specific fuel consumption is reduced from 701 g/kWh using MGO-DMA to 194 g/kWh using F1.
- Using sustainable fuels has reduced carbon emissions by 80% and improved energy efficiency by 14%, and exergy efficiency by 13%.
- The fuel, product, and destruction exergy rates are estimated to be 179 MW, 96 MW, and 83 MW, respectively, while the average of loss exergy rate is 0.7 MW.
- The average of exergetic efficiency and destruction ratio to be 53.6% and 46.4%, respectively.
- The normalized cost of the marine engine is \$16.8M based on CEPCI of May 2022. The levelized annual cost rate is 242.5\$/h.

- The relative cost difference in is within the range of 86.9 to 92.4%, and the exergoeconomic factor is the minimum of 2.5% for F4 and the maximum of 8.7% for F1.
- The total environmental impact, Y , and its rate, \dot{Y} , are 20kPt and 131.7mPt/h, respectively.
- The maximum specific fuel and product exergoenvironmental impacts are 16.11 and 29.8 mPt/MJ with F4, respectively, and the minimum impacts are 6.52 and 11.45 mPt/MJ occurring with F1.
- The relative environmental difference is an average of 84%, and the exergoenvironmental factor is about 0.006%.
- The SRC-SOFC-GT (M-2) is selected for the optimization study. The optimal output of this marine engine is increased to 16725 kW of the overall power and 70% of exoegetic efficiency and is decreased to 56% of relative cost difference and 51% of the relative environmental impact difference.

Finally, the proposed transportation engine can contribute to clean and sustainable aviation, rail, and marine transportation sectors. Using alternative fuels and advanced powering system indeed increased the net power of the engine and reduced the carbon emissions. Based on the exergoeconomic analysis, the economic aspects account mainly on the fuel prices. Also, the environmental impact of engines depends on the environmental impact of fuels, so if the fuels are produced by clean energy not fossil fuels, then the specific environment of fuels are reduced. However, using clean energy machines increases the fuel cost, which increases the economic aspects of the engine, since they still count on cost equations and increases yearly, as the rise of CEPCI. The possible solution is the government subsidy to the newly components for producing renewable fuels and making new transportation engine.

6.2 Recommendations

This thesis provides a comprehensive analysis of three transportation sectors for heavy and large engines. The thesis focuses on using five green fuels: such as green methane, methanol, ethanol, dimethyl ether, and hydrogen, in the form of five fuel blends as a hydrogen-based fuel. Also, the engine configurations have included fuel cells, gas turbines,

energy waste systems, internal combustion engines, and Rankine cycles. In addition, optimization has been implemented for four variables: compression ratio, expansion ratio, maximum pressure, and maximum temperature for light engines. Therefore, some recommendations can be fulfilled by future researchers in the following areas:

- A multi-criteria decision making (MCDM) tool can be used to the exiting data of different engines to determine the best choice by considering more than one criterion.
- Actual combustion reactions using traditional and alternative fuels can be investigated to determine other emissions such as SO_x, NO_x, and CO must be investigated.
- Experimental prototype for a hybrid fuel cell-engine, such as ICE combined with SOFC-GT is recommended to study the actual performance.
- More clean fuels can be investigated on the developed transportation engine to measure the engine power, engine efficiency, released emissions. The new clean fuels can form new clean fuel blends with different mass fractions. In addition, an optimization algorithm can be applied to select the high-quality fuel that gives maximum engine performance and less emissions.
- Hybridization of fuel cells with batteries can be implemented in some transportation engines. The sharing ratio of this hybridization can be investigated using the three methods and optimized to provide maximum engine power with less cost and less environmental impact.
- The geometry of different engine configurations can be built and designed including the safety protocols and spacious movement of workers in engine rooms.
- Multi-objective optimization can be studied on fuel cell parameters such as current density and losses to gain the maximum performance under high temperature and high pressure.

REFERENCES

- [1] WorldoMeter. Canada Population (2020). WorldoMeter n.d. <https://www.worldometers.info/world-population/canada-population/> (accessed December 25, 2020).
- [2] Transportation in Canada: Overview Report 2018. 2018.
- [3] Transportation | The Canadian Encyclopedia n.d. <https://www.thecanadianencyclopedia.ca/en/article/transportation> (accessed November 26, 2019).
- [4] El-Sayed AF. Aircraft Propulsion and Gas Turbine Engines. Florida, US: CRC Press; 2008. <https://doi.org/10.1201/9781420008777>.
- [5] Agarwal AK, Dhar A, Gautam A, Pandey A. Locomotives and rail road transportation: Technology, challenges and prospects. 2017. <https://doi.org/10.1007/978-981-10-3788-7>.
- [6] McBirnie SC. Marine Steam Engines and Turbines. London, UK: Butterworths; 1980.
- [7] Zamfirescu C, Dincer I. Ammonia as a green fuel and hydrogen source for vehicular applications. *Fuel Process Technol* 2009;90:729–37. <https://doi.org/10.1016/j.fuproc.2009.02.004>.
- [8] Dincer I, Høgerwaard J, Zamfirescu C. Clean Rail Transportation Options. Switzerland: Springer; 2016. <https://doi.org/10.2174/97816080528511120101>.
- [9] Natural Resources Canada. Energy Fact Book 2021-2022. 2021.
- [10] Energy Facts | Natural Resources Canada n.d. <https://www.nrcan.gc.ca/science-data/data-analysis/energy-data-analysis/energy-facts/20061> (accessed November 29, 2019).
- [11] Government of Canada. Progress towards Canada’s greenhouse gas emissions reduction target. 2019.
- [12] Home - Canada.ca n.d. <https://www.canada.ca/en.html> (accessed November 30, 2019).
- [13] Environment and natural resources - Canada.ca n.d. <https://www.canada.ca/en/services/environment.html> (accessed November 30, 2019).
- [14] Climate change - Canada.ca n.d. <https://www.canada.ca/en/services/environment/weather/climatechange.html> (accessed November 30, 2019).
- [15] Canada’s climate plan - Canada.ca n.d. <https://www.canada.ca/en/services/environment/weather/climatechange/climate-plan.html> (accessed November 30, 2019).
- [16] Our low carbon transportation future - Canada.ca n.d. <https://www.canada.ca/en/services/environment/weather/climatechange/climate->

- action/low-carbon-transportation-future.html (accessed November 30, 2019).
- [17] Transport Canada - Transport Canada n.d. <https://www.tc.gc.ca/en/transport-canada.html> (accessed November 30, 2019).
 - [18] Programs - Transport Canada n.d. <https://www.tc.gc.ca/en/programs-policies/programs.html> (accessed November 30, 2019).
 - [19] Hydrogen N, Hydrogen N, Vapor NH, Para- V, Entropy T, Conductivity T. III. Property of Hydrogen. Prop. Hydrog., n.d.
 - [20] Melaina M, Antonia O, Penev M. Blending Hydrogen into Natural Gas Pipeline Networks: A Review of Key Issues. Contract 2013;303:275–3000. <https://doi.org/10.2172/1068610>.
 - [21] Baratta M, d'Ambrosio S, Iemmolo D, Misul D. Method for the recognition of the fuel composition in CNG engines fed with natural gas/biofuel/hydrogen blends. J Nat Gas Sci Eng 2017;40:312–26. <https://doi.org/10.1016/j.jngse.2017.01.027>.
 - [22] Coker C. Food waste to renewable natural gas. Biocycle 2017;58:41–2.
 - [23] Parker N, Williams R, Dominguez-Faus R, Scheitrum D. Renewable natural gas in California: An assessment of the technical and economic potential. Energy Policy 2017;111:235–45. <https://doi.org/10.1016/j.enpol.2017.09.034>.
 - [24] Verhelst S, Turner JW, Sileghem L, Vancoillie J. Methanol as a fuel for internal combustion engines. Prog Energy Combust Sci 2019;70:43–88. <https://doi.org/10.1016/j.pecs.2018.10.001>.
 - [25] Methanol Institute. Methanol Gasoline Blends: Alternative Fuel For Today's Automobiles and Cleaner Burning Octane For Today's Oil Refinery. Methanol Inst 2016:1–18.
 - [26] Dogdibegovic E, Fukuyama Y, Tucker MC. Ethanol internal reforming in solid oxide fuel cells: A path toward high performance metal-supported cells for vehicular applications. J Power Sources 2020;449:227598. <https://doi.org/10.1016/j.jpowsour.2019.227598>.
 - [27] Greenwood JB, Erickson PA, Hwang J, Jordan EA. Experimental results of hydrogen enrichment of ethanol in an ultra-lean internal combustion engine. Int J Hydrogen Energy 2014;39:12980–90. <https://doi.org/10.1016/j.ijhydene.2014.06.030>.
 - [28] Jang J, Lee Y, Cho C, Woo Y, Bae C. Improvement of DME HCCI engine combustion by direct injection and EGR. Fuel 2013;113:617–24. <https://doi.org/10.1016/j.fuel.2013.06.001>.
 - [29] Semelsberger TA, Borup RL, Greene HL. Dimethyl ether (DME) as an alternative fuel. J Power Sources 2006;156:497–511. <https://doi.org/10.1016/j.jpowsour.2005.05.082>.
 - [30] Lee DS, Fahey DW, Skowron A, Allen MR, Burkhardt U, Chen Q, et al. The contribution of global aviation to anthropogenic climate forcing for 2000 to 2018. Atmos Environ 2021;244. <https://doi.org/10.1016/j.atmosenv.2020.117834>.
 - [31] Natural Resources Canada. Transportation Sector – Energy Use Analysis | Natural

- Resources Canada. Nat Resour Canada 2019.
<https://oee.nrcan.gc.ca/corporate/statistics/neud/dpa/showTable.cfm?type=AN§or=tran&juris=00&rn=1&page=0> (accessed January 14, 2021).
- [32] Natural Resources Canada. Energy Fact Book 2020-2021. 2020.
 - [33] Government of Canada. Canada's Action Plan to reduce greenhouse gas emissions from aviation. 2019.
 - [34] Kousoulidou M, Lonza L. Biofuels in aviation: Fuel demand and CO2 emissions evolution in Europe toward 2030. *Transp Res Part D Transp Environ* 2016;46:166–81. <https://doi.org/10.1016/j.trd.2016.03.018>.
 - [35] Schripp T, Grein T, Zinsmeister J, Oßwald P, Köhler M, Müller-Langer F, et al. Technical application of a ternary alternative jet fuel blend – Chemical characterization and impact on jet engine particle emission. *Fuel* 2021;288. <https://doi.org/10.1016/j.fuel.2020.119606>.
 - [36] Luo F, Song W, Chen W, Long Y. Investigation of kerosene supersonic combustion performance with hydrogen addition and fuel additive at low Mach inflow conditions. *Fuel* 2021;285:119139. <https://doi.org/10.1016/j.fuel.2020.119139>.
 - [37] Badami M, Nuccio P, Pastrone D, Signoretto A. Performance of a small-scale turbojet engine fed with traditional and alternative fuels. *Energy Convers Manag* 2014;82:219–28. <https://doi.org/10.1016/j.enconman.2014.03.026>.
 - [38] Petrescu RV V., Machín A, Fontánez K, Arango JC, Márquez FM, Petrescu FIT. Hydrogen for aircraft power and propulsion. *Int J Hydrogen Energy* 2020;45:20740–64. <https://doi.org/10.1016/j.ijhydene.2020.05.253>.
 - [39] Valera-Medina A, Morris S, Runyon J, Pugh DG, Marsh R, Beasley P, et al. Ammonia, Methane and Hydrogen for Gas Turbines. *Energy Procedia* 2015;75:118–23. <https://doi.org/10.1016/j.egypro.2015.07.205>.
 - [40] Bicer Y, Dincer I. Life cycle evaluation of hydrogen and other potential fuels for aircrafts. *Int J Hydrogen Energy* 2017;42:10722–38. <https://doi.org/10.1016/j.ijhydene.2016.12.119>.
 - [41] Ekici S, Altuntas O, Açikkalp E, Sogut MZ, Karakoc TH. Assessment of thermodynamic performance and exergetic sustainability of turboprop engine using mixture of kerosene and methanol. *Int J Exergy* 2016;19:295–314. <https://doi.org/10.1504/IJEX.2016.075666>.
 - [42] Ekici S. Thermodynamic mapping of A321-200 in terms of performance parameters, sustainability indicators and thermo-ecological performance at various flight phases. *Energy* 2020;202:117692. <https://doi.org/10.1016/j.energy.2020.117692>.
 - [43] Ekici S. Investigating routes performance of flight profile generated based on the off-design point: Elaboration of commercial aircraft-engine pairing. *Energy* 2020;193:116804. <https://doi.org/10.1016/j.energy.2019.116804>.
 - [44] Li Q, Wu G, Johnston CM, Zelenay P. Direct Dimethyl Ether Fuel Cell with Much Improved Performance. *Electrocatalysis* 2014;5:310–7.

<https://doi.org/10.1007/s12678-014-0196-z>.

- [45] Kim D, Park G, Choi B, Kim YB. Reaction characteristics of dimethyl ether (DME) steam reforming catalysts for hydrogen production. *Int J Hydrogen Energy* 2017;42:29210–21. <https://doi.org/10.1016/j.ijhydene.2017.10.020>.
- [46] Sato K, Tanaka Y, Negishi A, Kato T. Dual fuel type solid oxide fuel cell using dimethyl ether and liquefied petroleum gas as fuels. *J Power Sources* 2012;217:37–42. <https://doi.org/10.1016/j.jpowsour.2012.06.001>.
- [47] Sundmacher K, Kienle A, Pesch HJ, Berndt JF, Huppmann G. *Molten Carbonate Fuel Cells: Modeling, Analysis, Simulation, and Control*. Verlag, Weinheim, Germany: Wiley; 2007. <https://doi.org/10.1002/9783527611324>.
- [48] Ansarinasab H, Mehrpooya M. Investigation of a combined molten carbonate fuel cell, gas turbine and Stirling engine combined cooling heating and power (CCHP) process by exergy cost sensitivity analysis. *Energy Convers Manag* 2018;165:291–303. <https://doi.org/10.1016/j.enconman.2018.03.067>.
- [49] Hosseini SS, Mehrpooya M, Alsagri AS, Alrobaian AA. Introducing, evaluation and exergetic performance assessment of a novel hybrid system composed of MCFC, methanol synthesis process, and a combined power cycle. *Energy Convers Manag* 2019;197:111878. <https://doi.org/10.1016/j.enconman.2019.111878>.
- [50] Mehrpooya M, Ghorbani B, Moradi M. A novel MCFC hybrid power generation process using solar parabolic dish thermal energy. *Int J Hydrogen Energy* 2019;44:8548–65. <https://doi.org/10.1016/j.ijhydene.2018.12.014>.
- [51] Mehrpooya M, Ghorbani B, Bahnamiri FK. Basic design and thermodynamic analysis of a high helium content natural gas-fuel cell power plant. *J Clean Prod* 2020;262:121401. <https://doi.org/10.1016/j.jclepro.2020.121401>.
- [52] Mehrpooya M, Ghorbani B, Abedi H. Biodiesel production integrated with glycerol steam reforming process, solid oxide fuel cell (SOFC) power plant. *Energy Convers Manag* 2020;206:112467. <https://doi.org/10.1016/j.enconman.2020.112467>.
- [53] Ghorbani B, Mehrpooya M, Mousavi SA. Hybrid molten carbonate fuel cell power plant and multiple-effect desalination system. *J Clean Prod* 2019;220:1039–51. <https://doi.org/10.1016/j.jclepro.2019.02.215>.
- [54] Liu X, Reddi K, Elgowainy A, Lohse-Busch H, Wang M, Rustagi N. Comparison of well-to-wheels energy use and emissions of a hydrogen fuel cell electric vehicle relative to a conventional gasoline-powered internal combustion engine vehicle. *Int J Hydrogen Energy* 2019;45:972–83. <https://doi.org/10.1016/J.IJHYDENE.2019.10.192>.
- [55] Ahmadi P, Torabi SH, Afsaneh H, Sadegheih Y, Ganjehsarabi H, Ashjaee M. The effects of driving patterns and PEM fuel cell degradation on the lifecycle assessment of hydrogen fuel cell vehicles. *Int J Hydrogen Energy* 2019;1–14. <https://doi.org/10.1016/j.ijhydene.2019.01.165>.
- [56] Ji Z, Qin J, Cheng K, Liu H, Zhang S, Dong P. Performance evaluation of a turbojet engine integrated with interstage turbine burner and solid oxide fuel cell.

- Energy 2019;168:702–11. <https://doi.org/10.1016/j.energy.2018.11.088>.
- [57] Waters DF, Cadou CP. Engine-integrated solid oxide fuel cells for efficient electrical power generation on aircraft. *J Power Sources* 2015;284:588–605. <https://doi.org/10.1016/j.jpowsour.2015.02.108>.
 - [58] Jia T, Gong S, Pan L, Deng C, Zou JJ, Zhang X. Impact of deep hydrogenation on jet fuel oxidation and deposition. *Fuel* 2020;264:116843. <https://doi.org/10.1016/j.fuel.2019.116843>.
 - [59] Cai T, Zhao D. Effects of fuel composition and wall thermal conductivity on thermal and NO_x emission performances of an ammonia/hydrogen-oxygen micro-power system. *Fuel Process Technol* 2020;209:106527. <https://doi.org/10.1016/j.fuproc.2020.106527>.
 - [60] Ji Z, Qin J, Cheng K, Dang C, Zhang S, Dong P. Thermodynamic performance evaluation of a turbine-less jet engine integrated with solid oxide fuel cells for unmanned aerial vehicles. *Appl Therm Eng* 2019;160:114093. <https://doi.org/10.1016/j.applthermaleng.2019.114093>.
 - [61] Bakalis DP, Stamatis AG. Optimization methodology of turbomachines for hybrid SOFC-GT applications. *Energy* 2014;70:86–94. <https://doi.org/10.1016/j.energy.2014.03.093>.
 - [62] Verstraete D. Long range transport aircraft using hydrogen fuel. *Int J Hydrogen Energy* 2013;38:14824–31. <https://doi.org/10.1016/j.ijhydene.2013.09.021>.
 - [63] Wang B, Zhao D, Li W, Wang Z, Huang Y, You Y, et al. Current technologies and challenges of applying fuel cell hybrid propulsion systems in unmanned aerial vehicles. *Prog Aerosp Sci* 2020;116:100620. <https://doi.org/10.1016/j.paerosci.2020.100620>.
 - [64] Liu A, Wang B, Zeng W, Chen B, Weng Y. Catalytic combustion and system performance assessment of MCFC-MGT hybrid system. *Int J Hydrogen Energy* 2014;39:7437–46. <https://doi.org/10.1016/j.ijhydene.2014.02.175>.
 - [65] Devianto H, Li Z, Yoon SP, Han J, Nam SW, Lim TH, et al. The effect of electrolyte wettability on reforming catalyst in direct ethanol MCFC. *Curr Appl Phys* 2010;10:S26–8. <https://doi.org/10.1016/j.cap.2009.11.009>.
 - [66] Akram A, Jamil F, Alvi S. The effects of natural disasters on human development in developing and developed countries. *Int J Glob Warm* 2022;27:155–72. <https://doi.org/10.1504/IJGW.2022.123279>.
 - [67] Mostafa MM. World-wide concern for global warming: A stochastic cusp catastrophe analysis. *Int J Green Econ* 2019;13:19–39. <https://doi.org/10.1504/IJGE.2019.101449>.
 - [68] Singh OK. Combustion simulation and emission control in natural gas fuelled combustor of gas turbine. *J Therm Anal Calorim* 2016;125:949–57. <https://doi.org/10.1007/s10973-016-5472-0>.
 - [69] Mehri B, Pirouzfar V, Bagheri S, Pedram MZ. Modelling and optimization of exhaust pollutants and the properties and characteristics of ethanol-diesel through a statistical approach. *Can J Chem Eng* 2017;95:1054–62.

<https://doi.org/10.1002/cjce.22765>.

- [70] Xu Z, Liu J, Fu J. Experimental investigation on the urea injection and mixing module for improving the performance of urea-SCR in diesel engines. *Can J Chem Eng* 2018;96:1417–29. <https://doi.org/10.1002/cjce.23082>.
- [71] Hogerwaard J, Dincer I. Comparative efficiency and environmental impact assessments of a hydrogen assisted hybrid locomotive. *Int J Hydrogen Energy* 2016;41:6894–904. <https://doi.org/10.1016/j.ijhydene.2016.01.118>.
- [72] Marin GD, Naterer GF, Gabriel K. Rail transportation by hydrogen vs. electrification - Case study for Ontario Canada, I: Propulsion and storage. *Int J Hydrogen Energy* 2010;35:6084–96. <https://doi.org/10.1016/j.ijhydene.2010.03.098>.
- [73] Marin GD, Naterer GF, Gabriel K. Rail transportation by hydrogen vs. electrification - Case study for Ontario, Canada, II: Energy supply and distribution. *Int J Hydrogen Energy* 2010;35:6097–107. <https://doi.org/10.1016/j.ijhydene.2010.03.095>.
- [74] Hong Z, Li Q, Han Y, Shang W, Zhu Y, Chen W. An energy management strategy based on dynamic power factor for fuel cell/battery hybrid locomotive. *Int J Hydrogen Energy* 2018;43:3261–72. <https://doi.org/10.1016/j.ijhydene.2017.12.117>.
- [75] Meegahawatte D, Hillmans S, Roberts C, Falco M, McGordon A, Jennings P. Analysis of a fuel cell hybrid commuter railway vehicle. *J Power Sources* 2010;195:7829–37. <https://doi.org/10.1016/j.jpowsour.2010.02.025>.
- [76] Shinde AM, Dikshit AK, Singh RK, Campana PE. Life cycle analysis based comprehensive environmental performance evaluation of Mumbai Suburban Railway, India. *J Clean Prod* 2018;188:989–1003. <https://doi.org/10.1016/j.jclepro.2018.04.022>.
- [77] Zhang W, Li J, Xu L, Ouyang M, Liu Y, Han Q, et al. Comparison study on life-cycle costs of different trams powered by fuel cell systems and others. *Int J Hydrogen Energy* 2016;41:16577–91. <https://doi.org/10.1016/j.ijhydene.2016.03.032>.
- [78] Guo F, Qin J, Ji Z, Liu H, Cheng K, Zhang S. Performance analysis of a turbofan engine integrated with solid oxide fuel cells based on Al-H₂O hydrogen production for more electric long-endurance UAVs. *Energy Convers Manag* 2021;235:113999. <https://doi.org/10.1016/j.enconman.2021.113999>.
- [79] Sarma U, Ganguly S. Determination of the component sizing for the PEM fuel cell-battery hybrid energy system for locomotive application using particle swarm optimization. *J Energy Storage* 2018;19:247–59. <https://doi.org/10.1016/j.est.2018.08.008>.
- [80] Fan Y Van, Perry S, Klemeš JJ, Lee CT. A review on air emissions assessment: Transportation. *J Clean Prod* 2018;194:673–84. <https://doi.org/10.1016/j.jclepro.2018.05.151>.
- [81] Little DJ, Smith MR, Hamann TW. Electrolysis of liquid ammonia for hydrogen

- generation. *Energy Environ Sci* 2015;8:2775–81.
<https://doi.org/10.1039/c5ee01840d>.
- [82] Dong BX, Ichikawa T, Hanada N, Hino S, Kojima Y. Liquid ammonia electrolysis by platinum electrodes. *J Alloys Compd* 2011;509:S891–4.
<https://doi.org/10.1016/j.jallcom.2010.10.157>.
 - [83] Luo D, Sun Z, Wang R. Performance investigation of a thermoelectric generator system applied in automobile exhaust waste heat recovery. *Energy* 2022;238:121816. <https://doi.org/10.1016/j.energy.2021.121816>.
 - [84] Ma X, Hu S, Hu W, Luo Y, Cheng H. Experimental investigation of waste heat recovery of thermoelectric generators with temperature gradient. *Int J Heat Mass Transf* 2022;185:122342.
<https://doi.org/10.1016/j.ijheatmasstransfer.2021.122342>.
 - [85] Alegria P, Catalan L, Araiz M, Rodriguez A, Astrain D. Experimental development of a novel thermoelectric generator without moving parts to harness shallow hot dry rock fields. *Appl Therm Eng* 2022;200:117619.
<https://doi.org/10.1016/j.applthermaleng.2021.117619>.
 - [86] Uysal C, Keçebaş A. Advanced exergoeconomic analysis with using modified productive structure analysis: An application for a real gas turbine cycle. *Energy* 2021;223. <https://doi.org/10.1016/j.energy.2021.120085>.
 - [87] Chitgar N, Emadi MA. Development and exergoeconomic evaluation of a SOFC-GT driven multi-generation system to supply residential demands: Electricity, fresh water and hydrogen. *Int J Hydrogen Energy* 2021;46:17932–54.
<https://doi.org/10.1016/j.ijhydene.2021.02.191>.
 - [88] Aghbashlo M, Tabatabaei M, Khalife E, Roodbar Shojaei T, Dadak A. Exergoeconomic analysis of a DI diesel engine fueled with diesel/biodiesel (B5) emulsions containing aqueous nano cerium oxide. *Energy* 2018;149:967–78.
<https://doi.org/10.1016/j.energy.2018.02.082>.
 - [89] Cavalcanti EJC, Carvalho M, Ochoa AAV. Exergoeconomic and exergoenvironmental comparison of diesel-biodiesel blends in a direct injection engine at variable loads. *Energy Convers Manag* 2019;183:450–61.
<https://doi.org/10.1016/j.enconman.2018.12.113>.
 - [90] Lee YD, Ahn KY, Morosuk T, Tsatsaronis G. Exergetic and exergoeconomic evaluation of an SOFC-Engine hybrid power generation system. *Energy* 2018;145:810–22. <https://doi.org/10.1016/j.energy.2017.12.102>.
 - [91] Kumar P, Singh O. Thermoeconomic analysis of SOFC-GT-VARS-ORC combined power and cooling system. *Int J Hydrogen Energy* 2019;44:27575–86.
<https://doi.org/10.1016/j.ijhydene.2019.08.198>.
 - [92] Liu Y, Han J, You H. Performance analysis of a CCHP system based on SOFC/GT/CO₂ cycle and ORC with LNG cold energy utilization. *Int J Hydrogen Energy* 2019;44:29700–10. <https://doi.org/10.1016/j.ijhydene.2019.02.201>.
 - [93] Shi Y. Are greenhouse gas emissions from international shipping a type of marine pollution? *Mar Pollut Bull* 2016;113:187–92.

<https://doi.org/10.1016/j.marpolbul.2016.09.014>.

- [94] Khondaker AN, Rahman SM, Khan RA, Malik K, Muhyedeen MAR. Management of greenhouse gas emissions from maritime operations - Challenges and mitigation opportunities. *Int J Glob Warm* 2016;9:306–36. <https://doi.org/10.1504/IJGW.2016.075447>.
- [95] Chen J, Fei Y, Wan Z. The relationship between the development of global maritime fleets and GHG emission from shipping. *J Environ Manage* 2019;242:31–9. <https://doi.org/10.1016/j.jenvman.2019.03.136>.
- [96] Kanberoğlu B, Kökkülünk G. Assessment of CO₂ emissions for a bulk carrier fleet. *J Clean Prod* 2021;283. <https://doi.org/10.1016/j.jclepro.2020.124590>.
- [97] Einbu A, Pettersen T, Morud J, Tobiesen A, Jayarathna CK, Skagestad R, et al. Energy assessments of onboard CO₂ capture from ship engines by MEA-based post combustion capture system with flue gas heat integration. *Int J Greenh Gas Control* 2022;113:103526. <https://doi.org/10.1016/j.ijggc.2021.103526>.
- [98] Liu L, Tan F, Wu Z, Wang Y, Liu H. Comparison of the combustion and emission characteristics of NH₃/NH₄NO₂ and NH₃/H₂ in a two-stroke low speed marine engine. *Int J Hydrogen Energy* 2022;47:17778–87. <https://doi.org/10.1016/j.ijhydene.2022.03.239>.
- [99] Tipanluisa L, Thakkar K, Fonseca N, López JM. Investigation of diesel/n-butanol blends as drop-in fuel for heavy-duty diesel engines: Combustion, performance, and emissions. *Energy Convers Manag* 2022;255. <https://doi.org/10.1016/j.enconman.2022.115334>.
- [100] Zhao B, Wang H, Liao Y, Nasif O, Ali Alharbi S, Shanmugam S, et al. Effects of hydrocarbon liquid and HHO as the alternate fuel for unmodified compression ignition engines. *Fuel* 2022;324:124726. <https://doi.org/10.1016/j.fuel.2022.124726>.
- [101] Mueller CJ, Nilsen CW, Biles DE, Yraguen BF. Effects of fuel oxygenation and ducted fuel injection on the performance of a mixing-controlled compression-ignition optical engine with a two-orifice fuel injector. *Appl Energy Combust Sci* 2021;6:100024. <https://doi.org/10.1016/j.jaecs.2021.100024>.
- [102] Monsalve-Serrano J, Belgiorno G, Di Blasio G, Guzmán-Mendoza M. 1D simulation and experimental analysis on the effects of the injection parameters in methane–diesel dual-fuel combustion. *Energies* 2020;13:1–13. <https://doi.org/10.3390/en13143734>.
- [103] Xing H, Stuart C, Spence S, Chen H. Alternative fuel options for low carbon maritime transportation: Pathways to 2050. *J Clean Prod* 2021;297:126651. <https://doi.org/10.1016/j.jclepro.2021.126651>.
- [104] Wang Z, Cariveau R, Ting DSK, Xiong W, Wang Z. A review of marine renewable energy storage. *Int J Energy Res* 2019;43:6108–50. <https://doi.org/10.1002/ER.4444>.
- [105] Miretti F, Misul D, Gennaro G, Ferrari A. Hybridizing waterborne transport: Modeling and simulation of low-emissions hybrid waterbuses for the city of

- Venice. *Energy* 2022;244:123183. <https://doi.org/10.1016/j.energy.2022.123183>.
- [106] Long Y, Li G, Zhang Z, Wei W, Liang J. Hydrogen-rich gas generation via the exhaust gas-fuel reformer for the marine LNG engine. *Int J Hydrogen Energy* 2022;47:14674–86. <https://doi.org/10.1016/j.ijhydene.2022.02.188>.
 - [107] Yao S, Zhang Z, Huang H, Feng G, Xu J. Exergetic design and optimisation of LNG cold energy utilisation system for dual-fuel main engine of a container ship. *Int J Exergy* 2021;36:1–29. <https://doi.org/10.1504/IJEX.2021.117602>.
 - [108] Sürer MG, Arat HT. Advancements and current technologies on hydrogen fuel cell applications for marine vehicles. *Int J Hydrogen Energy* 2022;47:19865–75. <https://doi.org/10.1016/j.ijhydene.2021.12.251>.
 - [109] Ahn J, Noh Y, Park SH, Choi B Il, Chang D. Fuzzy-based failure mode and effect analysis (FMEA) of a hybrid molten carbonate fuel cell (MCFC) and gas turbine system for marine propulsion. *J Power Sources* 2017;364:226–33. <https://doi.org/10.1016/j.jpowsour.2017.08.028>.
 - [110] Lin L, Zhang L, Luo Y, Luo J, Chen C, Jiang L. Highly-integrated and Cost-efficient Ammonia-fueled fuel cell system for efficient power generation: A comprehensive system optimization and Techno-Economic analysis. *Energy Convers Manag* 2022;251:114917. <https://doi.org/10.1016/j.enconman.2021.114917>.
 - [111] Ahn J, Lee S, Jeong J, Choi Y. Comparative feasibility study of combined cycles for marine power system in a large container ship considering energy efficiency design index (EEDI). *Int J Hydrogen Energy* 2021;46:31816–27. <https://doi.org/10.1016/j.ijhydene.2021.07.068>.
 - [112] Mat Nawi Z, Kamarudin SK, Sheikh Abdullah SR, Lam SS. The potential of exhaust waste heat recovery (WHR) from marine diesel engines via organic rankine cycle. *Energy* 2019;166:17–31. <https://doi.org/10.1016/j.energy.2018.10.064>.
 - [113] Tian Z, Yue Y, Gu B, Gao W, Zhang Y. Thermo-economic analysis and optimization of a combined Organic Rankine Cycle (ORC) system with LNG cold energy and waste heat recovery of dual-fuel marine engine. *Int J Energy Res* 2020;44:9974–94. <https://doi.org/10.1002/ER.5529>.
 - [114] Liu C, Ye W, Li H, Liu J, Zhao C, Mao Z, et al. Experimental study on cascade utilization of ship's waste heat based on TEG-ORC combined cycle. *Int J Energy Res* 2021;45:4184–96. <https://doi.org/10.1002/ER.6083>.
 - [115] Vedachalam S, Baquerizo N, Dalai AK. Review on impacts of low sulfur regulations on marine fuels and compliance options. *Fuel* 2022;310:122243. <https://doi.org/10.1016/j.fuel.2021.122243>.
 - [116] Ampah JD, Yusuf AA, Afrane S, Jin C, Liu H. Reviewing two decades of cleaner alternative marine fuels: Towards IMO's decarbonization of the maritime transport sector. *J Clean Prod* 2021;320:128871. <https://doi.org/10.1016/j.jclepro.2021.128871>.
 - [117] Hountalas DT, Mavropoulos GC, Katsanos C, Daniolos S, Dolaptzis I, Mastorakis

- N. Potential for efficiency improvement of four-stroke marine diesel gensets by utilisation of exhaust gas energy. *Int J Glob Warm* 2016;10:133–57. <https://doi.org/10.1504/IJGW.2016.077910>.
- [118] Aghdoudchaboki Y, Khoshgard A, Salehi GR, Fazelpour F. Thermoeconomic assessment of a waste heat recovery system driven by a marine diesel engine for power and freshwater production. *Int J Exergy* 2020;33:231–53. <https://doi.org/10.1504/IJEX.2020.110841>.
- [119] Jafarzad A, Asgari N, Ranjbar F, Mohammadkhani F. Thermodynamic assessment and optimization of the influences of the steam-assisted turbocharging and organic Rankine cycle on the overall performance of a diesel engine-based cogeneration integrated with a reverse osmosis desalination unit. *Sustain Energy Technol Assessments* 2021;46:101175. <https://doi.org/10.1016/j.seta.2021.101175>.
- [120] Tsougranis EL, Wu D. A feasibility study of Organic Rankine Cycle (ORC) power generation using thermal and cryogenic waste energy on board an LNG passenger vessel. *Int J Energy Res* 2018;42:3121–42. <https://doi.org/10.1002/er.4047>.
- [121] Gonca G. Energy and exergy analyses of single and double reheat irreversible Rankine cycle. *Int J Exergy* 2015;18:402–22. <https://doi.org/10.1504/IJEX.2015.072907>.
- [122] Gude VG. Thermal desalination of ballast water using onboard waste heat in marine industry. *Int J Energy Res* 2019;43:6026–37. <https://doi.org/10.1002/ER.4647>.
- [123] Singh R, Singh O. Comparative study of combined solid oxide fuel cell-gas turbine-Organic Rankine cycle for different working fluid in bottoming cycle. *Energy Convers Manag* 2018;171:659–70. <https://doi.org/10.1016/j.enconman.2018.06.009>.
- [124] Lion S, Taccani R, Vlaskos I, Scrocco P, Vouvakos X, Kaiktsis L. Thermodynamic analysis of waste heat recovery using Organic Rankine Cycle (ORC) for a two-stroke low speed marine Diesel engine in IMO Tier II and Tier III operation. *Energy* 2019;183:48–60. <https://doi.org/10.1016/j.energy.2019.06.123>.
- [125] Chitgar N, Emadi MA, Chitsaz A, Rosen MA. Investigation of a novel multigeneration system driven by a SOFC for electricity and fresh water production. *Energy Convers Manag* 2019;196:296–310. <https://doi.org/10.1016/j.enconman.2019.06.006>.
- [126] Zhu S, Ma Z, Zhang K, Deng K. Energy and exergy analysis of the combined cycle power plant recovering waste heat from the marine two-stroke engine under design and off-design conditions. *Energy* 2020;210:118558. <https://doi.org/10.1016/j.energy.2020.118558>.
- [127] Wang E, Zhang M, Meng F, Zhang H. Zeotropic working fluid selection for an organic Rankine cycle bottoming with a marine engine. *Energy* 2022;243:123097. <https://doi.org/10.1016/j.energy.2021.123097>.
- [128] Liu C, Ye W, Li H, Liu J, Zhao C, Mao Z, et al. Experimental study on cascade utilization of ship's waste heat based on <sc>TEG-ORC</sc> combined cycle.

Int J Energy Res 2021;45:4184–96. <https://doi.org/10.1002/er.6083>.

- [129] Pallis P, Varvagiannis E, Braimakis K, Roumpedakis T, Leontaritis AD, Karellas S. Development, experimental testing and techno-economic assessment of a fully automated marine organic rankine cycle prototype for jacket cooling water heat recovery. *Energy* 2021;228:120596. <https://doi.org/10.1016/j.energy.2021.120596>.
- [130] Abbas WKA, Linnemann M, Baumhögger E, Vrabec J. Experimental study of two cascaded organic Rankine cycles with varying working fluids. *Energy Convers Manag* 2021;230. <https://doi.org/10.1016/j.enconman.2020.113818>.
- [131] Qu J, Feng Y, Zhu Y, Zhou S, Zhang W. Design and thermodynamic analysis of a combined system including steam Rankine cycle, organic Rankine cycle, and power turbine for marine low-speed diesel engine waste heat recovery. *Energy Convers Manag* 2021;245:114580. <https://doi.org/10.1016/j.enconman.2021.114580>.
- [132] Ahn J, Park SH, Lee S, Noh Y, Chang D. Molten carbonate fuel cell (MCFC)-based hybrid propulsion systems for a liquefied hydrogen tanker. *Int J Hydrogen Energy* 2018;43:7525–37. <https://doi.org/10.1016/j.ijhydene.2018.03.015>.
- [133] Choi CH, Yu S, Han IS, Kho BK, Kang DG, Lee HY, et al. Development and demonstration of PEM fuel-cell-battery hybrid system for propulsion of tourist boat. *Int J Hydrogen Energy* 2016;41:3591–9. <https://doi.org/10.1016/j.ijhydene.2015.12.186>.
- [134] Si Y, Wang R, Zhang S, Zhou W, Lin A, Zeng G. Configuration optimization and energy management of hybrid energy system for marine using quantum computing. *Energy* 2022;253:124131. <https://doi.org/10.1016/j.energy.2022.124131>.
- [135] EASA. Type-certificate data sheet for Trent 1000 series engines. vol. EASA.E.036. Blankenfelde-Mahlow, Germany: European Union Aviation Safety Agency; 2019.
- [136] Progress Rail: 710 series engines. Prog Rail n.d. <http://s7d2.scene7.com/is/content/Caterpillar/CM20170915-60253-59723> (accessed January 8, 2020).
- [137] EMD 710 diesel engine manual, specs and bolt torques n.d. <https://www.barringtondieselclub.co.za/emd/emd-710.html> (accessed January 9, 2020).
- [138] WARTSILA. Aframax tanker for oil and products: WSD42 111K 2014.
- [139] WARTSILA. WARTSILA Engines: WARTSILA X62 2014:1-2 datasheet.
- [140] Çengel YA, Boles MA. Thermodynamics: A Engineering Approach. Eighth. McGraw-Hill Education, USA; 2015. <https://doi.org/10.1109/MILCOM.2005.1605829>.
- [141] Ferguson CR, Kirkpatrick AT. Internal Combustion Engines: Applied Thermosciences. Third Edit. Sussex, UK: Wiley; 2016.
- [142] Kerrebrock JL. Aircraft Engines and Gas Turbines. Second Edi. Massachusetts,

- USA: The MIT Press; 2012. https://doi.org/10.1007/978-0-230-35686-3_1.
- [143] ASHRAE Technical Committee. ASHRAE Handbook: Refrigeration Inch-Pound Edition. 2014.
 - [144] Kennoy DH, Cunningham S, et al. ASHRAE Standard 34: Designation and Safety Classification of Refrigerants . 2019.
 - [145] Li ZL, Devianto H, Kwon HH, Yoon SP, Lim TH, Lee HI. The catalytic performance of Ni/MgSiO₃ catalyst for methane steam reforming in operation of direct internal reforming MCFC. *J Ind Eng Chem* 2010;16:485–9. <https://doi.org/10.1016/j.jiec.2010.01.058>.
 - [146] Vielstich W, Lamm A, Gasteiger HA. Handbook of Fuel Cells - Fundamentals, Technology and Applications. John Wiley & Sons, Ltd.; 2010. <https://doi.org/10.1002/9780470974001.f500032>.
 - [147] Koh JH, Kang BS, Lim HC. Analysis of temperature and pressure fields in molten carbonate fuel cell stacks. *AIChE J* 2001;47:1941–56. <https://doi.org/10.1002/aic.690470906>.
 - [148] Minutillo M, Perna A, Jannelli E. SOFC and MCFC system level modeling for hybrid plants performance prediction. *Int J Hydrogen Energy* 2014;39:21688–99. <https://doi.org/10.1016/j.ijhydene.2014.09.082>.
 - [149] Bessette NF, Wepfer WJ. A mathematical model of a tubular solid oxide fuel cell. *J Energy Resour Technol Trans ASME* 1995;117:43–9. <https://doi.org/10.1115/1.2835319>.
 - [150] Milewski J, Swirski K, Santarelli M, Leone P. Advanced methods of solid fuel cell modeling. Verlag London, UK: Springer-Verlag London Limited; 2011.
 - [151] Ji Z, Qin J, Cheng K, Guo F, Zhang S, Dong P. Thermodynamics analysis of a turbojet engine integrated with a fuel cell and steam injection for high-speed flight. *Energy* 2019;185:190–201. <https://doi.org/10.1016/j.energy.2019.07.016>.
 - [152] Carmo M, Fritz DL, Mergel J, Stolten D. A comprehensive review on PEM water electrolysis. *Int J Hydrogen Energy* 2013;38:4901–34. <https://doi.org/10.1016/j.ijhydene.2013.01.151>.
 - [153] Schröder M, Becker F, Kallo J, Gentner C. Optimal operating conditions of PEM fuel cells in commercial aircraft. *Int J Hydrogen Energy* 2021;46:33218–40. <https://doi.org/10.1016/j.ijhydene.2021.07.099>.
 - [154] Xing L, Das PK, Song X, Mamlouk M, Scott K. Numerical analysis of the optimum membrane/ionomer water content of PEMFCs: The interaction of Nafion® ionomer content and cathode relative humidity. *Appl Energy* 2015;138:242–57. <https://doi.org/10.1016/j.apenergy.2014.10.011>.
 - [155] O’Hayre R, Cha S-W, Colella WG, Prinz FB. Fuel cell fundamentals. Third Edit. Hoboken, New Jersey: John Wiley & Sons Inc.; 2016.
 - [156] Kocer AA, Ozturk M. Thermodynamic analysis of power and hydrogen production from renewable energy-based integrated system. *Int J Exergy* 2016;19:519–43. <https://doi.org/10.1504/IJEX.2016.075883>.

- [157] Godula-Jopek A. Hydrogen Production by Electrolysis. Weinheim, Germany: Wiley-VCH Verlag GmbH & Co.; 2015.
- [158] Hanada N, Kohase Y, Hori K, Sugime H, Noda S. Electrolysis of ammonia in aqueous solution by platinum nanoparticles supported on carbon nanotube film electrode. *Electrochim Acta* 2020;341:136027. <https://doi.org/10.1016/j.electacta.2020.136027>.
- [159] Boggs BK, Botte GG. On-board hydrogen storage and production: An application of ammonia electrolysis. *J Power Sources* 2009;192:573–81. <https://doi.org/10.1016/j.jpowsour.2009.03.018>.
- [160] Fernández-Yáñez P, Romero V, Armas O, Cerretti G. Thermal management of thermoelectric generators for waste energy recovery. *Appl Therm Eng* 2021;196. <https://doi.org/10.1016/j.applthermaleng.2021.117291>.
- [161] Wilbrecht S, Beitelschmidt M. The Potential of a Cascaded TEG System for Waste Heat Usage in Railway Vehicles. *J Electron Mater* 2018;47:3358–69. <https://doi.org/10.1007/s11664-018-6094-z>.
- [162] Xuan XC, Ng KC, Yap C, Chua HT. The maximum temperature difference and polar characteristic of two-stage thermoelectric coolers. *Cryogenics (Guildf)* 2002;42:273–8. [https://doi.org/10.1016/S0011-2275\(02\)00035-8](https://doi.org/10.1016/S0011-2275(02)00035-8).
- [163] Meddad M, Eddiai A, Farhan R, Benahadoug S, Mazroui M, Rguiti M. Design hybridization system of TEG/PZT for power generation: Modelling and experiments. *Superlattices Microstruct* 2019;127:86–92. <https://doi.org/10.1016/j.spmi.2018.03.007>.
- [164] Seyam S. Energy and Exergy Analysis of Refrigeration Systems. Low-temperature Technol., IntechOpen; 2019, p. 13. <https://doi.org/http://dx.doi.org/10.5772/57353>.
- [165] Dincer I. Refrigeration system and application. Third Edit. West Sussex, UK: Wiley& Sons Ltd; 2017.
- [166] Oil US, Co R. Ultra Low Sulfur Diesel Specifications n.d.;98421:98421.
- [167] Shehata MS, Elkotb MM, Salem H. Combustion characteristics for turbulent prevaporized premixed flame using commercial light diesel and kerosene fuels. *J Combust* 2014;2014. <https://doi.org/10.1155/2014/363465>.
- [168] Environment Canada Oil Properties Database. Marine Diesel Fuel Oil. Environ Canada, Emergencies Sci Technol Div 2010. <https://open.canada.ca/data/en/dataset/53c38f91-35c8-49a6-a437-b311703db8c5> (accessed October 1, 2022).
- [169] Guent MBV. Everything You Need to Know About Marine Fuels. *Chevron Prod Eng Dep* 2012;27:2009.
- [170] McCarty RD, Hord J, Roder HM. Selected Properties of Hydrogen (Engineering Design Data). US: U.S. Department of Commerce/National Bureau of Standards; 1981.
- [171] Pereira LG, Cavalett O, Bonomi A, Zhang Y, Warner E, Chum HL. Comparison of biofuel life-cycle GHG emissions assessment tools: The case studies of ethanol

- produced from sugarcane, corn, and wheat. *Renew Sustain Energy Rev* 2019;110:1–12. <https://doi.org/10.1016/j.rser.2019.04.043>.
- [172] Physical Property Data: Reference Manual. Version 10. Aspen Technology Inc.; 1999.
- [173] Sandler SI. Using Aspen Plus® in Thermodynamics Instruction: A step-by-step Guide. AICHE - Wiley; 2015.
- [174] Peng DY, Robinson DB. A New Two-Constant Equation of State. *Ind Eng Chem Fundam* 1976;15:59–64. <https://doi.org/10.1021/i160057a011>.
- [175] AspenTech. Aspen Physical Property System: Physical property data 11.1. Aspen Technology Inc.; 2001.
- [176] Seyam S, Dincer I, Agelin-Chaab M. Investigation of Potential Fuels for Hybrid Molten Carbonate Fuel Cell-Based Aircraft Propulsion Systems. *Energy & Fuels* 2021. <https://doi.org/10.1021/acs.energyfuels.1c00915>.
- [177] Seyam S, Dincer I, Agelin-Chaab M. Novel hybrid aircraft propulsion systems using hydrogen, methane, methanol, ethanol and dimethyl ether as alternative fuels. *Energy Convers Manag* 2021;238:114172. <https://doi.org/10.1016/j.enconman.2021.114172>.
- [178] Seyam S, Dincer I, Agelin-Chaab M. Development and assessment of a cleaner locomotive powering system with alternative fuels. *Fuel* 2021;185:120529. <https://doi.org/10.1016/j.applthermaleng.2020.116432>.
- [179] Seyam S, Dincer I, Agelin-Chaab M. Analysis of a newly developed locomotive engine employing sustainable fuel blends with hydrogen. *Fuel* 2022;319:123748. <https://doi.org/10.1016/j.fuel.2022.123748>.
- [180] Seyam S, Dincer I, Agelin-Chaab M. Development and assessment of a unique hybridized gas turbine locomotive engine operated by sustainable fuel blends. *Fuel* 2022;330:125638. <https://doi.org/10.1016/j.fuel.2022.125638>.
- [181] Seyam S, Dincer I, Agelin-Chaab M. An innovative study on a hybridized ship powering system with fuel cells using hydrogen and clean fuel blends. *Appl Therm Eng* 2023;221:119893. <https://doi.org/10.1016/j.applthermaleng.2022.119893>.
- [182] Seyam S, Dincer I, Agelin-Chaab M. Investigation of a hybridized combined cycle engine with SOFC system for marine applications. *J Therm Anal Calorim* 2022. <https://doi.org/10.1007/s10973-022-11765-y>.
- [183] Seyam S, Dincer I, Agelin-Chaab M. Investigation and comparative evaluation of a hybridized marine engine powered by eco-friendly fuels including hydrogen. *Int J Hydrogen Energy* 2022. <https://doi.org/10.1016/j.ijhydene.2022.11.008>.
- [184] Lazzaretto A, Tsatsaronis G. SPECO: A systematic and general methodology for calculating efficiencies and costs in thermal systems. *Energy* 2006;31:1257–89. <https://doi.org/10.1016/j.energy.2005.03.011>.
- [185] Turton R, Shaeiwitz JA, Bhattacharyya D, Whiting WB. Analysis, synthesis, and design of chemical processes. Fifth Edit. Pearson Education, Inc.; 2018.
- [186] Aji SS, Kim YS, Ahn KY, Lee YD. Life-cycle cost minimization of gas turbine

- power cycles for distributed power generation using sequential quadratic programming method. *Energies* 2018;11. <https://doi.org/10.3390/en11123511>.
- [187] EPA. Tool for the Reduction and Assessment of Chemical and Other Environmental Impacts (TRACI) User ' s Guide Tool for the Reduction and Assessment of Chemical and Other Environmental Impacts (TRACI). US Environ Prot Agency 2012;600/R-12/5:24.
- [188] Meyer L, Tsatsaronis G, Buchgeister J, Schebek L. Exergoenvironmental analysis for evaluation of the environmental impact of energy conversion systems. *Energy* 2009;34:75–89. <https://doi.org/10.1016/j.energy.2008.07.018>.
- [189] Sönnichsen N. Industrial electricity prices in major Canadian cities 2018. Statista 2020:Energy & Environmental Services/Electricity. <https://www.statista.com/statistics/579159/average-industrial-electricity-prices-canada-by-major-city/> (accessed September 22, 2020).
- [190] Tiseo I. Natural gas prices for industry globally by select country 2018. Statista 2020. <https://www.statista.com/statistics/253047/natural-gas-prices-in-selected-countries/> (accessed September 22, 2020).
- [191] Goedkoop M, Spriensma R. The Eco-indicator 99 - A damage oriented method for Life Cycle Impact Assessment. Amersfoort, The Netherlands: 2001.
- [192] Baayen H. The Eco-indicator 99: Manual for Designers. vol. 42. 2000. [https://doi.org/10.1016/S1359-6462\(99\)00348-6](https://doi.org/10.1016/S1359-6462(99)00348-6).
- [193] Hirschler R, Weidema B, Althaus H-J, Bauer C, Doka G, Dones R, et al. Implementation of Life Cycle Impact Assessment Methods Data v2.2 (2010). Zürich, Switzerland: 2010.
- [194] Ontario Energy Board. Historical electricity rates. Ontario Energy Board 2022. <https://www.oeb.ca/consumer-information-and-protection/electricity-rates/historical-electricity-rates> (accessed November 3, 2022).
- [195] City of Toronto. Water Rates & Fees. City Toronto 2022. <https://www.toronto.ca/services-payments/property-taxes-utilities/utility-bill/water-rates-fees/> (accessed November 3, 2022).
- [196] Gibb J, Horne W, Langdon C, Lui K, Nikolejsin D, O'Brien C. Power Perspectives 2022 - Hydrogen Overview. McCarthy Tétraut 2022. https://www.mccarthy.ca/en/insights/blogs/canadian-energy-perspectives/power-perspectives-2022-hydrogen-overview?utm_source=Mondaq&utm_medium=syndication&utm_campaign=LinkedIn-integration (accessed November 3, 2022).
- [197] US Energy Information Administration. US ammonia prices rise in response to higher international natural gas prices; up by a factor of 6 in two years. Green Car Congr 2022. <https://www.greencarcongress.com/2022/05/20220511-nh3.html> (accessed November 3, 2022).
- [198] ChemAnalyst. Methanol Price Trend and Forecast. ChemAnalyst 2022. <https://www.chemanalyst.com/Pricing-data/methanol-1> (accessed November 3, 2022).

- [199] ChemAnalyst. Ethanol Price Trend and Forecast. ChemAnalyst 2022.
<https://www.chemanalyst.com/Pricing-data/ethanol-13> (accessed November 3, 2022).
- [200] IndiaMART. Dimethyl Ether, 1 Kg . IndiaMART 2022.
<https://www.indiamart.com/proddetail/dimethyl-ether-16839018455.html>
(accessed November 3, 2022).
- [201] ChemAnalyst. Natural Gas Price Trend and Forecast. ChemAnalyst 2022.
<https://www.chemanalyst.com/Pricing-data/natural-gas-1339> (accessed November 3, 2022).
- [202] IndiaMart. Caustic Potash - Potassium Hydroxide KOH Latest Price. IndiaMART 2022. <https://dir.indiamart.com/impcat/caustic-potash.html> (accessed November 3, 2022).
- [203] Indiamart. Liquid n-pentane. Indiamart 2022.
<https://www.indiamart.com/proddetail/n-pentane-26470177388.html> (accessed December 4, 2022).
- [204] LPG Price. Butane price today. Gas Agency 2022. <https://lpg-price.com/butane> (accessed December 4, 2022).
- [205] CHEMI. Propylene market price & analysis. Chem Mark Price Insight 2022.
https://www.echemi.com/productsInformation/pid_Seven1855-propylene.html
(accessed December 4, 2022).
- [206] Bryan's Fuel. Propane tanks for sale in Ontario. Bryan's Fuel 2020.
<https://bryansfuel.on.ca/propane-tanks-for-sale/> (accessed December 4, 2022).
- [207] US Department of Energy. Alternative Fuel Price Report. US DOE Clean Cities 2020.
https://afdc.energy.gov/files/u/publication/alternative_fuel_price_report_april_2020.pdf.
- [208] Government of Canada. Fuel Consumption Levies in Canada. Nat Resour Canada 2022.
- [209] Turing Bot. TuringBot. TuringBot 2023. <https://turingbotsoftware.com/> (accessed February 1, 2023).
- [210] Maleki A, Nazari MA, Pourfayaz F. Harmony search optimization for optimum sizing of hybrid solar schemes based on battery storage unit. Energy Reports 2020;6:102–11. <https://doi.org/10.1016/j.egyr.2020.03.014>.
- [211] Coello CAC, Lechuga MS. MOPSO : A Proposal for Multiple Objective Particle Swarm Optimization. Proc 2002 Congr Evol Comput CEC'02 (Cat No 02TH8600), IEEE 2002;2:1051–6.
- [212] Seyam S, Dincer I, Agelin-Chaab M. Exergetic assessment of a newly designed solid oxide fuel cell-based system combined with a propulsion engine. Energy 2022;239:122314. <https://doi.org/10.1016/j.energy.2021.122314>.
- [213] Seyam S, Dincer I, Agelin-Chaab M. Environmental impact assessment of a newly developed solid oxide fuel cell-based system combined with propulsion engine

- using various fuel blends for cleaner operations. *Sustain Mater Technol* 2023;35:e00554. <https://doi.org/10.1016/j.susmat.2022.e00554>.
- [214] Lolis P. Development of a Preliminary Weight Estimation Method for Advanced Turbofan Engines. Cranfield University, 2014.
- [215] Seyam S, Dincer I, Agelin-Chaab M. Exergetic, exergoeconomic and exergoenvironmental analyses of a hybrid combined locomotive powering system for rail transportation. *Energy Convers Manag* 2021;245:114619. <https://doi.org/10.1016/j.enconman.2021.114619>.
- [216] Progress Rail. EMD 710 SERIES ENGINE BENEFITS ENGINES 710 n.d.
- [217] Arora CP. Refrigeration and Air Conditioning. Third. New Delhi: Tata McGraw-Hill Publishing Company Limited; 2009.
- [218] Jemaa R Ben, Issa N Ben, Issa S Ben, Bellagi A. Exergy analysis of a diffusion absorption refrigeration system. *Int J Exergy* 2008;5:626–37. <https://doi.org/10.1504/IJEX.2008.020829>.
- [219] Morosuk T, Tsatsaronis G, Koroneos C. On the Effect of Eco-indicator selection on the conclusions obtained from an exergoenvironmental analysis. *Proc. ECOS*, 2012, p. 1–13.
- [220] Morosuk T, Tsatsaronis G, Koroneos C. Environmental impact reduction using exergy-based methods. *J Clean Prod* 2016;118:118–23. <https://doi.org/10.1016/j.jclepro.2016.01.064>.
- [221] Ma Q, Zhang Q, Chen J, Huang Y, Shi Y. Effects of hydrogen on combustion characteristics of methane in air. *Int J Hydrogen Energy* 2014;39:11291–8. <https://doi.org/10.1016/j.ijhydene.2014.05.030>.
- [222] Yoon W, Park J. Parametric study on combustion characteristics of virtual HCCI engine fueled with methane–hydrogen blends under low load conditions. *Int J Hydrogen Energy* 2019;44:15511–22. <https://doi.org/10.1016/j.ijhydene.2019.04.137>.
- [223] Tian Z, Wang Y, Zhen X, Liu D. Numerical comparative analysis on performance and emission characteristics of methanol/hydrogen, ethanol/hydrogen and butanol/hydrogen blends fuels under lean burn conditions in SI engine. *Fuel* 2022;313:123012. <https://doi.org/10.1016/j.fuel.2021.123012>.
- [224] Londerville S, Colannino J, Baukal CE. Combustion fundamentals. John Zink Hamworthy Combust Handbook, Second Ed Vol 1 - Fundam 2012:79–124. <https://doi.org/10.1201/b11619>.
- [225] Seyam S, Dincer I, Agelin-chaab M. Efficiency, Economic and Environmental Impact Assessment of a Newly Developed Rail Engine using Hydrogen and Other Sustainable Fuel Blends. *E-Prime - Adv Electr Eng Electron Energy* n.d.:1–36.
- [226] Global Petrol Prices. Methane prices around the world. *Glob Pet Prices* 2022. https://www.globalpetrolprices.com/methane_prices/ (accessed November 5, 2022).
- [227] Solar Turbines. Centaur(R) 40: Gas Turbine Compressor Set. A Caterp Co

- 2021:1–2. <https://s7d2.scene7.com/is/content/Caterpillar/CM20150703-52095-02409> (accessed February 12, 2022).
- [228] Solar Turbines. Saturn 20 General Specifications. Sol Turbines A Caterp Companyurbines 2018:DS20PG/1118/EO.
- [229] Solar Turbines: A Caterpillar Company. TAURUS 65 Gas Turbine Generator Set 2018:DS65PG/1218/EO datasheet.
- [230] Solar Turbines. MARS® 100: Gas Turbine Generator Set 2021.
- [231] Alfa Laval. Aalborg MP-C 2018:MDD00248EN 1507 datasheet.
- [232] TURBODEN. TURBODEN gas expander 2021:1-14 datasheet.
- [233] Martinez I. Aerospace Engine Data. Isidoro Martinez 2021:2–6. <http://imartinez.etsiae.upm.es/~isidoro/bk3/c17/Propulsion.pdf>.

APPENDICES

Appendix A: Similarity of Papers

This thesis's high similarity is exclusively due to the candidate's 16 published journal papers, which are based on this thesis. As a result, some critical information, equations, and illustrations, which cannot be revised without losing the work's fundamental essence, are maintained. The similarity of the thesis and each of those papers is listed below. For this reason, permissions are duly obtained from the publishers to include this information in the thesis.

The following are the publishers' obtained permissions for the reuse of the published work based on this Ph.D. thesis.

1) Wiley: (International Journal of Energy Research)

Article C, in the Copyright transfer agreement:

“3. Final Published Version. The Owner hereby licenses back to the Contributor the following rights with respect to the final published version of the Contribution (the "Final Published Version"):”

“b. Re-use in other publications. The right to re-use the Final Published Version or parts thereof for any publication authored or edited by the Contributor (excluding journal articles) where such re-used material constitutes less than half of the total material in such publication. In such case, any modifications must be accurately noted.”

2) Elsevier:

Article: Submission declaration and verification in the Guide for authors:

“Submission of an article implies that the work described has not been published previously (except in the form of an abstract, a published lecture or academic thesis, see 'Multiple, redundant or concurrent publication' for more information), that it is not under consideration for publication elsewhere, that its publication is approved by all authors and tacitly or explicitly by the responsible authorities where the work was carried out, and that, if accepted, it will not be published elsewhere in the same form, in English or in any other language, including electronically without the written consent of the copyright-holder. To verify originality, your article may be checked by the originality detection service Crossref Similarity Check.”

Similarity of the thesis reaches the overall value of 59%, and the similarity of the published work that is based on the thesis.

Aviation Transportation:

S. Seyam, I. Dincer, M. Agelin-Chaab, Environmental impact assessment of a newly developed solid oxide fuel cell-based system combined with propulsion engine using various fuel blends for cleaner operations. *Sustain Mater Technol* 2023;35: e00554. <https://doi.org/10.1016/j.susmat.2022.e00554>.

with a similarity index of 2%

S. Seyam, I. Dincer, M. Agelin-Chaab, Economic and environmental impact assessments of hybridized aircraft engines with hydrogen and other fuels, *Int. J. Hydrogen Energy*. 47 (2022) 11669–11685. <https://doi.org/10.1016/j.ijhydene.2022.01.171>.

with a similarity index of 1%

S. Seyam, I. Dincer, M. Agelin-Chaab, Exergetic assessment of a newly designed solid oxide fuel cell-based system combined with a propulsion engine, *Energy*. 239 (2022) 122314. <https://doi.org/10.1016/j.energy.2021.122314>.

with a similarity index of 2%

S. Seyam, I. Dincer, M. Agelin-Chaab, Investigation of potential fuels for hybrid molten carbonate fuel cell-based aircraft propulsion systems, *Energy & Fuels*. (2021). <https://doi.org/10.1021/acs.energyfuels.1c00915>.

with a similarity index of 2%

S. Seyam, I. Dincer, M. Agelin-Chaab, Investigation of two hybrid aircraft propulsion and powering systems using alternative fuels, *Energy*. 232 (2021) 121037. <https://doi.org/10.1016/j.energy.2021.121037>.

with a similarity index of 2%

S. Seyam, I. Dincer, M. Agelin-Chaab, Novel hybrid aircraft propulsion systems using hydrogen, methane, methanol, ethanol and dimethyl ether as alternative fuels, *Energy Convers. Manag.* 238 (2021) 114172. <https://doi.org/10.1016/j.enconman.2021.114172>.

with a similarity index of 1%

Rail Transportation:

S. Seyam, I. Dincer, M. Agelin-Chaab, Modelling of a New Fuel Cell Based Rail Engine System Using Green Fuel Blends. *Appl Therm Eng* (2023) 120527.

<https://doi.org/10.1016/j.applthermaleng.2023.120527>. (Under publication process)

with a similarity index of 5%

S. Seyam, I. Dincer, M. Agelin-Chaab, Efficiency, economic and environmental impact assessments of a new integrated rail engine system using hydrogen and other sustainable fuel blends. E-Prime - Adv Electr Eng Electron Energy 3 (2023) 100109. <https://doi.org/10.1016/j.prime.2023.100109>.

with a similarity index of 4%

S. Seyam, I. Dincer, M. Agelin-Chaab, Analysis of a newly developed locomotive engine employing sustainable fuel blends with hydrogen, Fuel. 319 (2022) 123748. <https://doi.org/10.1016/j.fuel.2022.123748>.

with a similarity index of 2%

S. Seyam, I. Dincer, M. Agelin-Chaab, Development and assessment of a unique hybridized gas turbine locomotive engine operated by sustainable fuel blends, Fuel. 330 (2022) 125638. <https://doi.org/10.1016/j.fuel.2022.125638>.

with a similarity index of 4%

S. Seyam, I. Dincer, M. Agelin-Chaab, Exergetic, exergoeconomic and exergoenvironmental analyses of a hybrid combined locomotive powering system for rail transportation, Energy Convers. Manag. 245 (2021) 114619. <https://doi.org/10.1016/j.enconman.2021.114619>.

with a similarity index of 2%

S. Seyam, I. Dincer, M. Agelin-Chaab, Development and assessment of a cleaner locomotive powering system with alternative fuels, Fuel. 185 (2021) 120529. <https://doi.org/10.1016/j.applthermaleng.2020.116432>.

with a similarity index of 6%

Marine Transportation:

S. Seyam, I. Dincer, M. Agelin-Chaab, An innovative study on a hybridized ship powering system with fuel cells using hydrogen and clean fuel blends, Appl. Therm. Eng. 221 (2023) 119893. <https://doi.org/10.1016/j.applthermaleng.2022.119893>.

with a similarity index of 6%

S. Seyam, I. Dincer, M. Agelin-Chaab, Investigation of a hybridized combined cycle engine with SOFC system for marine applications. J Therm Anal Calorim (2022). <https://doi.org/10.1007/s10973-022-11765-y>.

with a similarity index of 5%

S. Seyam, I. Dincer, M. Agelin-Chaab, Investigation and comparative evaluation of a hybridized marine engine powered by eco-friendly fuels including hydrogen, Int. J. Hydrogen Energy. (2022). <https://doi.org/10.1016/j.ijhydene.2022.11.008>.

with a similarity index of 5%

Appendix B: Cost Equations of major components

This appendix displays the cost equations of major components that used in transportation engines.

Table B.1 Cost equations of major components used in the engine systems.

Components	Z_k	Year	CEPCI
Compressor	$Z_c = \left(\frac{44.71 \times \dot{m}_a}{0.95 - \eta_c} \right) r_c \ln(r_c)$	2003	402
Turbine	$Z_T = \left(\frac{301.45 \times \dot{m}_a}{0.94 - \eta_T} \right) \ln \left(\frac{P_{T,e}}{P_{T,i}} \right) \left[1 + \exp \left(0.035 (T_{T,i} - 1570K) \right) \right]$	2003	402
Pump	$Z_P = 705.48 P_P^{0.71} \left[1 + 5 \exp \left(\frac{0.2}{1 - \eta_P} \right) \right]$	2003	402
Combustion chamber	$Z_{CC} = \left(\frac{28.98 \times \dot{m}_a}{0.995 - \frac{P_{CC,e}}{P_{CC,i}}} \right) \left[1 + \exp \left(0.015K (T_{CC,i} - 1540K) \right) \right]$	2003	402
Regenerator	$Z_{REG} = 4122 \left(\frac{\dot{m}_g \dot{Q}_{reg}}{0.018 [W/(m^2K)] \times \Delta T_{LMTD}} \right)^{0.6}$	1996	381.7
Heat recovery steam generator	$Z_{HRSG} = 4131.8 \left[\left(\frac{\dot{Q}_{EC}}{\Delta T_{LMTD,EC}} \right)^{0.8} + \left(\frac{\dot{Q}_{EV}}{\Delta T_{LMTD,EV}} \right)^{0.8} + \left(\frac{\dot{Q}_{SH}}{\Delta T_{LMTD,SH}} \right)^{0.8} \right] + 13380 \dot{m}_w + 1489.7 \dot{m}_g^{1.2}$	2003	402
Steam turbine	$Z_{ST} = 3880.5 \dot{W}_{ST}^{0.7} \times \left[1 + \left(\frac{0.05}{1 - \eta_{ST}} \right)^3 \right] \times \left[1 + 5 \exp \left(\frac{T_{ST,i} - 866}{10.42} \right) \right]$	2003	402
Condenser	$Z_{COND} = 280.74 \times \frac{\dot{Q}_{COND}}{2.2 [kW/(m \cdot K)] (T_{h,i} - T_{cw,i})} + 746 \dot{m}_{CW} + 70.5 \times \dot{Q}_{COND} \times (-0.6936 \ln(T_{h,i} - T_{cw,e}) + 2.1989)$	2003	402
Fuel cell	$Z_{FC} = A_{FC} (2.96 - 1907 T_{FC}) + Z_{aux} + Z_{inv}$ $Z_{inv} = 10^5 \left(\frac{W_{FC}}{500} \right)^{0.7}$ $Z_{aux} = 0.1 \times Z_{FC}$	2010	579
ICE	$Z_{ICE} = \dot{W}_{ICE} \cdot (863.55 - 69.355 \cdot \ln \dot{W}_{ICE})$	2010	579

Appendix C: Life cycle analysis of material processing

This appendix displays the life cycle of material processing that used in the transportation engines in three sectors.

Table C.1 The EI-99 results of material processing

Material parts and processing	Description	EI-99 mPt/unit	Material/energy unit	Points mPt/kg
Compressors				
<i>Cast (33% wt)</i>				
- Forming: gas-fired heat with furnace	60% of Furnace efficiency, 0.47 MJ/kg of melting heat.	5.3 mPt/MJ	0.1551 MJ	0.82
- Brazing	0.5% of weight	4000 mPt/kg	0.00165 kg	6.60
<i>Axis (22% wt)</i>				
- Milling, turning, drilling	5% of weight	0.8 mPt/m ³	1.4 m ³	1.13
<i>Vane blades (45%)</i>				
- Forming: gas-fired heat with furnace	60% of Furnace efficiency, 0.47 MJ/kg of melting heat.	5.3 mPt/MJ	0.2115 MJ	1.12
- Milling 40%, turning, drilling	5% of weight	0.8 mPt/m ³	3 m ³	2.07
- Shearing/stamping-steel 4.5%	1mm thickness × perimeter	6E-05 mPt/mm ²	700 mm ²	0.04
Total				11.78
Turbines				
<i>Cast (33% wt)</i>				
- Forming: gas-fired heat with furnace	60% of Furnace efficiency, 0.47 MJ/kg of melting heat.	5.3 mPt/MJ	0.1551 MJ	0.82
- Brazing	0.5% of weight	4000 mPt/kg	0.00165 kg	6.60
<i>Axis (22% wt)</i>				
- Milling, turning, drilling	5% of weight	0.8 mPt/m ³	1.4 m ³	1.13
<i>Vane blades (45% wt)</i>				
- Forming: gas-fired heat with furnace	60% of Furnace efficiency, 0.47 MJ/kg of melting heat.	5.3 mPt/MJ	0.2115 MJ	1.12
- Milling 40%, turning, drilling	5% of weight	0.8 mPt/m ³	3 m ³	2.07
- Shearing/stamping-steel 4.5%	1mm thickness × perimeter	6E-05 mPt/mm ²	350 mm ²	0.02
Total				11.76
Reactors/ combustor				
Shearing/Stamping-steel	1 mm thickness × perimeter	6E-05 mPt/mm ²	0.14 mm ²	0.000085
Brazing	0.5% of weight	4000 mPt/kg	0.005 kg	20
Total				20.00
Fuel cell				
Steel 92%, Shearing	1mm thickness × perimeter	6E-05 mPt/mm ²	0.92 mm ²	5.5E-05
Copper 3%	Extrusion	72 mPt/kg	0.03 kg	2.16
Aluminum 5%, Forming: gas-fired heat with furnace	60% of Furnace efficiency, 0.60 MJ/kg of melting heat.	5.3 mPt/MJ	0.6 MJ	3.18
Zinc coating	0.1 m ² /kg surface per weight	49 mPt/m ²	0.1 m ²	4.90
Brazing	0.3% of weight	4000 mPt/kg	0.003 kg	12.00
Total				22.24

Appendix D: Life cycle analysis of material production

This appendix is describing the material production of major components of transportation engines that used in the thesis.

Table D.1 Material production of major components

#	Mat.	EI99 [mPt/kg]	Mat. [%]	EI99 [mPt/kg]	#	Mat.	EI99 [mPt/kg]	Mat. [%]	EI99 [mPt/kg]
FAN	Steel	86	33.0	28.4	S1	Steel	86	100	86.0
	Steel low al.	110	45.0	49.5	S2	Steel	86	100	86.0
	Cast iron	240	22.0	52.8	MX1	Steel	86	100	86.0
IPC			100	131	SR	Steel high al.	910	56	509.6
	Steel	86	33.0	28.4		Alumina	1,000	44	440.0
	Steel low al.	110	45.0	49.5				100	950
HPC	Cast iron	240	22.0	52.8	WGS	Steel high al.	910	84	764.4
			100	131		Alumina	1,000	1	10.4
	Steel	86	33.0	28.4		Cast iron	240	15	36.2
CC	Steel low al.	110	45.0	49.5		Nickel	1,200	0.010	0.1
	Cast iron	240	22.0	52.8				100	811
			100	131	SOFC	Steel	86	80	68.8
HPT	steel	86	33.0	28.4		Steel high al.	910	12.1	109.8
	steel high al.	910	67.0	609.7		Zinc	3,200	0.4	12.8
			100	638		Nickel	5,200	0.3	15.6
IPT						Purified silica	60	0.01	0.0
	Steel	86	25	21.5		Plastics	400	0.03	0.1
	Steel high al.	110	75	82.5		Copper	1,400	0.3	4.2
LPT			100	104		Microporous alumina-silica	450	0.75	3.4
	Steel	86	25	21.5		Alumina	1000	5.69	56.9
	Steel high al.	110	75	82.5		Aluminum	500	0.45	2.3
			100	104				100	274

al. .. alloy